Molecular modelling of MYC hyperfunction in plasma cell differentiation

Panagiota Vardaka

Submitted in accordance with the requirements for the degree of Doctor of Philosophy (PhD)

The University of Leeds

School of Medicine

October 2024

As the candidate, I confirm that the work submitted is my own, except where work which has formed part of a jointly authored publication has been included. My contribution and the other authors to this work has been explicitly indicated below. I confirm that appropriate credit has been given within the thesis where reference has been made to the work of others.

Results, data analysis, individual figures and graphs from Chapter 3, Chapter 4 and Chapter 5 of this thesis have also been utilised in a manuscript uploaded on bioRxiv and submitted for publication in an academic journal. This manuscript is currently under experimental revisions and its bioRxiv uploaded version is cited as 'Panagiota Vardaka, Eden Page, Matthew A Care, Sophie Stephenson, Ben Kemp, Michelle Umpierrez, Eleanor O'Callagan, Adam Mabbutt, Roger Owen, Daniel J Hodson, Gina M Doody, Reuben M Tooze. Enforced MYC expression selectively redirects transcriptional programs during human plasma cell differentiation. bioRxiv 2024.04.18.589889; doi: https://doi.org/10.1101/2024.04.18.589889'.

I confirm that the work contained in this thesis and included in the manuscript is my own and that appropriate credit has been given in the thesis where reference has been made to the work of others included as co-authors in the manuscript. In more detail, RNA-sequencing data analysis in Chapter 3, Chapter 4 and Chapter 5 was conducted by Dr. Matthew Care. IgM ELISAs in Chapter 3 were performed by Michelle Umpierrez. Sub-cloning of the MB deletion mutant retroviral constructs used in Chapter 4 and their validation by diagnostic digests were conducted by Eden Page. MSCV-backbone, pHIT60 and GALV-MTR plasmids as well as reagents and HEK-293 cells were on occasion shared with or provided by Ben Kemp, Adam Mabbutt, Ellie O'Callagan and Sophie Stephenson for the completion of experiments included in Chapter 3, Chapter 4 and Chapter 5. I can confirm that apart from otherwise stated in the text the work included is my own.

Acknowledgements

I would like to express my gratitude to my two patient and knowledgeable supervisors, Prof. Reuben Tooze and Dr. Gina Doody, for all their support during my PhD studies. Their suggestions and scientific guidance helped me learn and improve academically throughout the years. Also, they provided a supportive environment within the group for me to evolve and collaborate with other scientists, giving me space to explore while always providing their supervision. I am also very grateful to my sponsors from the Ella Dickinson Charitable Foundation without whom this PhD research would not have been possible. Next, I would like to thank my lab mates who were my best friends throughout this journey and were always understanding even when I was grumpy. A special thanks goes to Sophie Stephenson, who was always willing to help and share with me her knowledge and expertise in the field even when she was extremely busy herself. Also, I would like to thank Dr. Matthew Care for conducting the bioinformatic analysis of my RNA-sequencing experiments while always replying to my questions and emails trying to help me complete this journey. I am also very grateful to Dr. Alessio Lepore, Dr. Erica Wilson and Dr. Claire Taylor for all the guidance regarding containment class II work. Finally, a huge thank you goes to my parents and my sister for their consistent support, encouragement, and belief in me.

I acknowledge the use of Grammarly (Grammarly Inc., v1.2.106.1490, *https://www.grammarly.com/*) only for proofreading purposes as a grammar, punctuation and spelling check tool.

I. Abstract

c-MYC (MYC) is a major regulator of transcription and a critical transcription factor in the germinal centre (GC). Long-lived plasma cells (PCs) are generated mainly from a GC response and their differentiation requires MYC downregulation. MYC can also act as a potent oncogene when deregulated being involved in multiple mature B cell cancers. Tumour cells overexpressing MYC can also frequently deregulate the anti-apoptotic protein BCL2 for their survival. Thus, MYC and BCL2 oncogenes collaborate in cancers of the B lineage. The goal of this study was to investigate the impact of MYC overexpression on human PC differentiation. A previously established system was utilised to differentiate human memory B cells into PCs *in vitro*. *MYC* and *BCL2*, protecting from MYC-mediated apoptosis, were overexpressed utilising retroviral vectors. This experimental setting allowed the development of a novel model system where the effect of enforced MYC and BCL2 expression was assessed, for the first time to our knowledge, under conditions permissive for PC differentiation.

Acute overexpression of MYC and BCL2 at the stage of activated memory B cells did not result in transformation and PC differentiation arrest. MYC-BCL2 overexpressing cells acquired an abnormal plasmablast-like phenotype with impaired antibody secretion. In addition, MYC overexpression drove metabolic over secretory transcriptional reprogramming as differentiation progressed. Within the transactivation domain at the N-terminus of MYC, deletion of the MBI domain showed marginal differences to the MYCwt condition suggesting its dispensable role in MYC hyperfunction. On the contrary, deletion of the MB0 weakened the MYC hyperfunction effect while deletion of the MBII resulted in an almost non-functional MYC upon its overexpression. Thus, both the MBII and MB0 domains of MYC are required for its hyperfunction-mediated effect under conditions permissive for PC differentiation. Within MBII the results demonstrated a critical dependence on the DCMW motif and W135.

II. Table of contents

III. List of figures

IV. List of tables

V. Abbreviations

A	Alanine
aa	Amino acids
ABC	Activated B cell
ABC-DLBCL	Activated B cell-diffuse large B cell lymphoma
AID	Activation-induced cytidine deaminase
ANOVA	Analysis of variance
APC	Antigen presenting cell
APRIL	A proliferation-inducing ligand
ARID1A	AT-rich interaction domain 1A
ASC	Antibody secreting cell
ASCT	Autologous stem cell transplantation
ATF6	Activating transcription factor 6
ATP	Adenosine triphosphate
BACH2	BTB and CNC homolog 2
BAK	BCL2 antagonist/killer 1
BAX	BCL2 associated protein X
BCA	Bicinchoninic acid assay
BCL11A	B cell lymphoma/leukemia 11A
BCL2	B cell lymphoma 2
BCL6	B cell lymphoma 6
BCL-W	B cell lymphoma-w
BCL-xL	B cell lymphoma-extra large
BCR	B cell receptor
BH	BCL2 homology
BID	BH3 interacting-domain death agonist
BIK	BCL2 interacting killer
BIM	BCL2 interacting mediator of cell death
BIN1	Bridging integrator 1
BL	Burkitt lymphoma
BLIMP1	B lymphocyte-induced maturation protein 1

BMF	BCL2 modifying factor
BOK	BCL2 ovarian killer
bp	base pairs
BR	Basic region
BRAF	V-Raf murine sarcoma viral oncogene homolog B1
BRTC	Beta-transducin repeat containing E3 ubiquitin protein ligase
BSA	Bovine serum albumin
BTG1	B cell translocation gene 1
BTG2	B cell translocation gene 2
C	Cysteine
C/EBP	CCAAT/enhancer binding protein
CARD11	Caspase recruitment domain-containing protein 11
CCND1	Cyclin D1
CCND3	Cyclin D3
CD	Cluster of differentiation
CDC34	Cell division cycle 34
CDK	Cyclin-dependent kinase
CDKN1A	Cyclin-dependent kinase inhibitor 1A
CDKN2B	Cyclin-dependent kinase inhibitor 2B
cDNA	Complementary DNA
ChIP-seq	Chromatin immunoprecipitation sequencing
CHOP	Cyclophosphamide, doxorubicin, vincristine, prednisone
CLL	Chronic lymphocytic leukemia
CM	Complete medium
Co-IP	Co-immunoprecipitation
CREBBP	CREB binding protein
CSR	Class switch recombination
CYLD	Cylindromatosis lysine 63 deubiquitinase
D	Aspartic acid
D	Diversity segment
DAVID	Database for annotation, visualization and integrated discovery
DEG	Differentially expressed gene

DERL3	Derlin 3
DH	Double hit
dH_2O	Distilled water
DHL	Double hit lymphoma
DLBCL	Diffuse large B cell lymphoma
DMEM	Dulbecco's Modified Eagle Medium
DMSO	Dimethyl sulfoxide
DNA	Deoxyribonucleic acid
DRd	Daratumumab, lenalidomide, dexamethasone
DTX	Deltex
E	Glutamic acid
EBF1	Early B cell factor 1
eBL	Endemic Burkitt lymphoma
EBV	Epstein-Barr virus
EdU	5-ethynyl-2'-deoxyuridine
EEF1B2	Eukaryotic translation elongation factor 1 beta 2
eIF4B	Eukaryotic translation initiation factor 4B
ELISA	Enzyme-linked immunosorbent assay
ENO1	Enolase 1
EP300	E1A binding protein P300
EPRS1	Glutamyl-prolyl-tRNA synthetase 1
ER	Endoplasmic reticulum
ERG1	Early growth response 1
ERLEC1	Endoplasmic reticulum lectin 1
ERN1	Endoplasmic reticulum to nucleus signaling 1
EZH2	Enhancer of zeste homolog 2
F	Phenylalanine
FABP5	Fatty acid binding protein 5
FACS	Fluorescence-activating cell sorting
FAM46C	Family with sequence similarity 46 member C
FBXW7	F-box and WD repeat domain containing 7
FBXW8	F-box and WD repeat domain containing 8

FDC	Follicular dendritic cell
FDR	False discovery rate
FGFR3	Fibroblast growth factor receptor 3
FICD	FIC domain protein adenylyltransferase
FL	Follicular lymphoma
FSC-A	Forward scatter-area
G	Glycine
Gadd45a	Growth arrest and DNA damage-inducible 45 alpha
GALV-MTR	Gibbon ape leukemia virus-transmembrane region, cytoplasmic tail, R peptide
GALV-MULV	Gibbon ape leukemia virus-murine leukemia virus
GC	Germinal centre
GCB	Germinal centre B cell
GCB-DLBCL	Germinal centre B cell-diffuse large B cell lymphoma
GCN5	General control non-depressible 5
GLUT1	Glucose transporter protein type 1
GNA13	G protein subunit alpha 13
GNL3	G protein nucleolar 3
GO	Gene ontology
GSE	Gene signature enrichment
GSK3β	Glycogen synthase kinase 3 beta
h	hours
HAT	Histone acetyltransferase
HERPUD1	Homocysteine responsive endoplasmic reticulum resident ubiquitin like domain member 1
HGBL	High-grade B cell lymphoma
HIFBS	Heat-inactivated fetal bovine serum
HIV	Human immunodeficiency virus
HK2	Hexokinase 2
HLH-LZ	Helix-loop-helix-leucine zipper
HRK	Harakiri
HRP	Horseradish peroxidase
HSCs	Haematopoietic stem cells

HSPD1	Heat shock protein family D member 1
HUWE1	HECT, UBA and WWE domain containing E3 ubiquitin protein ligase 1
I	Isoleucine
iBL	Immunodeficiency-associated Burkitt lymphoma
ID3	Inhibitor of DNA-binding 3
IG	Immunoglobulin
IGH	Immunoglobulin heavy chain
IGK	Immunoglobulin light κ chain
IGL	Immunoglobulin light λ chain
IL	Interleukin
IMDM	Iscove's Modified Dulbecco's Medium
IRE1a	Inositol requiring enzyme 1 alpha
IRES	Ribosomal entry site
IRF4	Interferon regulatory factor 4
ISOs	Isotypes
ITAMs	Immunoreceptor tyrosine-based activation motifs
J	Joining segment
JAG2	Jagged canonical Notch ligand 2
K48	Lysine 48
kDa	Kilodalton
KDM2B	Lysine demethylase 2B
KDM6A	Lysine demethylase 6A
KISS1R	Kisspeptin 1 receptor
KMT2D	Lysine methyltransferase 2D
KRAS	Kirsten rat sarcoma viral oncogene homolog
L	Leucine
LB	Luria-Bertani
LDHA	Lactate dehydrogenase A
LPS	Lipopolysaccharide
LTB	Lymphotoxin B
LTR	Likelihood ratio test
LZ	Light zone

M	Methionine
M	Module
MACS	Magnetic-activated cell sorting
MAPK	Mitogen activated protein kinase
MAX	MYC associated factor X
MB	MYC homology box
MC29	Myelocytomatosis virus
MCL-1	Myeloid cell leukemia sequence 1
MDS	Multidimensional scaling
MEF2B	Myocyte enhancer factor 2B
MEV	Module expression value
MGUS	Monoclonal gammopathy of undetermined significance
MHC	Major histocompatibility complex
MIZ-1	Myc-interacting zinc-finger protein 1
MM	Multiple myeloma
MMSET	Multiple myeloma SET domain
MOMP	Mitochondrial outer membrane permeabilization
mRNA	messenger RNA
MS4A1	Membrane spanning 4-domains A1
MSCV	Murine stem cell virus
mTOR	Mammalian target of rapamycin
mTORC1	Mammalian target of rapamycin complex 1
mTORC2	Mammalian target of rapamycin complex 2
MYBBP1A	Myb-binding protein 1A
MYC	Myelocytomatosis oncogene
MYD88	Myeloid differentiation primary response 88
N	Asparagine
NF-κB	Nuclear factor kappa B
NGS	Next generation sequencing
NHSBT	NHS Blood and Transplant
NOS	Not otherwise specified
NOTCH1	Neurogenic locus notch homolog protein 1

NOTCH2	Neurogenic locus notch homolog protein 2
NRAS	Neuroblastoma RAS viral oncogene homolog
NuA4	Nucleosome acetyltransferase of H4
P	Proline
PAX5	Paired box 5
PBL	Plasmablastic lymphoma
PBMCs	Peripheral blood mononuclear cells
PBS	Phosphate saline buffer
PC	Plasma cell
PERK	Protein kinase R-like endoplasmic reticulum kinase
PGCNA	Parsimonious gene correlation network analysis
PI3K	Phosphoinositide 3-kinase
PIK3R1	Phosphoinositide 3-kinase regulatory subunit 1
PIN1	Peptidyl-prolyl cis-trans isomerase NIMA-interacting 1
pIRES2-EGFP	plasmid IRES2-enhanced green fluorescent protein
PNUTS	PP1 nuclear-targeting subunit
pola-R-CHP	Polatuzumab-rituximab-cyclophosphamide, doxorubicin, prednisone
PP1	Protein phosphatase 1
PP2A	Protein phosphatase 2A
PPIs	Protein protein interactions
PPP2R5A	Protein phosphatase 2 regulatory subunit B' alpha
PRDM1	PR domain zinc finger protein 1
P-TEFb	Positive transcription elongation factor b
PTM	Post-translational modification
PUMA	p53 upregulated modulator of apoptosis
RAG1	Recombination activating gene 1
RAG2	Recombination activating gene 2
RAS	Rat sarcoma
RB1	RB Transcriptional Corepressor 1/Retinoblastoma 1
R-CHOP	Rituximab-cyclophosphamide, doxorubicin, vincristine, prednisone
R-CHP	Rituximab-cyclophosphamide, doxorubicin, prednisone
REF	Rat embryonic fibroblasts

RET	Rearranged during transfection-receptor tyrosine kinase
RFTN1	Raftlin, lipid raft linker 1
RHOA	Ras homolog family member A
RNA	Ribonucleic acid
RNA-seq	RNA-sequencing
RRP12	Ribosomal RNA processing 12 homolog
RSL1D1	Ribosomal L1 domain-containing protein 1
RT	Room temperature
RUNX1	Runt-related transcription factor 1
S	Serine
S6K1	S6 kinase beta 1
sBL	Sporadic Burkitt lymphoma
SD	Standard deviation
SDC1	Syndecan 1
SDS	Sodium dodecyl sulfate
SGK1	Serum/glucocorticoid regulated kinase 1
SHM	Somatic hypermutation
SKP2	S-phase kinase associated protein 2
SLC20A1	Solute carrier family 20 member 1
SMM	Smouldering myeloma
SNPs	Single-nucleotide polymorphisms
SOCS1	Suppressor of cytokine signaling 1
SORD	Sorbitol dehydrogenase
SP1	Specificity protein 1
SP140	Speckled protein 140
SPEN	Spen family transcriptional repressor
SREBF1	Sterol regulatory element binding transcription factor 1
SSC-A	Side scatter-area
STAGA	SPT3-TAF9-GCN5L acetylase
T	Threonine
TAD	Transactivation domain
TBE	Tris-borate-EDTA

TBP	TATA box binding protein
TBS	Tris-buffered saline
TCF3	Transcription factor 3
TD	T-dependent
TdT	Terminal deoxynucleotidyl transferase
TE	Tris-EDTA
TERT	Telomerase reverse transcriptase
TET2	Tet methylcytosine dioxygenase 2
TF	Transcription factor
TFB1M	Mitochondrial transcription factor B1
T_{FH}	T follicular helper cells
TFIID	Transcription factor IID
TFIIF	Transcription factor IIF
TH	Triple hit
THL	Triple hit lymphoma
TI	T-independent
TIP60	Tat-interactive protein 60
TLR	Toll-like receptor
TMB	3,3’,5,5’-Tetramethylbenzidine
TNFRSF14	Tumor necrosis factor receptor superfamily member 14
TP53	Tumour protein P53
TRAF3	Tumor necrosis factor receptor-associated factor 3
TRAP1	Tumor necrosis factor receptor-associated protein 1
TRIM32	Tripartite motif-containing protein 32
TRPC4AP	Transient receptor potential cation channel subfamily C member 4 associated protein
TRRAP	Transformation-transactivation domain-associated protein
TRUSS	TNF receptor-associated ubiquitous scaffolding and signaling protein
TXNDC5	Thioredoxin domain-containing protein 5
UMAP	Uniform manifold approximation and projection
UPR	Unfolded protein response
UPS	Ubiquitin-proteasome system

UV	Ultraviolet
V	Variable segment
VCd	Bortezomib, cyclophosphamide, dexamethasone
VRd	Bortezomib, lenalidomide, dexamethasone
Vs	Versus
VST	Variance stabilizing transformation
VTd	Bortezomib, thalidomide, dexamethasone
W	Tryptophan
W135	Tryptophan 135
WDR5	WD repeat domain 5
WHO	World Health Organization
WT	Wild type
XBP1	X-box binding protein 1
XPOT	Exportin for tRNA

Chapter 1 – Introduction

1.1 Aggressive mature B cell cancers

B lymphocytes are cells of the haematopoietic lineage and develop in the bone marrow (1). Mature B cells enter the bloodstream to migrate into peripheral organs such as the lymph nodes and spleen. There, pathogen recognition drives their differentiation into memory B cells or effector cells termed plasma cells (PCs) providing long-lasting immunity against the same pathogens. During this process differentiating B cells in the periphery can acquire genetic aberrations that can result in their malignant transformation and ultimately cancer (2, 3). Mature B cells bearing genetic abnormalities are the cell of origin in multiple types of haematological cancers.

B cell lymphomas are haematological cancers developing from distinct B cell subtypes undergoing differentiation in the peripheral organs. They are divided into two discrete categories, Hodgkin and non-Hodgkin lymphomas (4). All the B cell lymphoma cases that do not belong in Hodgkin lymphoma are identified as non-Hodgkin lymphomas. There are several types of non-Hodgkin lymphomas which are subdivided into indolent (low-grade) and aggressive (high-grade) based on their clinical behavior and the rate of their tumour growth (5). Low-grade B cell lymphomas are characterized by slow growth with the most common being follicular lymphoma (FL) (5, 6). On multiple occasions, FL can transform into high-grade, or fast-growing, lymphomas such as diffuse large B cell lymphoma (DLBCL) (7). Characteristic examples of high-grade non-Hodgkin lymphomas are Burkitt lymphoma (BL), DLBCL and double-hit or triple-hit lymphomas (DHLs/THLs). All these types of non-Hodgkin lymphomas originate from B cells differentiating in distinct compartments of a germinal centre (GC) reaction happening in the follicles of a lymph node and described in detail in section 1.3.3.1. Thus, the cell of origin in most non-Hodgkin B cell lymphomas is considered a GC B cell.

Mature B cell-derived types of cancer can also originate from the terminal effectors of the B lineage and their precursors. These cells have completed and exited a GC reaction and differentiated first into plasmablasts and finally into terminal effector PCs. Plasmablastic lymphoma (PBL) and multiple myeloma (MM) are haematological cancers derived from plasmablast-like cells and PCs respectively (8, 9).

The stage of B cell differentiation in which a genetic abnormality manifests, is a critical factor in determining the cancer type that will be developed. Thus, the different mature B cell malignancies are

discriminated based on their cell of origin as GC or post-GC-derived (Figure 1.1). Extensive research and genomic sequencing studies have provided valuable insights into the cytogenetics and mutational profile in both high-grade non-Hodgkin B cell lymphoma and MM. Despite that, there are still unelucidated mechanisms contributing to the pathogenesis of these cancer types that limit current advances in treatment development. Genetic aberrations in the oncogene *c-MYC* (*MYC*) have been recurrently reported in combination with additional genetic alterations in these tumours (10-15). BL, DLBCL and MM will be described in more detail below as characteristic examples based on their dependence on *MYC* rearrangements and mutations, frequency and severity respectively.

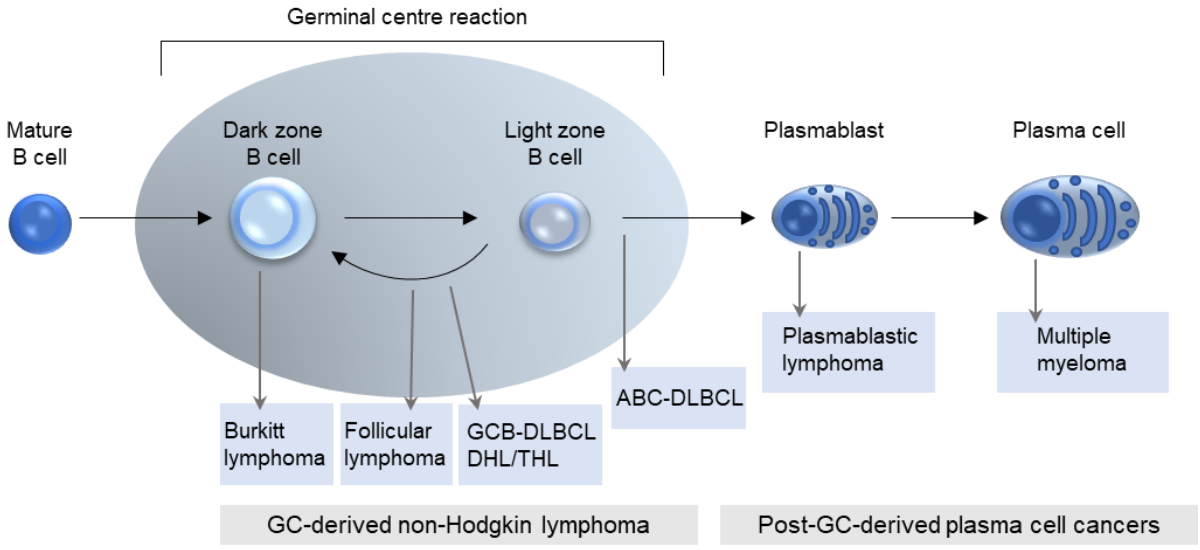

Figure 1.1: The cell of origin in non-Hodgkin lymphoma and PC cancers. Non-Hodgkin lymphomas originate from GC B cells localizing different compartments of the GC. BL originates from B cells in the dark zone of a GC. FL, a type of DLBCL (termed GCB-DLBCL) and DHL/THL originate from cells resembling GC B cells which have completed the GC reaction in the light zone and are reentering the dark zone. Another type of DLBCL (termed ABC-DLBCL) can develop from cells in the light zone compartment committed to a plasmablast fate. GC B cells that have differentiated into plasmablasts exit the GC and can be the cell of origin for PBL. Terminally differentiated plasmablasts turn into PCs, the cell of origin in MM (adaptation from Basso & Dalla-Favera, 2015 (3)).

1.1.1 Burkitt lymphoma

BL is a high-grade B cell lymphoma comprising 2% of the non-Hogdkin lymphoma cases every year. It can manifest at any age in both children and adults and it has three epidemiology-based variants (16). In regions with increased infection rates by the protozoan parasite *Plasmodium falciparum*, causing malaria, the main variant is the endemic BL (eBL). Regions with decreased cases of malaria infection are

characterized by non-endemic sporadic BL (sBL) while the immunodeficiency-associated BL (iBL) is related to the human immunodeficiency virus (HIV). Another critical risk factor mainly in eBL and sBL is the Epstein-Barr virus (EBV) infection. 90% of eBL and 10-30% of sBL patients are EBV-positive (16-18). Studies have shown that EBV^+ BL patients demonstrate biological differences from the EBV^- BL cases (16, 19, 20). EBV^+ BL carry more mutations and higher activity of the phosphoinositide 3-kinase (PI3K) pathway while the EBV^- BL cases have mutations in the *ID3-TCF3* axis which are also considered specific to BL and rarely detected in other types of B cell lymphomas (12, 16, 21-23). Thus, the detection of EBV infection is currently suggested as a new system to categorise BL cases regardless of their epidemiological classification (10, 16).

BL malignant cells are characterized by a high proliferation rate accompanied by increased cell death through apoptosis. Thus, they are highly positive for the Ki67 proliferation marker as the tumour cells grow rapidly forming extranodal masses (17). The manifestation of the disease for children is growing masses in the jaw or periorbital area as well as the abdomen while in adults, such regions are also the abdomen, the head and the neck (24, 25). Early clinical features linked with the disease are abdominal pain, nausea, and vomiting accompanied by manifestations known as B-symptoms which include weight loss, night sweating and high temperature. Even though BL is considered a highly curable disease, patients presenting BL symptoms must be urgently diagnosed and receive treatment. This includes different courses of chemotherapy and a combination with rituximab (anti-CD20) is a common course of action in first-line therapy (17, 26). Patients with relapsed BL usually have poor survival.

The cells of origin in BL are GC B cells of the dark zone that do not have upregulated expression of *MYC* (27, 28). Despite that, all types of BL present as primary genetic alteration the chromosomal translocation of *MYC* locus to the enhancer element of either of the immunoglobulin genes loci, *IGH, IGK* or *IGL* (17, 27, 29, 30). The juxtaposition of the regulatory element of an immunoglobulin gene locus by *MYC* results in overexpressed MYC protein demonstrating abnormally increased function. *MYC* chromosomal translocation is in the majority of cases the only genetic translocation to take place in BL (22). Thus, BL is characterized by a simple karyotype demonstrating t(8;14)(q24;q32), t(2;8)(p12;q24) or t(8;22)(q24;q11) chromosomal translocations of *MYC* in *IGH*, *IGK* or *IGL* locus respectively and considered a homogeneous disease (22, 27, 30-32).

MYC locus rearrangements do not suffice to drive lymphomagenesis. In addition, mutations of specific genes have been reported as recurrent events in BL patients and required for BL development. Genes such as *MYC, ID3, TP53, SMARCA4, RET, RHOA, PIK3R1, NOTCH1, ARID1A* and *GNA13* are recurrently mutated

(12, 22, 29, 33). Mutations in *ID3* and *TCF3* contribute to B cell receptor (BCR) signalling and PI3K pathway activation promoting survival in BL cells (23). 50-60% of BL cases carry such inactivating *ID3* mutations while activating mutations in *TCF3* have been identified in 10-25% of the cases (17, 22, 23). In normal B cell differentiation in the GC reaction, ID3 inhibits E2A, encoded by *TCF3* (23). Thus, inactivating mutations of ID3 block E2A inhibition while the activating mutations in *TCF3* induce E2A function promoting malignant cell survival via tonic BCR signalling (3, 23). In addition, *TCF3* expression in BL activates CCND3 promoting the cell cycle progression of malignant cells (3, 23, 33). Abnormal increase in CCND3 function has been recurrently observed in 30% of BL cases either because of activating mutations in *CCND3* or as a result of the cooperative signalling in PI3K and MYC pathways (3, 23, 33, 34). Thus, the initial MYC ectopic overexpression through chromosomal rearrangements requires the subsequently accumulated genetic mutations for lymphomagenesis and BL progression (Figure 1.2) (12, 22).

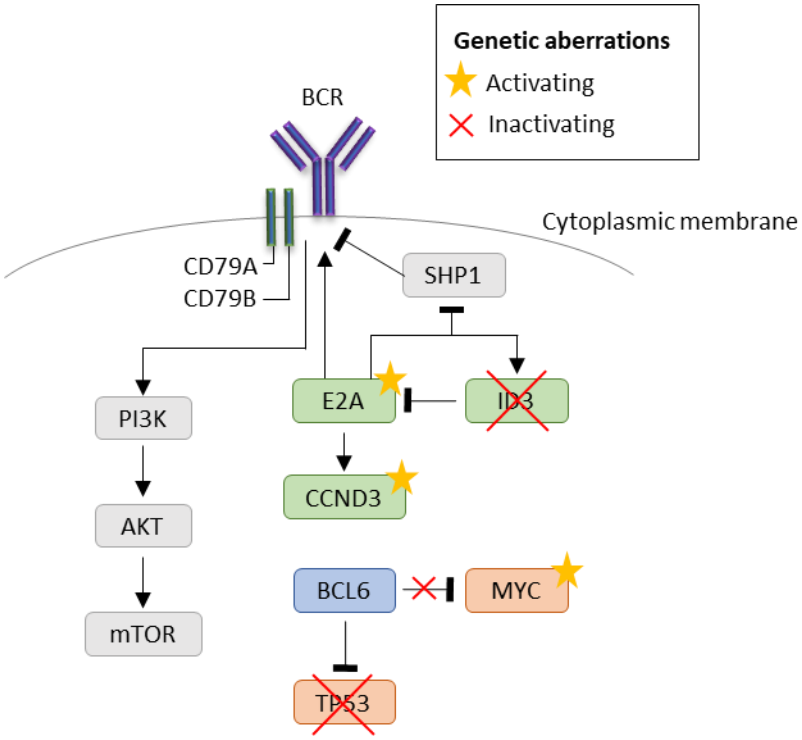

Figure 1.2: Deregulation of signalling pathways in BL. Activating genetic aberrations such as chromosomal translocations and subsequently acquired mutations result in abnormally increased MYC. Its combination with inactivating mutations of the tumour suppressors *TP53* and *ID3* promotes BL cell survival. Activating mutations of E2A induce PI3K pathway-mediated survival via tonic BCR signalling and CCND3-dependent cell cycle progression. In addition, activating mutations in *CCND3* induce increased proliferation in BL cells (adaptation from Basso & Dalla-Favera, 2015 (3)).

1.1.2 Diffuse large B cell lymphoma

DLBCL is the most common high-grade non-Hodgkin lymphoma in adults representing 40% of the cases (2, 3, 35). It is a highly heterogeneous disease with extended genetic diversity. Initially, DLBCL cases were classified into two distinct molecular subtypes based on their transcriptomic signature revealing their cell of origin, the GC B cell (GCB)-DLBCL and the activated B cell (ABC)-DLBCL (4). The gene expression profile in GCB-DLBCL is more consistent with a GC B cell undergoing somatic hypermutation (SHM) in the dark zone while ABC-DLBCL is dictated by gene expression signatures of B cell activation and PC differentiation (36, 37). An additional subtype was also identified as unclassified DLBCL demonstrating gene expression signatures that could not consistently be associated with either of the two previously identified subgroups (38). Thus, in DLBCL there is not a definite cell of origin, with its development rather depending on different B cell subtypes populating distinct GC compartments during their differentiation.

The DLBCL tumours are characterized by rapid growth developing nodal or extranodal masses in the lymph nodes (39). Enlarged masses can be detected in the neck, the armpit, or the groin as a result of lymphadenopathy which is usually painless (40). DLBCL is primarily a haematological cancer of the elderly population (39). Clinical manifestations include swelling, bleeding, and organ dysfunction of the liver or kidney (41). Also, the B-symptoms earlier mentioned in section 1.1.1, including high temperature, night sweats, uncontrolled weight loss and itching are clinical features in DLBCL as in BL (41). The standard therapy is a combination of chemotherapy based on cyclophosphamide, doxorubicin, vincristine, prednisone (CHOP) and rituximab (anti-CD20), termed R-CHOP (40, 42). A promising new treatment was recently tested in a phase 3 trial conducted on previously untreated DLBCL patients (43). The combination of rituximab, cyclophosphamide, doxorubicin and prednisone (R-CHP) with an anti-CD79B-drug conjugate (polatuzumab), pola-R-CHP, showed greater progression-free survival as a first-line therapy than R-CHOP treatment and thus, potential for clinical use. Despite that pola-R-CHP treatment showed promising tumour remissions in DLBCL patients, a longer follow-up is yet to be validated (43). Currently, around 50-70% of the DLBCL cases treated with R-CHOP are cured while the remaining relapse with 30% finally succumbing to this disease (35, 44). GCB-DLBCL and unclassified DLBCL have a better prognosis than ABC-DLBCL with all three DLBCL subtypes demonstrating different responses to the established R-CHOP treatment (2, 37, 40, 45).

Several studies have attempted to unravel the genetic profiling in DLBCL aiming to elaborate on its heterogeneity and complexity (13, 45-48). To do so whole genome or exome sequencing combined in

some of the studies with transcriptomic analysis have been applied in DLBCL patients. Samples from primary DLBCL tumours as well as tumour biopsies have been tested in cohorts consisting of GCB-DLBCL, ABC-DLBCL and unclassified DLBCL cases (13, 46-48). Characteristic examples of recurrent identified mutations involve genes such as *EZH2, CD79B, SGK1, BCL2, GNA13, TP53, CREBBP, CARD11, MLL2, TNFRSF14, MYD88, MEF2B, BTG1, BTG2, KDM2B, PRDM1, MYC, CCND3, NOTCH1* (13, 46, 47). Even though it is widely accepted that these mutated genes are associated with DLBCL pathology they do not present consistency in their occurrence in all of the different cohorts studied (13, 46-48). One study highlighted the small overlap in mutation recurrence in DLBCL, with only 10-20% of the identified mutations and genetic aberrations between four different studies overlapping (48). The complexity of this disease is also demonstrated by the different clinical outcomes between GCB-DLBCL and ABC-DLBCL as predicted in a genomic study of a 1,001 DLBCL cases cohort showing worse overall survival after initial treatment in the latter (45).

The heterogeneity of DLBCL has led to its classification into distinct molecular subsets with different transcriptional signatures (Table 1.1). Initial classification divided DLBCL cases into four groups (49). The two subgroups mostly associated with ABC-DLBCL are the MCD and N1. The MCD subgroup is characterized by *MYD88*^{L265P} or *CD79B* mutations while the N1 by *NOTCH1* mutations or aberrations. A mostly GCB-DLBCL-associated subgroup is the EZB characterized by translocation in *BCL2* and mutations in *EZH2*, *TNFRSF14*, *CREBBP*, *EP300*, *KMT2D* as well as amplification of *REL*. The fourth molecular subtype is BN2 bearing aberrations related to the NOTCH pathway in genes such as *NOTCH2*, *SPEN*, *DTX* and fusions of *BCL6*. In addition to these four molecular subgroups two new subtypes were proposed (50). The A53 subtype has recurrent *TP53* mutations and an ABC-DLBCL-like genetic profile and the ST2 subtype shows prevailing mutations in *SGK1* and *TET2* genes. The EZB subtype has also been subdivided into EZB MYC$^-$ and EZB MYC$^+$ tumours with enrichment for *MYC* mutations, amplifications and translocations resembling characteristic BL genetic aberrations but with distinct signatures (50). Relevant classifications were also observed in a population-based cohort of 928 DLBCL patients resolving five molecular subtypes characterized as MYD88, BCL2, TET2/SGK1, SOCS1/SGK1 and NOTHC2, based on their enriched genetic traits and signatures (51).

Table 1.1: Classification of the molecular subtypes in DLBCL. This table presents the classification of DLBCL cases into distinct molecular subtypes as has been established in two different studies in chronological order of publication (49, 50). The cell of origin in each molecular subtype as described by Schmitz et al., 2018 (49) is included and displayed in percentages based on the total number of donors tested and classified per subtype. Hallmark genetic

aberrations per subtype and percentages of their recurrence in the donors tested by Wright et al., 2020 (50), are included in the last column (adaptation from Shimkus & Nonaka, 2023 (36)).

Molecular classification			
Schmitz et al., 2018	**Wright et al., 2020**	**Cell of origin (Schmitz et al., 2018)**	**Genetic aberration (% prevalence) (Wright et al., 2020)**
BN2	BN2	N=98: Unclassified (40%) GCB (19%) ABC (41%)	BCL6 (72.8%), NOTCH2 (41.8%), TNFAIP3 (51.6%), DTX1 (50.0%), CD70 (41.3%), BCL10 (39.6%), UBE2A (30.4%), TMEM30A (26.7%), KLF2 (21.7%), SPEN (21.7%)
-	A53	-	TP53 (86.8%), B2M (34.2), TP53BP1 (27.0%), CNPY3 (23.7%), ING1 (15.8%), NFKBIZ (15.8%), TP73 (13.2%)
EZB	EZB MYC^- EZB MYC^+	N=69: Unclassified (9%) GCB (88%) ABC (3%)	BCL2 (68.4%), EZH2 (44.7%), TNFRSF14 (66.2%), KMT2D (53.9%), CREBBP (52.7%), REL (34.3%), FAS (30.1%), IRF8 (28.9%), EP300 (27.8%), MEF2B (26.3%), CIITA (25.0%), ARID1A (22.9%), GNA13 (22.5%), STAT6 (21.1%), PTEN (20.0%)
-	ST2	-	TET2 (48.1%), DUSP2 (44.4%), ZFP36L1 (40.7%), ACTG1 (37.0%), SGK1 (37.0%), ITPKB (33.3%), NFKBIA (33.3%), EIF4A2 (29.6%), JUNB (29.6%), STAT3 (29.6%), BCL2L1 (25.9%), CD83 (25.9%), DDX3X (25.9%), SOCS1 (25.9%), CD83 (25.9%), P2RY8 (22.2%), RFTN1 (22.2%)
MCD	MCD	N=71: Unclassified (3%) GCB (1%) ABC (96%)	MYD88 (66.2%), CD79B (50.0%), PIM1 (92.5%), HLA-B (73.8%), BTG1 (70.0%), CDKN2A (62.0%), ETV6 (55.0%), SPIB (51.9%), OSBPL10 (51.2%), TOX (48.1%), BCL2 (48.1%), BTG2 (43.8%), MPEG1 (43.8%), HLA-A (43.0%), HLA-C (42.5%), SETD1B (41.8%), KLHL14 (41.2%), TBL1XR1 (35.0%), GRHPR (33.8%), PRDM1 (32.5%), CD58 (31.6%), TAP1 (26.6%), PIM2 (25.0%), FOXC1 (21.2%), IRF4 (20.0%)
N1	N1	N=19: Unclassified (5%) ABC (95%)	NOTCH1 (100%), IRF2BP2 (43.8%), ID3 (25.0%), BCOR (25.0%), EPB41 (18.8%), IKBKB (18.8%), ALDH18A1 (18.8%)

Another set of genetic aberrations that is frequently associated with poor prognosis in DLBCL is characterized by chromosomal translocations or deregulation via overexpression of MYC in combination with BCL2 and/or BCL6 (45). Based on distinct genomic signatures, this type of DLBCL is currently considered a new entity of high-grade B cell lymphoma with *MYC* rearrangements combined with *BCL2* and/or *BCL6* translocations, termed DHL and THL respectively (35). This category is discussed in more detail in section 1.2.2. Overall, the classification of DLBCL cases aims to contribute to our understanding of its progression in patients sharing a similar genetic profile of the disease. Also, it sets the foundation for future research aiming at the discovery of novel therapeutic strategies that are of urgent need upon relapse and in refractory cases.

1.1.3 Multiple myeloma

MM is a haematological cancer originating from an abnormal clone of a long-lived PC in the bone marrow. It comprises 10% of the haematological malignancies and the diagnosed patients have a median age of 65 years old (52). It usually progresses from the pre-malignant condition of monoclonal gammopathy of undetermined significance (MGUS) with *de novo* MM development to a less frequent incident (53). MGUS is a benign PC disorder characterized by increased clonal bone marrow PC infiltration and monoclonal

immunoglobulin (M protein) production. MGUS patients are asymptomatic for the myeloma CRAB clinical features of end-organ damage, including hypercalcemia, renal insufficiency, anaemia or lytic bone lesions and do not show infection risks as in MM (54). Thus, their detection is based on incidental medical follow-ups as part of routine or irrelevant to their MGUS condition exams. An intermediate precursor stage with an advanced phenotype compared to MGUS is smouldering myeloma (SMM). SMM has higher M protein production and clonal PC bone marrow infiltration than MGUS ranging between 10% and 60% but remains asymptomatic (54). 1% of MGUS patients progress to symptomatic myeloma annually while 10% of the cases being diagnosed with SMM will result in myelomagenesis (52, 54, 55). MM progression rate depends on the cytogenetic profile of these precursor stages and differs for each patient. Thus, MM is a complex and highly heterogeneous disease (56-58). Upon MM progression the median survival is estimated at 5 years and a cure for this severe cancer is yet to be discovered (59).

Even though MM is an incurable disease up to date, treatment is available for newly diagnosed and relapsed patients to control and minimize their symptoms as well as to prolong their survival. The frontline therapy for MM patients is either a combination of a proteasome inhibitor with immunomodulatory drugs such as bortezomib with lenalidomide, dexamethasone (VRd) or an equivalent combination containing the anti-CD38 monoclonal antibody daratumumab with lenalidomide and dexamethasone (DRd) (52, 60, 61). Alternative VRd-based combinations excluding lenalidomide are the bortezomib, thalidomide, dexamethasone (VTd) and the bortezomib, cyclophosphamide, dexamethasone (VCd) (52). One of these drug combinations, known as triplet regimens, is the induction therapy choice before autologous stem cell transplantation (ASCT) (54). In addition, the triplet regimens are the standard therapy of choice for patients ineligible for ASCT. MM patients undergoing treatment experience adverse side effects including infections and neuropathy, on top of their severe clinical manifestations such as anaemia, hyperviscosity, nephropathy, persistent bone pain and bone disease (62). The majority will eventually relapse and succumb to their disease.

Driver cytogenetic aberrations and mutations in MM have been identified and characterized as primary and secondary genetic alterations driving its pathology. *MYC* rearrangements in MM act as secondary events associated with poor prognosis (14, 63). Primary genetic aberrations occur during DNA rearrangement in a GC reaction which is a required process for the terminal differentiation of long-lived PCs (63). Long-lived PCs bearing a primary oncogenic event localize the bone marrow and develop MGUS. Such primary oncogenic events could be either a chromosomal translocation of specific oncogenes in the *IGH* locus or aneuploidy (56, 64, 65). Chromosomal translocations acting as a primary oncogenic event in

myelomagenesis are characterized by rearrangements of the *IGH* enhancer element with the genes *CCND1* *t*(11;14), *FGFR3/MMSET* t(4;14), *MAF* t(14;16), *MAFB* t(14;20) and *CCND3* t(6;14) (54, 56, 65). The frequency of each of these five identified driver events in MM cases is estimated at 14%, 11%, 3%, 1.5% and <1% respectively (54). Primary events do not suffice for malignant transformation and indolent MGUS progression to MM thus, secondary events are required to drive the malignant transformation of the abnormal PC clone. Secondary events accumulate as the disease evolves (Figure 1.3) (65).

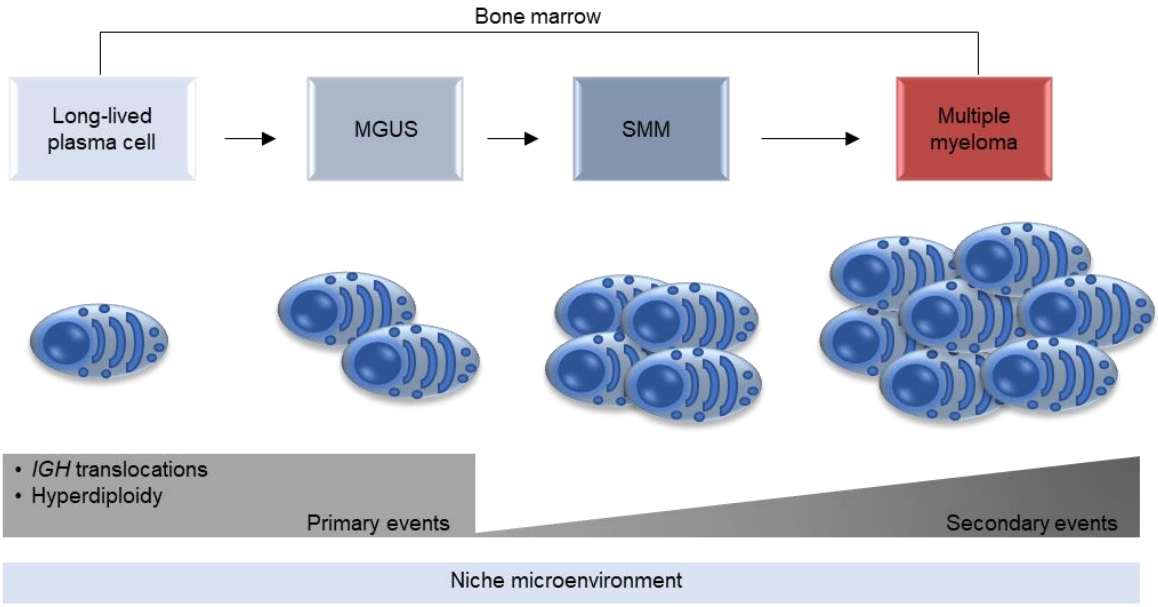

Figure 1.3: The progression of MM in the bone marrow. Two different types of primary oncogenic events can occur in MGUS and myelomagenesis. Such primary events are either hyperdiploidy or translocations of specific oncogenes in the regulatory elements of the *IGH* locus. These driver genetic aberrations have occurred in a single long-lived PC localizing the bone marrow and lead to MGUS. Secondary oncogenic events are required for progression to SMM and ultimately to MM or directly to MM. As the disease progresses the secondary events accumulate. SMM and MM patients carry the same primary oncogenic event as their MGUS predecessor condition. Despite their genetic aberrations MGUS and SMM are pre-malignant conditions and is uncertain if and when they will progress to MM. As the disease of these monoclonal gammopathies progresses the abnormal PC clone proliferates abnormally at a low rate competing with normal PCs for survival in the bone marrow niche.

A valuable insight into the complexity of this disease has been provided by multiple genome-wide and exome sequencing studies (57, 58, 65-67). Recurrently mutated genes acting as secondary events in MM are *KRAS*, *NRAS*, *TP53*, *BRAF*, *DIS3*, *FAM46C*, *TRAF3*, *CYLD*, *RB1*, *SP140, PRDM1*, *IRF4*, *ERG1*, *XBP1*, *LTB*, *MAX*, *CCND1*, *KDM6A* (57, 65-68). In addition, *MYC* translocations to the regulatory elements of *IGH* and

less frequently *IGL* or *IGK* loci are considered a secondary event in MM associated with disease progression (14, 56, 63, 65, 67).

Despite the known cytogenetic and mutational profile in MM the mechanism of symptomatic myeloma progression from the precursor conditions remains unknown. One of the challenges in the field of MM therapy is to accurately classify driver genetic aberration events and their associations with secondary mutations. A model of progression prediction based on the genetic landscape of SMM patients developing MM identified three main parameters as predictors, the presence of t(4;14), genetic abnormalities in the pathways of DNA repair and MAPK and finally the detection of *MYC* genetic alterations (69). In MM, *MYC* aberrations are associated with disease progression acting primarily as a late secondary oncogenic event (70). Current studies indicate its deregulation by the stage of SMM or even MGUS strengthening the case of *MYC* aberrations and/or signalling to be clinically relevant at an earlier stage of the disease than originally thought (69, 71).

1.2 c-MYC (MYC) oncogenic function in mature B cell cancers

In mature B cell cancers, *MYC* genetic aberrations occur in B cell subtypes generated during GC differentiation which normally have downregulated *MYC* expression. Thus, MYC is identified as a primary oncogenic event in BL and a secondary oncogenic event in DLBCL, DHL or THL, PBL, and MM (8, 22, 54). Identification of MYC as an oncogene took place in human BL where MYC chromosomal translocation t(8;14) was identified as the first recurrent chromosomal translocation in B cell lymphoid tumours (11, 15, 72). The juxtaposition of the regulatory elements of the immunoglobulin heavy chain locus on chromosome 14 (14q32) by *MYC*, which is normally located in chromosome 8 (8q24), is a frequent genetic aberration resulting in MYC overexpression. Translocation of *MYC* in the locus of light chain immunoglobulins has also been discovered as a genetic alteration in B cell lymphoma and myeloma (63, 73). Thus, chromosomal rearrangements and gene amplification of *MYC* comprise the main cytogenetic alterations leading to its deregulation in GC B cell and PC haematological cancers. Mutations in *MYC* can accompany an initial cytogenetic alteration of the *MYC* locus or occur first. Most frequently, they are acquired as secondary oncogenic events or in more progressed stages of the disease in conserved and non-conserved amino acids of MYC.

1.2.1 MYC in Burkitt lymphoma

MYC chromosomal translocation is the hallmark driver event in BL (Figure 1.4). In humans, *c-MYC* (*MYC*) contains three exons (74). Breakpoints in the first exon or first intron of *MYC* are identified as class I breakpoints, while breakpoints upstream of *MYC* at a close distance to its 5' end site belong to class II. Finally, class III breakpoints are identified upstream of the 5' end of *MYC* at a further distance than the class II allocated breakpoints (17). Depending on the breakpoint class in which each translocation event belongs different exons of MYC protein are encoded. Class III and II breakpoints translocate all three *MYC* exons while class I could result in translocation of only exon 2 and 3. *MYC* has translation initiation sites in both exon 1 and exon 2 encoding two different MYC isoforms, hence the breakpoint class will determine the MYC protein isoform being overexpressed (74). In the three clinical variants of BL, class II breakpoints are more represented in *MYC* translocations detected in eBL while sBL shows class I breakpoints more frequently (8). Somatic mutations can further develop into the translocated *MYC* allele in 60% of BL cases. Identified hot-spot locations are involved in epigenetic modifications of the gene such as acetylation or phosphorylation related to protein transactivation and protein stability respectively (75).

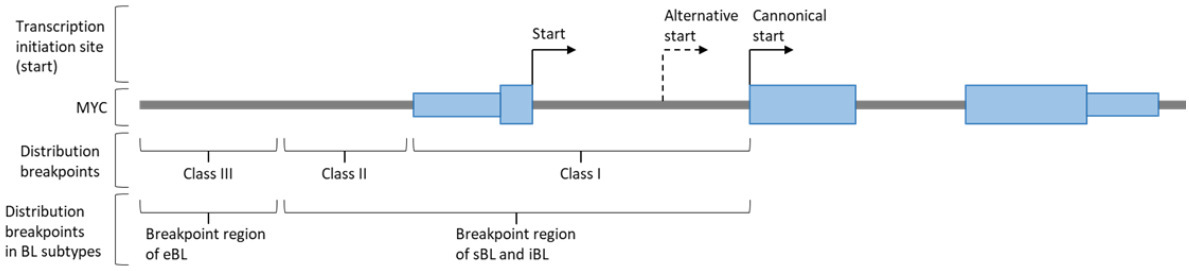

Figure 1.4: Breakpoint classes of the MYC chromosomal translocations in BL. Graphical representation of the *MYC* genomic sequence located in chromosome 8 (8q24). The three exons of *MYC* are represented as boxes (blue) with their untranslated regions (smaller boxes) and their coding sequence (bigger boxes). Exons 1, 2 and 3 are displayed from left to right in a 5' -> 3' direction. Exon 1 contains an alternative codon of transcription initiation while exon 2 contains a canonical transcription initiation codon. Transcription initiation from exon 1 produces MYC isoform 1 while MYC isoform 2 is encoded by exon 2. The distribution of *MYC* breakpoint sites in the BL variants is indicated as well as their classification as class I-III based on their distance from the *MYC* transcription initiation sites (adaptation from López et al., 2022 (17)).

1.2.2 MYC in other types of aggressive non-Hodgkin lymphomas

DLBCL and high-grade B cell lymphomas, DHL and THL, are types of high-grade non-Hodgkin lymphomas that carry *MYC* cytogenetic aberrations as secondary events in comparison to the BL where *MYC* chromosomal translocation is a driver of the disease. In contrast to a simple karyotype observed in BL,

DLBCL and DHL or THL manifest a more complex karyotype with *MYC* translocations to occur also in additional loci, and not uniquely to the immunoglobulin gene ones, as a result of a more heterogeneous genomic evolution (76). Identified partners of non-IG regulatory element rearrangements are *PAX5*, *BCL6*, *BCL11A*, *ICAROS49* and *RFTN1* (77, 78). Interestingly, DHL and THL carrying *MYC* rearrangements to an IG element showed poorer outcome than rearrangement to other genetic partners (29, 79). *MYC* genetic alterations were identified as the third most common in DLBCL being represented recurrently in 10% of the cases (2, 80). Originally, BCL2 deregulation combined with MYC ectopic expression via translocations was a hallmark of GCB-DLBCL (13, 81). Subsequently, cases of coexpression of MYC with BCL2 and/or BCL6 in abnormal levels because of chromosomal translocation events were defined as a new entity of DLBCL in the WHO classification of 2016 with intermediated features between BL and DLBCL and distinct genetic profile (82, 83). Identified as DHL and THL respectively, these DLBCL-derived subtypes were characterized by poor clinical outcome with less than a year of survival post-diagnosis (33, 81). Currently, B cell lymphomas with dual chromosomal translocations of *MYC* and *BCL2* comprise a separate entity entitled DLBCL/high-grade B cell lymphoma with *MYC* and *BCL2* re-arrangements (HGBL-*MYC*/*BCL2*) (10). DLBCL/HGBL-*MYC*/*BCL2* is a homogeneous entity, in contrast to lymphomas with dual *MYC* and *BCL6* translocations, characterized by a GC gene expression profile and pathogenic features related to FL and GCB-DLBCL derived molecular subsets (10). Thus, DLBCL/HGBL-*MYC*/*BCL2* tumour cells resemble a GC B cell phenotype but without comprising a subset of GCB-DLBCL (Figure 1.5) (84).

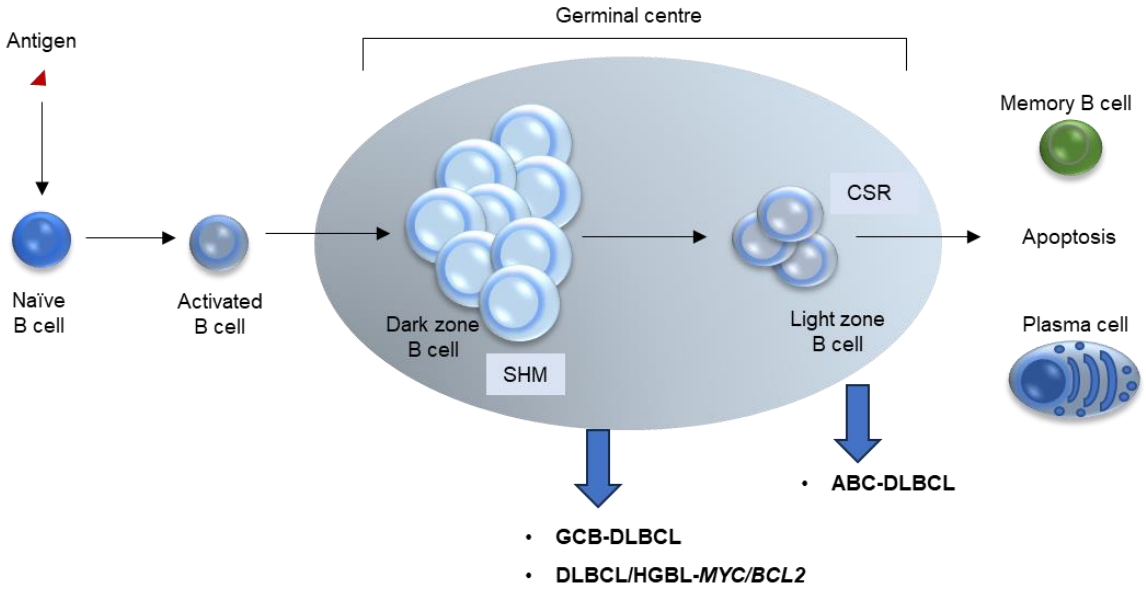

Figure 1.5: DLBCL/HGBL-*MYC*/*BCL2* tumour cells have a GC B cell phenotype and gene expression profile. Representation of a GC reaction formed upon antigen encounter with a naïve B cell. The naïve B cell gets activated

and differentiates in the GC into a memory B cell or PC. Genetic aberrations manifesting during the GC reaction can result in GCB-DLBCL or DLBCL/HGBL-*MYC*/*BCL2* originating from dark zone B cells. In contrast, ABC-DLBCL is considered light zone cell-derived and with distinct genetic features (adaptation from Pasqualucci & Dalla-Favera, 2018 (81)).

Lymphoma cases with *MYC* and *BCL6* rearrangements are less common than DLBCL/HGBL-*MYC*/*BCL2* and present greater heterogeneity classified as a subtype of DLBCL, not otherwise specified (NOS) based on the cytomorphology of the malignant cells (10). It remains unclear which of these two high-grade DHLs has a better outcome upon R-CHOP treatment (29, 35). Additional genetic aberrations of genes such as *TP53* add to their complexity (8). DHL with a *BCL2* translocation and THL can develop both *de novo* or as a transformed lymphoma originating from a pre-existed low-grade lymphoma such as FL (10, 80, 84, 85). Importantly, these high-grade B cell lymphomas are a distinct entity to DH and TH expressors in DLBCL where BCL2 and MYC co-overexpression is observed without translocations taking place (8, 81). These double-expressors B cell lymphomas show a more frequent occurrence in the ABC-DLBCL subtype as a result of constitutive BCR-mediated NF-κB signalling (13, 29, 35, 81). They are considered less aggressive but have a poorer clinical outcome than DLBCL after R-CHOP treatment (8, 86). This is an example of a B cell cancer subtype where the lack of MYC and BCL2 cytogenetic alterations defined its DLBCL classification.

1.2.3 MYC in plasma cell cancers

In the post-GC B cell-derived cancers of PBL and MM, MYC deregulation has been identified as a secondary oncogenic event. MYC genetic aberrations and oncogenic activity were detected in 49% of MM patients (54). *MYC* chromosomal translocation to the *IGH* enhancer (*IGH::MYC*) t(8;14) appears to be often combined with copy number amplification of *MYC* in MM (87). *IGK::MYC* and *IGL::MYC* translocations have also been detected in MM patients with only the latter having a poor prognosis (63, 87). Overall, chromosomal translocation of *MYC* is a late oncogenic event in MM associated with disease progression but it has also been detected in MGUS (14, 88). *In vivo* MGUS and MM mouse model studies showed that MGUS is a required pre-existed condition for *MYC* deregulation to induce MM progression (89). In such a model, a MYC-induced gene expression signature was identified only in the developed MM and not in MGUS highlighting the potential role of MYC deregulation in MGUS to MM transition. However, the exact mechanism of MGUS progression into MM remains unelucidated.

Additional mechanisms of MYC deregulation have also been detected in MM patients such as gene amplification, single-nucleotide polymorphisms (SNPs) or overexpression as a result of deregulation in upstream regulatory pathways of MYC (90, 91). Genetic aberrations in RAS family members *NRAS* and *KRAS* are secondary oncogenic events in MM, carrying mutations that activate the RAS pathway (90). Activation of MAPK pathway by mutated RAS stabilizes MYC protein via phosphorylation of S62 delaying its proteasomal degradation and enhancing its oncogenic function (63). In addition, myeloma malignant cells are addicted to *IRF4* activating mutations for their survival (92). A collaboration between *IRF4* and *MYC* has been described recurrently in MM cases where *MYC* overexpression is activated by its direct regulator IRF4 inducing a positive feedback loop with MYC to activate *IRF4* transcription (90, 92).

MYC rearrangements can also be found in PBL in 49% of the cases studied (93). The main chromosomal rearrangement partners of MYC in PBL are the immunoglobulins gene loci in contrast to MM where non-IG partners are more frequently rearranged (33). Originating from post-GC plasmablast-like cells, PBL is characterized by high proliferation and the transformed cells do not carry *BCL2* or *BCL6* translocations as in GC-derived lymphomas. In contrast, loss of function mutations have been detected in *PRDM1* which are associated with abnormally increased *MYC* expression since BLIMP1 shows a reduced ability to repress *MYC* (8). PBL is considered an aggressive disease with a poor prognosis, commonly diagnosed in HIV-positive individuals and associated with EBV infection with 74% of PBL cases carrying *MYC* translocations being EBV-positive (8).

1.3 B cell development and plasma cell differentiation

The immune system consists of two defence lines, innate and adaptive immunity. Different cell types of the haematopoietic lineage comprise the innate and the adaptive immune responses respectively. B cells are lymphocytes of the adaptive immunity developing in the bone marrow from haematopoietic stem cells (HSCs) (1). Mature B cells migrate in the periphery entering the naïve B cell pool. Upon antigen encounter, they can differentiate into memory B cells or PCs in a T-dependent (TD) response (94). Long-lived PCs return and localize the bone marrow receiving essential survival signals from the niche microenvironment (95, 96). Further exposures to the same pathogen activate a secondary immune response which is more effective based on the established immunological memory (96, 97). Also, the high amounts of antibody production from specialized long-lived PCs in the bone marrow contribute to the efficient elimination or even prevention of disease progression. This process of controlling infections conferred by the B lineage is known as humoral immunity.

1.3.1 B cell development in the bone marrow

The stages of B cell development and differentiation in the bone marrow are displayed in Figure 1.6. A BCR, made of two immunoglobulin heavy chains (IGH) and two immunoglobulin light chains (κ or λ), is composed, expressed on the surface and tested for its reactivity to self-antigens (98-101). Immature B cells reactive with high affinity to self-antigens are eliminated through apoptosis from the mature B cell pool (102).

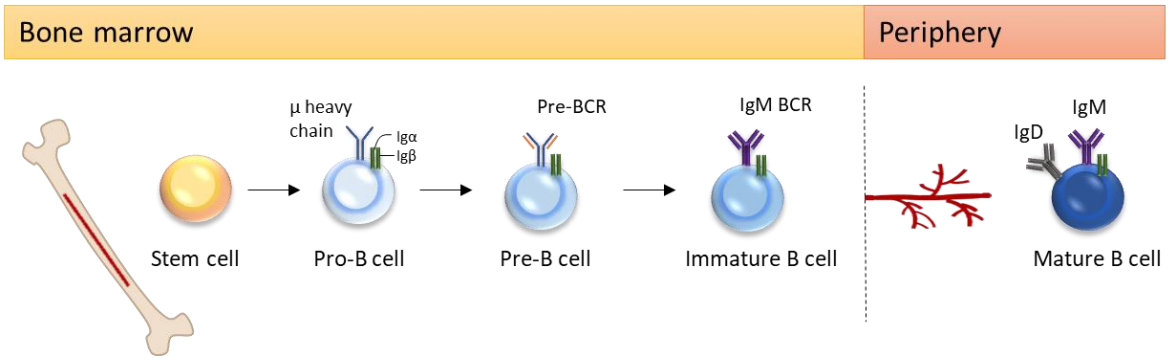

Figure 1.6: The stages of B cell development in the bone marrow. B cells originate from HSCs in the bone marrow which give rise to pro-B cells committed to the B lineage. A pro-B cell undergoes VDJ rearrangements in the *IGH* locus and expresses the μ heavy chains. Igα and Igβ receptors are also expressed on the surface of a pro-B cell as part of the BCR complex in preparation. Subsequently, a pro-B cell differentiates into a pre-B cell expressing a functional pre-BCR with surrogate light chains. Rearrangement of the light chain immunoglobulin locus completion and expression of an intact IgM BCR occur as a pre-B cell differentiates into an immature B cell. Immature B cells egress the bone marrow via the bloodstream and migrate into the peripheral lymphoid organs where they fully mature. Mature B cells enter the naïve B cell pool expressing IgM and IgD BCRs; Ig, immunoglobulin; BCR, B cell receptor.

At the pro-B cell stage, induction of the enzymes RAG1 and RAG2 signifies DNA rearrangements for the production of the *IGH* locus (98, 103). First, the diversity (D) gene segment gets rearranged with the joining (J) region of the heavy chain. D_H to J_H rearrangement is followed up by the rearrangement of the variable (V) segment to the DJ_H. V-DJ_H recombination results in the formation of μ heavy chains (98). The enzyme terminal deoxynucleotidyl transferase (TdT) is expressed by adding nontemplated nucleotides (N nucleotides) between the rearranged segments (104). This enhances the diversity of the heavy chain variable region, responsible for antigen recognition. In addition, pro-B cells express the CD79A and CD79B proteins on their surface corresponding to the Igα and Igβ molecules respectively. Igα and Igβ contain immunoreceptor tyrosine-based activation motifs (ITAMs) which are required for signal transduction upon BCR activation by antigen binding (99, 105). Thus, Igα and Igβ are essential for a functional BCR complex.

At this stage, a pro-B cell differentiates into a large pre-B cell with high proliferation potential. Two surrogate proteins (λ_5 and VpreB respectively) resembling the light chain of a BCR, are produced and attached to each of the μ chains forming the pre-BCR (106). Subsequently, the large pre-B cells undergo several rounds of cell division and differentiate into resting pre-B cells or the so-called small pre-B cells. Light chain rearrangement takes place for each of the small pre-B cells increasing further the BCR repertoire diversity. For a functional light chain to be produced two different gene segments need to be rearranged, the V and J, forming a VJ segment (100). Only one type of light chain, κ or λ, can be expressed in each B cell. Thus, small pre-B cells with rearranged light chains of either type differentiate into immature B cells expressing an intact IgM BCR on their surface. Immature IgM B cells also express low levels of IgD molecules and migrate in the spleen or other peripheral lymphoid organs such as the lymph nodes to complete their maturation (99, 107). Mature B cells enter the pool of the naïve B cells in the periphery expressing functional and non-self-reactive IgM BCR complex and IgD molecules (108).

1.3.2 Generation of plasma cells in T-independent and T-dependent responses

PCs are the terminal effectors of the B lineage and the antibody factory of humoral immunity. They develop upon antigen encounter with a naïve B cell. The naïve B cell gets activated and initiates its differentiation process in the peripheral lymphoid organs, such as the lymph nodes. Based on the nature of the antigen B cell responses leading to PC generation can be divided into T-independent (TI) and TD (109). TD responses require help from T cells in the follicles of the peripheral lymphoid organs while such help is not essential in a TI response. Antigens derived from bacterial components such as lipopolysaccharides (LPS) and unmethylated CpG DNA islands or polysaccharides from viral capsids can trigger a TI response (110, 111). During a TI response, the naïve B cells get activated either by their Toll-like receptor (TLR) resulting in polyclonal B cell differentiation or through their BCR, inducing antigen-specific PC generation (109, 112, 113). Synergistic activation of both BCR and TLR has also been described resulting in improved antibody production (111). On the contrary, a TD response is a result of the recognition of a protein antigen specifically through the BCR of a naïve B cell (110). Antibody affinity maturation and generation of long-lived bone marrow PCs producing high-affinity antibodies are characteristics of a TD response (114-116).

1.3.3 Plasma cell differentiation and germinal centre reaction

Long-lived PCs and short-lived PC-like blasts develop from a transient intrafollicular structure, the GC, and extrafollicular responses respectively, as a result of a TD response (Figure 1.7) (95). Naïve B cells

encountering antigen get activated through their BCR and turn into antigen presenting cells (APCs). They do so by internalizing the protein antigen and re-expressing antigenic peptides bound on MHC-II receptors on their surface (117). Thus, antigenic epitopes are presented to cognate $CD4^+$ helper T cells in the follicle (T follicular helper cells, T_{FH} cells). These $CD4^+$ T_{FH} cells are primed and have the same antigen specificity (117, 118). Naïve activated B cells with lower affinity for their antigen, demonstrate impaired antigen presentation and undergo an extrafollicular response differentiating into short-lived PCs (94, 119, 120). This type of cells complete their differentiation faster than their GC-derived counterparts and secrete antibodies with lower affinity (95). These antibodies comprise an important component of the early response of our adaptive immunity against infectious agents. DNA rearrangement processes such as SHM and class-switch recombination (CSR), mediated by the enzyme activation-induced cytidine deaminase (AID), can take place during the generation of short-lived PCs but not with the intensity observed in a GC reaction (95, 96, 121, 122). In addition, it is widely accepted that extrafollicular responses do not form immunological memory. This has been challenged with some short-lived PCs to generate IgM memory B cells through an extrafollicular response (123). Despite this valuable observation, immunological memory is primarily considered a result of a GC reaction in the B lineage.

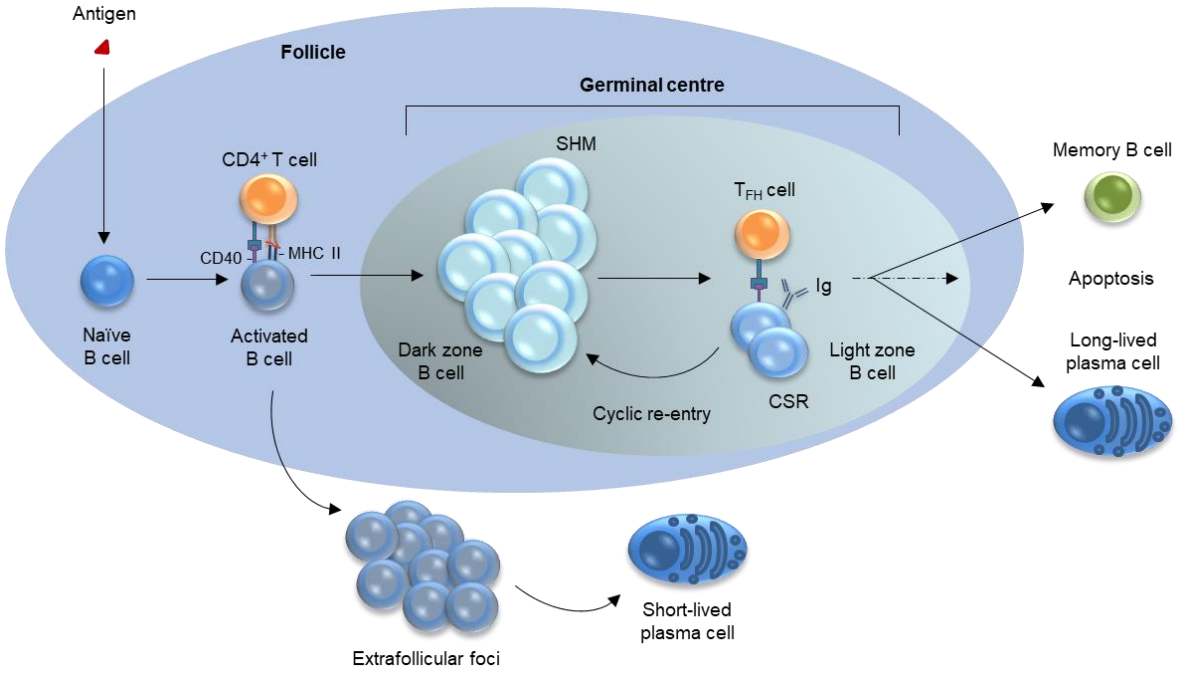

Figure 1.7: PC differentiation in a TD response. In the follicle of a lymph node, exogenous protein antigen interaction with the BCR of a naïve B cell results in its activation. Activated B cells act as APCs expressing antigenic peptides on their MHC-II surface molecules and presenting them to $CD4^+$ helper T cells. CD40:CD40L interaction of an activated

B cell with the $CD4^+$ helper T cells respectively induces further activation and proliferation. Activated B cells with low affinity for their antigen proliferate forming an extrafollicular reaction and producing short-lived PCs. Proliferating activated B cells with higher affinity for their antigen enter the dark zone of a GC and undergo several rounds of division and SHM. Migrating into the light zone they compete for T_{FH} cell-derived survival signal provided by the CD40:CD40L interaction. Failure to receive a survival signal results in apoptosis. Positively selected light zone B cells will undergo CSR and either re-enter the dark zone in a process called cyclic re-entry or they will exit the GC. Post-GC B cells either differentiate into memory B cells or PCs which are considered long-lived and localize the bone marrow niche; MHC, major histocompatibility complex; SHM, somatic hypermutation; CSR, class switch recombination; Ig, immunoglobulin.

1.3.3.1 The germinal centre

GCs are transient structures formed in a TD response by naïve B cells activated with higher affinity from their protein antigens. These B cells can internalize higher amounts of antigen and thus are considered more competent candidates for T_{FH} cell-derived signals during antigen presentation (94, 124-126). B cells and cognate T_{FH} cells also interact through their CD40:CD40L receptors respectively while essential cytokines such as IL-2, IL-4 and IL-21 are secreted by the T_{FH} cells (96, 109, 121, 127). CD40:CD40L interaction has a synergistic effect with IL-21 signalling inducing B cell activation and survival while IL-2 promotes proliferation (128-131). B cells that establish a longer-lasting interaction with cognate T_{FH} cells start proliferating and enter a GC reaction (116, 132). GC formation requires CD40 signalling driving differentiation toward the GC B cell fate and survival while it inhibits differentiation toward the PC lineage (133). On the contrary, IL-21 has a role in affinity maturation and the induction of PC differentiation (127, 128, 134).

A GC has two distinct compartments, the dark zone and the light zone (Figure 1.7) (135, 136). Activated B cells entering the GC differentiate into centroblasts and undergo vigorous proliferation and SHM in the dark zone to enhance their BCR affinity (116, 136). Then the dark zone B cells, characterized as $CXCR4^{hi}CD83^{low}CD86^{low}$, cease their proliferation and differentiate into smaller in size centrocytes migrating in the light zone characterized as $CXCR4^{low}CD83^{hi}CD86^{hi}$ (94, 137-139). There, follicular dendritic cells (FDCs) present antigen and activate the centrocytes which in turn act as APCs for the T_{FH} cells and compete for survival signal based on their BCR affinity (115, 116, 140). This process is described as affinity maturation and the centrocytes that fail the selection process die through apoptosis (115). In contrast, those that were successfully selected undergo CSR resulting in IgG, IgA, IgE or unswitched IgM isotype expression and can follow three potential fates (128, 141). They can either re-enter the dark zone for

additional rounds of mutations and division, a process controlled by MYC and called cyclic re-entry, or they exit the GC reaction and differentiate into memory B cells or PCs (139, 142-145). The DNA rearrangement processes of SHM and CSR that take place in a GC require the generation of double-strand breaks in the GC B cell DNA (89). Thus, they are prone to errors that can lead to genetic aberrations acting as drivers in lymphoma or myelomagenesis.

1.3.3.2 Long-lived plasma cells

Post-GC cells committed to the PC fate differentiate first into plasmablasts maintaining an active cell cycle (132). They mainly express CD19, CD27, CD38 and upregulate the PC hallmark protein syndecan 1 (CD138) (59, 121, 146, 147). PC differentiation is supported by IL-6 and IL-21 cytokines in a synergistic manner, as well as APRIL which facilitates PC differentiation and survival (134, 148, 149). Terminal differentiation into PCs is associated with cell cycle exit (122, 150). Plasmablasts and PCs produce high-affinity antibodies and are characterized as antibody secreting cells (ASCs). Plasmablasts generated from a GC reaction, will migrate through the bloodstream to the bone marrow and mature into terminally differentiated PCs localizing into the bone marrow niche for months to decades (56, 95, 96). Long-lived PC homing has also been detected to a lesser extent in the spleen (108). The bone marrow microenvironment provides essential signals for PC survival which is not an intrinsic PC feature (151, 152). Haematopoietic cells such as eosinophils co-localise the bone marrow and secrete IL-6 and APRIL supporting PC survival (96, 108). Thus, in re-call responses against the same pathogen these long-lived PCs secrete highly specialised neutralizing antibodies mediating long-lasting immunity (96, 108). Despite their crucial role in humoral immunity long-lived PCs are also the cell of origin in monoclonal gammopathies and MM.

1.3.4 Transcription factors in germinal centre and plasma cell differentiation

The stages of a GC reaction are tightly regulated by transcription factors (TFs) controlling PC differentiation. To do so these specialized TFs function as a balanced network to transcriptionally regulate the shift from a GC B cell state to the PC programme (Figure 1.8). PAX5 is a hallmark TF of the B cell lineage expressed during B cell development in the bone marrow at the pro-B cell stage, establishing a commitment to the B cell fate (153). It is required in GC to maintain B cell identity and acts as a repressor of the TF XBP1 which is essential in PC differentiation (154-156). BCL6 is a transcriptional repressor that is required for GC formation (157). IL-21 enhances *BCL6* expression known to repress the hallmark PC TF, BLIMP1 encoded

by *PRDM1* (96, 158, 159). BACH2 is another transcriptional repressor acting as a BLIMP1 inhibitor and sustaining the GC B cell programme over PC differentiation (160).

The PC transcriptional programme is dictated by IRF4, BLIMP1 and XBP1 TFs inducing ASC differentiation. *IRF4* expression in a GC is controlled in a dose-dependent fashion with low IRF4 levels to promote GC maintenance and CSR (161-164). The establishment of an ASC fate is controlled by higher IRF4 expression which subsequently leads to *BCL6* repression and induction of *PRDM1* (164). BLIMP1 functions as a master regulator of the PC fate repressing both *PAX5* and *BCL6* (159, 163, 165, 166). Also, genes related to the cell cycle, including *MYC*, are repressed by BLIMP1 (159, 163). Repression of *PAX5* by BLIMP1 induces *XBP1* expression driving PC differentiation and antibody secretion (96, 155, 159, 161).

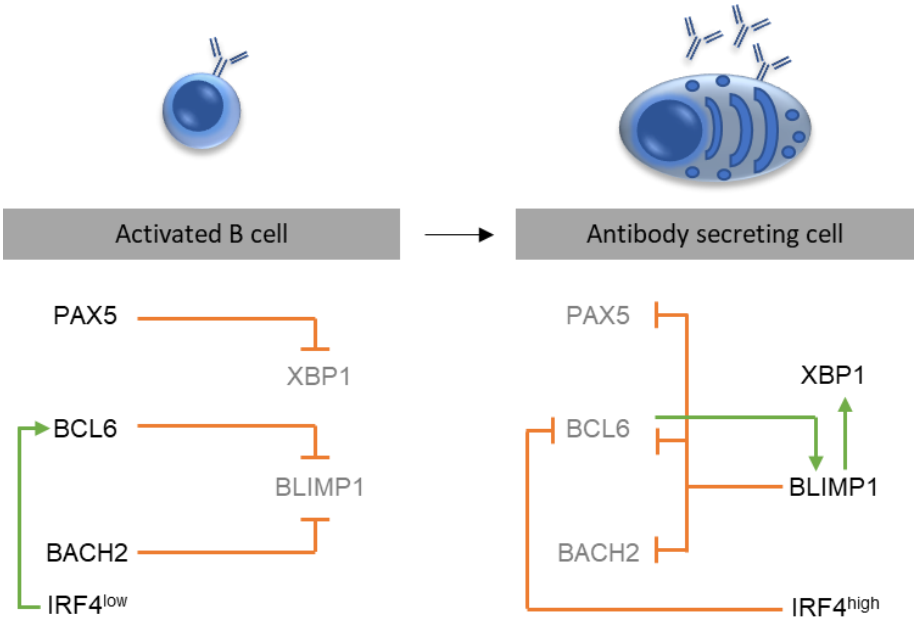

Figure 1.8: The network of the TFs regulating PC differentiation in a GC. During the activated B cell stage initiation and maintenance of the GC phenotype is regulated by the TFs PAX5, BCL6 and BACH2 while PC differentiation is driven by the expression of IRF4, BLIMP1 and XBP1. In an activated B cell, PAX5 represses XBP1. BLIMP1 is repressed by BCL6 and BACH2 ensuring retention of the GC phenotype as long as needed before progression to the ASC state. IRF4 at low levels induces BCL6 expression and contributes to GC maintenance and CSR. In an ASC, higher levels of IRF4 repress BCL6 leading to BLIMP1 induction. BLIMP1 upregulation subsequently represses PAX5, BCL6 and BACH2 while it also induces XBP1 establishing the PC transcriptional programme.

Deregulation of the established TF circuitry is observed in B cell and PC malignancies. Tumour cells in lymphoma block B cell differentiation acquiring *IGH* translocations of *PAX5* and *BCL6* loci (96). This results in their overexpression and thus abnormal retention of a GC phenotype observed in lymphomas. In

addition, *PRDM1*, *IRF4* and *XBP1* mutations are often detected in MM patients and are associated with disease progression in PC neoplasia (57, 65, 70). Thus, the stringent TF regulation taking place during PC differentiation in a GC can also be a great vulnerability contributing to lymphoma and myelomagenesis.

1.3.5 The role of MYC in mature B cell differentiation in the germinal centre

Activated naïve B cells in the periphery upregulate BCL6 and only transiently MYC which is essential for the formation of a GC reaction (142). Entering the dark zone of a GC the activated B cells differentiate into centroblasts characterized by vigorous proliferation. Despite MYC having an important role in activating cellular proliferation signalling and driving the cell cycle, *MYC* is not expressed in centroblasts of the dark zone (167). At this stage, BCL6 remains upregulated and directly represses *MYC*, while proliferation induction and regulation are associated with MYC-independent *CCND3* expression (142, 143, 168, 169). In addition, cyclin-dependent kinase (CDK) inhibitors are repressed by MIZ-1 function in a BCL6-dependent manner promoting cell cycle progression (170). These alternative mechanisms compensate for MYC absence and seem to play the main role in the ongoing proliferation in the dark zone of a GC.

As the differentiation of the GC progresses, a fraction of the centrocytes in the light zone upregulate MYC (138, 142, 143). These cells are positively selected bearing higher affinity BCR and undergo cyclic re-entry controlled by MYC (143). They return to the dark zone where they downregulate MYC and re-enter the cell cycle completing further rounds of SHM. In contrast, light zone B cells that do not re-express MYC either die through apoptosis failing selection or exit the GC to further differentiate into memory B cells or PCs. The same process will be followed by each of the MYC positive light zone B cells re-entering the dark zone (Figure 1.9). The MYC expression levels at the time of cyclic re-entry define their cell growth and thus proliferation rounds capacity in the dark zone before they undergo the selection process again (171). Thus, MYC re-expression in the light zone is required for GC maintenance but needs to be downregulated for proliferation to cease allowing differentiation into memory B cells or PCs (143). BLIMP1 upregulation upon positive selection at this stage can contribute to *MYC* repression in the light zone GC B cells inducing terminal differentiation toward PCs (33).

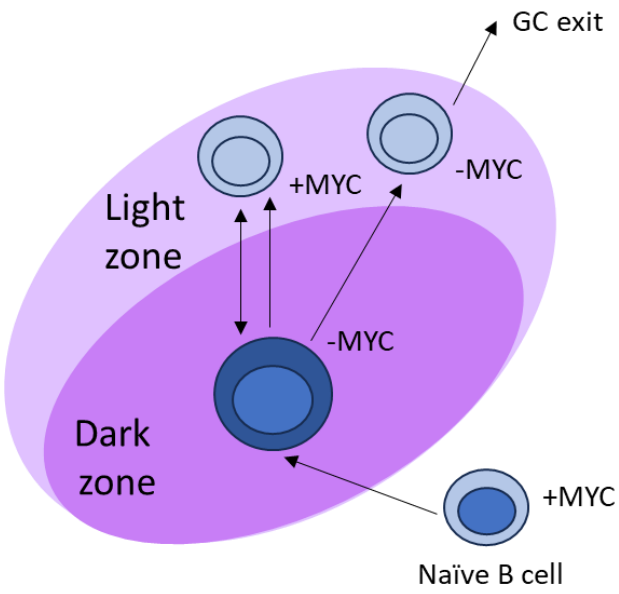

Figure 1.9: MYC expression in the GC reaction. Activated naïve B cells upregulate MYC as a result of the $CD4^+$ T cell signalling and BCR activation entering the GC reaction. MYC expression is downregulated in the dark zone. In the light zone, cells with downregulated MYC that have been positively selected exit the GC reaction to terminally differentiate into memory B cells or PCs. A fraction of light zone GC B cells derived from the dark zone having re-upregulated MYC will re-enter the dark zone in a process called cyclic re-entry. The outcome will be additional proliferation and SHM upon MYC downregulation resulting in higher BCR affinity.

1.3.6 XBP1 and the unfolded protein response

The main function of a PC is to produce and secrete high amounts of high-affinity antibodies. The production of immunoglobulin (Ig) protein molecules requires extensive use of the endoplasmic reticulum (ER) which can result in ER stress. Activation of the unfolded protein response (UPR) is a mechanism of the PCs (or plasmablasts as ASCs) to cope with ER stress and survive while remaining functional and secreting antibodies (172, 173). UPR is activated in a cell by proteins that are overexpressed or misfolded entering the ER (174). Three pathways of ER stress-induced UPR are known in eukaryotes mediated by three sensor proteins IRE1α, PERK and ATF6 respectively (172, 175).

XBP1 function is associated with the UPR via the IRE1α sensor (175, 176). XBP1 is a transcriptional activator required for PC differentiation and expressed in high levels in terminally differentiated PCs regulating their secretory pathway (155, 175, 177). Activation of XBP1 transcriptional activity requires a splicing event mediated by the IRE1α ribonuclease (172). IRE1α removes 26 nucleotides from the unspliced *XBP1* mRNA

containing a premature stop codon (176, 178). This modification results in the translation of the active XBP1s TF which induces the expression of genes related to protein synthesis, entry into the ER, folding and secretion (175, 176, 178, 179).

Two different studies based primarily on BL and breast cancer models showed that MYC overexpression induces activation of the IRE1α/XBP1-mediated UPR promoting tumour cell survival (178, 180). Inducible expression of MYC in a non-transformed breast epithelial cell line showed that its overexpression drives *XBP1* mRNA splicing by IRE1α (180). This MYC-specific induction of the IRE1α/XBP1 axis is driven by the direct binding of MYC on the regulatory elements of both *ERN1*, encoding for IRE1α, and *XBP1* regulating their expression (178, 180). In addition, MYC and XBP1s were found to form a complex in the nucleus resulting in enhanced XBP1s transcriptional activity (180). XBP1 can also directly activate *MYC* expression while the activity of XBP1s-mediated UPR has been associated with MYC oncogenic signalling in prostate cancer (181). Thus, in a MYC deregulation context, MYC and XBP1s activity through the UPR, seem to collaborate in driving cell survival. These studies have also proposed that the combination of standard chemotherapy with inhibitors of the pro-survival IRE1α/XBP1 pathway can be a promising therapeutic approach in MYC-associated cancers, including BL and MM (178, 180, 181).

1.4 BCL2 protein

B cell lymphoma 2 (BCL2) protein is a member of the BCL2 family of pro-apoptotic and anti-apoptotic proteins. It functions as an anti-apoptotic factor and it is expressed in progenitors of melanocytes, epithelial cells of the embryonic kidney, neuronal cell types and haematopoietic cells (182). BCL2 has a half-life of approximately 20 hours and its gene expression is regulated by different STAT proteins and members of the NF-κB pathway (182-184). B cells and PCs express and utilise BCL2 for their survival. Tumour cells of B cell and PC malignancies exploit the pro-survival role of BCL2, especially in DLBCL, DLBCL/HGBL-*MYC*/*BCL2*, THL and MM, thus BCL2 is a promising therapeutic target in mature B cell cancers.

1.4.1 BCL2 family proteins and function

Apoptosis is a process of programmed cell death activated by the extrinsic or intrinsic pathway (185). The intrinsic or mitochondrial pathway is regulated by the BCL2 family members. There are three categories of BCL2 family proteins, the pro-apoptotic members (BIM, BID, BIK, PUMA, NOXA, BIM, BMF, HRK), the anti-apoptotic members (BCL2, BCL-xL, MCL-1, BCL-W) and the effector members (BAX, BAK, BOK) (182). The balance in the protein-protein interactions (PPIs) between the pro-apoptotic and anti-apoptotic BCL2

family proteins determines cellular survival or apoptosis. The effector and anti-apoptotic BCL2 proteins have either three or all four of the BCL2 homology (BH) domains (BH1-3 or BH1-4 respectively) and are known as multi-BH domain proteins (186, 187). On the contrary, pro-apoptotic members with a critical role in apoptosis induction contain only the BH3 domain. The multi-BH domain BCL2 proteins can form a hydrophobic BH3 domain binding groove in their tertiary structure (186, 188). In healthy cells, the main role of anti-apoptotic proteins, such as BCL2 (BH1-4), is to inhibit activation of the effectors of apoptosis, BAX and BAK, promoting cell survival. When a cell experiences stresses including nutrient deprivation, DNA damage, hypoxia or oxidative stress, a process called mitochondrial outer membrane permeabilization (MOMP) is triggered leading to apoptosis (186). Cells responding to their stresses increase the levels of BH3-only pro-apoptotic proteins which bind with high affinity to anti-apoptotic proteins, such as BCL2. This interaction is conducted via the hydrophobic BH3-domain groove, promoting effector protein, BAX and BAK, function (Figure 1.10). MOMP is activated by BAX and BAK oligomerization forming pores in the outer mitochondrial membrane and releasing pro-apoptotic molecules such as cytochrome *c*, in the cytoplasm (182, 189). Cytochrome *c* release from the inner part of the mitochondria activates a cascade of caspases resulting finally in caspase 3 activation (5). Thus, the apoptotic machinery is activated cleaving cellular proteins and resulting in cell death.

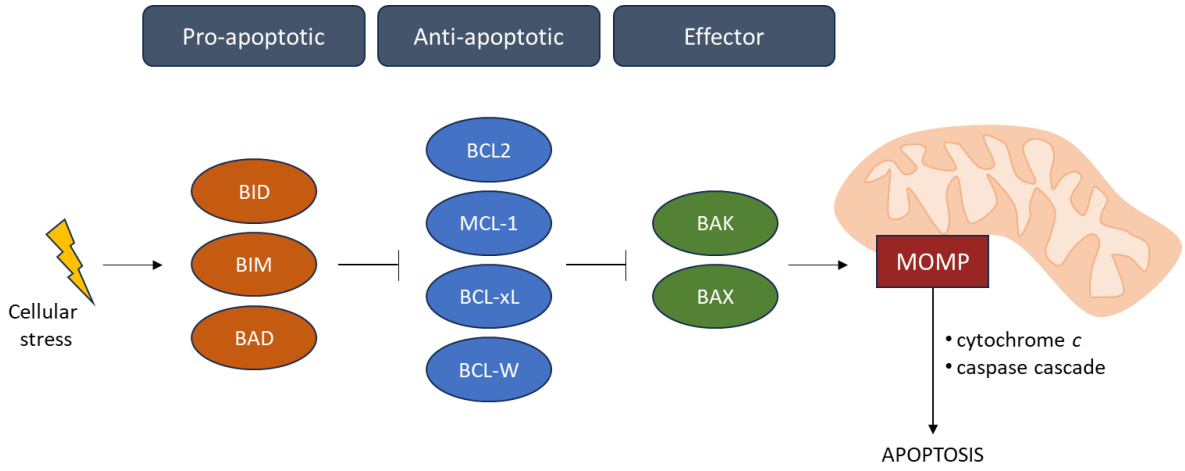

Figure 1.10: The regulation of the mitochondrial pathway of apoptosis by the BCL2 family proteins. Cells undergoing stress trigger increased levels of pro-apoptotic proteins of the BCL2 family to drive apoptosis. This increase disrupts the originally established balance between anti-apoptotic and pro-apoptotic BCL2 family members. The increased pro-apoptotic proteins bind with high affinity to the anti-apoptotic proteins promoting activation of the effector members BAK and BAX. This induces oligomerization of BAK and BAX activating MOMP and release of

cytochrome *c*. A cascade of caspases is in turn activated leading to cleavage of hundreds of cellular proteins and apoptosis (adaptation from Kaloni et al., 2023 (182)).

1.4.2 BCL2 protein deregulation in mature B cell cancers

Changes in the balance between anti-apoptotic and pro-apoptotic BCL2 family proteins is a normal process promoting apoptosis in cells aiming to maintain homeostasis. However, constitutive disruption of this balance can lead to aberrant survival, a mechanism that is frequently exploited by tumour cells. In healthy B cells, BCL2 is expressed in naïve and memory B cells playing a role in memory B cell fate selection post-GC exit (190-192). In contrast, GC B cells do not express BCL2 or its expression is observed at very low levels (191, 193, 194). Thus, anti-apoptotic BCL2 deregulation is a recurrent oncogenic event in GC B cell lymphomas while it has also been observed in MM but without detected DNA rearrangements (192, 195). Chromosomal translocations of *BCL2* to the *IGH* locus, t(14;18), are present in 80-90% of the FLs and are a driver event in FL pathogenesis (3, 7, 196). Cases with t(14;18) can acquire additional mutations in *BCL2* being usually associated with FL transformation to an aggressive disease such as DLBCL/HGBL-*MYC*/*BCL2* (46, 47, 189). *IGH::BCL2* chromosomal translocations are also driver events in THL while BCL2 overexpression because of gene amplification or constitutive NF-κB activation has been identified in patients with ABC-DLBCL (35, 189). Small molecule inhibitors ABT-263 (Navitoclax) and ABT-199 (Venetoclax) bind to the BH3 domain binding site of the multi-BH domain anti-apoptotic proteins promoting apoptosis of tumour cells (186). Venetoclax is a BCL2-specific inhibitor which has been approved for chronic lymphocytic leukemia (CLL) treatment (87). A subset of MM cases with t(11;14) chromosomal translocations are responsive to Venetoclax treatment indicating that these tumour cells are dependent on BCL2 for their survival (87, 197). Thus, further investigation of BCL2 inhibitors in t(11;14) MM is currently taking place in ongoing clinical trials with the promise of identifying the first MM-targeted therapy (197).

1.5 MYC protein family and c-MYC (MYC) overview

c-MYC (MYC) is a proto-oncogene of the MYC family which also contains MYCN and MYCL proteins (198). The different MYC family members manifest similar functions but are expressed in distinct cellular development or differentiation stages and tissues (199, 200). MYCN expression is restricted in the neural and neuroendocrine systems (201). MYCL expression is detected in the gastrointestinal tissues and the lungs while MYC is the most abundantly expressed member of the MYC protein family detected in multiple

tissues and cell types (198). MYC was discovered as a *v-gag-myc* homolog in the avian myelocytomatosis virus (MC29) causing avian leukaemia while MYCN and MYCL were discovered later in neuroblastoma and lung cancer respectively (202-204).

All three MYC family proteins are associated with a wide range of tumours when deregulated. MYCN deregulation has been reported in neuroblastoma, rhabdomyosarcoma, medulloblastoma and retinoblastoma (199, 205). Small cell lung carcinomas and intestinal cancers are associated with MYCL deregulation (199). MYC is a bona fide oncoprotein involved in almost 70% of human cancers (206). Its deregulation by overexpression has been reported in many haematological cancers such as leukaemia, lymphoma and MM as well as in solid tumours with some examples being colon, breast, lung, liver, prostate and ovarian cancers (205, 207, 208).

In healthy cells, MYC is a major regulator of transcription regulating 15% of the genome (204, 206, 209). MYC *in vivo* knockout in the germline is embryonically lethal (142, 198). All three RNA polymerases as well as non-coding, ribosomal and transfer RNAs are regulated by MYC during transcription (204). Thus, MYC function is associated with many cellular processes such as cell growth, cell cycle, metabolism, ribosome and protein synthesis, glycolysis, mitochondrial biogenesis, and apoptosis in normal tissues. MYC deregulation induces angiogenesis, genomic instability, and differentiation blockade (Figure 1.11). Despite the example of an *in vivo* Myc overexpression-mediated B cell lymphoma model, it is widely accepted that MYC genetic aberrations do not suffice to drive cellular transformation and neoplastic formation requires secondary events (205). Mutations in oncogenes and tumour suppressors, such as RAS proteins and p53 respectively, have been frequently used in combination with MYC overexpression in cancer model development (210-213). As a homeostatic mechanism, MYC overexpression drives cellular death by apoptosis and tumour cells frequently acquire translocations in the genetic locus of BCL2 anti-apoptotic protein in lymphomas to establish their survival (203, 211). In MYC-associated cancers, malignant cells depend for their survival on the signalling downstream of overexpressed MYC, a phenomenon known as oncogenic addiction (205).

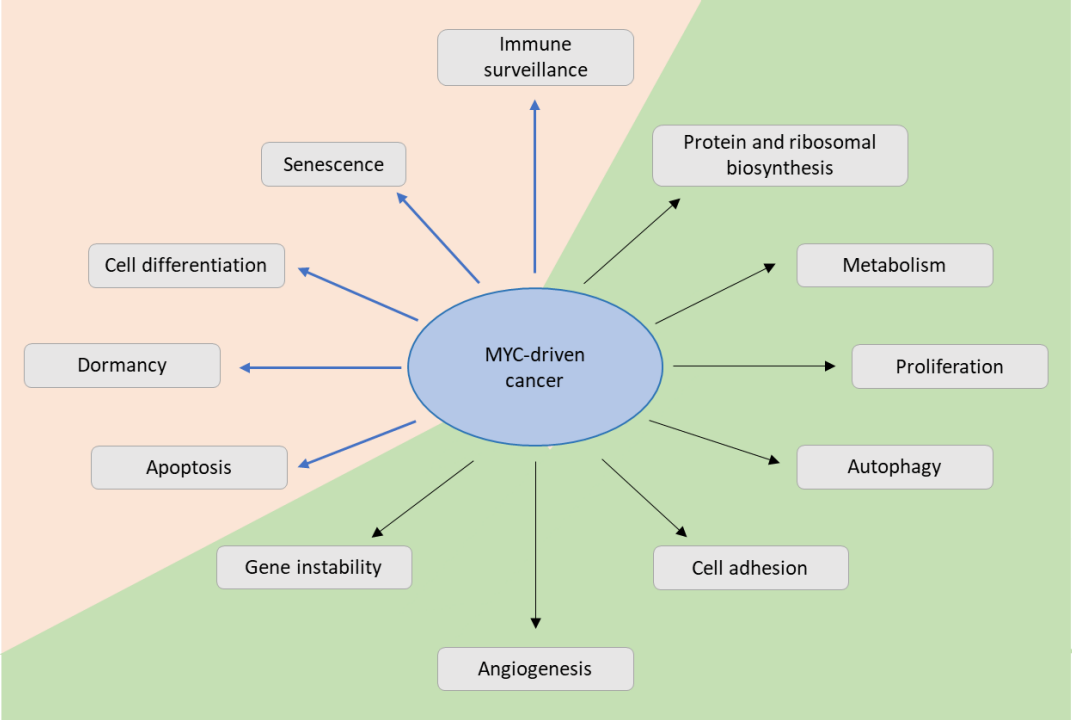

Figure 1.11: MYC deregulation in cancer. Cellular processes regulated by MYC in normal cells are highjacked upon its overexpression in cancer. Augmented pathways related to malignant cell survival (green background) are responsible for tumour establishment and dependent on MYC oncogenic signalling. In addition, critical MYC-driven processes are blocked in cancer (red background) to promote tumour progression (adaptation from Dhanasekaran et al., 2022 (205)).

The ability of a single gene to drive such numerous effects on multiple cellular processes in healthy and tumour cells has defined MYC as a key oncoprotein for therapeutic targeting in cancer. Extensive research has provided several candidate molecules for MYC targeting over the years but with no promising results *in vivo* leading to fewer clinical trials than originally expected (199). MYC complex tertiary protein structure and lack of an enzymatic site have proven challenging in the drug discovery process for direct MYC inhibitors. Currently, MYC targeting is still an ongoing struggle for the scientific community with Omomyc, an inhibitor of the MYC:MAX complex DNA binding required for MYC function, being one of the most promising molecules discovered up to date (204, 205). A novel theory has evolved with MYC being considered “undruggable” and alternative strategies of indirect MYC targeting via its PPIs have been highlighted as a possible solution (199, 214). Thus, despite MYC being established as a major contributor to cancer development and maintenance and a promising target for cancer treatment, its efficient clinically applicable targeting is still pending. A more in-depth understanding of the molecular mechanisms of MYC

function and protein characteristics in a deregulation context is a requirement for the development of successful MYC-focused therapeutic strategies.

1.5.1 MYC protein function as a transcription factor

MYC acts as a TF upon dimerization with its obligate partner MAX (215). MYC:MAX DNA binding preferably occurs in DNA sites called E-boxes carrying a CACGTG motif (198). Alternative E-boxes CANNTG binding has also been reported for the MYC:MAX complex as well as unspecific DNA binding in non-canonical E-box consensus sequences especially upon MYC deregulation (204, 208, 216). MYC, after its complex formation with MAX, acts as a transcription activator while also transcriptional repression is mediated upon its interaction with co-factors such as MIZ-1 and SP1 (217, 218). CDK cell cycle inhibitors, $p15^{INK4b}$ and $p21^{Cip1}$, are transcriptionally repressed in a MYC-dependent manner. *CDKN2B* encodes for the CDK inhibitor $p15^{INK4b}$ and *CDKN1A* encodes for $p21^{Cip1}$ (219, 220). MYC interaction with MIZ-1 antagonises MIZ-1 binding to the *CDKN2B* or *CDKN1A* promoters repressing their expression and inducing cell cycle progression (204).

Open chromatin domains are considered a requirement for MYC transcriptional activity but MYC cannot open condensed chromatin regions without its indispensable co-factors (221). Thus, transcriptional activation driven by MYC signalling is associated with increased levels of histone acetylation mediated by co-factors with histone acetyltransferase (HAT) activity (222, 223). Transcriptional regulation by MYC is also facilitated by its interaction with the kinase P-TEFb which phosphorylates RNA Pol II activating transcriptional elongation (224, 225). Through this mechanism, MYC has been attributed a role in RNA polymerase II pause and release, a critical process in gene expression implicated in the general amplification of RNA transcription observed as a MYC effect in healthy and transformed cells. This generalized increase in RNA transcripts has been a reason for debate regarding the specificity of MYC function in regulating genomic expression (204). The original mechanism of MYC function as a TF has been implicated with a distinct gene expression signature (226-228). Through regulating specific gene sets MYC was considered to consistently manifest its function affecting discrete pathways of cell growth, cell cycle, metabolism, DNA replication, apoptosis, and differentiation blockade. An alternative hypothesis derived from two ChIP-seq genomic studies challenges the MYC-specific target gene mechanism (229, 230). This so-called global or general amplifier model suggests that instead of regulating specific gene sets MYC functions as a direct amplifier of all active loci in the genome (221, 229, 230). To explain the global RNA amplification observed upon MYC binding especially when deregulated, the general amplifier model has provided a reasonable alternative to the original specific target gene mechanism proposing that all the

open chromatin regulatory elements can be transcribed via a MYC-dependent mechanism. Such a model does not take into consideration the MYC-mediated transcriptional repression and currently seems to have been sidelined by additional genomic studies concluding that MYC functions in a target gene-specific fashion (221).

Additional hypotheses have been proposed to explain the phenomenon of wide RNA amplification as a downstream effect of MYC signalling and its targets in a cell and context-dependent manner. In one instance, RNA amplification has been suggested to be a secondary result of MYC function originating from the downstream targets of MYC-activated genes and recruited co-factors (221). Another hypothesis exploring the idea of MYC binding to an abundant number of promoters resulted in the model of "level-dependent regulation" (226). It proposes that the affinity of MYC binding is a critical contributor to gene expression levels. Promoters with high-affinity MYC binding appear more expressed under physiological MYC activity conditions while they become saturated upon MYC overexpression. Thus, lower affinity promoters get activated as frequently as the higher affinity ones upon MYC deregulation. While the two original specific target gene or global amplifier models dominated our current understanding of MYC-mediated transcriptional regulation such additional theoretical approaches provide intermediate alternatives essential to be experimentally proven to unravel the unelucidated MYC function as a TF.

1.5.2 MYC protein structure and its domains

MYC protein has two major isoforms (74, 231). Isoform 1 or p67, consists of 454 amino acids and is transcribed from an alternative CTG transcription initiation codon in exon 1 (74). The shorter isoform 2, p64 with 439 amino acids, is transcribed from a conventional ATG transcription initiation site located in exon 2 (74). MYC isoforms contain a basic region (BR) next to a helix-loop-helix-leucine zipper (HLH-LZ) sequence at the C-terminus of MYC where MAX interaction with the latter and subsequent DNA binding via the former MYC region occur (Figure 1.12) (215, 232). BR-HLH-LZ domains are required for MYC function and transformation upon heterodimerization with MAX (212, 232-234). Deletion of the BR-HLH domain inhibits MAX interaction and DNA binding leading to abolished MYC activity (235).

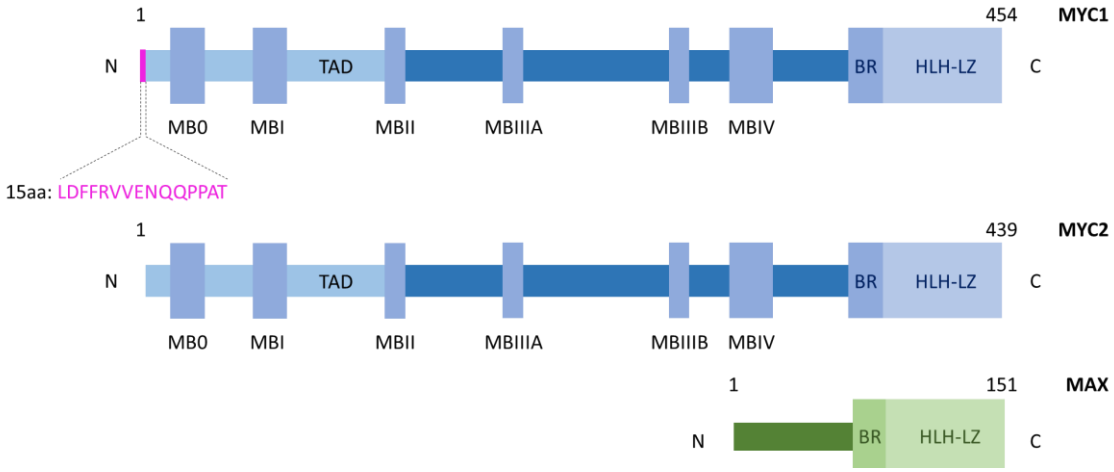

Figure 1.12: MYC isoforms and MAX protein structure. MYC isoform 1 (top) contains 15 amino acids (aa, peptide sequence in magenta) more than isoform 2 (middle), which are located at the N-terminus. MB0, MBI and MBII are in the transactivation domain (TAD) of MYC for both isoforms while MBIIIa, MBIIIb and MBIV domains are located in the core of the protein structure. At the C-terminus is the HLH-LZ domain where MYC interacts with MAX (bottom) and upon dimerization binds to the DNA via its basic region (BR) (adaptation from Meyer & Penn, 2008 (203)).

MYC function is associated with six additional domains conserved in the MYC family termed MYC boxes (MBs) (Figure 1.12). The central region of MYC contains three conserved MB domains, MBIIIa, MBIIIb and MBIV with a nuclear localization signal accommodating MYC transfer to the nucleus (203). A critical region for MYC function located at its N-terminus is the transactivation domain (TAD), amino acids 1-143 (203). TAD contains three MB domains, MB0, MBI and MBII, with essential and distinct functions. MBI is associated with protein stability and proteasomal degradation as a phosphodegron (236-239). MB0 was the latest discovered MB domain in TAD and has been implicated with transactivation and tumour growth-related MYC functions (240). MBII is considered an indispensable MYC domain essential for all its biological activities and MYC-mediated cellular transformation (212). More specifically, MBII has been suggested to play a role in epigenetic modifications conferred by MYC interactors through this domain and thus in the process of tumour initiation (240).

1.5.3 MYC interactome

In healthy and transformed cells, MYC function as a TF or an oncoprotein respectively is dependent on MYC interactions with its co-factors. Apart from MYC:MAX complex required for DNA binding multiple additional interactors have been identified for MYC in particular via its MB domains (204, 241, 242). More than 300 known partners have been identified that form complexes with MYC in distinct MBs (198, 240).

WDR5 protein, a component of chromatin remodelling complexes, interacts directly with MYC through its MBIIIb domain (208). WDR5 is bound to chromatin prior to MYC:MAX DNA binding (208, 243). ChIP-seq showed that 80% of the DNA sites bound by MYC wild type were lost in the WDR5 mutant, WBM (208). These findings suggested that WDR5 interaction with MYC via its MBIIIb may play a role in MYC:MAX complex recruitment to the DNA sites of MYC targets in the context of chromatin binding. MYC:MAX cannot bind to condensed chromatin. Thus, the activity of co-factors facilitating chromatin remodelling is required prior to MYC:MAX DNA binding (221). The PPIs between these co-factors and MYC have been suggested to play a role in MYC:MAX complex recruitment to the open chromatin (221). Based on this hypothesis a model of three succeeding modes of MYC:MAX recruitment has been proposed (244). Initially, MYC:MAX recruitment is accomplished only via PPIs and no DNA binding leading subsequently to MYC:MAX binding to MYC non-specific DNA sites. Finally, MYC:MAX binding to consensus E-boxes occurs locally after scanning of the bound DNA sequence by the MYC:MAX complex. Such a model attempted to explain how TFs identify their DNA binding sites in the genome based on pre-existing co-factors bound on DNA facilitating their recruitment (244). Thus, MYC interactors could be implicated in its function via their PPIs both prior to and after its recruitment to chromatin and DNA binding.

A bona fide region for MYC function is its TAD with indispensable interactions to take place via the MB0, MBI or MBII conserved domains. MYC PPIs in MBI include the TATA box binding protein (TBP), a component of TFIID and TFIIF of the RNA polymerase II complex, the tumour suppressor BIN1 and E3 ligases such as FBXW7 and TRUSS (214, 245, 246). Another component of the RNA polymerase II complex, TFIIF, has been identified to directly interact with MYC via its MB0 domain in a BioID-mediated mass spectrometry study of the MYC interactome identifying 336 high-confidence interactors (240). Through its MB0:TFIIF interaction, MYC has been associated with transcriptional elongation regulation as a critical contributor to tumour growth (240). MB0 also directly interacts with the PP1 nuclear-targeting subunit (PNUTS) recruiting the PP1 serine-threonine phosphatase which inhibition results in MYC hyperphosphorylation and MBI-mediated proteasomal degradation as described below in section 1.5.5 (247).

The MBII domain of MYC is critical for its biological activity and transformation with multiple identified co-factors. A critical co-factor of MYC via the MBII domain is the transformation-transactivation domain-associated protein (TRRAP) (248). MYC:TRRAP interaction recruits to the promoters of MYC target genes the STAGA or NuA4 histone acetylation complexes containing the HATs GCN5 and TIP60 respectively (249-251). Acetylation of histone by the recruited HATs contributes to the retention of chromatin accessibility by the RNA I-III polymerases required for MYC-mediated regulation of transcription (252). GCN5 has been

also reported to directly interact with the MBII domain (253). TIP48/TIP49 are co-factors of MYC via the MBII and act as ATPases facilitating chromatin remodelling (251). The E3-ubiquitin ligase SKP2 interaction with MYC is mediated by the MBII and accommodates MYC ubiquitination and degradation in a phosphorylation-independent manner as well as transactivation (254).

An interesting theory of MYC function is described by the 'coalition model' (214). It is based on the paradoxical observation that a single protein such as MYC can drive such a variety of effects in a cell and proposes that the main driver is the established MYC PPIs. Based on the unelucidated mechanism of the distinct MYC molecules' function, this model suggests that different MYC molecules can interact with different co-factors mediating distinct effects in parallel. The combination of all these MYC complexes acting at the same time deliver collectively the MYC function. This model originated from *in vivo* experiments showing that the co-overexpression of *Δ*MB0 and *Δ*MBII MYC mutant conditions was essential to drive tumour growth (240). Even though it needs to be further experimentally proven, such a model challenges how MYC molecules form complexes with their interactors. Importantly, it suggests novel molecular avenues in future research aiming at MYC indirect targeting for cancer treatment.

1.5.4 The role of MYC in glycolysis and mTOR pathway

MYC downstream signalling drives cellular processes that require enhanced energy and nutrient resources to facilitate cell growth, proliferation, and increased oxidative stress challenges. Thus, MYC function is interconnected with nucleotide and protein synthesis, ribosome and mitochondrial biogenesis and increased biomass. For adaptation to deregulated cell division or transformation, a cell is dependent on metabolic reprogramming and MYC is a major contributor to such adaptations. Increased metabolism is controlled by direct MYC regulation of glycolytic genes such as *GLUT1*, *HK2*, *PFKM*, *ENO1* and *LDHA* which are involved in glucose metabolism (209, 252, 255). The increased metabolic demands in a cell can be met by an exchange into aerobic glycolysis otherwise described as the Warburg effect, utilizing the conversion of glucose to lactate in highly proliferating cells (209, 256). Exploiting the Warburg effect MYC-associated cancer cells facilitate their metabolic demands both in sufficient oxygen and hypoxic environments.

MYC is an upstream regulator of the mammalian target of rapamycin (mTOR) which regulates cell growth, metabolism, protein synthesis and survival (257). mTOR Complex 1 (mTORC1) and mTOR Complex 2 (mTORC2) share the catalytic subunit mTOR and display distinct functions via localizing into different cellular compartments (258, 259). Also, a positive feedback loop has been observed with the mTORC1 pathway to regulate *MYC* mRNA translation in an S6K1-dependent manner via phosphorylation of eIF4B

(260). Activation of protein and lipid synthesis and ribosomal biogenesis are induced by the mTOR complex in high-nutrient environments (261). Thus, mTOR pathway activation further facilitates the induction of downstream anabolic pathways associated with MYC function.

1.5.5 MYC degradation in the proteasome

MYC protein has a short half-life of approximately 20-30 minutes upon its synthesis (262). To ensure effective MYC proteostasis the ubiquitin-proteasome system (UPS) regulates MYC degradation with multiple ubiquitin-ligases to control the protein turnover of MYC. FBXW7, HECTH9, SKP2, TRIM32, TRUSS, FBXW8 are known E3-ligases involved in MYC proteostasis regulating the increase or decrease of its levels (263). SKP2 and FBXW8 interact with MYC via its MBII domain while FBXW7 and TRUSS via its MBI (263, 264). FBXW7 is the most widely studied E3 ubiquitin ligase related to MYC protein reduction and interacts with a phosphodegron sequence in the MYC MBI domain containing threonine 58 (T58) and serine 62 (S62) (265). FBXW7 interaction with MYC via these two residues regulates MYC protein levels via UPS degradation (239).

UPS is completed in three steps by an E1 ubiquitin-activating enzyme, an E2 ubiquitin-conjugating enzyme and an E3-ubiquitin ligase (263). In MYC degradation MYC acts as the target substrate bound to an E3-ubiquitin ligase. While E1 adenylates the ubiquitin molecules via an ATP-dependent process, the E2 enzyme is responsible for transporting the activated ubiquitin to a lysine 48 (K48) residue of the substrate MYC (263). RING-FINGER/U-box family E3-ligases, such as FBXW7, bind to MYC and collaborate with E2 enzymes to ubiquitinate the first K48 residue (263). Subsequent poly-ubiquitination to the K48 residue forming a chain of at least four or more ubiquitin molecules, is required for efficient recognition and degradation by the 26S proteasome (266). CDC34 is the E2 enzyme cooperating with FBXW7 in MYC UPS-based degradation (267).

MYC degradation via the ubiquitin/26S proteasome pathway is regulated by sequential phosphorylation steps of S62 and T58 in the MBI phosphodegron (268). RAS-activated/MAPK/ERK and/or CDKs phosphorylate the S62 increasing MYC protein stability and recruiting the GSK3β kinase to phosphorylate T58 (205, 269). Upon T58 phosphorylation, dephosphorylation of S62 is required, to generate an unstable MYC protein (269). Subsequently, phosphorylated T58 in the phosphodegron sequence of MBI allows FBXW7 E3 ubiquitin ligase recognition and ubiquitination of MYC activating its proteasomal degradation (Figure 1.13) (263, 270).

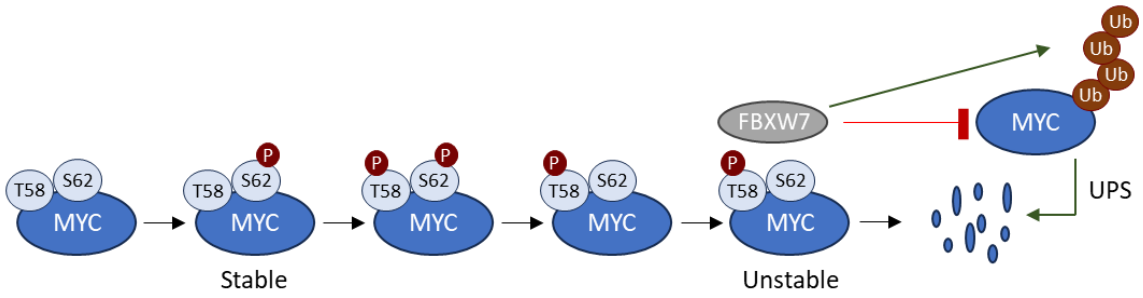

Figure 1.13: The FBXW7-mediated MYC degradation through the UPS. MYC contains two critical residues in a phosphodegron sequence of its MBI domain, T58 and S62. Phosphorylation of S62 forms a stable MYC protein and induces sequential phosphorylation of T58. Upon dephosphorylation of S62, unstable MYC protein can interact with the E3 ubiquitin ligase FBXW7 via its phosphorylated T58. This interaction induces poly-ubiquitination of MYC and activates the UPS for its degradation (adaptation from Boi et al., 2023 (266)).

Mutations that deregulate the tightly controlled MYC degradation process have been identified in both T58 and S62 critical residues of MYC and in proteins associated with its UPS-based protein turnover. Substitution of MYC T58 is a recurrent and driver oncogenic event in BL while multiple MYC-associated lymphomas and solid cancers also carry mutations in these two critical MBI residues (266, 271, 272). Recurrent missense substitutions disrupting normal MYC protein degradation are T58I or T58A (213, 272). They lead to constitutive phosphorylation of S62 resulting in increased MYC protein stability or blockade of FBXW7 interaction and thus inhibition of degradation (205, 266, 271, 273). Deregulation of the MYC protein degradation process also occurs when the required E3-ligases acquire loss of function mutations. FBXW7 is an identified tumour suppressor which can acquire inactivating mutations in MYC-associated cancers such as uterine, colon and cervical cancer (198, 205). Thus, FBXW7 plays a critical role in the UPS-mediated proteostasis of MYC.

1.5.6 Amino acid conservation in MYC

MYC protein contains highly conserved amino acids primarily in the MB domains (204). The MBI domain of MYC contains the critical residues T58 and S62 within its phosphodegron sequence. These two amino acids are conserved between the MYC family members. In the MBII domain, the consensus motif DCMW, represented by the amino acids 132-135, is characterized by the highest conservation verified in MYC TAD with W135 being the most highly conserved residue. Two studies have explored this conserved part of the MBII domain in MYC (274, 275). DCMW motif substitutions in U2OS osteosarcoma cells and Drosophila melanogaster *in vitro* and *in vivo* experiments respectively, have shown that loss of its function suffices to

impair MYC function in a similar manner to a complete deletion of the MBII domain (274, 275). Point mutations of the MBII highly conserved residues have been assessed by the Cole laboratory, testing C133A, M134A, W135A, W135E, S136A, F138A and S146L in cancer cell lines or primary human colon organoids in the context of MYC:TRRAP interaction (213, 276). Such substitutions showed a critical role of W135 in MYC:TRRAP complex formation, a result which was also recently verified by computational-based analysis of *in silico* W135G mutants (264). M134A and F138A also reduced MYC:TRRAP interaction while S136A achieved that to a lesser extent and C133A played no significant role in the complex formation (276). In contrast, S146L augmented the affinity of MYC and TRRAP binding. Such findings highlight that specific amino acids in the MYC protein sequence can have synergistic or uniquely distinct roles in MYC function.

1.5.7 Identified MYC mutations in mature B cell cancers

MYC oncogenic activity is more rarely characterized by mutations than other oncogenes with *MYC* translocation events being the main genetic aberration detected in MM (67, 69, 252). However, recurrent mutations of *MYC* genomic locus have been identified in BL and DLBCL (12, 23, 75). A single substitution in *MYC* considered a 'hot spot' mutation in B cell lymphoma occurs in T58 and has been identified to be associated with increased MYC protein stability because of impaired ubiquitin/proteasomal degradation, as previously mentioned in section 1.5.5 (271). Several alternative residues have been detected to replace the T58 in cancer such as alanine (A), isoleucine (I), leucine (L) and asparagine (N) (213). Substitution T58I has been identified as the most recurrent with T58A being the second most common (272). Despite their frequency difference in case studies of patients with BL or other haematological malignancies, both substitutions seem to affect the pathway of MYC degradation via its MBI domain recognition. Thus, it is suggested that the main mechanism of their function leads to MYC overexpression via increased protein half-life and stability inhibiting its ubiquitination and proteasomal recognition for degradation. In addition, T58A has been associated with increased transformation activity in comparison to T58I and is known to induce B cell lymphomas *in vivo* in mouse models (272).

Additional mutations have been discovered in the MBI domain of MYC in both BL and DLBCL patients with T58 substitutions existing in 2% of DLBCL cases (35). T58 is surrounded by a series of proline (P) residues. P57 is a residue with identified mutations in BL also associated with impaired MYC degradation (75, 271). BL mutations in *MYC* have been extensively studied since it is the primary event driving disease initiation with a wide range of mutations to have been reported (75). When data of the mutational profile in BL were compared to the mutational profile of DLBCL there was an overlap of the mutations identified in *MYC*

between the two cancer types (12). T58N was one of the point mutations in BL compared to the mutational profile of the DLBCL-derived data. In a more recent study, focusing on DLBCL genetic profiling, no T58 substitutions were identified as drivers of the disease in the patients tested (45). These conflicting results in combination with the number of different point mutations identified in *MYC* in these studies highlight the complexity of haematological tumour progression. Also, it verifies that as previously mentioned BL is less heterogenic than DLBCL and *MYC* mutations are no exception.

In comparison to the number of point mutations occurring in the MBI domain of MYC, significantly fewer are the single substitutions identified in its MBII domain. Two residues in the MBII domain carrying recurrent mutations are F138 and S146 (75, 213, 276). An interesting observation is that the frequency of point mutations in the DCMW highly conserved core of the MBII domain is remarkably low (75, 213, 271). This can indicate its critical role in MBII function and could be associated with MBII requirement in MYC biological activities and mediated transformation.

1.6 Model system for overexpression of oncogenic sequences in *in vitro* differentiated human plasma cells

In vitro modelling of B cell and plasma cell transformation could unravel critical unelucidated molecular mechanisms contributing to the initiation or progression of neoplasms. An *in vitro* system of human GC B cell transformation was developed by the Hodson group to model DLBCL (277, 278). Samples from pediatric tonsils were utilised to isolate GC B cells which were cultured under constitutive CD40 and IL-21 signalling inducing differentiation blockade. This primary culture was transduced with retroviral vectors carrying a combination of oncogenes. *MYC* and *BCL2* oncogenic sequences were inserted into an MSCV retroviral backbone bearing a CD2 reporter (Appendix 3 and Appendix 4). In the retroviral vector, *MYC* and *BCL2* were merged with a *t2A* sequence while *BCL2* and *CD2* sequences were merged with an internal ribosome entry site (IRES) element. This vector configuration resulted in a single mRNA transcript. During protein synthesis, the t2A-cleaving peptide allows the production of MYC protein separated from the BCL2 protein while *CD2* mRNA is translated independently via the IRES element (279-281). Thus, from a single mRNA three different proteins, MYC, BCL2 and CD2, are overexpressed simultaneously in the transduced cells. The retroviruses had a pseudotyped envelope of GALV-MULV fusion binding to a SLC20A1 B cell receptor to infect the primary GC B cells (277, 278). SLC20A1 is highly expressed in B cells and the usage of these optimised pseudotyped retroviruses resulted in enhanced transduction efficiency. Thus,

overexpression of MYC and BCL2 in human GC B cells was achieved and under constitutive CD40 and IL-21 signalling resulted in their persistent cell growth, modelling successfully a DLBCL phenotype.

An equivalent model of primary B cell culture has been developed by the Doody-Tooze laboratory aiming to model human PC differentiation *in vitro* (149, 282, 283). In this system, naïve and memory B cells were isolated from the peripheral blood of healthy individuals. These total B cells were activated through their BCR with $F(ab')_2$ fragments to avoid the potential inhibitory effect mediated by the Fc fragments which could reduce the activated B cell numbers at an early stage of the *in vitro* culture. Simultaneously, T_{FH} cell-derived signals were also provided. The cells received CD40 signalling upon co-culture with CD40L-expressing stromal cells. Additional soluble cytokines, IL-2 and IL-21, were used to induce further activation and proliferation. Upon removal of the CD40 signalling, differentiation toward PCs was accommodated with the addition of IL-6 and APRIL while IL-21 signalling was sustained up to the PC stage. Long-lived *in vitro* differentiated PCs were maintained in the culture without IL-21, utilising the bone marrow niche-derived cytokines IL-6 and APRIL and essential lipids and amino acids. Under these conditions differentiation and long-term PC survival were achieved *in vitro*.

The combination of these two experimental approaches would provide a novel *in vitro* model system aiming at the overexpression of specific oncogenes during PC differentiation. Such a model has been developed and utilised in this study.

1.7 Aims and Objectives

MYC is a potent oncogene in aggressive B cell lymphomas and a secondary event in MM (12-14, 45, 50, 65, 284). MYC deregulation frequently co-operates with BCL2 deregulation in high-grade lymphomas characterized by poor outcome. In addition, even though BCL2 is not a driver oncogene in PC neoplasia, its overexpression can promote cell viability protecting from MYC hyperactivity-mediated apoptosis in a primary culture. Thus, in this study, MYC overexpression is combined with BCL2 protecting from deregulated MYC-mediated apoptosis. Utilising the retroviral vectors developed by the Hodson group, MYC and BCL2 overexpression is studied in a forced toward PC differentiation culture environment as established by the Doody-Tooze laboratory (149, 277, 278, 282, 283). GC B cells were the initial population transduced for MYC and BCL2 overexpression and cultured under sustained CD40 and IL-21 signalling by the Hodson group to model DLBCL (277, 278). In this study, memory B cells are used as the initial B cell population to undergo PC differentiation *in vitro* upon MYC and BCL2 overexpression. Memory B cells have undergone CSR similar to PCs (132). Thus, the evaluation of MYC and BCL2 overexpression impact under

conditions permissive for PC differentiation is conducted on cells expressing different isotypes mimicking the normal PC pool.

A series of established experiments is employed to assess the changes mediated in the *in vitro* human PC differentiation by MYC overexpression combined with BCL2, promoting cell survival. The established set of experiments utilised in this study includes i) the characterization of the immunophenotypic changes using flow cytometry, ii) the evaluation of the transcriptional changes with RNA-sequencing and iii) the assessment of the functionality of the differentiated cells based on antibody secretion using ELISAs. The goal of the study is to investigate the effect of enforced MYC under conditions permissive for PC differentiation in the model system and to unravel regions of MYC contributing to this effect.

A reductionist approach is followed to investigate regions in MYC protein that drive the observed changes in the model system. Starting from a general understanding of the MYC-BCL2 overexpression effect this study ends up revealing specific domains in MYC protein driving its effect in a deregulation context, downsizing the findings to a single amino acid, tryptophan 135 (W135). A summary of the experimental approach of this study is displayed in Figure 1.14.

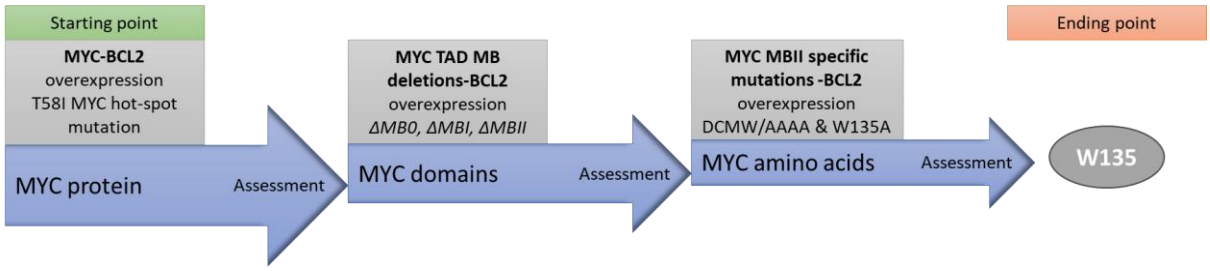

Figure 1.14: The experimental approach and layout summary of the study. This study is categorized into three sections based on the experimental setting and findings summary. Each of the sections interrogates a different aspect of MYC overexpression contribution with section one focusing on the general protein level, section two assessing protein domains and section three highlighting specific amino acids in MYC. Characterization of the immunophenotype, gene expression and antibody secretion takes place consistently for each of the sections (assessment) leading to the next goals of the study and final findings.

Initially, the hot spot mutation T58I of MYC is tested to stabilize its protein levels. MYC T58I and BCL2 are overexpressed upon retroviral transductions at a stage between activated B cell and pre-plasmablast differentiation. Following up the PC differentiation protocol, key questions to be addressed are if the enforced MYC oncogenic signalling in combination with BCL2 overexpression drives i) PC differentiation

blockade, and ii) cellular transformation in an equivalent manner to the DLBCL model developed by the Hodson group (277, 278).

Subsequently, based on the established MYC T58I-BCL2 overexpression effect on PC differentiation, the next goal of the study is to provide an insight into the contribution of each of the three MBs (MB0, MBI or MBII) of the TAD in MYC protein, to the observed changes. Each of the domains is deleted from the MYC protein. These MB deletion MYC mutants are overexpressed in the *in vitro* system with BCL2 and characterized accordingly.

The final goal of this study is to identify specific residues in the MBII domain of MYC driving the observed effect. Based on their high conservation in MYC protein the motif DCMW (132-135 residues) and its W135 are mutated into alanine to lose their functionality, and tested with BCL2 in the model system. This approach addresses whether the DCMW motif and specifically its W135 play a critical role in driving the MYC overexpression effect on the *in vitro* PC differentiation.

Chapter 2 – Methods

2.1 Bacterial work and plasmid preparation

In this study, ten plasmids were utilised in total. A brief introductory summary of the ten plasmids used is in Table 2.1. The preparation of the plasmids was conducted in three different batches and generated bigger and validated stocks. The original plasmids in batch 1 were provided by the Hodson group in Cambridge and *T58I-t2A-BCL2* plasmid is also available on Addgene (Plasmid 135306) (277). Upon bacterial transformation and propagation, they were purified generating bigger stocks. The sequences of the inserts in batch 2 and batch 3 plasmids were designed. Custom cDNA cloning of the inserts into a pIRES2-EGFP vector was performed commercially (MRC PPU Reagents and Services, University of Dundee). Subcloning of the inserts into the MSCV-backbone vector took place in-house for the generation of the final plasmid stocks in batch 2 and batch 3. The subcloning of the batch 2 plasmids was conducted by the master student, Eden Page.

Table 2.1: The plasmids used in this study and their total and insert sizes in base pairs (bp).

Batch	Plasmid	Vector size (bp)	Insert size (bp)	Appendix
1	pHIT60	12,227	-	Vector map- Appendix 1
	GALV-MTR	9,356	-	Vector map- Appendix 2
	MSCV-backbone	6,574	-	Vector map- Appendix 3
	T58I-t2A-BCL2	8,784	2,210	Vector map- Appendix 4 & Insert sequence- Appendix 5
2	*WT-t2A-BCL2*	8,739	2,165	Insert sequence- Appendix 6
	ΔMB0-t2A-BCL2	8,688	2,114	Insert sequence- Appendix 7
	ΔMBI-t2A-BCL2	8,682	2,108	Insert sequence- Appendix 8
	ΔMBII-t2A-BCL2	8,691	2,117	Insert sequence- Appendix 9
3	*MBII-4aa mut-t2A-BCL2*	8,739	2,165	Insert sequence- Appendix 10
	MBII-W135A-t2A-BCL2	8,739	2,165	Insert sequence- Appendix 11

2.1.1 Plasmid propagation

Luria-Bertani (LB) broth (LBX0102, Formedium) was prepared by dissolving 10 g of powdered growth medium in 500 ml of distilled water (dH_2O). The mixture was briefly stirred with a magnet and sterilized by autoclaving.

LB agar (LBX0202, Formedium) was prepared by dissolving 35 g of powdered agar in 1 L of dH_2O. The mixture was briefly stirred with a magnet and autoclaved.

2.1.1.1 Bacterial transformation with pIRES2-EGFP-backbone-based constructs

Propagation took place using the Subcloning Efficiency DH5α Competent Cells (18265-017, Invitrogen). Plasmids were diluted at 1 ng/ml and 5 µl of each was added to 25 µl of defrosted bacteria. Tubes were gently flicked and incubated on ice for 30 minutes without mixing. Heat shock was conducted at 42°C for 20 seconds and the tubes were directly placed on ice and incubated for 2 minutes. 950 µl of LB broth were added and the tubes were incubated on a shaking platform at 225 rpm for 60 minutes at 37°C.

Overnight prepared agar plates, containing 30 mg/ml kanamycin (K-4000, Sigma-Aldrich), were prewarmed in advance at 37°C for at least 30 minutes. 25 µl and 50 µl of transformed bacteria were spread onto the kanamycin selection plates including empty plate control. The selection plates were incubated overnight at 37°C.

2.1.1.2 Bacterial transformation with MSCV-backbone-based constructs

Propagation took place using the NEB Stable Competent E. coli (High Efficiency) (C3040H, New England Biolabs) bacteria. Plasmids were diluted at 100 ng/ml and 5 µl of each was added to 25 µl of defrosted bacteria. Tubes were gently flicked and incubated on ice for 30 minutes without mixing. Heat shock was conducted at 42°C for 30 seconds and the tubes were directly placed on ice and incubated for 5 minutes. 950 µl of outgrowth medium, included in the kit, were added and the tubes were incubated on a shaking platform at 250 rpm at 30°C for 60 minutes.

Overnight prepared agar plates, containing 100 mg/ml ampicillin (A9518, Sigma-Aldrich), were prewarmed in advance at 30°C for at least 30 minutes. 25 µl, 50 µl, and 100 µl of transformed bacteria were spread onto ampicillin selection plates including empty agar plate control. The selection plates were incubated for 24 hours at 30°C.

2.1.1.3 Single colonies selection and propagation

Three to six single colonies were selected per condition and experimental round. Each single colony was transferred to a 15 ml falcon tube containing 3 ml LB broth with appropriate antibiotic (30 mg/ml kanamycin or 100 mg/ml ampicillin). Tubes were incubated on a shaking platform at 225 rpm overnight at 30°C. 1 ml glycerol stocks were prepared by mixing 500 ml of 50% glycerol with 500 ml bacterial culture per condition and stored at -80°C. The remaining bacterial cultures were centrifuged at 4,000 x g for 1 hour at 4°C. The supernatant was removed, and the bacterial pellets were stored at -20°C for plasmid purification and validation.

2.1.2 Plasmid purification

Miniprep kit (K210002, Invitrogen) was utilised according to the manufacturer's instructions to purify plasmids from the frozen bacterial pellets. Upon validation with diagnostic digests, as described below in section 2.1.4, single colony-derived plasmids were selected. Bacterial propagation of the corresponding glycerol stocks was conducted to acquire higher concentrations of the purified plasmids. 100 ml LB broth containing the appropriate antibiotic (30 mg/ml kanamycin or 100 mg/ml ampicillin) were prepared and glycerol stock-derived transformed bacteria were added with a tip and incubated at 37°C overnight on a bacterial shaker at 225-250 rpm. The overnight bacterial cultures were centrifuged at 4,000 x g for 1 hour at 4°C in 50 ml falcon tubes. The supernatant was discarded and the bacterial pellets were either stored at -20°C or immediately processed for plasmid purification with a Midiprep kit (K210005, Invitrogen) according to the manufacturer's instructions. Purified plasmids were resuspended either in RNase/DNase-free water or in Tris-EDTA (TE) buffer provided with the plasmid purification kit.

2.1.3 Plasmid quantification

The concentration of the purified plasmids was quantified with Nanodrop (ND-100 spectrophotometer, Nanodrop Technologies, Inc.) at least one day after the purification protocol completion. 2 µl of plasmid were used per Nanodrop reading.

2.1.4 Diagnostic digests

Restriction enzymes were selected as described in Table 2.2 based on the maps of the vectors (Appendix 3 and Appendix 4). The digest reaction was performed for 30 minutes at 37°C in a thermocycler and restriction enzyme inactivation was included for 20 minutes at 65°C, as described in Table 2.3.

Table 2.2: Restriction enzymes and the size of the expected bands in base pairs (bp) after double digest.

Plasmid	Vector size (bp)	Enzyme 1	Enzyme 2	Expected bands at double digest (bp)
MSCV-empty	6,574	XhoI	SalI	5,120 and 1,454
T58I-t2A-BCL2	8,784	XhoI	SalI	5,120 and 3,664
WT-t2A-BCL2	8,739	EcoRI	XhoI	6,574 and 2,165
ΔMB0-t2A-BCL2	8,688	EcoRI	XhoI	6,574 and 2,114
ΔMBI-t2A-BCL2	8,682	EcoRI	XhoI	6,574 and 2,108
ΔMBII-t2A-BCL2	8,691	EcoRI	XhoI	6,574 and 2,117
MBII-4aa mut-t2A-BCL2	8,739	EcoRI	XhoI	6,574 and 2,165
MBII-W135A-t2A-BCL2	8,739	EcoRI	XhoI	6,574 and 2,165

Table 2.3: Restriction enzyme diagnostic digest reaction.

Reagent	Volume per reaction (µl)
0.5 µg plasmid	variable
CutSmart 10X NEB buffer	2.5
Restriction enzyme 1	2.5
Restriction enzyme 2	2.5
RNase/DNase-free water	variable
Total volume	50
Incubation °C -Time	37°C for 60 minutes
Heat inactivation	65°C for 20 minutes

2.1.5 Agarose electrophoresis and gel extraction

1% agarose gel was prepared by mixing 1.2 g agarose with 120 ml 1X Tris-borate-EDTA (TBE) buffer. The mixture was microwaved until the agarose was completely dissolved. 16 µl of Ethidium bromide was added and mixed. Gel imaging was performed under UV light using the ChemiDoc MP Imaging System (BioRad). For the desired inserts' DNA band isolation, the Qiagen QIAquick gel extraction kit (28706, QIAGEN) was used, and DNA purification was conducted following the manufacturer's instructions.

2.1.6 Design of the MYC TAD deletion and the MBII mutants

For the design of the MYC TAD MB deletion mutants, the *MYC* sequence encoding for MYC isoform 2 was used (Appendix 6, Appendix 7, Appendix 8 and Appendix 9) (74). The nucleotides encoding for each of the domains MB0 (YDSVQPYFYCDEEENFY), MBI (PSEDIWKKFELLPTPPLSP) or MBII (IIIQDCMWSGFSAAAK) were removed from the *MYC* cDNA sequence (Figure 2.1). In the MYC protein sequence, the position of each amino acid corresponding to MB0 (aa 16-32), MBI (aa 45-63), and MBII (aa 128-143) domains was identified as previously published (240).

Figure 2.1 MYC TAD and the MB0, MBI and MBII domains. The TAD contains 1-143 amino acids (aa) in MYC isoform 2 protein and is located at its N terminus. The highlighted aa indicate each of the MB0, MBI and MBII domains deleted in each of the mutants. MB0 occupying 16-32 aa is indicated with green, MBI occupying 45-63 aa is indicated with blue and MBII occupying 128-143 aa is indicated with grey. The 4 aa motif mutated into alanine in the MBII occupies 132-135 aa and is indicated with red capital letters.

For the design of the MYC MBII mutants, the *MYC* sequence encoding for MYC isoform 2 was utilised (Appendix 10 and Appendix 11) (74). The codons encoding for the amino acids 132-135 (DCMW) or W135, as depicted in Figure 2.1, were substituted with a GCC codon (5' -> 3') encoding for alanine.

2.1.7 Cloning

The gel-extracted inserts were cloned into linearised MSCV-backbone plasmid, digested in its cloning site. Eden Page (master student in the laboratory) conducted the cloning of *WT-t2A-BCL2*, *ΔMB0-t2A-BCL2*, *ΔMBI-t2A-BCL2* and *ΔMBII-t2A-BCL2* plasmids of batch 2 as described in Table 2.1 of section 2.1. For the cloning of the Batch 3 plasmids *MBII-4αα mut-t2A-BCL2* and *MBII-W135A-t2A*-BCL2, as described in Table 2.1 of section 2.1, Ben Kemp (master and PhD student in the laboratory) provided the linearly digested MSCV-backbone construct. The ligation reaction was performed as described in Table 2.4 followed by 2

hours of incubation at RT. Sub-cloned plasmids were validated with diagnostic digests and/or Sanger sequencing as described in sections 2.1.4 and 2.1.8 respectively.

Table 2.4: Ligation reaction of digested MSCV-backbone and inserts of interest.

Reagent	Volume per reaction (µl)
MSCV-backbone linear plasmid	1
Insert DNA	4
Ligase Buffer	1
T4 Ligase enzyme	0.5
RNase/DNase-free water	3.5

2.1.8 Sanger sequencing

MBII-4αα mut-t2A-BCL2 and *MBII-W135A-t2A-BCL2* plasmids were validated with Sanger sequencing. Forward and reverse primers, 5'- ACCAGCTGGAGATGGTGAC -3' and 5'- AGAGGGTAGGGGAAGACCAC -3' respectively, were designed as displayed in Figure 2.2. Their oligos were commercially synthesized by Sigma Aldrich. The samples of plasmids and primers were shipped to Source BioScience for Sanger sequencing and the chromatograms were viewed and analysed with SnapGene Viewer version 5.2.4.

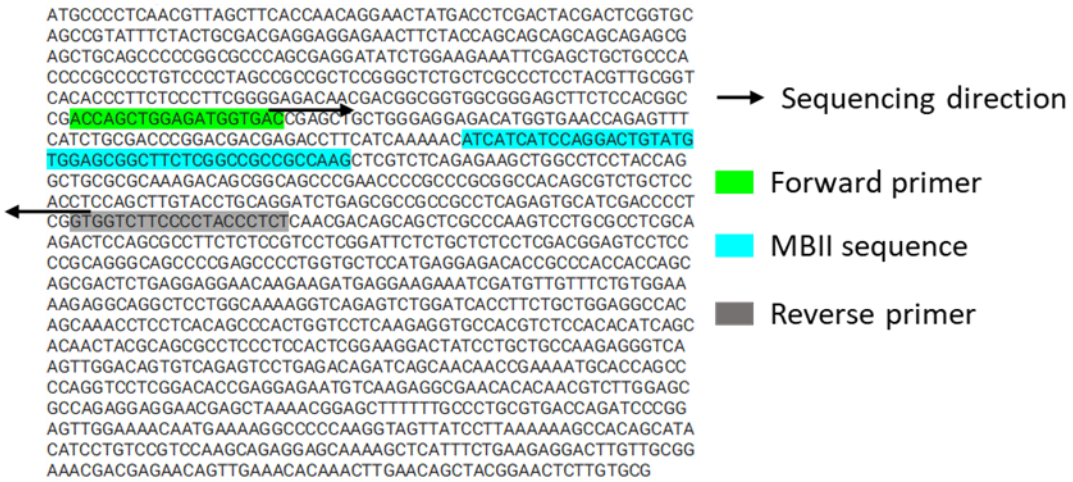

Figure 2.2: Primers design for Sanger sequencing. The DNA sequence (5' -> 3') of the gene encoding for MYC isoform 2 is illustrated. In green is the sequence of the forward primer and in grey is the sequence corresponding to the reverse primer. In light blue is the sequence of the MBII domain of *MYC* containing the nucleotides modified by mutations. Arrows indicate the direction of sequencing based on the designed oligos of the primers.

2.2 *In vitro* differentiation of human plasma cells

2.2.1 Isolation of PBMCs

Peripheral blood mononuclear cells (PBMCs) were isolated from either 80 ml peripheral blood or leukocyte cones of healthy anonymous donors. Blood material was diluted with sterile phosphate saline buffer (PBS) at RT up to 180 ml final volume. The diluted blood material was distributed in three 50 ml falcon tubes containing 15 ml Lymphoprep at RT creating a layer at the top. Lymphoprep density gradient centrifugation was performed at 2,400 rpm (for peripheral blood-derived tubes) or 800 x g (for leukocyte cone-derived tubes) (acceleration 5, brake 0) for 20 minutes at 22°C. The buffy coat containing the isolated PBMCs was collected in 50 ml tubes with sterile cold PBS followed by centrifugation at 1,800 rpm (for peripheral blood-derived tubes) or 200 x g (for leukocyte cone-derived tubes) for 20 minutes at 4°C. Cell pellets were resuspended in 50 ml falcon tubes with cold magnetic-activated cell sorting (MACS) buffer up to 50 ml. Resuspended cells were mixed and counted using a hemocytometer and trypan blue exclusion while cells were stored on ice.

The desired number of isolated PBMCs per experiment was labelled with antibodies for magnetic selection as described in the sections below. The remaining cells were aliquoted at $2x10^8$ PBMCs per tube in heat-inactivated fetal bovine serum (HIFBS) with 10% dimethyl sulfoxide (DMSO) and stored at -80°C.

2.2.1.1 Population and ethical approval

Whole blood was collected from healthy individuals volunteering to participate as donors after informed consent. Leukocyte cones were obtained from the NHS Blood and Transplant (NHSBT) services. Ethical approval was provided by the UK National Research Ethics Service via the Leeds East Research Ethics Committee (approval reference: 07/Q1206/47, IRAS reference 187050) (Appendix 12, Appendix 13 and Appendix 14).

2.2.2 Isolation of total B cells

The following protocol was used for total B cell negative selection from PBMCs with a Miltenyi memory B cell isolation kit. The quantities described correspond to cell counts up to $1x10^8$ cells. All quantities of reagents were doubled if the PBMCs yield exceeded $1x10^8$ cells.

PBMCs were pelleted with centrifugation at 1,500 rpm for 5 minutes at 4°C. The cell pellet was resuspended in 400 µl cold MACS buffer. 100 µl B cell biotin-antibody cocktail was added and incubated

for 20 minutes at 4°C. 200 µl anti-biotin beads and 300 µl cold MACS buffer were added followed by incubation for 20 minutes at 4°C. The labelled cells were washed with 10 ml cold MACS buffer and centrifuged at 1,500 rpm for 10 minutes at 4°C. Cell pellets were resuspended in 1 ml cold MACS buffer and run through gravity flow in an equilibrated LD column under an applied magnetic field. The effluent containing the total B cells was collected. The column was washed twice with 1 ml cold MACS buffer to collect residual unlabelled B cells. Cells were counted using a hemocytometer and trypan blue exclusion. 10 ml of cold MACS buffer was added, and the cells were centrifuged at 1,500 rpm for 5 minutes at 4°C.

2.2.3 Isolation of memory B cells

The following protocol was used for $1x10^7$ or fewer cells to negatively select $CD23^-$ memory B cells from the total B cell isolated population. All centrifugation steps were conducted at 1,500 rpm for 5 minutes at 4°C.

10 µl CD23 biotin-conjugated antibody and 90 µl cold MACS buffer were added per sample. The mixture was incubated for 15 minutes at 4°C and centrifuged. 20 µl anti-biotin microbeads and 80 µl cold MACS buffer were pipetted per sample. The mixture was incubated for 15 minutes at 4°C, washed with 2 ml cold MACS buffer, and centrifuged. The cell pellet was resuspended in 500 µl cold MACS buffer and run through gravity flow in an equilibrated MS column under a magnetic field. The flow through containing unlabelled memory B cells was collected. The column was washed three times with 0.5 ml MACS buffer. Cells were counted using a hemocytometer and trypan blue exclusion. Subsequently, cells were pelleted with centrifugation at 1,500 rpm for 5 minutes at 4°C and resuspended at $5x10^5$ cells/ml in Iscove's Modified Dulbecco's Medium (IMDM) containing 10% HIFBS (IMDM CM). The memory B cell suspension was stored at 4°C until seeded for differentiation, later on the same experimental day, following the *in vitro* system conditions described below in section 2.2.5.

2.2.4 Preparation of CD40L-L fibroblasts

CD40L-L stromal cells were generated by transfecting murine L fibroblasts to stably express human CD40L. Irradiation of the CD40L-L was performed in a gamma irradiator. The irradiated stromal cells were aliquoted at $1x10^6$ or $2x10^6$ per tube and stored at -80°C for short-term storage and in liquid nitrogen for long-term storage.

2.2.5 B cell differentiation culture conditions

An aliquot of $2x10^6$ irradiated CD40L-L stromal cells was thawed and added dropwise in 9 ml IMDM CM followed by a centrifugation at 1,500 rpm for 5 minutes at 22°C. CD40L-L stromal cells were seeded 24 hours in advance in 24 well-plates at a ratio of $2x10^4$ cells/well/500 µl IMDM CM and incubated overnight at 37°C with 5% CO_2. The culture conditions followed for *in vitro* PC differentiation are described in Figure 2.3 (149, 282, 283). Cells were incubated at 37°C with 5% CO_2 in 24 well-plates.

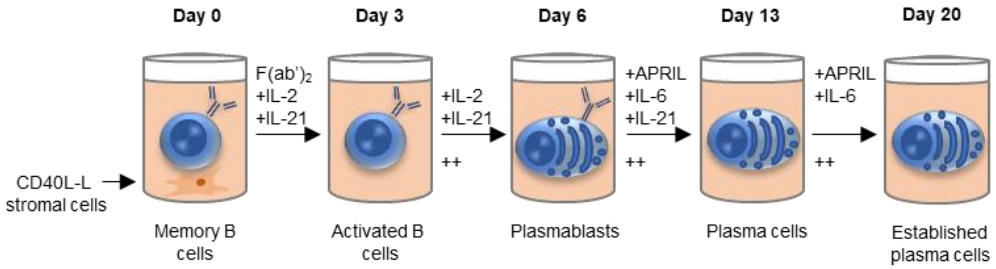

Figure 2.3: Conditions and time points of the *in vitro* human PC differentiation system. Memory B cells isolated from the peripheral blood of healthy individuals were activated on day 0 of the *in vitro* system through their BCR with F(ab)'$_2$ fragments. CD40:CD40L interaction of B cells with modified stromal cells as well as IL-2 and IL-21 addition promoted further activation and proliferation. On day 3, activated memory B cells were re-seeded without CD40L-L stromal cells allowing their differentiation into plasmablasts by day 6. At this stage, IL-6 and APRIL cytokines were added to induce PC differentiation. The PC phenotype was anticipated from day 13 onwards. The *in vitro* differentiated PCs were maintained up to day 20 in growth medium containing APRIL and IL-6 cytokines as well as supplements (++) of essential amino acids and lipids.

At day 0, 500 µl/well of IMDM CM with cytokines hIL-2 (40 U/ml), hIL-21 (100 ng/ml) and F(ab')$_2$ goat anti-human IgG, IgM and IgA fragments (20 µg/ml) replaced the growth medium of the pre-seeded CD40L-L stromal cells. Memory B cells were resuspended at $5x10^5$ cells/ml in IMDM CM. 500 µl of memory B cell suspension were added per well in co-culture with the CD40L-L stromal cells.

At day 3, activated B cells were collected and counted with a hemocytometer and trypan blue exclusion. They were seeded in new 24 well-plates at $0.33x10^5$ cells/ml for the *T58I-t2A-BCL2*, *WT-t2A-BCL2* and *ΔMBI-t2A-BCL2* conditions and at $1x10^5$ cells/ml for the rest of the conditions in IMDM CM containing hIL-2 (20 U/ml), hIL-21 (50 ng/ml) and supplements of lipid mixture 1; chemically defined (200X) and MEM amino acids solution (50X).

At day 6, plasmablasts were counted with a hemocytometer and trypan blue exclusion. Then they were seeded at $0.66x10^5$ cells/ml for the *T58I-t2A-BCL2*, *WT-t2A-BCL2* and *ΔMBI-t2A-BCL2* conditions, and for the rest of the conditions at $2x10^6$ cells/ml in IMDM CM containing APRIL (100 ng/ml), hIL-21 (10 ng/ml), hIL-6 (10 ng/ml) and supplements of lipids and amino acids.

At day 9, the *T58I-t2A-BCL2*, *WT-t2A-BCL2* and *ΔMBI-t2A-BCL2* cells were passaged following a 1:2 ratio (or higher if needed). Appropriate volume of the day 6 complete medium was added to all the conditions aiming at a final volume of 2 ml per well.

At day 13, the *T58I-t2A-BCL2*, *WT-t2A-BCL2* and *ΔMBI-t2A-BCL2* cells were re-seeded at $0.33x10^5$ cells/ml and the rest of the conditions at $1x10^6$ cells/ml in IMDM CM containing APRIL (100 ng/ml), hIL-6 (10 ng/ml) and supplements at 1 ml final volume per well.

From day 13 onwards and up to day 20, the cell growth rate was monitored and if needed the cells were passaged following a 1:2 ratio (or higher if essential). Appropriate volume of the day 13 complete medium was added to all the conditions which were subcultured aiming at a final volume of 1 ml per well.

2.2.6 Cytokines and reagents

Table 2.5: Cytokines and supplements used in the *in vitro* differentiation system.

Reagent name	Company	Catalog number
hIL-2 (human IL-2)	Miltenyi Biotec	130-097-746
hIL-6 (human IL-6)	PeproTech	200-06
hIL-21 (human IL-21)	PeproTech	200-21
APRIL	Biotechne	5860-AP
Goat anti-human $F(ab')_2$ anti-IgM, IgG and IgA	Jackson Immunoresearch	109-006-064
MEM Amino Acids Solution	Sigma-Aldrich	M5550-100ML
Lipid Mixture 1 chemically defined	Sigma-Aldrich	L0288-100ML

2.3 HEK-293 cells

The HEK-293 adherent cell line was maintained in the culture using Dulbecco's Modified Eagle Medium (DMEM) (41965039, Thermofisher Scientific) with 10% HIFBS and 1:100 penicillin/streptomycin (15140122, Gibco) (DMEM CM). HEK-293 cells were used for transfections as packaging cells to produce retrovirus. Also, they were transduced with retroviruses as part of a validation assay evaluating the produced viral stocks as described in the section below.

2.4 Retroviral transduction of *in vitro* activated memory B cells

The workflow followed for GALV-MTR pseudotyped retrovirus production and transduction of memory B cells is displayed in Figure 2.4A and Figure 2.4B respectively.

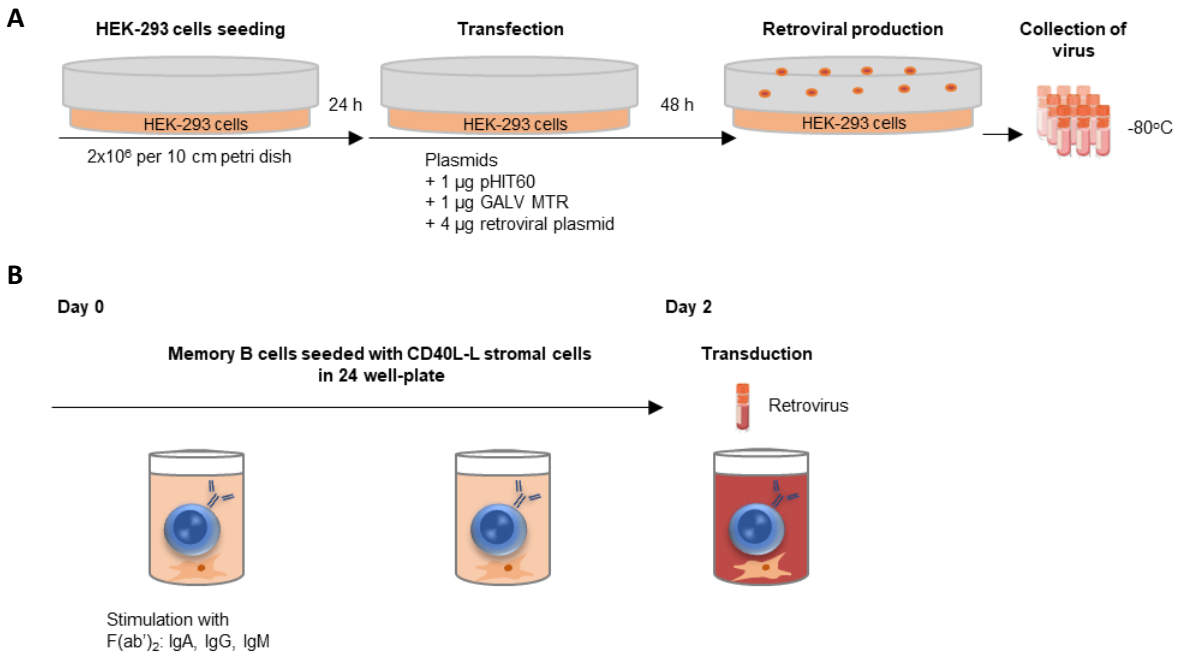

Figure 2.4: Virus production and transduction of *in vitro* activated memory B cells at day 2. (**A**) HEK-293 cells were seeded 24 hours (h) in advance and transfected with the packaging (pHIT60), envelop (GALV-MTR), and retroviral constructs at the indicated amounts. The produced virus was collected 48 h later and divided into 1 ml aliquots. The aliquots were either used immediately for transductions or stored at -80˚C as bigger viral stocks of 1 ml virus per aliquot. (**B**) On day 0 of the *in vitro* system, memory B cells isolated from human PBMCs were activated through their BCR with $F(ab')_2$ fragments in a co-culture with CD40L-L stromal cells and appropriate cytokines. On day 2, retroviral transductions took place transducing cells in each well of the *in vitro* system with one aliquot of 1 ml virus. (A, B) Images of the tubes representing the viral 1 ml aliquots were created in BioRender.com.

2.4.1 Virus preparation

$2x10^6$ HEK-293 adherent cells were seeded in 10 cm Petri dishes 24 hours in advance. Transfection of HEK-293 cells took place using 1 ml Opti-MEM (31985062, Invitrogen) mixed with 18 µl Transit-293T (MIR 2700, Mirus) transfection reagent containing 1 µg pHIT60 packaging, 1 µg GALV-MTR envelop and 4 µg retroviral constructs, as previously described (142, 277). The produced virus was collected and filtered through a

0.22 µm sterile filter unit after 48 hours of incubation at 37°C with 5% CO_2. Collected and filtered virus was either used fresh for transductions or aliquoted at 1 ml and stored at -80°C.

2.4.2 Virus validation by transduction of HEK-293 cells

The frozen viral stocks were validated before long-term storage at -80°C. HEK-293 adherent cells were seeded in 6 well plates 24 hours in advance. They were transduced with 1 ml frozen virus per well mixed with 10 µg/ml polybrene (sc134220, INSIGHT biotechnology). A spinfection step at 2,500 rpm for 60 minutes at 30°C was followed to augment the efficiency of retroviral infection. The growth medium was replaced with fresh DMEM CM, and the transduced cells were incubated at 37°C with 5% CO_2. Live/dead and CD2 staining were conducted 24 hours, 72 hours and/or 96 hours post-transduction for flow cytometry assessment as described below in section 2.5.

2.4.3 Viral transductions of activated memory B cells

Activated memory B cells co-cultured with CD40L-L at day 2 of the *in vitro* differentiation system, were centrifuged at 400 x g for 4 minutes at RT. 80% of the existing growth medium per well was aspirated. 1 ml fresh or frozen retrovirus mixed with 25 µM HEPES (15630-056, Thermofisher Scientific) and 10 µg/ml polybrene (sc134220, INSIGHT biotechnology) were added. A spinfection step at 1,500 x g for 90 minutes at 32°C was followed. Subsequently, 70% of the medium was replaced with fresh IMDM CM containing hIL-2 (20 U/ml), and hIL-21 (50 ng/ml). The transduced cells were incubated at 37°C with 5% CO_2 up to day 3 of the *in vitro* differentiation system.

2.5 Flow cytometry

2.5.1 Staining for flow cytometry assessment

In vitro differentiating cells growing in 24 well-plates or 96 well-plates were mixed and combined in one falcon tube corresponding to each condition tested on the day. Cells were counted with a hemocytometer and trypan blue exclusion. $2x10^4$ cells were collected in flow tubes followed by surface and/or intracellular staining and flow cytometry assessment.

2.5.1.1 Surface staining

Collected cells were washed with 2 ml PBS at RT. A centrifugation step at 1,500 rpm for 5 minutes at RT was performed and cell pellets were gently mixed. Live/dead fixable viability stain (565388, BD Biosciences) was prepared 1:1000 in PBS at RT. Cell pellets were resuspended in 500 µl of the viability stain mixture and incubated for 15 minutes at RT protected from light. 2 ml fluorescence-activating cell sorting (FACS) buffer was added to each tube and cells were centrifuged at 1,500 rpm for 5 minutes at RT. 25 µl blocking buffer was added to the cell pellet and incubation of 15 minutes took place at RT. Antibody and isotype control mixtures were prepared, as described in Table 2.6 in section 2.5.3, and 10 µl was added to each sample respectively. Cells were incubated for 20 minutes at RT and then washed with 2 ml FACS buffer and centrifuged at 1,500 rpm for 5 minutes at RT. The stained cell pellets were fixed with 150 µl 2% paraformaldehyde and stored at 4°C.

2.5.1.2 Intracellular staining

Fixed and stored at 4°C cells were washed with 2 ml FACS buffer and centrifuged at 1,500 rpm for 5 minutes at RT. 1X saponin-based permeabilization buffer was prepared with RT PBS containing 1% HIFBS. 200 µl 1X permeabilization buffer were added to the cell pellets and an incubation step of 20 minutes at RT was conducted. Cells were washed with 2 ml 1X permeabilization buffer and centrifuged at 1,500 rpm for 5 minutes at RT. Antibody mixtures were prepared at a final volume of 100 µl of 1X permeabilization buffer and added to the cell pellets (Table 2.7 in section 2.5.3). Samples were incubated for 1.5 hours at 4°C and mixed every 30 minutes. Intracellularly stained cells were washed with 1X permeabilization buffer and centrifuged at 1,500 rpm for 5 minutes at RT. Cell pellets were resuspended in 150 µl of FACS buffer and samples were stored on ice or at 4°C for immediate or less than 24 hours flow cytometry assessment respectively.

2.5.2 Flow cytometry

Counting beads master mix was prepared prior to the flow cytometry assessment. 5 µl counting beads reagent (C36950, Invitrogen) containing 5,200 beads were added per 45 µl FACS buffer. 50 µl counting beads mixture was added per sample and the tubes were gently mixed. Flow cytometry data collection was conducted using Cytoflex S and Cytoflex LX analysers (Beckman Coulter). Flow cytometry data analysis was performed using FlowJo v.10.7.2 and v.10.8.1 (Treestar) and GraphPad Prism 10 software.

2.5.3 Antibody panels

Table 2.6: Flow cytometry panel of antibodies and their isotype controls for surface staining.

Antigen	Fluorochrome	Antibody volume/sample	Isotype volume/sample	Company	Catalog number
Live/Dead	780 nm	500 µl of 1:1000	-	BD Biosciences	565388
CD19	PE	0.4 µl	2 µl	Miltenyi	130-113-169
CD20	ef450 or BV421	2.5 µl	1.25 µl	eBioscience BD Biosciences	48-0209-42 562873
CD27	FITC	2 µl	2 µl	BD Pharmingen	555440
CD38	PE-Cy7	0.5 µl	0.25 µl	BD Biosciences	335825
CD138	APC	0.4 µl	0.4 µl	Miltenyi	130-117-395
CD2	BUV395	1.2 µl	2 µl	BD Biosciences	563819

Table 2.7: Flow cytometry panel for intracellular staining.

Antigen	Fluorochrome	Antibody volume/sample	Isotype volume/sample	Company	Catalog number
EdU	Alexa Fluor 647 nm	-	-	Invitrogen	C10635
Ki67	Alexa Fluor 488 nm	7 µl	7 µl	BD Biosciences	558616

2.5.4 Gating strategy

The gating strategy used in this study for the *in vitro* PC differentiation and transductions model system is displayed below (Figure 2.5):

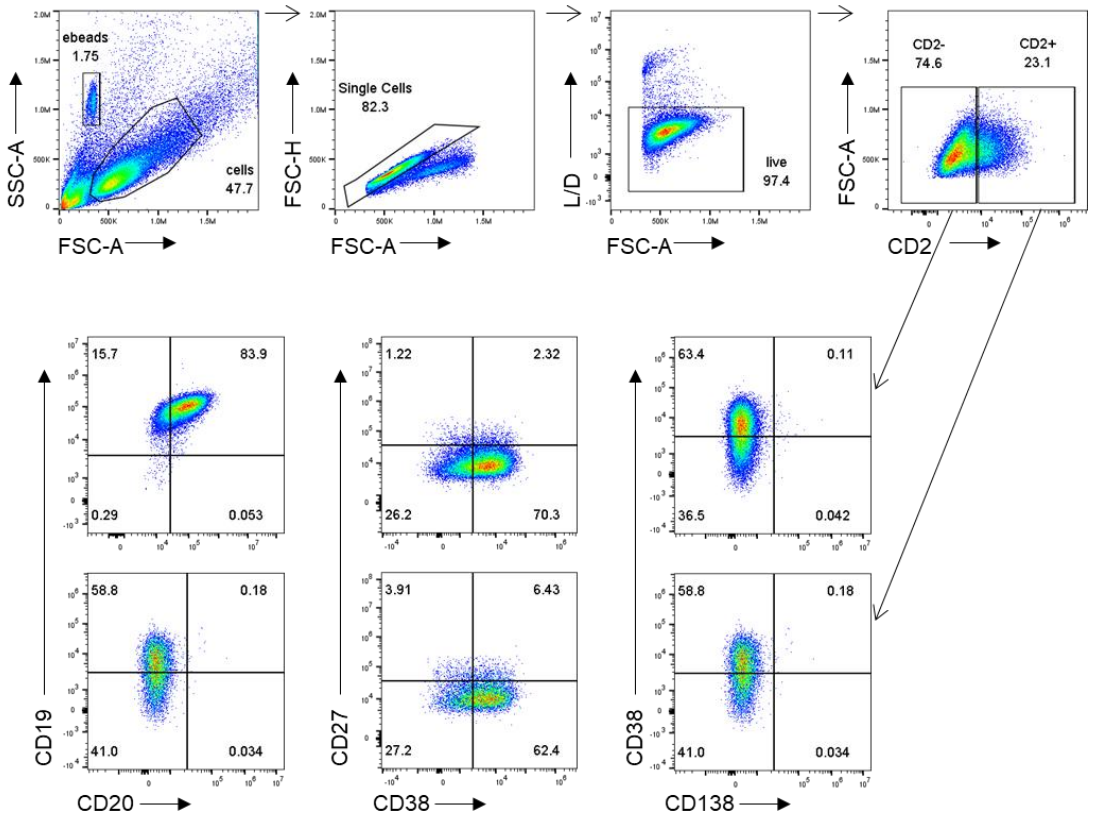

Figure 2.5 Gating strategy. The viable cells were initially gated based on their FSC-A and SSC-A parameters and apart from the counting beads gate (ebeads). Single cells discrimination was conducted next and was followed by a live cell gate based on the viability stain. The viable cells are negative for the viability stain used. In this live cell gate, CD2 negative and positive populations were distinctively gated. Immunophenotyping was conducted for each of these two populations assessing the expression of CD19 versus CD20, CD27 versus CD38 and CD38 versus CD138 on the y-axis and x-axis respectively. All gates were placed based on the untransduced samples and validated with isotype controls. Arrows indicate the gating strategy flow between each population and its ancestry. The flow plots used in this figure are representative of a day 3 MSCV-backbone transduced sample.

2.6 5-ethynyl-2'-deoxyuridine (EdU) proliferation assay

$1x10^6$ day 21 or $1x10^5$ day 21 and day 31 cells of the *in vitro* differentiation system were collected and centrifuged at 1,500 rpm for 5 minutes at RT. Fresh growth medium (equivalent to the day 13 conditions) was prepared and the cell pellets were resuspended in 1 ml or 100 µl respectively. Resuspended cells were seeded per condition in a 24 well-plate or a 96 well-plate. EdU (5-ethynyl-2'-deoxyuridine) concentrations of 1.5 µM and 5 µM were prepared and added to the EdU-treated conditions appropriately. 1-hour pulse EdU incorporation was followed with incubation of the treated and untreated cells at 37°C with 5% CO_2.

Subsequently, the cells were washed with RT PBS and centrifuged at 1,500 rpm for 5 minutes at RT. Live/dead and CD2 surface staining was performed as described in section 2.5.1.1.

Click-iT EdU detection took place according to the manufacturer's instructions (Click-iT Plus EdU Alexa fluor 647 kit, C10635, Invitrogen). Cells were fixed with 100 µl Click-iT fixative for 15 minutes at RT protected from light. Cells were washed with 3 ml RT PBS containing 1% bovine serum albumin (BSA) and centrifuged at 1,500 rpm for 5 minutes at RT to form pellets. 1X saponin-based permeabilization buffer was prepared and shared at 100 µl per cell pellet. Cells were permeabilized following a 15-minute incubation at RT. For the EdU detection reaction, 1X Click-iT EdU buffer additive was prepared as well as the Click-iT Plus reaction cocktail as described in Table 2.8 below:

Table 2.8: Click-iT Plus reaction cocktail components and volumes.

Reaction components	Number of reactions			
	1	2	5	10
PBS	438 µl	875 µl	2.19 ml	4.38 ml
Copper protectant	10 µl	20 µl	50 µl	100 µl
Fluorescent stain picol azide	2.5 µl	5 µl	12.5 µl	25 µl
Reaction buffer	50 µl	100 µl	250 µl	500 µl

500 µl of the Click-iT Plus reaction cocktail were immediately added upon its preparation to the appropriate samples followed by an incubation of 30 minutes at RT protected from light. Samples were washed with 3 ml 1X permeabilization buffer and centrifuged at 1,500 rpm for 5 minutes at RT.

Next, Ki67 intracellular staining took place. Cells were re-permeabilized with 200 µl 1X permeabilization buffer for 15 minutes at RT. 2 ml of 1X permeabilization buffer was added and the cells were centrifuged at 1,500 rpm for 5 minutes at RT. Ki67 intracellular staining was performed as described in sections 2.5.1.2 and 2.5.3 (Table 2.7). Cellular proliferation based on EdU/Ki67 staining was assessed with flow cytometry analysers as described in section 2.5.2.

2.7 RNA-sequencing

2.7.1 Samples collection

Cells under *in vitro* differentiation were collected, counted using a hemocytometer and trypan blue exclusion and centrifuged at 1,500 rpm for 5 minutes at RT. The supernatants were completely removed

from the collected samples and cells were lysed with 800 µl (or 1 ml for cell counts exceeding $5x10^6$) TRIzol reagent. Samples were incubated for 10 minutes at RT and stored at -80°C.

2.7.2 RNA extraction

Frozen cell pellets in TRIzol were defrosted at 25°C in a heat block. Chloroform (C2432-26ML, Honeywell) was added at 160 µl (or 200 µl for samples with cell count exceeding $5x10^6$), followed by vigorous shaking for 15 seconds and incubation for 3 minutes at RT. This was followed by centrifugation at 11,000 rpm for 15 minutes at 4°C and the aqueous phase containing the RNA was collected into RNase/DNase-free tubes. 400 µl isopropanol and 10 µl or 20 µl glycogen (AM9510, Invitrogen) were added based on the initial cell counts. The mixture was incubated for 10 minutes at RT. Samples were centrifuged at 11,000 rpm for 10 minutes at 4°C. The pellet was washed three times with 75% ethanol followed by a centrifugation step at 9,000 rpm for 5 minutes at 4°C. RNA pellets were air-dried for 10 minutes and dissolved in 30 µl RNase-free water. RNA was incubated at 55°C for 10 minutes to be properly dissolved.

2.7.3 DNase treatment of extracted RNA

Extracted RNA was treated with DNases for genomic DNA removal (AM1906, Invitrogen). 3.5 µl of 10X buffer and 1 µl DNaseI were added to 30 µl of RNA. Samples were gently mixed and incubated at 37°C in a heat block for 30 minutes. 4 µl of vortexed inactivated beads were added per sample and an incubation step at RT for 2 minutes took place. The samples were gently mixed and incubated for another 2 minutes. Inactivated beads were pelleted with a centrifugation step at 14,000 rpm for 1 minute and the supernatant containing the treated RNA was transferred to a new RNase/DNase-free tube. The RNA samples were stored at -20°C.

2.7.4 RNA quantification

High sensitivity RNA Qubit quantification kit (Q32852, Thermo Fisher Scientific) was utilised to quantify the extracted RNA concentration. According to the manufacturer's instructions, 1ml of high-sensitivity buffer was mixed with 5 µl concentrated assay reagent (Q32852A, Invitrogen) per 5 samples. 198 µl of this mixture was shared in appropriate tubes and 2 µl of RNA was added. The samples were vortexed and upon calibration with appropriate standards provided by the kit, RNA measurements took place with Qubit 3.0 Fluorometer (Invitrogen).

2.7.5 RNA-sequencing data analysis

RNA-sequencing was conducted on a Novoseq6000 platform (Illumina), using 150-bp paired-end sequencing. Bioinformatic data analysis was performed by Dr. Matthew Care. The text below as well as the text in section 2.7.6 were written and provided by Dr. Matthew Care. Also, this text has been utilised for the methods section corresponding to this study's manuscript uploaded on bioRxiv (285). Appropriate adjustments have been made. All analyses were undertaken on ARC4, part of the High Performance Computing facilities at the University of Leeds, UK.

The fastq files were assessed for initial quality using FastQC v0.11.8, trimmed for adapter sequences using TrimGalore v0.6.10 and aligned to GRCh38.p13/hg38 with STAR aligner (v2.6.0c) (286). Transcripts were re-annotated with the MyGene.info API using all available references and any ambiguous mappings manually assigned. Transcript abundance was estimated in RSEM v1.3.1 and imported into R v4.1.2 with txImport v1.22.0 and then processed using DESeq2 v1.34.0 (287-290). Software DESeq2 determined differential gene expression (DEG) between every contrast and a total DEG carried out with a likelihood ratio test (LRT). Quality visualised using MA plots and shrinkage of log fold estimated using the apeglm method (291). Software DESeq2 also provided $\log_2$-transformed expression values that were normalized and stabilized with respect to variance via variance stabilizing transformation (VST) (288).

Parsimonious Gene Correlation Network Analysis (PGCNA) approach was utilised, as previously published (292). The transcripts differentially expressed between any contrast or across the timeseries data (DESeq2 FDR < 0.01) were retained for PGCNA analysis. 15,941 genes giving a 15,941 x 32 matrix were analysed with PGCNA in the RNA-sequencing experiment in Chapter 3. The equivalent numbers for Chapter 4 were 14,360 genes giving a 14,360 x 48 matrix and 7,148 genes resulting in a 7,148 x 18 matrix for Chapter 5. These were used for a PGCNA2 analysis (-n 1000, -b 100) giving a network with multiple modules. The median expression per condition/time was visualized as Z-scores mapped onto the network. For each gene in the network a strength (edge-weight x degree) was calculated and used to select the top 10 genes per module. These were converted to Module Expression Values (MEVs) by taking their median Z-scores (across samples) and visualised as a hierarchically clustered heatmap. The optimal PGCNA networks were converted to a list of edges and nodes and uploaded into the Gephi package (version 0.9.2). Betweenness Centrality and degree were calculated, and the latter used to adjust node sizes. The network layout was generated using the ForceAtlas2 approach, and interactive visualizations were generated from GraphML files using the Ouestware Retina tool.

2.7.6 Gene ontology terms and signature enrichment

A data set of 21,456 gene signatures was created by merging multiple different signatures downloaded from gene sets such as SignatureDB, MSigDB V7.4 (MSigDB C1-C8 and H; excluding C5), Human CORUM complexes with > 2 genes and UniProt keywords (parsed XML). In-house generated signatures based on previous RNA-sequencing experiments performed in the laboratory using the established *in vitro* human PC differentiation system were assigned in LEEDS_GOLD gene set. A gene ontology (GO) gene set was created using an in-house Python script. This parses a gene association file (geneontology.org/page/download-annotations) to link genes with ontology terms, then uses the ontology structure (.obo file; purl.obolibrary.org/obo/go.obo) to propagate these terms up to the root. The resultant gene set contained 22,865 terms. The gene ontology and gene signatures sets were merged to give a final signature set of 44,321 terms.

The gene signature enrichment (GSE) was assessed using a hypergeometric test, in which the draw is the gene list genes, the successes are the signature genes, and the population is the genes present on the platform. The resultant p-values are then adjusted for multiple testing using Benjamini and Hochberg correction. For the PGCNA networks GSE analyses, the genes per module were compared against the 43,572-signature database (background: 15,941 or 14,360 or 7,148 genes in the network for RNA-sequencing analysis in Chapter 3, Chapter 4 and Chapter 5 respectively). Only signatures that contain at least 3 genes in the background set were retained. GSE graphs were plotted with GraphPad Prism 10 software.

2.7.7 Gene ontology analysis with DAVID software

Generated lists of DEGs provided by Dr. Matthew Care were utilised for multiple pairwise comparisons using Venn diagrams (online tool: https://bioinformatics.psb.ugent.be/webtools/Venn/). The resolved gene lists were analysed in DAVID Functional Annotation Bioinformatics online tool (2021, Knowledgebase v2023q4) to conduct GO analysis (293, 294). GO analysis was also conducted using Enrichr online gene set enrichment analysis tool for validation purposes (295-297). The results from DAVID analysis provided clusters of enriched signatures in the assessed gene lists. The first cluster provided the highest enrichment score for the gene lists analysed and was used for interpretation and further analysis. Genes from all the signatures enriched in this first cluster were collected generating a new gene list. This was re-analysed in DAVID to generate a more detailed representation of the ontologies identified in the DEGs originally

analysed. Heatmaps of this re-analysis were generated based on data provided by DAVID using MORPHEUS software (BROAD Institute, https://software.broadinstitute.org/morpheus).

2.8 Western blotting

2.8.1 Protein extraction and quantification

Collected cells were washed with sterile PBS and centrifuged at 1,500 rpm for 5 minutes at 4°C. Protein was extracted with 30 µl RIPA buffer with protease inhibitors. Lysed cells were kept on ice for 15 minutes followed by a centrifugation step at 12,000 rpm for 30 minutes at 4°C and supernatant collection. Protein quantification was conducted with Bicinchoninic acid assay (BCA) (AR0146, Boster or 23250, Thermo Scientific) following the manufacturer's instructions. Absorbance reading was performed with a Cytation 5 imaging plate reader (BioTek). Protein lysates were normalised and 2X Laemmli buffer was added at 1:1 ratio. Samples were vortexed and boiled for 5 to 10 minutes at 99°C and stored at -20°C.

2.8.2 Immunoblotting

Normalised lysates were loaded in 10% sodium dodecyl sulfate (SDS)-polyacrylamide gel (Table 2.9) and transferred to a nitrocellulose membrane with 120 Volts for 60 minutes. The membrane was incubated in blocking buffer for 60 minutes on a shaking platform at RT. Primary antibodies were diluted in blocking buffer for the detection of c-MYC (D3N8F rabbit, 1:1000 13987S, Cell Signalling Technology), BLIMP1 (PRDM1a form mouse, 1:1000), BCL2 (2870S, Cell Signalling Technology, 1:1000) or (2872, Cell Signalling Technology, 1:1000) and β-ACTIN (A1978-200UL mouse, 1:10,000). The membrane was incubated in the primary antibody mixture overnight on a shaking platform at 4°C. Subsequently, washing buffer was applied on the membrane for 5 minutes at RT on a shaking platform. This step was repeated five times. Horseradish peroxidase (HRP) conjugated rabbit or mouse secondary antibodies were used at 1:10,000 in blocking buffer and the membrane was incubated on a shaking platform for 60 minutes at RT. Five washing steps were performed and the membrane was developed using enhanced chemiluminescent HRP substrate (34580, Thermo Fisher Scientific) incubation. Images were taken with ChemiDoc MP Imaging System (BioRad). Membranes were stripped using stripping buffer (46430, Thermo Fisher Scientific) for 10 minutes at RT. Densitometry measurements were conducted with ImageJ 1.54d software to quantify the protein band sizes upon membrane development and imaging.

Table 2.9: The components and volumes used in a 10% SDS-polyacrylamide gel.

Components	For 20 ml of resolving gel	For 10 ml of stacking gel
Resolving buffer	5 ml	-
Stacking buffer	-	2.5 ml
Polyacrylamide 30% (w/v): 0.8% (w/v) Bis-Acrylamide stock solution (EC-890)	6.6 ml	1.3 ml
Distilled H_2O	8.2 ml	6.1 ml
10% ammonium persulfate (APS) (1 g/10 ml)	0.2 ml	0.1 ml
TEMED	0.02 ml	0.01 ml

2.9 Enzyme-Linked Immunosorbent Assay (ELISA)

2.9.1 UV irradiation of class II supernatants

Class II viral supernatants (virus), right after collection or defrosted from -80°C stock, were handled in a class II biosafety cabinet. 1 ml virus was pipetted per condition and added per well in 6 well-plates. Following the biosafety II regulations, the 6 well-plates containing the viruses were irradiated in a UV Stratalinker apparatus for 2, 3, 5 or 10 minutes. UV-treated samples were used to transduce HEK-293 cells. Upon flow cytometry assessment based on CD2 reporter levels UV irradiation for 5 minutes was selected and used to inactivate potential viral particles in future assays. 1 ml B cell-derived supernatants, collected as class II reagents, were transferred in 6 well-plates and irradiated with UV in the Stratalinker apparatus for 5 minutes. Then they were collected in new tubes and handelled as class I reagents stored at -80°C.

2.9.2 Human IgM and total human IgG antibody detection

ELISA-specific 96 well-plates (F96 Maxisorp NUNC-Immuno plate, 442404, Thermo Scientific) were coated with 100 µl per well of 1 µl affinity purified antibody in 99 µl coating buffer for IgM (A80-100A, Bethyl) or IgG (A80-104A, Bethyl) detection. The plates were incubated at RT for 60 minutes and washed five times. 200 µl of blocking buffer were added per well and the plate was incubated at RT for 30 minutes and washed five times. Dilutions of standard samples in sample/conjugate buffer were performed as described in Table 2.10 and Table 2.11. Serial dilutions of 1:10, 1:100 and 1:1000 took place in IMDM CM for the testing samples.

Table 2.10: Dilutions of standard samples for the generation of the standard curve for IgM concentrations.

Standard (std)	ng/ml	0.44 mg/ml IgM	Sample Diluent

1	1000	5 µl	5 ml
2	500	500 µl from std 1	500 µl
3	250	500 µl from std 2	500 µl
4	125	500 µl from std 3	500 µl
5	62.5	500 µl from std 4	500 µl
6	31.25	500 µl from std 5	500 µl
7	15.6	500 µl from std 6	500 µl
8	0	Blank	500 µl

Table 2.11: Dilutions of standard samples for the generation of the standard curve for IgG concentrations.

Standard (std)	ng/ml	4.4 mg/ml IgG	Sample Diluent
Initial	1000	5 µl	5 ml
1	500	500 µl from std initial	500 µl
2	250	500 µl from std 1	500 µl
3	125	500 µl from std 2	500 µl
4	62.5	500 µl from std 3	500 µl
5	31.25	500 µl from std 4	500 µl
6	15.6	500 µl from std 5	500 µl
7	7.8	500 µl from std 6	500 µl
8	0	Blank	500 µl

100 µl of diluted standards and testing samples were loaded to the corresponding wells in duplicates including blank condition. The plates were incubated at RT for 60 minutes and washed five times. HRP antibodies for IgM (A80-100P, Bethyl) and IgG (A80-104P, Bethyl) detection were diluted at 1:100,000 and 1:150,000 in sample/conjugate diluent respectively. 100 µl of diluted HRP antibodies were added per well followed by RT incubation for 60 minutes. The plates were washed five times and 100 µl 3,3',5,5'-Tetramethylbenzidine (TMB) substrate (E102, Bethyl) were added per well. The plates were incubated at RT protected from light for 5-8 minutes. 100 µl stop solution was directly added per well. Absorbance readings were performed within the next 15 minutes at 450 nm with a Cytation 5 imaging plate reader (BioTek). Analysis was conducted using MyAssays Ltd online data analysis tool and GraphPad Prism 10 software.

2.10 Statistical analysis

One-way analysis of variance (ANOVA) and unpaired two-tailed Student's *t*-test were utilised for the statistical analysis of the data. Tukey's multiple comparisons test was conducted as a follow-up test of the

one-way ANOVA performed in cell counts' data for further assessment of the statistical analysis. GraphPad Prism 10 software was used to perform the statistical tests.

2.11 Reagents

Table 2.12: Summary of reagents used in this study per type of experiment.

Experiment	Item	Company	Catalog number
Tissue culture	IMDM	Gibco	31980-022
	DMEM	Thermofisher Scientific	41965039
	FBS	Gibco	10270-106
	DMSO	Sigma-Aldrich	D2650-100ML
	Penicillin/Streptomycin	Gibco	15140122
	Memory B cell isolation kit, human	Miltenyi Biotec	130-093-546
	autoMACS rinsing solution	Miltenyi Biotec	130-091-376
	MACS BSA stock solution	Miltenyi Biotec	130-091-222
	MS columns	Miltenyi Biotec	130-042-201
	LD columns	Miltenyi Biotec	130-042-901
	CD23 antibody	Miltenyi Biotec	130-094-510
	$F(ab')_2$ fragments	Jackson Immunoresearch	109-006-064
	MEM Amino Acids Solution	Sigma-Aldrich	M5550-100ML
	Lipid Mixture 1 chemically defined	Sigma-Aldrich	L0288-100ML
Virus production & transductions	Opti-MEM	Invitrogen	31985062
	TransIT-293	Mirus	MIR 2700
	Polybrene infection reagent	INSIGHT biotechnology	sc134220
	HEPES buffer	Thermofisher Scientific	15630-056
Flow cytometry	Fixable Viability stain 780 nm	BD Biosciences	565388
	PE Isotype	Miltenyi Biotec	130-113-200
	ef450 Isotype	Invitrogen	48-4732-82
	PE-Cy7 Isotype	BD Biosciences	348808
	APC Isotype	Miltenyi Biotec	130-113-196
	BUV395 Isotype	BD Biosciences	563547
	FITC Isotype	BD Biosciences	555748
	Alexa 488 nm Isotype	BD Biosciences	557702
	OneComp eBeads Compensation beads	Invitrogen	01-1111-42
	CountBright Absolute counting beads	Invitrogen	C36950
	Paraformaldehyde	Alfa Aesar	J61899
	FACS Flow Sheath Fluid	BD Biosciences	342003
	Click-iT Plus EdU Alexa fluor 647 kit	Invitrogen	C10635
Bacteria & plasmids	DH5a E. coli	Invitrogen	C36950
	NEB Stable Competent E. coli	New England Biolabs	C3040H
	LENNOX agar	Formedium	LBX0202

	LENNOX broth	Formedium	LBX0102
	T4 ligase	Invitrogen	15224-017
	Ampicillin sodium salt	Sigma-Aldrich	A9518
	Kanamycin	Sigma-Aldrich	K-4000
	Miniprep kit	QIAGEN	27106
	Midiprep kit	Invitrogen	K210005
Diagnostic digests & DNA	Agarose	MP	AGAH0500
	TBE 10X	Invitrogen	15581-028
	DNA Ladder	New England Biolabs	N3232S
	Gel Loading Dye, Purple (6X), no SDS	New England Biolabs	B7025S
	EcoRI	New England Biolabs	R3101S
	SalI	New England Biolabs	R0138S
	XhoI	New England Biolabs	R0146S
	CutSmart Buffer	New England Biolabs	B7204S
Western blot	ProtoGel	National Diagnostics	EC-890
	TEMED	Sigma-Aldrich	T9281-50ML
	2-Mercaptoethanol	Sigma-Aldrich	63689-100ML
	Precision Plus Protein Standards (Ladder)	Bio-Rad	161-0374
	c-Myc (D3N8F) Rabbit mAb	Cell Signalling Technology	13987S
	BCL2 antibody	Cell Signalling Technology	2870S
	BCL2 antibody	Cell Signalling Technology	2872
	β-ACTIN antibody	Sigma-Aldrich	A1978
	ECL	Thermo Scientific	34580
	Stripping buffer	Thermo Scientific	21059
RNA-extraction	Gel extraction kit	QIAGEN	28706
	TRIzol	Invitrogen	15596018
	Chloroform	Honeywell	C2432-26ML
	Glycogen	Invitrogen	AM9510
	DNase/RNase-Free Water	Invitrogen	AM9937
	DNase kit	Invitrogen	AM1906
	Qubit RNA High Sensitivity (HS) assay kit	Invitrogen	Q32852
ELISAs	Goat anti-Human IgG-Fc-antibody	BETHYL	A80-104-A
	Purified Human IgG normal serum	BETHYL	P80-105
	Anti-Human IgG Fc-HRP-antibody	BETHYL	A80-104P
	Anti-Human IgM	BETHYL	A80-100A
	IgM Human serum	BETHYL	18260-1MG
	Anti-Human IgM, HRP-antibody	BETHYL	A80-100P
	TMB One Component Substrate	BETHYL	E102
General	Lymphoprep	Axis-Shield	1114547
	PBS tablets	Sigma-Aldrich	P4417-1000TAB

2.12 Buffers composition

- MACS buffer: 12.5 ml MACS BSA stock solution, 250 ml autoMACS rinsing solution
- FACS buffer: FACS Flow Sheath Fluid, 0.5% HIFBS
- Blocking buffer (flow cytometry): 932 µl MACS buffer, 16.6 µl hIgG, 50 µl natal mouse serum
- RIPA buffer: 50 mM Tris-HCl (pH 8.0), 150 mM NaCl, 1 mM EDTA, 1% NP-40, 0.5% sodium deoxycholate (NaDOC), 0.1% SDS
- Stacking buffer: 6.06 g Tris Base, 2 ml 20% SDS, dH_2O 0.1 ml (pH 6.8)
- Resolving buffer: 90.9 g Tris Base, 10 ml 20% SDS, dH_2O 0.5 ml (pH 8.8)
- 10X Transfer buffer: 30 g Tris Base, 144 g glycine, dH_2O 1 L
- Running buffer (1X): 100 ml 10X Transfer Buffer, 10 ml 10% SDS, dH_2O up to 1 L
- Transfer buffer (1X): 100 ml 10X Transfer Buffer, 200 ml (20%) methanol, dH_2O up to 1 L
- 10X Tris-buffered saline (TBS): 80 g NaCl, 2 g KCl, 30 g Tris Base, dH_2O up to 1 L (pH 7.4)
- Blocking buffer (western blot): 5% of milk powder (containing casein) in 1X TBS
- Wash buffer (western blot): 1X TBS and 0.1% Tween-20
- PBS-T: 1X PBS, 0.1% Tween-20
- Laemmli buffer: 100 mM Tris-HCl (pH 6.8), 2% SDS, 20% glycerol, 4% β-mercaptoethanol
- ELISA coating buffer: 0.05 M carbonate-bicarbonate (pH 9.6)
- ELISA wash buffer: 50 mM Tris Base, 0.14 M NaCl, 0.05% Tween-20 (pH 8.0)
- ELISA blocking solution: 50 mM Tris Base, 0.14 M NaCl, 1% BSA (pH 8.0)
- ELISA sample/conjugate diluent: 50 mM Tris Base, 0.14 M NaCl, 1% BSA, 0.05% Tween-20
- ELISA stop solution: 0.18 M H_2SO_4

Chapter 3 – Acute MYC T58I-BCL2 hyperfunction interferes with *in vitro* human plasma cell differentiation and forces metabolic over secretory reprogramming

3.1 Introduction

MYC is a crucial TF involved in the T-dependent response-driven B cell differentiation in a GC. Its downregulation is required for the light zone B cells to further differentiate into PCs (143). In contrast to MYC, the anti-apoptotic protein BCL2 remains downregulated in a GC reaction (191, 193). In healthy cells, deregulation of MYC induces apoptosis as a protection mechanism against malignant transformation. Tumour cells exploit the deregulation of anti-apoptotic proteins such as BCL2 in combination with deregulated MYC to overcome MYC-mediated apoptosis (13, 35, 211). Both MYC and BCL2 are known oncogenic events in B cell and PC neoplasia (14, 35, 45, 298, 299). Upon their deregulation in GC B cells, MYC and BCL2 oncogenic combination can result in high-grade B cell lymphoma and differentiation arrest. Here the BCL2 protein was utilised to confer its protection effect from MYC-mediated cell death. The hypothesis tested was if MYC overexpression, in combination with BCL2, can interfere with PC differentiation in an *in vitro* model system with permissive for PC differentiation conditions.

To test this hypothesis, MYC and BCL2 were overexpressed at an activated B cell stage utilising a retroviral vector (277). Combining the transduction approach developed by the Hodson group (277, 278) and an *in vitro* system of human PC differentiation established in the Doody-Tooze laboratory, a novel model system was generated and utilised in this study (149, 282, 283). A hot spot mutation equivalent to T58I in the MBI domain of MYC, was introduced to stabilise MYC protein via defective proteasomal degradation and was combined with BCL2 overexpression (213, 272, 277). It was reasoned that the activating point mutation T58I in MYC protein would provide a more robust and consistent phenotype upon MYC deregulation. This would be beneficial to verify the robustness of any observed changes in an *in vitro* setting. In addition, the MYC T58I point mutant was also used in the system developed by the Hodson group assessing MYC deregulation in human GC B cells *in vitro*, modelling DLBCL (277). Utilising MYC carrying the T58I substitution would facilitate a direct comparison of our model to the system developed by the Hodson group. Thus, in the present study, a MYC T58I point mutant was initially used instead of a wild type MYC protein.

Fundamental proteins CD19, CD20, CD27, CD38 and CD138, expressed in B cells and/or PCs, were evaluated to determine the resulting immunophenotype by flow cytometry. Further analysis of the MYC T58I-BCL2 overexpression impact in the established model system was performed assessing the transcriptomic and proteomic profile of the cells under differentiation by RNA-sequencing and western blots, respectively. Finally, PC features such as BLIMP1 expression, cell cycle exit, PC gene expression programme, and antibody secretion were evaluated in the model system to further explore the findings.

3.2 Retroviral vectors preparation and validation

In order to overexpress MYC and BCL2 proteins in the model system a retroviral vector containing their cDNA sequences was obtained by the Hodson laboratory. The retroviral construct was based on a murine stem cell virus (MSCV) backbone containing an internal ribosomal entry site (IRES) element prior to a *CD2* reporter cDNA sequence. CD2 protein functioned as a marker of successful transduction. *MYC* and *BCL2* sequences were included in front of the IRES-*CD2* insert and combined with a t2A cleavage element resulting in a single mRNA transcript of the whole insert (Appendix 5). The *MYC* sequence contained the known and recurring T58I mutation while the wild type sequence of *BCL2* was used. Two retroviral vectors, with XhoI and SalI unique restriction enzyme sites, were utilised in the established model system. The MSCV-backbone (Appendix 3), used as a transduction and phenotype control, and the test vector namely MSCV-*T58I-t2A-BCL2* carrying the *MYC* T58I and *BCL2* sequences (Appendix 4), are displayed in Figure 3.1A and Figure 3.1B respectively.

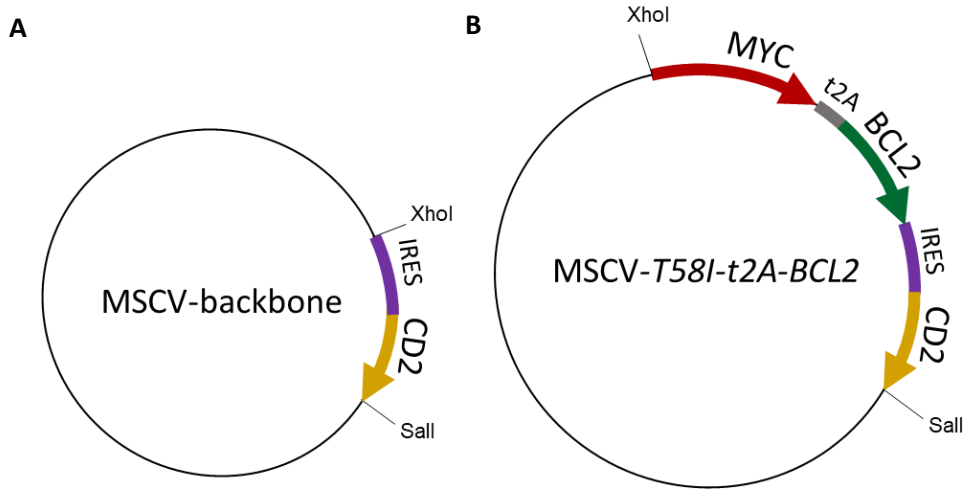

Figure 3.1 A representation of the retroviral vectors used in the model system. A map of each of the retroviral vectors, (**A**) MSCV-backbone and (**B**) the test vector MSCV-*T58I-t2A-BCL2*, showing that both contain unique

restriction enzyme sites of XhoI and SalI in the backbone vector cloning site. The MSCV-backbone had integrated only the *IRES-CD2* cDNA sequence while *MYC T58I-t2A-BCL2* sequences were included in the test vector insert.

The two retroviral vectors were propagated in commercially optimised competent E. coli bacteria suitable for lentiviral and retroviral constructs to ensure high bacterial transformation efficiency. Verification of single colony-derived plasmid purification was performed with diagnostic digests and on an agarose gel. Unique restriction enzyme sites for XhoI and SalI (Figure 3.1) were selected to verify the inserts in the two vectors. Conditions of undigested construct, single and double digests were tested for both vectors and the results are shown in Figure 3.2. The expected DNA bands were confirmed for both plasmids tested. The double digest condition for the MSCV-backbone vector showed the anticipated 5,120 bp and 1,454 bp DNA bands while the MSCV-*T58I-t2A-BCL2* construct had a 5,120 bp band followed by a 3,664 bp band as expected. These results validated the correct identity of the propagated vectors.

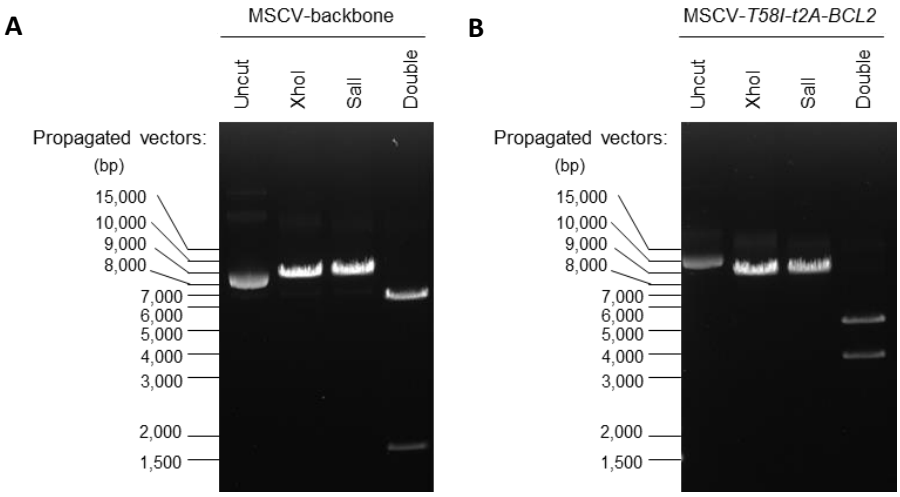

Figure 3.2 Diagnostic digests of the propagated retroviral vectors. Representative images of ethidium bromide-stained 1% agarose gel of the undigested (uncut), single digest with XhoI, single digest with SalI, or double digest conditions for (**A**) the MSCV-backbone vector and (**B**) the test MSCV-*T58I-t2A-BCL2* vector. The displayed DNA bands are located on the gel at the expected size. The molecular weights of the DNA ladder are indicated on the left side of each gel; bp, base pairs.

3.3 Virus preparation and validation

Virus for the MSCV-*T58I-t2A-BCL2* retroviral construct (*T58I-t2A-BCL2*) was generated in a big stock batch fashion and stored at -80°C. The viral stock was used to transduce HEK-293 cells and was validated based

on the resulting CD2 reporter expression by flow cytometry. Two different time points were tested post-transduction as shown in Figure 3.3.

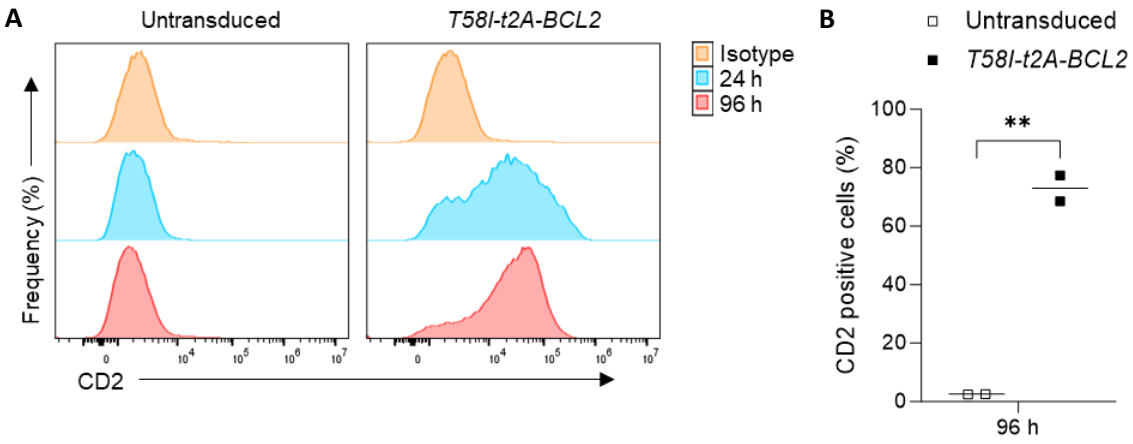

Figure 3.3 Validation of frozen *T58I-t2A-BCL2* viral batch. HEK-293 cells were transduced with *T58I-t2A-BCL2* virus produced in a big batch and stored at -80°C, including an untransduced control. (**A**) Representation of the CD2 expression in histograms for the indicated time points and samples tested. Two subsequent time points of 24 hours and 96 hours post-transduction were assessed to test viral transduction efficiency based on the CD2 reporter levels. Untransduced HEK-293 cells and CD2 isotype control were included. (**B**) Graph of CD2 positivity in percentages at the 96 hours post-transduction time point for the indicated samples. Unpaired two-tailed Student's *t*-test (B). Data are representative of two independent experiments. Bars and error represent mean and standard deviation (SD); ** $P < 0.01$; h, hours.

CD2 expression was increased at 24 hours post-transduction in comparison to the untransduced and CD2 isotype controls (Figure 3.3A). Its expression remained significantly high 96 hours post-transduction (Figure 3.3A and 3.3B). This experiment showed reproducibly, in two independent experimental repeats, that the generated and frozen *T58I-t2A-BCL2* viral batch of interest was established.

3.4 Development of the retroviral transduction and plasma cell differentiation *in vitro* system

The next aim was to develop the model system of retroviral transductions for MYC T58I and BCL2 overexpression in *in vitro* differentiated human PCs. The initial population utilised to acquire *in vitro* differentiated PCs was memory B cells. Memory B cells are class-switched B cells and thus provide both a better representation of a PC pool upon *in vitro* differentiation and a greater B cell activation and thus

survival potential in a primary culture. CD23 antibody was utilized to label total B cells derived from isolated PBMCs. Naïve $CD23^+$ B cells were depleted resulting in $CD23^-$ memory B cell enrichment. A negative selection strategy was important to maintain intact the purified memory B cell population and avoid B cell activation and intrinsic signalling initiation due to the isolation process.

At day 0 of the model system, the isolated memory B cells were co-cultured with CD40L expressing fibroblasts mimicking a B cell/T_{FH} cell interaction via CD40:CD40L receptors respectively. In parallel, the memory B cells received signals from soluble cytokines of IL-2 and IL-21 mimicking help from T_{FH} cell-derived cytokine secretion. $F(ab)_2$' IgG, IgM, and IgA antibody fragments were used to activate BCR signalling in the memory B cells. By day 2, an activated memory B cell phenotype was established in the culture and at this stage the cells were transduced with the retroviral vectors. Upon transduction, the growth medium was replenished containing IL-2 to promote survival and proliferation as well as IL-21 inducing proliferation and differentiation.

The main focus of the developed model system was to assess the impact of MYC T58I and BCL2 sustained overexpression under conditions permissive for PC differentiation. In the light zone of a GC reaction, CD40:CD40L interaction between a centrocyte and a T_{FH} cell, delivers a survival signal to the centrocytes that are subsequently able to further differentiate into memory B cells or PCs. To allow PC differentiation to proceed in the model system the CD40L fibroblasts were removed from the culture on day 3. Thus, cells collected and assessed at day 6 are anticipated to have a plasmablast phenotype. At day 6 to support further differentiation from plasmablast to PC IL-2 was replaced by IL-6 and APRIL, which support PC survival. These culture conditions suffice to establish an *in vitro* PC phenotype by day 13 (149, 282). From day 13 onwards, the *in vitro* differentiated PC population was maintained in a growth medium containing only IL-6, APRIL, and supplements as described in the Methods section 2.2.5, for long-term culture.

Based on the above cell culture conditions inducing PC differentiation, the phenotype of the cells in each of the key time points of the model system is displayed in Figure 3.4. On day 3, the activated memory B cells are characterized as $CD19^+CD20^+CD27^-CD38^+CD138^-$. This phenotype changes at day 6 with plasmablasts to be defined as $CD19^+CD20^{lo}CD27^+CD38^+CD138^{+/-}$ while the day 13 PCs have clear CD138 upregulation, and they phenotypically are $CD19^+CD20^-CD27^+CD38^+CD138^{++}$.

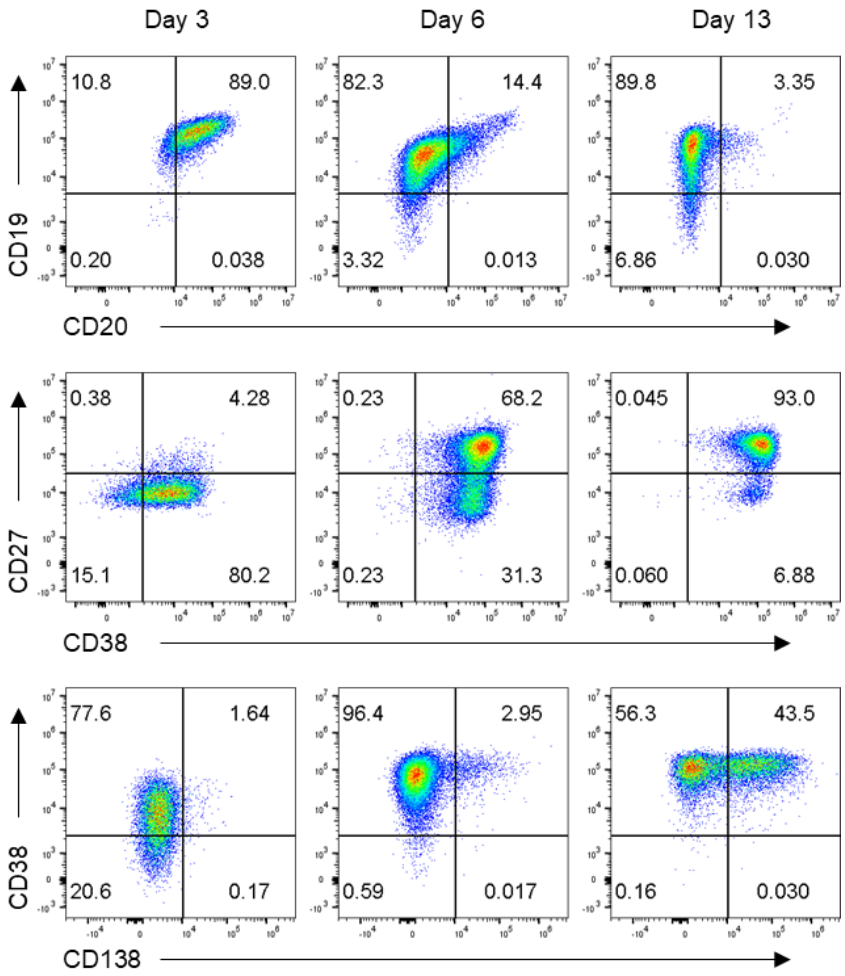

Figure 3.4 Immunophenotyping of the *in vitro* differentiated cells. Representative flow cytometry plots of selected protein markers expression for the indicated time points of the model system (top). Evaluation of CD19, CD27 and CD38 (y-axis) versus CD20, CD38 and CD138 (x-axis) respectively. Data are representative of four independent experiments with two biological replicates (N= 2) and no technical replicates per experiment. The total number of donors tested as biological replicates was eight (N= 8).

Utilizing these PC differentiation conditions, previously established by the Doody-Tooze laboratory (149, 282, 283), MYC T58I and BCL2 overexpression effect on PC differentiation was next assessed *in vitro*.

3.4.1 Purity check of the isolated memory B cell population

At day 0 of the model system, the isolated memory B cells were stained and assessed by flow cytometry for their purity before co-culture with the CD40L-L stromal cells under differentiation conditions. CD19 and CD20 B cell markers were evaluated for their expression to verify the B cell population purity at the

starting point of the culture on day 0. Viability dye was also used to exclude dead cells from the analysis. A cut-off of around 95% of $CD19^{+}CD20^{+}$ cells was desirable to verify adequate B cell enrichment of the isolated population at day 0. The samples tested for the three independent experiments included in this Chapter were verified with at least 95% $CD19^{+}CD20^{+}$ B cells upon isolation at day 0 as depicted in Figure 3.5. The sample collected from donor 2 in experiment 1 was lost during experimental processing. Donor 2 memory B cells were isolated in parallel with donor 1 following the same protocol, incubation timings and reagents. Given the high purity of 97.1% B cells in donor 1, donor 2 was also included in the experiment.

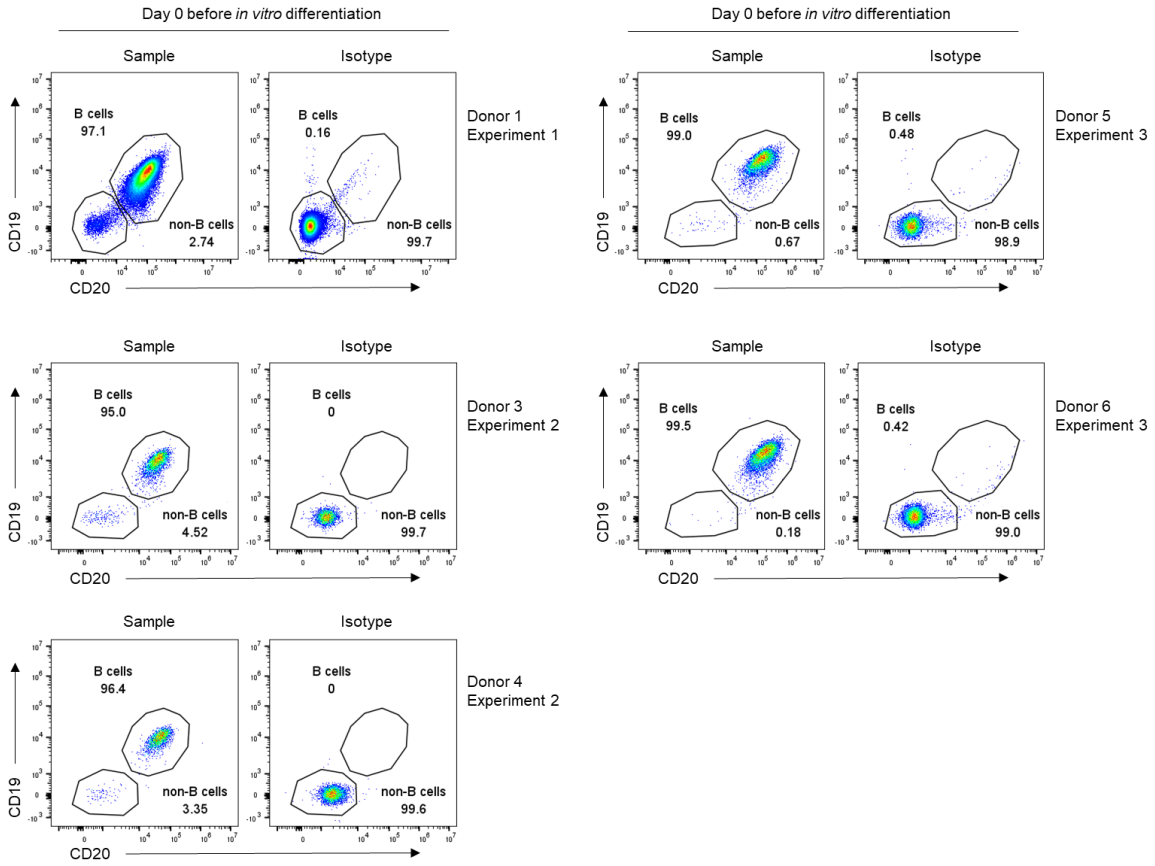

Figure 3.5 Verification of $CD19^{+}CD20^{+}$ B cell isolation prior to co-culture and differentiation at day 0. Flow cytometry plots of day 0 isolated memory B cells being assessed for their CD19 (y-axis) and CD20 (x-axis) expression to verify their purity. The $CD19^{+}CD20^{+}$ gated B cells and $CD19^{-}CD20^{-}$ non-B cells are indicated. Isotype control was included to verify the staining specificity. Data represent memory B cells isolated from five different donors tested as biological replicates (N= 5), in three independent experiments as indicated on the right side of the flow plots. No technical replicates were included.

3.4.2 Transduction of the B cells under *in vitro* differentiation

Utilising the *in vitro* PC differentiation system, memory B cells were cultured and differentiated up to day 20. At day 2, activated memory B cells were transduced with either MSCV-backbone or the *T58I-t2A-BCL2* retroviruses. Day 3 activated memory B cells were assessed for their CD2 expression levels. As displayed in Figure 3.6A, successful transduction was achieved 24 hours post-transduction with 23.1% and 35.6% CD2 positive cells for MSCV-backbone and *T58I-t2A-BCL2* samples respectively. In contrast, the untransduced control showed only 1.2% CD2 positive cells representing the background. Importantly, high transduction efficiency was validated by significantly increased CD2 expression in the transduced cells of both MSCV-backbone and *T58I-t2A-BCL2* conditions on day 6. An even more obvious increase was established by day 13 and maintained up to day 20 (Figure 3.6B and Figure 3.6C).

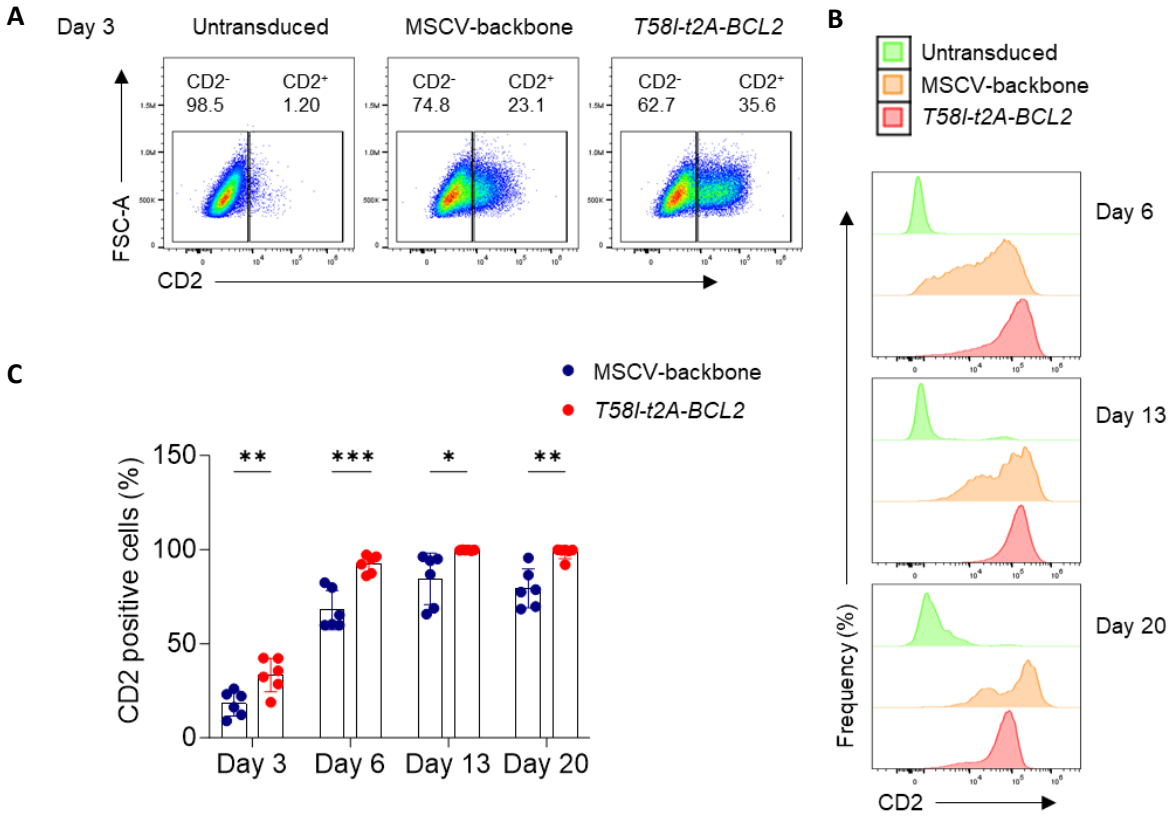

Figure 3.6 Transduction efficiency validation in the model system based on the CD2 reporter expression. (**A**) Flow cytometry plots representing day 3 cells of the indicated conditions assessed for FSC-A parameter (y-axis) against CD2 (x-axis). The $CD2^-$ and $CD2^+$ applied gates indicate the calculated frequencies. (**B**) Representative histograms of CD2 expression frequencies assessed by flow cytometry in the indicated conditions and time points. (**C**) Graph representing the summary of frequencies of the CD2 positive cells at the indicated time points for the MSCV-

backbone and the *T58I-t2A-BCL2* samples. Unpaired two-tailed Student's *t*-test (C). Data are representative of three independent experiments with two biological replicates (N= 2) and no technical replicates per experiment. The total number of donors tested as biological replicates was six (N= 6). Bars and error represent mean and standard deviation (SD); * P < 0.05; ** P < 0.01; *** P < 0.001.

In addition, *T58I-t2A-BCL2* $CD2^+$ cells showed a competitive advantage at day 6 against the $CD2^-$ cells with almost 100% of the cells in the sample being $CD2^+$. This competitive advantage was observed in all the time points tested in the *T58I-t2A-BCL2* cells (Figure 3.6B and Figure 3.6C). These results validated that CD2 protein overexpression was reproducibly detected in the transduced cells at the time points of interest.

3.4.3 Validation of MYC and BCL2 protein overexpression

Having established the transduction step, the overexpression of MYC T58I and BCL2 proteins was next evaluated in the model system. Transduced cells with either MSCV-backbone or *T58I-t2A-BCL2* were collected at day 6 and total protein lysates were assessed for MYC and BCL2 expression by western blot including a β-actin loading control. As Figure 3.7A shows, both MYC and BCL2 expression was detected at higher levels in *T58I-t2A-BCL2* than in the MSCV-backbone control transduced cells, as anticipated. In Figure 3.7B, this result was validated in two independent experiments verifying increased protein expression of MYC with a significant trend and in a statistically significant manner for BCL2 in the *T58I-t2A-BCL2* samples.

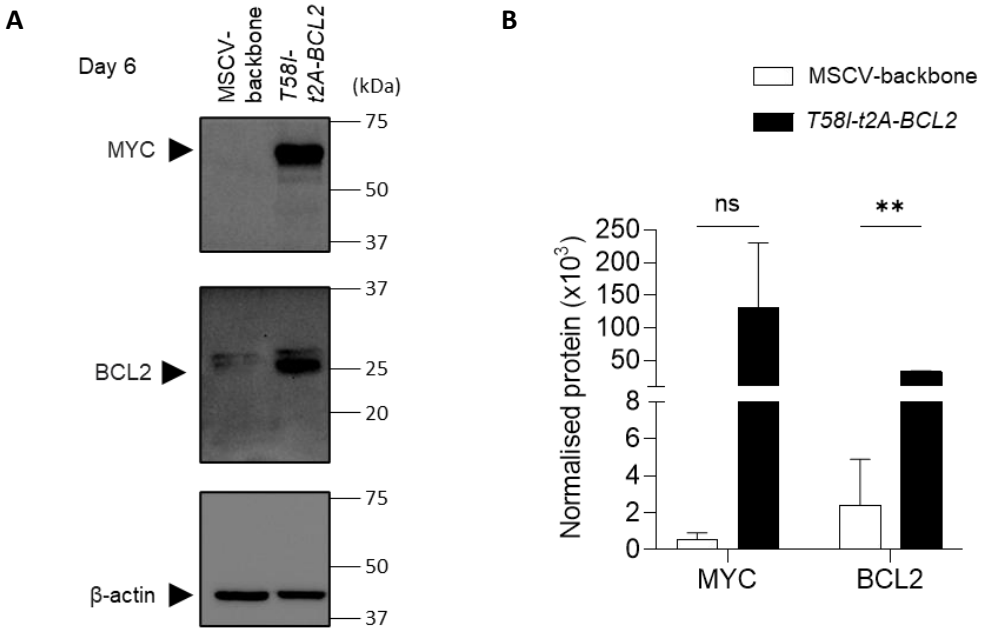

Figure 3.7 MYC and BCL2 protein overexpression validation. (**A**) Total protein lysates of day 6 transduced cells with either MSCV-backbone or *T58I-t2A-BCL2* were stained and assessed by western blots for MYC (62 kDa), BCL2 (26 kDa) and β-actin (42 kDa) expression; kDa, kilodalton. (**B**) Graph of the quantification of MYC and BCL2 protein expression, in the indicated day 6 samples, after normalisation to their β-actin loading control expression values. Densitometry values of the quantified protein bands were obtained with ImageJ software. Unpaired two-tailed Student's *t*-test (B). Data are representative of two independent experiments with one biological replicate (N= 1) and no technical replicates per experiment. The total number of donors tested as biological replicates was two (N= 2). Bars and error represent mean and standard deviation (SD); ns, not significant; ** $P < 0.01$.

Assessment of MYC and BCL2 protein levels, with western blots, at different time points would have been beneficial in further validating the model. However, in the two control conditions, adequate protein sample collection was not possible at later time points of the culture due to their low cell numbers. That made the comparison between the three conditions under assessment not feasible. Thus, no western blots were conducted for later time points than day 6. Despite that, MYC T58I and BCL2 overexpression were successfully validated upon transductions in the model system.

3.5 Acute MYC T58I-BCL2 overexpression interferes with plasma cell differentiation

To understand the effect of MYC T58I and BCL2 overexpression on the model system assessment of the *in vitro* differentiated cells took place upon transduction with *T58I-t2A-BCL2* virus on day 2. Key time points in the differentiation process of day 3, day 6, day 13 and day 20, as previously established (149, 282, 283), were tested for immunophenotyping by flow cytometry. In addition, the cell cycle status, protein expression and antibody secretion were evaluated in the model system.

3.5.1 *T58I-t2A-BCL2* transduced cells have increased cell number, survival and size

Initially, the main cellular characteristics of the *in vitro* culture were assessed post-transduction. As displayed in Figure 3.8A, at day 3 and day 6 time points, no differences were observed in the cell size and survival of the *T58I-t2A-BCL2* cells compared to the control MSCV-backbone and untransduced conditions. In contrast, on day 13, MYC T58I-BCL2 overexpressing cells showed increased survival and cell size, based on the SSC-A versus FSC-A parameters of flow cytometry. 28.7% of the events constituted the viable cells shown in the 'cells' gate of the *T58I-t2A-BCL2* sample. In contrast, only 5.17% and 1.47% of the cells were viable in the untransduced and the MSCV-backbone conditions respectively. A similar pattern but with reduced percentages in the gate of the viable cells was observed in all samples mentioned above, at day

20, with the corresponding frequencies being 21.7% versus 1.52% and 0.67%. This analysis indicates that MYC in combination with BCL2 does not drive cellular apoptosis upon its overexpression in the model system.

Calculation of the geometric mean of the FSC-A parameter from all the donors tested in Figure 3.8B, validated the increased cell size upon MYC T58I-BCL2 overexpression from day 6 onwards, as anticipated by MYC function promoting cell growth.

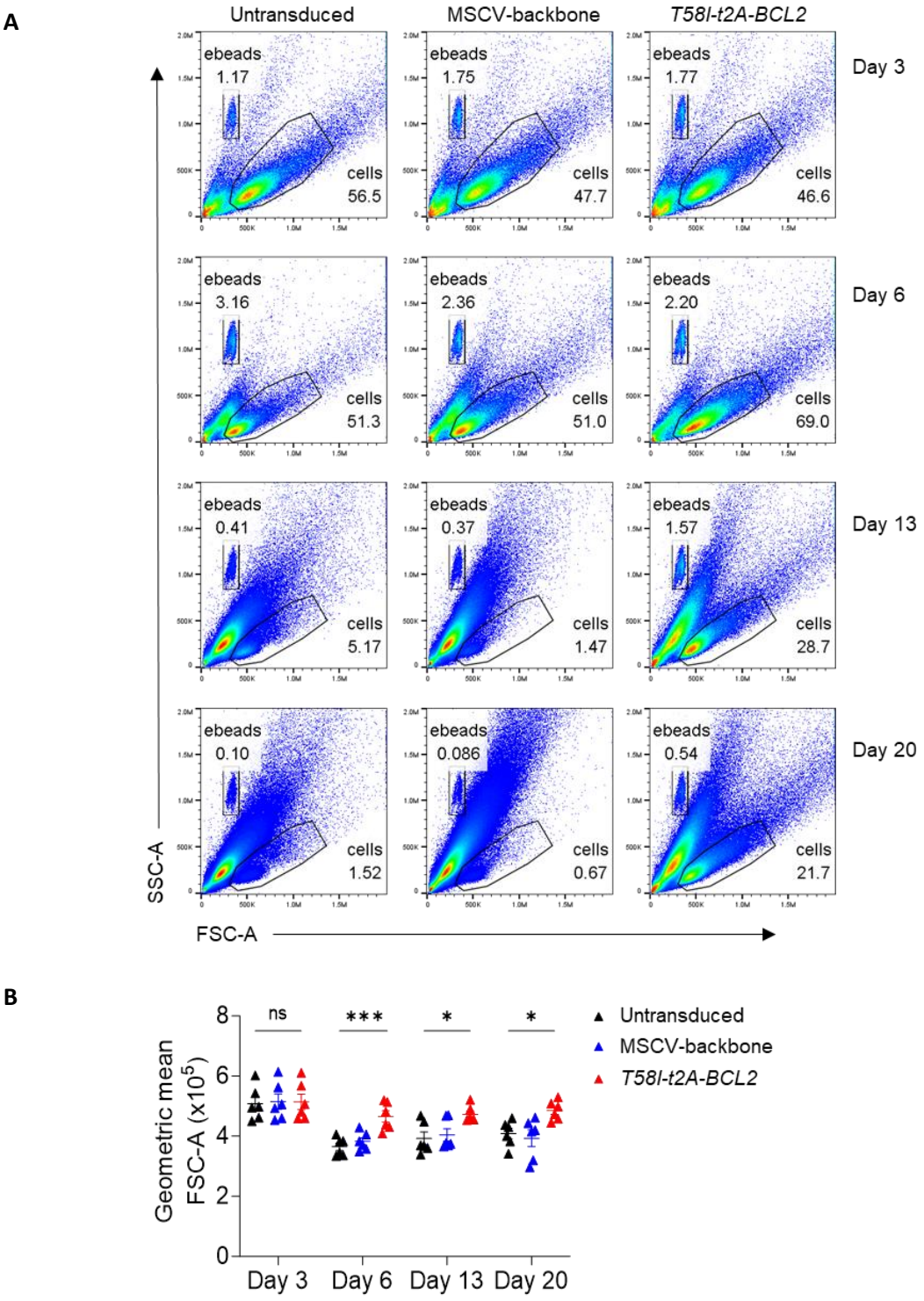

Figure 3.8 Survival and cell size evaluation by flow cytometry after transduction. (**A**) Flow cytometry plots representing SSC-A (y-axis) versus FSC-A (x-axis) parameters for the indicated time points and samples. Gate labelled as cells, shows percentages of the viable population while the gate indicated as ebeads represents the absolute counting beads population added for further sample analysis. (**B**) Graph representing the summary values of the

geometric mean of FSC-A parameter as calculated by the flow cytometry data analysis software FlowJo for the indicated time points and conditions. One-way ANOVA (B). Data are representative of three independent experiments with two biological replicates (N= 2) and no technical replicates per experiment. The total number of donors tested as biological replicates was six (N= 6). Bars and error represent mean and standard deviation (SD); ns, not significant; * P < 0.05; *** P < 0.001.

By absolute cell counts, no significant changes were observed at day 3 and day 6 between the controls and *T58I-t2A-BCL2* samples (Figure 3.9). Interestingly, at day 13, the *T58I-t2A-BCL2* cells had significantly higher absolute cell counts compared to their counterparts. This increase in cell numbers was also observed at day 20 for the MYC T58I-BCL2 overexpressing cells.

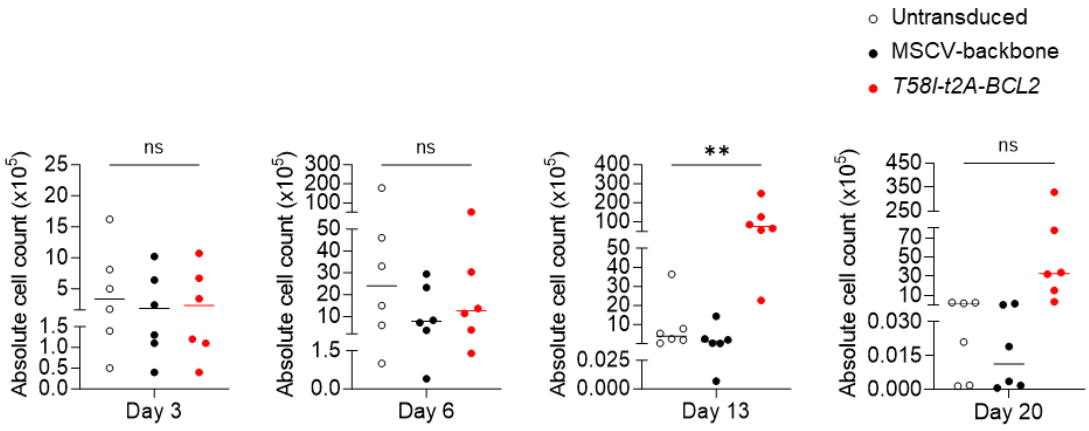

Figure 3.9 Increased cell numbers in the culture upon MYC T58I-BCL2 overexpression. Absolute cell counts of the indicated samples at day 3, day 6, day 13 and day 20. Cell counts were performed using a hemocytometer and trypan blue exclusion. Day 13 and day 20 control samples with low cell numbers were counted using counting beads and flow cytometry assessment. One-way ANOVA. Data are representative of three independent experiments with two biological replicates (N= 2) and no technical replicates per experiment. The total number of donors tested as biological replicates was six (N= 6). Bars and error represent mean and standard deviation (SD); ns, not significant; ** P < 0.01.

Statistical analysis did not verify statistical significance in the day 20 absolute cell counts (Figure 3.9). This result contradicted the statistical significance observed in the day 13 cell counts and the observed increase in cell numbers for the *T58I-t2A-BCL2* condition in both time points. The generated p-values, upon the comparison of the untransduced, MSCV-backbone and *T58I-t2A-BCL2* conditions on day 13 and day 20, using one-way ANOVA, are provided in Table 3.1. With a threshold of P < 0.05, a p-value of 0.0041 was obtained for the day 13 cell counts indicating statistical significance. No statistically significant difference was observed on day 20 with a p-value of 0.1084.

Table 3.1 The acquired p-values upon statistical analysis of the day 13 and day 20 absolute cell counts using one-way ANOVA. Details of the p-values generated upon statistical analysis using one-way ANOVA are illustrated for the day 13 and day 20 absolute cell counts depicted in Figure 3.9. The p-value threshold of significance for the statistical test was $P < 0.05$ as indicated. Data are representative of three independent experiments with two biological replicates (N= 2) and no technical replicates per experiment. The total number of donors tested as biological replicates was six (N= 6); vs, versus; ns, not significant; ** $P < 0.01$.

One-way ANOVA summary	Day 13	Day 20
P value	0.0041	0.1084
P value summary	**	ns
Significant difference among means (P < 0.05)?	Yes	No

To further assess this result, Tukey's test was performed to correct for multiple comparisons upon one-way ANOVA. In Table 3.2, statistical significance was confirmed only on day 13 for the untransduced versus *T58I-t2A-BCL2* and MSCV-backbone versus *T58I-t2A-BCL2* comparisons. These two comparisons were the ones that contributed to the overall statistical significance that was confirmed on day 13 using one-way ANOVA. The equivalent comparisons showed no statistical significance on day 20 as verified by their adjusted p-values (Table 3.2).

Table 3.2 Summary of Tukey's test correcting for multiple comparisons upon one-way ANOVA. Details of the adjusted p-values generated upon statistical analysis using Tukey's multiple comparisons test in combination with one-way ANOVA. Tukey's test was performed for the day 13 and day 20 absolute cell counts depicted in Figure 3.9. Pairwise comparisons of the indicated conditions were assessed per time point. The p-value threshold of significance for the statistical test was $P < 0.05$. Data are representative of three independent experiments with two biological replicates (N= 2) and no technical replicates per experiment. The total number of donors tested as biological replicates was six (N= 6); vs, versus; ns, not significant; * $P < 0.05$; ** $P < 0.01$.

Day 13 - Tukey's multiple comparisons test	Below threshold?	Summary	Adjusted P Value
Untransduced vs. MSCV-backbone	No	ns	0.9752
Untransduced vs. *T58I-t2A-BCL2*	Yes	*	0.0109
MSCV-backbone vs. *T58I-t2A-BCL2*	Yes	**	0.0071
Day 20 - Tukey's multiple comparisons test	**Below threshold?**	**Summary**	**Adjusted P Value**
Untransduced vs. MSCV-backbone	No	ns	0.9998
Untransduced vs. *T58I-t2A-BCL2*	No	ns	0.1568
MSCV-backbone vs. *T58I-t2A-BCL2*	No	ns	0.1515

The day 13 absolute cell counts demonstrated values closer to the calculated mean for each condition tested (Figure 3.9). This phenomenon was not observed in the day 20 values that were characterized by a

wider spread, especially in the control samples. A characteristic of the *in vitro* culture is that low cell numbers are acquired for the untransduced control on day 20 due to the differentiation process resulting in reduced survival and a cease in proliferation. A similar phenotype with low cell numbers was also observed for the MSCV-backbone control at day 20. These low cell numbers may have contributed to the variability observed in the day 20 cell counts within the control conditions and in comparison to day 13, as they have increased the difficulty of the handling and counting process of the cells. Thus, based on the data assessed here, statistical significance using one-way ANOVA was only achieved in the day 13 comparison. Despite the absence of statistical significance on day 20, the absolute cell counts remained higher in the *T58I-t2A-BCL2* condition than in the controls following a similar pattern to day 13. These results indicate that the *T58I-t2A-BCL2* cells demonstrate increased proliferation and survival potential in the windows between day 6 to day 13 and day 13 to day 20 compared to their counterparts.

3.5.2 Immunophenotyping

Having established the overexpression of MYC T58I-BCL2 combination in the model system and its initial effect on cell survival, growth and proliferation based on cell numbers, the phenotype of the transduced cells was next evaluated. Immunophenotyping assessment was completed by flow cytometry as displayed in Figure 3.10.

Activated B cells, at day 3 of the *in vitro* model system, are characterized as $CD19^{+}CD20^{+}CD27^{-}CD38^{+}CD138^{-}$ cells. This phenotype was observed, as displayed in Figure 3.10A, in the untransduced cells tested on day 3 as well as in the transduced cells of both the MSCV-empty and the *T58I-t2A-BCL2* conditions. This result indicated that overexpression of MYC T58I-BCL2 did not affect the activated B cell phenotype at day 3 and the transduced cells were similar to the controls 24 hours post-transduction.

At day 6, the cells are anticipated to acquire the plasmablast phenotype of $CD19^{+}CD20^{lo}CD27^{+}CD38^{+}CD138^{+/-}$ expression. As shown in Figure 3.10B, marginal changes were observed in the CD19 versus CD20 evaluation. A greater shift toward the $CD19^{+}$ cells was detected in addition to an increased $CD19^{-}CD20^{-}$ population in the *T58I-t2A-BCL2* cells in comparison to the two controls which were more similar with each other regarding their CD19 and CD20 expression. Interestingly, there was a significant reduction in the CD27 upregulation with 31.2% $CD27^{+}CD38^{+}$ cells in the *T58I-t2A-BCL2* condition versus 62.2% and 69.6% in each of the controls having differentiated as expected. Despite the CD27 downregulated phenotype, CD38 expression in the *T58I-t2A-BCL2* cells was increased similarly to the

controls. In contrast, the CD138 PC hallmark protein showed reduced upregulation in the MYC T58I-BCL2 overexpressing cells.

The establishment of the PC phenotype in the *in vitro* system is expected from day 13 onwards (282). Cells acquired at day 13 are anticipated to be $CD19^{+}CD20^{-}CD27^{+}CD38^{+}CD138^{++}$ when assessed by flow cytometry. While the untransduced and MSCV-backbone controls differentiated as expected acquiring the PC phenotype, MYC T58I-BCL2 overexpression interfered with normal PC differentiation as Figure 3.10C shows. Abnormal CD19 and CD20 expression was observed in the *T58I-t2A-BCL2* sample with a shift toward the $CD19^{-}CD20^{-}$ population. Also, enhanced expression of CD20 in comparison to the controls and reduction of the $CD19^{+}CD20^{-}$ cells were detected. Importantly, CD27 and CD138 upregulation was significantly inhibited while the cells maintained high CD38 expression. In more detail, only 22.6% of the assessed population were $CD27^{+}CD38^{+}$ in contrast to the 93.1% and 86.8% of the untransduced and MSCV-backbone controls respectively. Remarkable inhibition of CD138 expression was reported with only 3.01% of the cells being $CD38^{+}CD138^{+}$ in comparison to the anticipated frequency which reached more than 45% for both the controls.

In the *in vitro* system, day 20 cells have already acquired the PC phenotype which they maintain when cultured consistently in the growth medium described in the Methods section 2.2.5. As Figure 3.10D shows, the two control samples had normal and even enhanced PC phenotype at day 20, in comparison to the day 13 cells. On the other side, the *T58I-t2A-BCL2* cells did not reach a similar PC differentiation phenotype. In contrast, upon MYC T58I-BCL2 overexpression, at day 20 aberrant increase of $CD19^{-}CD20^{-}$ cells was observed reaching 62.6% of the total population and maintaining also low and abnormal levels of $CD19^{-}CD20^{+}$ cells. Additionally, the majority of the cells were $CD27^{-}CD38^{+}$. They did not upregulate their CD27 expression with only 11.3% $CD27^{+}CD38^{+}$ in comparison to the controls with 97.4% and 87.7% respectively. CD138 upregulation followed a similar trend and was maintained significantly reduced. Only 7.91% of events were $CD38^{+}CD138^{+}$ in the MYC T58I-BCL2 overexpressing cells in contrast to 77.6% and 58.6% in the two controls. Interestingly, the day 20 *T58I-t2A-BCL2* cells showed a greater than two-fold increase in their $CD38^{+}CD138^{+}$ population reaching 7.91%, in comparison to the day 13 sample with 3.01%. This latter result suggested that CD138 expression is significantly delayed but not completely inhibited by MYC T58I-BCL2 overexpression in the model system.

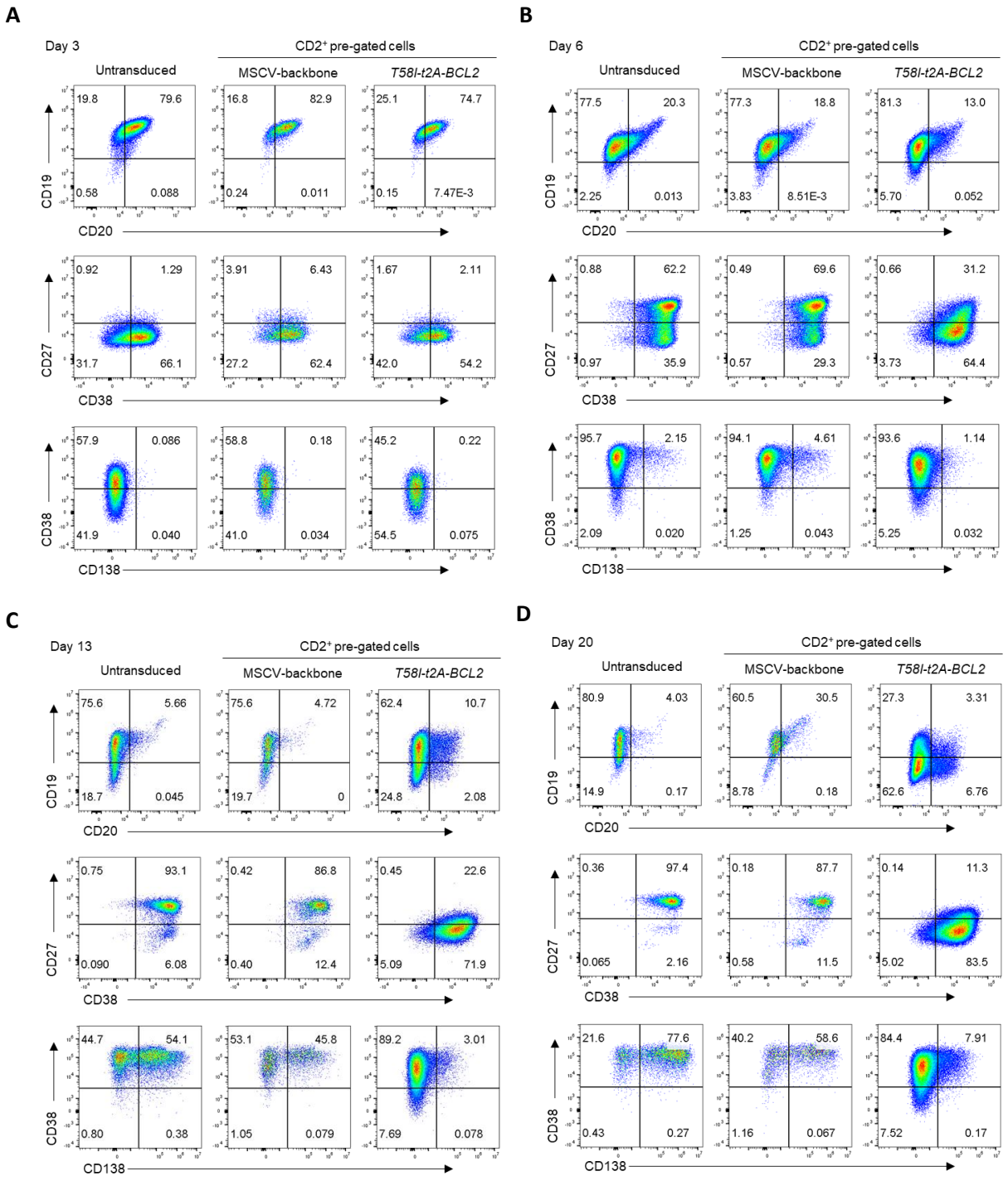

Figure 3.10 Flow cytometry analysis revealing the immunophenotyping in the model system. Representative flow cytometry plots of selected protein markers expression for the indicated conditions (top). Evaluation of CD19, CD27 and CD38 (y-axis) versus CD20, CD38 and CD138 (x-axis) respectively for (**A**) day 3 samples, (**B**) day 6 samples, (**C**) day 13 samples, and (**D**) day 20 samples. The assessed cells in MSCV-backbone and *T58I-t2A-BCL2* conditions are $CD2^+$ pre-gated as indicated at the top of each figure. An untransduced control condition was included for all the time

points tested. Data are representative of three independent experiments with two biological replicates (N= 2) and no technical replicates per experiment. The total number of donors tested as biological replicates was six (N= 6).

The immunophenotyping described above was consistent and reproducible in all the donors tested as displayed in the data summary Figure 3.11. This analysis verified that overall day 3 was characterized by no to marginal differences between the controls and the *T58I-t2A-BCL2* condition. The main phenotypically driven changes were detected from the plasmablast stage of the differentiation namely day 6 onwards. In Figure 3.11A, the MYC T58I-BCL2 overexpression resulted in a gradually increased reduction of the $CD19^{+}CD20^{-}$ cells from day 6 up to day 20. Even greater was the effect of the enforced MYC T58I-BCL2 overexpression in the $CD27^{+}CD38^{+}$ population. Figure 3.11B showed its significant decrease from day 6 to day 13 reaching a peak of reduction at day 20, consistently in all donors tested. In contrast, in Figure 3.11C, despite its statistically significant decrease at day 13, the $CD38^{+}CD138^{+}$ population appeared slightly improved at day 20 supporting a MYC T58I-BCL2 overexpression-driven delay rather than persistent inhibition of CD138 upregulation in the time course tested.

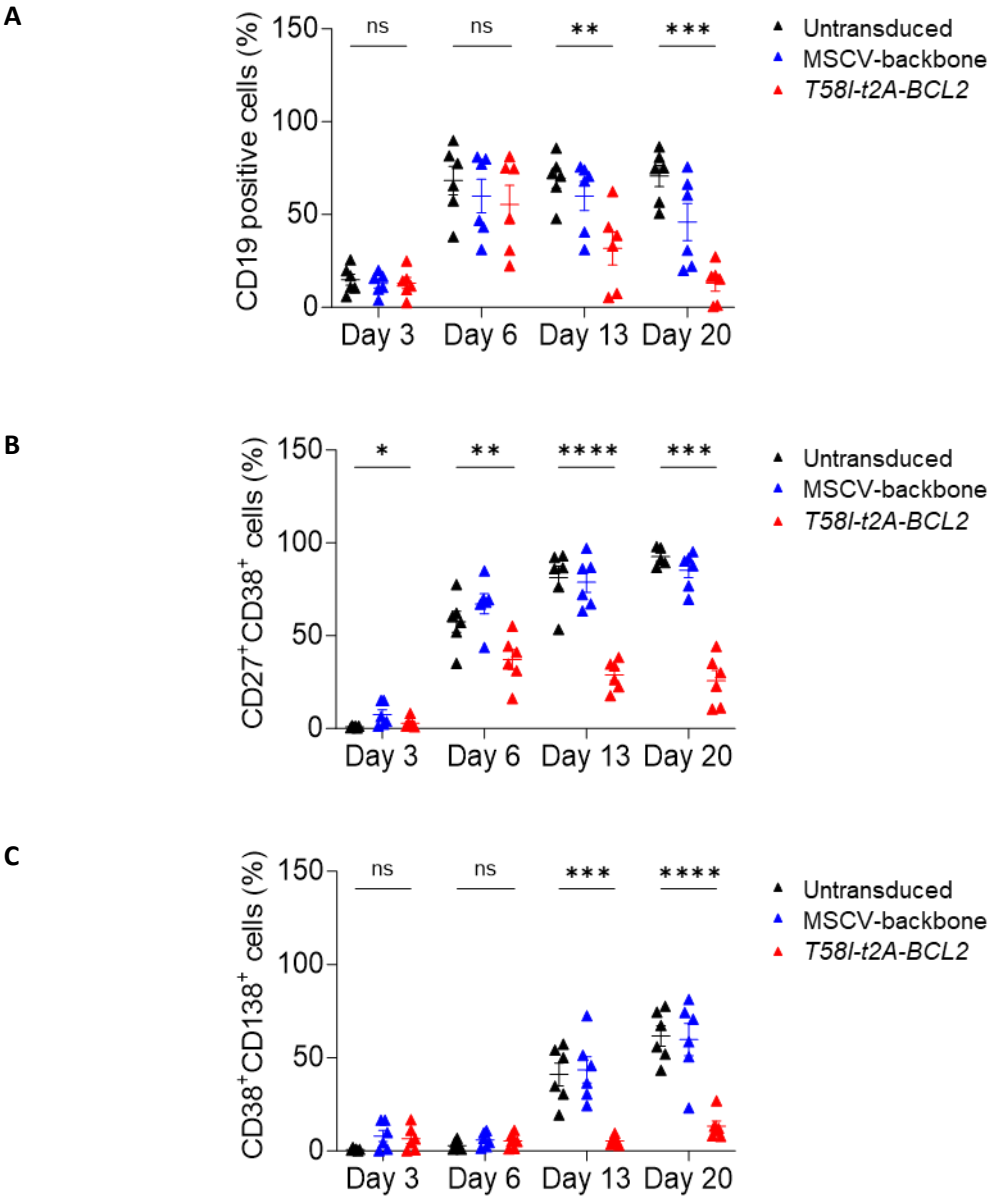

Figure 3.11 Summary graphs of flow cytometry data-based immunophenotyping. Graphs of untransduced, MSCV-backbone and *T58I-t2A-BCL2*-derived flow cytometry data representing the frequencies of (**A**) the CD19 positive cells ($CD19^+CD20^-$), (**B**) $CD27^+CD38^+$ cells and (**C**) $CD38^+CD138^+$ cells, at the indicated time points. The assessed cells in MSCV-backbone and *T58I-t2A-BCL2* conditions are $CD2^+$ pre-gated. One-way ANOVA (A, B, C). Data are representative of three independent experiments with two biological replicates (N= 2) and no technical replicates per experiment. The total number of donors tested as biological replicates was six (N= 6). Bars and error represent mean and standard deviation (SD); ns, not significant; * $P < 0.05$; ** $P < 0.01$; *** $P < 0.001$; **** $P < 0.0001$.

Combining the analysis shown in Figure 3.10 and Figure 3.11, MYC T58I-BCL2 overexpression resulted in an abnormal population of transduced cells that did not acquire the expected day 13 PC phenotype. The

T58I-t2A-BCL2 transduction affected CD19, CD20, CD27 and CD138 expression while the cells maintained high CD38 levels in the time points tested.

3.5.3 Extended cell cycle with no transformation upon MYC T58I-BCL2 overexpression

In comparison to plasmablasts which maintain an active cell cycle, differentiation to PCs is usually accompanied by cell cycle exit (282, 300). Thus, the cell cycle status of the *in vitro* differentiated cells with and without transductions was assessed in our model system. The anticipated time point of cell cycle exit in the untransduced cells was between day 10 to day 13 as previously established in the laboratory (282). As described in the Results sections 3.5.1 and 3.5.2, MYC T58I-BCL2 overexpression altered the PC features of the *in vitro* cells and enhanced their survival, size and cell number at day 13. Based on these observations, the later time point of day 21 was selected for cell cycle status assessment in the model system.

To evaluate the cell cycle status an EdU 1 hour pulse incorporation assay was performed followed by EdU detection and Ki67 intracellular staining. The aim of the assay was to detect new DNA synthesis ongoing in the samples at the time point of collection. Ki67 further validated the cell cycle stage of the cells under evaluation. Initially, as displayed in Figure 3.12, two different concentrations of EdU, 1.5 µM and 5 µM, were tested to assess EdU-associated cytotoxicity. Both EdU concentrations tested resulted in around 10% $EdU^{+}Ki67^{+}$ cells. This analysis indicated that upon EdU 1 hour pulse incorporation assay the day 21 *T58I-t2A-BCL2* cells were synthesizing new DNA while the untransduced control had no $EdU^{+}Ki67^{+}$ cells, in keeping with cell cycle exit.

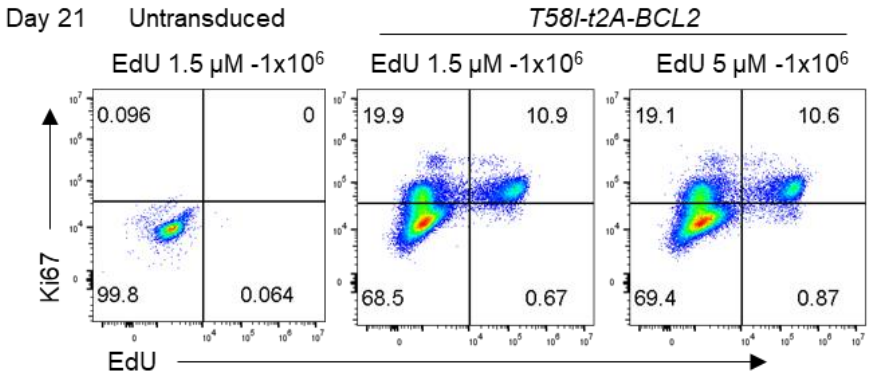

Figure 3.12 EdU 1 hour pulse incorporation assay experimental setup. Day 21 untransduced or *T58I-t2A-BCL2* cells were treated for 1 hour with 1.5 µM and 1.5 µM or 5 µM of EdU respectively. Upon fixation and EdU detection protocol, Ki67 intracellular staining took place followed by flow cytometry analysis. The assessed cells in *T58I-t2A-*

BCL2 condition are $CD2^+$ pre-gated. $1x10^6$ indicates the cell number seeded during the 1 hour EdU treatment and subsequent flow cytometry assessment.

These results verified that 1.5 µM of EdU suffices in limiting EdU-associated cytotoxicity without compromising the performance of the 1 hour pulse incorporation assay. Thus, 1.5 µM of EdU was used in subsequent assays.

Since day 21 cells overexpressing MYC T58I-BCL2 contained cells with retained evidence of active cell cycle, an additional later time point was included in the EdU 1 hour pulse incorporation assay to assess cellular transformation. Day 21 and day 31 cells were treated with 1.5 µM EdU for 1 hour, followed by detection assay, Ki67 staining and flow cytometry assessment. As presented in Figure 3.13A, *T58I-t2A-BCL2* cells were 8.11% EdU^+KI67^+ in contrast to 0.00% in the untransduced control at day 21 verifying active DNA synthesis as previously observed. However, at day 31, the EdU^+KI67^+ cells were 0.00% and 0.00% respectively in both conditions. In Figure 3.13B, EdU 1 hour pulse incorporation assays followed by Ki67 staining were repeated in multiple donors at day 21 and day 31. Only day 21 *T58I-t2A-BCL2* cells had an EdU^+Ki67^+ population while day 31 was similar to the untransduced cells, characterized by EdU^-Ki67^- cells. These findings suggest that the MYC T58I-BCL2 cells have exited the cell cycle by day 31 of the model system. This is consistent with a prolonged proliferative window in comparison to the untransduced samples, but the cells were not transformed and eventually exited cell cycle.

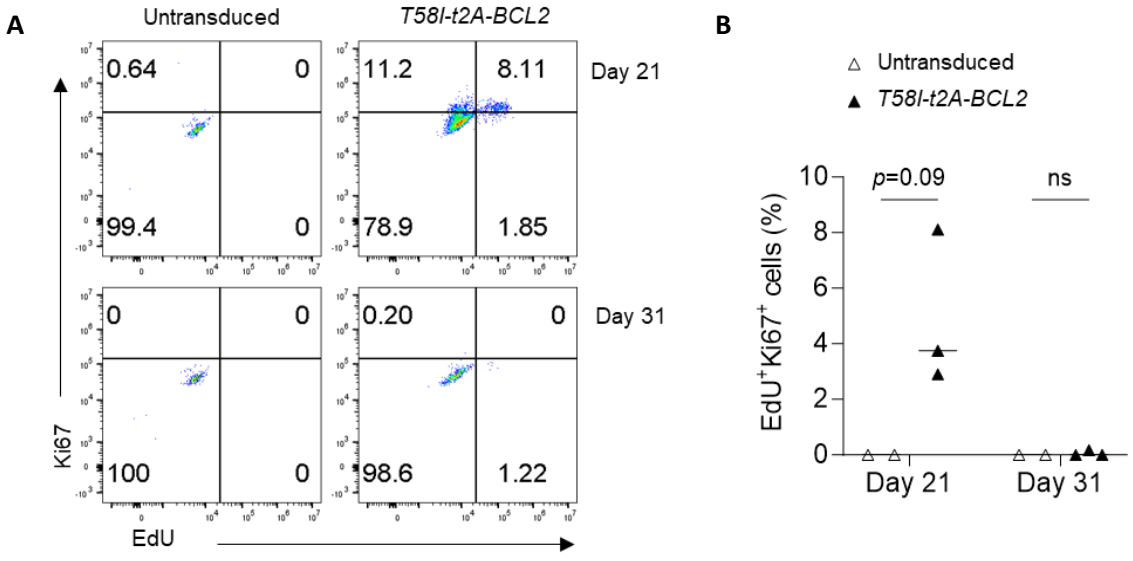

Figure 3.13 Evaluation of cell cycle status at day 21 and day 31 of the model system. The established EdU 1 hour pulse incorporation and Ki67 staining assay was used to assess the cell cycle of untransduced and *T58I-t2A-BCL2* cells. (**A**) Flow cytometry plots show Ki67 (y-axis) versus EdU (x-axis) evaluation upon assay completion at the indicated

time points. (**B**) Summary of flow cytometry data representing the percentages of $EdU^{+}Ki67^{+}$ cells at day 21 and day 31 for the indicated samples. The assessed cells in *T58I-t2A-BCL2* condition are $CD2^{+}$ pre-gated. Unpaired two-tailed Student's *t*-test. Data are representative of two independent experiments with no technical replicates per experiment. The total number of donors tested as biological replicates was three (N= 3). Bars and error represent mean and standard deviation (SD); ns, not significant.

3.5.4 BLIMP1 upregulation in transduced *T58I-t2A-BCL2* cells

Based on the results mentioned above, the day 6, day 13 and day 20 cells show a perturbed phenotype with inhibited CD27 and delayed CD138 expression, while they also have extended cell cycle with increased survival and cell size. Since MYC T58I-BCL2 overexpression altered the PC differentiation process without resulting in cell transformation *in vitro*, the next question was how the MYC T58I-BCL2 deregulation affected other hallmark PC features.

A key TF required for PC differentiation is BLIMP1. To test BLIMP1 expression upon transductions, the anticipated differentiation stage of plasmablasts at day 6 was selected. Total protein lysates of day 6 cells were evaluated by western blot for BLIMP1 expression with β-actin, as loading control. As displayed in Figure 3.14A and Figure 3.14B, BLIMP1 expression was detected at similar levels in the MSCV-backbone and the *T58I-t2A-BCL2* transduced cells at day 6. This finding indicated that this key regulator of PC differentiation remained equivalently expressed between the MSCV-backbone control and the MYC T58I-BCL2 overexpressing cells.

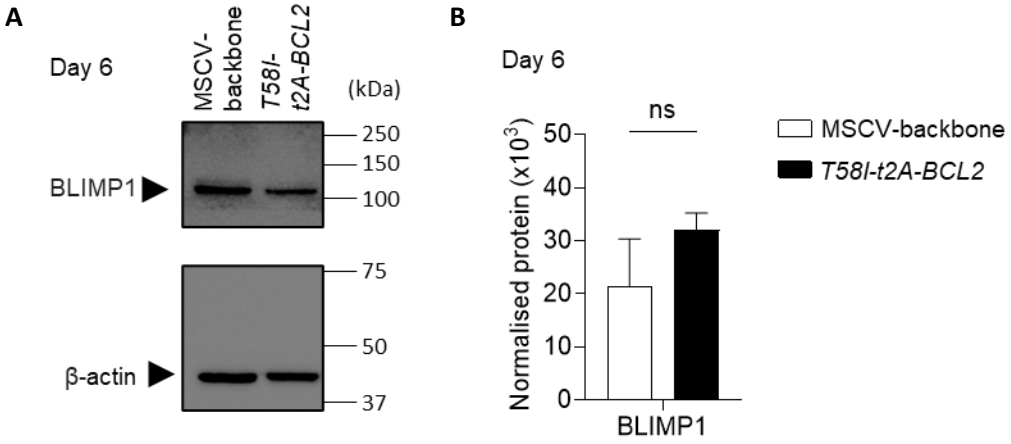

Figure 3.14 BLIMP1 detection in *T58I-t2A-BCL2* cells at day 6 with western blot. (**A**) Representative images of a developed membrane of total protein lysates collected at day 6 cells for the indicated samples. Lysates were probed for BLIMP1 and β-actin detection and assessed with western blot; kDa, kilodalton. (**B**) Graph of BLIMP1 protein

quantification upon normalisation to β-actin loading control for the day 6 indicated samples. Densitometry values of the quantified protein bands were obtained with ImageJ software. Unpaired two-tailed Student's *t*-test (B). Data are representative of two independent experiments with one biological replicate (N= 1) and no technical replicates per experiment. The total number of donors tested as biological replicates was two (N= 2). Bars and error represent mean and standard deviation (SD); ns, not significant.

3.5.5 The MYC T58I-BCL2 overexpressing cells acquire an abnormal antibody secreting cell phenotype

The main function of a PC is antibody secretion. *In vitro* generated plasmablasts at day 6 and PCs at day 13 onwards have been previously validated in the laboratory for their antibody secretion capacity (282). To test the impact of MYC T58I-BCL2 overexpression on antibody secretion, ELISAs were performed for human IgG and IgM. First, UV irradiation for 5 minutes was conducted on class II biosafety-derived supernatants to allow their handling under class I biosafety regulations. UV-treated supernatants were compared to untreated supernatants for their antibody concentrations with ELISAs under class II biosafety regulations. This validated that the UV treatment does not affect the integrity of the antibodies (data not shown) and allowed us to establish the ELISAs in the model system.

Human total IgG and IgM antibody secretion would be evaluated with the established ELISAs in supernatants collected at day 6, day 13 and day 20 of the model system. The heat-inactivated fetal bovine serum (HIFBS) in the growth medium collected with the supernatants is associated with cow-specific antibodies. The ELISA kits used in this study were specific to human IgG and IgM, as mentioned in Table 2.12 of the Methods section 2.11. Thus, no detection of cow-specific immunoglobulins of the integrated HIFBS was anticipated. To validate this experimentally, a preliminary ELISA experiment was conducted assessing the concentration of IgG and IgM antibodies in the no-cell-derived growth medium containing 10% HIFBS (IMDM CM). In this experiment, supernatants from untransduced day 6 and day 13 test samples were also included. Obtained raw data from the IgG- and IgM-specific ELISAs showed that the absorbance readings of the IMDM CM samples were similar to the absorbance readings of the blank control included in each of the assays (Table 3.3 and Table 3.4). The blank control was the no-cell-derived buffer used in the dilutions of the standard curve-associated control samples namely, sample/conjugate buffer. This blank control was expected to give a low absorbance reading corresponding to the assay background and with no specificity to any of the immunoglobulins tested. Figure 3.15 shows that the absorbance readings

acquired from the blank controls and the IMDM CM samples had no statistically significant differences in the IgG- and IgM-specific ELISAs, verifying their similarity.

Table 3.3 Similar absorbance readings for the blank control and the IMDM CM sample using ELISA to evaluate human IgG concentration. The raw data values of the absorbance readings, obtained with ELISA assessing the concentration of human IgG antibodies, are provided for the blank control sample (sample/conjugate buffer) and the IMDM CM sample (growth medium with 10% HIFBS). Both samples were tested in duplicates as indicated. Absorbance readings were conducted at 450 nm. Data are representative of one experiment with two technical replicates per condition.

IgG-specific ELISA				
Sample	**Blank control replicate 1**	**Blank control replicate 2**	**IMDM CM (medium with 10% HIFBS) replicate 1**	**IMDM CM (medium with 10% HIFBS) replicate 2**
Absorbance reading (450nm)	0.046	0.043	0.048	0.045

Table 3.4 Similar absorbance readings for the blank control and the IMDM CM sample using ELISA to evaluate human IgM concentration. The raw data values of the absorbance readings, obtained with ELISA assessing the concentration of human IgM antibodies, are provided for the blank control sample (sample/conjugate buffer) and the IMDM CM sample (growth medium with 10% HIFBS). Both samples were tested in duplicates as indicated. Absorbance readings were conducted at 450 nm. Data are representative of one experiment with two technical replicates per condition.

IgM-specific ELISA				
Sample	**Blank control replicate 1**	**Blank control replicate 2**	**IMDM CM (medium with 10% HIFBS) replicate 1**	**IMDM CM (medium with 10% HIFBS) replicate 2**
Absorbance reading (450nm)	0.050	0.051	0.051	0.043

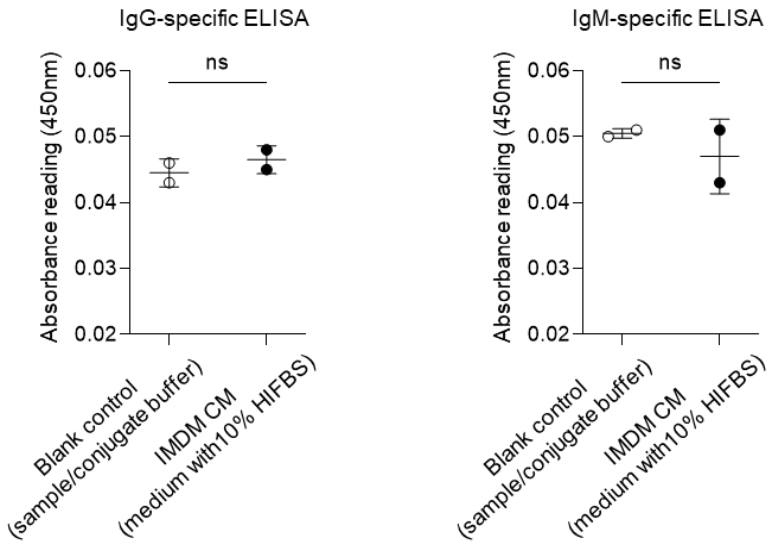

Figure 3.15 Comparison of the absorbance readings from the blank controls and the IMDM CM samples showed no statistically significant differences using human IgG- and human IgM-specific ELISAs. Statistical analysis confirmed no statistical significance between the absorbance readings of the blank controls (sample/conjugate buffer) and the IMDM CM samples (growth medium with 10% HIFBS). The compared absorbance values are illustrated in Table 3.3 for the IgG-specific ELISA (left), and in Table 3.4 for the IgM-specific ELISA (right). Unpaired two-tailed Student's *t*-test. Data are representative of one experiment with two technical replicates per condition. Bars and error represent mean and standard deviation (SD); ns, not significant.

Next, we aimed to show that there was no substantial contribution of this assay background to the calculated IgG and IgM antibody concentrations in supernatants collected from untransduced day 6 and day 13 samples. IgG and IgM antibody concentrations were quantified for both IMDM CM and untransduced test samples. Analysis of the raw data derived from the above preliminary ELISAs showed that the calculation of IgG and IgM antibody concentrations was not successful for the IMDM CM samples. This was because of their low absorbance readings which did not fit the range of the generated standard curves. On the contrary, the collected untransduced supernatants gave higher absorbance readings ranging from 0.478 to 2.213 and from 1.378 to 3.957 for the IgG- and IgM-specific ELISAs, respectively. These absorbance values allowed the quantification of IgG and IgM secretion in the untransduced supernatants. These results suggested that there was no significant contribution of the assay background to the quantified IgG and IgM concentrations in untransduced supernatants. Also, no significant detection of human IgG and IgM antibodies was confirmed for the neat growth medium containing HIFBS (IMDM CM) and phenocopying the absorbance readings of the blank control. Thus, the human specificity of the ELISA kits utilsed in this study was verified experimentally.

The supernatants collected on day 6, day 13 and day 20 from the samples of interest were assessed next with ELISAs. To complete the experimental plan within the required timeframe, the IgM ELISAs were conducted by Michelle Umpierrez under my supervision. As displayed in Figure 3.16, the initial analysis of the generated ELISA data was based on assessing IgG and IgM antibody concentrations (ng/ml) in the collected supernatants. On day 6, the time point of plasmablast differentiation in the model system, the MYC T58I-BCL2 overexpressing cells appeared to secrete less IgG and IgM antibodies than the controls which showed relatively similar antibody concentrations. On day 13, this effect was lost, and higher antibody concentrations were observed than on day 6 for both IgG and IgM in all the conditions tested. Day 20 supernatants had similar antibody concentrations between the conditions. This result indicated that at day 13 and day 20 MYC T58I-BCL2 overexpressing cells demonstrate similar secretory capacity to the controls.

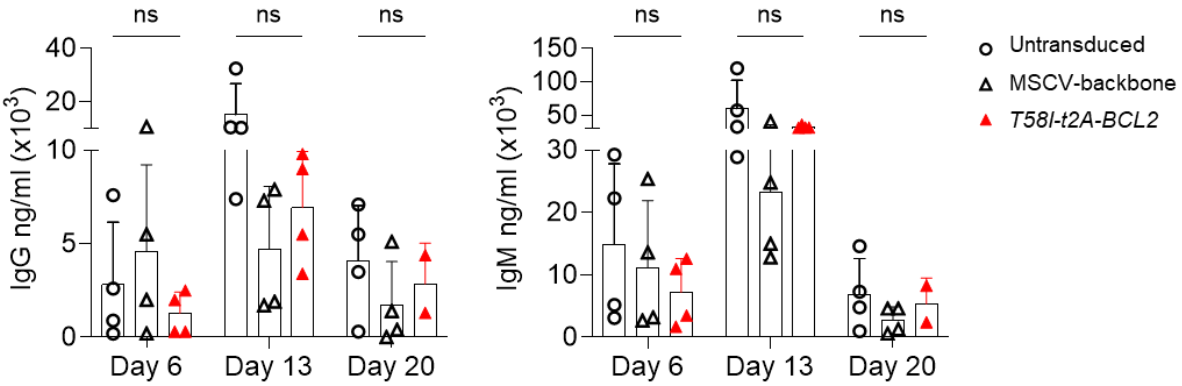

Figure 3.16 Evaluation of IgG and IgM antibody concentration in the model system. Supernatants of day 6, day 13 and day 20 samples of the indicated conditions were assessed for their secreted antibody concentration. Human total IgG and IgM ELISAs were performed, and quantification of the detected antibody secretion was calculated at ng/ml per time point tested. One-way ANOVA. Data are representative of two independent experiments with two biological replicates (N= 2) per experiment for all the conditions and time points apart from the day 20 *T58I-t2A-BCL2*. Data are representative of one of the two independent experiments with two biological replicates (N= 2) in total for the *T58I-t2A-BCL2* condition on day 20. Each sample was tested in two technical replicates per assay. Bars and error represent mean and standard deviation (SD); ns, not significant.

The antibody concentrations evaluated on day 6 represented cumulative antibody secretion of 72 hours (reseeding on day 3 and supernatant collection on day 6). In contrast, 144 hours were mediated between reseeding and supernatant collection on day 13 and day 20 time points. Thus, ELISAs performed on day 13 and day 20 evaluated a bigger time window of potential antibody accumulation than the one assessed in

the day 6 supernatants. In addition, as described in the Results section 3.5.1, an increase in viable cell numbers was observed in the *T58I-t2A-BCL2* transduced cells at day 13 and day 20 compared to the controls (Figure 3.9). Given the increased cell numbers in the MYC T58I-BCL2 overexpressing cells at the PC stages of the *in vitro* system, it would be anticipated that higher antibody concentrations could be established in a 144-hour window in comparison to the controls. Thus, the IgG and IgM antibody concentrations were also assessed per cell based on the absolute cell counts depicted in Figure 3.9. As displayed in Figure 3.17, the total human IgG and IgM antibody concentration per cell showed a reduction in the MYC T58I-BCL2 overexpressing cells from day 6 up to day 20. Despite the variation observed in the secretory capacity of the control conditions at day 13 and day 20, the *T58I-t2A-BCL2* transduced cells had a consistent delay in secreting either IgG or IgM at all three-time points tested. These results support a deficient phenotype in secretion capacity driven by MYC T58I-BCL2 overexpression. This finding further supported that MYC T58I-BCL2 overexpression mediated aberrant PC differentiation of the initial memory B cell population indicating perturbed antibody secreting cell features.

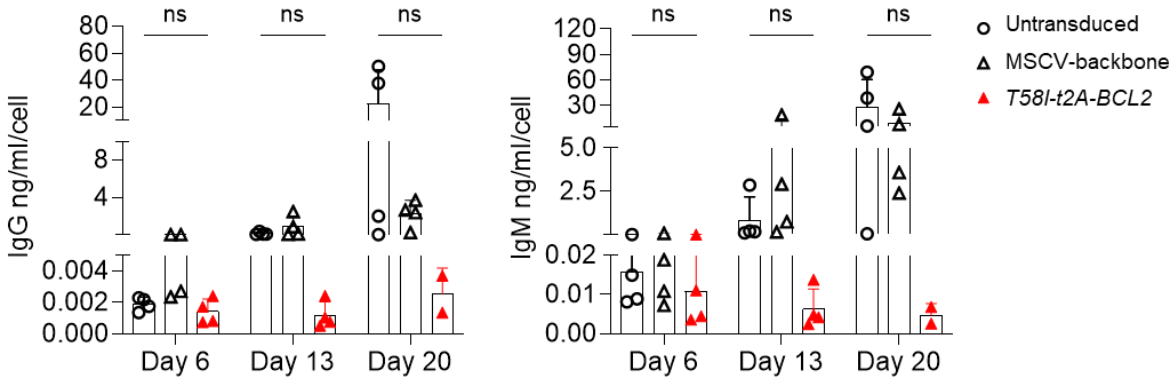

Figure 3.17 Reduced IgG and IgM antibody secretion per cell upon MYC T58I-BCL2 overexpression. Supernatants of day 6, day 13 and day 20 cells untransduced or transduced with MSCV-backbone or *T58I-t2A-BCL2* virus, were assessed for their antibody secretion with ELISAs. Antibody concentration of human total IgG and IgM was normalised to the absolute cell count of each sample per time point and condition to quantify ng/ml/cell. One-way ANOVA. Data are representative of two independent experiments with two biological replicates (N= 2) per experiment for all the conditions and time points apart from the day 20 *T58I-t2A-BCL2*. Data are representative of one of the two independent experiments with two biological replicates (N= 2) in total for the *T58I-t2A-BCL2* condition on day 20. Each sample was tested in two technical replicates per assay. Bars and error represent mean and standard deviation (SD); ns, not significant.

3.6 MYC T58I-BCL2 overexpression drives transcriptional metabolic over secretory reprogramming

To briefly summarise the previously described results overexpression of MYC T58I-BCL2 drove an aberrant phenotype of differentiation characterized by prolonged cell cycle exit and no transformation. In addition, the PC hallmark TF BLIMP1 was successfully detected at a protein level on day 6 and active but impaired antibody secretion was verified in the differentiating cells upon MYC T58I-BCL2 overexpression. These findings indicate that enforced expression of MYC carrying T58I and BCL2 at an activated memory B cell stage drives changes without blocking the differentiation process.

To evaluate the overall extent of MYC impact on differentiation the transcriptomic profile of the *in vitro* cells after MYC T58I-BCL2 overexpression was investigated next. To assess if MYC-BCL2-mediated transcriptional changes follow similar patterns to our previously verified phenotypes, a gene expression study was performed in samples collected from a complete time course of the differentiation key stages. Day 0 isolated memory B cells pre-co-culture, day 3 activated memory B cells, day 6 plasmablasts, day 13 PCs and day 20 PCs with enhanced survival potential were the hallmark time points tested with RNA-sequencing. Thus, *T58I-t2A-BCL2* cells versus their MSCV-backbone and untransduced counterparts were collected at each of the above time points. Total RNA was extracted, and the transcriptome of the prepared samples was assessed with next-generation sequencing (NGS). The total number of donors tested as biological replicates fluctuated per time point in the three different conditions. This was due to the low cell number collected for some of the donors, during sample collection, for RNA extraction. In samples where a low cell number was collected the concentration of the extracted RNA was not adequate for NGS. Thus, RNA-sequencing was conducted only in samples suitable for sequencing based on their RNA concentrations. RNA-sequencing bioinformatic data analysis was performed by Dr. Matthew Care as described in the Methods section 2.7. Additional downstream analysis took place to fully understand the MYC T58I-BCL2-driven changes in the gene expression of the tested samples.

3.6.1 Identification of differentially expressed genes upon MYC T58I-BCL2 overexpression

The differentially expressed genes (DEGs) in the conditions tested were identified upon RNA-sequencing data analysis. As displayed in Table 3.5, no DEGs were present in the day 3 samples. This finding is in accordance with previous flow cytometry-based results showing no differences between MYC T58I-BCL2 overexpressing cells and the controls at this time point of the model system.

Transcriptional differences were observed from day 6 (the plasmablast stage) onwards. Pairwise comparisons of relative gene expression between the untransduced and the MSCV-backbone control showed a low number to no DEGs on days 6 and 13 respectively. This result indicated that the MSCV-backbone control demonstrated a similar transcriptional profile to the untransduced cells in the model system. On the contrary, high numbers of DEGs were calculated for the pairwise comparisons of either one of the control conditions to the *T58I-t2A-BCL2* samples. This finding verified that enforced MYC T58I-BCL2 expression in the model system resulted in transcriptional changes which were detected on day 6, day 13 and day 20.

Table 3.5 Counts of differentially expressed genes in pairwise comparisons between samples. RNA-sequencing data were analysed and transcript abundance was calculated in each sample and between conditions. Pairwise comparisons, as indicated, resulted in an accurate estimation of the differentially expressed genes (DEGs) on day 3, day 6, day 13 and day 20 of the model system. Data are representative of two independent experiments with two biological replicates (N= 2) and no technical replicates per experiment. The total number of donors tested as biological replicates was four (N= 4) out of which: two (N= 2) were assessed on day 0; three (N= 3) were assessed on day 3; two (N= 2) for the untransduced condition, three (N= 3) for each of the MSCV-backbone and *T58I-t2A-BCL2* transductions were assessed on day 6; three (N= 3) for the untransduced control, two (N= 2) for the MSCV-backbone and four (N= 4) for the *T58I-t2A-BCL2* condition were assessed on day 13; one (N= 1) for the untransduced condition and three (N= 3) for the *T58I-t2A-BCL2* transductions were assessed on day 20. No donors were assessed for the MSCV-backbone control on day 20. Missing donors in the different conditions per time point were not evaluated due to low collected cell numbers and inadequate RNA concentrations for RNA-sequencing.

Time point	Comparison	DEGs
Day 3	Untransduced vs MSCV-backbone	0
Day 3	Untransduced vs *T58I-t2A-BCL2*	0
Day 3	MSCV-backbone vs *T58I-t2A-BCL2*	0
Day 3	MSCV-backbone vs Untransduced	0
Day 3	*T58I-t2A-BCL2* vs Untransduced	0
Day 3	*T58I-t2A-BCL2* vs MSCV-backbone	0
Day 6	Untransduced vs MSCV-backbone	2
Day 6	Untransduced vs *T58I-t2A-BCL2*	354
Day 6	MSCV-backbone vs *T58I-t2A-BCL2*	1131
Day 6	MSCV-backbone vs Untransduced	4
Day 6	*T58I-t2A-BCL2* vs Untransduced	548
Day 6	*T58I-t2A-BCL2* vs MSCV-backbone	1118
Day 13	Untransduced vs MSCV-backbone	0
Day 13	Untransduced vs *T58I-t2A-BCL2*	1904
Day 13	MSCV-backbone vs *T58I-t2A-BCL2*	1358
Day 13	MSCV-backbone vs Untransduced	0
Day 13	*T58I-t2A-BCL2* vs Untransduced	1820
Day 13	*T58I-t2A-BCL2* vs MSCV-backbone	1345
Day 20	Untransduced vs *T58I-t2A-BCL2*	620
Day 20	*T58I-t2A-BCL2* vs Untransduced	843

To get a better understanding of the transcriptional similarities between the different conditions, the data were explored with a uniform manifold approximation and projection (UMAP) analysis to reduce their dimensionality variation. In Figure 3.18, based on their DEGs on day 3, all conditions clustered together at the left bottom corner of the plot next to the day 0 included samples. These two time points generated an independent cluster to the remaining three time points tested which displayed separate clusters located at the right top side of the plot. Day 6 control samples generated a cluster close to day 6 MYC T58I-BCL2 overexpressing samples. In more detail, day 6 *T58I-t2A-BCL2* generated a distinctive cluster to the day 13 and day 20 controls and closer to the day 13 and day 20 *T58I-t2A-BCL2* samples which produced a separate cluster at the top right corner of the plot.

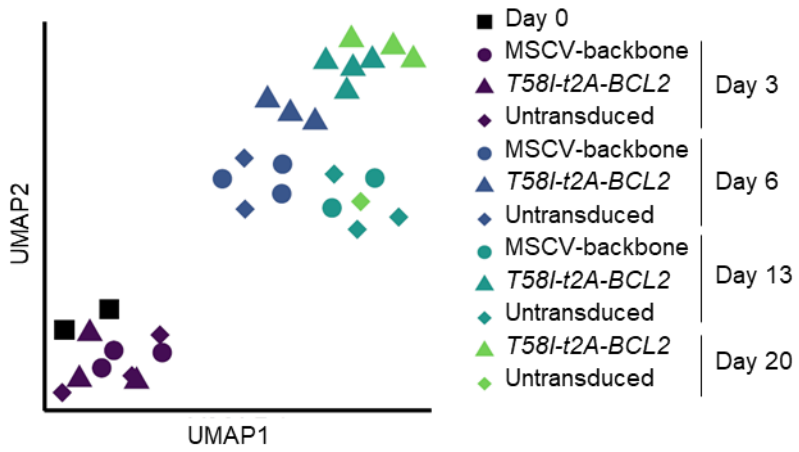

Figure 3.18 Clustering of the DEGs with a dimensionality reduction approach. Samples collected at day 0, day 3, day 6, day 13 and day 20 were studied with bulk RNA-sequencing to characterize their gene expression profile. RNA-sequencing data were analysed and the DEGs were used for dimensionality reduction analysis of the indicated samples using the uniform manifold approximation and projection (UMAP) approach. The illustrated plot was generated by Dr. Matthew Care. Data are representative of two independent experiments with two biological replicates (N= 2) and no technical replicates per experiment. The total number of donors tested as biological replicates was four (N= 4) out of which: two (N= 2) were assessed on day 0; three (N= 3) were assessed on day 3; two (N= 2) for the untransduced condition, three (N= 3) for each of the MSCV-backbone and *T58I-t2A-BCL2* transductions were assessed on day 6; three (N= 3) for the untransduced control, two (N= 2) for the MSCV-backbone and four (N= 4) for the *T58I-t2A-BCL2* condition were assessed on day 13; one (N= 1) for the untransduced condition and three (N= 3) for the *T58I-t2A-BCL2* transductions were assessed on day 20. No donors were assessed for the MSCV-backbone control on day 20. Missing donors in the different conditions per time point were not evaluated due to low collected cell numbers and inadequate RNA concentrations for RNA-sequencing.

These data suggested transcriptional similarities of the day 3 samples between each other and also with day 0 derived cells. Following the normal differentiation process, day 6 samples succeeded the day 0 and day 3 cluster. The day 13 and day 20 control samples were located close to each other and represented the sequential PC differentiation occurring in the *in vitro* model system. There was a separation of the samples with MYC T58I-BCL2 overexpression which became more pronounced from day 6 to day 13 and finally day 20. This indicates that the impact of MYC T58I-BCL2 on gene expression becomes more distinct as the differentiation proceeds.

3.6.2 Gene signature enrichment of the differentially expressed genes

The functional annotation of the resulting DEGs upon MYC T58I-BCL2 was assessed using GO analysis. First, to get a better understanding of the anticipated PC differentiation process, the DEGs with higher expression in the untransduced samples over the *T58I-t2A-BCL2* were analysed based on their overlap with known gene expression signatures. As Table 3.6 (top) shows, on day 6 signatures related to the transition of a GC B cell to a light zone (LZ) B cell transcriptional profile were enriched. ER and Golgi apparatus-associated signatures indicated gene expression related to an active secretory pathway. These findings agreed with the anticipated plasmablast-like phenotype of the day 6 time point. Subsequently, the day 13 and day 20 comparisons, Table 3.6 (middle and bottom respectively), showed a significant enrichment of signatures related to immune response, PC features and immunoglobulin production and secretion. These findings demonstrated, in all three time points tested, the anticipated biological annotation of the upregulated genes in the untransduced control.

Table 3.6 Gene signature enrichment of DEGs higher expressed in untransduced than *T58I-t2A-BCL2* condition on day 6, day 13 and day 20. Gene sets of GeneOntology_BP, GeneOntology_CC, GeneOntology_MF, SignatureDB, UniProt-Keyword and MSigDB_H were compared to evaluate functional annotation of the DEGs upregulated in the untransduced samples versus (vs) the *T58I-t2A-BCL2* condition at the indicated time points. The displayed signatures are the ten most highly enriched based on their Z-score. Data are representative of two independent experiments with two biological replicates (N= 2) and no technical replicates per experiment. The total number of donors tested as biological replicates was four (N= 4) out of which: two (N= 2) for the untransduced condition, three (N= 3) for each of the MSCV-backbone and *T58I-t2A-BCL2* transductions were assessed on day 6; three (N= 3) for the untransduced control, two (N= 2) for the MSCV-backbone and four (N= 4) for the *T58I-t2A-BCL2* condition were assessed on day 13; one (N= 1) for the untransduced condition and three (N= 3) for the *T58I-t2A-BCL2* transductions were assessed on day 20. No donors were assessed for the MSCV-backbone control on day 20. Missing donors in the different conditions per time point were not evaluated due to low collected cell numbers and inadequate RNA concentrations for RNA-sequencing; FDR, false discovery rate.

Day 6 Untransduced vs *T58I-t2A-BCL2*

Gene Signature	Gene Set	Overlapping	Gene Set Size	Z-score	p-value	FDR
organelle subcompartment [GoID:GO:0031984]	GeneOntology_CC	67	1396	9.0761	1.13E-19	4.33E-17
BCL6_ChIPSeq_Basso_GC_low (PMID:19965633)	SignatureDB	60	1175	8.8808	6.64E-19	2.36E-16
Quiescence_heme_all (PMID:15075390)	SignatureDB	30	269	8.8496	8.78E-19	3.03E-16
XBP1_target_secretory (PMID:15345222)	SignatureDB	16	49	8.7470	2.19E-18	7.35E-16
endoplasmic reticulum membrane [GoID:GO:0005789]	GeneOntology_CC	54	1080	8.2860	1.17E-16	3.37E-14
endoplasmic reticulum subcompartment [GoID:GO:0098827	GeneOntology_CC	54	1084	8.2672	1.37E-16	3.86E-14
Golgi membrane [GoID:GO:0000139]	GeneOntology_CC	40	605	8.2461	1.64E-16	4.46E-14
scGC_cluster1_LZ (PMID:30104629)	SignatureDB	36	490	8.2090	2.23E-16	6.04E-14
Golgi apparatus	UniProt-Keyword	48	879	8.1991	2.42E-16	6.37E-14
nuclear outer membrane-endoplasmic reticulum membrane network [GoID:GO:0042175]	GeneOntology_CC	54	1101	8.1880	2.66E-16	6.94E-14

Day 13 Untransduced vs *T58I-t2A-BCL2*

Gene Signature	Gene Set	Overlapping	Gene Set Size	Z-score	p-value	FDR
Immunoglobulin	UniProt-Keyword	92	145	17.4420	3.96E-68	2.13E-65
immunoglobulin complex [GoID:GO:0019814]	GeneOntology_CC	96	160	17.3881	1.02E-67	5.38E-65
adaptive immune response [GoID:GO:0002250]	GeneOntology_BP	179	597	16.9074	3.97E-64	1.96E-61
Adaptive immunity	UniProt-Keyword	137	357	16.8843	5.87E-64	2.86E-61
Immunity	UniProt-Keyword	197	715	16.8717	7.27E-64	3.50E-61
antigen binding [GoID:GO:0003823]	GeneOntology_MF	89	167	15.8659	1.09E-56	3.91E-54
cell activation [GoID:GO:0001775]	GeneOntology_BP	226	1004	15.7767	4.50E-56	1.57E-53
leukocyte activation [GoID:GO:0045321S]	GeneOntology_BP	208	877	15.6901	1.77E-55	6.10E-53
lymphocyte activation [GoID:GO:0046649]	GeneOntology_BP	188	735	15.6818	2.01E-55	6.82E-53
regulation of immune system process [GoID:GO:0002682]	GeneOntology_BP	264	1330	15.5063	3.15E-54	1.03E-51

Day 20 Untransduced vs *T58I-t2A-BCL2*

Gene Signature	Gene Set	Overlapping	Gene Set Size	Z-score	p-value	FDR
Immunoglobulin	UniProt-Keyword	61	145	16.3866	2.38E-60	7.92E-57
immunoglobulin complex [GoID:GO:0019814]	GeneOntology_CC	63	160	16.3512	4.26E-60	1.30E-56
Adaptive immunity	UniProt-Keyword	72	357	14.1746	1.32E-45	2.00E-42
adaptive immune response [GoID:GO:0002250]	GeneOntology_BP	85	597	13.4732	2.25E-41	2.65E-38
antigen binding [GoID:GO:0003823]	GeneOntology_MF	50	167	13.3963	6.35E-41	7.04E-38
Immunity	UniProt-Keyword	88	715	12.8429	9.43E-38	9.08E-35
Immunoglobulin domain	UniProt-Keyword	80	605	12.6288	1.46E-36	1.25E-33
B cell activation [GoID:GO:0042113]	GeneOntology_BP	53	316	11.2839	1.58E-29	8.73E-27
immunoglobulin complex, circulating [GoID:GO:0042571]	GeneOntology_CC	30	75	11.2501	2.31E-29	1.26E-26
B cell receptor signaling pathway [GoID:GO:0050853]	GeneOntology_BP	36	126	11.1655	6.01E-29	3.19E-26

When the reverse comparison was performed, the DEGs with higher expression in the *T58I-t2A-BCL2* samples over the untransduced, overlapped with signatures highly correlated with MYC function and less with B cell and PC differentiation. As displayed in Table 3.7, in all three time points tested, gene expression associated with upregulation of MYC-signalling, MYC targets, ribosome biogenesis, RNA-processing and translation dominated the more enriched signatures identified by this analysis. These findings supported that on a transcriptional level, the overexpressed MYC function dominated the most enriched signatures in the reverse comparisons made. Although the enforced MYC activity was validated through this analysis, no specific conclusions could be reached regarding its effect on the *in vitro* PC differentiation process.

Table 3.7 Gene signature enrichment of DEGs upregulated in *T58I-t2A-BCL2* over the untransduced condition on day 6, day 13 and day 20. Gene sets of GeneOntology_BP, GeneOntology_CC, GeneOntology_MF, SignatureDB, UniProt-Keyword and MSigDB_H were compared to evaluate functional annotation of the DEGs with higher expression in the *T58I-t2A-BCL2* condition versus (vs) the untransduced samples at the indicated time points. The displayed signatures are the ten most highly enriched based on their Z-score. Data are representative of two independent experiments with two biological replicates (N= 2) and no technical replicates per experiment. The total

number of donors tested as biological replicates was four (N= 4) out of which: two (N= 2) for the untransduced condition, three (N= 3) for each of the MSCV-backbone and *T58I-t2A-BCL2* transductions were assessed on day 6; three (N= 3) for the untransduced control, two (N= 2) for the MSCV-backbone and four (N= 4) for the *T58I-t2A-BCL2* condition were assessed on day 13; one (N= 1) for the untransduced condition and three (N= 3) for the *T58I-t2A-BCL2* transductions were assessed on day 20. No donors were assessed for the MSCV-backbone control on day 20. Missing donors in the different conditions per time point were not evaluated due to low collected cell numbers and inadequate RNA concentrations for RNA-sequencing; FDR, false discovery rate.

Day 6 *T58I-t2A-BCL2* vs Untransduced

Gene Signature	Gene Set	Overlapping	Gene Set Size	Z-score	p-value	FDR
Myc_ChIP_PET_Expr_Up (PMID:17093053)	SignatureDB	89	403	16.9679	1.42E-64	1.79E-61
ribonucleoprotein complex biogenesis [GoID:GO:002261]	GeneOntology_BP	91	429	16.9434	2.15E-64	2.63E-61
JAK2_upregulated_PMBL (PMID:21156283)	SignatureDB	124	964	16.6141	5.51E-62	5.75E-59
ribosome biogenesis [GoID:GO:004225]	GeneOntology_BP	73	296	15.8452	1.52E-56	1.09E-53
HALLMARK_MYC_TARGETS_V1	MSigDB_H	63	200	15.7927	3.49E-56	2.37E-53
Mitochondrion	UniProt-Keyword	123	1182	15.0348	4.34E-51	2.52E-48
rRNA processing [GoID:GO:0006364]	GeneOntology_BP	60	224	14.6838	8.19E-49	4.22E-46
rRNA metabolic process [GoID:GO:0016072]	GeneOntology_BP	60	235	14.4707	1.85E-47	9.04E-45
ncRNA metabolic process [GoID:GO:0034660]	GeneOntology_BP	78	473	14.3124	1.83E-46	8.69E-44
ribonucleoprotein complex [GoID:GO:1990904]	GeneOntology_CC	89	658	14.1969	9.57E-46	4.38E-43

Day 13 *T58I-t2A-BCL2* vs Untransduced

Gene Signature	Gene Set	Overlapping	Gene Set Size	Z-score	p-value	FDR
ribonucleoprotein complex [GoID:GO:1990904]	GeneOntology_CC	250	658	23.3394	1.76E-120	1.65E-117
ribonucleoprotein complex biogenesis [GoID:GO:0022613]	GeneOntology_BP	197	429	22.5695	8.64E-113	5.76E-110
Myc_ChIP_PET_Expr_Up (PMID:17093053)	SignatureDB	184	403	21.7277	1.12E-104	6.22E-102
HALLMARK_MYC_TARGETS_V1	MSigDB_H	125	200	20.4820	3.12E-93	1.41E-90
translation [GoID:GO:0006412]	GeneOntology_BP	216	633	20.4502	5.98E-93	2.67E-90
ribosome biogenesis [GoID:GO:0042254]	GeneOntology_BP	149	296	20.3767	2.69E-92	1.16E-89
Ribonucleoprotein	UniProt-Keyword	140	268	20.0659	1.47E-89	5.89E-87
peptide biosynthetic process [GoID:GO:0043043]	GeneOntology_BP	216	656	20.0611	1.61E-89	6.35E-87
amide biosynthetic process [GoID:GO:0043604]	GeneOntology_BP	228	778	19.3255	3.28E-83	1.19E-80
cytoplasmic translation [GoID:GO:0002181]	GeneOntology_BP	102	148	19.2654	1.05E-82	3.76E-80

Day 20 *T58I-t2A-BCL2* vs Untransduced

Gene Signature	Gene Set	Overlapping	GeneSetSize	Z-score	p-value	FDR
cytoplasmic translation [GoID:GO:0002181]	GeneOntology_BP	98	148	22.2660	7.89E-110	7.40E-107
ribonucleoprotein complex [GoID:GO:1990904]	GeneOntology_CC	168	658	21.5760	3.02E-103	2.45E-100
Ribonucleoprotein	UniProt-Keyword	117	268	21.4394	5.73E-102	4.46E-99
structural constituent of ribosome [GoID:GO:0003735]	GeneOntology_MF	95	161	21.1441	3.12E-99	2.20E-96
cytosolic ribosome [GoID:GO:0022626]	GeneOntology_CC	79	100	21.1111	6.30E-99	4.34E-96
Ribosomal protein	UniProt-Keyword	96	167	21.0877	1.03E-98	6.99E-96
ribosomal subunit [GoID:GO:0044391]	GeneOntology_CC	96	178	20.6771	5.57E-95	3.23E-92
ribosome [GoID:GO:0005840]	GeneOntology_CC	103	219	20.5482	7.98E-94	4.42E-91
translation [GoID:GO:0006412]	GeneOntology_BP	156	633	20.4621	4.69E-93	2.52E-90
peptide biosynthetic process [GoID:GO:0043043]	GeneOntology_BP	156	656	20.1801	1.46E-90	7.75E-88

3.6.3 The function of overexpressed MYC on day 6 and day 13 of the model system

Next, the effect of MYC T58I overexpression on gene expression under permissive for PC differentiation conditions was further investigated. The analysis described in the previous section 3.6.2, indicated that MYC function-related transcriptional signatures were enriched at day 6 onwards in the *T58I-t2A-BCL2* transduced cells. As previously shown in Table 3.5, MYC T58I overexpression induced higher expression at day 13 (1820 genes) than day 6 (548) in genes that were upregulated in the *T58I-t2A-BCL2* samples over

the untransduced control. To get a better insight on the functional annotation characterizing these genes a Venn diagram-based approach was utilized to resolve the genes being upregulated at both time points. As displayed in Figure 3.19, 110 DEGs with higher expression in the *T58I-t2A-BCL2* samples than in the untransduced condition were identified to be uniquely expressed on day 6 (Gene set B) and 1382 to be upregulated at day 13 and not day 6 (Gene set C). The genes that were upregulated at both time points were 438 (Gene set A).

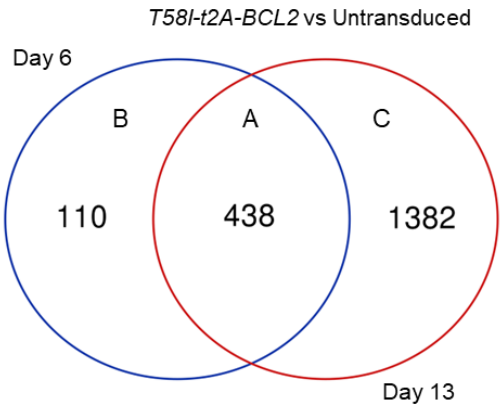

Figure 3.19 Classification of DEGs upregulated in the MYC T58I-BCL2 overexpressing cells over the untransduced into uniquely expressed or shared between day 6 and day 13 time points. Venn diagram comparing the day 6 and day 13 DEGs with higher expression in the *T58I-t2A-BCL2* condition versus (vs) the untransduced samples. DEGs shared between day 6 and day 13 represent Gene set A. DEGs induced uniquely on day 6 represent Gene set B while uniquely induced DEGs on day 13 belong to Gene set C. Data are representative of two independent experiments with two biological replicates (N= 2) and no technical replicates per experiment. The total number of donors tested as biological replicates was four (N= 4) out of which: two (N= 2) for the untransduced condition, three (N= 3) for each of the MSCV-backbone and *T58I-t2A-BCL2* transductions were assessed on day 6; three (N= 3) for the untransduced control, two (N= 2) for the MSCV-backbone and four (N= 4) for the *T58I-t2A-BCL2* condition were assessed on day 13. Missing donors in the different conditions per time point were not evaluated due to low collected cell numbers and inadequate RNA concentrations for RNA-sequencing.

Next, GO analysis using DAVID software was performed on the Gene sets A, B and C, generated in Figure 3.19. Upon functional annotation-based clustering performed with DAVID, the first cluster representing GO terms and signatures with the highest enrichment was selected and displayed in Table 3.8 for each of the three Gene sets. Similar GO terms were more highly enriched in Gene set A and Gene set B, related to mitochondrion function and activity, a hallmark of MYC function. The remaining annotation clusters also showed GO terms related to known MYC functions (data not shown). GO of the Gene set C, representing day 13 only, showed different GO terms to be enriched, in its first cluster, that were associated with

ribosomal activity and translation. This analysis suggested that only the DEGs associated with MYC overexpression on day 13 show a distinct high enrichment for GO terms which is mostly related to protein synthesis. This finding could support the hypothesis that the transcriptional profile observed in the day 13 *T58I-t2A-BCL2* cells, showing increased gene expression, is partially a result of ongoing MYC T58I overexpression function but also of downstream and earlier activated MYC overexpression-mediated signalling.

Table 3.8 Protein synthesis-related GO terms were enriched on the day 13 DEGs with higher expression in *T58I-t2A-BCL2* versus the untransduced. Gene ontology analysis was performed by functional annotation and clustering of enriched GO terms based on their enrichment using DAVID software. The Gene sets A, B and C (identified in Figure 3.19) were analysed to compare day 6 and day 13 GO terms enriched in each of the three Gene sets. Data are representative of two independent experiments with two biological replicates (N= 2) and no technical replicates per experiment. The total number of donors tested as biological replicates was four (N= 4) out of which: two (N= 2) for the untransduced condition, three (N= 3) for each of the MSCV-backbone and *T58I-t2A-BCL2* transductions were assessed on day 6; three (N= 3) for the untransduced control, two (N= 2) for the MSCV-backbone and four (N= 4) for the *T58I-t2A-BCL2* condition were assessed on day 13. Missing donors in the different conditions per time point were not evaluated due to low collected cell numbers and inadequate RNA concentrations for RNA-sequencing; FDR, false discovery rate; %, percentage of overlap.

Gene set A: common genes expressed at day 6 and day 13

Annotation Cluster 1	Enrichment Score: 26.7144149643926					
Category	**Term**	**Count**	**%**	**p-value**	**Benjamini**	**FDR**
GOTERM_CC_DIRECT	GO:0005739~mitochondrion	105	24.48	1.25E-31	5.34E-29	4.77E-29
UP_KW_CELLULAR_COMPONENT	KW-0496~Mitochondrion	102	23.78	2.99E-30	1.26E-28	1.08E-28
UP_KW_DOMAIN	KW-0809~Transit peptide	60	13.99	7.31E-30	1.83E-28	1.76E-28
UP_SEQ_FEATURE	TRANSIT:Mitochondrion	60	13.99	2.16E-26	4.12E-23	4.10E-23
GOTERM_CC_DIRECT	GO:0005759~mitochondrial matrix	44	10.26	4.54E-19	9.74E-17	8.70E-17

Gene set B: unique genes at day 6

Annotation Cluster 1	Enrichment Score: 3.471566001141157					
Category	**Term**	**Count**	**%**	**p-value**	**Benjamini**	**FDR**
UP_KW_CELLULAR_COMPONENT	KW-0496~Mitochondrion	24	23.08	9.51E-07	2.19E-05	2.19E-05
UP_KW_DOMAIN	KW-0809~Transit peptide	11	10.58	2.43E-04	0.0034	0.0034
UP_SEQ_FEATURE	TRANSIT:Mitochondrion	11	10.58	3.81E-04	0.1854	0.1854
GOTERM_CC_DIRECT	GO:0005759~mitochondrial matrix	5	4.81	0.1471	1	0.9830

Gene set C: unique genes at day 13

Annotation Cluster 1	Enrichment Score: 43.01502277132832					
Category	**Term**	**Count**	**%**	**p-value**	**Benjamini**	**FDR**
GOTERM_BP_DIRECT	GO:0002181~cytoplasmic translation	73	5.64	1.28E-68	4.90E-65	4.88E-65
GOTERM_CC_DIRECT	GO:0022626~cytosolic ribosome	68	5.26	1.48E-62	1.08E-59	9.96E-60
UP_KW_MOLECULAR_FUNCTION	KW-0687~Ribonucleoprotein	114	8.81	1.83E-55	1.59E-53	1.48E-53
GOTERM_MF_DIRECT	GO:0003735~structural constituent of ribosome	88	6.80	2.43E-55	1.63E-52	1.61E-52
UP_KW_MOLECULAR_FUNCTION	KW-0689~Ribosomal protein	91	7.03	6.82E-55	2.97E-53	2.76E-53
GOTERM_BP_DIRECT	GO:0006412~translation	88	6.80	4.17E-54	7.97E-51	7.94E-51
KEGG_PATHWAY	hsa03010:Ribosome	83	6.41	5.52E-50	1.82E-47	1.78E-47
GOTERM_CC_DIRECT	GO:0022625~cytosolic large ribosomal subunit	46	3.55	3.80E-36	1.39E-33	1.28E-33
KEGG_PATHWAY	hsa05171:Coronavirus disease - COVID-19	73	5.64	2.05E-28	3.38E-26	3.30E-26
GOTERM_CC_DIRECT	GO:0022627~cytosolic small ribosomal subunit	32	2.47	6.53E-26	7.97E-24	7.34E-24
GOTERM_CC_DIRECT	GO:0005840~ribosome	43	3.32	3.51E-23	3.67E-21	3.38E-21
GOTERM_CC_DIRECT	GO:0005925~focal adhesion	60	4.64	2.80E-10	1.46E-08	1.35E-08

3.6.4 Immunophenotyping markers and MYC targets gene expression

Variance stabilizing transformation (VST) log-like units were used to normalise and stabilize in respect to variance the count data derived from our gene expression study. VST data, adjusted to remove mean-dependent variance, were generated from DESeq2 software as log_2-transformed gene expression values (288, 301). VST data in log-like scale are suitable for visualization of changes in gene expression across samples and time-series data. Thus, normalised and log_2-transformed VST values were plotted for selected genes to provide a better understanding of the MYC T58I-BCL2 overexpression effect on gene expression across the time points tested and in comparison to the controls.

In the developed *in vitro* model system overexpression of MYC carrying the T58I substitution and BCL2 was achieved with a retroviral vector containing a CD2 reporter. In Figure 3.20, analysis of the normalised gene expression values showed the successful overexpression of *CD2* in the transduced samples, for both MSCV-

backbone or *T58I-t2A-BCL2* transductions. In addition, *MYC* and *BCL2* were successfully overexpressed after day 3 in the *T58I-t2A-BCL2* condition. Endogenous *MYC* expression represented in the control samples of untransduced, and MSCV-backbone conditions showed a gradual decrease in expression from day 3 onwards. In contrast, endogenous *BCL2* expression slightly fluctuated remaining consistently lower than its day 0 expression from day 3 onwards. This analysis showed that successful overexpression of *MYC* and *BCL2* was achieved which was maintained up to day 20 at higher levels than their endogenous expression.

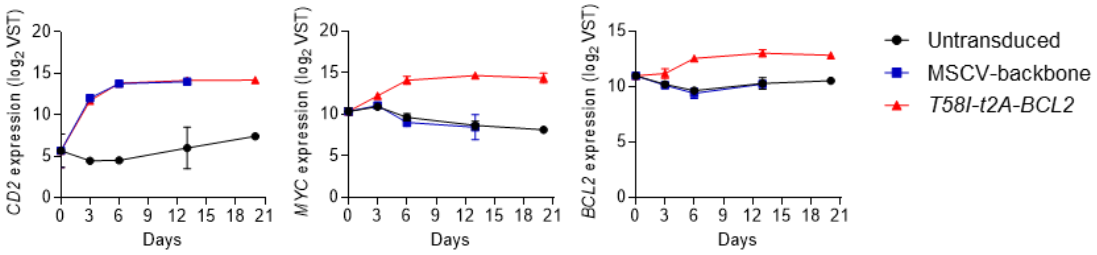

Figure 3.20 Validation of the model system on a transcriptional level. Graphs of the normalised expression values of *CD2*, *MYC* and *BCL2* genes at day 0, day 3, day 6, day 13 and day 20 for the indicated conditions. Software DESeq2 performed variance stabilizing transformation (VST) analysis generating the normalized log_2-transformed gene expression values, with stabilized variance, that are visualized in the graphs. Data are representative of two independent experiments with two biological replicates (N= 2) and no technical replicates per experiment. The total number of donors tested as biological replicates was four (N= 4) out of which: two (N= 2) were assessed on day 0; three (N= 3) were assessed on day 3; two (N= 2) for the untransduced condition, three (N= 3) for each of the MSCV-backbone and *T58I-t2A-BCL2* transductions were assessed on day 6; three (N= 3) for the untransduced control, two (N= 2) for the MSCV-backbone and four (N= 4) for the *T58I-t2A-BCL2* condition were assessed on day 13; one (N= 1) for the untransduced condition and three (N= 3) for the *T58I-t2A-BCL2* transductions were assessed on day 20. No donors were assessed for the MSCV-backbone control on day 20. Missing donors in the different conditions per time point were not evaluated due to low collected cell numbers and inadequate RNA concentrations for RNA-sequencing.

Having verified *MYC* and *BCL2* overexpression, the expression of genes encoding the immunophenotyped surface proteins, previously assessed with flow cytometry, were evaluated next alongside known MYC targets. Each of the selected genes was plotted and compared between untransduced and transduced with MSCV-backbone or *T58I-t2A-BCL2* conditions. As displayed in Figure 3.21, *CD19* expression was reduced from day 3 onwards upon MYC T58I-BCL2 overexpression in comparison to the controls. On the contrary, *CD20* showed an increase in expression in the *T58I-t2A-BCL2* samples from day 6. *CD27* had a decreased expression at day 6, 13 and 20 while *CD38* remained relatively close to the controls' levels of

expression showing a slight decrease in the MYC T58I-BCL2 overexpressing cells. Importantly, *CD138* showed differences in expression on day 13 with a significant decrease in comparison to the controls while it increased slightly on day 20. These results were in agreement with the flow cytometry findings suggesting that MYC T58I-BCL2-mediated changes in the immunophenotypic proteins tested were transcriptionally regulated.

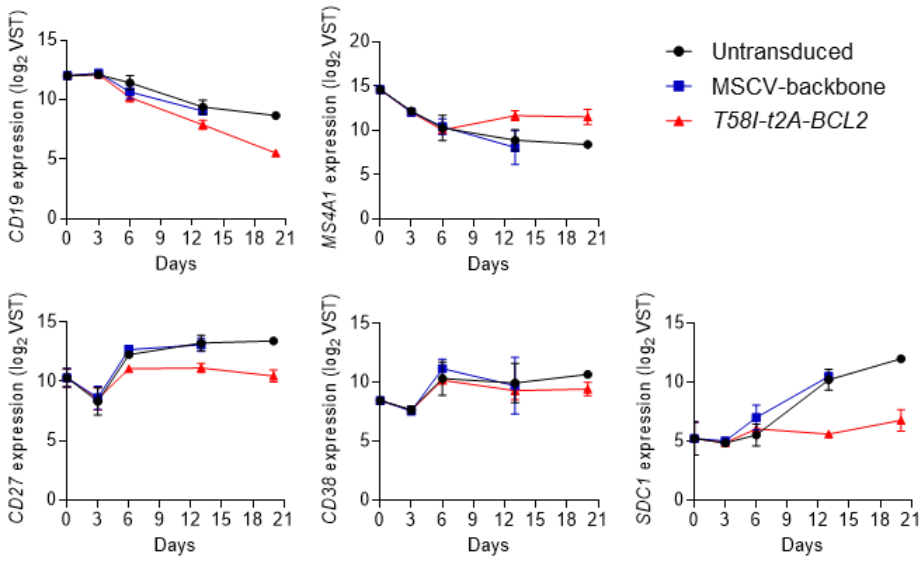

Figure 3.21 Gene expression of the flow cytometry immunophenotypic markers utilised in the model system. Normalised expression values of DEGs were plotted at day 0, day 3, day 6, day 13 and day 20 for the indicated conditions evaluating *CD19*, *MS4A1* (CD20), *CD27*, *CD38*, and *SDC1* (CD138) expression. Software DESeq2 performed variance stabilizing transformation (VST) analysis generating the normalized log_2-transformed gene expression values, with stabilized variance, that are visualized in the graphs. Data are representative of two independent experiments with two biological replicates (N= 2) and no technical replicates per experiment. The total number of donors tested as biological replicates was four (N= 4) out of which: two (N= 2) were assessed on day 0; three (N= 3) were assessed on day 3; two (N= 2) for the untransduced condition, three (N= 3) for each of the MSCV-backbone and *T58I-t2A-BCL2* transductions were assessed on day 6; three (N= 3) for the untransduced control, two (N= 2) for the MSCV-backbone and four (N= 4) for the *T58I-t2A-BCL2* condition were assessed on day 13; one (N= 1) for the untransduced condition and three (N= 3) for the *T58I-t2A-BCL2* transductions were assessed on day 20. No donors were assessed for the MSCV-backbone control on day 20. Missing donors in the different conditions per time point were not evaluated due to low collected cell numbers and inadequate RNA concentrations for RNA-sequencing.

The increase observed in *MYC* expression was followed by an increase in MYC activity. As Figure 3.22 shows, several direct MYC targets (302-306) had a significant increase in their expression in the *T58I-t2A-BCL2* samples from day 3 up to day 20 and in comparison, to their levels in the control conditions. These

findings suggested that the enforced MYC T58I expression resulted in increased MYC function in the model system.

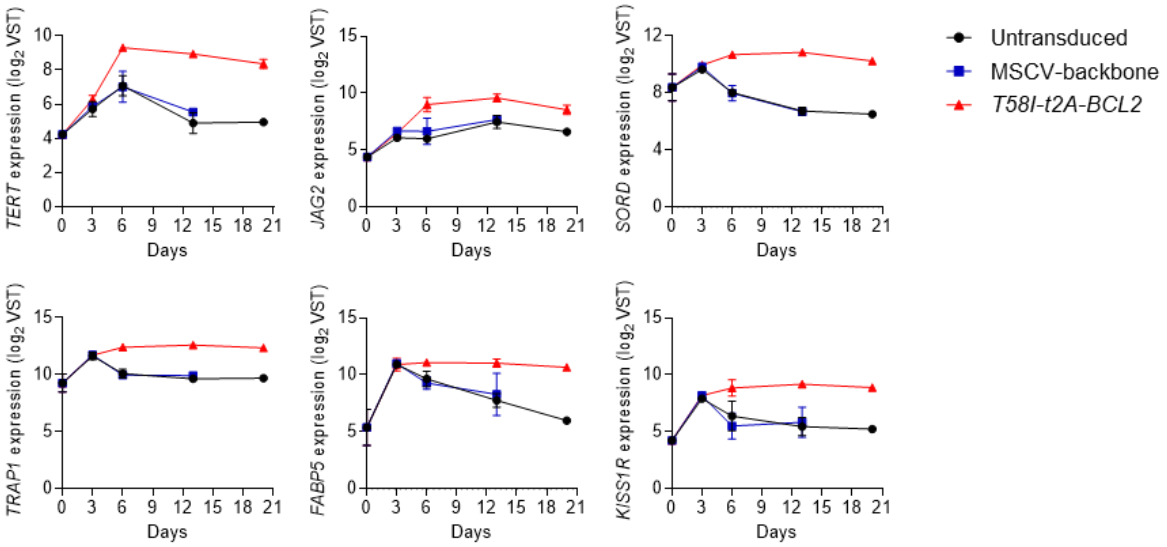

Figure 3.22 MYC targets gene expression analysis. Normalised expression values of differentially expressed MYC targets were plotted at day 0, day 3, day 6, day 13 and day 20 for the indicated conditions evaluating *TERT*, *JAG2*, *SORD, TRAP1, FABP5* and *KISS1R* expression. Software DESeq2 performed variance stabilizing transformation (VST) analysis generating the normalized log_2-transformed gene expression values, with stabilized variance, that are visualized in the graphs. Data are representative of two independent experiments with two biological replicates (N= 2) and no technical replicates per experiment. The total number of donors tested as biological replicates was four (N= 4) out of which: two (N= 2) were assessed on day 0; three (N= 3) were assessed on day 3; two (N= 2) for the untransduced condition, three (N= 3) for each of the MSCV-backbone and *T58I-t2A-BCL2* transductions were assessed on day 6; three (N= 3) for the untransduced control, two (N= 2) for the MSCV-backbone and four (N= 4) for the *T58I-t2A-BCL2* condition were assessed on day 13; one (N= 1) for the untransduced condition and three (N= 3) for the *T58I-t2A-BCL2* transductions were assessed on day 20. No donors were assessed for the MSCV-backbone control on day 20. Missing donors in the different conditions per time point were not evaluated due to low collected cell numbers and inadequate RNA concentrations for RNA-sequencing.

3.6.5 Gene expression of transcription factors

TFs strictly regulate the process of PC differentiation. To better understand the differentiation status upon MYC T58I-BCL2 overexpression, key TFs were analysed for their expression levels in the model system. As displayed in Figure 3.23, PAX5 and EBF1, two main TFs for the maintenance of the B cell state showed a reduction in their gene expression independently of MYC T58I-BCL2 overexpression. The same pattern was

observed for the gene expression of *BCL6*, a regulator of the GC B cell phenotype. BACH2 inhibits PC differentiation progression and directly represses the PC hallmark TF BLIMP1 (307). Despite its overall downregulation after day 3, an aberrant increase was observed in the levels of *BACH2* expression on day 13 and day 20 in the *T58I-t2A-BCL2* samples in comparison to the controls. The gene expression of additional TFs such as RUNX1 and SREBF1 was also perturbed in the MYC T58I-BCL2 overexpressing samples. Importantly, upregulation of the PC state regulators *PRDM1* (BLIMP1) and *IRF4* was detected reaching similar levels to the controls with only a slight reduction in their expression levels in the MYC T58I-BCL2 overexpressing samples. Interestingly, XBP1, the key TF regulating antibody secretion in PCs, showed a reduction in its gene expression after day 6 in the *T58I-t2A-BCL2* condition compared to the controls. These results suggest that on a transcriptional level, MYC T58I-BCL2 overexpression does not inhibit the downregulation of TFs such as PAX5 and BACH2 acting as antagonists of the PC differentiation. In parallel, the upregulation of *PRDM1, IRF4* indicated that enforced MYC T58I allowed PC differentiation progression but drove aberrant expression levels of key TFs and repression of *XBP1*.

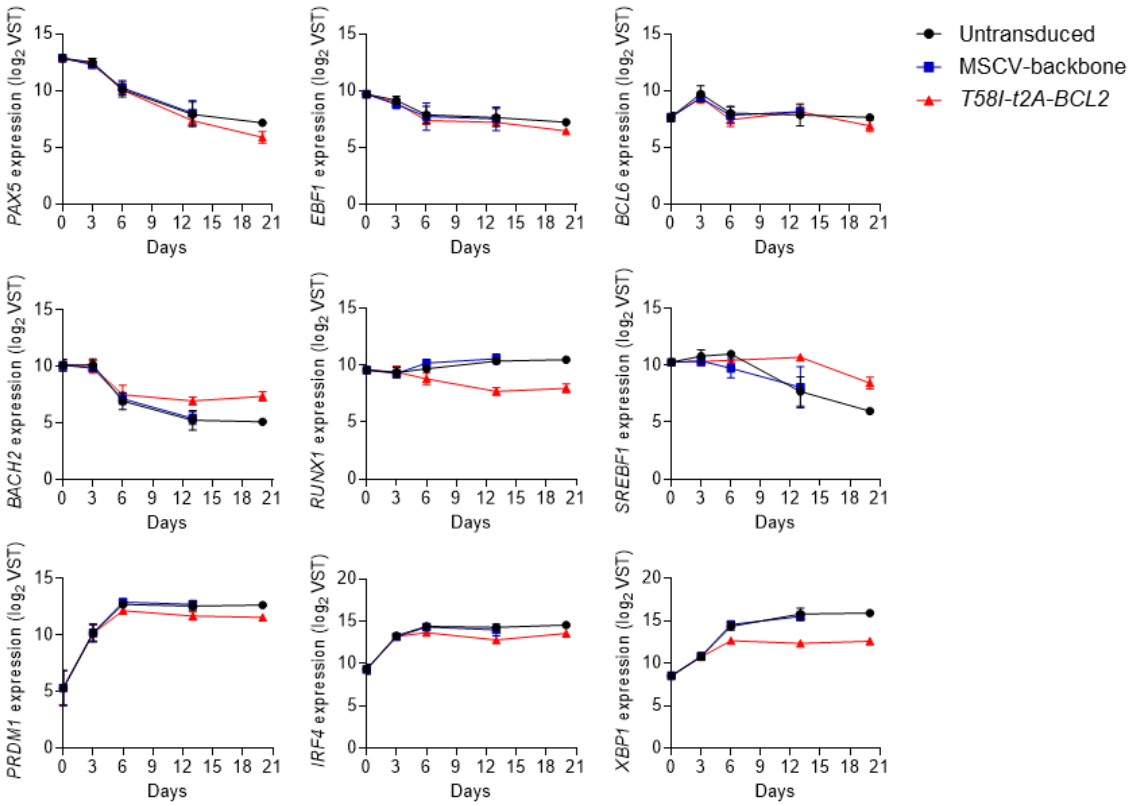

Figure 3.23 Gene expression of key TFs. Normalised expression values of differentially expressed TFs were plotted at day 0, day 3, day 6, day 13 and day 20 for the indicated conditions evaluating gene expression of the *PAX5*, *EBF1*, *BCL6*, *BACH2*, *RUNX1*, *SREBF1*, *PRDM1*, *IRF4* and *XBP1*. Software DESeq2 performed variance stabilizing

transformation (VST) analysis generating the normalized log_2-transformed gene expression values, with stabilized variance, that are visualized in the graphs. Data are representative of two independent experiments with two biological replicates (N= 2) and no technical replicates per experiment. The total number of donors tested as biological replicates was four (N= 4) out of which: two (N= 2) were assessed on day 0; three (N= 3) were assessed on day 3; two (N= 2) for the untransduced condition, three (N= 3) for each of the MSCV-backbone and *T58I-t2A-BCL2* transductions were assessed on day 6; three (N= 3) for the untransduced control, two (N= 2) for the MSCV-backbone and four (N= 4) for the *T58I-t2A-BCL2* condition were assessed on day 13; one (N= 1) for the untransduced condition and three (N= 3) for the *T58I-t2A-BCL2* transductions were assessed on day 20. No donors were assessed for the MSCV-backbone control on day 20. Missing donors in the different conditions per time point were not evaluated due to low collected cell numbers and inadequate RNA concentrations for RNA-sequencing.

3.6.6 XBP1 targets and immunoglobulins gene expression

To further investigate the *XBP1* reduction, specific XBP1 target genes associated with the UPR (308-310) were assessed for their expression in the model system. As displayed in Figure 3.24, a consistent pattern of reduction was observed in all the analysed XBP1 targets at the *T58I-t2A-BCL2* condition when compared to the untransduced and MSCV-backbone conditions across the time course.

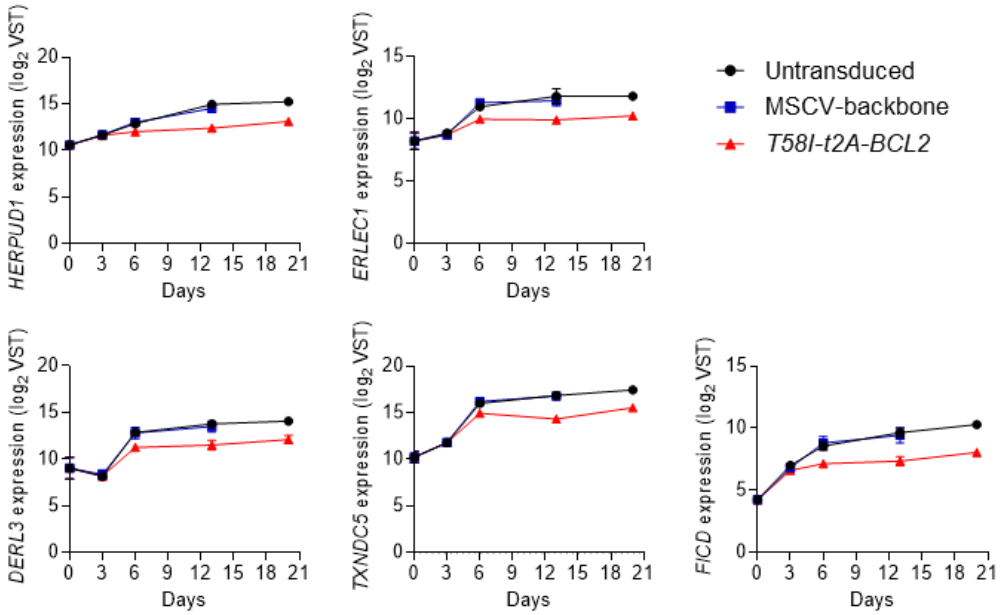

Figure 3.24 Gene expression of XBP1 target genes. Normalised expression values of differentially expressed XBP1 targets associated with UPR-pathway, were plotted at day 0, day 3, day 6, day 13 and day 20 for the indicated conditions evaluating *HERPUD1*, *ERLEC1*, *DERL3*, *TXNDC5* and *FICD* expression. Software DESeq2 performed variance stabilizing transformation (VST) analysis generating the normalized log_2-transformed gene expression values, with

stabilized variance, that are visualized in the graphs. Data are representative of two independent experiments with two biological replicates (N= 2) and no technical replicates per experiment. The total number of donors tested as biological replicates was four (N= 4) out of which: two (N= 2) were assessed on day 0; three (N= 3) were assessed on day 3; two (N= 2) for the untransduced condition, three (N= 3) for each of the MSCV-backbone and *T58I-t2A-BCL2* transductions were assessed on day 6; three (N= 3) for the untransduced control, two (N= 2) for the MSCV-backbone and four (N= 4) for the *T58I-t2A-BCL2* condition were assessed on day 13; one (N= 1) for the untransduced condition and three (N= 3) for the *T58I-t2A-BCL2* transductions were assessed on day 20. No donors were assessed for the MSCV-backbone control on day 20. Missing donors in the different conditions per time point were not evaluated due to low collected cell numbers and inadequate RNA concentrations for RNA-sequencing.

Given the crucial role of XBP1 in immunoglobulin secretion to further investigate this finding gene expression profiling of the immunoglobulin genes was performed. A consistent reduction in expression was observed in the immunoglobulin genes upon MYC T58I-BCL2 overexpression. Genes, responsible for the heavy chain compartments of immunoglobulin molecules as well as for their light chains, were shown to have decreased expression in the *T58I-t2A-BCL2* condition from day 6 (the plasmablasts stage) onwards in comparison to both the control conditions, as displayed in Figure 3.25 and Figure 3.26 respectively.

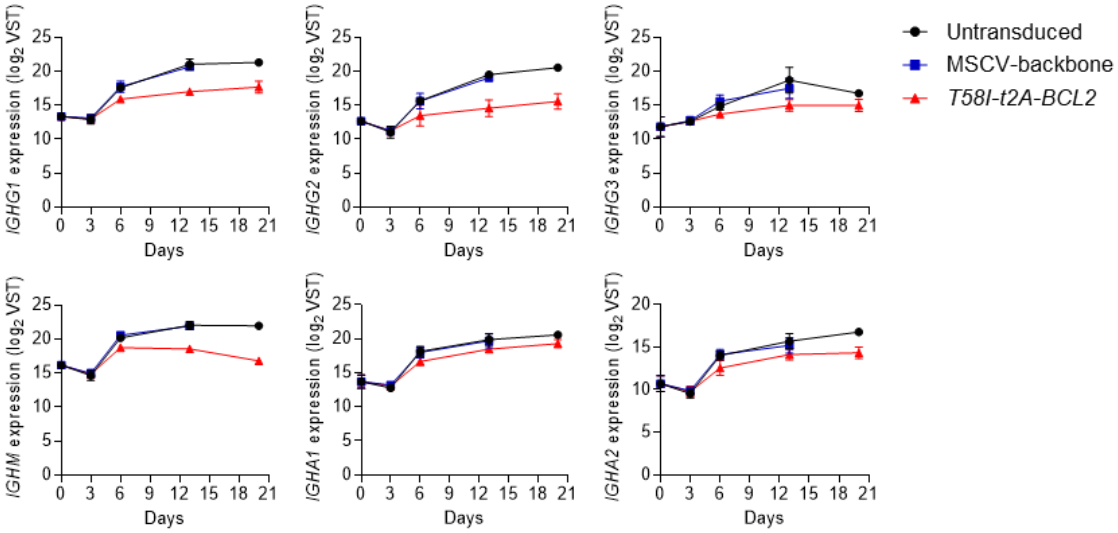

Figure 3.25 Heavy chain immunoglobulins gene expression. Normalised expression values of DEGs were plotted at day 0, day 3, day 6, day 13 and day 20 for the indicated conditions evaluating *IGHG1*, *IGHG2*, *IGHG3*, *IGHM*, *IGHA1* and *IGHA2* expression. Software DESeq2 performed variance stabilizing transformation (VST) analysis generating the normalized log_2-transformed gene expression values, with stabilized variance, that are visualized in the graphs. Data are representative of two independent experiments with two biological replicates (N= 2) and no technical replicates per experiment. The total number of donors tested as biological replicates was four (N= 4) out of which: two (N= 2) were assessed on day 0; three (N= 3) were assessed on day 3; two (N= 2) for the untransduced condition, three (N=

3) for each of the MSCV-backbone and *T58I-t2A-BCL2* transductions were assessed on day 6; three (N= 3) for the untransduced control, two (N= 2) for the MSCV-backbone and four (N= 4) for the *T58I-t2A-BCL2* condition were assessed on day 13; one (N= 1) for the untransduced condition and three (N= 3) for the *T58I-t2A-BCL2* transductions were assessed on day 20. No donors were assessed for the MSCV-backbone control on day 20. Missing donors in the different conditions per time point were not evaluated due to low collected cell numbers and inadequate RNA concentrations for RNA-sequencing.

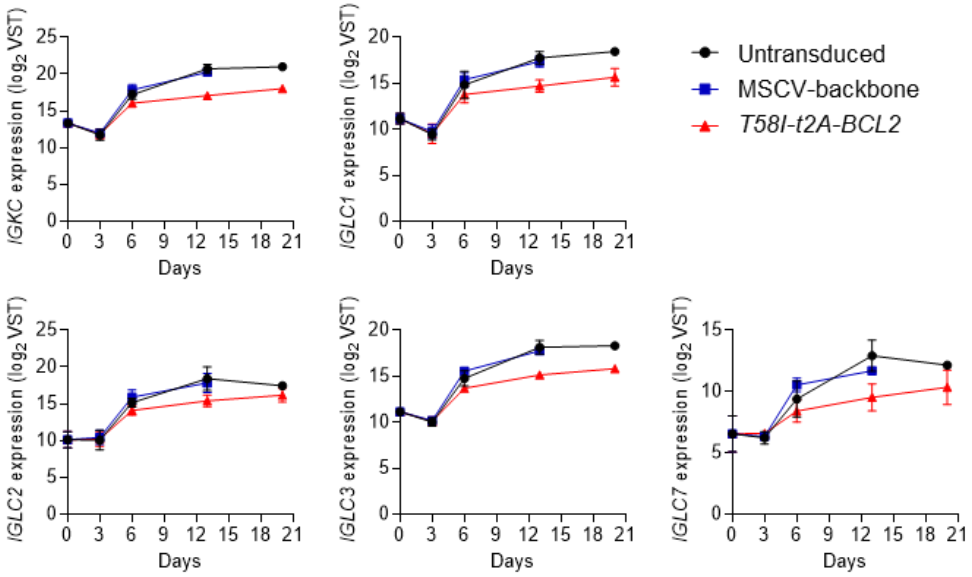

Figure 3.26 Light chain immunoglobulins gene expression. Normalised expression values of DEGs were plotted at day 0, day 3, day 6, day 13 and day 20 for the indicated conditions evaluating *IGKC*, *IGLC1*, *IGLC2*, *IGLC3* and *IGLC7* expression. Software DESeq2 performed variance stabilizing transformation (VST) analysis generating the normalized log_2-transformed gene expression values, with stabilized variance, that are visualized in the graphs. Data are representative of two independent experiments with two biological replicates (N= 2) and no technical replicates per experiment. The total number of donors tested as biological replicates was four (N= 4) out of which: two (N= 2) were assessed on day 0; three (N= 3) were assessed on day 3; two (N= 2) for the untransduced condition, three (N= 3) for each of the MSCV-backbone and *T58I-t2A-BCL2* transductions were assessed on day 6; three (N= 3) for the untransduced control, two (N= 2) for the MSCV-backbone and four (N= 4) for the *T58I-t2A-BCL2* condition were assessed on day 13; one (N= 1) for the untransduced condition and three (N= 3) for the *T58I-t2A-BCL2* transductions were assessed on day 20. No donors were assessed for the MSCV-backbone control on day 20. Missing donors in the different conditions per time point were not evaluated due to low collected cell numbers and inadequate RNA concentrations for RNA-sequencing.

These findings suggest that the transcriptional repression observed in *XBP1* upon MYC T58I overexpression resulted in a reduction in XBP1 transcriptional activity. In addition, enforced MYC T58I in the model system

had a general effect on the immunoglobulin genes expression mediating their repression via an unknown mechanism.

3.6.7 Parsimonious Gene Correlation Network Analysis (PGCNA)

To get a better understanding of the biological processes that MYC T58I-BCL2 overexpression affected across the time course tested, Parsimonious Gene Correlation Network Analysis (PGCNA) was performed. PGCNA is an agnostic correlation-based method that generates modules of co-expressed genes comparing the shifting patterns between the conditions of interest throughout the time points tested. Pairwise correlations between all the DEGs analysed resulted in correlation matrices that were utilised to generate a network (Figure 3.27, left). In PGCNA only the 3 highest correlations per gene (represented as network edges) are maintained to reduce the issue of high connectivity between the genes analysed and represented in the network (292). Clustering of the genes and their correlations in the network resulted in 16 modules based on co-expression patterns (Figure 3.27). Each module was labelled based on the number and function of the genes assigned to it. As displayed in Figure 3.27 (right), the module (M) with the highest number of genes was M1 followed by M2 with 1628 and 1625 genes respectively. Accordingly, the last identified cluster of co-expression, M16, had the lowest number of assigned genes (499 genes).

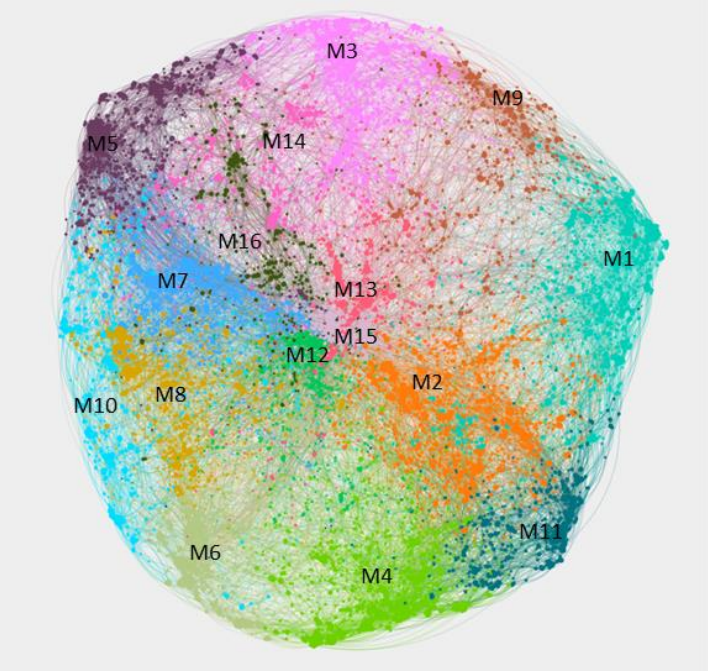

Module	Module Size
M1	1628
M2	1625
M3	1367
M4	1300
M5	1143
M6	1118
M7	1072
M8	1039
M9	844
M10	804
M11	768
M12	723
M13	721
M14	666
M15	624
M16	499

Figure 3.27 The number of genes assigned to each of the 16 identified modules upon PGCNA. 16 modules derived from the generated network (left) using Parsimonious Gene Correlation Network Analysis (PGCNA) were named

based on the number of genes they were comprised of (right). The higher number was 1628 genes assigned to the first module followed by the second bigger module with 1625 genes up to the last module (module 16) with 499 genes. The PGCNA-derived network (left) was generated by Dr. Matthew Care. Data are representative of two independent experiments with two biological replicates (N= 2) and no technical replicates per experiment. The total number of donors tested as biological replicates was four (N= 4) out of which: two (N= 2) were assessed on day 0; three (N= 3) were assessed on day 3; two (N= 2) for the untransduced condition, three (N= 3) for each of the MSCV-backbone and *T58I-t2A-BCL2* transductions were assessed on day 6; three (N= 3) for the untransduced control, two (N= 2) for the MSCV-backbone and four (N= 4) for the *T58I-t2A-BCL2* condition were assessed on day 13; one (N= 1) for the untransduced condition and three (N= 3) for the *T58I-t2A-BCL2* transductions were assessed on day 20. No donors were assessed for the MSCV-backbone control on day 20. Missing donors in the different conditions per time point were not evaluated due to low collected cell numbers and inadequate RNA concentrations for RNA-sequencing; M, module.

GO and signature enrichment were performed for each of the generated modules to unravel the functional annotation of their co-expression patterns. GO terms and signatures that were highly represented in each module are displayed in Table 3.9. M1 showed enrichment in signatures related to B cell activation, differentiation and migration as well as to genes related to NF-κB signalling. Cell migration and NF-κB signalling-related signatures were represented also in the M2, while B cell differentiation and quiescence were the main terms enriched in M3. Additional modules related to PC differentiation were the M5 and M7 where immunoglobulin, XBP1 and UPR-associated genes were enriched in the represented signatures.

On the contrary to M1, M2, M3, M5 and M7, the modules M4 and M6 showed enrichment for signatures containing genes involved in RNA-binding, ribosome biogenesis, mitochondrial function and MYC function-derived gene upregulation and targets. Another module with enriched signatures related to ribosome and translation was the M13. M10 showed enrichment in antibody secreting cell differentiation-associated genes as well as metabolic-related signatures. Cell cycle-associated signatures were enriched in M11. This analysis provided an overview of the distinct co-expression patterns identified in the modules. Also, it validated that each module demonstrated a distinct GO enrichment.

Table 3.9 Signature enrichment analysis for the 16 identified modules by PGCNA. The 16 modules derived by PGCNA were tested for their functional annotation. Representative highly enriched signatures per module are illustrated. Data are representative of two independent experiments with two biological replicates (N= 2) and no technical replicates per experiment. The total number of donors tested as biological replicates was four (N= 4) out of which: two (N= 2) were assessed on day 0; three (N= 3) were assessed on day 3; two (N= 2) for the untransduced condition, three (N= 3) for each of the MSCV-backbone and *T58I-t2A-BCL2* transductions were assessed on day 6; three (N= 3) for the untransduced control, two (N= 2) for the MSCV-backbone and four (N= 4) for the *T58I-t2A-BCL2* condition

were assessed on day 13; one (N= 1) for the untransduced condition and three (N= 3) for the *T58I-t2A-BCL2* transductions were assessed on day 20. No donors were assessed for the MSCV-backbone control on day 20. Missing donors in the different conditions per time point were not evaluated due to low collected cell numbers and inadequate RNA concentrations for RNA-sequencing; FDR, false discovery rate.

Module 1						
Gene Signature	**Gene Set**	**Overlapping**	**Gene Set Size**	**Z-score**	**p-value**	**FDR**
BcellD0-D41_PGCNA_M2 Bcell Blimp1Repressed MHC	LEEDS_GOLD	204	409	20.3435	5.31E-92	1.81E-87
BcellDiff_upBC	LEEDS_GOLD	243	576	20.1609	2.16E-90	3.69E-86
IRF4_ABC_induced_panB (PMID:22698399)	SignatureDB	69	144	11.3561	6.91E-30	8.75E-27
cell migration [GoID:GO:0016477]	GeneOntology_BP	166	950	6.6767	2.44E-11	3.25E-09
IRF4_ABC_induced_NFkB (PMID:22698399)	SignatureDB	49	196	5.7920	6.95E-09	5.58E-07
Module 2						
Gene Signature	**Gene Set**	**Overlapping**	**Gene Set Size**	**Z-score**	**p-value**	**FDR**
locomotion [GoID:GO:0040011]	GeneOntology_BP	196	1134	7.5496	4.37E-14	7.86E-11
cell migration [GoID:GO:0016477]	GeneOntology_BP	169	950	7.3191	2.50E-13	3.71E-10
cell adhesion [GoID:GO:0007155]	GeneOntology_BP	151	921	5.9624	2.49E-09	1.02E-06
HALLMARK_INFLAMMATORY_RESPONSE	MSigDB_H	40	145	5.9016	3.60E-09	1.33E-06
HALLMARK_TNFA_SIGNALING_VIA_NFKB	MSigDB_H	43	176	5.4551	4.89E-08	1.13E-05
Module 3						
Gene Signature	**Gene Set**	**Overlapping**	**Gene Set Size**	**Z-score**	**p-value**	**FDR**
TotalBcell-D0-D6_minCI50_PGCNA_M1 UpD0 UpD6 Quiescence Vesicle SerumResponse	LEEDS_GOLD	129	427	12.8643	7.15E-38	2.72E-34
Blood_Module-3.8_Undetermined (PMID:18631455)	SignatureDB	66	178	10.4120	2.18E-25	4.43E-22
BcellDiff_upBC	LEEDS_GOLD	112	576	8.1105	5.04E-16	3.25E-13
Quiescence_heme_all (PMID:15075390)	SignatureDB	60	244	7.3953	1.41E-13	6.79E-11
Quiescence_heme_cluster1 (PMID:15075390)	SignatureDB	38	146	6.1548	7.52E-10	1.82E-07
Module 5						
Gene Signature	**Gene Set**	**Overlapping**	**Gene Set Size**	**Z-score**	**p-value**	**FDR**
BcellDiff_upPC	LEEDS_GOLD	259	765	22.0973	3.35E-108	2.86E-104
Immunoglobulin	UniProt-Keyword	108	132	21.1387	3.51E-99	2.40E-95
immunoglobulin complex [GoID:GO:0019814]	GeneOntology_CC	110	141	20.8673	1.06E-96	6.04E-93
MM_PGCNA_M5 PC ER XBP1_Targets UnfoldedProteinResponse	LEEDS_GOLD	150	636	13.0513	6.25E-39	4.45E-36
BcellD3-D20-TGFBconditions_PGCNA_M14 ER-Golgi_Autophagy	LEEDS_GOLD	114	396	12.9372	2.78E-38	1.79E-35
Module 7						
Gene Signature	**Gene Set**	**Overlapping**	**Gene Set Size**	**Z-score**	**p-value**	**FDR**
GSE12366_PLASMA_CELL_VS_NAIVE_BCELL_UP	MSigDB_C7	28	160	5.1402	2.74E-07	4.99E-05
BcellD0-D41_PGCNA_M1 Immunoglobulins PC	LEEDS_GOLD	28	193	4.3718	1.23E-05	0.0013
Secreted	UniProt-Keyword	81	869	4.0886	4.34E-05	0.0038
BcellDiff_upPC	LEEDS_GOLD	70	765	3.6617	0.0003	0.0152
TotalBcell-D0-D6_minCI50_PGCNA_M8 UpD5on PlasmaCell ER Golgi UPR_XBP1	LEEDS_GOLD	45	447	3.5094	0.0004	0.0232
Module 4						
Gene Signature	**Gene Set**	**Overlapping**	**Gene Set Size**	**Z-score**	**p-value**	**FDR**
RNA binding [GoID:GO:0003723]	GeneOntology_MF	301	1404	16.1224	1.78E-58	6.74E-55
WEI_MYCN_TARGETS_WITH_E_BOX	MSigDB_C2	178	678	14.2436	4.92E-46	8.40E-43
ribonucleoprotein complex biogenesis [GoID:GO:0022613]	GeneOntology_BP	121	394	12.9765	1.66E-38	2.03E-35
ribosome biogenesis [GoID:GO:0042254]	GeneOntology_BP	93	277	11.9906	3.98E-33	3.32E-30
HALLMARK_MYC_TARGETS_V1	MSigDB_H	69	196	10.5920	3.25E-26	1.39E-23
Module 6						
Gene Signature	**Gene Set**	**Overlapping**	**Gene Set Size**	**Z-score**	**p-value**	**FDR**
mitochondrial matrix [GoID:GO:0005759]	GeneOntology_CC	99	401	11.161	6.36E-29	5.44E-25
Mitochondrion	UniProt-Keyword	170	990	11.064	1.88E-28	1.29E-24
Myc_ChIP_PET_Expr_Up (PMID:17093053)	SignatureDB	90	375	10.414	2.15E-25	8.16E-22
mitochondrion [GoID:GO:0005739]	GeneOntology_CC	196	1329	10.150	3.33E-24	1.14E-20
ribosome biogenesis [GoID:GO:0042254]	GeneOntology_BP	67	277	8.992	2.43E-19	3.46E-16
Module 13						
Gene Signature	**Gene Set**	**Overlapping**	**Gene Set Size**	**Z-score**	**p-value**	**FDR**
REACTOME_EUKARYOTIC_TRANSLATION_ELONGATION	MSigDB_C2	77	89	20.2152	7.20E-91	1.23E-86
KEGG_RIBOSOME	MSigDB_C2	71	83	19.2995	5.42E-83	3.71E-79
REACTOME_EUKARYOTIC_TRANSLATION_INITIATION	MSigDB_C2	80	115	18.9654	3.30E-80	1.61E-76
cytoplasmic translation [GoID:GO:0002181]	GeneOntology_BP	80	133	18.0012	1.91E-72	5.92E-69
structural constituent of ribosome [GoID:GO:0003735]	GeneOntology_MF	77	152	16.5934	7.78E-62	1.40E-58
Module 10						
Gene Signature	**Gene Set**	**Overlapping**	**Gene Set Size**	**Z-score**	**p-value**	**FDR**
ASC_plasma_cell_high (PMID:27525369)	SignatureDB	143	469	17.9634	3.77E-72	1.29E-67
mitochondrial protein-containing complex [GoID:GO:0098798]	GeneOntology_CC	87	236	15.0421	3.89E-51	4.43E-47
Mitochondrion	UniProt-Keyword	173	990	14.6384	1.60E-48	9.10E-45
oxidative phosphorylation [GoID:GO:0006119]	GeneOntology_BP	56	121	13.1592	1.51E-39	2.71E-36
HALLMARK_OXIDATIVE_PHOSPHORYLATION	MSigDB_H	63	181	12.4185	2.07E-35	2.29E-32

Module 11						
Gene Signature	**Gene Set**	**Overlapping**	**Gene Set Size**	**Z-score**	**p-value**	**FDR**
HALLMARK_E2F_TARGETS	MSigDB_H	119	198	21.6102	1.44E-103	1.59E-100
Cell_cycle_Liu (PMID:15123814)	SignatureDB	118	211	20.9505	1.86E-97	1.81E-94
cell cycle [GoID:GO:0007049]	GeneOntology_BP	265	1339	20.6059	2.43E-94	1.98E-91
Cell_cycle_Whitfield (PMID:12058064)	SignatureDB	181	609	20.4093	1.38E-92	1.01E-89
Cell cycle	UniProt-Keyword	168	552	19.8067	2.61E-87	1.62E-84

Based on the most highly enriched signatures and GO terms identified, a name was assigned to each module to describe its distinctive pattern of co-expression. The summary name of each module is depicted in Table 3.10.

Table 3.10 Labelling of the 16 modules identified by PGCNA. Each module was assigned a short description based on the GO terms and signatures that overrepresented their assigned genes. The short description of the functional annotation characterizing each module is indicated as module ID. Data are representative of two independent experiments with two biological replicates (N= 2) and no technical replicates per experiment. The total number of donors tested as biological replicates was four (N= 4) out of which: two (N= 2) were assessed on day 0; three (N= 3) were assessed on day 3; two (N= 2) for the untransduced condition, three (N= 3) for each of the MSCV-backbone and *T58I-t2A-BCL2* transductions were assessed on day 6; three (N= 3) for the untransduced control, two (N= 2) for the MSCV-backbone and four (N= 4) for the *T58I-t2A-BCL2* condition were assessed on day 13; one (N= 1) for the untransduced condition and three (N= 3) for the *T58I-t2A-BCL2* transductions were assessed on day 20. No donors were assessed for the MSCV-backbone control on day 20. Missing donors in the different conditions per time point were not evaluated due to low collected cell numbers and inadequate RNA concentrations for RNA-sequencing; M, module.

Module	Module_ID
M1	upBC BLIMP1_Repressed CellMigration IFN TNFA_Via_NFkB
M2	UpD3 CellMigration TNFA_Via_NFkB IFN EMT
M3	UpD0.D6on Quiescence
M4	UpD3 D6&D13_MYCinduced MYC_overexpression MTORC1_SIG RibosomeBiogenesis
M5	UpPC Ig XBP1_Targets UPR ER_Golgi
M6	D6&D13&D20_MYCinduced Mitochondria MYC_overexpression
M7	UpPC
M8	MM_CD1_UP
M9	UpD0.D6on ZincFinger Quiescence
M10	UpPC Mitochondria OxPhos
M11	CellCycle
M12	Novel1
M13	Ribosome_Translation
M14	Lysosome
M15	Golgi Autophagy
M16	Novel2

The PGCNA-based network generation allowed the clustering of the examined genes into modules of co-expression across the time course and between the conditions tested. To further explore the MYC T58I-BCL2 overexpression effect per condition and time point a module expression value (MEV) was assigned

to each of the 16 clusters in the network. The contribution of each gene to the network through its strength and median Z-score was calculated and the ten top genes per module were used to generate a MEV. As displayed in Figure 3.28, based on the MEV allocated per module for each of the conditions tested, five different categories of co-expression modules were observed. In the first category were modules that behaved similarly between the control conditions and the *T58I-t2A-BCL2* samples across the time course. Such modules were the M1, M2 and M11 which showed enrichment at day 3 while they were depleted by day 13. Genes associated with B cell activation, BLIMP1 repressed targets, NF-κB signalling, cell migration and cell cycle process were assigned to M1, M2 and M11, suggesting that T58I-BCL2 overexpression did not result in differential regulation of these genes compared to the controls.

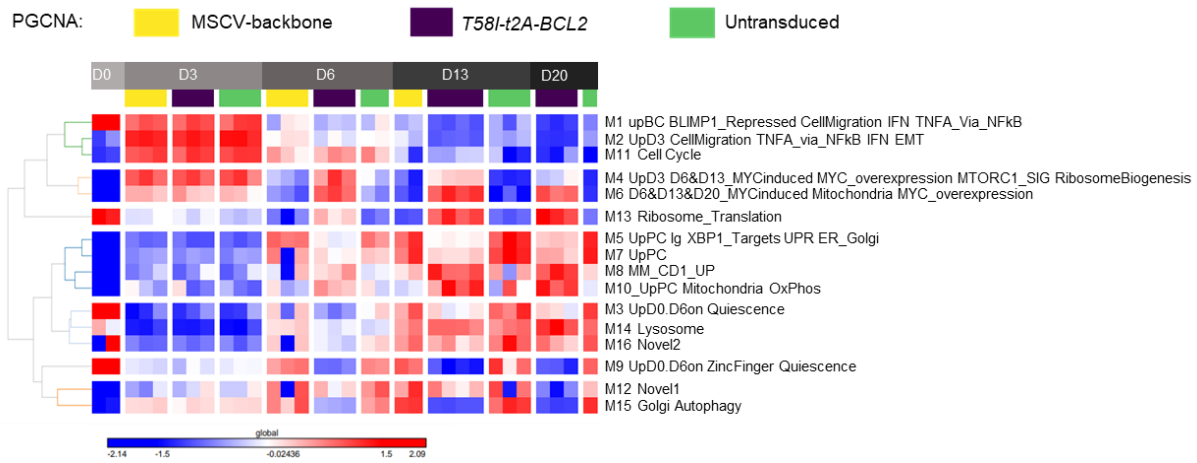

Figure 3.28 Modular gene expression across the time course and between conditions. Using Parsimonious Gene Correlation Network Analysis (PGCNA) 16 modules of gene co-expression were identified in the RNA-sequencing data. Hierarchically clustered heatmap of module expression values (MEVs) represents modular gene expression averaged to the rest of the genes assigned in the module based on Z-scores (-2.14 blue to +2.09 red) for the indicated conditions and time points. The 16 modules (indicated on the right) were labelled based on their enrichment for GO terms and signatures and the number of genes assigned per module. The analysis took place for day 0, day 3, day 6, day 13 and day 20 indicated samples. The PGCNA-derived heatmap was generated by Dr. Matthew Care. Data are representative of two independent experiments with two biological replicates (N= 2) and no technical replicates per experiment. The total number of donors tested as biological replicates was four (N= 4) out of which: two (N= 2) were assessed on day 0; three (N= 3) were assessed on day 3; two (N= 2) for the untransduced condition, three (N= 3) for each of the MSCV-backbone and *T58I-t2A-BCL2* transductions were assessed on day 6; three (N= 3) for the untransduced control, two (N= 2) for the MSCV-backbone and four (N= 4) for the *T58I-t2A-BCL2* condition were assessed on day 13; one (N= 1) for the untransduced condition and three (N= 3) for the *T58I-t2A-BCL2* transductions were assessed on day 20. No donors were assessed for the MSCV-backbone control on day 20. Missing donors in the

different conditions per time point were not evaluated due to low collected cell numbers and inadequate RNA concentrations for RNA-sequencing; D, day; M, module.

A second category contained modules with depleted expression in the controls and enrichment in the *T58I-t2A-BCL2* samples. M4, M6 and M13 with functional annotation related to known MYC-induced biological processes, showed enrichment only in the *T58I-t2A-BCL2* samples from day 6 onwards. On the contrary, M9, M12 and M15 showed the exact opposite pattern of enrichment and were induced in the controls and depleted upon MYC T58I-BCL2 overexpression.

The last two categories consisted of modules which were induced during normal PC differentiation represented by the control conditions and either had higher expression in the *T58I-t2A-BCL2* (M8, M10, M14) or showed reduced enrichment in comparison to the controls (M5, M7, M3, M16).

This analysis suggested that MYC T58I-BCL2 overexpression resulted in reduced, but not depleted, expression of DEGs assigned in M5, M7, and M3 related to PC differentiation and importantly immunoglobulin secretion. On the other side, DEGs assigned in M4, M6, M13 as well as M8, M10, M14 or M15, related to metabolic, ribosomal, and mitochondrial processes based on their functional annotations, showed increased expression mediated by MYC T58I-BCL2 overexpression. Thus, an abnormal gene expression profile was established in the *T58I-t2A-BCL2* samples characterized by induction of genes promoting aberrant PC differentiation and metabolic over secretory reprogramming.

3.6.8 Representation of MYC T58I-BCL2 overexpression-induced genes in the PGCNA modules

In previous analysis described in section 3.6.3 (Figure 3.19), 438 genes with higher expression in the *T58I-t2A-BCL2* samples in comparison to the untransduced were identified to maintain their upregulation at both day 6 and day 13 time points. It was reasoned that these 438 genes (Gene set A) comprised an interesting gene set demonstrating a consistent association with MYC T58I-BCL2 hyperfunction in the model system. Thus, their contribution to the modular co-expression resolved by PGCNA was assessed next across the time course and between conditions. Pairwise comparisons were performed between the gene set of interest and each of the gene lists derived from the 16 modules. As displayed in Table 3.11, the modules with the highest number of genes belonging to Gene set A were M6, M4, M13 and M10. These modules were the four most highly associated modules with MYC function-derived signatures. In addition, M1, M8, M14, M11 and M2 had lower counts of the Gene set A genes. No association was verified with the remaining modules and importantly with M5 and M7, associated with PC and antibody secretion-

related terms. This analysis further supported that MYC T58I overexpression is negatively affecting the secretory pathway of the transduced cells by not inducing regulation of its target genes.

Table 3.11 The contribution of an identified gene set in modular co-expression. Pairwise comparisons were used to assign the 438 common genes between day 6 and day 13 as identified using Venn diagrams in Figure 3.19, to each of the 16 modules (Table 3.10). The gene set of interest comprised DEGs with higher expression in the *T58I-t2A-BCL2* condition versus (vs) the untransduced and was indicated as Gene set A. Modules with no overlap were not included. Data are representative of two independent experiments with two biological replicates (N= 2) and no technical replicates per experiment. The total number of donors tested as biological replicates was four (N= 4) out of which: two (N= 2) were assessed on day 0; three (N= 3) were assessed on day 3; two (N= 2) for the untransduced condition, three (N= 3) for each of the MSCV-backbone and *T58I-t2A-BCL2* transductions were assessed on day 6; three (N= 3) for the untransduced control, two (N= 2) for the MSCV-backbone and four (N= 4) for the *T58I-t2A-BCL2* condition were assessed on day 13; one (N= 1) for the untransduced condition and three (N= 3) for the *T58I-t2A-BCL2* transductions were assessed on day 20. No donors were assessed for the MSCV-backbone control on day 20. Missing donors in the different conditions per time point were not evaluated due to low collected cell numbers and inadequate RNA concentrations for RNA-sequencing; M, module.

T58I-t2A-BCL2 vs Untransduced comparison

PGCNA-derived module	Genes per module
M6: D6&D13&D20_MYCinduced Mitochondria MYC_overexpression	202
M4: UpD3 D6&D13_MYCinduced MYC_overexpression MTORC1_SIG RibosomeBiogenesis	139
M13: Ribosome_Translation	51
M10: UpPC Mitochondria OxPhos	21
M1: upBC BLIMP1_Repressed CellMigration IFN TNFA_Via_NFkB	11
M8: MM_CD1_UP	8
M14:Lysosome	3
M11: CellCycle	2
M2: UpD3 CellMigration TNFA_Via_NFkB IFN EMT	1

3.7 Discussion

This Chapter aimed to investigate if overexpression of MYC protein combined with BCL2 would result in differentiation arrest and transformation of *in vitro* differentiated human PCs. A novel model system was established to overexpress MYC with BCL2 under conditions permissive for PC differentiation and tested for up to 20 days. MYC is a potent oncogene involved in many cancer types including B cell and PC malignancies (54, 311). In BL, MYC deregulation is identified as a primary oncogenic event while in DLBCL, and DHL MYC is a secondary genomic aberration often in combination with BCL2 (8, 17). T58I is a recurrent

mutation in these B cell cancer types and was utilised in the model system to verify increased MYC protein stability *in vitro* upon its deregulation. To our knowledge, MYC overexpression has not been previously studied in the context of normal human PC differentiation.

In the developed model system, the aim was to interrogate the effect of MYC overexpression during the process of differentiation from an activated B cell stage toward the PC phenotype. To achieve that the selected time point for the retroviral transductions was day 2 of the *in vitro* differentiation. This time point provided a 48-hour time frame for the initial memory population to acquire an activated B cell phenotype. It also allowed an additional 24-hour window for the transduced cells to be cultured under sustained T_{FH}-derived signals. In this post-transduction 24-hour window, CD40-mediated signalling supported by replenished IL-2 promoted survival and transduction recovery in the *in vitro* culture. In addition, to ensure successful MYC and BCL2 overexpression, high efficiency of the retroviral transductions was necessary. Retroviral constructs can only transduce cells that undergo active cell division. Activated B cell blasts are generated at an increased rate by day 2 in the model system. Thus, day 2 was considered an ideal time point to overexpress MYC and BCL2 at a pre-plasmablast stage and assess the original hypothesis.

Initially, it was hypothesised that MYC T58I and BCL2 hyperfunction might result in cellular transformation. In general, MYC deregulation alone is considered to not suffice to drive transformation (205). In an *in vitro* system modelling DLBCL, MYC combination with BCL2 overexpression resulted in the transformation and immortalization of GC B cells maintained under constitutive CD40 and IL-21 signalling (277). This effect was not observed in our model system assessing MYC-BCL2 overexpression under conditions permissive for PC differentiation. EdU 1 hour pulse assays showed that MYC T58I-BCL2 overexpressing cells had prolonged proliferation and eventually exit cell cycle. Thus, MYC T58I-BCL2 hyperfunction could not suffice to transform the transduced culture as originally hypothesised. Interestingly, MYC T58I-BCL2 overexpression induced an increase in the cell size and number of the transduced population accompanied by metabolic transcriptional reprogramming. A potential explanation for the observed prolonged cell cycle exit lies in overexpressed MYC acting as a determining factor of an aberrant number of divisions in the transduced cells while being unable to fully confer its oncogenic activity. Re-expression of MYC in the light zone B cells in the GC fuels their metabolic repertoire according to the strength of the T_{FH} cell signal they have received (171). Thus, the downstream MYC signalling determines the rounds of divisions they will undergo in the dark zone upon cyclic re-entry. Given that no transformation was observed in our model system, MYC overexpression might play a similar role under conditions permissive for PC differentiation. Enforced MYC-mediated metabolic reprogramming of the cells resulted in prolonged proliferation and

delayed cell cycle exit by approximately 18 days. A potential explanation could be that the absence of essential signals mimicking T_{FH} cell help, from the day 31 growth medium, could not support additional re-fuelling effect by the enforced MYC and the proliferation ceased. Another explanation could lie in the limitations of the retroviral transduction to adequately overexpress MYC long-term. Based on our gene expression study *MYC* and *BCL2* transcripts were more abundant than in the controls up to day 20. Although it is not expected, a potential loss of MYC-BCL2 overexpression between day 21 to day 31 could also result in the observed cell cycle exit. Such a technical limitation of the system would validate that acute MYC-BCL2 overexpression cannot mediate transformation under the assessed conditions permissive for PC differentiation.

MYC T58I-BCL2 acute overexpression resulted in an abnormal immunophenotype at the PC stage. Flow cytometry assessment showed inhibition of CD27 expression, severely delayed CD138 upregulation and abnormal CD19 and CD20 profiling. These changes were also observed at a transcriptional level favouring MYC T58I-BCL2-driven perturbation via transcriptional deregulation over post-transcriptional. In agreement with our observed phenotype, malignant plasmablasts and PCs could lose CD27 expression and maintain higher CD20 expression than in healthy counterparts (312, 313). Thus, MYC T58I-BCL2 overexpression resulted in changes in the composition of the surface proteins of the transduced cells that have been previously observed in abnormal PCs. This further supports the aberrant antibody secreting cell phenotype acquired in the model system upon MYC T58I-BCL2 overexpression.

A valuable finding was that the PC transcriptional programme was not inhibited although perturbed. Gene expression of *PAX5* and *PRDM1*, driving the B cell and the PC programmes respectively, showed the anticipated transcriptional regulation of repression and upregulation respectively as the time course proceeded. In addition to that, BLIMP1 protein was expressed at the plasmablast day 6 stage upon MYC T58I-BCL2 overexpression and in agreement with the gene expression data. Thus, MYC T58I and BCL2 overexpression did not block but perturbed the PC differentiation in the model system. As already mentioned above, overexpression of MYC and BCL2 was also tested in a previously established *in vitro* system modelling DLBCL (277). In this model, MYC and BCL2 were overexpressed in paediatric tonsil-derived GC B cells, instead of memory B cells used in our model, and the transduced cells received constitutive CD40 and IL-21 signalling (277). Under these conditions, persistent cell growth mimicking immortalisation and an intermediate GC B cell and plasmablast-like phenotype with a blockage toward terminal PC differentiation were established. In contrast, the findings of the present study, suggest that the equivalent oncogenic event combination when overexpressed in memory B cells under conditions

permissive for PC differentiation did not suffice to either immortalise or block the differentiation capacity of the transduced population. Thus, the current study further supports that MYC T58I in combination with BCL2 hyperfunction impact is cell-type and context-dependent (314).

An unclear concept regarding MYC function, frequently debated in recent literature, is its ability to act as a global gene expression amplifier over a target-specific one. The most broadly accepted hypothesis is that by default, MYC as a TF binds the DNA upon dimerization with its obligate partner MAX, at E-boxes (CACGTG) regulating the expression of specific target genes (215, 315). Upon MYC deregulation the MYC:MAX complex has also been identified to bind alternative E-boxes (CANNTG) and non-consensus motifs (204, 224, 316). As an alternative model of MYC function in cancer, the hypothesis of MYC acting as a global amplifier of actively and highly transcribed genes in an E-box-independent manner has been suggested (229, 230, 274). In our model of enforced MYC-T58I overexpression in combination with BCL2, enrichment of signatures and GO terms associated with well-defined MYC-related biology and classical E-box binding, was observed at a transcriptional level. Thus, the deregulation of MYC T58I-BCL2 via overexpression resulted in the regulation of MYC targets favouring the specific-targets MYC function hypothesis over its alternative.

An interesting finding of the present study was the secretory deficiency observed in the differentiating cells overexpressing MYC T58I-BCL2. Despite MYC T58I-BCL2-mediated hyperfunction, a perturbed but active PC differentiation programme and BLIMP1 expression and target regulation, such as *PAX5* and *BCL6* downregulation, remained intact. The key functionality of a plasmablast differentiating into a PC is the transition to secrete high amounts of antibodies (108, 122). This functional characteristic of the differentiated cells in the model system appeared to be compromised in the MYC T58I-BCL2 condition. This observation was coupled with noticeable *XBP1* repression driven by the MYC T58I-BCL2 hyperactivity while XBP1 targets were also transcriptionally repressed. Furthermore, MYC T58I-BCL2 overexpressing cells showed repression of the immunoglobulin genes for heavy and light chain production of the different isotypes. In addition to the repression observed in genes related to the secretory pathway, MYC T58I-BCL2 overexpressing cells also showed enrichment for known MYC function-associated metabolic pathways. Thus, an exchange of cellular resources seems to be at the core of MYC T58I-BCL2 overexpression impact. Hence, perturbed but not blocked PC differentiation, accompanies a switch in metabolic pathways away from the anticipated secretory reprogramming. With a focus on MYC protein, it was crucial to next investigate which regions of its protein structure are contributing to the observed aberrant PC phenotype and impaired antibody secretion.

Chapter 4 – MBII and MB0 domains of MYC are crucial for its overexpression-mediated effect on the plasma cell differentiation

4.1 Introduction

The effect of MYC T58I-BCL2 overexpression on human PC differentiation *in vitro* has been established. MYC protein both at physiological levels and upon deregulation requires interaction with its obligatory partner MAX for DNA binding (215, 221). MYC and MAX interaction takes place at the C-terminal site of MYC protein where MAX binds to the HLH-LZ motifs of MYC to generate the MYC:MAX complex. A DNA binding domain, BR, lies next to the HLH-LZ motifs at the C terminus of MYC. Upon MYC:MAX heterodimerization MYC interacts with the DNA through its BR domain at canonical and non-canonical E boxes (317). Disruption of MYC:MAX complex formation results in the abolishment of MYC function (274, 318). In addition to its DNA binding and HLH-LZ domains, MYC protein contains six highly conserved MYC homology boxes (MBs) (203). Interactors of MYC via these MB domains confer downstream molecular activities to mediate the regulation of its targets and function. Three of these MB domains are located in the core of MYC protein MBIIIa, MBIIIb and MBIV. MBIIIb has been identified to contribute to the DNA binding of MYC on target genes via its interactor WDR5 (208).

A transactivation domain (TAD) is located at the N-terminal site of MYC. TAD contains the remaining three MYC MBs, namely MB0, MBI and MBII. TAD MB domains have been of central interest in MYC studies and identified to have distinct and synergistic roles in MYC function. MB0 directly interacts with TFIIF, one of the general TFs participating in the formation of the RNA polymerase II transcription preinitiation complex (240). Thus, MB0 has been associated with tumour growth via mechanisms related to the regulation of transcription elongation (240). MBI acts as a phosphodegron for MYC protein containing two critical amino acids regulating its proteasomal degradation, T58 and S62 (199, 319). Phosphorylated T58 interacts with PIN1 and PP2A mediating dephosphorylation of S62 resulting in unstable MYC (204, 320, 321). At this stage, recognition of phosphorylated T58 by the ubiquitin E3 ligase FBXW7 initiates MYC ubiquitination activating its degradation in the proteasome (239, 270). Deletion of the MBI of MYC has shown small differences in MYC-mediated transformation to MYC WT upon ectopic overexpression (234, 240). On the contrary, deletion of the MB0 indicated impaired cellular proliferation and tumour growth and a requirement for full MYC oncogenic activity (240). Both MB0 and MBI were required for the transformation

of rat embryonic fibroblasts (REF) upon MYC and RAS overexpression (322). Thus, differential roles in MYC oncogenic activity have been previously described for the MB0 and MBI domains.

The MBII domain of MYC is considered indispensable for all its biological activities and is required for MYC-mediated transformation (212, 234, 314). MYC DNA binding and target gene expression have been associated with chromatin remodelling mediated by MYC interactors with histone acetyltransferase (HAT) activity (323). TRRAP is a MYC co-factor interacting with its MBII domain and a component in complexes such as TRRAP/GCN5 (STAGA) and TRRAP/TIP60 (NuA4 in yeast) (204, 248, 323, 324). HAT activity of these complexes is conferred via GCN5 and TIP60 which acetylate histone H3 and H4 respectively and facilitate MYC target transcription initiation (323). Additional MBII interactors have been reported such as TIP48 and TIP49 ATP-ases which can be recruited either as components of TRRAP complexes or bind directly to the MBII domain of MYC (251, 323). Deletion of MBII in overexpressed MYC lacked interaction with TRRAP and other co-factors of the TRRAP/GCN5 and TRRAP/TIP60 complexes and showed no tumour growth in a breast cancer mouse model (240). Thus, MYC-mediated tumour initiation depends on the activity of complexes with HAT components upon their recruitment to the MBII domain.

Here, deletion mutants for each of the MB0, MBI and MBII domains of MYC were overexpressed in the established model system in combination with BCL2. Their effect on MYC function was examined in an overexpression context and under conditions permissive for PC differentiation. In addition, the impact of a MYC wild type (WT) ectopically expressed protein was investigated and compared to the MB deletion mutants in the model system.

4.2 Generation of constructs with MYC wild type or ΔMB0, ΔMBI, ΔMBII mutants, and BCL2

MYC protein has two major isoforms, isoform 1 and isoform 2 which differ in their initiation of transcription codons with the former having an alternative CTG and the latter a canonical ATG (74). MYC isoform 1 has a 15 amino acid extension at the N-terminal site of the protein which has been implicated with its ability to regulate gene expression via a C/EBP-DNA binding site in addition to the canonical E-box (231). Both MYC isoforms 1 and 2 have been reported as deregulated in BL, but genetic aberrations such as translocations or mutations in exon 1 have resulted in the loss of MYC isoform 1 in many BL-derived cell lines (74, 231). In addition, MYC isoform 2 has been more frequently associated with tumorigenesis inducing aberrant cell growth upon its deregulation (231, 325, 326). Initial results on MYC-BCL2

overexpression in the *in vitro* differentiation system were described in the results of Chapter 3. The retroviral vector used to achieve MYC overexpression was provided by the Hodson group and contained the isoform 1 of the MYC protein and an equivalent to T58I substitution. In addition, its non-canonical CTG codon had been modified into an ATG encoding methionine. To ensure a more physiological initiation of transcription of the *MYC* sequence and the optimum MYC-mediated hyperactivity and cell growth, all the additionally generated retroviral vectors described in this Chapter and in the next one, Chapters 4 and 5 respectively, were based on the WT sequence of *MYC* encoding for isoform 2.

To test the contribution of MB0, MBI or MBII domains in the MYC overexpression-driven changes on PC differentiation, each of their sequences were deleted in *MYC* cDNA prior to the *t2A-BCL2* sequence (Appendix 7, Appendix 8 and Appendix 9). In addition, the WT *MYC* isoform 2 sequence, encoding a T58 intact and no T58I substitution, was generated and included to test the MYC overexpression effect in combination with BCL2 in the model system (Appendix 6). As displayed in Figure 4.1A and Figure 4.1B, new vectors based on the MSCV-IRES-human CD2 backbone were designed containing the inserts of either *MYC* WT or *Δ*MB0, *Δ*MBI, *Δ*MBII and *BCL2* cDNA sequences.

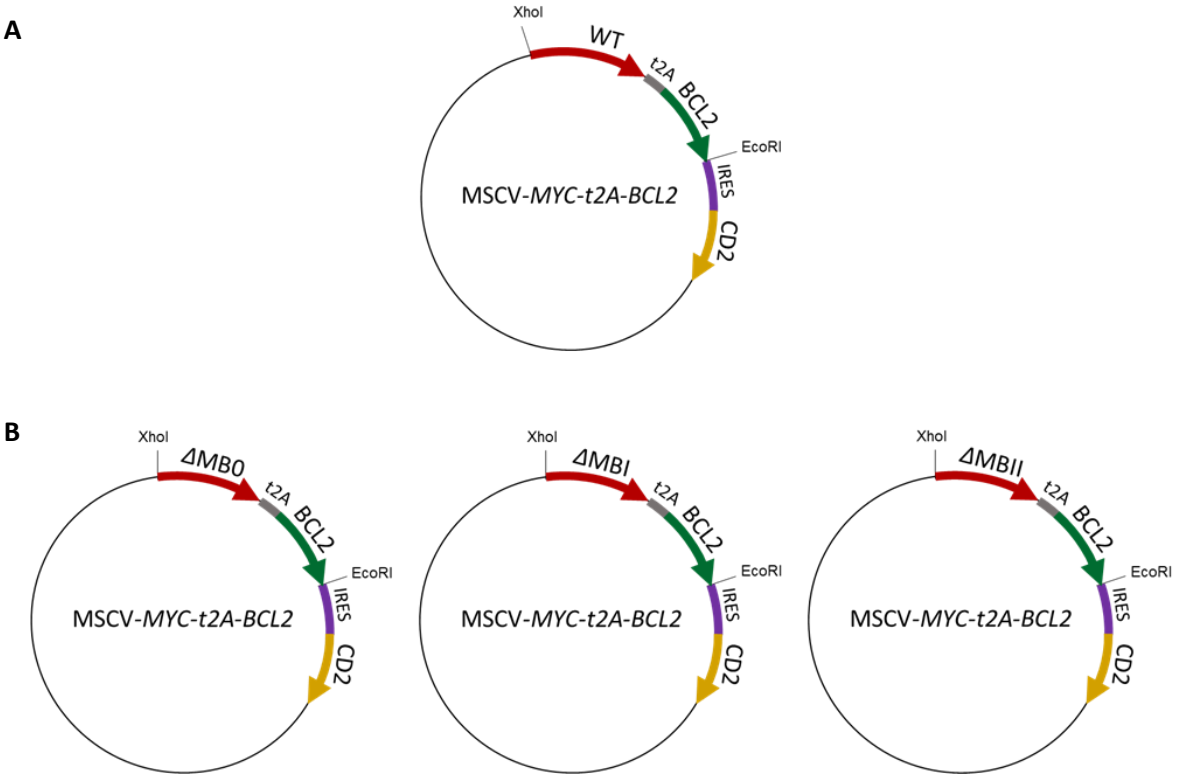

Figure 4.1 MYC WT and MB0, MBI, MBII deletion mutants' vectors. Graphical representation of the constructs designed for overexpression of (**A**) MYC WT and (**B**) *Δ*MB0 (left), *Δ*MBI (middle) and *Δ*MBII (right). The inserts

contained the cDNA sequence encoding for MYC isoform 2 and were cloned into the MSCV-IRES-human CD2 backbone vector. The unique sites of the restriction enzymes XhoI and EcoRI were utilised as indicated on the map of each construct at the start and end site of their inserts respectively.

4.2.1 Cloning into the MSCV-IRES-human CD2 backbone

Inserts of MYC *WT-t2A-BCL2*, *ΔMB0-t2A-BCL2*, *ΔMBI-t2A-BCL2* and *ΔMBII-t2A-BCL2* were designed and then synthesized and cloned commercially into pIRES2-EGFP plasmid by MRC PPU Reagents and Services, University of Dundee. Subcloning of the inserts into the retroviral MSCV-IRES-human CD2 constructs and subsequent diagnostic digests were conducted by the master's student, Eden Page. Bacterial transformations were performed with the sub-cloned constructs and multiple single colonies were selected. To validate the correct insert for each vector, diagnostic digests were performed on the selected single colonies using the unique restriction enzymes XhoI and EcoRI. As depicted in Figure 4.2, digests with both enzymes validated the anticipated DNA band size when compared to the molecular size of the DNA ladder on agarose gel electrophoresis. Single digests and undigested samples were included as controls. Thus, for each of the vectors tested both the single digest conditions showed the full vector size in a linear plasmid formation including the insert of interest. For the *WT-t2A-BCL2*, *ΔMB0-t2A-BCL2*, *ΔMBI-t2A-BCL2* and *ΔMBII-t2A-BCL2*, the total vector size was 8,739 bp, 8,688 bp, 8,682 bp and 8,691 bp. In the double digests, the size of the insert was also validated as anticipated being 2,165 bp, 2,114 bp, 2,108 bp and 2,117 bp respectively. These results verified the correct insert size for the four generated retroviral vectors.

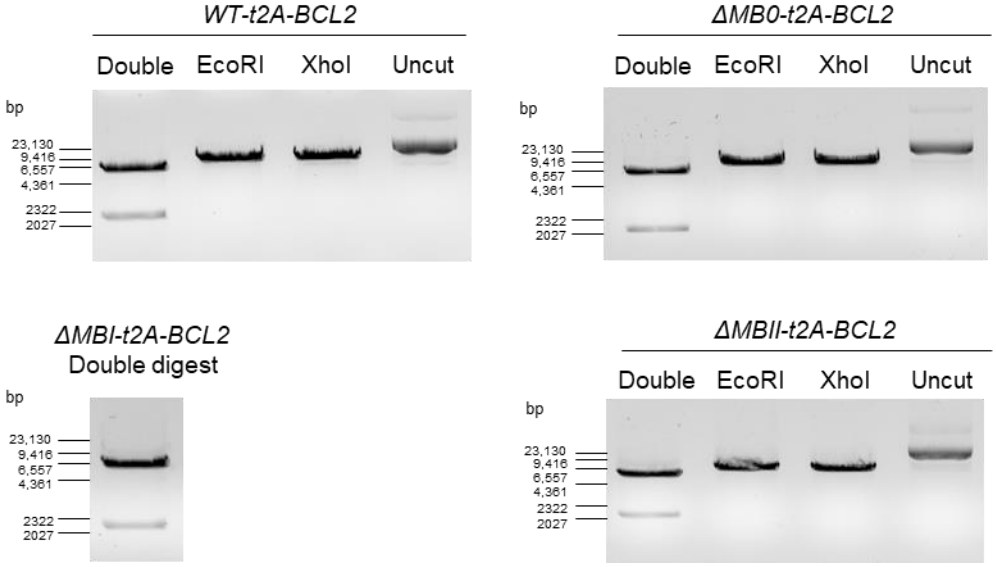

Figure 4.2 Subcloning validation of the MYC WT and deletion MB0, MBI, MBII mutant vectors into the MSCV-backbone retroviral plasmid. Representative images of ethidium bromide-stained diagnostic digests run on 1% agarose gel. As indicated above the gel image - double digest with both EcoRI and XhoI, single digests with either EcoRI or XhoI and undigested (uncut) conditions were assessed for the new retroviral vectors *WT-t2A-BCL2* (top left), *ΔMB0-t2A-BCL2* (top right), *ΔMBI-t2A-BCL2* (bottom left), with only a double digest sample, and *ΔMBII-t2A-BCL2* (bottom right). Data of diagnostic digests were generated by Eden Page. Ladder DNA band sizes are indicated at the left side of each gel; bp, base pairs.

4.2.2 Virus generation and validation

Having confirmed the cloned inserts of the retroviral constructs containing *MYC* WT, ΔMB0, ΔMBI or ΔMBII, in combination with *BCL2*, the next step was to produce viral stocks. Validation of the produced virus was conducted by transducing HEK-293 cells and evaluating the transduction efficiency based on CD2 expression levels assessed with flow cytometry 72 hours later. As displayed in Figure 4.3, the untransduced negative control had 0.38% of CD2 positive cells, representing background staining, while a previously validated MSCV-backbone virus was used as a positive control with transduction efficiency at 60.9% of $CD2^+$ cells. High transduction efficiency was verified for all the viral preparations with CD2 positivity to be quite higher than in the untransduced condition or at least as good as in the MSCV-backbone positive control. The *WT-t2A-BCL2* and *ΔMB0-t2A-BCL2* samples had more than 90% CD2 positive cells, while the *ΔMBI-t2A-BCL2* and *ΔMBII-t2A-BCL2* viruses reached 78.4% and 72.2% in CD2 positivity respectively. These results validated the generated viral stocks which were stored at -80°C and used in all the following experiments described in this Chapter.

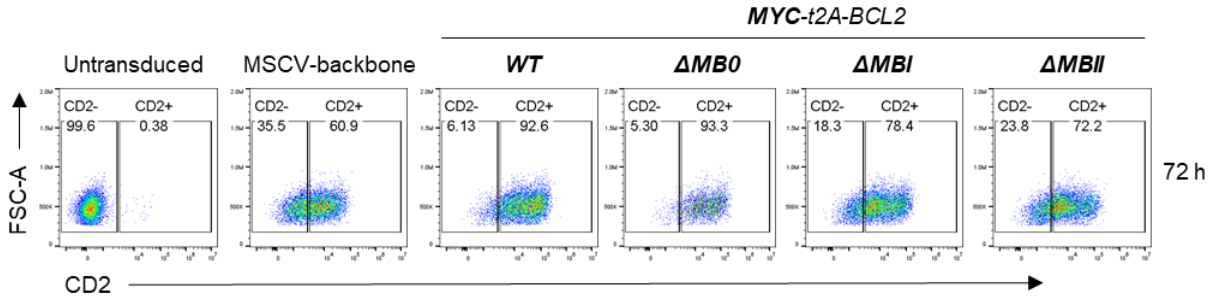

Figure 4.3 Transduction of HEK-293 cells for generated viral stocks validation. HEK-293 adherent cells were seeded 24 hours in advance and transduced with either of the *WT-t2A-BCL2*, *ΔMB0-t2A-BCL2*, *ΔMBI-t2A-BCL2* or *ΔMBII-t2A-BCL2* viruses containing the sequence encoding for MYC isoform 2. MSCV-backbone already validated frozen virus and untransduced controls were also included. Assessment of CD2 positivity levels was conducted 72 hours post-transduction with flow cytometry; h, hours.

4.3 *In vitro* screening of MYC ΔMB0, ΔMBI and ΔMBII domain mutants with BCL2 overexpression in the model system

The next goal was to assess overexpression of the MYC WT, and the TAD MB deletion mutants in combination with BCL2 in the *in vitro* differentiation. As described in Chapter 3, differentiating memory B-cells were transduced on day 2 after activation to overexpress the new retroviral construct sequences of interest. The *in vitro* differentiation conditions were followed up to day 13. Assessment of phenotypic changes mediated by transduction was conducted in each condition at the activated B cell- day 3, plasmablast- day 6 and PC- day 13 stages. In this new experimental set-up, untransduced cells and MSCV-backbone transductions provided the controls against which to compare MYC WT-BCL2 and each of the *ΔMB-t2A-BCL2* conditions. The *in vitro* model system provided a valuable platform to explore the solely driven contribution of each of the MB0, MBI and MBII domains in MYC function in a hyperactivity context during PC differentiation.

4.3.1 MYC wild type and MB0, MBI, MBII deletion mutants with BCL2 overexpression in the model system

Upon transductions with MSCV-backbone, *WT-t2A-BCL2*, *ΔMB0-t2A-BCL2*, *ΔMBI-t2A-BCL2* and *ΔMBII-t2A-BCL2,* the CD2 reporter expression levels were assessed on day 3, day 6 and day 13 with flow cytometry. A summary of the flow cytometry CD2 expression data, collected from all the donors tested, is displayed in Figure 4.4.

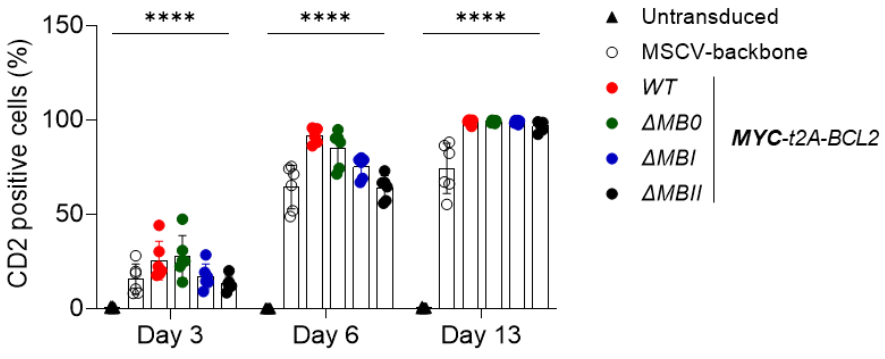

Figure 4.4 Evaluation of CD2 reporter expression levels upon transduction with the MYC WT and MB deletion-BCL2 mutants. Flow cytometry data summary of the CD2 expression percentages on day 3, day 6 and day 13 for the indicated conditions. One-way ANOVA. Data are representative of three independent experiments with two

biological replicates (N= 2) and no technical replicates per experiment. The total number of donors tested as biological replicates was six (N= 6). Bars and error represent mean and standard deviation (SD); **** P < 0.0001.

At day 3, CD2 frequency was observed in all the transduced conditions to be higher than the untransduced control confirming successful transduction after 24 hours. In comparison to the day 3 CD2 percentages that were below 50%, a gradual increase in the CD2 positive cells was observed for the next two time points tested. On day 6 the CD2 expression levels appeared significantly increased and consistently above 60% for all the transduced conditions. The differences observed in CD2 expression between the transductions at day 3 and day 6 were not maintained at day 13 where an even greater increase was observed in the transduced samples. These results validated that all the performed viral transductions resulted in a consistent increase in CD2 protein expression between the time points tested establishing high CD2 levels by day 13 of the model system.

4.3.2 Validation of protein overexpression

To confirm MYC and BCL2 protein overexpression, upon transduction, protein lysates were collected from the *in vitro* cells at day 6, the plasmablast anticipated stage of the model system. As displayed in Figures 4.5A and 4.5B, western blot experiments validated that MYC and BCL2 were overexpressed in the *WT-t2A-BCL2* and the three TAD MB domain deletion mutant conditions in comparison to the MSCV-backbone sample. MYC WT protein consists of 439 amino acids with its MB0 domain (aa 16-32) occupying 17 residues, its MBI domain (aa 45-63) occupying 19 residues and its MBII domain (aa 128-143) composed of 16 residues. Thus, deletion of the MBI domain of MYC was anticipated to generate the smallest in size MYC mutant protein (aa 420) followed by the *Δ*MB0 (aa 422) and *Δ*MBII (aa 423). The detected MYC protein bands agreed with the anticipated size for each of the MB deletion mutants in comparison to the MYC WT band as displayed in Figure 4.5A. Also, BLIMP1 expression was detected at similar levels across all the conditions tested verifying the findings described in the Results section 3.5.4. This analysis confirmed that the *WT-t2A-BCL2* and the MB deletion mutants performed as anticipated upon their introduction to the model system.

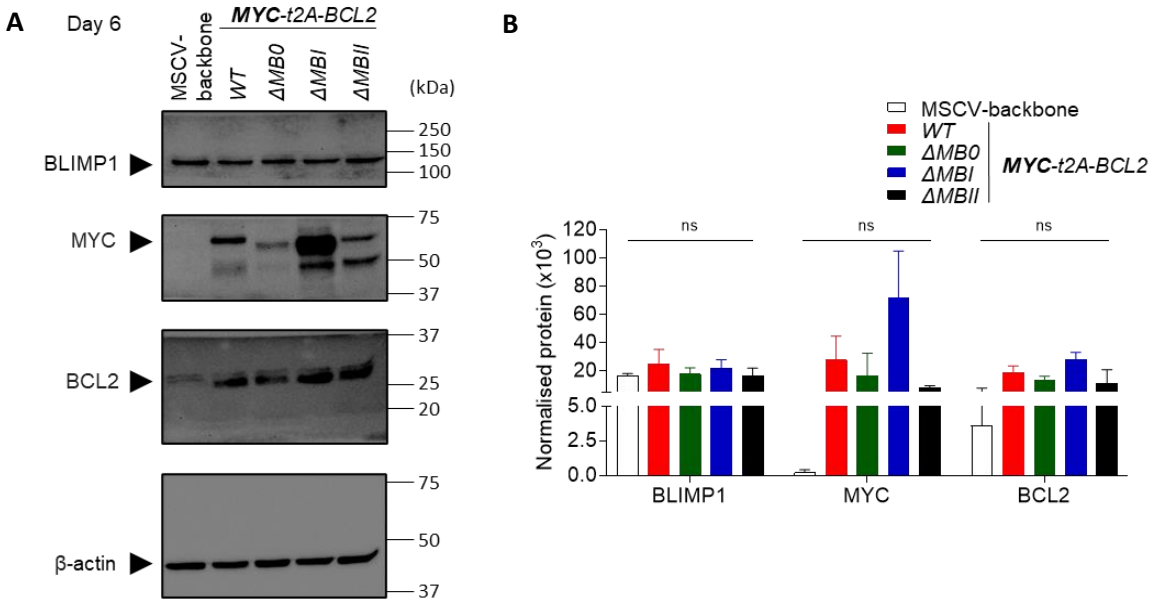

Figure 4.5 Protein detection via western blot validated successful overexpression in the MB deletion mutants. Day 6 total protein lysates were generated and assessed for their BLIMP1, MYC, BCL2 and β-actin expression levels with western blot. (**A**) Representative image of the SDS-polyacrylamide gel performed to detect protein expression at the indicated conditions; kDa, kilodalton. (**B**) Summary graph of the quantified protein expression upon normalisation to the β-actin loading control for each of the conditions as indicated per gel lane. Densitometry values of the quantified protein bands were obtained with ImageJ software. One-way ANOVA (B). Data are representative of two independent experiments with one biological replicate (N= 1) and no technical replicates per experiment. The total number of donors tested as biological replicates was two (N= 2). Bars and error represent mean and standard deviation (SD); ns, not significant.

Loss of function for the MBI domain via deletion resulted in a 3-fold increase in MYC protein levels in comparison to WT. As previously mentioned in section 1.5.5 of Chapter 1, MBI acts as a crucial domain regulating MYC protein degradation through the proteasome. Thus, it was reasoned that the deletion of critical residues associated with this process such as T58 and S62, resulted in the increased amount of MYC protein in the *ΔMBI-t2A-BCL2* condition upon overexpression in comparison to the *WT-t2A-BCL2* lysates. In parallel, reduced was the MYC protein detected upon its overexpression in the *ΔMB0-t2A-BCL2* and *ΔMBII-t2A-BCL2* conditions. This decrease indicates that the MB0 and MBII domains have a role in the levels of MYC WT protein expression in the model system. The different levels of overexpressed MYC protein observed in the three MB deletion mutants could affect the MYC hyperfunction effect on *in vitro* PC differentiation. In combination with the disruption of its MB0, MBI or MBII domains via deletion, different MYC protein expression levels in the assessed deletion mutants could contribute to distinct

phenotypes in comparison to the *WT-t2A-BCL2* condition. Despite the differences observed in the intensity of the MYC protein bands between the MB deletion mutants, these results validated the successful overexpression of MYC compared to the MSCV-backbone samples in all the conditions tested.

4.3.3 Increase in cell survival and number upon MYC WT-BCL2 hyperactivity

In the *in vitro* differentiation system, the time window between day 3 and day 6 is characterized by extensive proliferation up to the plasmablast stage. The proliferation rate from day 6 onwards is reduced and the cells end up exiting the cell cycle completely by day 13 representing the PC stage (282). Thus, absolute cell counts were performed to get a better understanding of the effect of MYC WT or MYC MB deletion mutants with BCL2 overexpression on cell numbers and proliferation rate. Total sample collection allowed the calculation of absolute cell numbers per time point tested. As depicted in Figure 4.6, at day 3 similar cell numbers were observed throughout the conditions. At day 6 higher cell numbers were detected for the *WT-t2A-BCL2* condition in four out of the six donors tested in three independent experiments. The two donors with the lowest day 6 cell count, derived from the same experiment suggesting experimental and maybe donor variation. Also, they were identified as the donors resulting consistently in the lowest cell counts in all the conditions tested on day 6. On day 13, cell counts of these two donors were incidentally not performed during experimental processing because of time limitations faced on the day. The cell counts of the remaining four donors from two independent experiments showed a more established pattern of cell numbers between the different conditions than the day 3 and day 6 samples. The *WT-t2A-BCL2* had the highest number of cells on day 13 followed by the *ΔMBI-t2A-BCL2* and then by the *ΔMB0-t2A-BCL2* transductions. Notably, overexpression of MYC ΔMBII-BCL2 had similar cell counts to the controls. These results suggest that MBII and MB0 loss of function abrogated and reduced respectively, the ability of the overexpressed MYC protein to drive an increase in cell numbers at day 13 of the model system.

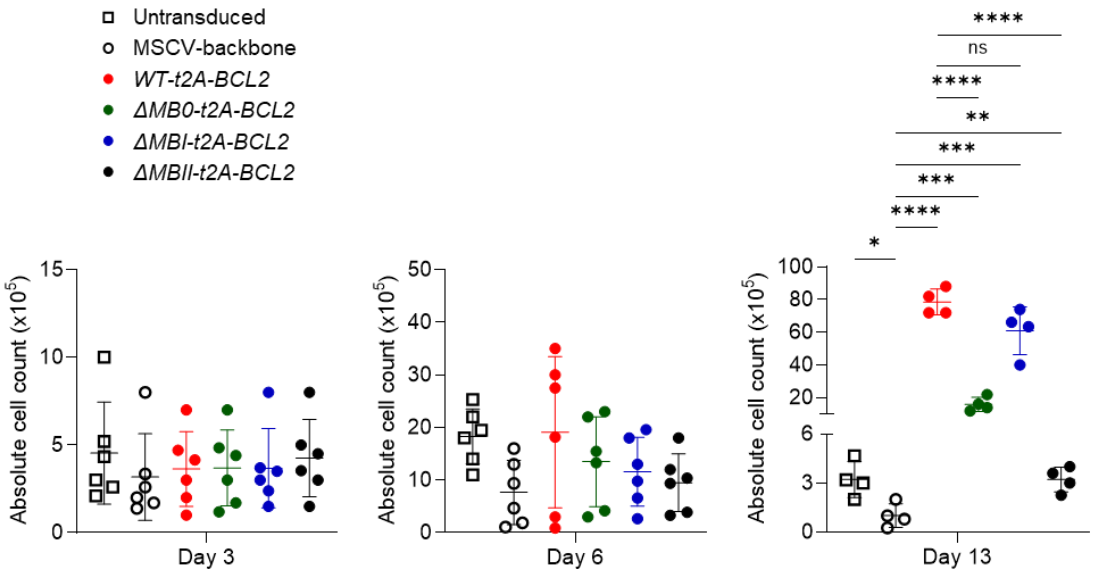

Figure 4.6 Calculation of absolute cell counts upon transduction. Samples were collected and cell counting, using a hemocytometer and trypan blue exclusion, was conducted on day 3, day 6 and day 13 for the indicated conditions tested. The figure shows summary graphs of the cell counts performed from all the donors tested. Unpaired two-tailed Student's *t*-test. For day 3 and day 6 time points, data are representative of three independent experiments with two biological replicates (N= 2) and no technical replicates per experiment. The total number of donors tested as biological replicates was six (N= 6). For the day 13 time point, data are representative of two out of the three independent experiments with two biological replicates (N= 2) and no technical replicates per experiment. The total number of donors tested as biological replicates was four (N= 4). Bars and error represent mean and standard deviation (SD); ns, not significant; * $P < 0.05$; ** $P < 0.01$; *** $P < 0.001$; **** $P < 0.0001$.

4.3.4 MYC-mediated cell growth increase was reduced in the ΔMBII and ΔMB0 mutants

Having shown that MYC WT-BCL2 overexpression led to higher cell numbers followed by the *ΔMBI-*, *ΔMB0-* and *ΔMBII-t2A-BCL2* conditions in a hierarchical order, the effect of MYC MB mutants on cell growth was evaluated next. Based on previous observations made in section 3.5.1 of Chapter 3, *T58I-t2A-BCL2* drove increased cell size. Flow cytometry analysis with FSC-A versus SSC-A parameters showed a similar effect being observed in the *WT-t2A-BCL2* condition. In detail, as Figures 4.7A and 4.7B show, no differences were detected on day 3 between the controls and the transduced cells. Interestingly though at day 6 and day 13, differences were observed following a similar hierarchy to the Figure 4.6 day 13 samples. MYC WT-BCL2 overexpression resulted in increased survival and cell size at a similar rate to the *ΔMBI-t2A-BCL2* samples. In contrast, slightly decreased was the cell size in the *ΔMB0-t2A-BCL2* samples followed by the

ΔMBII-t2A-BCL2 condition which was more similar to the controls. These results agreed with the previously observed hierarchal importance of the MBII, MB0 and lastly the MBI domains to the overexpressed MYC effect on the *in vitro* culture.

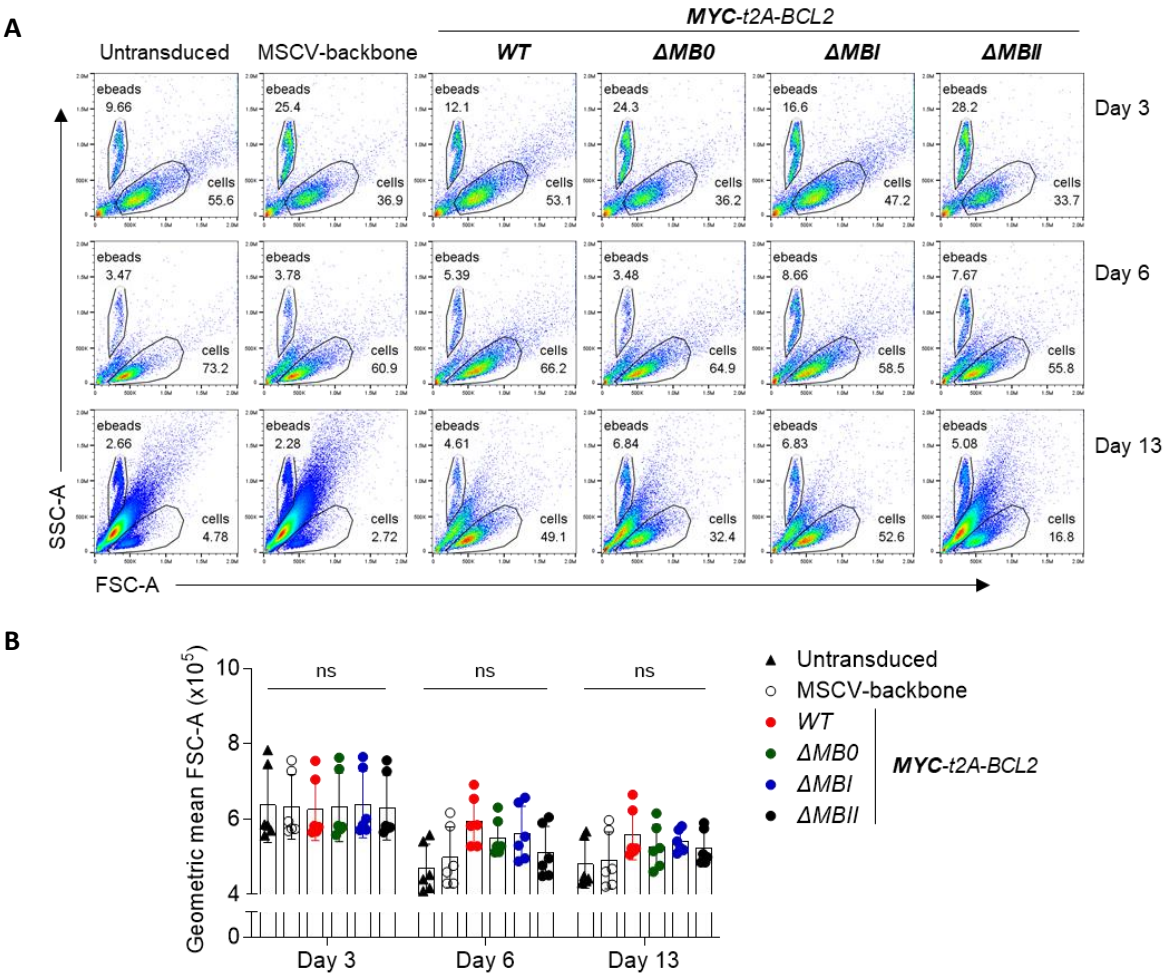

Figure 4.7 Cell size estimation based on FSC-A and SSC-A flow cytometry parameters. (**A**) Representative flow cytometry plots from day 3, day 6 and day 13 samples of the indicated conditions. The cellular populations were assessed under comparison of the FSC-A versus SSC-A parameters on the viable gate named as cells in the figure plots. A gate named ebeads existed to distinguish the cell sample from the counting beads added to the sample and was not included in the current analysis. (**B**) Graph of the summary data from all donors tested with flow cytometry to calculate the geometric mean of the FSC-A parameter assessing cell size changes in the indicated conditions and time points. One-way ANOVA (B). Data are representative of three independent experiments with two biological replicates (N= 2) and no technical replicates per experiment. The total number of donors tested as biological replicates was six (N= 6). Bars and error represent mean and standard deviation (SD); ns, not significant.

4.3.5 The overexpressed MYC-mediated effect is dependent on its MBII and MB0 domains

To investigate the immunophenotype of the transduced cells flow cytometry was conducted upon MYC WT-BCL2 or MYC MB deletion mutants-BCL2 overexpression. In Figure 4.8, the cells were assessed for their CD19 and CD20 expression.

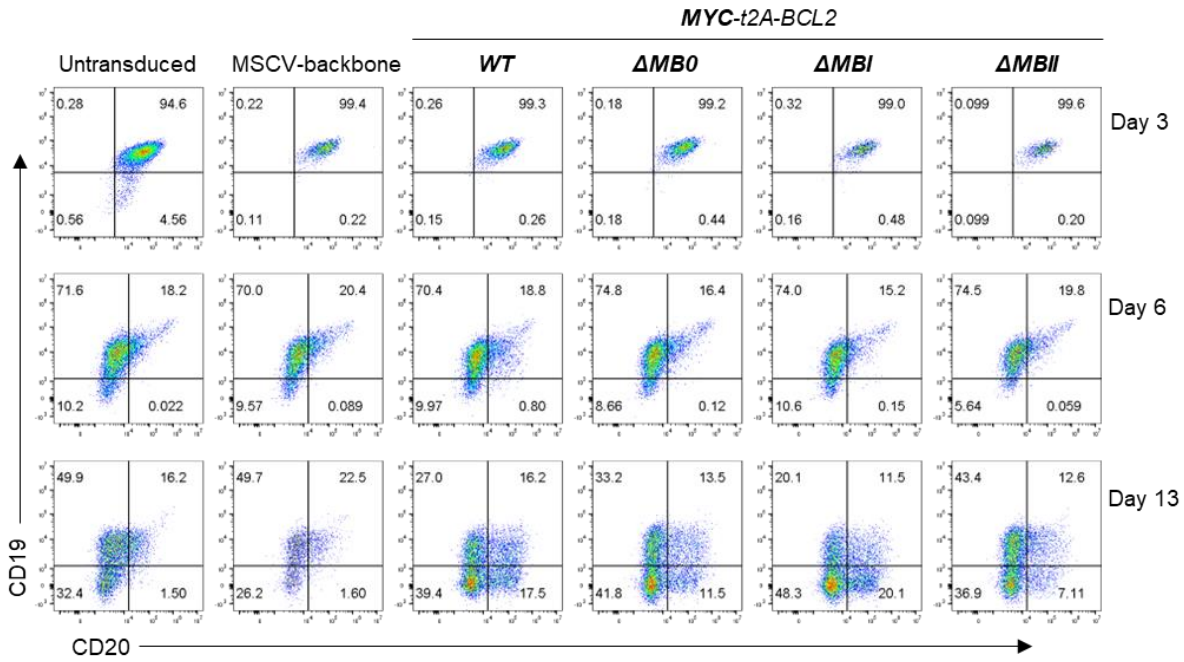

Figure 4.8 MYC WT and MB deletion mutants driven changes in CD19 and CD20 expression assessed with flow cytometry. Representative flow cytometry plots from day 3, day 6 and day 13 samples of the indicated conditions. The cellular populations were assessed under CD19 (y-axis) versus CD20 (x-axis) expression. The cells assessed in the transduced conditions were $CD2^+$ pre-gated. Data are representative of three independent experiments with two biological replicates (N= 2) and no technical replicates per experiment. The total number of donors tested as biological replicates was six (N= 6).

As previously observed in an overexpression context, the day 3 time point showed no differences between the controls and the MYC-BCL2 conditions tested with 94% to 99% of the population being $CD19^+CD20^+$ as anticipated. At the plasmablast stage of day 6, approximately 70% of the cells were $CD19^+CD20^-$ in both the untransduced and MSCV-backbone controls indicating successful differentiation based on these two markers. A similar fraction of the cells appeared to be $CD19^+CD20^-$ in the *WT-t2A-BCL2* and the three MB deletion mutant conditions. The PC $CD19^+CD20^-$ population at day 13 was around 49% in the untransduced and MSCV-backbone controls. A significant decrease was observed upon MYC WT-BCL2 or *Δ*MBI-BCL2 overexpression with only 27% and 20.1% of the cells being $CD19^+CD20^-$ respectively. An increase in the

$CD19^{-}CD20^{-}$ cells was observed while also the $CD19^{+}CD20^{+}$ and $CD19^{-}CD20^{+}$ populations were maintained at higher frequencies showing an abnormal phenotype. The *ΔMB0-t2A-BCL2* condition resulted in 33.2% $CD19^{+}CD20^{-}$ PCs and showed higher frequencies of $CD19^{-}CD20^{-}$ and $CD19^{-}CD20^{+}$ populations than the controls. Upon deletion of the MBII domain, 43.4% of the cells were $CD19^{+}CD20^{-}$ approaching the percentage of the control conditions. At the same time slightly increased was the $CD19^{-}CD20^{-}$ population in comparison to the controls.

As displayed in Figure 4.9, normal levels of CD27 and CD38 expression were observed on day 3 for all the conditions tested, representing the activated memory B cell phenotype. At day 6, approximately 73%-76% of the cells differentiated into $CD27^{+}CD38^{+}$ in the control samples. A reduction of this population was observed in the *WT-t2A-BCL2* condition showing impaired CD27 upregulation with increased $CD27^{-}CD38^{+}$ cells at 50.4%. The deletion mutants of MYC showed marginal changes at day 6 but at day 13 a more perturbed CD27 expression was observed. In agreement with the previously identified hierarchical order, at day 13 CD27 expression was inhibited in the MYC WT-BCL2 overexpressing cells and this was also observed in the *ΔMBI-t2A-BCL2* condition. Deletion of MB0 resulted in a reduction of the CD27 levels at 64.6% in the $CD38^{+}$ compartment. Deletion of the MBII domain allowed normal differentiation into a $CD27^{+}CD38^{+}$ population similarly to the controls.

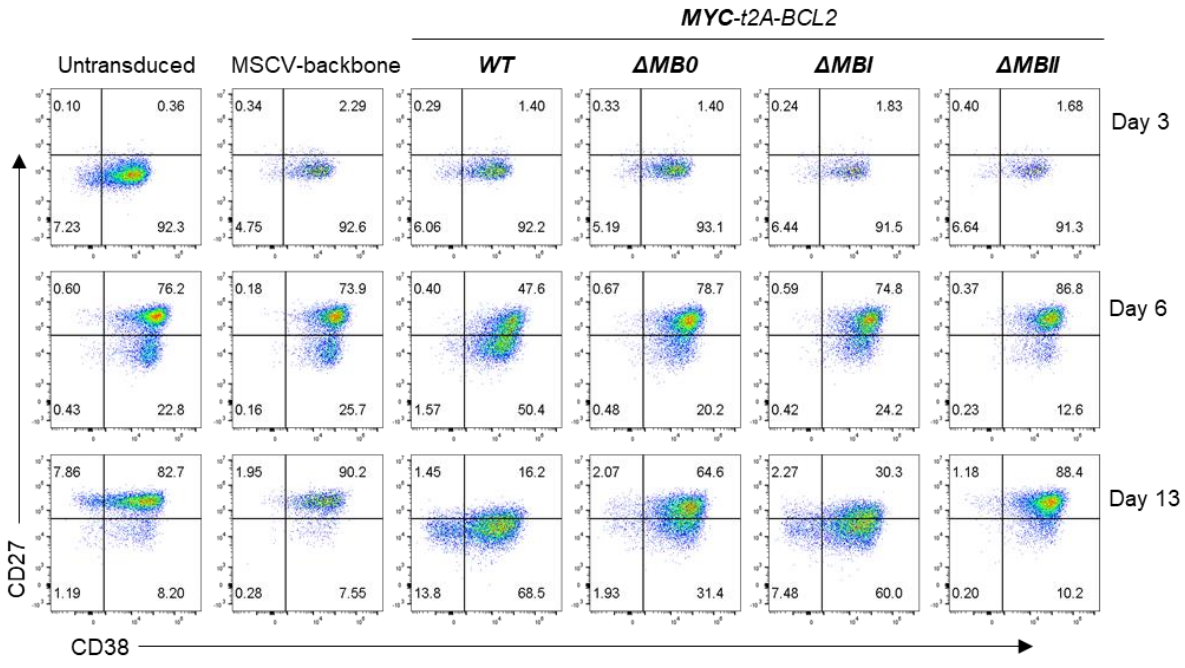

Figure 4.9 MYC WT and MB deletion mutants driven changes in CD27 and CD38 expression assessed with flow cytometry. Representative flow cytometry plots from day 3, day 6 and day 13 samples of the indicated conditions.

The cellular populations were assessed under CD27 (y-axis) versus CD38 (x-axis) expression. The cells assessed in the transduced conditions were $CD2^+$ pre-gated. Data are representative of three independent experiments with two biological replicates (N= 2) and no technical replicates per experiment. The total number of donors tested as biological replicates was six (N= 6).

PC differentiation is characterized by CD138 expression. As Figure 4.10 represents, on day 3 all the conditions tested were similar to the controls with a $CD38^+CD138^-$ phenotype. In addition, no differences appeared upon MYC WT-, *Δ*MB0-, *Δ*MBI-, or *Δ*MBII-BCL2 overexpression at day 6 with very few cells expressing CD138. CD138 upregulation is a key feature of the day 13 differentiated PC population. MYC WT- and *Δ*MBI-BCL2 overexpression showed a significant reduction in CD138 upregulation with a partial decrease in the *ΔMB0-t2A-BCL2* condition while greater was the observed CD138 expression after deletion of the MBII domain.

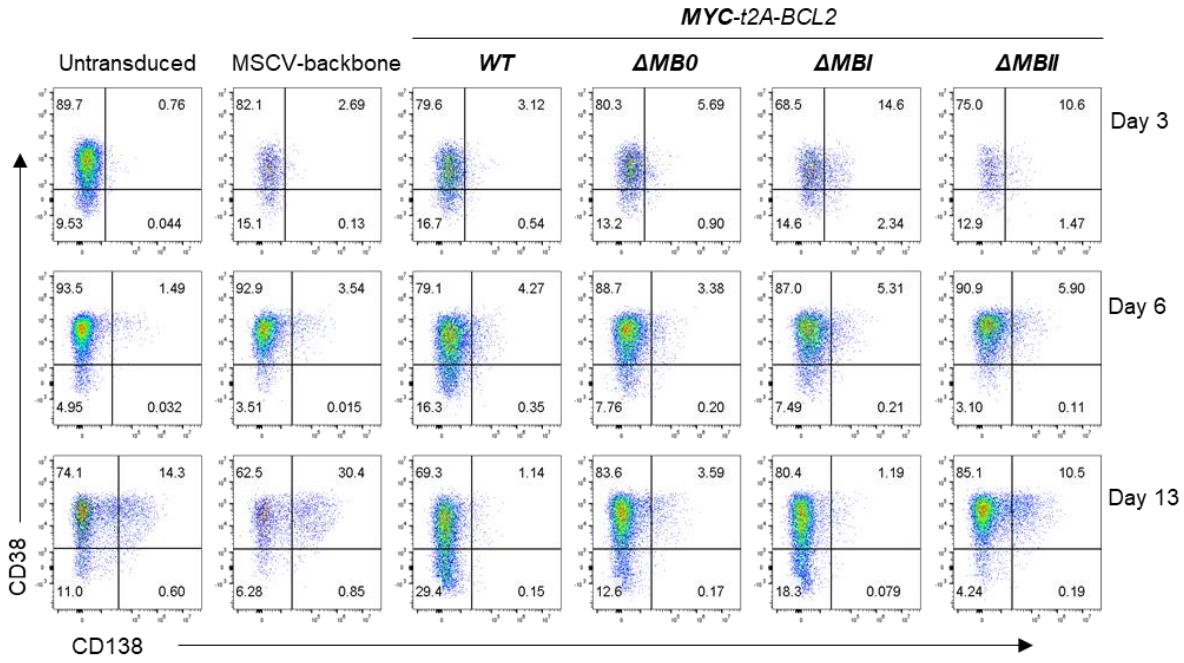

Figure 4.10 MYC WT and MB deletion mutants driven changes in CD38 and CD138 expression assessed with flow cytometry. Representative flow cytometry plots from day 3, day 6 and day 13 samples of the indicated conditions. The cellular populations were assessed under CD38 (y-axis) versus CD138 (x-axis) expression. The cells assessed in the transduced conditions were $CD2^+$ pre-gated. Data are representative of three independent experiments with two biological replicates (N= 2) and no technical replicates per experiment. The total number of donors tested as biological replicates was six (N= 6).

These results indicated that MYC WT-BCL2 overexpression drove an abnormal and perturbed phenotype at the day 13 PC stage. The cells had aberrant CD19 and CD20 expression, inhibition of CD27 upregulation and delay of CD138 expression. These findings agreed with the phenotype observed for *T58I-t2A-BCL2* and were also similar in the *ΔMBI-t2A-BCL2* condition. Deletion of MB0 partially impaired the MYC WT-BCL2-mediated phenotype while the MBII domain deletion almost entirely abolished the impact of MYC overexpression on the day 13 phenotype.

To further verify the above findings the summary flow cytometry data of all the donors tested were plotted in Figure 4.11A for the $CD19^{+}CD20^{-}$ cells, Figure 4.11B for the $CD27^{+}CD38^{+}$ cells, and Figure 4.11C for the $CD38^{+}CD138^{+}$ cells. This analysis revealed the kinetics of all the phenotypical changes observed and described above. Upon MYC WT-BCL2 or MYC MB deletion mutants-BCL2 overexpression, day 3 showed no differences between the conditions. Phenotypical changes were identifiable at day 6 showing an established pattern at day 13 of the model system. In Figure 4.11, the day 13-time point verified, in all the donors tested, that the MBII has a critical contribution to the MYC WT-BCL2 overexpression-mediated effect on PC differentiation. MB0 domain also showed a substantial contribution while MBI domain was marginally involved in the observed changes upon MYC overexpression in the model system.

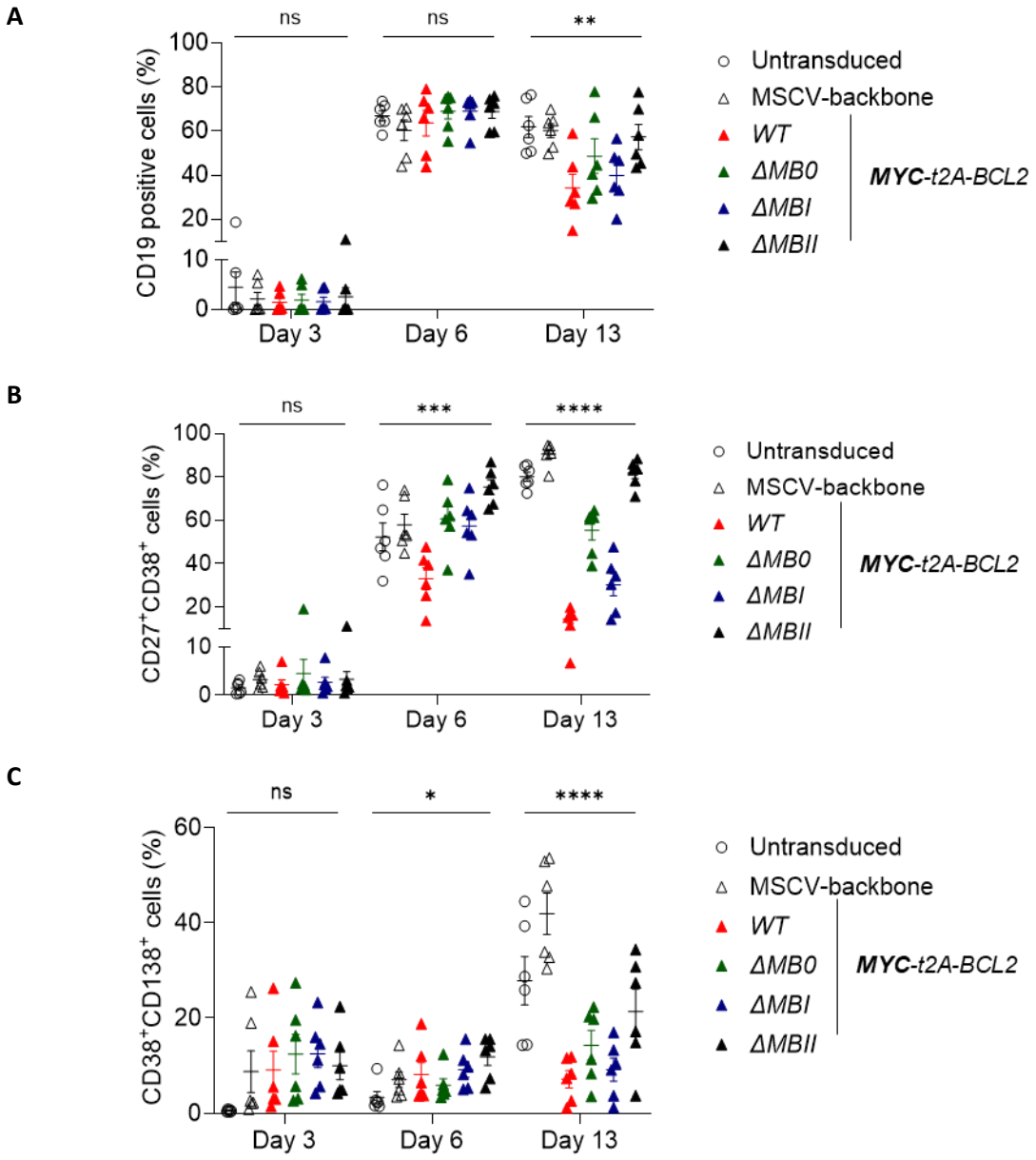

Figure 4.11 Summary flow cytometry data of MYC WT and MB deletion screening. Graphs of the summary data from all donors tested with flow cytometry assessing population percentages of (**A**) $CD19^{+}CD20^{-}$, (**B**) $CD27^{+}CD38^{+}$, and (**C**) $CD38^{+}CD138^{+}$ cells at the indicated time points. One-way ANOVA (A, B, C). The cells assessed in the transduced conditions were $CD2^{+}$ pre-gated. Data are representative of three independent experiments with two biological replicates (N= 2) and no technical replicates per experiment. The total number of donors tested as biological replicates was six (N= 6). Bars and error represent mean and standard deviation (SD); ns, not significant; * $P < 0.05$; ** $P < 0.01$; *** $P < 0.001$; **** $P < 0.0001$.

4.4 T58I mutant overexpression drives a similar effect with the MYC WT and ΔMBI

Having identified the effect of MYC WT and MB deletion mutants' overexpression with BCL2 on the PC differentiation, additional analysis was conducted to validate that the *WT-t2A-BCL2* and *ΔMBI-t2A-BCL2* conditions drive a similar impact on the differentiation process as in the *T58I-t2A-BCL2* samples, described in the results of Chapter 3. As displayed in Figure 4.12, the MYC isoform 1 with a modified ATG transcription initiation codon and a T58I substitution (top) was compared to the MYC WT isoform 2 (middle) and the MYC ΔMBI isoform 2 (bottom), contained in each of the retroviral vectors tested.

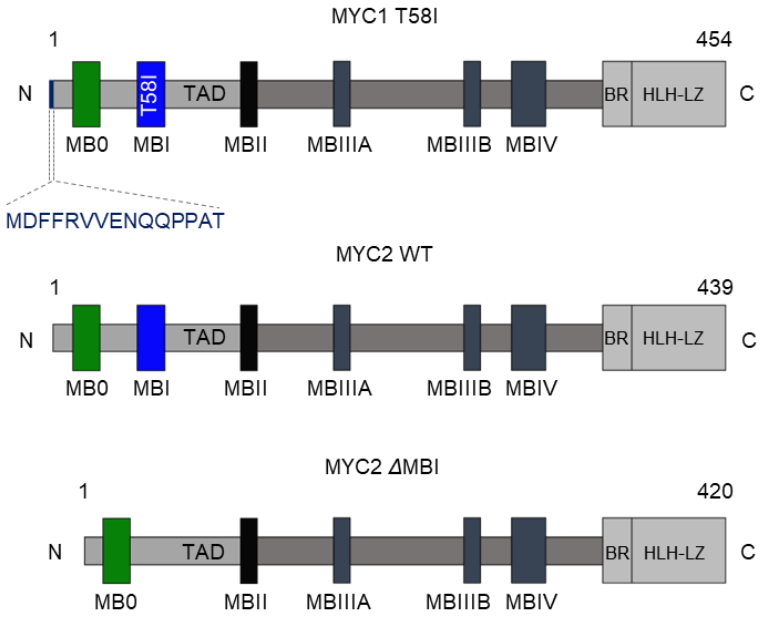

Figure 4.12 Representation of the MYC protein structure used per retroviral vector. *T58I-t2A-BCL2* contains MYC isoform 1 with an equivalent to T58I substitution (top), its additional 15 amino acid sequence at the N-terminus is represented in blue capital letters. Its translation initiation residue is a modified methionine (M) encoded by an ATG codon instead of a CTG (74). *WT-t2A-BCL2* contains MYC isoform 2 without the additional 15 amino acids (middle), similarly *ΔMBI-t2A-BCL2* condition contains MYC isoform 2 with a deleted MBI domain (bottom).

Flow cytometry data were merged between experiments and utilized to compare the immunophenotypic differences between the MYC *T58I-*, *WT-*, and *ΔMBI-t2A-BCL2* conditions. As depicted in Figure 4.13, while the *T58I-t2A-BCL2* condition had a higher percentage of CD19-positive cells on day 3, there were no significant differences at the $CD19^{+}CD20^{-}$ cells of day 6 and day 13 between the three conditions. In addition, no significant differences were observed at day 3, day 6 and day 13 for the $CD38^{+}CD138^{+}$ population, being consistently lower than anticipated in all the three MYC proteins tested for their

overexpression in the system. These results so far indicate that MYC *T58I-*, *WT-*, and *ΔMBI-t2A-BCL2* conditions do not differ in their MYC-mediated effect, especially on the plasmablast and PC stage of day 6 and day 13 respectively. When the frequencies of the $CD27^{+}CD38^{+}$ cells were compared between the three conditions a significant difference was observed on day 6 and day 13. The *WT-t2A-BCL2* cells showed reduced $CD27^{+}CD38^{+}$ frequencies in comparison to either of the two MBI-associated mutants. These findings validate that from the phenotypic factors tested only CD27 expression is inhibited in a more significant manner upon MYC WT isoform 2-BCL2 overexpression than in any of the other two MBI-BCL2 mutants.

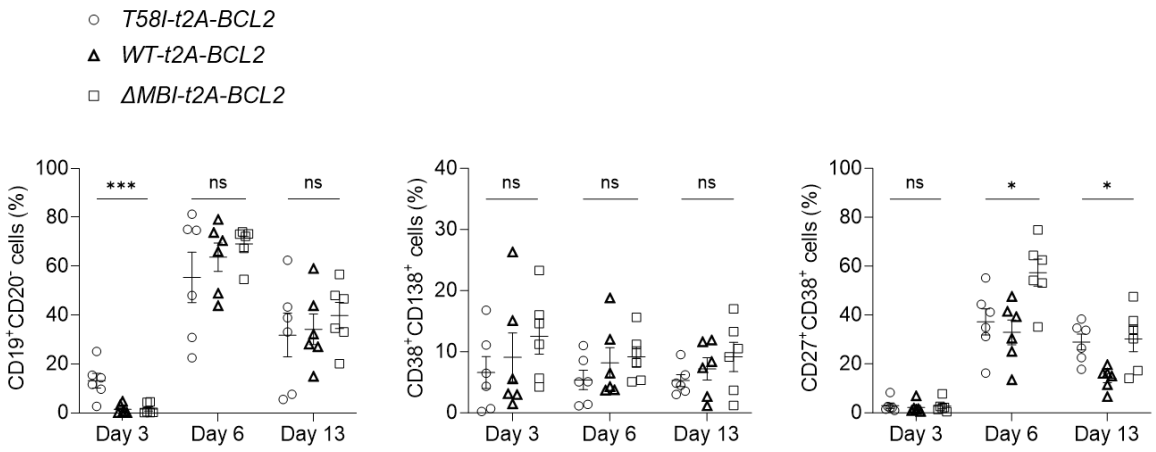

Figure 4.13 Comparison of immunophenotyping between the *T58I-*, *WT-* and *ΔMBI-t2A-BCL2* conditions. Graphs of the merged between distinct experiments data from all donors tested with flow cytometry assessing the population percentages of $CD19^{+}CD20^{-}$ (left), $CD38^{+}CD138^{+}$ (middle), $CD27^{+}CD38^{+}$ (right) cells at the indicated time points and conditions. One-way ANOVA. For this analysis data were merged between experiments described in Chapter 3 for the *T58I-t2A-BCL2* condition and in results from this Chapter for the *WT-t2A-BCL2* and *ΔMBI-t2A-BCL2* transductions. The cells assessed in the transduced conditions were $CD2^{+}$ pre-gated. Data are representative of three independent experiments with two biological replicates (N= 2) and no technical replicates per experiment for the *T58I-t2A-BCL2* samples and three additional independent experiments with two biological replicates (N= 2) and no technical replicates per experiment for the *WT-t2A-BCL2* and *ΔMBI-t2A-BCL2* conditions. Bars and error represent mean and standard deviation (SD); ns, not significant; * $P < 0.05$; $P < 0.01$; ***.

4.5 Gene expression upon MYC TAD MBs deletion screening in the model system

Having identified that MBII and MB0 had a critical role in the phenotypic impact of overexpressed MYC in the model system, the next aim was to interrogate changes in gene expression. RNA-sequencing was conducted, and the selected time points were day 6 and day 13 of plasmablasts and PCs respectively.

Bioinformatic analysis of the RNA-sequencing data was conducted by Dr. Matthew Care. Gene expression analysis took place to further explore if the transcriptional profile in the *ΔMB-t2A-BCL2* conditions would be in agreement with the flow cytometry-derived phenotype described above.

4.5.1 Identification of differentially expressed genes in the MBs deletion *in vitro* screening

Gene expression study revealed the pattern of transcriptional changes on PC differentiation driven by overexpression of MYC WT or the MB deletion mutants. DEGs were counted in the conditions tested upon RNA-sequencing. As displayed in Table 4.1, both at day 6 and day 13, comparison between the untransduced and MSCV-backbone samples showed only a few DEGs as a result of the gene expression analysis. The two controls had a high number of DEGs when compared with the *WT-t2A-BCL2* and *ΔMBI-t2A-BCL2* samples. Considerably less but still at a high number were the DEGs identified between either of the two controls and the *ΔMB0-t2A-BCL2* condition. Importantly, negligible was the difference in the count of DEGs between untransduced or MSCV-backbone and the *ΔMBII-t2A-BCL2* samples with only 4 and 3 genes to be estimated respectively.

A different pattern was observed in the distribution of DEGs count upon pairwise comparisons between *WT-t2A-BCL2* samples and the remaining conditions. Samples overexpressing MYC WT-BCL2 showed a higher number of DEGs with the MSCV-backbone, the untransduced and the *ΔMBII-t2A-BCL2* samples both at day 6 and day 13. Relatively high was the number of DEGs between the samples carrying a deleted MB0 domain, while marginal to no differences were observed with the *ΔMBI-t2A-BCL2* condition.

When the DEGs count was estimated for the *ΔMB0-t2A-BCL2* and the *ΔMBI-t2A-BCL2* conditions in a pairwise comparison manner greater differences were observed with the MSCV-backbone and untransduced controls followed by the *ΔMBII-t2A-BCL2* samples. *ΔMB0-t2A-BCL2* also displayed differences at a lower level with the *WT-t2A-BCL2* and *ΔMBI-t2A-BCL2* conditions. Importantly, marginal differences in DEGs count were detected between *ΔMBI-t2A-BCL2* and *WT-t2A-BCL2* suggesting their transcriptional similarities. When pairwise comparisons were conducted for the *ΔMBII-t2A-BCL2* samples with the remaining conditions, a similar pattern to the untransduced and MSCV-backbone controls was observed on day 6 while its differences to these two controls slightly increased on day 13. A higher absolute count of DEGs was confirmed upon comparison to the *WT-t2A-BCL2* and *ΔMBI-t2A-BCL2* samples.

Table 4.1 Distribution of DEGs count between all the conditions tested on day 6 and day 13. Accurate calculation of the DEGs between the indicated conditions was performed in a pairwise comparison manner. The table represents these counts for day 6 and day 13 samples after RNA-sequencing data analysis. Data are representative of two

independent experiments with two biological replicates (N= 2) and no technical replicates per experiment. The total number of donors tested as biological replicates was four (N= 4).

Day 6

Condition 1	Condition 2	DEGs
Untransduced	MSCV-backbone	63
Untransduced	MYC WT.BCL2	2365
Untransduced	MYC ΔMB0.BCL2	773
Untransduced	MYC ΔMBI.BCL2	1423
Untransduced	MYC ΔMBII.BCL2	4
MSCV-backbone	Untransduced	35
MSCV-backbone	MYC WT.BCL2	2844
MSCV-backbone	MYC ΔMB0.BCL2	1330
MSCV-backbone	MYC ΔMBI.BCL2	2005
MSCV-backbone	MYC ΔMBII.BCL2	3
MYC WT.BCL2	Untransduced	2797
MYC WT.BCL2	MSCV-backbone	3158
MYC WT.BCL2	MYC ΔMB0.BCL2	708
MYC WT.BCL2	MYC ΔMBI.BCL2	36
MYC WT.BCL2	MYC ΔMBII.BCL2	2696
MYC ΔMB0.BCL2	Untransduced	1554
MYC ΔMB0.BCL2	MSCV-backbone	2170
MYC ΔMB0.BCL2	MYC WT.BCL2	806
MYC ΔMB0.BCL2	MYC ΔMBI.BCL2	40
MYC ΔMB0.BCL2	MYC ΔMBII.BCL2	1424
MYC ΔMBI.BCL2	Untransduced	1981
MYC ΔMBI.BCL2	MSCV-backbone	2503
MYC ΔMBI.BCL2	MYC WT.BCL2	86
MYC ΔMBI.BCL2	MYC ΔMB0.BCL2	30
MYC ΔMBI.BCL2	MYC ΔMBII.BCL2	1870
MYC ΔMBII.BCL2	Untransduced	21
MYC ΔMBII.BCL2	MSCV-backbone	41
MYC ΔMBII.BCL2	MYC WT.BCL2	2268
MYC ΔMBII.BCL2	MYC ΔMB0.BCL2	642
MYC ΔMBII.BCL2	MYC ΔMBI.BCL2	1311

Day 13

Condition 1	Condition 2	DEGs
Untransduced	MSCV-backbone	114
Untransduced	MYC WT.BCL2	2517
Untransduced	MYC ΔMB0.BCL2	997
Untransduced	MYC ΔMBI.BCL2	2400
Untransduced	MYC ΔMBII.BCL2	136
MSCV-backbone	Untransduced	32
MSCV-backbone	MYC WT.BCL2	2779
MSCV-backbone	MYC ΔMB0.BCL2	1297
MSCV-backbone	MYC ΔMBI.BCL2	2633
MSCV-backbone	MYC ΔMBII.BCL2	218
MYC WT.BCL2	Untransduced	3140
MYC WT.BCL2	MSCV-backbone	3349
MYC WT.BCL2	MYC ΔMB0.BCL2	602
MYC WT.BCL2	MYC ΔMBI.BCL2	0
MYC WT.BCL2	MYC ΔMBII.BCL2	2456
MYC ΔMB0.BCL2	Untransduced	1545
MYC ΔMB0.BCL2	MSCV-backbone	2019
MYC ΔMB0.BCL2	MYC WT.BCL2	742
MYC ΔMB0.BCL2	MYC ΔMBI.BCL2	411
MYC ΔMB0.BCL2	MYC ΔMBII.BCL2	769
MYC ΔMBI.BCL2	Untransduced	2951
MYC ΔMBI.BCL2	MSCV-backbone	3216
MYC ΔMBI.BCL2	MYC WT.BCL2	4
MYC ΔMBI.BCL2	MYC ΔMB0.BCL2	356
MYC ΔMBI.BCL2	MYC ΔMBII.BCL2	2308
MYC ΔMBII.BCL2	Untransduced	314
MYC ΔMBII.BCL2	MSCV-backbone	521
MYC ΔMBII.BCL2	MYC WT.BCL2	1908
MYC ΔMBII.BCL2	MYC ΔMB0.BCL2	256
MYC ΔMBII.BCL2	MYC ΔMBI.BCL2	1681

To get a better understanding of the MYC WT-BCL2 overexpression and the effect of MB0, MBI and MBII in MYC hyperfunction between the conditions at the two time points tested, dimensionality reduction analysis was performed. As Figure 4.14 shows, all day 6 samples were plotted at the right corner of the graph. The day 6 untransduced and MSCV-backbone controls occupied their own cluster at the bottom of the plot. The MYC WT-BCL2 overexpressing cells formed a distinct cluster at the opposite top site indicating their differences in gene expression to the controls. The *ΔMBI-t2A-BCL2* cluster was close to the *WT-t2A-*

BCL2 followed by the *ΔMB0-t2A-BCL2* samples, indicating their similarities. Importantly, the MYC ΔMBII-BCL2 samples clustered next to the controls and separated from the *WT-t2A-BCL2* condition.

A similar placement in the order of clusters was observed on day 13 but at the opposite side of the plot. This validated enhanced differences between the two time points. In detail, the untransduced and MSCV-backbone controls remained at the bottom end of the clusters' allocation and close to the *ΔMBII-t2A-BCL2* samples. All day 13 clusters showed a greater distance between each other in comparison to day 6. The *ΔMB0-t2A-BCL2* samples appeared in the middle of the day 13 clusters equivalently to their position on day 6. A noticeable change was observed for the *ΔMBI-t2A-BCL2* samples which clustered together with the *WT-t2A-BCL2* condition at the top.

These findings suggest that the *WT-t2A-BCL2* samples share significant similarities in gene expression with the *ΔMBI-t2A-BCL2* condition followed by the *ΔMB0-t2A-BCL2*. On the contrary, deletion of the MBII domain showed more similarities to the controls on a transcriptional level at both time points tested.

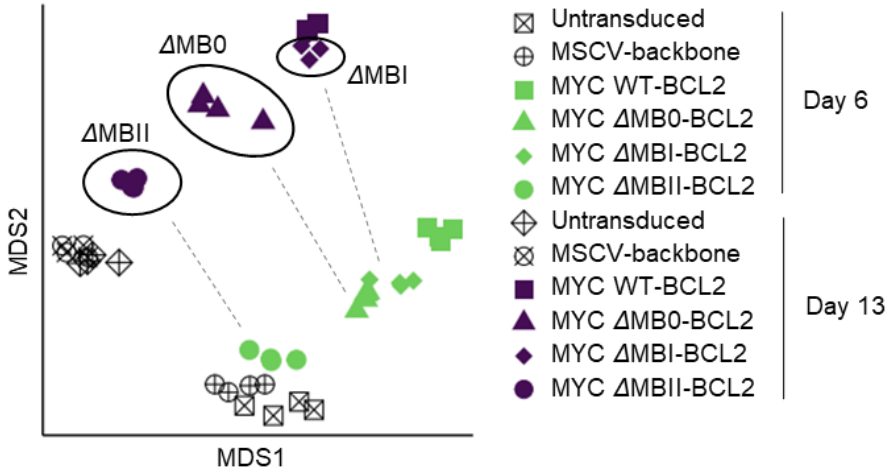

Figure 4.14 Clustering of the DEGs with a dimensionality reduction approach. RNA-sequencing data collected at day 6 and day 13 were analysed and the identified DEGs were used for dimensionality reduction analysis of the indicated samples using the multidimensional scaling (MDS) approach. The illustrated plot was generated by Dr. Matthew Care. Data are representative of two independent experiments with two biological replicates (N= 2) and no technical replicates per experiment. The total number of donors tested as biological replicates was four (N= 4).

4.5.2 Gene signature enrichment using the HALLMARK-MSigDB gene set

The analysis above provided an overall idea of the similarities and differences between the conditions tested on a transcriptional level. The DEGs identified between the *WT-t2A-BCL2* and *ΔMBII-t2A-BCL2*

condition were substantially high as the *ΔMBII-t2A-BCL2* samples shared very few DEGs with the controls. Thus, deletion of the MBII seems to generate a distinctive transcriptional profile to the MYC WT in an overexpression context when tested using the model system.

To get a better insight into the annotation of the genes identified as differentially expressed upon deletion of the MB0 or MBI domains, gene ontology analysis was employed. Several gene sets were evaluated and the HALLMARK-MSigDB was selected containing signatures highly associated with MYC function which was the scope of this analysis (327). The ten more highly enriched signatures in the HALLMARK_MsigDB gene set were selected and evaluated per condition and time point for the identified DEGs. As displayed in Figure 4.15, twelve different signatures were identified from the pairwise comparisons of DEG relative expression to the MSCV-backbone control acting as a reference point. At day 6, DEGs with higher relative expression in *WT-t2A-BCL2*, *ΔMB0-t2A-BCL2*, *ΔMBI-t2A-BCL2*, over the MSCV-backbone samples showed similar representation with the three most highly enriched signatures to be the same in all three conditions (MYC_TARGETS_V1, OXIDATIVE_PHOSPHORYLATION and MYC_TARGETS_V2). Subsequently, signatures related to cell cycle, DNA repair, and metabolic activity such as FATTY_ACID_METABOLISM, ADIPOGENESIS and GLYCOLYSIS were enriched with small differences between the compared conditions. At day 13, the *WT-t2A-BCL2* and *ΔMBI-t2A-BCL2* comparisons to MSCV-backbone displayed more similarities than the *ΔMB0-t2A-BCL2*. All three comparisons showed higher enrichment for the MYC_TARGETS_V1, E2F_TARGETS and G2M_CHECKPOINT signatures. Differences were observed in the *ΔMB0-t2A-BCL2* comparison to MSCV-backbone control displaying enrichment for MITOTIC_SPINDLE instead of the metabolism-related FATTY_ACID_METABOLISM and ADIPOGENESIS signatures. Also, enrichment for the UNFOLDED_PROTEIN_RESPONSE signature was maintained only in the *ΔMB0-t2A-BCL2* condition at day 13.

Statistical significance and high overlap were confirmed for all the enriched signatures described above, as displayed in Table 4.2. These findings provided a greater understanding of the changes driven in MYC hyperfunction upon deletion of the MB0 and MBI domains during *in vitro* PC differentiation. Also, this analysis was in agreement with the findings described earlier in section 4.5.1 showing that deletion of the MBI resembled the MYC WT condition in an overexpression context. Interestingly, loss of function of the MB0 showed differences, especially on day 13 of the system, while still maintaining the main signatures enriched in the *WT-t2A-BCL2* comparison to the MSCV-backbone.

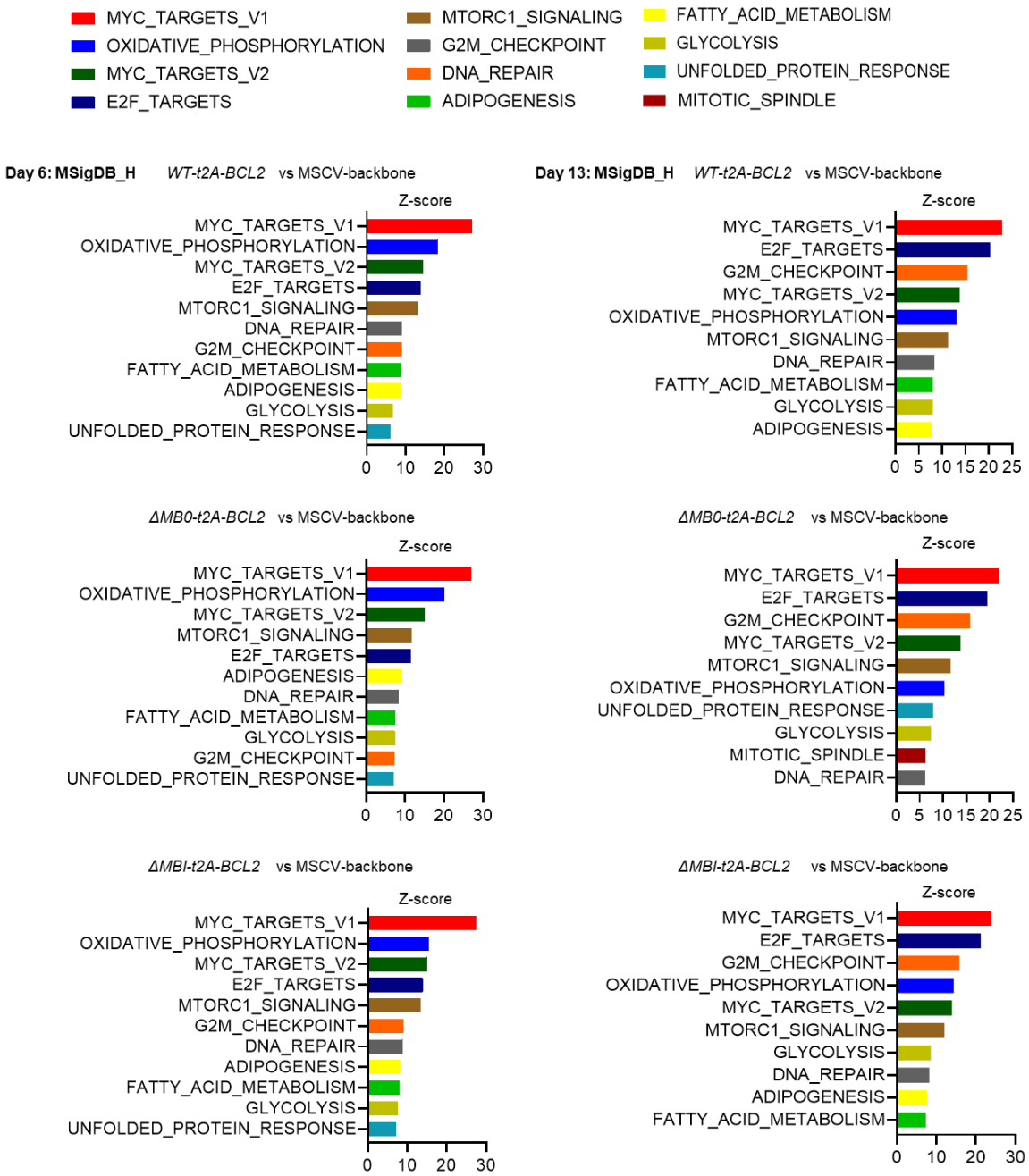

Figure 4.15 Gene ontology of the *WT, ΔMB0* and *ΔMBI -t2A-BCL2* conditions based on the MSigDB_HALLMARK gene set. Pairwise comparisons of the *WT-t2A-BCL2*, *ΔMB0-t2A-BCL2* and *ΔMBI-t2A-BCL2* versus (vs) the MSCV-backbone control resolved lists of DEGs. GO analysis provided an overlap of the identified DEGs per comparison to the signatures comprising the MSigDB_HALLMARK gene set. The most highly represented signatures for each comparison on day 6 and day 13 were plotted based on their Z-scores. Data are representative of two independent experiments with two biological replicates (N= 2) and no technical replicates per experiment. The total number of donors tested as biological replicates was four (N= 4).

Table 4.2 Overlap of the DEGs identified by comparison of the *WT*, *ΔMB0* and *ΔMBI -t2A-BCL2* conditions to the MSCV-backbone, with the MSigDB_HALLMARK signatures. Gene ontology analysis provided overlap of the identified DEGs per indicated comparison to the signatures comprising the MSigDB_HALLMARK gene set. The most highly overlapped signatures per comparison on day 6 and day 13 were selected based on their Z-scores. The overlap is presented as a percentage (%). Data are representative of two independent experiments with two biological replicates (N= 2) and no technical replicates per experiment. The total number of donors tested as biological replicates was four (N= 4); vs, versus; FDR, false discovery rate.

Day 6

WT-t2A-BCL2 vs MSCV-backbone

Gene Signature	% Overlap	p-value	FDR
MYC_TARGETS_V1	94.50	1.0647E-162	3.7491E-160
OXIDATIVE_PHOSPHORYLATION	66.33	1.05571E-74	1.28439E-72
MYC_TARGETS_V2	94.83	5.13003E-48	3.4344E-46
E2F_TARGETS	51.50	8.68835E-44	5.20732E-42
MTORC1_SIGNALING	49.50	3.58926E-40	1.94724E-38
DNA_REPAIR	40.94	6.01616E-20	1.41316E-18
G2M_CHECKPOINT	36.18	1.28413E-19	2.96687E-18
FATTY_ACID_METABOLISM	39.47	1.02645E-18	2.23343E-17
ADIPOGENESIS	35.38	2.92977E-18	6.16599E-17
GLYCOLYSIS	28.93	3.33572E-11	4.29365E-10
UNFOLDED_PROTEIN_RESPONSE	33.63	5.66229E-10	6.53904E-09

ΔMB0-t2A-BCL2 vs MSCV-backbone

Gene Signature	% Overlap	p-value	FDR
MYC_TARGETS_V1	86.50	6.3744E-161	2.3819E-158
OXIDATIVE_PHOSPHORYLATION	64.32	5.52324E-90	9.07E-88
MYC_TARGETS_V2	89.66	1.31654E-50	1.00339E-48
MTORC1_SIGNALING	37.50	1.33764E-31	6.13069E-30
E2F_TARGETS	36.50	6.55294E-30	2.84323E-28
ADIPOGENESIS	30.26	9.15762E-20	2.41434E-18
DNA_REPAIR	31.54	7.89465E-17	1.73739E-15
FATTY_ACID_METABOLISM	28.29	1.17352E-13	2.09223E-12
GLYCOLYSIS	25.38	1.29856E-13	2.3073E-12
G2M_CHECKPOINT	24.62	7.77798E-13	1.30716E-11
UNFOLDED_PROTEIN_RESPONSE	30.97	1.21843E-12	2.01713E-11

ΔMBI-t2A-BCL2 vs MSCV-backbone

Gene Signature	% Overlap	p-value	FDR
MYC_TARGETS_V1	91.00	5.5172E-167	2.2701E-164
OXIDATIVE_PHOSPHORYLATION	51.76	2.68968E-53	2.41412E-51
MYC_TARGETS_V2	93.10	2.60477E-51	2.18276E-49
E2F_TARGETS	47.00	4.58253E-44	3.10764E-42
MTORC1_SIGNALING	45.00	2.58401E-40	1.59304E-38
G2M_CHECKPOINT	32.16	1.30192E-19	3.3789E-18
DNA_REPAIR	35.57	1.14155E-18	2.81886E-17
ADIPOGENESIS	29.74	3.73849E-16	7.89525E-15
FATTY_ACID_METABOLISM	32.24	2.12482E-15	4.22656E-14
GLYCOLYSIS	27.92	4.19351E-14	7.56112E-13
UNFOLDED_PROTEIN_RESPONSE	33.63	6.50916E-13	1.0689E-11

Day 13

WT-t2A-BCL2 vs MSCV-backbone

Gene Signature	% Overlap	p-value	FDR
MYC_TARGETS_V1	82.00	1.584E-114	4.83E-112
E2F_TARGETS	74.00	1.1235E-91	2.298E-89
G2M_CHECKPOINT	57.79	1.11436E-53	1.038E-51
MYC_TARGETS_V2	91.38	5.25542E-43	3.564E-41
OXIDATIVE_PHOSPHORYLATION	50.25	1.53772E-39	9.262E-38
MTORC1_SIGNALING	44.00	1.83722E-29	7.851E-28
DNA_REPAIR	38.93	7.20261E-17	1.628E-15
FATTY_ACID_METABOLISM	37.50	9.55158E-16	2E-14
GLYCOLYSIS	34.01	9.6098E-16	2.005E-14
ADIPOGENESIS	33.33	7.72615E-15	1.493E-13

ΔMB0-t2A-BCL2 vs MSCV-backbone

Gene Signature	% Overlap	p-value	FDR
MYC_TARGETS_V1	68.00	1.433E-105	4.64E-103
E2F_TARGETS	60.50	7.88185E-85	1.659E-82
G2M_CHECKPOINT	48.74	3.16755E-56	3.558E-54
MYC_TARGETS_V2	81.03	3.17753E-43	2.476E-41
MTORC1_SIGNALING	36.00	2.12035E-31	1.111E-29
OXIDATIVE_PHOSPHORYLATION	32.16	6.56934E-25	2.618E-23
UNFOLDED_PROTEIN_RESPONSE	32.74	2.79153E-15	6.617E-14
GLYCOLYSIS	24.37	8.98963E-14	1.891E-12
MITOTIC_SPINDLE	21.11	4.13238E-10	6.311E-09
DNA_REPAIR	23.49	5.73045E-10	8.611E-09

ΔMBI-t2A-BCL2 vs MSCV-backbone

Gene Signature	% Overlap	p-value	FDR
MYC_TARGETS_V1	84.50	2.1776E-125	6.93E-123
E2F_TARGETS	76.00	9.9483E-100	2.143E-97
G2M_CHECKPOINT	58.29	1.38151E-56	1.265E-54
OXIDATIVE_PHOSPHORYLATION	53.27	1.21531E-46	8.477E-45
MYC_TARGETS_V2	91.38	6.12808E-44	3.889E-42
MTORC1_SIGNALING	45.50	3.55223E-33	1.614E-31
GLYCOLYSIS	35.03	7.32973E-18	1.644E-16
DNA_REPAIR	37.58	2.50727E-16	5.153E-15
ADIPOGENESIS	32.31	1.55144E-14	2.781E-13
FATTY_ACID_METABOLISM	34.21	2.35714E-13	3.878E-12

4.5.3 Gene ontology analysis for the MB0 and MBI deletion mutants

The next aim was to specify the DEGs shared between the *WT-t2A-BCL2*, *ΔMB0-t2A-BCL2* and *ΔMBI-t2A-BCL2* versus DEGs that are uniquely regulated in each of these conditions. The main focus of this analysis was to unravel the GO of genes that are more highly differentially expressed in each of the conditions in comparison to the MSCV-backbone control. MYC function-related transcripts would be analysed upon its overexpression in the model system and thus, day 6 and day 13 pairwise comparisons were performed. As displayed in Figure 4.16A, at day 6 1814 genes were shared between the three conditions tested

representing genes that were expressed upon MYC overexpression in the system despite deletion of MB0 and MBI. 566 were the genes expressed only when MB0 and MBI were intact indicating the requirement of both these domains for their regulation by MYC. The genes that were expressed independently of the presence of the MB0 were 179 while the genes that were expressed independently of the MBI were 599. This finding indicated that the MB0 was more required than the MBI for full MYC WT function in an overexpression context at day 6.

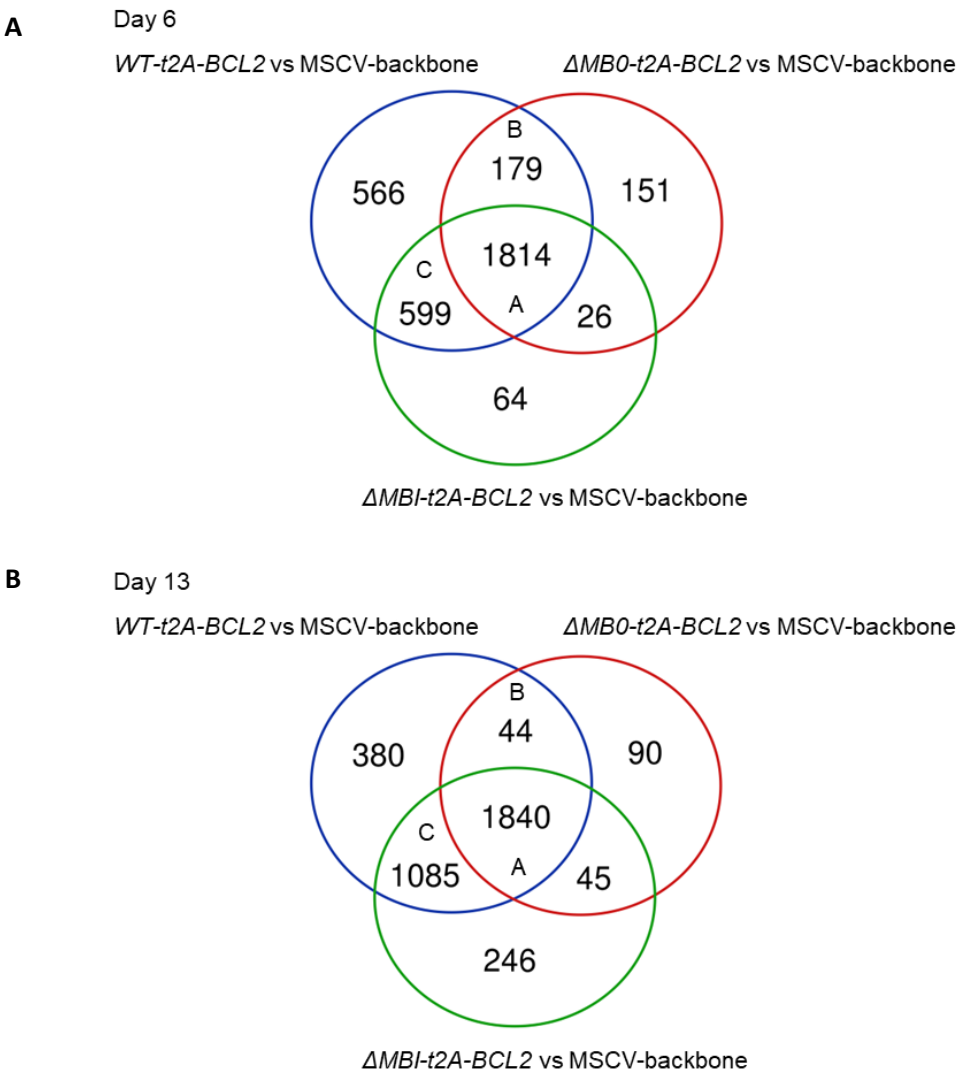

Figure 4.16 MB0 is more essential than MBI for overexpressed MYC to induce gene expression. Venn diagrams of the DEGs upregulated in *WT-t2A-BCL2*, *ΔMB0-t2A-BCL2* and *ΔMBI-t2A-BCL2* versus (vs) the MSCV-backbone control (**A**) at day 6 and (**B**) at day 13. Gene counts are depicted in each comparison of the Venn diagram. Capital letters A, B, C on the plots indicate their corresponding identified gene sets. Data are representative of two independent

experiments with two biological replicates (N= 2) and no technical replicates per experiment. The total number of donors tested as biological replicates was four (N= 4).

The same order of contribution to MYC overexpression-mediated gene expression was observed at day 13 for the MB0 and MBI domains. As Figure 4.16B shows, on day 13 a smaller number of genes compared to day 6 required both the MB0 and MBI domains for their induction (380 genes), while an almost two-fold increase was observed in the genes that were expressed independently of the MBI but not the MB0 (1085 genes). In accordance with this change, only 44 genes required the MBI domain supporting that MYC function on a transcriptional level at day 13 is not primarily driven by its MBI domain in comparison to its MB0. Also, roughly the same number of genes to day 6 were expressed independently to the loss of function of both the MB0 and MBI (1840 genes) at day 13. This analysis further supported that MB0 was more essential for the overexpressed MYC effect on a transcriptional level than MBI.

GO analysis was performed for the genes identified as shared between all three conditions (Gene set A) at day 6. Using the DAVID GO analysis software, the GO terms representing the genes of interest generated clusters based on their similarities in gene annotations. The most enriched clusters were selected from the analysis conducted by DAVID annotation software. As displayed in Table 4.3, the most enriched cluster identified upon analysis of Gene set A was characterized by GO terms related to mitochondrial function. Similar analysis of the 179 genes that were expressed independently of the MB0 but not of the MBI (Gene set B), resulted in GO terms associated with ribosomal activity, translation and RNA binding. Nucleus-related GO terms were identified in the most enriched cluster of the 599 genes dependent on MB0 but not on MBI (Gene set C).

Table 4.3 GO analysis of Gene set A, B and C at day 6 showed enrichment of different GO terms. The gene lists generated by the Venn diagram in Figure 4.16A, were labelled as Gene set A (representing the 1814 identified genes), Gene set B (representing the 179 identified genes) and Gene set C (representing the 599 identified genes). Functional annotation analysis took place for each of these three gene sets using DAVID software. The most highly enriched GO terms were estimated by the software upon clustering. The tables represent the cluster of GO terms with the highest enrichment score as provided by DAVID (Cluster 1); %, overlap of genes tested with the enriched GO terms. Data are representative of two independent experiments with two biological replicates (N= 2) and no technical replicates per experiment. The total number of donors tested as biological replicates was four (N= 4); FDR, false discovery rate.

Day 6: Gene set A

Annotation Cluster 1	Enrichment Score: 114.69035186116179					
Category	Term	Count	%	PValue	Benjamini	FDR
GOTERM_CC_DIRECT	GO:0005739~mitochondrion	429	24.38	6.33E-137	5.31E-134	4.62E-134
UP_KW_DOMAIN	KW-0809~Transit peptide	239	13.58	1.08E-134	2.91E-133	2.69E-133
UP_KW_CELLULAR_COMPONENT	KW-0496~Mitochondrion	421	23.92	2.79E-134	1.42E-132	1.09E-132
UP_SEQ_FEATURE	TRANSIT:Mitochondrion	235	13.35	1.99E-111	1.17E-107	1.16E-107
GOTERM_CC_DIRECT	GO:0005759~mitochondrial matrix	152	8.64	9.33E-60	1.57E-57	1.36E-57

Day 6: Gene set B

Annotation Cluster 1	Enrichment Score: 15.409816290768733					
Category	Term	Count	%	PValue	Benjamini	FDR
UP_KW_MOLECULAR_FUNCTION	KW-0689~Ribosomal protein	26	15.57	3.45E-26	1.38E-24	1.38E-24
GOTERM_MF_DIRECT	GO:0003735~structural constituent of ribosome	26	15.57	4.13E-24	8.58E-22	8.46E-22
GOTERM_BP_DIRECT	GO:0006412~translation	25	14.97	1.36E-22	7.75E-20	7.60E-20
UP_KW_MOLECULAR_FUNCTION	KW-0687~Ribonucleoprotein	27	16.17	2.55E-22	5.11E-21	5.11E-21
GOTERM_BP_DIRECT	GO:0002181~cytoplasmic translation	18	10.78	3.13E-19	8.95E-17	8.78E-17
KEGG_PATHWAY	hsa03010:Ribosome	22	13.17	3.71E-18	1.12E-16	1.07E-16
GOTERM_CC_DIRECT	GO:0022625~cytosolic large ribosomal subunit	13	7.78	3.48E-13	2.40E-11	2.25E-11
KEGG_PATHWAY	hsa05171:Coronavirus disease - COVID-19	19	11.38	5.70E-12	5.76E-11	5.51E-11
GOTERM_CC_DIRECT	GO:0022626~cytosolic ribosome	12	7.19	7.50E-11	3.88E-09	3.64E-09
GOTERM_MF_DIRECT	GO:0003723~RNA binding	29	17.37	3.36E-06	2.33E-04	2.29E-04
GOTERM_CC_DIRECT	GO:0045202~synapse	10	5.99	1.09E-02	1.32E-01	1.24E-01

Day 6: Gene set C

Annotation Cluster 1	Enrichment Score: 20.174343816861082					
Category	Term	Count	%	PValue	Benjamini	FDR
GOTERM_CC_DIRECT	GO:0005654~nucleoplasm	216	37.31	4.02E-29	2.17E-26	2.10E-26
UP_KW_CELLULAR_COMPONENT	KW-0539~Nucleus	255	44.04	2.05E-18	8.41E-17	6.16E-17
GOTERM_CC_DIRECT	GO:0005634~nucleus	246	42.49	3.63E-15	6.54E-13	6.32E-13

The GO terms detected in these three most enriched clusters for each gene set were associated with distinctive MYC function-associated processes. To acquire a more in-depth understanding of the genes involved in MBI or MB0 contribution to MYC overexpression-mediated changes in the transcriptome, additional GO was conducted in the genes derived from the enriched clusters. In Figure 4.17A, similar GO terms to the original cluster were further enriched for the Gene set B and were associated with cytoplasmic translation and ribosomal protein. Interestingly, when this analysis was conducted for the Gene set C, a more descriptive annotation of GO terms was observed. As depicted in Figure 4.17B, the GO terms of the original cluster were associated with the nucleus and were also enriched for GO terms specifically related to mRNA processing, splicing and gene transcription. These findings indicate distinctive roles of the MB0 and the MBI domains in overexpressed MYC function apart from different contributions to the full MYC effect in the overexpression context tested in the model system.

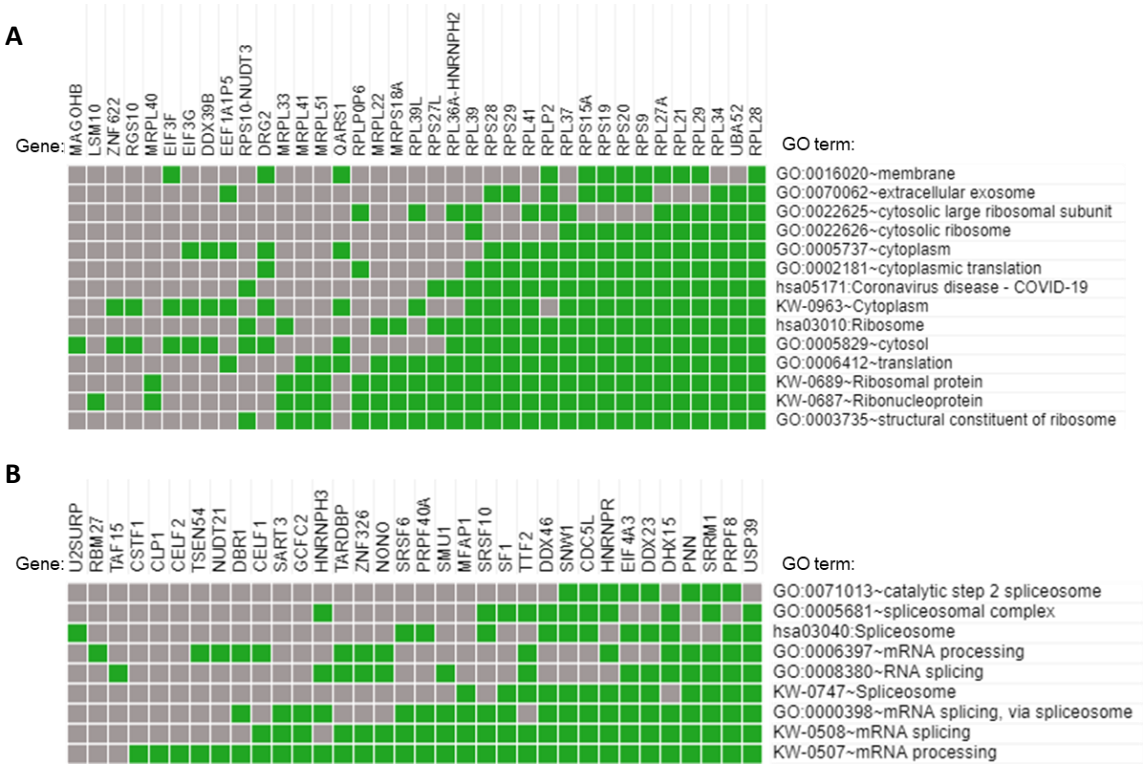

Figure 4.17 GO analysis with DAVID on the genes represented by the first most highly enriched cluster in the original GO analysis. Day 6 DEGs overlapping with the GO terms derived from the most highly enriched cluster upon DAVID analysis were collected in a new gene list and re-analysed for their GO with DAVID. Heatmaps of the most highly enriched GO terms corresponding to cluster 1 in this analysis were generated for (**A**) Gene set B and (**B**) Gene set C. Green corresponds to genes associated with a GO term while grey represents no association. Data are representative of two independent experiments with two biological replicates (N= 2) and no technical replicates per experiment. The total number of donors tested as biological replicates was four (N= 4).

Subsequently, the functional annotation of the genes shared between the *WT-t2A-BCL2* and *ΔMBI-t2A-BCL2* at day 13 was investigated. This gene set, being dependent on an intact MB0 based on the analysis presented in Figure 4.16B, was the equivalent of Gene set C on day 6. GO analysis was conducted in Table 4.4 and the most enriched cluster showed significant overlap of genes with GO terms associated with the mitochondrion in the cells. To get a better insight the GO analysis was repeated in the genes provided by DAVID for each of the GO terms in cluster 1. This analysis verified association with translation, ribosomal protein and mitochondrial translation (Figure 4.18).

Table 4.4 GO analysis of Gene set C at day 13. The gene list generated by the Venn diagram in Figure 4.16B, representing the 1085 genes shared between *WT-t2A-BCL2* and *ΔMBI-t2A-BCL2* conditions, was equivalent to Gene set C from Figure 4.16A. Functional annotation analysis took place for this day 13 gene set using DAVID software. The

most highly enriched GO terms were estimated by the software upon clustering. The table represents the cluster of GO terms with the highest enrichment score as provided by DAVID (Cluster 1); %, overlap of genes tested with the enriched GO terms. Data are representative of two independent experiments with two biological replicates (N= 2) and no technical replicates per experiment. The total number of donors tested as biological replicates was four (N= 4); FDR, false discovery rate.

Day 13: Gene set C

Annotation Cluster 1	Enrichment Score: 27.280485099146308					
Category	**Term**	**Count**	**%**	**PValue**	**Benjamini**	**FDR**
GOTERM_CC_DIRECT	GO:0005739~mitochondrion	182	18.12749	1.81E-38	1.25E-35	1.21E-35
UP_KW_CELLULAR_COMPONENT	KW-0496~Mitochondrion	175	17.43028	4.98E-36	2.49E-34	2.04E-34
UP_KW_DOMAIN	KW-0809~Transit peptide	88	8.76494	1.66E-27	4.99E-26	4.99E-26
UP_SEQ_FEATURE	TRANSIT:Mitochondrion	86	8.565737	1.03E-23	3.89E-20	3.89E-20
GOTERM_CC_DIRECT	GO:0005759~mitochondrial matrix	58	5.776892	2.56E-14	4.41E-12	4.29E-12

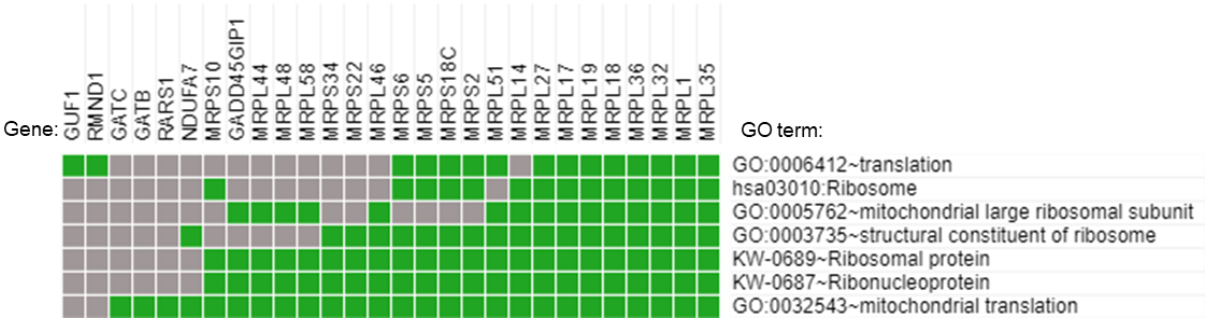

Figure 4.18 GO terms related to ribosomal protein, translation and the mitochondria in Gene set C genes. Heatmap of the day 13 DEGs overlapping with the indicated GO terms derived from the GO analysis of the most highly enriched cluster in Gene set C (Figure 4.16B). Green corresponds to genes associated with a GO term while grey represents no association. Data are representative of two independent experiments with two biological replicates (N= 2) and no technical replicates per experiment. The total number of donors tested as biological replicates was four (N= 4).

These results suggest that the MB0 domain is a critical contributor to known MYC function on a transcriptional level based on its overexpression-mediated impact on the model system. In addition, on day 6 the enriched GO terms for the DEGs related to MB0 presence were associated with RNA processing and transcription in the nucleus. Interestingly, the main GO terms on day 13 were related to mitochondrial translation and the ribosome. Thus, potentially distinctive roles of the MB0 between the two time points tested were highlighted through this analysis.

4.5.4 Gene expression of immunophenotypic markers and MYC targets

The analysis above sets a proof of principle for the role of MB0 and MBI domains in MYC function upon its overexpression in the model system but provided little information on the ongoing PC differentiation

process. To get a better understanding of the impact of MYC overexpression and the contribution of each of the MB domains of interest on PC differentiation the normalised values of vignette DEGs were plotted at day 6 and day 13. First, CD2 and MYC overexpression were confirmed at a transcriptional level upon transductions. As displayed in Figure 4.19, at day 6 and day 13 higher was the expression of *CD2* in the MSCV-backbone and the MYC *WT* and *ΔMB* mutant conditions in comparison to the untransduced. In parallel, higher expression of *MYC* was validated in the *WT* and *ΔMB* mutants in comparison to both the untransduced and the MSCV-backbone controls at day 6 and day 13 as anticipated.

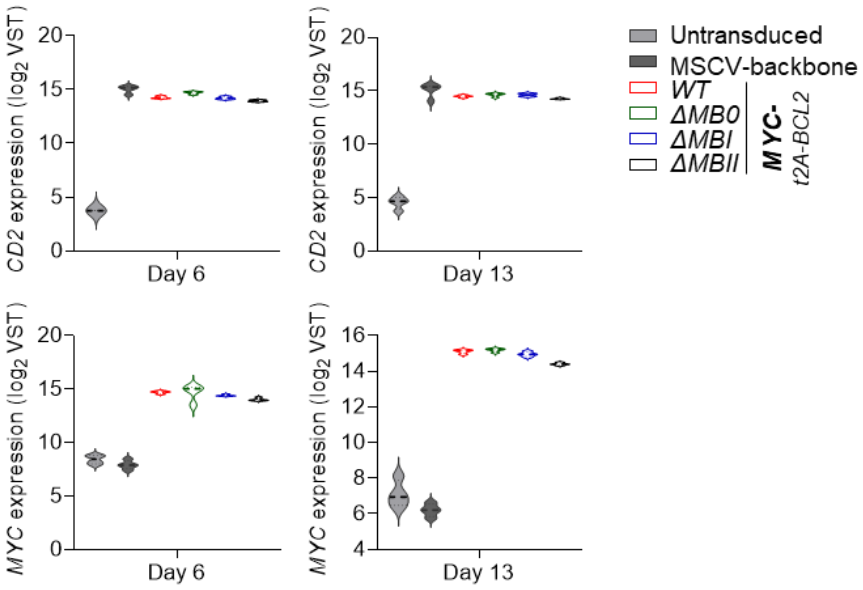

Figure 4.19 Gene expression of *CD2* and *MYC* in the MYC TAD MB deletion screening. Graphs of normalised expression values of differential expression for *CD2* and *MYC* as analysed for the indicated conditions at day 6 and day 13. Software DESeq2 conducted variance stabilizing transformation (VST) analysis generating the normalized log_2-transformed gene expression values, with stabilized variance, that are visualized in the graphs. Data are representative of two independent experiments with two biological replicates (N= 2) and no technical replicates per experiment. The total number of donors tested as biological replicates was four (N= 4).

When CD19, CD20, CD27, CD38 and CD138 were analysed for their gene expression a similar effect was observed per deletion mutant with their corresponding flow cytometry results described in section 4.3.5. In detail, as depicted in Figure 4.20, on day 6 *CD19* showed a significant reduction in expression in the *WT-t2A-BCL2* (henceforth also referred to as MYCwt) condition in comparison to the controls. A smaller decrease in its gene expression was observed at day 13. At both time points deletion of the MB0 and MBII reduced the effect mediated by MYC overexpression while deleting the MBI showed no differences. In contrast to *CD19*, the expression of *MS4A1* (CD20) was increased upon MYC WT-BCL2 overexpression on

day 13. Deletion of the MB0 and MBII domains resulted in a reduction of the overexpressed MYC-driven effect on *MS4A1* expression. Similarly, the repression observed for *CD27*, *CD38* and *CD138* in the MYCwt samples was partially and significantly reduced when the MB0 and MBII domains were deleted from the overexpressed MYC respectively. The *ΔMBI-t2A-BCL2* condition phenocopied the effect observed in MYC WT overexpressing samples.

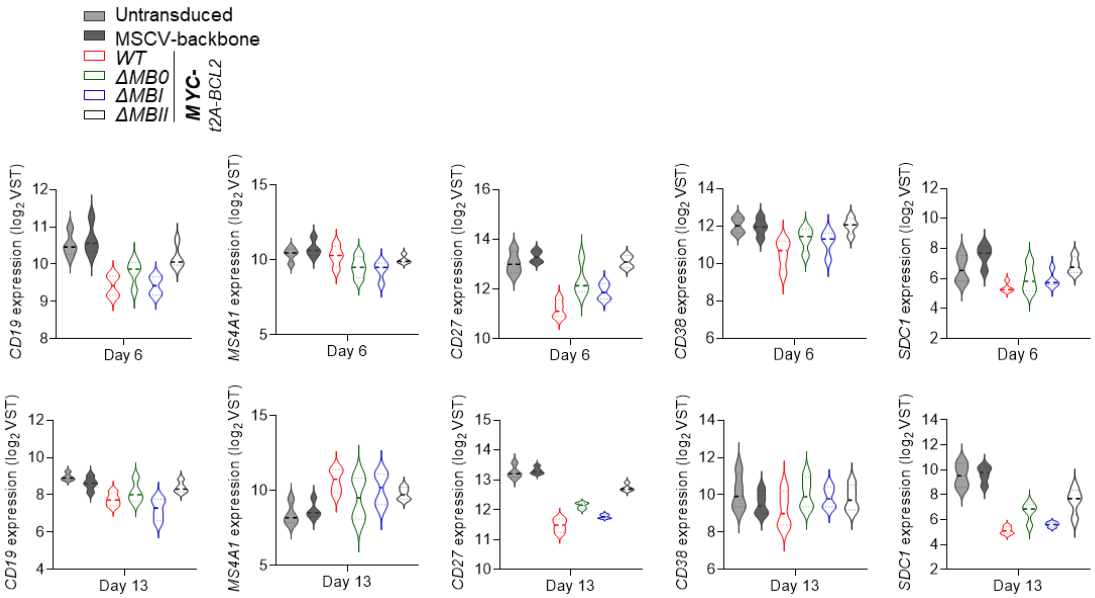

Figure 4.20 Gene expression of the flow cytometry immunophenotypic markers in the model system. Normalised expression values of DEGs were plotted for the indicated conditions at day 6 and day 13 evaluating *CD19*, *MS4A1*, *CD27*, *CD38* and *SDC1* expression. Software DESeq2 conducted variance stabilizing transformation (VST) analysis generating the normalized log_2-transformed gene expression values, with stabilized variance, that are visualized in the graphs. Data are representative of two independent experiments with two biological replicates (N= 2) and no technical replicates per experiment. The total number of donors tested as biological replicates was four (N= 4).

To validate MYC hyperfunction and its effect after deletion of either MB0, MBI or MBII, specific MYC target genes were analysed per condition for their expression. As shown in Figure 4.21, on day 6 a similar pattern of expression was represented for all the genes tested. The highest expression was observed in MYC WT-BCL2 conditions. Slightly lower expression levels in comparison to MYCwt were observed in the *ΔMBI-t2A-BCL2* conditions and a further reduction was observed for *ΔMB0-t2A-BCL2*. *ΔMBII-t2A-BCL2* showed expression levels close to those of the controls. The impact of the *ΔMB0-t2A-BCL2* condition was arguably more suggestive of gene-specific effects in this limited target gene set. The *ΔMB0-t2A-BCL2* condition showed a loss of impact on *JAG2* expression but retained more similar regulation of *TERT* and *SORD* when compared to MYCwt.

At day 13 these results were recapitulated with the *WT-t2A-BCL2* and *ΔMBI-t2A-BCL2* conditions showing the most similar impact on the MYC-target gene expression. The already mentioned hierarchy of *ΔMBII*> *ΔMB0*> *ΔMBI* was validated regarding the contribution of each domain deletion mutant to the loss of the observed MYC hyperfunction.

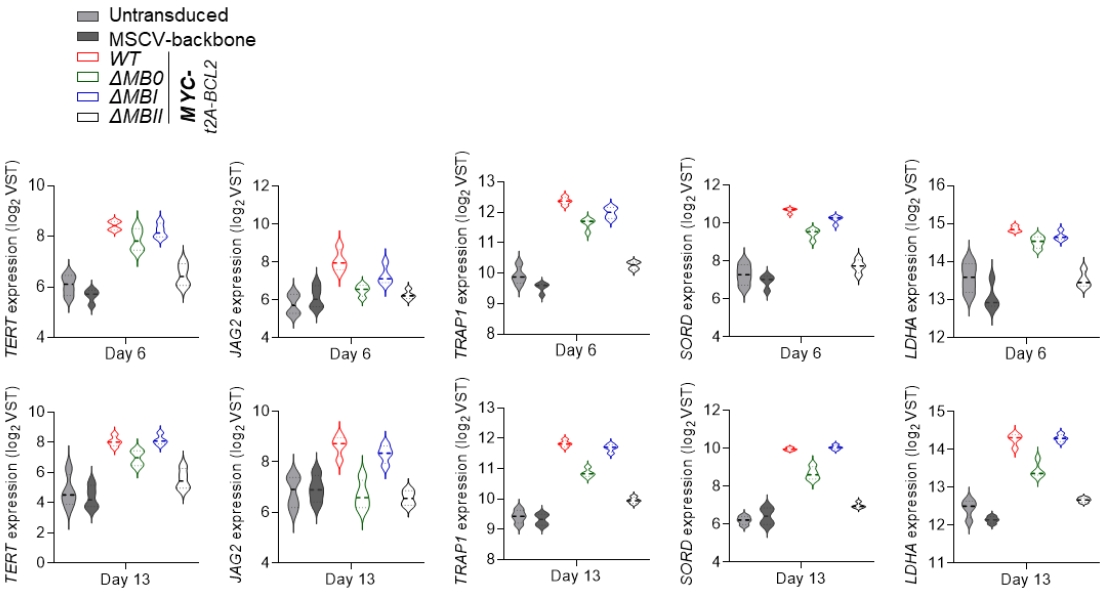

Figure 4.21 Gene expression of MYC targets in the MYC TAD MB deletion screening. Normalised expression values of differentially expressed MYC targets were plotted for the indicated conditions at day 6 and day 13 evaluating *TERT*, *JAG2*, *TRAP1*, *SORD* and *LDHA* expression. Software DESeq2 conducted variance stabilizing transformation (VST) analysis generating the normalized log_2-transformed gene expression values, with stabilized variance, that are visualized in the graphs. Data are representative of two independent experiments with two biological replicates (N= 2) and no technical replicates per experiment. The total number of donors tested as biological replicates was four (N= 4).

4.5.5 Gene expression of key transcription factors

The TFs assessed for their gene expression in Figure 3.23 of Chapter 3 were assessed next. At day 6, as shown in Figure 4.22A, *PAX5* and *BACH2* expression appeared similar in all the conditions tested while *SREBF1* showed a small increase in the *WT-t2A-BCL2* and *ΔMB0-t2A-BCL2* transductions. Deletion of the MB0 and MBII domains partially and significantly decreased the overexpressed MYC ability to repress *EBF1* respectively. At day 6, the same trend was observed in the gene expression of PC-related TFs such as *PRDM1*, *IRF4* and *RUNX1*. A significant repression of *XBP1* was detected in the MYCwt condition as also observed upon MYC T58I-BCL2 overexpression in Figure 3.23 of Chapter 3. Loss of MBI and MB0 function

reduced the MYC-mediated repression of its expression while deletion of the MBII almost revoked it as also observed for other genes tested.

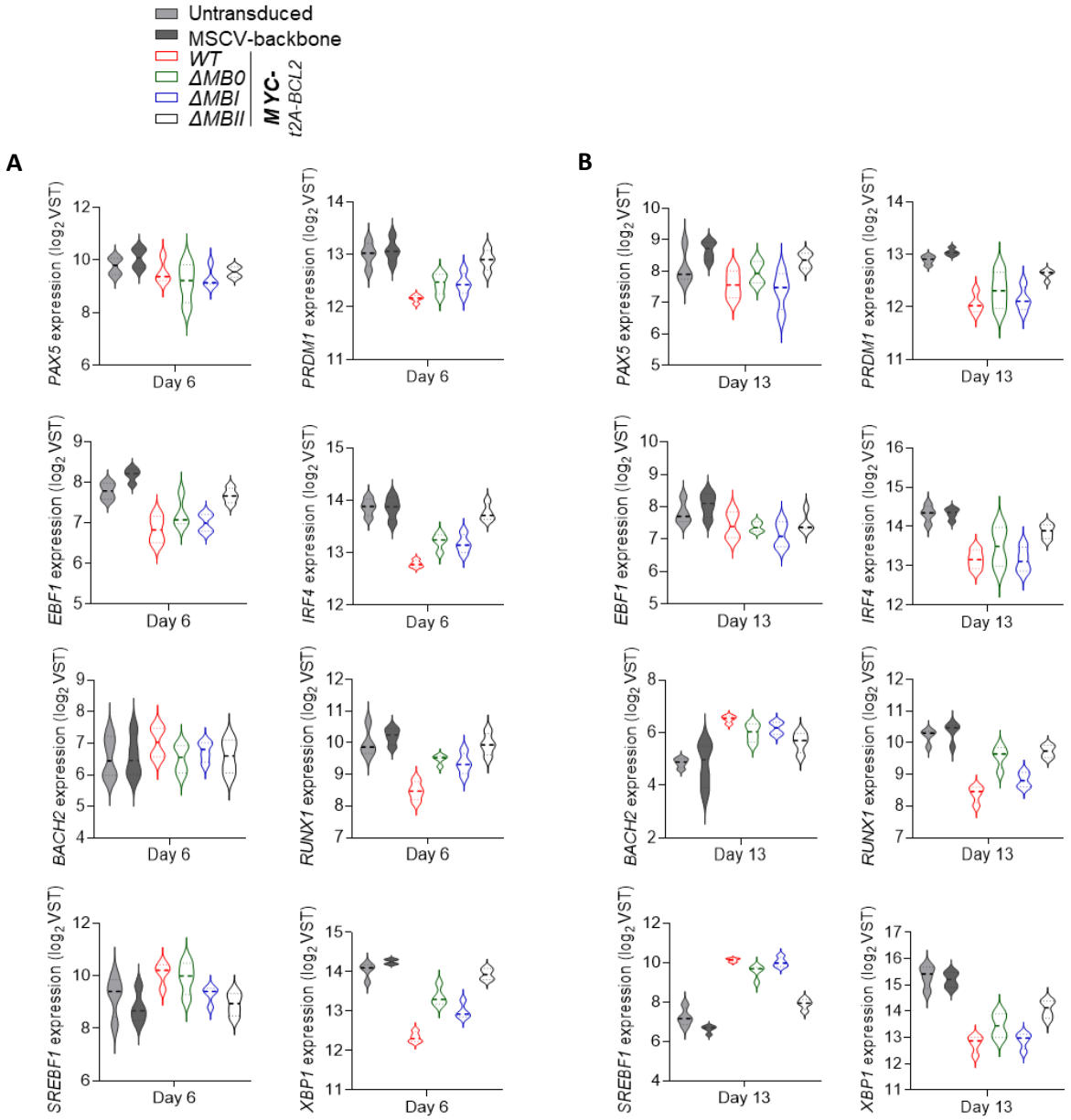

Figure 4.22 Gene expression of B cell state and PC programme TFs upon MYC TAD MB deletion screening. Normalised expression values of differentially expressed TFs were plotted for the indicated conditions at (**A**) day 6 and (**B**) day 13, evaluating gene expression of *PAX5*, *EBF1*, *BACH2*, *SREBF1*, *PRDM1*, *IRF4*, *RUNX1* and *XBP1*. Software DESeq2 conducted variance stabilizing transformation (VST) analysis generating the normalized log_2-transformed gene expression values, with stabilized variance, that are visualized in the graphs. Data are representative of two

independent experiments with two biological replicates (N= 2) and no technical replicates per experiment. The total number of donors tested as biological replicates was four (N= 4).

As displayed in Figure 4.22B, at day 13 a more consistent phenotype of gene expression was established for the selected TFs. In all the TFs tested the MYCwt effect observed in their expression was partially and significantly reduced upon deletion of its MB0 and MBII respectively. On the contrary and as previously observed in other genes tested, loss of MBI function resulted in marginal differences compared to the MYCwt. An interesting observation in the day 13 data was that while deletion of the MBII resulted in a significant reduction of MYC activity in the overexpression context examined here, it did not completely abolish MYC activity for TFs such as *PRDM1*, *IRF4*, *RUNX1*, *SREBF1*, and *XBP1*. This result suggested that some MYC hyperfunction might be maintained in the *ΔMBII-t2A-BCL2* condition although the main effect mediated by MYC overexpression appeared to be impaired for the TFs shown.

Importantly, this analysis revealed that *XBP1* expression remained negatively affected by MYC WT- and *Δ*MBI-BCL2 overexpression showing a significant reduction in comparison to the controls at both the time points tested. Again, the deletion of MB0 showed a decrease in the hyperfunctioning MYC and a higher reduction was attributed to the loss of function in the MBII domain.

4.5.6 XBP1 targets and immunoglobulin gene expression

We previously saw that overexpression of MYC T58I impacted both the gene expression of *XBP1* and its target genes. Thus, a similar analysis to the Results section 3.6.6 of Chapter 3 was conducted in Figure 4.23. XBP1 selected target genes associated with the UPR, were analysed for their gene expression upon MYC WT and the MB deletion mutants with BCL2 overexpression. A clear repression of their expression was observed upon MYC WT-BCL2 overexpression in both time points tested in comparison to the controls. This indicated a stronger impact of the MYC WT-BCL2 overexpression on their expression as cells progressed toward the PC stage. A similar effect was verified upon deletion of the MBI in both time points tested. On the contrary, the suppression of XBP1 target expression was significantly less in the *ΔMB0-t2A-BCL2* conditions and was lost in *ΔMBII-t2A-BCL2* samples. This analysis indicated that the repression observed in *XBP1* expression in the MYCwt affected the gene expression of its target genes tested here in a similar manner to the MYC T58I hyperfunction, previously addressed in Chapter 3. In addition, the abrogation of MBII functionality sufficed to abolish the observed repression in the XBP1 targets.

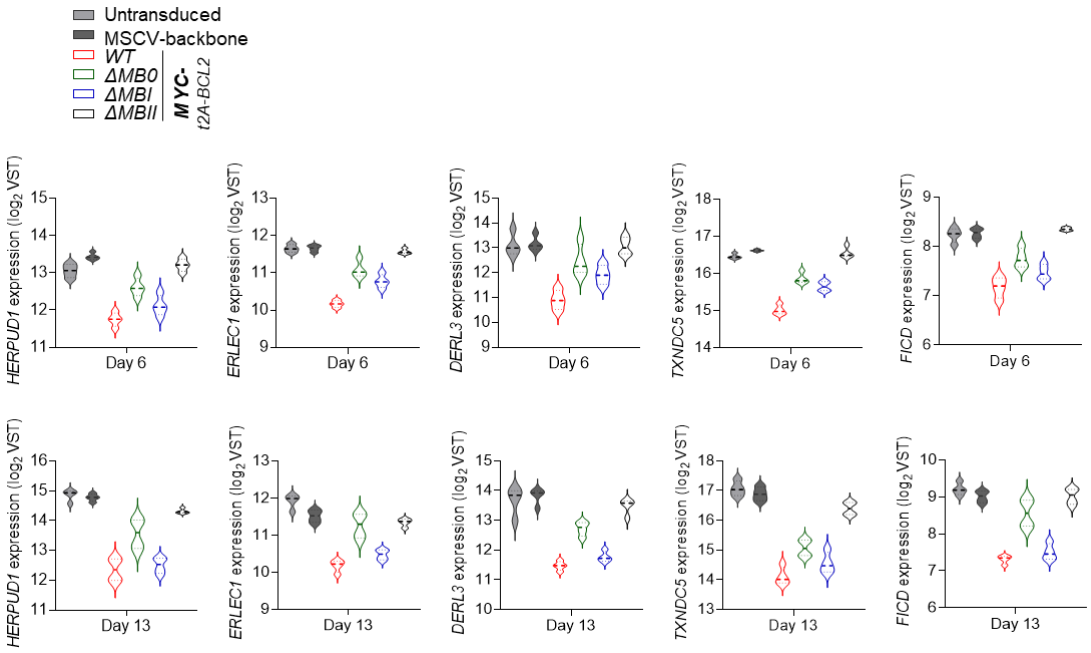

Figure 4.23 XBP1 gene targets expression in the MYC TAD MB mutants. Normalised expression values of differentially expressed XBP1 targets associated with the UPR were plotted for the indicated conditions at day 6 and day 13 evaluating *HERPUD1*, *ERLEC1*, *DERL3*, *TXNDC5* and *FICD* expression. Software DESeq2 conducted variance stabilizing transformation (VST) analysis generating the normalized log_2-transformed gene expression values, with stabilized variance, that are visualized in the graphs. Data are representative of two independent experiments with two biological replicates (N= 2) and no technical replicates per experiment. The total number of donors tested as biological replicates was four (N= 4).

Subsequently, transcriptional changes in the immunoglobulin gene expression were evaluated. As displayed in Figure 4.24A and 4.24B, MYCwt repressed the immunoglobulin genes similarly to the MYC-T58I overexpression (Figure 3.25 and Figure 3.26 of Chapter 3). Deletion of the MBI domain showed marginal differences to the MYCwt observed effect. On the contrary, the absence of MB0 and MBII domains progressively reduced the MYC-mediated impact on immunoglobulin gene expression. Deletion of MB0 reduced the observed repression while the *ΔMBII-t2A-BCL2* samples demonstrated normal immunoglobulin gene expression in similar levels to the controls.

Together these results indicate that there is a critical role of MBII and MB0 domains of MYC protein in its overexpression-driven effect on the transcriptional profile of the cells undergoing PC differentiation *in vitro*. Based on our gene expression analysis, loss of function for the MBII domain of MYC almost completely abolished its hyperfunction indicating its requirement for MYC protein function when

overexpressed in our system. In parallel, the absence of its MB0 showed also a crucial contribution to MYC hyperactivity by weakening its impact under conditions permissive for PC differentiation.

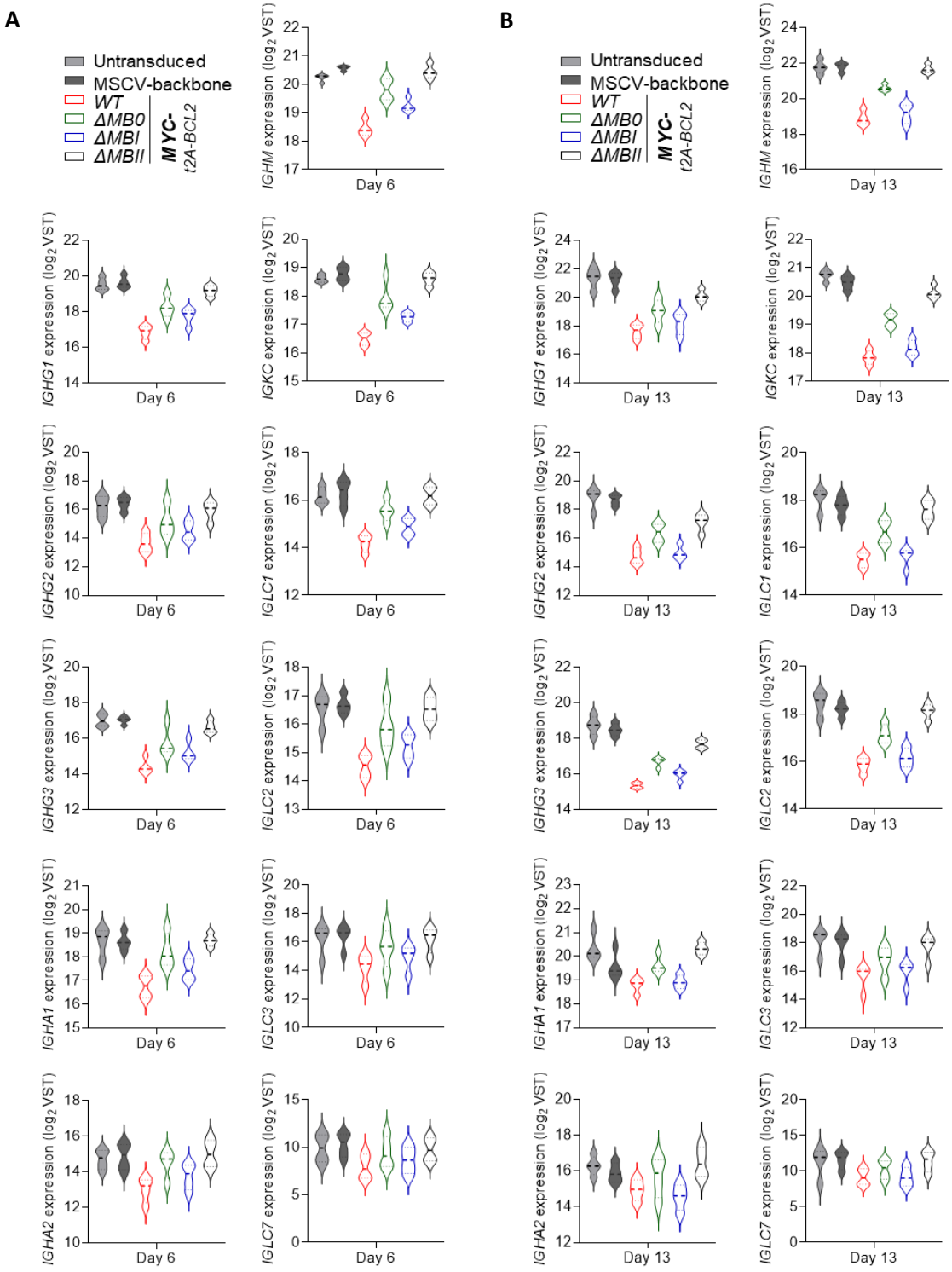

Figure 4.24 Heavy and light chain immunoglobulins gene expression. Normalised expression values of DEGs were plotted for the indicated conditions at day 6 and day 13 evaluating heavy chain *IGHG1*, *IGHG2*, *IGHG3*, *IGHA1*, *IGHA2* and *IGHM* and light chain *IGKC*, *IGLC1*, *IGLC2*, *IGLC3* and *IGLC7* expression. Software DESeq2 conducted variance stabilizing transformation (VST) analysis generating the normalized log_2-transformed gene expression values, with stabilized variance, that are visualized in the graphs. Data are representative of two independent experiments with two biological replicates (N= 2) and no technical replicates per experiment. The total number of donors tested as biological replicates was four (N= 4).

4.5.7 Parsimonious Gene Correlation Network Analysis (PGCNA)

To understand the role of MBII and MB0 in the biological processes impacted by MYC WT-BCL2 hyperfunction during PC differentiation the PGCNA approach was utilised for additional gene expression data analysis. As displayed in Table 4.5, the analysed DEGs gave 13 modules of coregulation associated with distinct cellular processes. The module (M) with the most assigned genes in it was M1 with 1598 genes, while the smaller module, in terms of gene counts, was M13 with 257 genes.

Table 4.5 PGCNA identified 13 modules of co-expression. Each module was assigned a summary description based on the GO terms and signatures that were overrepresented by their assigned genes. The short description of the functional annotation characterizing each module is indicated as Module ID. The number of genes assigned per module is in the column indicated as Module Size. Data are representative of two independent experiments with two biological replicates (N= 2) and no technical replicates per experiment. The total number of donors tested as biological replicates was four (N= 4); M, module.

Module	Module ID	Module Size
M1	Mitochondrian MYC_Targets	1598
M2	ZincFinger	1522
M3	IRF4-ChIP upBC Myc_ChIP_PET_Expr_DN scGC_cluster1_LZ	1420
M4	Ribosome Translation	1341
M5	MATRISOME EMT	1249
M6	ZHAN_MM_CD1_VS_CD2_UP ZBTB7B_TARGET_GENES	1157
M7	upPC Golgi ER	1125
M8	CellCycle	1072
M9	upPC Ig	1069
M10	mRNA-Splicing Mitochondrian MYC_Targets scGC_cluster1_DZ MYC_ChIP_Exp_DN	971
M11	chr7q35	904
M12	PA700_complex REACTOME_PCP_CE_PATHWAY BCR_DownstreamSig	675
M13	Tcell_Like	257

A summary description was used for each of the 13 modules upon GO analysis and signature enrichment of the genes they contained. This summary is depicted in Table 4.5 under Module ID, and was further

explored in Table 4.6, where highly enriched signatures and GO terms per module are presented. As previously observed in section 3.6.7 of the Results Chapter 3, each module was assigned to genes with distinctive functional annotations. M4 and M10 were overrepresented by GO terms and signatures associated with known MYC-mediated function. M4 was enriched for translation and ribosome-related signatures. In M10, RNA-processing, transcription and the HALLMARK_MYC TARGETS V1 signatures were significantly enriched. A combination of the enriched signatures in M4 and M10 was observed in M1, while M6 showed enrichment in RNA-processing and Myeloma CD-1 subgroup signatures.

A module with distinct ontologies was the M8 which showed enrichment in cell cycle-related terms and signatures. M3 was overrepresented by genes involved in B cell activation, Blimp repressed and NF-κB target regulation as well as reduced induction of MYC targets. Significant enrichment in PC-associated signatures related to the ER and Golgi apparatus was observed in M7 while immunoglobulin-associated GO terms were overrepresented in M9. M2 was characterized by enrichment in transcription-associated signatures followed by M5 representing enrichment in extracellular matrix and B cell activation-related genes. Expression of genes associated with T cell activation as well as B cell differentiation and reduced induction of MYC targets was detected in M13.

Table 4.6 GO and signature enrichment analysis for the 13 identified modules using PGCNA. The 13 modules derived by Parsimonious Gene Correlation Network Analysis (PGCNA) were tested for their functional annotation based on highly enriched signatures and GO terms. Data are representative of two independent experiments with two biological replicates (N= 2) and no technical replicates per experiment. The total number of donors tested as biological replicates was four (N= 4); FDR, false discovery rate.

Module 4						
Gene Signature	**Gene Set**	**Overlapping**	**Gene Set Size**	**Z-score**	**p-value**	**FDR**
cytosolic ribosome [GoID:GO:0022626]	GeneOntology_CC	80	91	17.7806	9.98E-71	5.62E-67
cytoplasmic translation [GoID:GO:0002181]	GeneOntology_BP	95	137	17.1491	6.39E-66	2.16E-62
Ribonucleoprotein	UniProt-Keyword	87	253	11.0736	1.69E-28	9.33E-26
translation [GoID:GO:0006412]	GeneOntology_BP	128	575	9.4807	2.53E-21	9.58E-19
Ribosomal_protein (PMID:11567628)	SignatureDB	17	18	8.3864	5.01E-17	1.50E-14
Module 10						
Gene Signature	**Gene Set**	**Overlapping**	**Gene Set Size**	**Z-score**	**p-value**	**FDR**
RNA splicing [GoID:GO:0008380]	GeneOntology_BP	86	341	10.7202	8.18E-27	9.53E-24
RNA processing [GoID:GO:0006396]	GeneOntology_BP	139	784	10.5229	6.78E-26	6.93E-23
mRNA splicing, via spliceosome [GoID:GO:0000398]	GeneOntology_BP	69	246	10.2323	1.42E-24	1.04E-21
HALLMARK_MYC_TARGETS_V1	MSigDB_H	47	200	7.4905	6.86E-14	1.43E-11
gene expression [GoID:GO:0010467]	GeneOntology_BP	387	4096	7.3835	1.54E-13	3.04E-11
Module 1						
Gene Signature	**Gene Set**	**Overlapping**	**Gene Set Size**	**Z-score**	**p-value**	**FDR**
DLBCL_PGCNA_M8 Mitochondrian MYC_Overexpression RibosomeBiogenesis	LEEDS_GOLD	351	795	24.0163	1.88E-127	3.17E-123
mitochondrion [GoID:GO:0005739]	GeneOntology_CC	421	1365	20.2634	2.70E-91	1.14E-87
DLBCL-WithBL_PGCNA_M1 Mitochondrian RibosomeBiogenesis MYC_Overexpression	LEEDS_GOLD	441	1521	19.6727	3.69E-86	1.39E-82
RNA binding [GoID:GO:0003723]	GeneOntology_MF	408	1441	18.3671	2.41E-75	6.25E-72
ribonucleoprotein complex biogenesis [GoID:GO:0022613]	GeneOntology_BP	188	396	18.0112	1.59E-72	3.36E-69

Module 6						
Gene Signature	**Gene Set**	**Overlapping**	**Gene Set Size**	**Z-score**	**p-value**	**FDR**
Methyltransferase	UniProt-Keyword	26	151	3.7522	0.0002	0.0135
Myeloma_CD-1_subgroup_up (PMID:16728703)	SignatureDB	10	37	3.4701	0.0005	0.0284
tRNA processing [GoID:GO:0008033]	GeneOntology_BP	19	113	3.1436	0.0017	0.0619
RNA modification [GoID:GO:0009451]	GeneOntology_BP	21	143	2.7889	0.0053	0.1235
tRNA methyltransferase activity [GoID:GO:0008175]	GeneOntology_MF	7	28	2.7626	0.0057	0.1287

Module 8						
Gene Signature	**Gene Set**	**Overlapping**	**Gene Set Size**	**Z-score**	**p-value**	**FDR**
Cell_cycle_Liu (PMID:15123814)	SignatureDB	123	221	18.8981	1.18E-79	1.11E-76
HALLMARK_E2F_TARGETS	MSigDB_H	117	199	18.8791	1.69E-79	1.55E-76
Cell_cycle_Whitfield (PMID:12058064)	SignatureDB	190	590	18.0178	1.41E-72	1.08E-69
cell cycle [GoID:GO:0007049]	GeneOntology_BP	294	1318	18.0149	1.49E-72	1.12E-69
HALLMARK_G2M_CHECKPOINT	MSigDB_H	100	192	16.4649	6.56E-61	3.16E-58

Module 3						
Gene Signature	**Gene Set**	**Overlapping**	**Gene Set Size**	**Z-score**	**p-value**	**FDR**
Myc_ChIP_PET_Expr_Down (PMID:17093053)	SignatureDB	63	239	7.4371	1.03E-13	7.09E-11
IRF4_ABC_induced_ABCDLBCL (PMID:22698399)	SignatureDB	42	149	6.4151	1.41E-10	4.17E-08
Blimp_Bcell_repressed (PMID:12150891)	SignatureDB	22	60	5.6222	1.89E-08	2.72E-06
HALLMARK_TNFA_SIGNALING_VIA_NFKB	MSigDB_H	40	161	5.6051	2.08E-08	2.95E-06
IRF4_ABC_induced_all (PMID:22698399)	SignatureDB	69	387	5.0114	5.40E-07	4.64E-05

Module 7						
Gene Signature	**Gene Set**	**Overlapping**	**Gene Set Size**	**Z-score**	**p-value**	**FDR**
BcellDiff_upPC	LEEDS_GOLD	167	745	12.8527	8.31E-38	9.35E-34
BcellD0-D41_PGCNA_M4 ER Golgi UPR_XBP1	LEEDS_GOLD	77	327	8.8879	6.23E-19	1.00E-15
Golgi apparatus	UniProt-Keyword	111	672	7.6630	1.82E-14	1.28E-11
Golgi organization [GoID:GO:0007030]	GeneOntology_BP	28	121	5.2513	1.51E-07	3.17E-05
ER-Golgi transport	UniProt-Keyword	22	85	5.0624	4.14E-07	7.90E-05

Module 9						
Gene Signature	**Gene Set**	**Overlapping**	**Gene Set Size**	**Z-score**	**p-value**	**FDR**
Immunoglobulin	UniProt-Keyword	91	119	18.8837	1.55E-79	5.25E-75
immunoglobulin complex [GoID:GO:0019814]	GeneOntology_CC	93	127	18.7266	3.01E-78	5.08E-74
BLCA_PGCNA_M41 Immunoglobulins	LEEDS_GOLD	98	152	18.1839	6.93E-74	7.79E-70
immunoglobulin complex, circulating [GoID:GO:0042571A]	GeneOntology_CC	41	58	12.1313	7.21E-34	1.22E-30
humoral immune response mediated by circulating immunoglobulin [GoID:GO:0002455]	GeneOntology_BP	39	81	9.9504	2.51E-23	2.12E-20

Module 2						
Gene Signature	**Gene Set**	**Overlapping**	**Gene Set Size**	**Z-score**	**p-value**	**FDR**
Zinc-finger	UniProt-Keyword	195	1276	5.8714	4.32E-09	9.46E-07
Zinc	UniProt-Keyword	230	1636	5.1782	2.24E-07	3.24E-05
Blood_Module-3.8_Undetermined (PMID:18631455)	SignatureDB	38	186	4.1788	2.93E-05	0.0022
DNA-binding	UniProt-Keyword	163	1282	3.0466	0.0023	0.0609
Transcription regulation	UniProt-Keyword	192	1578	2.7039	0.0069	0.1267

Module 5						
Gene Signature	**Gene Set**	**Overlapping**	**Gene Set Size**	**Z-score**	**p-value**	**FDR**
DLBCL_PGCNA_M4 EMT_Angiogenesis	LEEDS_GOLD	107	625	7.3661	1.76E-13	5.93E-11
extracellular matrix [GoID:GO:0031012]	GeneOntology_CC	40	228	4.5982	4.26E-06	0.0004
extracellular matrix structural constituent [GoID:GO:0005201]	GeneOntology_MF	16	67	3.9238	8.71E-05	0.0045
ABC_upGCB	LEEDS_GOLD	40	283	3.4374	0.0006	0.0194
HALLMARK_EPITHELIAL_MESENCHYMAL_TRANSITION	MSigDB_H	19	103	3.3799	0.0007	0.0224

Module 13						
Gene Signature	**Gene Set**	**Overlapping**	**Gene Set Size**	**Z-score**	**p-value**	**FDR**
Myc_ChIP_PET_Expr_Down (PMID:17093053)	SignatureDB	16	239	4.6317	3.63E-06	0.0028
Tcell_cytokine_induced_IL4only (PMID:12435740)	SignatureDB	3	6	3.9012	9.57E-05	0.0267
BcellDiff_upPB	LEEDS_GOLD	11	161	3.8827	0.0001	0.0277
T cell activation [GoID:GO:0042110]	GeneOntology_BP	17	357	3.8014	0.0001	0.0342
IRF4_ABC_induced_panB (PMID:22698399)	SignatureDB	10	146	3.7082	0.0002	0.0425

Next, the transcriptional landscape of the biological processes affected by MYC WT, *Δ*MB0, *Δ*MBI or *Δ*MBII overexpression was examined using the resolved modules at day 6 and day 13. The modular co-expression of DEGs was assessed generating a hierarchically clustered heatmap of MEVs for each condition tested. As displayed in Figure 4.25, the untransduced and MSCV-backbone samples show obvious differences in

enrichment with the MYC WT, ΔMBI and ΔMB0 in this order. In contrast, the enrichment pattern in the *ΔMBII-t2A-BCL2* condition was overall more similar to the controls.

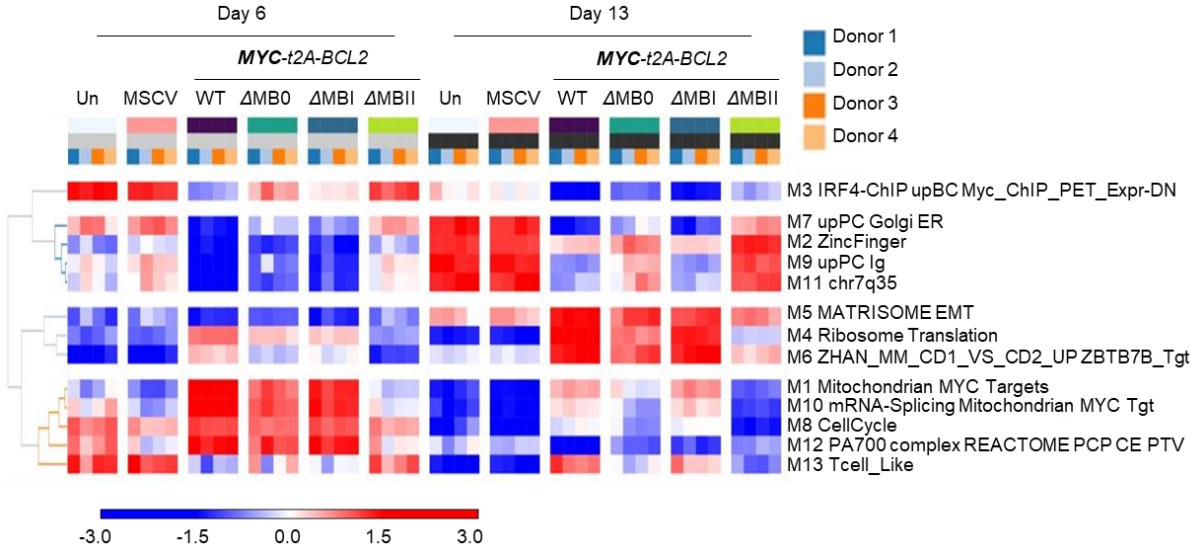

Figure 4.25 PGCNA modular analysis supported higher expression of genes associated with PC differentiation than MYC function upon deletion of the MB0 or the MBII domains in overexpressed MYC. Using Parsimonious Gene Correlation Network Analysis (PGCNA) 13 modules of gene co-regulation were resolved. Hierarchical clustering was used to generate a heatmap of module expression values (MEVs) for each condition tested. MEVs represent the modular gene expression averaged to all the genes assigned in the module based on Z-scores (-3 blue to +3 red). The 13 modules are indicated on the right and were labelled based on their enrichment for GO terms and signatures and the number of genes assigned per module. The analysis took place on day 6 and day 13 for the indicated samples (top). The PGCNA-derived heatmap was generated by Dr. Matthew Care. Data are representative of two independent experiments with two biological replicates (N= 2) and no technical replicates per experiment. The total number of donors tested as biological replicates was four (N= 4); M, module.

Specifically, modules that represent PC pathways, M7 and M9, are depleted for the *WT-t2A-BCL2* and *ΔMBI-t2A-BCL2* conditions, slightly enriched in the *ΔMB0-t2A-BCL2* condition and enriched in the *ΔMBII-t2A-BCL2* condition in a similar level to the untransduced and MSCV-backbone controls. The exact reverse effect is observed in modules M4, M5, M6, M1 and M10, related to metabolic processes and MYC targets, where depletion is observed in the controls and *ΔMBII-t2A-BCL2* samples and enrichment in the MYC WT> *ΔMBI*> *ΔMB0*-BCL2 overexpression. These results further validated the previous findings.

4.5.8 Representation of genes upregulated in MYC WT and ΔMB0 or MYC WT and ΔMBI over the MSCV-backbone control in the PGCNA resolved modules

Venn diagrams performed in section 4.5.3 (Figure 4.16) classified DEGs with higher expression in the MYC WT and ΔMB0 or ΔMBI conditions versus the MSCV-backbone in seven distinct gene sets. Gene set B contained shared genes upregulated in *WT-t2A-BCL2* and *ΔMB0-t2A-BCL2* and not induced in the *ΔMBI-t2A-BCL2* condition. Gene set C contained highly induced genes which were identified in both *WT-t2A-BCL2* and *ΔMBI-t2A-BCL2* but not in *ΔMB0-t2A-BCL2*.

To evaluate the contribution of these gene sets in the PGCNA resolved modules pairwise comparisons were performed between Gene set B or Gene set C and the genes assigned to each of the 13 modules. As depicted in Table 4.7, when this analysis was conducted for day 6 identified gene sets, the DEGs belonging to Gene set B were mainly assigned to the MYC function-related modules M4, M1, M6, M10 as well as in M12 and the cell cycle module M8. MYC function-associated modules M1, M10 and M6 were the modules represented by the highest gene count from DEGs in Gene set C followed by M8, M12 and M4. Ten genes were present in M2 and only one in M5. This analysis suggested that at day 6, the modular co-expression patterns of Gene sets B and C are relatively similar and primarily associated with MYC function signatures.

Table 4.7 Overlap with the PGCNA modules for the genes identified to depend either on MB0 or on MBI for their day 6 upregulation in *T58I-t2A-BCL2* versus the MSCV-backbone. Using Parsimonious Gene Correlation Network Analysis (PGCNA) 13 modules of gene co-regulation were resolved. The gene lists of each of the 13 modules were compared using pairwise comparisons with the Gene sets B and C at day 6, identified using Venn diagrams in Figure 4.16A. Gene set B was assigned shared genes with higher expression in *WT-t2A-BCL2* and *ΔMB0-t2A-BCL2* over the MSCV-backbone. Gene set C was assigned shared genes with higher expression in *WT-t2A-BCL2* and *ΔMBI-t2A-BCL2* over the MSCV-backbone. Gene counts resulting from the pairwise comparisons are in the column named Genes per module (right). Modules with no overlap were not included. Data are representative of two independent experiments with two biological replicates (N= 2) and no technical replicates per experiment. The total number of donors tested as biological replicates was four (N= 4); M, module.

Genes compared between:
WT-t2A-BCL2
ΔMB0-t2A-BCL2
ΔMBI-t2A-BCL2

Common genes only in *WT-t2A-BCL2* and *ΔMB0-t2A-BCL2* – **day 6 Gene set B**

PGCNA-derived module	Genes per module
M4: Ribosome Translation	60
M1: Mitochondrian MYC_Targets	52
M6: ZHAN_MM_CD1_VS_CD2_UP ZBTB7B_TARGET_GENES	27
M10: mRNA-Splicing Mitochondrian MYC_Targets scGC_cluster1_DZ MYC_ChIP_Exp_DN	25
M12: PA700_complex REACTOME_PCP_CE_PATHWAY BCR_DownstreamSig	6
M8: CellCycle	5
M2: ZincFinger	2
M5: MATRISOME EMT	1
M13: Tcell_Like	1

Common genes only in *WT-t2A-BCL2* and *ΔMBI-t2A-BCL2* – **day 6 Gene set C**

PGCNA-derived module	Genes per module
M1: Mitochondrian MYC_Targets	204
M10: mRNA-Splicing Mitochondrian MYC_Targets scGC_cluster1_DZ MYC_ChIP_Exp_DN	124
M6: ZHAN_MM_CD1_VS_CD2_UP ZBTB7B_TARGET_GENES	90
M8: CellCycle	57
M12: PA700_complex REACTOME_PCP_CE_PATHWAY BCR_DownstreamSig	57
M4: Ribosome Translation	52
M2: ZincFinger	10
M5: MATRISOME EMT	1

At day 13, higher was the contribution of Gene set C than Gene set B in the modular co-expression patterns identified by PGCNA (Table 4.8). Both gene sets represented MYC function-associated modules but with different preferences in contribution while again no gene counts were identified in the PC-related modules M7 and M9. Gene set B contributed the most in M5, M6, M1 and M4 whereas Gene set C was more represented by M1, M4, M10 and M6 of the MYC function-associated modules. In addition, the cell cycle module M8 and T cell-associated module M13 were represented with lower gene counts by both Gene sets. Overall, Gene set B showed a more MYC function-restricted representation in the modules. Gene set C, with genes requiring MB0 for their expression, showed additional contribution in M3, M2 and M12 but with very low gene counts. Also, the number of genes induced independently of the MBI but only in the presence of MB0 (Gene set C) was higher, indicating that MB0 was more critical for MYC-mediated transcriptional regulation than the MBI. This agreed with a higher representation of Gene set C in the resolved modules than Gene set B on day 13.

Table 4.8 Overlap with the PGCNA modules for the genes identified to depend either on MB0 or on MBI for their day 13 upregulation *in T58I-t2A-BCL2* versus the MSCV-backbone. Using Parsimonious Gene Correlation Network Analysis (PGCNA) 13 modules of gene co-regulation were resolved. The gene lists of each of the 13 modules were

compared using pairwise comparisons with the Gene sets B and C at day 13, identified using Venn diagrams in Figure 4.16B. Gene set B was assigned shared genes with higher expression in *WT-t2A-BCL2* and *ΔMB0-t2A-BCL2* over the MSCV-backbone. Gene set C was assigned shared genes with higher expression in *WT-t2A-BCL2* and *ΔMBI-t2A-BCL2* over the MSCV-backbone. Gene counts resulting from the pairwise comparisons are in the column named Genes per module (right). Modules with no overlap were not included. Data are representative of two independent experiments with two biological replicates (N= 2) and no technical replicates per experiment. The total number of donors tested as biological replicates was four (N= 4); M, module.

Genes compared between:
WT-t2A-BCL2
ΔMB0-t2A-BCL2
ΔMBI-t2A-BCL2

Common genes only in *WT-t2A-BCL2* and *ΔMB0-t2A-BCL2* – **day 13 Gene set B**

PGCNA-derived module	Genes per module
M5: MATRISOME EMT	11
M6: ZHAN_MM_CD1_VS_CD2_UP ZBTB7B_TARGET_GENES	10
M1: Mitochondrian MYC_Targets	9
M4: Ribosome Translation	5
M8: CellCycle	4
M13: Tcell_Like	3
M10: mRNA-Splicing Mitochondrian MYC_Targets scGC_cluster1_DZ MYC_ChIP_Exp_DN	2

Common genes only in *WT-t2A-BCL2* and *ΔMBI-t2A-BCL2* – **day 13 Gene set C**

PGCNA-derived module	Genes per module
M1: Mitochondrian MYC_Targets	300
M4: Ribosome Translation	264
M10: mRNA-Splicing Mitochondrian MYC_Targets scGC_cluster1_DZ MYC_ChIP_Exp_DN	205
M6: ZHAN_MM_CD1_VS_CD2_UP ZBTB7B_TARGET_GENES	131
M8: CellCycle	98
M5: MATRISOME EMT	60
M13: Tcell_Like	23
M3: IRF4-ChIP upBC Myc_ChIP_PET_Expr_DN scGC_cluster1_LZ	2
M2: ZincFinger	1
M12: PA700_complex REACTOME_PCP_CE_PATHWAY BCR_DownstreamSig	1

4.6 Impairment of antibody secretion upon MYC-BCL2 overexpression is dependent on MYC MBII and MB0 domains

Having established the critical role of MB0 and MBII in the effect observed upon MYC-BCL2 overexpression at a transcriptional level, the contribution of MB0, MBI or MBII domains in the antibody secretion of the differentiated cells was assessed next. ELISAs were conducted for day 6 and day 13 collected supernatants from *WT-*, *ΔMB0-*, *ΔMBI-*, *ΔMBII-t2A-BCL2* transductions and the untransduced and MSCV-backbone

controls. Initial quantification of human IgG and IgM concentrations (ng/ml) was performed. Day 6 supernatants showed reduced concentrations of IgG and IgM in the *WT-t2A-BCL2* and *ΔMBI-t2A-BCL2* transductions while small differences were observed in secretion between the remaining conditions (Figure 4.26A). However, this effect was not observed on day 13 (Figure 4.26B).

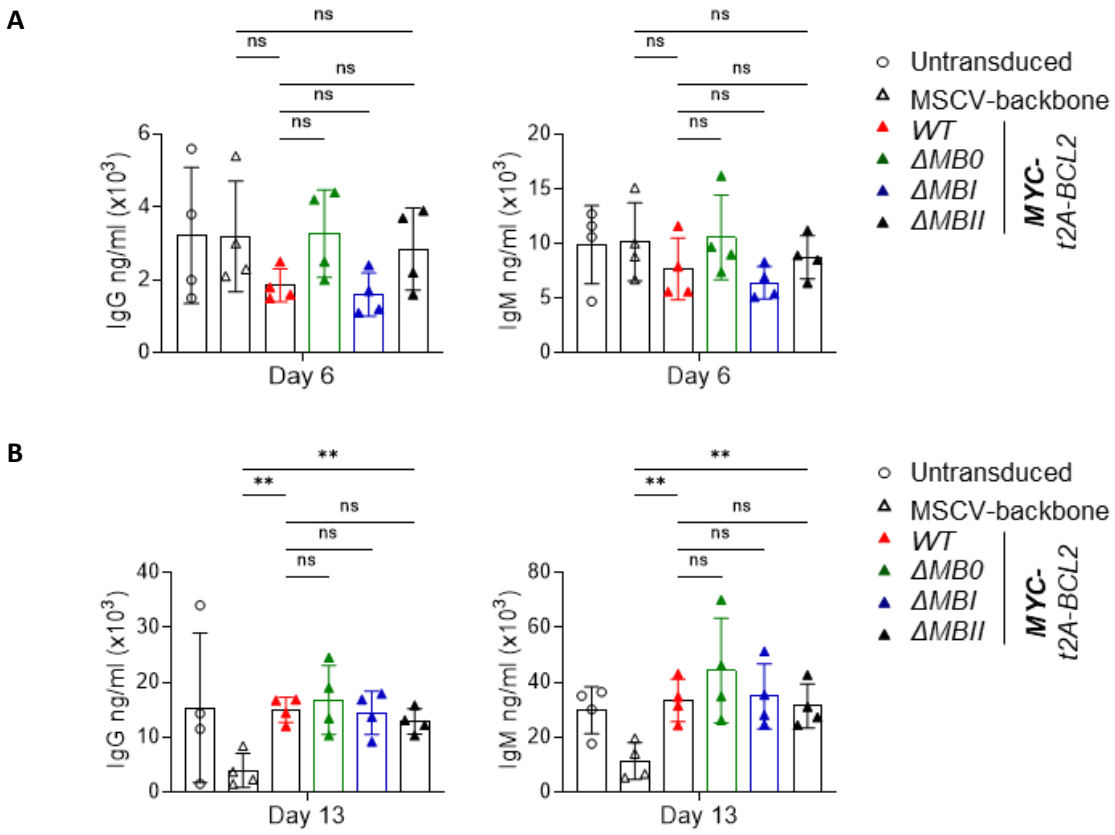

Figure 4.26 IgG and IgM antibody concentrations evaluated by ELISAs. Supernatants of (**A**) day 6 and (**B**) day 13 untransduced or transduced with the indicated retroviral conditions samples, were assessed for their antibody secretion. Human total IgG and IgM ELISAs were performed, and quantification of the detected antibody secretion was calculated at ng/ml per time point tested as indicated. Unpaired two-tailed Student's *t*-test. Data are representative of two independent experiments with two biological replicates (N= 2) per experiment. The total number of donors tested as biological replicates was four (N= 4). Each sample was tested in two technical replicates per assay. Bars and error represent mean and standard deviation (SD); ns, not significant; ** P < 0.01.

When the analysis was performed by quantifying antibody concentration per cell the previously established hierarchical pattern of importance to the hyperfunctional MYC-mediated effect was observed for the deletion mutants. As displayed in Figure 4.27A, overexpression of MYC WT-BCL2 significantly reduced the antibody secretion per cell of either the IgG or the IgM at day 6 in comparison to the MSCV-

backbone as well as the untransduced. Deletion of the MBI domain showed a slight improvement in the MYC overexpression impact on the antibody secretion capacity per cell. Interestingly, deletion of the MB0 or MBII domain reduced the MYC overexpression effect showing higher antibody secretion more similar to the controls. In Figure 4.27B, representing the day 13 PC stage of the system, the secretion per cell for the controls was enhanced in comparison to day 6, Figure 4.27A, and even more profoundly reduced between the controls and the MYC WT-BCL2 derived supernatants. At this time point of the model system, the *ΔMBI-t2A-BCL2* condition showed marginal differences to the *WT-t2A-BCL2* samples with the cells secreting less IgG and IgM than the controls. In contrast, deletion of the MB0 domain resulted in increased secretory output in comparison to the *WT-t2A-BCL2* and *ΔMBI-t2A-BCL2* transductions. Importantly, loss of MBII function significantly reduced the ability of overexpressed MYC to impair both IgG and IgM secretion.

These results confirm that the cells populating the culture at both day 6 and day 13 secrete significantly less IgG and IgM antibodies when they overexpress WT MYC protein. The domains MBII and MB0, but not the MBI, were critical contributors to the impaired secretory output observed upon MYC WT overexpression in the model system.

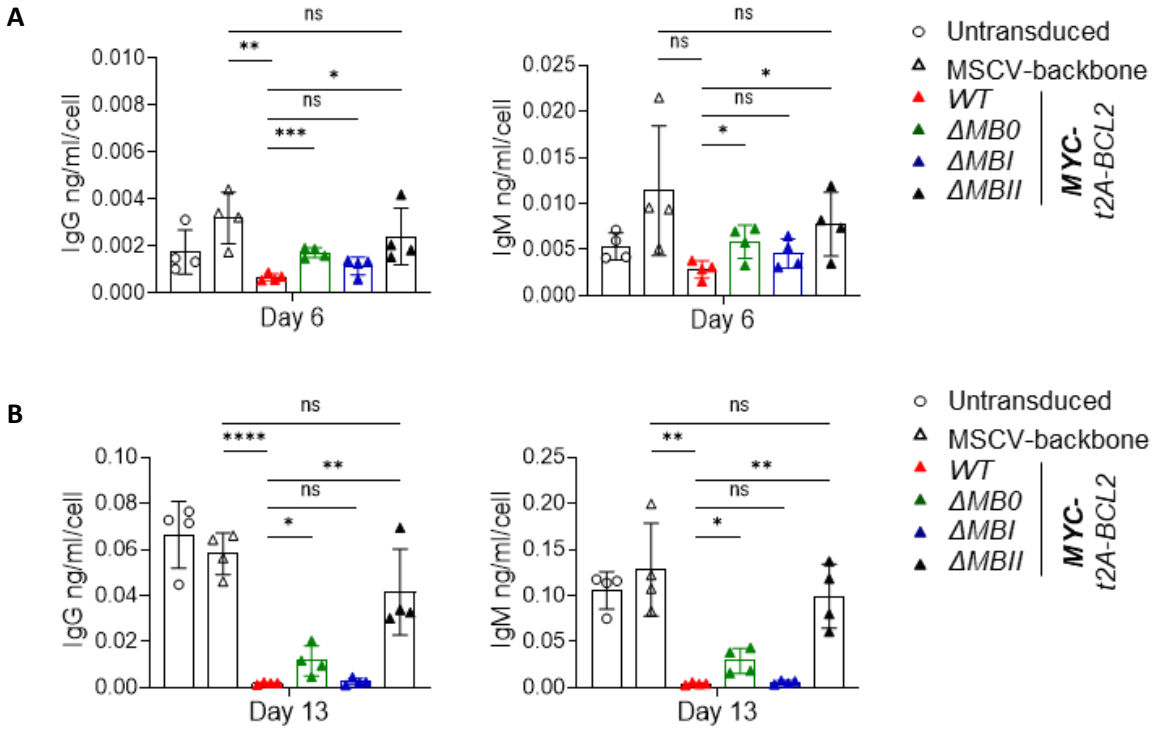

Figure 4.27 Significantly reduced MYC hyperfunction effect on IgG and IgM antibody secretion upon ΔMBII-BCL2 overexpression. Supernatants of (**A**) day 6 and (**B**) day 13 untransduced or transduced with the indicated retroviral

conditions samples, were assessed for their antibody secretion. Human total IgG and IgM ELISAs were performed, and quantification of the detected antibody secretion was calculated at ng/ml/cell per time point tested as indicated. Unpaired two-tailed Student's *t*-test. Data are representative of two independent experiments with two biological replicates (N= 2) per experiment. The total number of donors tested as biological replicates was four (N= 4). Each sample was tested in two technical replicates per assay. Bars and error represent mean and standard deviation (SD); ns, not significant; * $P < 0.05$; ** $P < 0.01$; *** $P < 0.001$; **** $P < 0.0001$.

4.7 Discussion

In this Chapter, a WT MYC protein was overexpressed in the developed model system in combination with BCL2. Having established its effect on PC differentiation, its comparison to MYC deletion mutants of ΔMB0, ΔMBI or ΔMBII allowed a clear confirmation of their contribution individually to the PC differentiation effect. The combination of MYC overexpression with the anti-apoptotic protein BCL2 was initially selected to avoid MYC-mediated apoptosis (203, 211). In addition, during PC differentiation in the model system limitations in survival and cell number had to be considered, especially in cells that had undergone a transduction procedure. In an overexpression context, the anti-apoptotic function conferred by BCL2 augmented the enhanced survival observed in the MYC-BCL2 transductions. On the contrary, the cells that were transduced with the MSCV-backbone virus, lacking BCL2 overexpression, showed decreased survival in comparison to the untransduced and the different *MYC-t2A-BCL2* conditions, with a more profound effect to be observed at the later time points of the culture. Hence, BCL2 overexpression was maintained throughout to overcome these primary culture-associated challenges, in addition to protecting from MYC overexpression-mediated apoptosis (272).

In the context of enforced MYC and BCL2 co-overexpression, both MYC and BCL2 could affect the PC differentiation process. Based on our results, when MYC function was impaired by overexpressing its ΔMB0 or ΔMBII mutants, the PC differentiation appeared less perturbed or almost normal respectively, despite sustained BCL2 overexpression. Also, our gene expression study showed that the cells overexpressing MYC WT and BCL2 were skewed toward a MYC hyperfunction-related transcriptional profile. This enforced MYC effect was lost in *ΔMBII-t2A-BCL2* samples, and despite intact BCL2 overexpression, this condition showed marginal differences in gene expression to the controls. Thus, we could conclude that the BCL2 overexpression did not play a critical role in the perturbed PC differentiation observed upon MYC WT overexpression.

With a focus on MYC transactivation and transformation activity, ΔMBI has been shown to have a similar effect to full MYC (240). This has been previously attributed to its crucial role in MYC protein stability. MBI containing T58 and S62 residues regulates MYC protein degradation via the proteasome upon a series of sequential phosphorylation steps (199, 272, 319). The immunophenotypic changes observed in MYC T58I-BCL2 samples were similar to the *ΔMBI-t2A-BCL2* condition which also showed moderate differences to the *WT-t2A-BCL2*, especially at day 13. In other models, gene expression data suggested that MYC WT, T58I, and T58A have significant differences primarily because of the chemical interactions formed upon the exchange of the different residues tested or because of differences in protein stability (272). Conformational differences between WT, T58I, or ΔMBI MYC protein are to be expected also in the present model system. However, these did not yield considerable differences to the observed phenotype, and marginally affected the MYC impact on PC differentiation in an overexpression context.

In contrast to the loss of MBI function, which resulted in a similar impact to MYC WT, deletion of the MB0 resulted in reduced function of the overexpressed MYC and thus an intermediate effect on PC differentiation. MB0 was the most recently discovered of the TAD MBs and hence maybe the least studied (322). Its role in MYC function has been associated with MYC transactivation and recruitment of TFIIF interactor driving transcriptional elongation (240, 322). Our results showed that the DEGs upregulated on MYC WT over the MSCV-backbone control in an MB0-dependent fashion were enriched for GO terms associated with activity in the nucleus and RNA transcription. Also, our flow cytometry data showed that overexpression of a ΔMB0 mutant is weakening but does not abolish MYC hyperfunction. Thus, PC differentiation was partially allowed to take place upon ΔMB0 MYC overexpression while MYC-mediated metabolic reprogramming was also observed. When deletion of the MB0 was tested in different experimental settings, ΔMB0 overexpression also sustained a significant part of MYC function. Partial reduction was observed in its ability to induce gene expression in comparison to the WT (240). In the same study when tested for its transformation activity, ΔMB0 overexpression could maintain its oncogenic activity and transform TET21, Rat1a and MCF10A cells, with constitutive $PIK3CA^{H1047R}$ expression modeling triple-negative breast cancer, upon MYC deregulation (240). The oncogenic effect of MYC driving transformation was not observed in our system, however, our findings were in agreement with the reduction of ectopically expressed MYC function upon deletion of its MB0.

The impact of ΔMBII in the model system was detrimental to the MYC hyperactivity-mediated effect on the PC differentiation. MBII being the most well-studied domain in MYC, has been strongly implicated as required for MYC function and transformation activity (212, 214, 240, 275, 314). Of similar importance

was the MBII domain for the MYC overexpression-driven effect on PC differentiation. Deletion of MBII from the *MYC* sequence had a significant impact on MYC function which despite its overexpression showed marginal differences to the controls in cell survival and number. Importantly, both gene expression and antibody secretion capacity per cell were dramatically restored upon MBII loss of function rendering MYC almost non-functional. A critical role in DNA binding and thus transactivation activity has been attributed to the MBIIIb domain of MYC via interaction with the WDR5 co-factor (208, 214). No similar role in DNA binding has been associated with the MBII domain. In addition, the MBII is located at the N terminus of MYC protein, and its deletion is not expected to have affected the MYC DNA binding domain and its interaction with MAX. Based on these it was reasoned that overexpressed ΔMBII MYC can successfully interact with MAX and bind to the DNA. The present study suggests marginal maintenance of MYC-mediated function on MYC target genes accompanied by a small impact on the PC differentiation process upon ΔMBII overexpression in the model system. Thus, the loss of MYC function observed upon ΔMBII overexpression is potentially an effect of lost PPIs with its co-factors (214). In this context, MBII-mediated MYC interactions, such as with TRRAP and STAGA (containing GCN5) or TIP60, could provide a promising avenue for MYC therapeutic targeting in B cell and PC transformation.

The recruitment of GCN5 or TIP60 HATs upon direct MYC interaction with TRRAP via its MBII domain drives epigenetic regulation of condensed chromatin (204, 240, 248). Recruited GCN5 and TIP60 confer histone H3 and H4 acetylation, respectively, resulting in chromatin remodelling to an open state (323). This has been described as an essential mechanism for MYC-mediated transcription initiation and function dependent on its MBII domain (221, 323). The present study showed that deletion of the MBII had a detrimental effect on MYC hyperfunction. Thus, it was reasoned that the interaction between MYC and TRRAP was affected in the *ΔMBII-t2A-BCL2* condition. Loss of MYC:TRRAP interaction in the MBII deletion mutant could inhibit the recruitment of HATs resulting in reduced histone H3 and H4 acetylation as previously shown (240). In this setting, condensed chromatin would persist around the loci of MYC targets impeding overexpressed MYC-mediated transcriptional regulation in the model system. Evaluation of the acetylation levels of histone H3 and H4 for the MYC ΔMBII mutant in comparison to MYC WT could provide useful information regarding the involvement of TRRAP/HAT complexes to the observed MYC overexpression effect on *in vitro* PC differentiation through these epigenetic marks.

Protein expression assessment with western blot verified successful MYC overexpression for the *WT-*, *ΔMBI-*, *ΔMB0-* and *ΔMBII-t2A-BCL2* transductions at day 6 of the model system, in comparison to the MSCV-backbone control (Figure 4.5 of the Results section 4.3.2). These results validated that its

overexpression was achieved as anticipated for the MYC-associated retroviral transductions. In parallel, the MYC protein expression levels differed between the *MYC-t2A-BCL2* conditions. Deletion of the MBI domain resulted in increased MYC protein overexpression compared to the *WT-t2A-BCL2* condition. It was reasoned that deletion of the MBI, and hence of the amino acids T58 and S62, would disrupt MYC degradation through the proteasome resulting in elevated MYC protein stability (199). Thus, in the *ΔMBI-t2A-BCL2* condition, the observed increase in MYC protein levels was an anticipated result in the model system. Interestingly though, this increase did not correlate with enhanced MYC hyperfunction. Based on cell counts, cell size, immunophenotyping, gene expression and antibody secretion results of our downstream analyses, the *ΔMBI-t2A-BCL2* condition was slightly less effective in mediating the MYC overexpression effect in comparison to the *WT-t2A-BCL2* condition. This could indicate that deleted amino acids in the MBI domain of MYC play a role in MYC WT function in an overexpression setting. In addition, the elevated protein levels observed in *ΔMBI-t2A-BCL2* condition might correspond to excess protein unable to drive an enhanced MYC hyperfunction effect. Hence, it could be possible that the deregulated MYC ΔMBI also reached a plateau of function in the model system.

In contrast to the increased MYC protein levels observed upon deletion of its MBI domain, reduced levels of expression were detected in the *ΔMB0-t2A-BCL2* and *ΔMBII-t2A-BCL2* conditions in comparison to *WT-t2A-BCL2*. This reduction might contribute to the disrupted MYC hyperfunction observed in these two conditions. Specifically, deletion of the MB0 domain resulted in impaired MYC hyperfunction and deletion of the MBII in an almost non-functional MYC. The reduced MYC protein levels upon MYC ΔMB0 or MYC ΔMBII overexpression could indicate inadequate production of the protein amount required for MYC to confer its effect in the deregulation setting tested here. In this context, lower levels of overexpressed MYC protein in the model system could be a critical determinant contributing to the impaired and severely disrupted MYC overexpression effect observed in *ΔMB0-t2A-BCL2* and *ΔMBII-t2A-BCL2* conditions, respectively.

The original perception of MYC function is based on MYC:MAX binding to canonical E-boxes in regulatory elements of specific MYC targets (208, 215). This idea has been challenged by an alternative MYC function hypothesis suggesting that MYC acts as a global amplifier of all actively transcribed genes (221). The main idea behind the global amplifier model stands on the potential ability of MYC to confer its hyperfunction in an overexpression context by expanding its effect on gene transcription (221, 227). The gene expression data presented in this study, in combination with additional studies, support that overexpressed MYC activates the transcription of specific targets, hence regulating specific processes (221, 227). MYC WT

showed enrichment in transcriptional pathways previously associated exclusively with MYC function such as, cell growth, cell cycle, glycolysis, mitochondrial biogenesis, ribosome biogenesis, protein and nucleotide synthesis, RNA synthesis and processing (221). Importantly, upon deletion of MBII and MB0 the restoration of these MYC-associated processes was observed and exchanged to the PC-related signatures without showing additional or unexpected transcriptional differences. These findings suggest that MYC overexpression regulates specific gene expression pathways to carry out its function.

The metabolic reprogramming observed in Chapter 3 upon MYC T58I-BCL2 overexpression was also confirmed in the findings of the present Chapter, in the context of MYC WT-BCL2 hyperactivity. MYC-mediated gene expression favoured metabolic signatures over PC terminal differentiation processes and antibody secretion. *LDHA* is a known MYC target involved in glycolysis (328). *LDHA* expression showed a significant increase upon MYC WT-BCL2 overexpression which was not observed upon MBII domain deletion. This indicated that MYC targets regulating processes with a central role in MYC function were not expressed in *Δ*MBII and highlighted the requirement of MBII in MYC hyperactivity. Further investigation on the amino acid sequence comprising the MBII domain could provide valuable insight into its critical role in the observed MYC hyperfunction effect on *in vitro* PC differentiation.

Chapter 5 – DCMW motif and W135 of the MBII domain are critical for the MYC hyperfunction effect on human plasma cell differentiation

5.1 Introduction

In Chapter 4, deletion of the MBII domain profoundly compromised the ability of overexpressed MYC to impact PC differentiation. One potential explanation for this is that the MBII domain is required for efficient MYC protein folding. Another explanation could be that the amino acids comprising the MBII have essential properties for MYC to drive aberrant gene expression when overexpressed in differentiating human PCs. To further investigate this hypothesis, it was reasoned that specific residues are likely to be responsible for the observed MBII importance in MYC hyperfunction.

The MBII domain contains a highly conserved amino acid sequence at residues 132-135, DCMW (204). Interrogation of the role of DCMW motif in the MYC-overexpression impact on PC differentiation would be of interest because it demonstrates the highest conservation in the MBII domain of MYC and its TAD (204, 329). Mutation of this motif into sequential alanine has previously shown a significant reduction of MYC transactivation ability in synthetic reporters but no loss of DNA binding (274). U2OS cells were co-transfected with luciferase reporter plasmids and constructs with inducible expression of MYCwt or MYC MB mutants. Sequential alanine sequences were used to substitute the core amino acids in the MBI, MBII, MBIII and MBIV domains of MYC. DCMW/AAAA in the MBII of MYC resulted in reduced luciferase gene expression in comparison to MYCwt and the lowest luciferase signal compared to the rest of the MB mutants tested. This study highlighted the requirement of MBII in MYC-driven transactivation in comparison to other MB domains of MYC. Also, it indicated the DCMW motif as critical for MBII-dependent MYC function. In another study, point mutations C133A, M134A and W135A or W135E in the DCMW motif, showed significant impairment in MYC transformation activity *in vitro* utilizing a MYC-dependent triple-negative breast cancer model based on the MCF10A cell line (276). Thus, the DCMW sequence has been previously reported to confer a critical role in normal and oncogenic MYC activity.

W135 in humans or W136 in mice is the most highly evolutionary conserved amino acid in the DCMW motif (204, 210, 234). W135 is a critical amino acid in the interaction of TRRAP with the MBII domain of MYC. Co-IP experiment in HEK-293 cells has shown that its point mutation into glycine led to disruption of

the MYC:TRRAP complex formation (330). More recently, an *in silico* model predicted that W135G sufficed to reduce the interaction of the MBII peptide with TRRAP (264). Previous studies have indicated its critical role in MYC transactivation and transformation activity (210, 314). Overexpression of W136G and W136E Myc in REFs showed impaired foci formation and transcriptional activity (210). Similarly, W135E MYC overexpression almost abolished colony formation in Rat1a cells while W135A MYC showed a slight reduction in comparison to MYCwt (234). Different W135 point mutations seem to impact MYC transactivation and oncogenic function with differential intensities and in a context-dependent manner. In an attempt to pinpoint specific MBII residues responsible for the effect of overexpressed MYC on PC differentiation, based on their critical role, mutation of the DCMW motif into a sequential alanine sequence and a single substitution of W135A, were generated and introduced to the model system.

5.2 Generation of *MYC* MBII mutants in combination with *BCL2* sequence

To generate new retroviral constructs containing MBII mutations the MYC *WT-t2A-BCL2* construct was utilised and mutations were commercially added to its sequence with PCR mutagenesis by MRC PPU Reagents and Services, University of Dundee. The new inserts were cloned in pIRES2-EGFP plasmids and sub-cloning was conducted in-house into the retroviral construct of MSCV-backbone carrying the IRES and *CD2* reporter sequences. As Figure 5.1A and Figure 5.1B show, two new retroviral constructs were generated, one carrying a mutated DCMW motif into an alanine sequence, namely MBII-4aa mut (Appendix 10), and the second carrying a W135A substitution, namely MBII-W135A (Appendix 11), respectively.

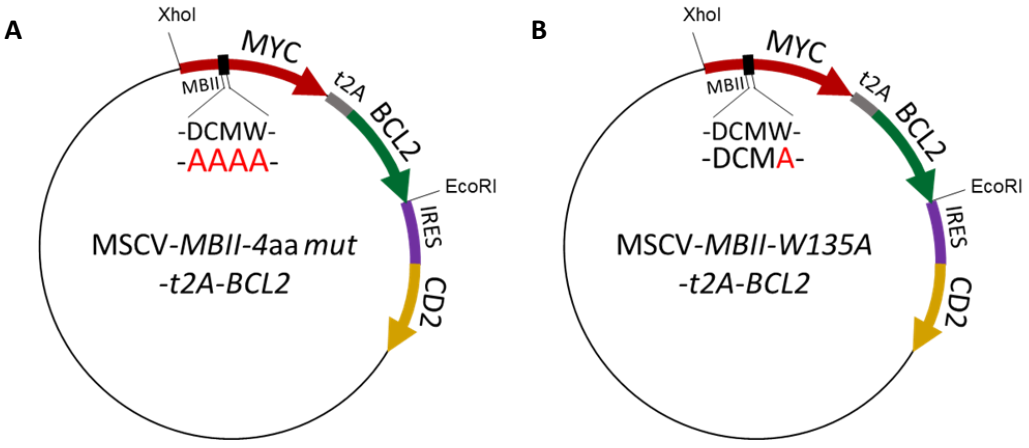

Figure 5.1 MYC MBII mutants' retroviral constructs. Graphical representation of the constructs designed for overexpression of (**A**) MYC MBII-4aa mut and (**B**) MYC MBII-W135A. The inserts, including a *-t2A-BCL2* sequence,

were sub-cloned into the MSCV-IRES-human CD2 backbone vector utilizing the unique sites of the restriction enzymes XhoI and EcoRI, as indicated on the map of each construct at the start and the end site of their inserts respectively.

5.2.1 Cloning and validation of *MYC* MBII mutants with *BCL2* into the MSCV-backbone

New pIRES2-EGFP vectors with the *MBII-4aa mut-t2A-BCL2* or *MBII-W135A-t2A-BCL2* inserts were propagated and purified plasmids were validated with diagnostic digests as displayed in Figure 5.2A. Unique restriction enzymes XhoI and EcoRI were used to isolate the insert DNA. The insert DNA bands were validated based on an anticipated size of 2,165 bp. Gel extraction method was utilised to isolate their DNA. In Figure 5.2B, the purified insert DNA size was validated on an agarose gel with a single band confirming that only the desired insert DNA has been purified before sub-cloning into the MSCV-backbone vector.

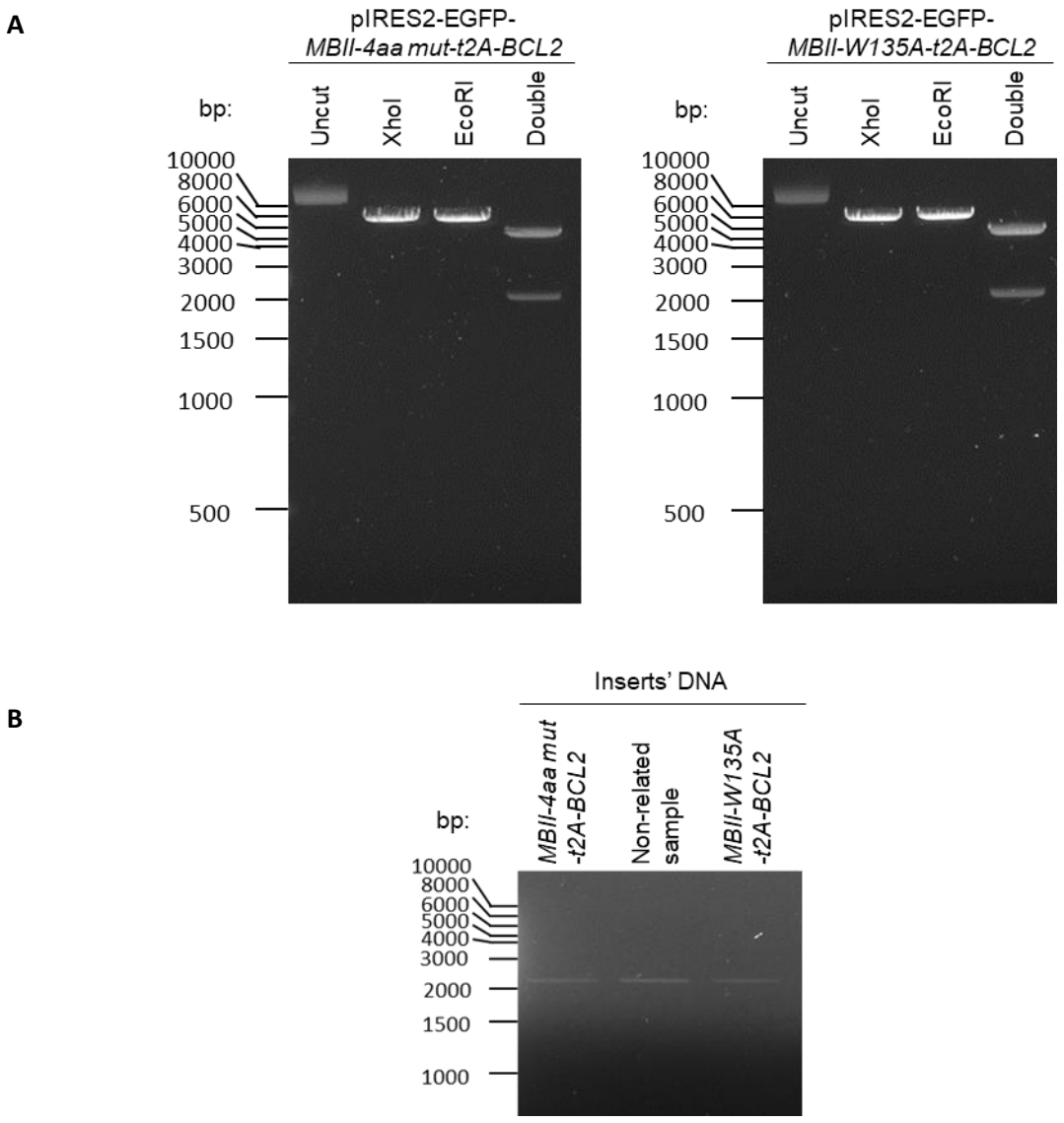

Figure 5.2 Inserts DNA isolation for the MBII mutant plasmids before sub-cloning into the retroviral vectors. (**A**) Images of diagnostic digests on 1% agarose gels for the *MBII-4aa mut-t2A-BCL2* (left) and the *MBII-W135A-t2A-BCL2* (right) inserts in pIRES2-EGFP plasmids. Undigested (uncut), single digests with either XhoI or EcoRI and double digest with both XhoI and EcoRI, conditions were assessed to validate insert size. The validated inserts' DNA was extracted from the gel. (**B**) Inserts gel purified DNA on a 1% agarose gel for purity validation prior to subcloning. Ladder DNA band sizes are indicated at the left side of each gel; bp, base pairs.

These results verified the anticipated DNA size of 2,165 bp for both inserts and allowed their sub-cloning into the MSCV-backbone retroviral vectors to proceed. As displayed in Figure 5.3A and Figure 5.3B, single colony-derived MSCV-based retroviral constructs were successfully generated carrying the inserts of interest with the anticipated DNA size in colonies 1 and 2 for the MSCV-*MBII-4aa mut-t2A-BCL2* vector and

in colonies 1 and 3 for the MSCV-*MBII-W135A-t2A-BCL2* vector respectively. Colony 2 of the latter vector failed to integrate the desired insert since multiple cuts were observed in all the conditions and not in the anticipated size. Thus, this colony was not used further in this Chapter.

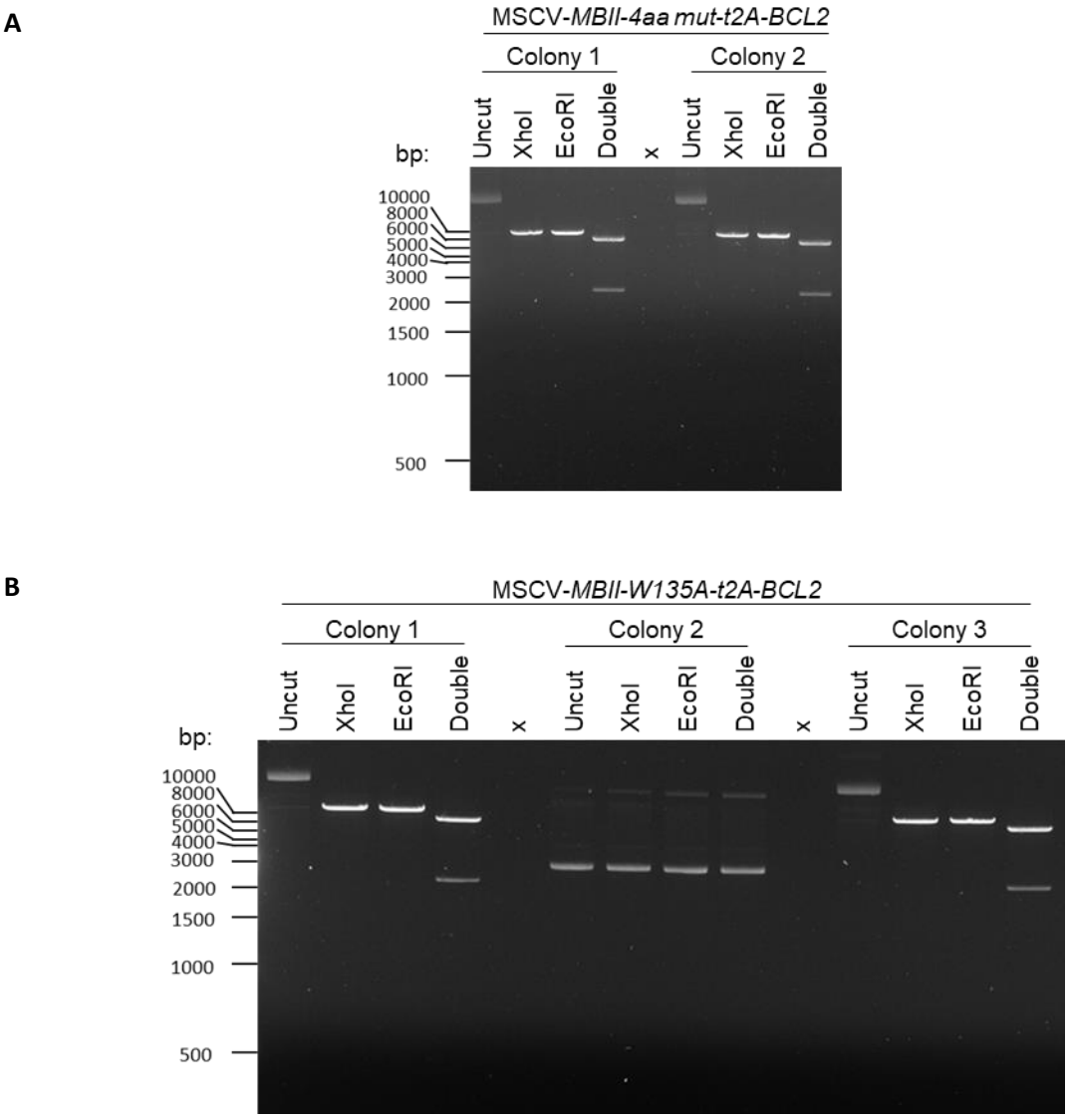

Figure 5.3 Validation of MBII mutants' inserts sub-cloning into MSCV-backbone retroviral plasmid. Images of the diagnostic digests on 1% agarose gels for the single colony derived from (**A**) *MBII-4aa mut-t2A-BCL2* and (**B**) *MBII-W135A-t2A-BCL2*, MSCV-based retroviral constructs upon cloning. Undigested (uncut), single digests with either XhoI or EcoRI and double digest with both XhoI and EcoRI, conditions were assessed to validate insert size at 2,165 bp and backbone vector at 6,574 bp in the double digest condition. The total construct size was 8,739 bp for the single digests as anticipated. Ladder DNA band sizes are indicated at the left side of each gel; x, empty well; bp, base pairs.

Additional validation of the mutated DCMW/AAAA and W135A sequences sub-cloning in the MSCV-backbone constructs was conducted with Sanger sequencing. Both MSCV-*MBII-4aa mut-t2A-BCL2* and MSCV-*MBII-W135A-t2A-BCL2* retroviral vectors were successfully generated carrying the anticipated substitutions (Figure 5.4A and Figure 5.4B).

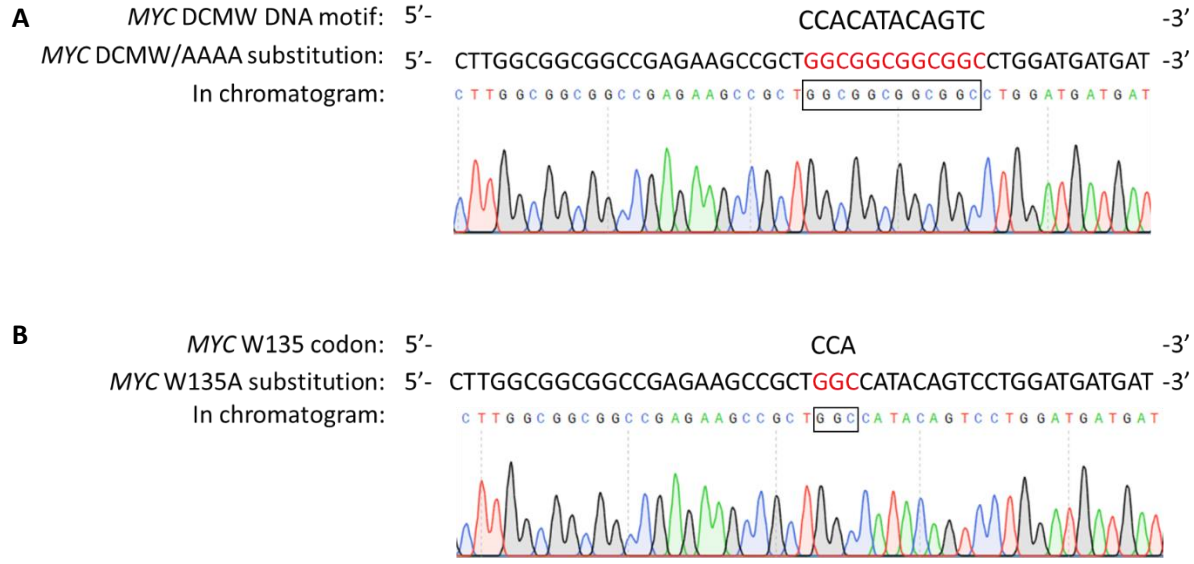

Figure 5.4 Sanger sequencing trace of the MBII mutants' inserts upon their sub-cloning into MSCV-backbone retroviral constructs. Images representing a fraction of the chromatogram generated upon Sanger sequencing with the reverse primers. The mutated nucleotides for (**A**) *MBII-4aa mut-t2A-BCL2* and (**B**) *MBII-W135A-t2A-BCL2* plasmids were visualised and compared to the wild type sequence of *MYC* in a 5'-> 3' orientation for the noncoding DNA strand (top line). The nucleotides originally mutated into 5'- GCC -3' codons in the coding DNA strand encoding for alanine, correspond to 5'- GGC -3' codons of the reverse primer generated sequence and are highlighted with red in each anticipated substituted sequence (middle line) and with a black box at the top of the chromatogram (bottom line). Visualization of the chromatograms was performed with SnapGene Viewer 5.2.4 software.

5.2.2 Virus generation and validation of the MYC MBII mutants

The two new retroviral constructs carrying MBII mutations in the *MYC* sequence and combined with *BCL2*, were used to generate viral stocks. Frozen viral stocks were validated for their transduction efficiency based on the CD2 reporter levels expressed in HEK-293 transduced cells. In addition, new stocks of *WT-t2A-BCL2* and *ΔMBII-t2A-BCL2* virus were generated and validated for the following set of experiments. As displayed in Figure 5.5, all the new retroviruses showed higher transduction efficiency than 40% and greater CD2 positivity than the MSCV-backbone virus included as a positive control 72 hours post-transduction. The untransduced control had only 0.26% $CD2^+$ cells which was very similar to the negligible

CD2 positivity observed in the isotype controls. These results validated the transduction efficiency of all the generated viruses of interest.

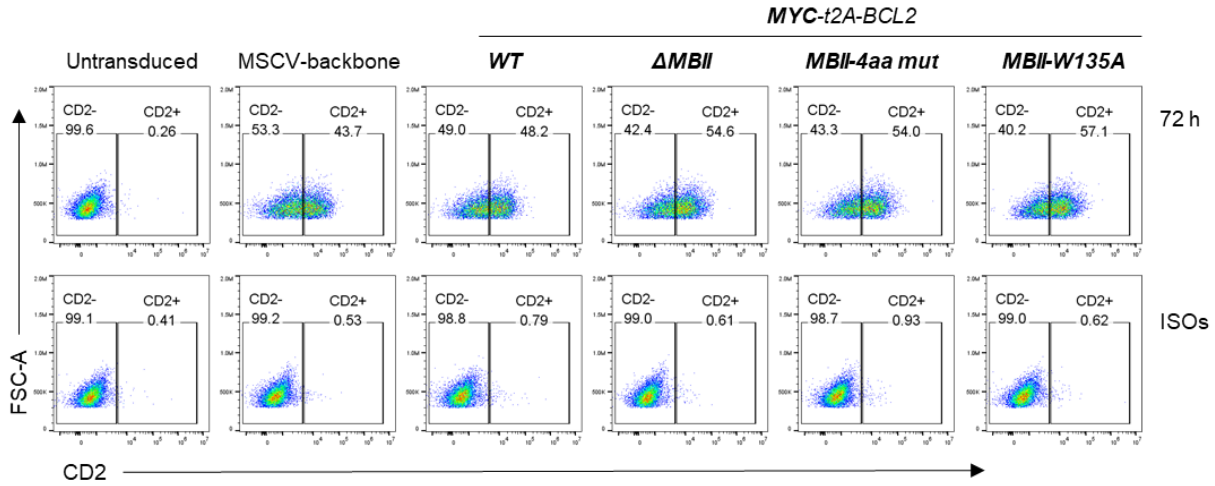

Figure 5.5 Transduction of HEK-293 cells for generated viral stocks validation. HEK-293 adherent cells were seeded 24 hours in advance and transduced with either of the *WT-t2A-BCL2*, *ΔMBII-t2A-BCL2*, MBII-4aa mut-*t2A-BCL2* or *MBII-W135A-t2A-BCL2* viruses. MSCV-backbone already validated frozen virus, untransduced and isotype staining controls (ISOs) were also included. Assessment of CD2 positivity levels was conducted 72 hours post-transduction with flow cytometry; h, hours.

5.3 Introduction of the MBII mutants in the model system

Memory B cells isolated from the peripheral blood of healthy individuals were transduced with the MBII mutants' retroviral constructs to study their effect on MYC hyperactivity in the model system. Additional control conditions of untransduced and transduced cells with MSCV-backbone, as well as *WT-t2A-BCL2* and *ΔMBII-t2A-BCL2* viruses, were included. This allowed a direct comparison between the MBII deletion and point mutants. Key time points of the plasmablast stage at day 6 and PC stage at day 13 were evaluated for the viral transduction efficiency based on CD2 reporter expression. As displayed in Figure 5.6, high transduction efficiency was achieved for all the transduced conditions at both time points tested in comparison to the untransduced control. Also, the CD2 expression frequencies were increased at day 13 in comparison to day 6. This phenomenon was previously observed in the model system indicating that the expression of the reporter was established and maintained in all the transduced donors tested by day 13.

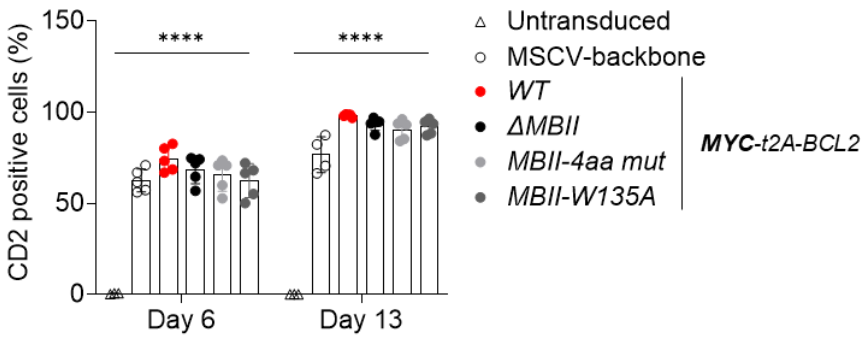

Figure 5.6 Evaluation of CD2 reporter expression levels upon transduction with MYC MBII mutants. Flow cytometry data summary of the CD2 expression percentages on days 6 and 13 for the indicated conditions. One-way ANOVA. Data are representative of three independent experiments with no technical replicates per experiment. The total number of donors tested as biological replicates was: three (N= 3) for the untransduced samples of day 6 and day 13, collected from two out of the three independent experiments; five (N= 5) for the remaining conditions apart from the day 13 MSCV-backbone transductions with four biological replicates in total (N= 4) due to processing error of the fifth sample during manual handling. Bars and error represent mean and standard deviation (SD); **** $P < 0.0001$.

5.3.1 Substitutions of DCMW motif or W135 into alanine residues mimic the MYC ΔMBII-BCL2 overexpression effect on the differentiated cells

Previously characterized cell features impacted by overexpressed MYC during the differentiation were assessed upon retroviral transductions with the MYC MBII mutants. Flow cytometry comparison of the SSC-A and FSC-A parameters were used to evaluate cell survival and size between the different samples tested. As Figure 5.7A represents, at day 6, all the conditions showed similar frequencies of viable cells with similar cell size indicating marginal differences. On the contrary, on day 13 a decrease in cell survival, number and size was detected in the *ΔMBII-*, *MBII-4aa mut-*, and *MBII-W135A-t2A-BCL2* transductions, in comparison to the MYC WT-BCL2 overexpressing cells. In addition, the frequencies of the gated viable cells for the MBII mutants resembled more the untransduced and MSCV-backbone controls.

This finding was further verified when the geometric mean of FSC-A parameter was calculated to evaluate the cell size in the culture. In Figure 5.7B, FSC-A geometric mean data of all the donors tested in this set of experiments showed a trend of decrease in cell size for the *ΔMBII-*, *MBII-4aa mut-*, and *MBII-W135A-t2A-BCL2* transductions to a similar level to the controls at day 6 when compared to the *WT-t2A-BCL2* condition. At day 13, a greater decrease in their size was observed in comparison to the *WT-t2A-BCL2* and the controls. These results suggest that abrogation of DCMW or W135 residues via substitution into alanine

suffices to mimic the deletion of the MBII domain phenotype and restore the survival and size of the cells under conditions permissive for PC differentiation back to the controls' level.

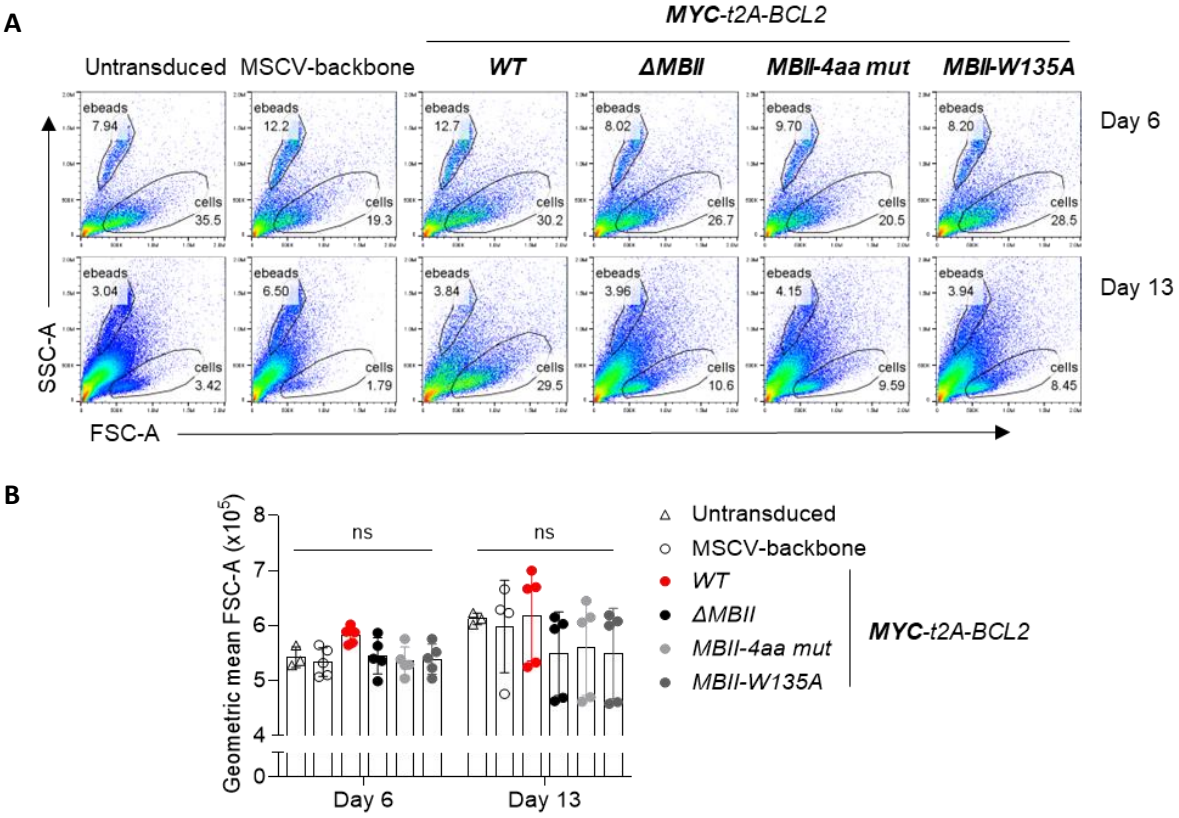

Figure 5.7 Cell size estimation based on FSC-A and SSC-A flow cytometry parameters. (**A**) Representative flow cytometry plots from day 6 and day 13 samples of the indicated conditions. The cellular populations were assessed under FSC-A versus SSC-A parameters comparison on the viable gate named as cells in the figure plots. A gate named ebeads existed to distinguish the cell sample from the counting beads added to the sample and was not included in the current analysis. (**B**) Graph of the summary data from all donors tested with flow cytometry showing the calculated geometric mean of the FSC-A parameter assessing cell size changes in the indicated conditions and time points. One-way ANOVA. Data are representative of three independent experiments with no technical replicates per experiment. The total number of donors tested as biological replicates was: three (N= 3) for the untransduced samples of day 6 and day 13, collected from two out of the three independent experiments; five (N= 5) for the remaining conditions apart from the day 13 MSCV-backbone transductions with four biological replicates in total (N= 4) due to processing error of the fifth sample during manual handling. Bars and error represent mean and standard deviation (SD); ns, not significant.

To get a better understanding of the impact of MYC MBII mutants on the outcome of MYC overexpression in the model system, absolute cell numbers were calculated upon transductions across the time course. In

Figure 5.8, as previously observed in the results of Chapters 3 and 4, at day 3 the activated memory B cell numbers were similar for all the conditions 24 hours post-transduction. Differences were detected in cell number at the plasmablast stage of day 6, where increased cell counts were acquired only for the *WT-t2A-BCL2* transduction. Importantly, at the PC stage of day 13, MYC WT-BCL2 overexpressing cells showed a statistically significant increase in cell numbers with their cell counts to generate a significantly higher mean than the controls and the three different MBII mutant conditions.

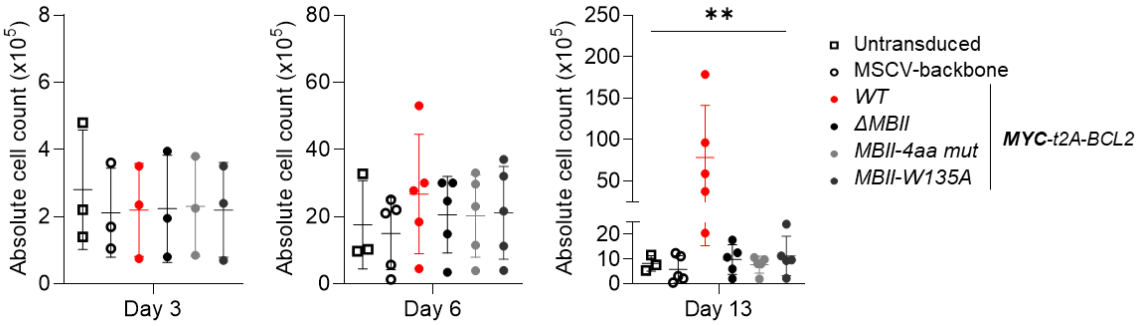

Figure 5.8 Calculation of absolute cell counts upon transduction for MYC MBII-4aa mut- or MBII-W135A-BCL2 overexpression. Samples were collected and cell counting was conducted at day 3 (left), day 6 (middle) and day 13 (right) for the indicated conditions. The figure shows summary graphs of the cell counts performed with a hemocytometer and trypan blue exclusion from all the donors tested. One-way ANOVA (Day 13, right). Data are representative of three independent experiments with no technical replicates per experiment. The total number of donors tested as biological replicates was: three (N= 3) for all the untransduced samples, collected from two out of the three independent experiments; three (N= 3) for the remaining conditions on day 3, collected from two out of the three independent experiments; five (N= 5) for all the conditions apart from the untransduced on day 6 and day 13. Bars and error represent mean and standard deviation (SD); ** $P < 0.01$.

This analysis showed that from day 6 onwards the loss of function for the MBII domain by deletion, resembled the control conditions as previously observed (Chapter 4). This was recapitulated in the context of either MYC MBII-4aa mut-BCL2 or MYC MBII-W135A-BCL2 overexpression. Thus, the DCMW/AAAA and the W135A mutations yielded normal cell size and survival in the model system, similarly to the control populations at each time point tested.

5.3.2 MBII domain substitutions in the DCMW motif and W135 into alanine abrogate the MYC overexpression effect on plasma cell differentiation

Having established that *MBII-4aa mut-t2A-BCL2* and *MBII-W135A-t2A-BCL2* transductions resulted in similar cell growth characteristics to the *ΔMBII-t2A-BCL2* condition, their immunophenotype was assessed next by flow cytometry.

As displayed in Figure 5.9A, CD19 and CD20 expression were evaluated at day 6 and the majority of the cells for all the conditions were $CD19^{+}CD20^{-}$ as anticipated with frequencies over 60% similarly to the untransduced. At day 13, *in vitro* PCs were produced for the untransduced and MSCV-backbone conditions characterized by $CD19^{+}CD20^{-}$ at 84.7% and 83.5% (an increase relative to day 6 percentages). When MYC WT-BCL2 was overexpressed, a decrease was observed at 62.3% $CD19^{+}CD20^{-}$ cells, with a noticeable increase in the $CD19^{-}CD20^{-}$ population in comparison to the controls. This phenotype was compared to the three MBII mutants. Deletion of the MBII increased the $CD19^{+}CD20^{-}$ cells reaching 86.5% and validating previous findings. Interestingly, a similar effect in MYC hyperfunction was observed in either of the MBII alanine substitution mutants with 79.9% for the MBII-4aa mut-BCL2 and 82.6% for the MBII-W135A-BCL2 conditions.

An equivalent trend was detected for the CD27 and CD38 expression. In Figure 5.9B, at day 6 no significant differences were observed between the untransduced and the transduced cells for the conditions tested. However, at day 13, only MYC WT-BCL2 overexpression resulted in perturbation of the expected phenotype with a significant decrease in CD27 upregulation within the $CD38^{+}$ population. On the contrary, the levels seen in the controls were also observed in the *MBII-4aa mut-t2A-BCL2* and *MBII-W135A-t2A-BCL2* transductions with 89.2% and 87.6% $CD27^{+}CD38^{+}$ cells respectively. *ΔMBII-t2A-BCL2* condition resulted in 88.5% of double positive CD27 and CD38 cells validating that DCMW and especially W135 mutations sufficed to abrogate the effect of overexpressed MYC on CD27 expression.

When CD38 and CD138 expression was evaluated, as displayed in Figure 5.9C, at day 6 all the conditions had differentiated equivalently to the untransduced and MSCV-backbone controls with the anticipated $CD38^{+}CD138^{-}$ plasmablast population. At the PC day 13 stage, CD138 upregulation was observed as expected for the untransduced and MSCV-backbone controls as well as the *ΔMBII-t2A-BCL2* condition. Similarly, MBII-4aa mut-BCL2 and MBII-W135A-BCL2 overexpression resulted in 37.7% and 44.8% of $CD38^{+}CD138^{+}$ cells close to the control frequencies. This contrasted with MYC WT-BCL2 overexpression which had a 3-fold decrease in the $CD38^{+}CD138^{+}$ population.

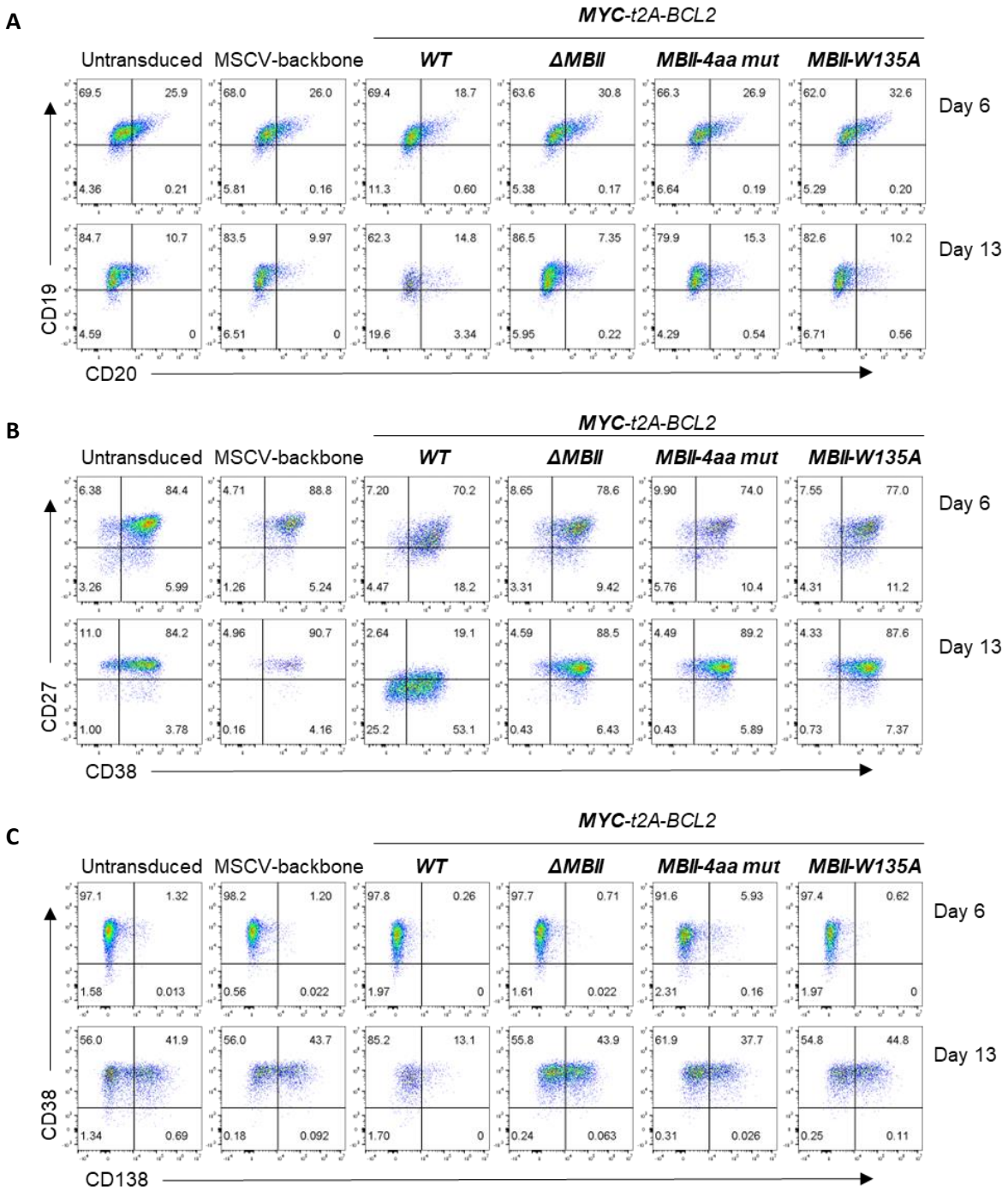

Figure 5.9 Immunophenotyping upon MBII mutants' overexpression. Representative flow cytometry plots of selected protein markers expression for the indicated conditions. Evaluation of (**A**) CD19 against CD20, (**B**) CD27 against CD38, and (**C**) CD38 against CD138, on the y-axis and x-axis respectively, for day 6 and day 13 samples. The cells assessed in the transduced conditions were $CD2^+$ pre-gated. Data are representative of three independent experiments with no technical replicates per experiment. The total number of donors tested as biological replicates was: three (N= 3) for the untransduced samples of day 6 and day 13, collected from two out of the three independent

experiments; five (N= 5) for the remaining conditions apart from the day 13 MSCV-backbone transductions with four biological replicates in total (N= 4) due to processing error of the fifth sample during manual handling.

To further validate these results summary graphs of the immunophenotyping conducted by flow cytometry were generated for all the donors tested in this set of experiments. As Figure 5.10 shows, day 6 was a time point with little to no differences between the conditions tested, with MYC WT-BCL2 overexpression driving no statistically significant differences for either of the evaluated populations. At the day 13 time point, a significant reduction was observed in the MYC WT-BCL2 overexpressing transduced cells for the $CD19^{+}CD20^{-}$, $CD27^{+}CD38^{+}$ and $CD38^{+}CD138^{+}$ populations. In addition, the *ΔMBII-*, *MBII-4aa mut-* and *MBII-W135A-t2A-BCL2* conditions of interest showed almost a complete resemblance to the control levels in comparison to the *WT-t2A-BCL2*.

These findings validated that the MYC WT-mediated overexpression effect on PC differentiation is highly dependent on the MBII domain and specifically on its DCMW conserved motif. W135 of this motif is critical and its mutation into alanine sufficed to impair MYC WT overexpression impact in a similar manner to the MBII domain deletion.

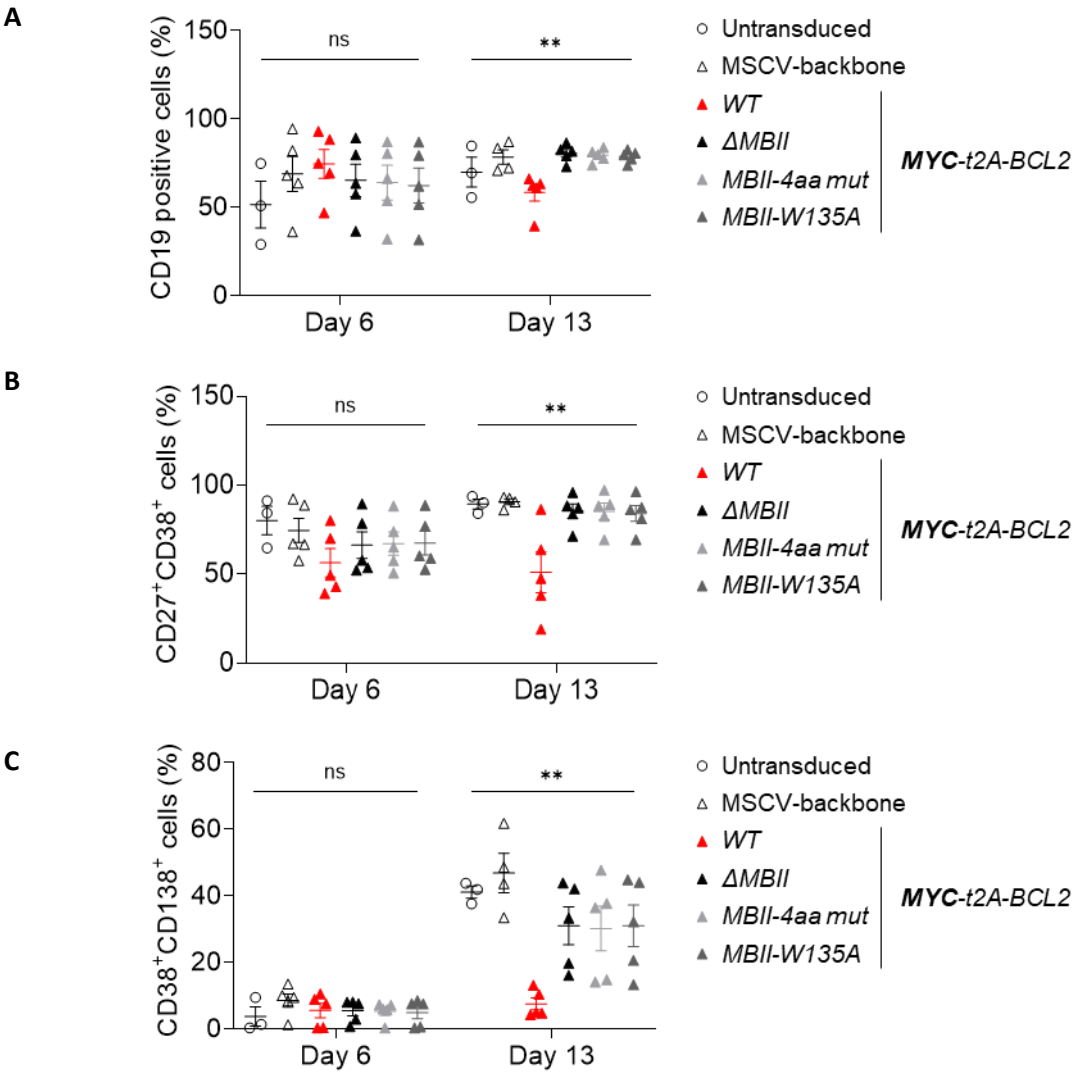

Figure 5.10 Summary flow cytometry data for the MBII mutants' overexpression in the model system. Graphs of the summary data from all donors tested with flow cytometry assessing population percentages of (**A**) $CD19^{+}CD20^{-}$, (**B**) $CD27^{+}CD38^{+}$, and (**C**) $CD38^{+}CD138^{+}$, cells at the indicated time points and conditions. One-way ANOVA. The cells assessed in the transduced conditions were $CD2^{+}$ pre-gated. Data are representative of three independent experiments with no technical replicates per experiment. The total number of donors tested as biological replicates was: three (N= 3) for the untransduced samples of day 6 and day 13, collected from two out of the three independent experiments; five (N= 5) for the remaining conditions apart from the day 13 MSCV-backbone transductions with four biological replicates in total (N= 4) due to processing error of the fifth sample during manual handling. Bars and error represent mean and standard deviation (SD); ns, not significant; ** $P < 0.01$.

5.4 Assessment of MYC protein overexpression in the MBII mutants

Having identified the importance of DCMW and W135 of MBII, their contribution to MYC protein expression was next evaluated. Day 6 cells were collected, and total protein lysates were extracted and assessed by western blot for their MYC protein levels using β-actin as a loading control. In addition, BLIMP1 and BCL2 expression were included in the evaluation to confirm PC programme activation and co-overexpression of BCL2 as anticipated in the model system respectively.

As Figure 5.11A and Figure 5.11B display, similar levels for BLIMP1 expression were detected in all the conditions relative to MSCV-backbone, verifying that BLIMP1 upregulation occurs in a MYC-BCL2 overexpression-independent manner. MYC and BCL2 overexpression was also verified at day 6 in comparison to the MSCV-backbone negative control.

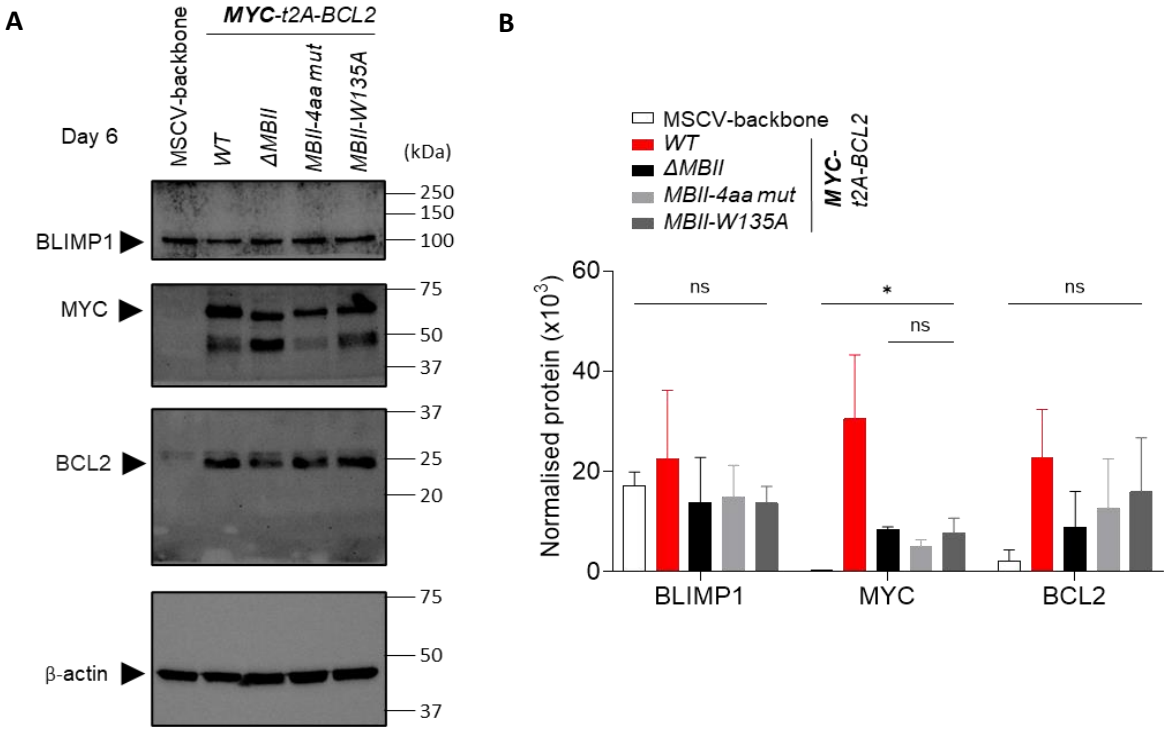

Figure 5.11 Protein detection via western blot upon overexpression of the MBII mutants. Day 6 total protein lysates were generated and probed against BLIMP1, MYC, BCL2 and β-actin to assess their expression levels with western blot. (**A**) Representative image of the SDS-polyacrylamide gel performed to detect protein expression at the indicated conditions; kDa, kilodalton. (**B**) Summary graph of the quantified protein expression upon normalisation to the β-actin loading control for each of the conditions as indicated per gel lane. Densitometry values of the quantified protein bands were obtained with ImageJ software. One-way ANOVA. Data are representative of two independent experiments with one biological replicate (N= 1) and no technical replicates per condition. The total number of

donors tested as biological replicates was two (N= 2). Bars and error represent mean and standard deviation (SD); ns, not significant; * P < 0.05.

As shown in Figure 5.11A, the molecular size of the identified MYC protein band was similar for the *WT-t2A-BCL2* condition and the two MBII mutants. That was anticipated as no amino acids were deleted from MYC protein in these conditions. In contrast, a slight decrease was observed in the *ΔMBII-t2A-BCL2* condition indicating deletion of the MBII domain. This verified that the MYC proteins were overexpressed as expected in each of the indicated conditions. A second band was observed in the *MYC-t2A-BCL2* conditions, with lower molecular size compared to the identified MYC protein band. This lower band could be a product of post-translational modifications (PTMs). It is known that MYC can undergo different PTMs, including phosphorylation, ubiquitination, acetylation, glycosylation, methylation and SUMOylation (331, 332). Such PTMs regulate MYC function and protein turnover after adding chemical groups or proteins to the synthesized MYC usually resulting in slight increases in its molecular size. The decreased size of the detected lower band indicates the occurrence of a PTM that did not result in the anticipated increased size. A PTM that adds a negative charge to the overexpressed MYC protein could promote its faster migration on the SDS-polyacrylamide gel resulting in a lower band. Even though that could be a possibility for phosphoproteins like MYC, such a PTM would not usually result in such a noticeable reduction of the modified protein's size. An additional PTM previously identified in MYC is proteolytic cleavage. A characteristic example is the truncated Myc protein, Myc-nick, which is generated upon calpain protease-mediated proteolysis of full Myc in the cytoplasm in mice and humans (333, 334). The molecular size of MYC-nick is 42kDa (333), thus it could not correspond to the detected lower band which has an intermediate size between MYC and MYC-nick of approximately 50kDa. Despite that, a similar proteolytic event happening in the overexpressed MYC in the model system could produce the truncated form of MYC detected in Figure 5.11A.

The expression levels of the identified MYC protein bands appeared higher in the *WT-t2A-BCL2* transduced cells than in *ΔMBII-t2A-BCL2* and the two MBII mutants (Figure 5.11A). When quantification and normalisation of MYC took place, as depicted in Figure 5.11B, MYC WT protein expression was significantly higher than in the rest of the conditions including the MBII mutants. Mutation of the DCMW motif or W135A resulted in a similar decrease in MYC protein levels to the *ΔMBII-t2A-BCL2* condition when compared to the *WT-t2A-BCL2*. Despite the differences between the *WT-t2A-BCL2* and the three MBII mutants, MYC protein overexpression was confirmed in comparison to the MSCV-backbone control.

5.5 Gene expression upon MYC MBII mutants' introduction in the model system

Mutation of DCMW MBII domain motif into sequential alanine residues and W135A single substitution almost abolished the phenotypic impact of MYC overexpression on PC differentiation. To further assess the extent of this effect, gene expression study was performed for the two MBII mutants, *ΔMBII-*, *WT-t2A-BCL2,* and MSCV-backbone and untransduced controls.

Previous findings of gene expression described in the results sections 3.6 and 4.5, showed that the impact of MYC overexpression on the PC differentiation at a transcriptional level was greatest at day 13. Hence, only this time point was evaluated upon overexpression of the MBII mutants with RNA-sequencing. The bioinformatic analysis of the gene expression data was performed by Dr. Matthew Care.

5.5.1 Differentially expressed genes in the transcriptome of the MBII mutants

Global RNA-sequencing data analysis provided an accurate count of the DEGs between the six conditions examined here. As displayed in Table 5.1, the higher number of upregulated DEGs in the untransduced condition was identified upon pairwise comparison to the MYCwt samples (1756 genes). Only 10 were the genes that were induced between the untransduced and the *ΔMBII-t2A-BCL2* samples. Even less were the genes showing upregulation in the untransduced in comparison to the *MBII-4aa mut-t2A-BCL2 and MBII-W135A-t2A-BCL2* transductions, being 1 and 5 genes respectively.

Pairwise comparisons between the MSCV-backbone samples and the *WT-t2A-BCL2* condition resulted in 2272 genes being differentially expressed. On the other hand, only 353 genes were differentially expressed between the MSCV-backbone and the untransduced samples with a similar number of DEGs being calculated for the comparison to either the *MBII-4aa mut-* or *MBII-W135A- t2A-BCL2* samples, indicating their transcriptional similarities.

For the pairwise comparisons performed in the samples overexpressing MYC protein, the number of DEGs estimated as upregulated in the *WT-t2A-BCL2* samples over the remaining five conditions was higher than 1600 genes. Subsequently, when the MBII mutants were compared to the untransduced and MSCV-backbone controls small number of genes were calculated as differentially expressed. Importantly, a striking lack of DEGs was observed for all the pairwise comparisons performed between the *ΔMBII-t2A-BCL2*, *MBII-4aa mut-t2A-BCL2* and *MBII-W135A-t2A-BCL2* samples resulting in no DEGs identified between these three conditions.

Table 5.1 Counts of DEGs between the conditions tested. Pairwise comparisons, as indicated, revealed the number of DEGs between the conditions examined on day 13 of the model system. Data are representative of two independent experiments with three biological replicates in total (N= 3) and no technical replicates.

Day 13

Condition 1	Condition 2	DEGs
Untransduced	MSCV-backbone	469
Untransduced	MYC WT.BCL2	1756
Untransduced	MYC ΔMBII.BCL2	10
Untransduced	MBII 4aa mut.BCL2	1
Untransduced	MBII W135A.BCL2	5
MSCV-backbone	Untransduced	353
MSCV-backbone	MYC WT.BCL2	2272
MSCV-backbone	MYC ΔMBII.BCL2	372
MSCV-backbone	MBII 4aa mut.BCL2	520
MSCV-backbone	MBII W135A.BCL2	408
MYC WT.BCL2	Untransduced	1977
MYC WT.BCL2	MSCV-backbone	2727
MYC WT.BCL2	MYC ΔMBII.BCL2	1659
MYC WT.BCL2	MBII 4aa mut.BCL2	1614
MYC WT.BCL2	MBII W135A.BCL2	1617

Condition 1	Condition 2	DEGs
MYC ΔMBII.BCL2	Untransduced	58
MYC ΔMBII.BCL2	MSCV-backbone	513
MYC ΔMBII.BCL2	MYC WT.BCL2	1476
MYC ΔMBII.BCL2	MBII 4aa mut.BCL2	0
MYC ΔMBII.BCL2	MBII W135A.BCL2	0
MBII 4aa mut.BCL2	Untransduced	32
MBII 4aa mut.BCL2	MSCV-backbone	648
MBII 4aa mut.BCL2	MYC WT.BCL2	1365
MBII 4aa mut.BCL2	MYC ΔMBII.BCL2	0
MBII 4aa mut.BCL2	MBII W135A.BCL2	0
MBII W135A.BCL2	Untransduced	53
MBII W135A.BCL2	MSCV-backbone	613
MBII W135A.BCL2	MYC WT.BCL2	1443
MBII W135A.BCL2	MYC ΔMBII.BCL2	0
MBII W135A.BCL2	MBII 4aa mut.BCL2	0

The identified DEGs were analyzed next with a dimensionality reduction approach to get a better insight into their similarities. As displayed in Figure 5.12, on day 13, the samples overexpressing MYC WT-BCL2 proteins clustered separately from the rest of the conditions, at the right side of the plot. The *ΔMBII-*, *MBII-4aa mut-*, and *MBII-W135A-t2A-BCL2* conditions formed a unified cluster at the opposite top side of the *WT-t2A-BCL2* samples indicating distinct gene expression. The untransduced and one of the MSCV-backbone samples clustered together with the MBII mutants. These results showed a profound difference between MYC WT and its counterpart MBII mutants which appear to share more similarities with the controls at a transcriptional level.

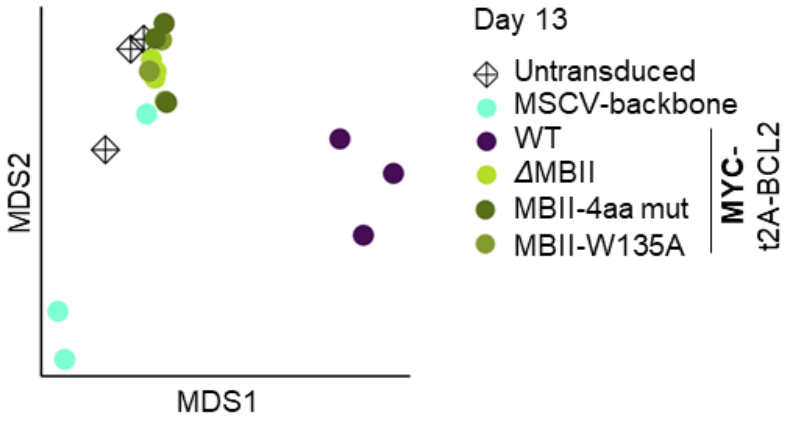

Figure 5.12 Clustering of the DEGs with a dimensionality reduction approach at day 13. RNA-sequencing data from day 13 samples were analysed and the DEGs were used for dimensionality reduction analysis of the indicated conditions using a multidimensional scaling (MDS) approach. The illustrated plot was generated by Dr. Matthew Care. Data are representative of two independent experiments with three biological replicates in total (N= 3) and no technical replicates.

5.5.2 Gene ontology of the differentially expressed genes detected upon MBII mutants' overexpression

Having an overview of the differences between MYCwt and the MBII mutants in inducing gene expression, GO analysis was performed next to assess the functional annotation of the identified DEGs. Lists of DEGs with higher expression in each of the *WT-t2A-BCL2*, *ΔMBII-t2A-BCL2*, *MBII-4aa mut-t2A-BCL2* and *MBII-W135A-t2A-BCL2* conditions compared to the MSCV-backbone were analyzed for their GO. The six most highly enriched GO terms were used to assess GO enrichment for the pairwise comparisons tested between samples. As displayed in Table 5.2, the DEGs analysed in the *WT-t2A-BCL2* condition showed distinctive GO terms in comparison to the remaining comparisons. The most highly overlapping GO terms were associated with LZ B cells, ribosome and nucleoprotein biogenesis, and MYC targets. The description of these GO terms was correlated to MYC function as expected from our previous findings. Quite different were the enriched signatures of the identified GO terms in the comparisons of the MBII mutants. Importantly, some signatures, such as Pan_B_U133plus and Myeloma_CD1_subgroup_up, were shared between the *ΔMBII-t2A-BCL2* and the *MBII-W135A-t2A-BCL2* conditions. The signature Protein biosynthesis was common for all three *ΔMBII-t2A-BCL2*, *MBII-4aa mut-t2A-BCL2* and *MBII-W135A-t2A-BCL2* comparisons.

From this analysis, the signatures identified in the *MBII-4aa mut-t2A-BCL2* condition showed a higher association with active PC differentiation. In addition, *MBII-W135A-t2A-BCL2* had great similarities with the *ΔMBII-t2A-BCL2* condition previously shown to abrogate MYC hyperfunction under conditions permissive for PC differentiation. Thus, these findings further supported the distinctive transcriptional changes driven by MYCwt in comparison to the MBII mutants in an overexpression context, as well as the similarities that the two MBII mutant conditions shared with *ΔMBII-t2A-BCL2* samples.

Table 5.2 GO analysis of the DEGs. The DEGs showing higher expression in *WT-t2A-BCL2*, *ΔMBII-t2A-BCL2*, *MBII 4aa mut-t2A-BCL2*, or *MBII W135A-t2A-BCL2* in comparison to MSCV-backbone control were analysed with GO. The six GO terms with the higher Z-score that overlapped with the examined DEGs were selected. Data are representative

of two independent experiments with three biological replicates in total (N= 3) and no technical replicates; vs, versus; FDR, false discovery rate.

Day 13

WT-t2A-BCL2 vs MSCV-backbone

Gene Signature	Gene Set	%Overlap	Z-score	p-value	FDR
LZ_Bach2high_downreg (PMID:32619424)	SignatureDB	44.53	27.1365	3.7E-162	1.20E-159
ribonucleoprotein complex biogenesis [GoID:GO:0022613]	GeneOntology_BP	52.45	23.3893	5.5E-121	1.22E-118
Proliferation_DLBCL (PMID:12075054)	SignatureDB	43.94	23.0093	3.8E-117	8.04E-115
Myc_ChIP_PET_Expr_Up (PMID:17093053)	SignatureDB	54.80	22.4579	1.1E-111	2.20E-109
HALLMARK_MYC_TARGETS_V1	MSigDB_H	76.53	22.1915	4.1E-109	8.30E-107
OCT2_shRNA_OCT2_ChIP (PMID:26993806)	SignatureDB	43.59	22.1471	1.1E-108	2.21E-106

ΔMBII-t2A-BCL2 vs MSCV-backbone

Gene Signature	Gene Set	%Overlap	Z-score	p-value	FDR
regulation of amide metabolic process [GoID:GO:0034248]	GeneOntology_BP	5.53	5.1006	3.4E-07	0.0001
regulation of translation [GoID:GO:0006417]	GeneOntology_BP	5.59	4.8568	1.2E-06	0.0004
Myeloma_CD-1_subgroup_up (PMID:16728703)	SignatureDB	18.18	4.8395	1.3E-06	0.0005
Protein biosynthesis	UniProt-Keyword	9.52	4.6031	4.2E-06	0.0013
post-transcriptional regulation of gene expression [GoID:GO:0010608]	GeneOntology_BP	4.77	4.3622	1.3E-05	0.0035
Leucine_starve_up (PMID:12101249)	SignatureDB	9.09	4.3108	1.6E-05	0.0042

MBII 4aa mut-t2A-BCL2 vs MSCV-backbone

Gene Signature	Gene Set	%Overlap	Z-score	p-value	FDR
Pan_B_U133plus	SignatureDB	14.81	5.0506	4.4E-07	0.0001
Protein biosynthesis	UniProt-Keyword	9.52	4.0739	4.6E-05	0.0085
IRF4_ABC_repressed_all (PMID:22698399)	SignatureDB	5.61	3.8170	1.4E-04	0.0200
ABCgtGCB_U133AB	SignatureDB	6.43	3.8158	1.4E-04	0.0200
Blood_Module-1.3_B_cells (PMID:18631455)	SignatureDB	13.21	3.6728	2.4E-04	0.0311
BCL6_ChIPSeq_Basso_GC_low (PMID:19965633)	SignatureDB	3.99	3.5292	4.2E-04	0.0483

MBII W135A-t2A-BCL2 vs MSCV-backbone

Gene Signature	Gene Set	%Overlap	Z-score	p-value	FDR
Myeloma_CD-1_subgroup_up (PMID:16728703)	SignatureDB	18.18	4.5674	4.9E-06	0.0017
Protein biosynthesis	UniProt-Keyword	9.52	4.2136	2.5E-05	0.0069
choline catabolic process [GoID:GO:0042426]	GeneOntology_BP	75	4.0916	4.3E-05	0.0106
choline metabolic process [GoID:GO:0019695]	GeneOntology_BP	60	3.8779	1.1E-04	0.0233
Notch_T-ALL_up_Weng (PMID:16847353)	SignatureDB	13.46	3.8003	1.4E-04	0.0302
Pan_B_U133plus	SignatureDB	9.88	3.5166	4.4E-04	0.0733

5.5.3 The similarities of differentially expressed genes between ΔMBII and W135A mutation in overexpressed MYC

Next, the similarities of the *MBII-W135A-t2A-BCL2* condition to the samples with deleted MBII domain in MYC were further investigated. The analysis conducted so far suggested that the single mutation of W135 into an alanine sufficed to phenocopy the results observed in *ΔMBII-t2A-BCL2* samples. The finding that no DEGs were identified from the pairwise comparisons performed between *ΔMBII-t2A-BCL2* and *MBII-W135A-t2A-BCL2* conditions on day 13 (Table 5.1), indicated absolute resemblance. However, different GO terms and signatures were enriched in the two conditions for the DEGs showing upregulation in each of them upon comparison to the MSCV-backbone (Table 5.2). Thus, to examine potential transcriptional

differences as well as additional similarities, GO was conducted in a different set of DEGs associated with these two conditions of interest. To explore this idea the DEGs with higher expression in the *WT-t2A-BCL2* or *ΔMBII-t2A-BCL2* or *MBII-W135A-t2A-BCL2* than in the MSCV-backbone were used this time. Venn diagrams were utilized to resolve genes uniquely or commonly expressed in each of the comparisons. As Figure 5.13 shows, this approach gave 285 genes shared in all three conditions and 98 genes shared only between *ΔMBII-t2A-BCL2* and *MBII-W135A-t2A-BCL2* comparison. The majority of the genes in this analysis were uniquely expressed in the *WT-t2A-BCL2* versus the MSCV-backbone comparison (2247 genes). This further supported that even though both the deletion of the MBII or W135A substitution drove reduced transcriptional changes compared to MYCwt, they demonstrated some distinct patterns of gene regulation.

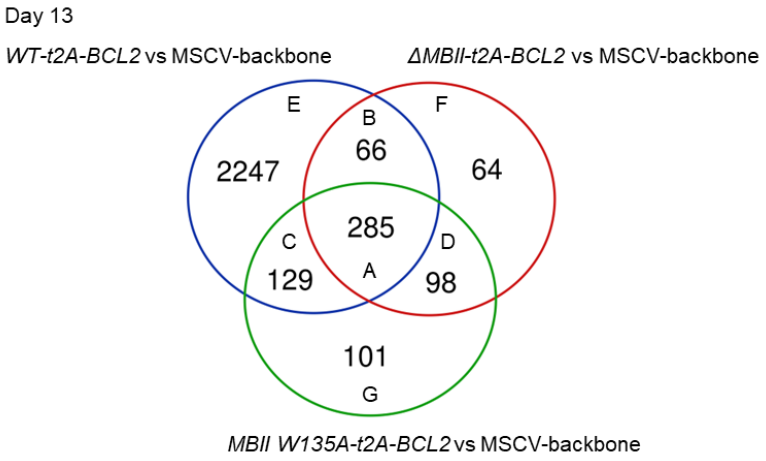

Figure 5.13 Analysis of DEGs with higher expression in *ΔMBII*- or *MBII W135A-t2A-BCL2* relative to MSCV-backbone condition revealed shared genes between the two conditions. Venn diagrams of the DEGs upregulated in *WT-t2A-BCL2*, *ΔMBII-t2A-BCL2* or *MBII W135A-t2A-BCL2* versus (vs) the MSCV-backbone control at day 13. Gene counts are depicted in each comparison of the Venn diagram. Capital letters A-G label each of the generated gene lists in this analysis. Data are representative of two independent experiments with three biological replicates in total (N= 3) and no technical replicates.

To get a better insight on the upregulated DEGs in MYCwt and *MBII-W135A-t2A-BCL2* but not in *ΔMBII-t2A-BCL2* over the MSCV-backbone, GO analysis was conducted using DAVID software for the generated gene lists in Figure 5.13. GO analysis of Gene set E, gave significant enrichments of GO terms related to MYC function as anticipated (data not shown as previously discussed). On the contrary, as displayed in Table 5.3, only the first two GO terms, identified as overrepresented in Gene set A, showed significant enrichment. No significant enrichment was confirmed for the identified GO terms of Gene sets B and C. To

validate this result also, the Enrichr GO analysis software was used. This alternative analysis also provided a similar result showing poor enrichment in the proposed GO terms (data not shown). The number of genes comprising gene sets A, B and C was significantly lower than in Gene set E represented by genes related to fundamental MYC function (Figure 5.13). Thus, functional annotation of gene sets A, B and C using GO analysis indicated their unique and unelucidated function, not being associated yet with known GO terms with high confidence. The generated gene lists (Figure 5.13) were provided in Table 5.4 as valuable information generated by our analysis.

Table 5.3 GO analysis of the generated gene sets in Figure 5.13. The gene lists generated by the Venn diagram in Figure 5.13 were analysed using the functional annotation software DAVID. The most highly enriched cluster (Annotation Cluster 1) of GO terms associated with the imported genes is displayed here per Gene set tested. Gene sets A, B, and C, indicate the identified gene sets in Figure 5.13. Data are representative of two independent experiments with three biological replicates in total (N= 3) and no technical replicates; FDR, false discovery rate; %, percentage of overlap.

Day 13: Gene set A

Annotation Cluster 1	**Enrichment Score: 2.6894417349926067**					
Category	**Term**	**Count**	**%**	**p-value**	**Benjamini**	**FDR**
UP_KW_PTM	KW-0832~Ubl conjugation	39	19.5	3.3E-04	0.0059	0.0059
UP_KW_PTM	KW-1017~Isopeptide bond	27	13.5	4.6E-03	0.0417	0.0417
UP_SEQ_FEATURE	CROSSLNK:Glycyl lysine isopeptide (Lys-Gly) (interchain with G-Cter in SUMO2)	20	10	5.7E-03	1	1

Day 13: Gene set B

Annotation Cluster 1	**Enrichment Score: 1.1459369350554152**					
Category	**Term**	**Count**	**%**	**p-value**	**Benjamini**	**FDR**
UP_KW_CELLULAR_COMPONENT	KW-0963~Cytoplasm	19	39.58	0.0045	0.0980	0.0980
UP_KW_PTM	KW-0597~Phosphoprotein	18	37.50	0.2423	0.6338	0.6338
GOTERM_CC_DIRECT	GO:0005829~cytosol	12	25	0.3381	1	1

Day 13: Gene set C

Annotation Cluster 1	**Enrichment Score: 1.5746091520074064**					
Category	**Term**	**Count**	**%**	**p-value**	**Benjamini**	**FDR**
GOTERM_MF_DIRECT	GO:0005178~integrin binding	5	4.59	0.0067	1	1
GOTERM_BP_DIRECT	GO:0007155~cell adhesion	7	6.42	0.0280	1	1
UP_KW_BIOLOGICAL_PROCESS	KW-0130~Cell adhesion	7	6.42	0.0375	1	1
KEGG_PATHWAY	hsa04510:Focal adhesion	4	3.67	0.0713	1	1

Table 5.4 The gene lists generated in Figure 5.13. Gene sets A, B, C, D, F and G correspond to the identified gene sets as indicated in Figure 5.13. The 'Count' column represents the number of genes comprising each gene set. Data are representative of two independent experiments with three biological replicates in total (N= 3) and no technical replicates; vs, versus.

Genes ID	Count	Genes
Gene set A: Common genes between WT.BCL2, ΔMBII.BCL2 and MBII W135A.BCL2 vs MSCV-backbone	285	CIPC, AC007262.2, SNHG16, AL590064.1, GDF15, AL137058.2, KBTBD8, ANKRD13B, XK, LRRC37A4P, ANKRD20A10P, AC005052.1, UTRN, EVI2A, AP4B1-AS1, AC008966.1, AL358473.1, AP003108.2, HSPD1, AC093642.2, TRIM2, BCL2, ERLIN2, LINC02334, AC026412.3, AL050343.2, AC009283.1, AL928654.4, AC004980.1, COL7A1, NUDT16P1, AL079338.1, KISS1R, AC012184.2, RPL4, IRAG2, BTK, RPS6KA6, GDF9, ZNF709, H2BC18, FAM185BP, VWA2, AP003392.1, SLC4A5, NFRKB, C5, LINC01237, RAB9B, TBC1D8, PHC1P1, TEX9, MIR17HG, AP002490.1, AC234775.3, BCL7A, PARD6G, TPI1P2, AC009107.2, AC005261.5, AC245060.5, ZNF681, MSTO2P, FASTKD2, XPOT, SLC7A11, ZXDC, MYC, KIF9-AS1, RHBDL1, HEXD-IT1, LINC02193, HSD17B7P2, ZNF33B, TMEM268, PTCD2, AL035252.3, MIR4453HG, C1S, AL049830.3, AC025031.4, AC007098.1, DRC3, SLC22A23, C5orf63, AC118344.1, AC093866.1, GHRLOS, CEP63, TNK1, AC107027.3, LINC02352, AC004076.2, EIF3A, AC010522.1, C12orf77, SMAD1, ENPP7, RTCA, CHST7, MTHFD1L, GALNT14, WFDC2, AL031009.1, INHBE, GOLGA6L4, MBNL3, LINC01275, AL022328.1, AC099332.2, C2orf68, AP001267.5, C2orf15, SLC7A1, AC006058.4, UPF3B, AIG1, SBF2-AS1, EIF3E, SLC25A51, KCNIP2, AL031600.1, AC063949.2, CNNM2, ZNF804A, TRIM16L, RSL1D1, MACROD2, AC106897.1, MYBBP1A, EPHB4, GPR75, SNHG29, TTC26, STEAP1, AL731566.2, COBLL1, AP001160.1, C12orf42, PXT1, CLGN, MID1IP1, NETO2, AL596244.1, AL020996.1, LINC01772, AC091390.4, LARS1, LINC02043, ZNF581, CDK12, SLC16A7, AC009084.2, RPL7L1, AC023818.1, CR769775.2, EIF4EBP3, NLRP6, RIOX2, EXD2, ARFGEF3, ZNF117, CCSER1, AC018665.1, GRK3, TNFRSF10A-AS1, COIL, LINC01136, Z93930.2, TRIM65, ECM1, TEKT3, HECW2, RNF227, CCN2, POC1B-GALNT4, AC087741.1, AC002310.1, MARVELD1, AC005052.2, ZNF587B, EFNA1, TIMM10B, ACRBP, KYNU, DCAF1, MAP6D1, AC092117.2, RPL4P4, CRLF1, AL359715.1, TUB, AL512770.1, GRHL3, LRRC14B, AC138866.1, AL035696.4, RBM12B, AC099332.1, IPO5P1, ELP3, NSUN3, KCNK12, MUC4, FAM157C, MAP3K1, ZNF761, ZMAT3, EEF1A1, KLHL32, AL117344.2, EIF4B, RBKS, SPINK2, SPESP1, TGM1, DLL3, AC015813.1, UHRF1BP1, KLHL7-DT, EEF2, AC138035.1, AL162258.2, SOCS7, UVRAG, BCL2L11, TFB2M, CD80, B3GNT4, AC234031.1, ZBTB33, AC124944.3, ZNF460-AS1, HSPA5, Z95115.1, RNF144B, ATG4C, PDZK1P1, TTC34, AC124016.1, MRE11, CAV1, STRBP, AL109976.1, LYL1, FAM86EP, AC107375.1, AC139795.1, AL110114.1, USP32P3, CMBL, DEPTOR, AC126177.6, TMEM220, AC004771.4, FAR2P2, ARHGEF17, CLEC18A, MRPL45P2, QSER1, ACTA2-AS1, RRM2B, AL357079.1, YBX3, SHISA2, AC108488.2, SPATA13, AC116913.1, C3orf35, STC2, AL031595.3, KCTD12, ZBTB5, FGF7P6, ZNF324B, SEC14L1P1, AC025164.1, TGFBI, RASSF6, AC123768.2, ZNF562, AL353796.1, UBE2Q2P1, AC012676.1, LINC01806
Gene set B: Unique between WT.BCL2 and ΔMBII.BCL2 vs MSCV-backbone	66	GAS5, ZSWIM1, IGKV2-26, FRY, CDK20, CCDC66, RRN3P2, DESI1, AF127577.4, AL590714.1, AL031670.1, GRTP1, EIF3H, AP000350.6, AC006160.1, AC109460.1, LRRC70, RPL3, AC025283.2, MBTPS2, NOP14, MRPS31P5, SPTBN2, MANEA-DT, SSPN, CFAP97, SUZ12P1, ZNF789, AL133493.2, PLA2G12A, ZSCAN20, CBY3, MEF2C-AS1, TOMM20, RSL24D1, VWA8, AC092119.2, C12orf76, WTIP, LSG1, AC026979.4, MTHFD2, MMACHC, SUMF2, EEF1B2, EPRS1, AL162151.2, H2AC15, RIN1, AC133644.1, USP6, RPL5, AL117339.4, SHROOM3, ALG1L9P, MYRIP, AC245060.4, AL033527.2, ZNF28, AC011476.3, AL161452.1, UBE3C, AL049795.1, PEX5L, SUGT1-DT, DPY19L2P3
Gene set C: Unique between WT.BCL2 and MBII W135A.BCL2 vs MSCV-backbone	129	GNL3, MACROD1, TNNT3, TNXB, PPP1R9A, AC233280.1, C3orf52, AC007842.1, HES7, CRPPA, IMMT, DZANK1, SCN3A, BMS1P2, CHAMP1, PSTK, AL158055.1, LINC02614, SPP1, IL13RA1, SLC9A2, TOX, TEX10, EDNRB-AS1, SHANK3, PJVK, AC091057.6, CR1, CATSPER2P1, ZNF287, NME9, MRPS18AP1, GAREM1, UXT-AS1, TLN2, FNIP2, PDLIM1, AL031717.1, SLC25A27, AL513327.1, TMEM38B, HPDL, CCDC136, DDX21, CACNB2, KIF13A, AC126474.1, AC108704.2, AL353135.2, UBE2E2, SLC39A10, LZIC, PCDHGC3, SLC25A1P5, NSUN7, PTPRU, BEND3, AKAP11, FBXL4, PPARGC1B, AC132872.3, PSD3, ZNRF2P2, MPZL2, ELFN1-AS1, SETD2, IQCK, AC093525.4, AC006059.1, ZNF202, ABITRAM, ZNF704, ARL5B, PM20D2, AL136981.3, KTN1-AS1, CROT, HUWE1, PEAK1, MORF4L2, WWC1, AC025287.3, ANK2, PDPR, TTC5, PRR5-ARHGAP8, LNCOC1, PER2, AC025569.1, MSANTD1, GREM1, AC093890.1, AC087521.2, SCLY, SAP30L-AS1, GNL3L, NIPSNAP3A, TASOR2, MXI1, GRIK5, AC092645.2, RPL23AP53, CCDC144CP, TP53INP1, MTMR7, IGF1R, IPO7, NAV1, GPR146, SDHAF4, CCNH, ATP6V1G2-DDX39B, PHF14, RRP12, CHRD, SLC45A3, PABPC1, FCRLA, MORN2, ADAM22, AC069547.1, RANBP2, DAAM1, EMSLR, ICAM5, BCKDHB, VARS1, N4BP3, AC104066.5
Gene set D: Unique between ΔMBII.BCL2 and MBII W135A.BCL2 vs MSCV-backbone	98	FARP1, AC022239.1, AC012313.2, TMC3-AS1, PAPSS2, N4BP2L2, MARF1, ASS1, ZBTB18, AC009318.1, SPDYE5, ZNF417, PTCRA, KLF2, AC093525.6, SLC30A7, DMGDH, ZBTB41, SLC37A1, WNT10B, AC008074.2, AC012313.5, ZNNT1, FAM238C, FLT1, AC079880.1, AC021242.3, MRPL23-AS1, CFAP54, TRIM52, EVI2B, PDE5A, C16orf72, TAPT1-AS1, NPIPB6, AC135782.3, PNPLA7, AC092301.1, AL121917.1, LTK, ATXN2L, LINC02078, MBNL2, ZBED3, AL117339.3, KCNT1, AL356488.3, LILRB4, CEBPB-AS1, AC007686.3, ZNF527, CD180, CCNL2, AL669831.1, AC012358.3, AC120114.3, SDHAP1, MBD4, PLEKHA7, AL355388.1, DRAM1, MUC20P1, AC104472.4, AC092070.2, POU5F1P3, AC095057.3, NXPH4, CILK1, SS18, SNX29P2, ADM2, AC092145.1, MTMR9LP, CCDC18-AS1, STRCP1, PLEKHN1, PSAT1, ZNF841, SNX30, PDCL3P4, OXER1, CAMK1D, AL353593.1, AC105020.6, PLLP, AL121772.1, SLC6A9, RAP2C-AS1, AL132800.1, HEPACAM2, CACNA2D4, DERL1, KIF21B, ERN1, SESN2, PINK1-AS, PARM1, LINC00891
Gene set F: Unique in ΔMBII.BCL2 vs MSCV-backbone	64	BANK1, SERPINF1, PDIA3, PLEKHG4, LINC02777, CROCCP3, HABP4, ZNF70, ZNF432, SYTL1, TPT1, ZNF137P, CFAP44, ZNRD2-AS1, TNKS2-AS1, AC159540.2, ERCC4, TMEM181, TNFSF8, AC009113.1, SLC3A2, LINC01480, FILIP1L, ZMYM2, PMS2P3, LRRC27, TSSK6, AC079174.2, ALMS1, AC006378.1, TBX6, AC138409.2, AANAT, SHMT2, SLC22A18, NMRK1, ZNF274, AL683813.2, ADCY5, ZNF81, SLC1A5, AC016747.1, ZNF540, AL732372.3, NPIPB11, SNORC, AC233723.2, ATP1B2, ATF5, AC011468.1, HSDL1, RAB39B, SIAH1, DNAH10OS, LINC00899, RPS10P7, GRID2IP, FNBP4, ASNS, SARS1, ACVR1B, AP001057.1, AL021707.2, VSIG10
Gene set G: Unique in MBII W135A.BCL2 vs MSCV-backbone	101	PLCE1, DLG1, AP001033.2, AL122035.2, AC005674.2, AP3S2, PPP3CA, AC022306.2, CEP120, ALDH1L2, ZNF805, ZC3H6, SMIM38, PIEZO2, TTC3, AC008764.8, TLK1, DNAJC16, ZNF561, AL627171.2, IL4I1, CHDH, DPY19L3, GTF2IP13, SETBP1, AC027682.1, KIAA1841, TRPV1, AC004951.1, ZNF664, HECTD1, Z83843.1, H3P37, PTOV1-AS1, RINL, UPB1, LINC01126, GRK4, ZSCAN31, RCCD1-AS1, ZMYM4, AL031595.1, TMEM262, AC004233.2, MARS1, NKILA, TIGD3, AL360270.1, TARS3, AC105036.3, ZNF233, BACH2, AC108449.2, AC016586.1, PLXNA3, METTL14-DT, PDC-AS1, AC007614.1, AC009163.7, DNAH6, BCL9, SRPK3, AC097637.2, ENAM, ZNF765, PLXNC1, STOX2, ABCC4, RTL5, AC004943.1, AC005288.1, ZNF221, RPS11P5, AC063950.1, TSSK3, SLC44A1, DND1P1, KANSL1L, TMEM154, CREBL2, AL357033.3, OGT, PPARA, AL627309.5, KLF7, MYO15A, ZNF451, ZNF674, TVP23C-CDRT4, ADCY6, LINC00909, FCRL4, LINC00707, PRKAR1B-AS1, PTPRO, TTLL7-IT1, RHOQ-AS1, AC112220.2, SS18L1, AC137932.3, PRKAR2A-AS1

As GO analysis did not result in a further understanding of our data, we next aimed to identify distinct MYC targets in the Gene sets A, B and C. Genes from the signatures HALLMARK_MYC_TARGETS_V1 (MYC_V1_H) and HALLMARK_MYC_TARGETS_V2 (MYC_V2_H) (MigSDB_HALLMARK GO term) induced in the MYCwt over the MSCV-backbone were utilized and compared to each of the gene lists generated by Gene set A, B and C. In Gene set A the MYC targets *RSL1D1*, *XPOT*, *HSPD1* (MYC_V1_H) and *TFB1M*, *MYBBP1A*, *HSPD1* (MYC_V2_H) were identified. In Gene set B, only *EEF1B2* and *EPRS1* were identified in MYC_V1_H. Lastly, in Gene set C, *GNL3* was a MYC target identified in both signatures while *PAPPC1* and *RRP12* belonged in MYC_V1_H and MYC_V2_H respectively. Thus, even though no representation of the MYC_V2_H existed in Gene set B, MYC targets were identified in all three Gene sets A, B and C between the DEGs shared with the *WT-t2A-BCL2* condition.

When this analysis was performed for Gene set E, 19 MYC targets were identified in total from both the signatures tested. Thus, even though MYC targets were identified as induced in the Gene sets A, B and C their gene count was reduced in comparison to Gene set E, suggesting a significant impairment of MYC activity upon W135A introduction in an overexpression context.

5.5.4 Immunophenotypic markers and MYC targets gene expression

The expression of genes encoding the immunophenotypic markers selected for flow cytometry assessment in the model system was explored. As depicted in Figure 5.14, *CD2* reporter expression was successfully verified in all the transduced samples at day 13 in comparison to the untransduced.

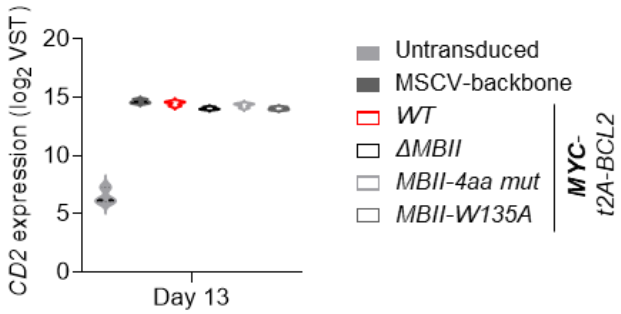

Figure 5.14 Gene expression of *CD2* reporter. Graphs of normalised expression values of *CD2* as analysed for the indicated conditions at day 13. Software DESeq2 performed variance stabilizing transformation (VST) analysis generating the normalized log_2-transformed gene expression values, with stabilized variance, that are visualized in the graph. Data are representative of two independent experiments with three biological replicates in total (N= 3) and no technical replicates.

The corresponding genes to the immunophenotypic proteins were analysed and similarities with the flow cytometry data were confirmed at a transcriptional level. In Figure 5.15, *CD19* expression appeared downregulated in the *WT-t2A-BCL2* condition and slightly upregulated in the MBII mutants in comparison to the untransduced and MSCV-backbone conditions. *MS4A1* encoding for CD20 showed expression closer to the control levels and lower expression than in the MYC WT-BCL2 overexpressing samples. *CD27* and *SDC1* expression followed a similar pattern. They showed significant but not complete upregulation upon overexpression of the *ΔMBII-*, *MBII-4aa mut-*, and *MBII-W135A-t2A-BCL2* conditions in comparison to their reduced expression in the *WT-t2A-BCL2* transduction. *CD38* expression was similar to the control levels upon MYC MBII mutants' overexpression.

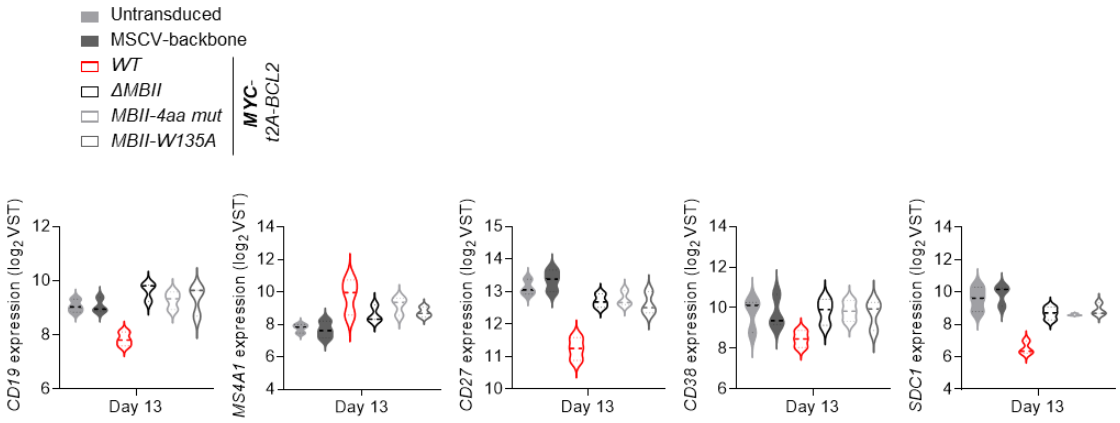

Figure 5.15 Expression of the flow cytometry immunophenotypic protein genes. Normalised expression values of DEGs were plotted for the indicated conditions at day 13 evaluating *CD19*, *MS4A1*, *CD27*, *CD38* and *SDC1* expression. Software DESeq2 performed variance stabilizing transformation (VST) analysis generating the normalized log_2-transformed gene expression values, with stabilized variance, that are visualized in the graphs. Data are representative of two independent experiments with three biological replicates in total (N= 3) and no technical replicates.

Next, the gene expression of known MYC targets was assessed. Differentially expressed MYC targets were selected and as displayed in Figure 5.16, MYC WT-BCL2 overexpression significantly increased their expression at day 13 in comparison to their expression levels in the controls. The effect of hyperfunctional MYC was significantly lower for the MBII deletion and mutation conditions for *TERT*, *TRAP1, SORD, JAG2* and *LDHA* expression. Thus, DCMW mutation into alanine and W135A showed a profound loss of impact on canonical MYC target gene expression in the model system.

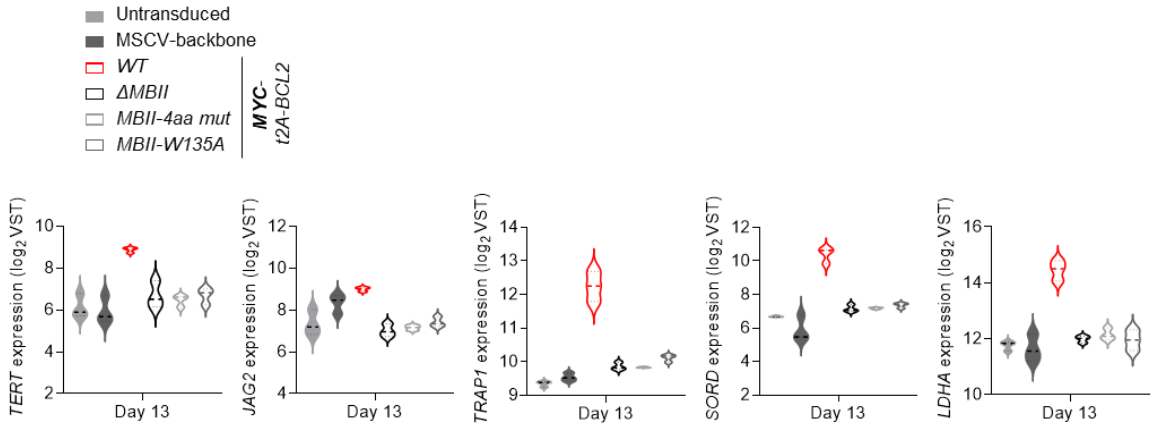

Figure 5.16 Gene expression of MYC targets after DCMW and W135 alanine-based substitutions in the MBII of overexpressed MYC. Normalised expression values of differentially expressed MYC targets were plotted for the indicated conditions at day 13 evaluating *TERT*, *JAG2*, *TRAP1*, *SORD* and *LDHA* expression. Software DESeq2 performed variance stabilizing transformation (VST) analysis generating the normalized log_2-transformed gene expression values, with stabilized variance, that are visualized in the graphs. Data are representative of two independent experiments with three biological replicates in total (N= 3) and no technical replicates.

5.5.5 Gene expression of transcription factors

Key TFs that regulate the transition of a B cell to the PC state were assessed next upon overexpression of the MYC MBII mutants. Overall, gene expression of B cell-associated TFs such as PAX5, EBF1, BACH2 and SREBF1 was reduced at day 13 and in comparison to the expression levels of PC-related TFs, BLIMP1, IRF4, RUNX1 and XBP1, as previously observed in sections 3.6.5 and 4.5.5.

In detail, as displayed in Figure 5.17, *MYC* overexpression was verified in all the transduced conditions in the model system apart from MSCV-backbone which lacked *MYC-t2A-BCL2*-related cDNA sequences. No significant differences were observed in *PAX5* expression between the conditions tested. In contrast, the differences established in *EBF1* showed higher expression in the MBII mutants than in the *WT-t2A-BCL2* samples. MYC WT overexpression drove an aberrant increase in *BACH2* and *SREBF1* expression. Marginal differences were observed in *BACH2* expression upon overexpression of the MBII mutants maintaining higher levels of expression to the controls. Closer to the controls' levels appeared the expression of *SREBF1* for the *ΔMBII-*, *MBII-4aa mut-*, and *MBII-W135A-t2A-BCL2* conditions.

Also in Figure 5.17, the repression observed in MYCwt for the PC-related TFs' genes *PRDM1*, *IRF4* and *RUNX1* was abolished in the MBII mutant conditions. *XBP1* expression was significantly reduced in the *WT-*

t2A-BCL2 samples recapitulating and verifying previous findings in sections 3.6.5 and 4.5.5. Importantly, the *MBII-4aa mut-t2A-BCL2* and *MBII-W135A-t2A-BCL2* conditions significantly revoked the repression of *XBP1* expression observed in MYCwt. This result indicates that MYC overexpression significantly regulates the expression of key TFs involved in PC differentiation, and DCMW motif and W135 play a critical role in this regulation in the model system.

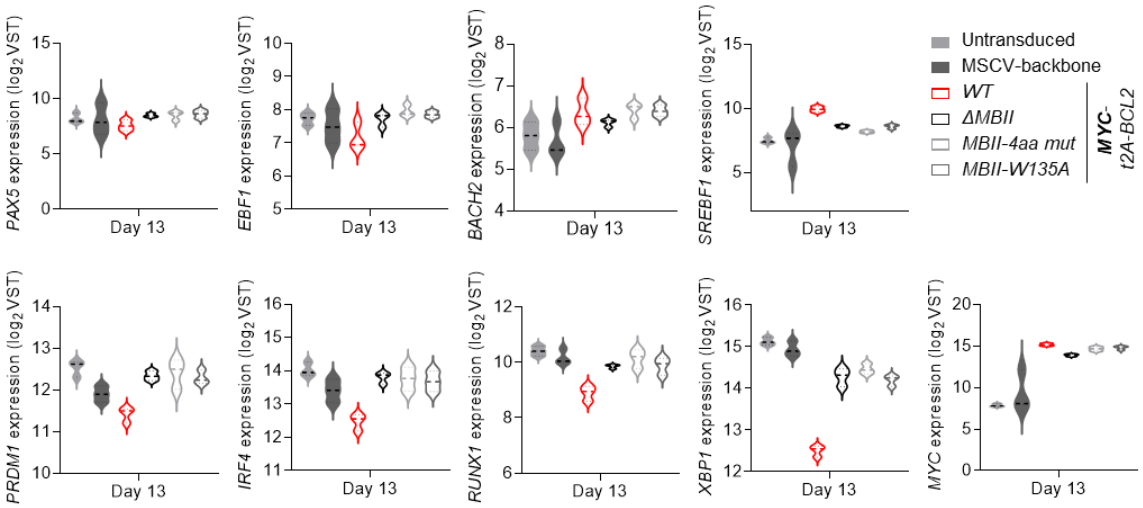

Figure 5.17 Gene expression of TFs upon MBII mutants' introduction to the model system. Normalised expression values of differentially expressed TFs were plotted for the indicated conditions at day 13, evaluating the expression of *PAX5*, *EBF1*, *BACH2*, *SREBF1*, *PRDM1*, *IRF4*, *RUNX1*, *XBP1* and *MYC*. Software DESeq2 performed variance stabilizing transformation (VST) analysis generating the normalized log_2-transformed gene expression values, with stabilized variance, that are visualized in the graphs. Data are representative of two independent experiments with three biological replicates in total (N= 3) and no technical replicates.

5.5.6 XBP1 targets and immunoglobulin gene expression

Next, we assessed the effect of MYC MBII mutants on XBP1 activity. Specific genes identified as XBP1 targets were evaluated and as displayed in Figure 5.18, repression in their expression was observed in MYCwt. Overexpression of either of the *ΔMBII-*, *MBII-4aa mut-*, and *MBII-W135A-t2A-BCL2* conditions significantly reduced the MYCwt effect on the XBP1 targets expression. This result indicated that the repression observed in *XBP1* upon MYC WT overexpression resulted in its reduced TF activity. Substitution of DCMW motif into sequential alanine residues or W135A sufficed to abolish this hyperfunctioning MYC-mediated effect on the XBP1-driven gene expression.

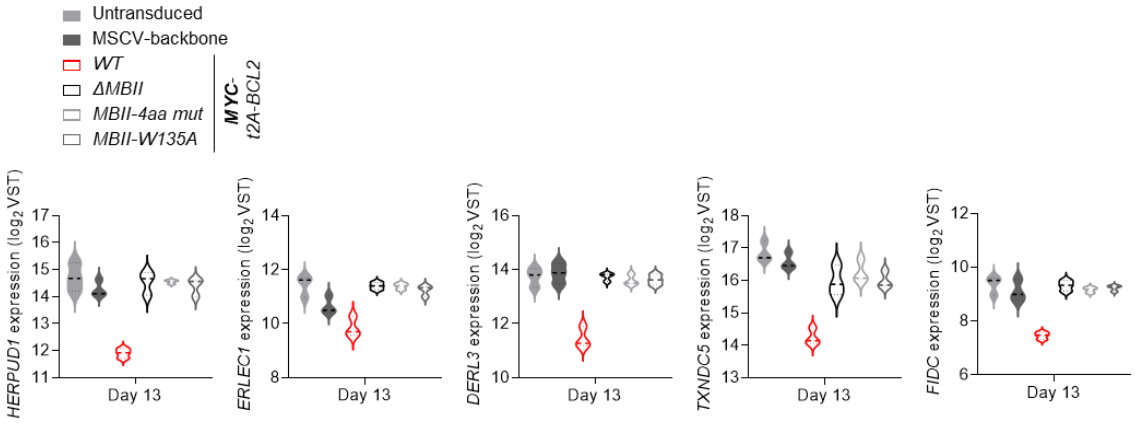

Figure 5.18 MYC-mediated XBP1 function impairment was restored in the conditions carrying the MBII mutants. Normalised expression values of differentially expressed XBP1 targets were plotted for the indicated conditions at day 13 evaluating *HERPUD1*, *ERLEC1*, *DERL3*, *TXNDC5* and *FIDC* expression. Software DESeq2 performed variance stabilizing transformation (VST) analysis generating the normalized log_2-transformed gene expression values, with stabilized variance, that are visualized in the graphs. Data are representative of two independent experiments with three biological replicates in total (N= 3) and no technical replicates.

Previous findings in sections 3.6.6 and 4.5.6 showed impaired transcription of immunoglobulin genes upon MYC WT-BCL2 overexpression which was significantly abolished by deletion of the MYC MBII domain. Thus, immunoglobulin gene expression was assessed to get a better understanding of MYC-BCL2 hyperactivity effect at a transcriptional level after DCMW motif and W135 alanine substitutions.

All the heavy and light chain genes assessed in Figure 5.19 showed similar gene expression to the controls in the *ΔMBII-*, *MBII-4aa mut-*, and *MBII-W135A-t2A-BCL2* conditions in comparison to the MYCwt. This analysis further supported that the MBII domain of MYC is crucial for its hyperfunction effect observed on PC differentiation at a transcriptional level. The DCMW motif and W135 are essential in the context of MYC overexpression to mediate its impact on gene expression under conditions permissive for PC differentiation as examined here.

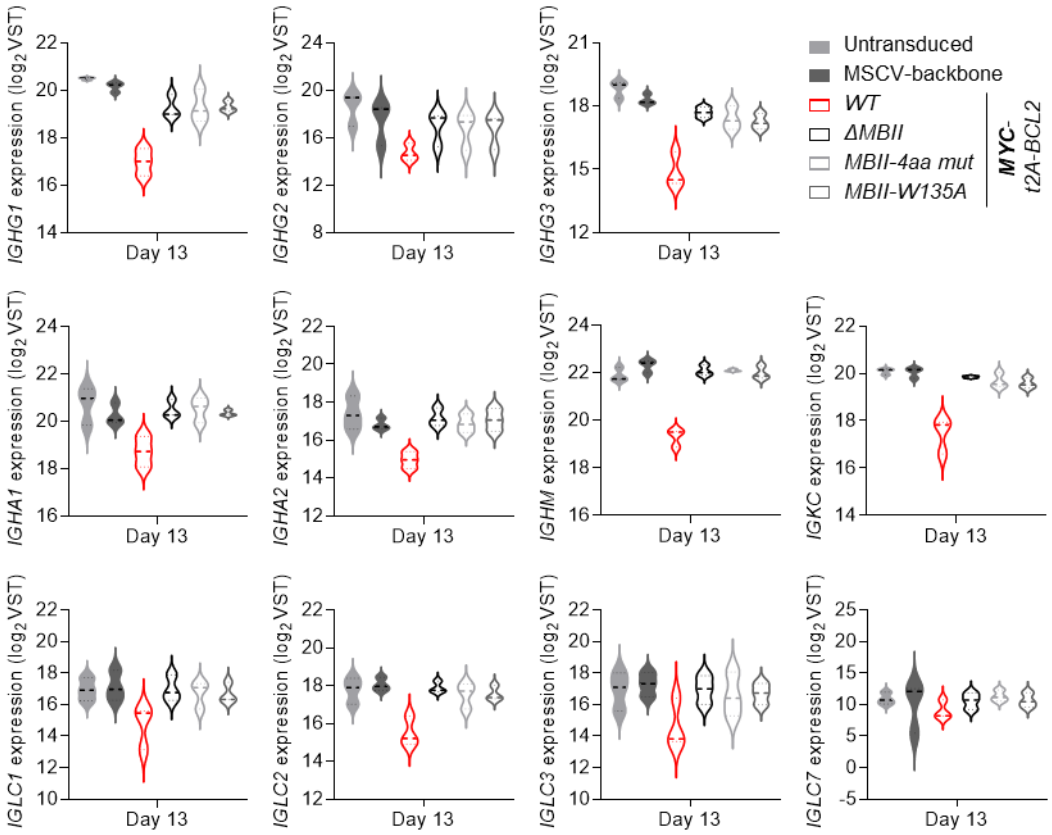

Figure 5.19 Heavy and light chain immunoglobulins gene expression is not repressed in the MBII mutants. Normalised expression values of DEGs were plotted for the indicated conditions at day 13 evaluating heavy chain *IGHG1*, *IGHG2*, *IGHG3*, *IGHA1*, *IGHA2* and *IGHM* and light chain *IGKC*, *IGLC1*, *IGLC2*, *IGLC3* and *IGLC7* expression. Software DESeq2 performed variance stabilizing transformation (VST) analysis generating the normalized log_2-transformed gene expression values, with stabilized variance, that are visualized in the graphs. Data are representative of two independent experiments with three biological replicates in total (N= 3) and no technical replicates.

5.5.7 Transcriptional expression of MYC degradation-associated genes and the role of DCMW motif and W135 in the hyperfunctioning MYC-mediated effect

To explore the protein expression decrease observed in the *MBII-4aa mut*- and *MBII-W135A-t2A-BCL2* conditions it was reasoned that MBII disruption could result in transcriptional expression changes of genes involved in MYC degradation. MYC protein has been associated with direct interactions by E3 ubiquitin ligases (263). Genes encoding for known E3 ubiquitin ligases interacting with MYC were analysed for their differential expression in Figure 5.20. FBXW7 and TRUSS, encoded by *FBXW7* and *TRPC4AP*, interact with

MYC via its MBI and showed transcriptional repression in the *WT-t2A-BCL2* condition which was abolished in the MBII mutants. HECTH9, SKP2, FBXW8, TRIM32 and β-TRCP E3 ubiquitin ligases encoded by *HUWE1*, *SKP2*, *FBXW8*, *TRIM32*, and *BRTC* respectively, interact with MYC via other regions rather than the MBI including the MBII domain. *HUWE1*, *SKP2* and *TRIM32* showed an increase in expression in MYCwt which was lost in the MBII mutant conditions mimicking the gene expression levels of the controls. Negligible differences in gene expression were observed for the *FBXW8* and *BRTC* between all the conditions tested. These results indicated a differential effect of MYC WT overexpression in the transcription of genes encoding for the E3 ubiquitin ligases shown in Figure 5.20. Importantly, the role of DCMW motif and W135 in hyperfunctioning MYC was only observed in genes affected by MYC WT overexpression such as *FBXW7* or *SKP2,* and not in genes unaffected in the MYCwt such as *BRTC*.

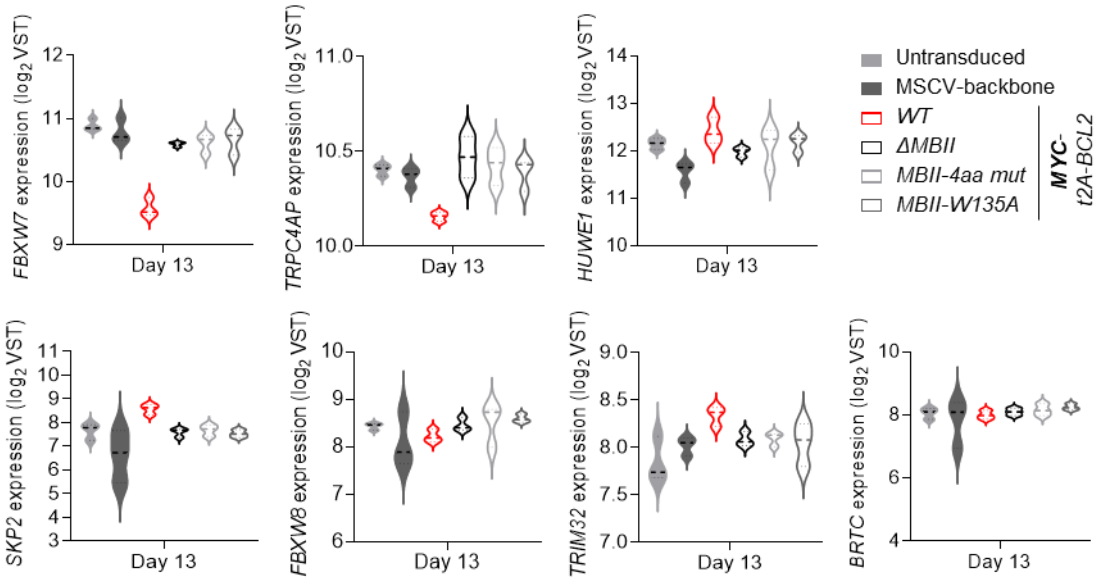

Figure 5.20 MYC WT represses E3 ubiquitin ligases *FBXW7* and *TRPC4AP,* interacting with its MBI domain, only when MBII is intact in an overexpression context. Normalised expression values of DEGs were plotted for the indicated conditions at day 13 evaluating *FBXW7, TRPC4AP*, *HUWE1*, *SKP2*, *FBXW8*, *TRIM32* and *BRTC* expression. Software DESeq2 performed variance stabilizing transformation (VST) analysis generating the normalized log_2-transformed gene expression values, with stabilized variance, that are visualized in the graphs. Data are representative of two independent experiments with three biological replicates in total (N= 3) and no technical replicates.

In the results discussed to this point, most of the genes showed perturbed gene expression patterns upon MYC WT overexpression in comparison to their counterparts. Despite this being the overall effect observed in our data, a smaller set of genes also show no significant differences in gene expression upon MYC WT

overexpression. Deletion of the MBII and substitutions of its DCMW motif and W135 into alanine have consistently resulted in abolishing the effect driven by MYC WT overexpression at a transcriptional level.

Next, we aimed to further validate this contribution of DCMW and W135 in MYC hyperfunction-mediated transcriptional changes in the model system. To achieve that, vignette genes involved in a particular process showing marginal differences in MYCwt were to be exclusively examined. The analysis above showed that MYC WT induces transcriptional repression of E3 ubiquitin ligases interacting with its MBI and specifically repression of *FBXW7*. As displayed in Figure 5.21, a set of genes encoding for critical proteins involved in the S62 and T58 mediated MYC proteasomal degradation, upon its ubiquitination by SCF^{FBXW7}, showed marginal differences in gene expression upon MYC WT overexpression. This set of genes included *CDC34*, encoding for the CDC34 E2 ubiquitin-conjugating enzyme of FBXW7, *PIN1*, *GSK3B* and *PPP2R5A*. Importantly, no differences were observed in their gene expression in either of the MBII mutants.

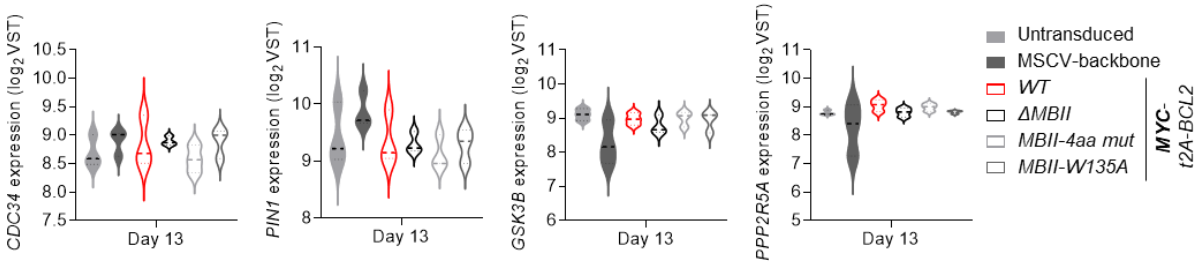

Figure 5.21 Assessment of key genes involved in FBXW7-associated MYC proteasomal degradation pathway. Normalised expression values of DEGs were plotted for the indicated conditions at day 13 evaluating *CDC34, PIN1, GSK3B* and *PPP2R5A* expression. Software DESeq2 performed variance stabilizing transformation (VST) analysis generating the normalized log_2-transformed gene expression values, with stabilized variance, that are visualized in the graphs. Data are representative of two independent experiments with three biological replicates in total (N= 3) and no technical replicates.

This analysis confirmed that the DCMW motif and W135 were critical for the MYC-mediated effect on gene expression in the model system examining a group of genes involved in the process of MYC proteasomal degradation. The contribution of the DCMW motif and W135 to MYC hyperfunction did not confer alternative regulation patterns to the anticipated and previously observed MYC overexpression-mediated changes in gene expression. Thus, no novel or differential regulation is enforced by the MBII mutants tested here if MYC WT hyperfunction does not affect the expression of DEGs in the first place.

5.5.8 Parsimonious Gene Correlation Network Analysis (PGCNA)

To explore the changes in different biological processes between the controls, MYC WT-BCL2 and MBII mutants' overexpression, PGCNA was performed for the genes identified as differentially expressed at day 13. Clustering of the generated network resulted in 19 modules (M) of co-expression for the analysed DEGs. As Table 5.5 shows, M1, M2 and M3 contained more than 550 genes each while the smaller module in absolute gene count was comprised of 96 genes and was the only cluster with less than 160 genes. Each of the 19 modules was allocated a summary description based on enriched GO terms and signatures identified upon functional annotation analysis.

Table 5.5 PGCNA identified 19 modules of co-expression. Each module derived by Parsimonious Gene Correlation Network Analysis (PGCNA) was assigned a summary description based on the GO terms and signatures that overrepresented their assigned genes. The short description of the functional annotation characterizing each module is indicated as Module_ID. The number of genes assigned per module is in the column indicated as Module Size. Data are representative of two independent experiments with three biological replicates in total (N= 3) and no technical replicates; M, module.

Module	Module_ID	Module Size
M1	upPC Golgi ER Bcell_Ecotyper_S02 ASC_plasma_cell_high	581
M2	MIR WEI_MYCN_TARGETS_WITH_E_BOX	576
M3	LZ_Bach2high_upreg Bcell_Ecotyper_S03	550
M4	Ig Membrane Secreted	450
M5	JAK2_upregulated_PMBL MYC_UP.V1_UP RibosomeBiogenesis HIF1_DN	438
M6	THAKAR_PBMC_INACTIVATED_DN	428
M7	Ig Membrane Secreted RegulationOfImmuneResponse	421
M8	Extracellular_Matrix ZHAN_MULTIPLE_MYELOMA_CD1_VS_CD2_UP	416
M9	ProteinBiosynthesis Translation	397
M10	Ribosome Mitochondria	396
M11	JAK2_upregulated_PMBL CACGTG_MYC_Q2	387
M12	Mitochondria_OxPhos scGC_cluster1_DZ ASC_plasma_cell_high	345
M13	LZ_Bach2high_downreg WEI_MYCN_TARGETS_WITH_E_BOX Mitochondria	333
M14	MIR	324
M15	CellCycle	318
M16	CellMembrane ZHAN_MULTIPLE_MYELOMA_CD1_DN	273
M17	CellCycle	250
M18	IL15_UP.V1_UP Immediate_early	169
M19	Tcells	96

In Table 5.6, modules with enriched signatures and GO terms associated with PC differentiation and immunoglobulin secretion were the M7, M1, M3, M4. The overrepresentation of cell cycle-related genes was confirmed upon GO and signature enrichment analysis in M15 and M17. Modules with high enrichment in MYC function-associated terms and gene signatures were the M9, M10, M12, M13 and M5.

Table 5.6 GO analysis and signature enrichment for modules identified by PGCNA. Signature enrichment and GO analysis were conducted in the 19 modules identified using PGCNA. Tables of modules demonstrating enrichment in PC differentiation, MYC-function or cell cycle-related GO terms and signatures are provided here. In total, five significantly enriched signatures and GO terms per module are displayed. Data are representative of two independent experiments with three biological replicates in total (N= 3) and no technical replicates; FDR, false discovery rate.

Module 7

Gene Signature	Gene Set	Overlapping	Gene Set Size	Z-score	p-value	FDR
Secreted	UniProt-Keyword	76	467	8.3442	7.17E-17	1.78E-14
Immunoglobulin	UniProt-Keyword	34	111	8.1747	2.97E-16	6.97E-14
regulation of immune response [GoID:GO:0050776]	GeneOntology_BP	62	376	7.5532	4.25E-14	8.81E-12
plasma membrane [GoID:GO:0005886]	GeneOntology_CC	158	1579	7.4116	1.25E-13	2.46E-11
immunoglobulin production [GoID:GO:0002377]	GeneOntology_BP	31	113	7.3589	1.85E-13	3.51E-11

Module 1

Gene Signature	Gene Set	Overlapping	Gene Set Size	Z-score	p-value	FDR
BcellDiff_upPC	LEEDS_GOLD	105	470	9.9696	2.07E-23	4.33E-21
ER-Golgi transport	UniProt-Keyword	20	41	6.8769	6.12E-12	7.45E-10
XBP1_target_secretory (PMID:15345222)	SignatureDB	14	32	5.4310	5.60E-08	4.53E-06
ASC_plasma_cell_high (PMID:27525369)	SignatureDB	49	296	4.9128	8.98E-07	6.06E-05
Bcell_Ecotyper_S02_3pct (PMID:34597589)	SignatureDB	9	20	4.4003	1.08E-05	5.91E-04

Module 3

Gene Signature	Gene Set	Overlapping	Gene Set Size	Z-score	p-value	FDR
Bcell_Ecotyper_S03_20pct (PMID:34597589)	SignatureDB	66	321	7.5362	4.84E-14	7.48E-12
LZ_Bach2high_upreg (PMID:32619424)	SignatureDB	71	465	5.7295	1.01E-08	1.07E-06
BcellDiff_upPC	LEEDS_GOLD	69	470	5.3594	8.35E-08	8.01E-06
IRF4_ABC_induced_all (PMID:22698399)	SignatureDB	35	218	4.2324	2.31E-05	0.0014
IRF4_ABC_induced_PC (PMID:22698399)	SignatureDB	14	61	3.7543	1.74E-04	0.0083

Module 4

Gene Signature	Gene Set	Overlapping	Gene Set Size	Z-score	p-value	FDR
Secreted	UniProt-Keyword	69	467	6.8194	9.15E-12	2.05E-09
immunoglobulin complex [GoID:GO:0019814]	GeneOntology_CC	27	116	6.0042	1.92E-09	3.25E-07
Immunoglobulin	UniProt-Keyword	26	111	5.9138	3.34E-09	5.51E-07
Cell membrane	UniProt-Keyword	102	945	5.6988	1.21E-08	1.79E-06
secretory granule [GoID:GO:0030141]	GeneOntology_CC	35	293	3.7463	0.0002	0.0110

Module 15

Gene Signature	Gene Set	Overlapping	Gene Set Size	Z-score	p-value	FDR
cell cycle [GoID:GO:000704]	GeneOntology_BP	140	777	15.5465	1.68E-54	7.38E-52
mitotic cell cycle [GoID:GO:0000278]	GeneOntology_BP	102	429	14.8037	1.39E-49	5.00E-47
Cell_cycle_Whitfield (PMID:12058064)	SignatureDB	91	373	14.0451	8.26E-45	2.45E-42
Cell cycle	UniProt-Keyword	81	325	13.2942	2.50E-40	6.42E-38
Cell_cycle_Liu (PMID:15123814)	SignatureDB	55	143	12.9215	3.40E-38	7.99E-36

Module 17

Gene Signature	Gene Set	Overlapping	Gene Set Size	Z-score	p-value	FDR
DLBCL_PGCNA_M7 CellCycle E2F_EGFR	LEEDS_GOLD	69	516	10.0733	7.25E-24	1.16E-20
HALLMARK_E2F_TARGETS	MSigDB_H	31	169	7.7181	1.18E-14	3.77E-12
Cell cycle	UniProt-Keyword	39	325	6.8778	6.08E-12	1.28E-09
REACTOME_CELL_CYCLE	MSigDB_C2	41	361	6.8084	9.87E-12	2.02E-09
cell cycle process [GoID:GO:0022402]	GeneOntology_BP	53	576	6.6735	2.50E-11	4.76E-09

Module 9

Gene Signature	Gene Set	Overlapping	Gene Set Size	Z-score	p-value	FDR
Protein biosynthesis	UniProt-Keyword	27	89	7.4186	1.18E-13	3.20E-11
translation [GoID:GO:0006412]	GeneOntology_BP	52	408	5.7312	9.97E-09	1.72E-06
peptide biosynthetic process [GoID:GO:0043043]	GeneOntology_BP	52	419	5.5742	2.49E-08	4.19E-06
cytoplasmic translational initiation [GoID:GO:0002183]	GeneOntology_BP	10	24	5.1557	2.53E-07	3.68E-05
ribosome biogenesis [GoID:GO:0042254]	GeneOntology_BP	30	236	4.3016	1.70E-05	0.0019

Module 10

Gene Signature	Gene Set	Overlapping	Gene Set Size	Z-score	p-value	FDR
cytosolic ribosome [GoID:GO:0022626]	GeneOntology_CC	72	94	18.1008	3.14E-73	4.33E-70
Ribosomal protein	UniProt-Keyword	78	127	17.3416	2.28E-67	2.16E-64
ribonucleoprotein complex [GoID:GO:1990904]	GeneOntology_CC	108	457	13.6283	2.72E-42	8.50E-40
ribosome biogenesis [GoID:GO:0042254]	GeneOntology_BP	61	236	10.4722	1.16E-25	2.07E-23
DLBCL_PGCNA_M8 Mitochondrian MYC_Overexpression RibosomeBiogenesis	LEEDS_GOLD	81	498	9.0972	9.27E-20	1.23E-17

Module 12						
Gene Signature	**Gene Set**	**Overlapping**	**Gene Set Size**	**Z-score**	**p-value**	**FDR**
scGC_cluster1_DZ (PMID:30104629)	SignatureDB	79	441	10.5296	6.31E-26	3.03E-23
ASC_plasma_cell_high (PMID:27525369)	SignatureDB	61	296	9.9275	3.16E-23	1.28E-20
Mitochondrion	UniProt-Keyword	88	608	9.6810	3.63E-22	1.28E-19
oxidative phosphorylation [GoID:GO:0006119]	GeneOntology_BP	31	74	9.6455	5.14E-22	1.79E-19
HALLMARK_OXIDATIVE_PHOSPHORYLATION	MSigDB_H	35	109	9.2103	3.25E-20	9.57E-18

Module 13						
Gene Signature	**Gene Set**	**Overlapping**	**Gene Set Size**	**Z-score**	**p-value**	**FDR**
LZ_Bach2high_downreg (PMID:32619424)	SignatureDB	84	586	9.6421	5.31E-22	2.17E-19
WEI_MYCN_TARGETS_WITH_E_BOX	MSigDB_C2	71	473	9.0649	1.25E-19	4.29E-17
Mitochondrion	UniProt-Keyword	76	608	8.1853	2.72E-16	6.58E-14
mitochondrial gene expression [GoID:GO:0140053]	GeneOntology_BP	28	109	7.5350	4.88E-14	9.67E-12
mitochondrial matrix [GoID:GO:0005759]	GeneOntology_CC	40	285	6.3356	2.36E-10	3.01E-08

Module 5						
Gene Signature	**Gene Set**	**Overlapping**	**Gene Set Size**	**Z-score**	**p-value**	**FDR**
DLBCL-WithBL_PGCNA_M1 Mitochondrian RibosomeBiogenesis MYC_Overexpression	LEEDS_GOLD	134	852	10.8655	1.68E-27	8.64E-25
JAK2_upregulated_PMBL (PMID:21156283)	SignatureDB	81	505	8.2825	1.21E-16	2.90E-14
ribosome biogenesis [GoID:GO:0042254]	GeneOntology_BP	42	236	6.3620	1.99E-10	3.13E-08
HIF1alpha_1.5x_down (PMID:15374877)	SignatureDB	30	155	5.7020	1.18E-08	1.68E-06
MYC_UP.V1_UP	MSigDB_C6	22	90	5.6798	1.35E-08	1.88E-06

Having unraveled the ontologies that govern critical modules, a heatmap of the MEVs calculated for each of the 19 modules was generated to allow comparison of modular co-expression across all the conditions tested at day 13. As displayed in Figure 5.22, modules that showed enrichment in normal PC differentiation such as M4, M3, M7 and M1 were depleted in the *WT-t2A-BCL2* samples. Importantly, an enrichment similar to the controls was observed in all three *ΔMBII-*, *MBII-4aa mut-*, and *MBII-W135A-t2A-BCL2* conditions supporting our previous findings. In agreement with this result modules such as M5, M12, M10, M9, and M13, which showed enrichment for MYC function-related signatures, were less enriched or depleted in both the controls while they showed significant enrichment in MYCwt. Their enrichment was reduced in both the MBII mutants and the *ΔMBII-t2A-BCL2* samples which appeared to be consistently more similar to the controls. The same pattern was observed in M15 and M17, related to cell cycle, where only MYCwt showed enrichment from all the conditions tested on day 13.

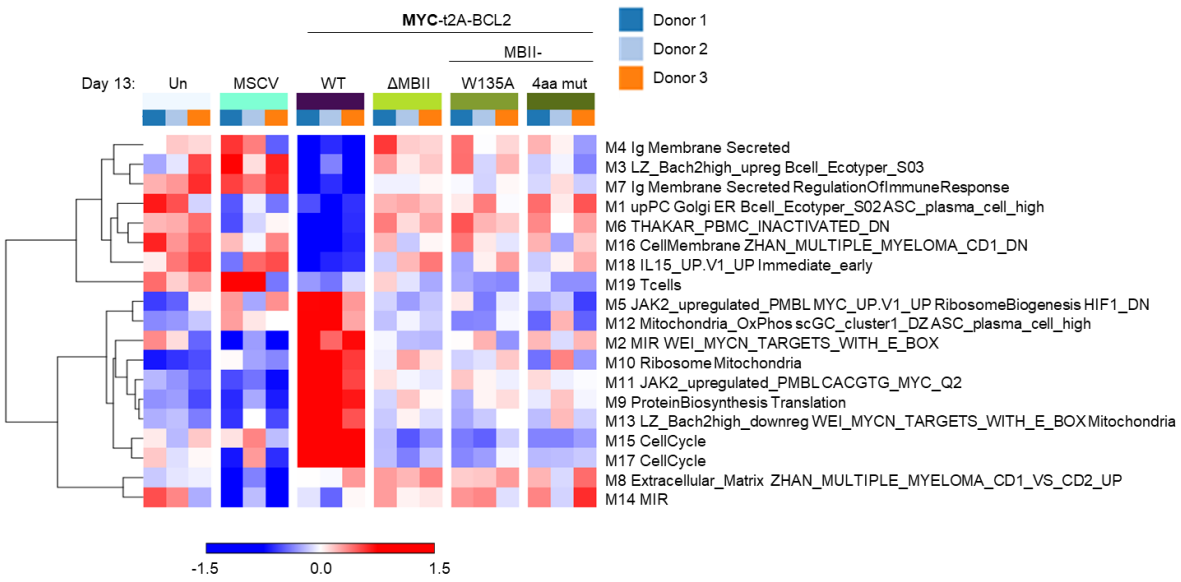

Figure 5.22 Modular enrichment in PC and immunoglobulin secretion over MYC function-associated genes in the MBII mutants. PGCNA network-based analysis was conducted and 19 modules of gene co-regulation were identified. Each module was assigned a module expression value (MEV) which was used to generate the displayed hierarchically clustered heatmap (Z-score scale indicates depletion to enrichment, -1.5 blue to 1.5 red). Short summary of the indicated modules is on the right. All the conditions compared and used to generate the heatmap of MEVs are indicated at the top. Dr. Matthew Care generated the PGCNA-derived heatmap. Data are representative of two independent experiments with three biological replicates in total (N= 3) and no technical replicates; M, module.

These results suggest that overexpression of MYC with alanine-based modifications in the MBII DCMW motif or W135 resulted in the abolishment of MYC hyperfunction and allowed PC differentiation at a transcriptional level to proceed similarly to the controls. In addition, negligible differences were observed between *ΔMBII-*, *MBII-4aa mut-*, and *MBII-W135A-t2A-BCL2* conditions regarding their signature enrichment patterns. This result strongly suggested that the MYC hyperfunction attributed to its MBII domain is dependent on the highly conserved W135 in the DCMW motif for the model system tested.

5.5.9 Modular co-expression showed marginal differences in the differentially expressed genes induced upon overexpression of MYC with ΔMBII or MBII W135A

The representation of the Gene sets identified in Figure 5.13 (Results section 5.5.3) to the modular co-expression was assessed next. In Gene set B were assigned DEGs upregulated in *WT-t2A-BCL2* and *ΔMBII-t2A-BCL2* compared to MSCV-backbone but not in the *MBII-W135A-t2A-BCL2* condition. The reverse comparison was shown in Gene set C, where DEGs upregulated in *WT-t2A-BCL2* and *MBII-W135A-t2A-*

BCL2 compared to MSCV-backbone but not in the *ΔMBII-t2A-BCL2* were identified. In Table 5.7, MYC function-associated modules showed overlap with both Gene sets B and C. M8 was the most highly represented followed by M9, M2 and M11 for Gene set B while M11, M2 and M9 showed overlap for Gene set C in this order. This indicated that both Gene sets were highly represented by similar modules of co-expression but with slightly different contributions. Interestingly, Gene set C showed representation in three additional modules, M13, M1 and M5. This analysis suggested that the modifications of ΔMBII domain and W135A in MYC showed some differences in the co-regulation of their identified DEGs with the *MBII-W135A-t2A-BCL2* condition to show a more diverse modular overlap. However, these differences were based on very low absolute gene counts suggesting that the overall representation of both conditions in the modules showed no significant differences. These results further validated our previous analysis and highlighted the critical role of W135 in the MBII-dependent MYC function in an overexpression context and during PC differentiation.

Table 5.7 Modular representation of upregulated genes in *WT-*, *ΔMBII-*, and *MBII W135A-t2A-BCL2* condition in comparison to MSCV-backbone. The 19 identified modules, using PGCNA, were used to evaluate co-expression patterns of gene sets resolved in Figure 5.13 with Venn diagrams. Gene set B was assigned shared genes with higher expression in *WT-t2A-BCL2* and *ΔMBII-t2A-BCL2* but not in the *MBII W135A-t2A-BCL2* over the MSCV-backbone. Gene set C was assigned shared genes with higher expression in *WT-t2A-BCL2* and *MBII W135A-t2A-BCL2* but not in the *ΔMBII-t2A-BCL2* over the MSCV-backbone. Gene sets B and C were compared to the gene lists of each of the 19 modules using pairwise comparisons. Gene counts resulting from the pairwise comparisons are in the column named Genes per module (right). Modules with no overlap were not included. Data are representative of two independent experiments with three biological replicates in total (N= 3) and no technical replicates; M, module.

Genes compared between:
WT-t2A-BCL2
ΔMBII-t2A-BCL2
MBII 4aa mut-t2A-BCL2

Common genes only in *WT-t2A-BCL2* and *ΔMBII-t2A-BCL2*- **day 13 Gene set B**

PGCNA-derived module	Genes per module
M8: Extracellular_Matrix ZHAN_MULTIPLE_MYELOMA_CD1_VS_CD2_UP	19
M9: ProteinBiosynthesis Translation	9
M2: MIR WEI_MYCN_TARGETS_WITH_E_BOX	7
M11: JAK2_upregulated_PMBL CACGTG_MYC_Q2	5
M17: CellCycle	3
M10: Ribosome Mitochondria	2
M14: MIR	1
M15: CellCycle	1

Common genes only in *WT-t2A-BCL2* and *MBII W135A-t2A-BCL2*- **day 13 Gene set C**

PGCNA-derived module	Genes per module
M8: Extracellular_Matrix ZHAN_MULTIPLE_MYELOMA_CD1_VS_CD2_UP	32
M11: JAK2_upregulated_PMBL CACGTG_MYC_Q2	30
M2: MIR WEI_MYCN_TARGETS_WITH_E_BOX	20
M9: ProteinBiosynthesis Translation	20
M14: MIR	17
M17: CellCycle	4
M13: LZ_Bach2high_downreg WEI_MYCN_TARGETS_WITH_E_BOX Mitochondria	2
M1: upPC Golgi ER Bcell_Ecotyper_S02 ASC_plasma_cell_high	1
M5: JAK2_upregulated_PMBL MYC_UP.V1_UP RibosomeBiogenesis HIF1_DN	1
M10: Ribosome Mitochondria	1
M15: CellCycle	1

5.6 Impairment of antibody secretion upon MYC WT-BCL2 overexpression requires an intact DCMW motif and the amino acid W135 in the MBII domain

As described in sections 5.5.5 and 5.5.6, MYC WT overexpression in the model system repressed *XBP1* and immunoglobulin gene expression. On the contrary, overexpressed MYC carrying DCMW alanine substitutions or the W135A mutation did not confer such an effect on a transcriptomic level. Thus, it was crucial to explore the effects of MBII mutants on the antibody secretion capacity of the differentiated cells testing their functionality. To do so ELISAs of collected day 6 and day 13 supernatants were performed evaluating total IgG and IgM secretion per cell. As depicted in Figure 5.23, at day 6 a similar pattern of

antibody secretion per cell was observed for both IgG and IgM showing the anticipated secretion in the untransduced and MSCV-backbone controls at the plasmablast stage. On the contrary, reduced secretion was observed in the *WT-t2A-BCL2* condition being consistent with previous results in sections 3.5.5 and 4.6. Secretion similar to the control levels was detected per cell for the IgG at day 6 in the MBII mutants while the difference in the IgM levels was negligible.

Interestingly, at day 13 a significant improvement in IgG secretion per cell was established in the *MBII-4aa mut-*, and *MBII-W135A-t2A-BCL2* conditions verified also by the *ΔMBII-t2A-BCL2* compared to *WT-t2A-BCL2*. In addition, an increase in IgM secretion per cell was also verified for the *MBII-4aa mut-*, and *MBII-W135A-t2A-BCL2* conditions following a similar trend to the IgG.

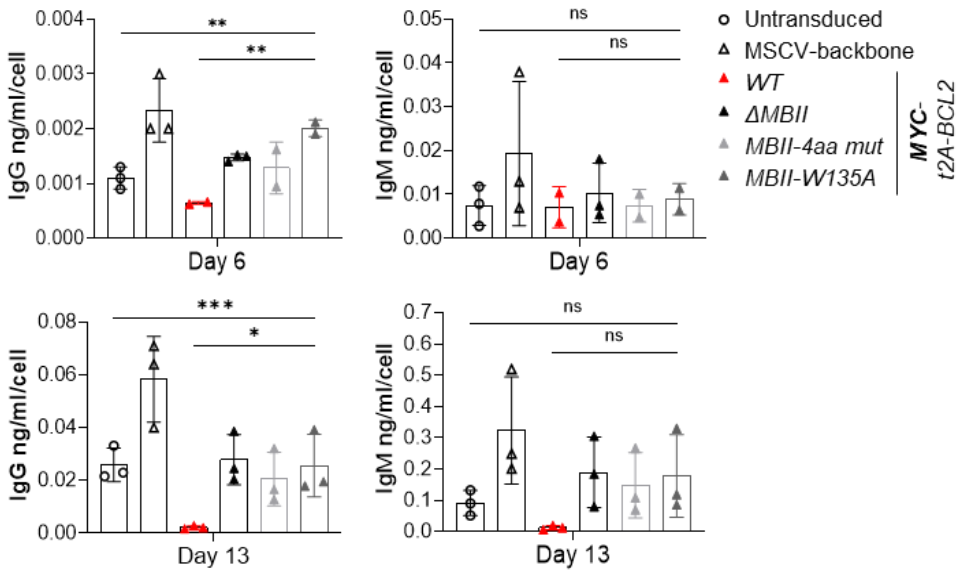

Figure 5.23 Efficient IgG and IgM antibody secretion capacity per cell upon overexpression of *MYC* with *MBII-4aa mut* or *MBII-W135A* and *BCL2* sequences. Supernatants of day 6 (top) and day 13 (bottom) untransduced or transduced with the indicated retroviruses samples, were assessed for their antibody concentration per cell. Human total IgG and IgM ELISAs were performed, and quantification of the detected antibody secretion was calculated at ng/ml/cell per time point tested as indicated. One-way ANOVA. Data are representative of two independent experiments. On day 6, the total number of donors tested as biological replicates was three (N= 3) for each of the untransduced, MSCV-backbone and *ΔMBII-t2A-BCL2* conditions and two (N= 2) for the remaining conditions, *WT-t2A-BCL2*, *MBII 4aa mut-t2A-BCL2* and *MBII W135A-t2A-BCL2*. On day 13, the total number of donors tested as biological replicates was three (N= 3) for all the conditions. Each sample was tested in two technical replicates per assay. Bars and error represent mean and standard deviation (SD); ns, not significant; * $P < 0.05$; ** $P < 0.01$; *** $P < 0.001$.

Similar findings but with less established differences between conditions were confirmed when IgG and IgM concentrations were calculated as ng/ml and assessed between conditions on day 6 and day 13 (data not shown). These findings indicated that the PC secretory state was efficiently established when MYC carrying a DCMW/AAAA or a single W135A mutation was overexpressed in the model system.

5.7 Discussion

Based on previous observations in Chapter 4, disruption of the MBII domain by its deletion led to a striking impact on the ability of overexpressed MYC to perturb PC differentiation. In the context of *ΔMBII-t2A-BCL2* condition cell growth, numbers and immunophenotypic features as well as secretory gene signatures were similar to control differentiations. Also, the metabolic reprogramming driven by MYC WT-BCL2 overexpression was not observed. Thus, MBII was identified as a critical domain for the hyperfunctional MYC-mediated impact on *in vitro* PC differentiation. This Chapter explored the importance of the conserved DCMW motif, 132-135 aa, located in the core of the MBII domain, and its most highly conserved amino acid, W135. Overexpression of MYC carrying a DCMW/AAAA phenocopied the effect observed in *ΔMBII-t2A-BCL2* condition phenotypically, functionally based on ELISAs assessing antibody secretion and transcriptionally. A similar impact on gene expression was observed upon DCMW/AAAA in MYC binding on synthetic reporters resulting in significantly impaired transactivation (274). Thus, DCMW substitutions into alanine sufficed to drive the observed *Δ*MBII effect on PC differentiation in the MYC overexpression context tested here.

Investigating the effect of MYC overexpression upon MBII DCMW/AAAA or W135A resulted in significant restoration of both *XBP1* and immunoglobulins gene expression as well as of the secretory output per cell under differentiation in the model system. Despite W135 being the only residue of the DCMW motif tested with a point mutation, W135A sufficed to mimic both the DCMW/AAAA and *Δ*MBII restored phenotype in the model system. In addition, W135A alone could phenocopy the gene expression signatures observed in *Δ*MBII condition and associated with PC differentiation and secretory reprogramming rather than metabolic and MYC targets-related signatures. Also, despite being remarkably similar to the untransduced and MSCV-backbone controls of normally differentiated PCs, *MBII-W135A-t2A-BCL2* transduced cells maintained MYC targets gene expression and slightly reduced *CD138* and *XBP1* upregulation which was not completely restored. These findings further supported that MYC overexpression drives distinct and selective target transcriptional regulation and that W135 plays a critical role in the transcriptional regulation observed upon MYC WT hyperfunction.

Several point mutations have been previously described for W135 including substitutions into glutamic acid (E), glycine (G), phenylalanine (F), or alanine (A) (210, 213, 234, 264, 276, 314, 330, 335). Differential results have been observed between the W135 point mutations tested in these studies regarding the contribution of W135 in the MBII-dependent MYC function. In experimental settings evaluating W135 point mutations in non-tumorigenic or acute MYC-dependent transformation models, W135E has repeatedly shown disruption of MYC function and of MYC-mediated transformation in an overexpression context (210, 213, 234, 276, 314, 335). In cell lines of rat fibroblasts, the effect of W135E on MYC function was not phenocopied by W135F and W135A which had no significant differences from the MYCwt (234). In a more recent study using the MCF10A human breast epithelial cell line, both W135E and W135A significantly impaired MYC-mediated transformation (276). Here, W135A showed an absolute resemblance with *Δ*MBII condition at a transcriptional level as well as a similar phenotype. Although no transformation was established in the model system, an increased cell number was observed in MYCwt and not in *Δ*MBII or W135A overexpression. Thus, our findings suggest that W135 was a critical residue for overexpressed MYC function in non-transformed human B cells. The fact that MYC hyperfunction was almost revoked in our model system upon W135A but not in a rat fibroblast-based *in vitro* model (234) indicates that W135 point mutations could be of benefit in future studies to unravel MBII-dependent MYC hyperfunction in a cell-type dependent context.

Disruption of the MBII via domain deletion or DCMW motif alanine substitutions or W135A resulted in decreased levels of MYC protein expression when total protein lysates were assessed with western blots. This could be a result of the viral stocks used for transductions and their efficiency in transcribing *MYC*. Another explanation could be that MBII may be involved in overexpressed MYC protein stability. A critical role in MYC protein turnover has been attributed to its MBI domain via well-described sequential phosphorylation steps of S62 and T58 leading to MYC ubiquitination and proteasomal degradation (263). In the context of the *MBII-4aa mut-*, and *MBII-W135A-t2A-BCL2* conditions as well as the *ΔMBII-t2A-BCL2* overexpression, the MBI domain remained intact allowing S62 and T58 dependent proteasomal degradation of MYC to theoretically proceed as normal. Transcriptomic study in this Chapter showed that genes encoding for E3 ubiquitin ligases, FBXW7 and TRUSS, interacting with MYC via the MBI domain are specifically repressed in the *WT-t2A-BCL2* condition. This indicates that a strict and balanced regulation between MYC protein production and degradation should be established, probably in a defined time frame, for overexpressed MYC to undertake its function. Importantly, loss of MBII integrity in the DCMW/AAAA and W135A mutants restored the expression of E3 ubiquitin ligases genes, *FBXW7* and *TRPC4AP*, to the controls' level. Similar was the effect upon DCMW/AAAA or W135A overexpression in

most of the genes identified as DEGs for the *WT-t2A-BCL2* condition. This suggests that *FBXW7* expression was affected by hyperfunctional MYC-mediated regulation in the model system in an MBII-dependent but not MBII-specific fashion.

MYC:TRRAP interaction through the MBII domain results in the formation of bigger complexes with HAT activity, such as the MYC:TRRAP-TIP60 or MYC:TRRAP-GCN5 (204, 276). W135 occupies the core of MBII domain and MYC-TRRAP interaction. Several combinations of glycine substitutions for the hydrophobic amino acids comprising the MBII domain were assessed in an *in silico* model (264). The single mutation of W135G sufficed to predict reduction of MBII:TRRAP interaction (264). The same substitution of W135, resulted in disruption of MYC:TRRAP binding also in a Co-IP setting (330). In addition, a protein complex formation-based luminescence assay has also shown reduced MYC:TRRAP interaction upon W135E or W135A utilizing minimal binding domains of these proteins (276). In the same study, W135E and W135A also led to reduced transformation activity assessing *in vitro* proliferation and growth of MCF10A cells (276). This finding correlated the reduced TRRAP interaction of MYC because of W135E or W135A, with reduced MYC-mediated transformation activity (276). Our findings support that MYC W135A mutant sufficed to confine MYC overexpression function and thus its effect on PC differentiation. Thus, the present study indicates that W135 is a critical residue in the DCMW motif of MBII when no transformation is established and in a PC setting.

Recent literature has identified MYC as an undruggable protein with no enzymatic sites (199). An alternative approach suggested MYC therapeutic targeting through its interactome (214). Our model system comprises the first to our knowledge study investigating a point mutation of W135 upon MYC overexpression in an *in vitro* model of human B cells. Even though co-factors binding to the MBII were not addressed here, TRRAP/HATs complexes interaction with MYC is highly likely to be affected by the MBII alanine substitutions tested in the model system. Also, despite the lack of MYC-driven transformation in our model, the findings of this study provide further evidence that W135 is a promising MYC site to be targeted via its indispensable interactions for MYC oncogenic activity. In this context, our model system suggests that such an undertaking could be of benefit in the context of MYC deregulation and potentially MYC-dependent transformation also in B cells.

A current hypothesis of MYC function is based on the coalition model in which MYC molecules in a cell complete different activities with their effect in total to constitute the overall known MYC function (214, 240). Unelucidated questions of this model regarding specific MYC molecule activities distribution and abundance required for the full MYC effect to be completed are beyond the scope of this study. Our

findings showed a repression in *XBP1* and *FBWX7* upon MYC WT hyperfunction. Although no experiments were conducted to examine their direct or indirect repression by MYC, the MYC WT hyperactivity effect was reversed in the MBII mutants tested here similarly to the *Δ*MBII. In addition, MYC protein overexpression was reduced in the MBII mutants. All these findings together could suggest four different hypotheses of MYC hyperactivity effect on PC differentiation. The first one could be that despite less MYC protein in the MBII mutants the restoration in PC functionality and reprogramming observed is not a result of reduced MYC protein but of a significant loss in the overexpressed MYC function. The second hypothesis, driven by the coalition model, supports the exact opposite, namely, MYC carrying the MBII mutations does not produce an efficient amount of MYC protein to achieve the threshold of molecules completing the full MYC function. Hence, PC differentiation progresses, and the restoration is a result of inadequate MYC protein rather than loss of MYC function through mechanisms or interactions dependent on W135 or DCMW of MBII. A third hypothesis would suggest that a combination of the previous two hypotheses drove the progression of PC differentiation upon the MBII mutants overexpression. In this context, both impaired MYC protein levels and significant loss of function occur in parallel when MBII is not intact, because of the mutations tested, and cooperate resulting in PC differentiation progression. A final hypothesis could lie in the previously observed role of ubiquitin ligases to control MYC transactivation upon inducing its proteasomal degradation (336, 337). An example of a candidate protein conferring such regulation on MYC hyperfunction via the MBII domain is the ubiquitin ligase SKP2. SKP2 has been identified to interact with MYC via its MBII domain (336, 338). Thus, loss of MBII function either through deletion or through the specific amino acid substitutions tested in this Chapter could result in loss of efficient SKP2 interaction in addition to TRRAP/HAT complexes. Importantly, SKP2 acts as a co-activator of MYC function through its ubiquitination and activation of proteasomal degradation (339). SKP2 and MYC co-operate to drive MYC transcriptional activation and elongation (339). Loss of transcription co-activators of MYC, such as the SKP2, via a disrupted MBII, could partially explain the significantly reduced gene expression observed in the MBII mutants tested here. Future studies unravelling such intriguing questions regarding MYC hyperfunction and its MBII domain would be essential and valuable in understanding unknown molecular mechanisms of B cell and PC differentiation progression versus transformation.

Chapter 6 – Discussion

6.1 MYC-BCL2 overexpression did not result in transformation and differentiation arrest

In this study, the effect of MYC overexpression was investigated in human memory B cells differentiating into PCs *in vitro*. MYC overexpression did not suffice to drive transformation when combined with the anti-apoptotic protein and oncogene BCL2. MYC-BCL2 overexpression had previously been utilized by the Hodson group to model DLBCL *in vitro* (277). In this system, constitutive CD40 and IL-21 signalling was used and supported an intermediate phenotype between a GC B cell and a plasmablast upon MYC-BCL2 overexpression. Under these conditions, the combination of these two oncogenes led to persistently prolonged cell growth *in vitro*. In B cells, CD40:CD40L interaction provides a survival signal and promotes proliferation (133). However, constitutive CD40 signalling inhibits PC differentiation favoring a memory B cell fate (133, 340-342). Also, previous *in vitro* models have shown that disruption of CD40:CD40L interaction was essential after day 3 in culture to allow differentiation toward the PC state while IL-21 promotes PC differentiation (340, 341, 343, 344). Synergy has been observed between IL-21 and CD40 which could explain the centrocyte and plasmablastic features observed in the GC B cells differentiated *in vitro* by the Hodson group (343). However, no PC differentiation was established upon MYC-BCL2 overexpression under indefinitely sustained CD40 and IL-21 signalling in their system, successfully modelling DLBCL (277).

In the present study, MYC-BCL2 overexpression acted for 24 hours under the presence of CD40 signalling which was removed from the culture after day 3 in order to promote PC differentiation (149, 282, 283, 340, 341). At this stage sustained IL-21 signalling initially augmented by IL-2 and then by APRIL and IL-6 accompanied the MYC-BCL2 hyperfunction *in vitro* for an additional 10-day window. Under these conditions MYC-BCL2 overexpression increased cell growth and cell numbers for a significantly shorter period than the one observed by the Hodson group system in Caeser et al., 2019 (277). Here, MYC-BCL2 overexpressing cells exited the cell cycle by day 31 consistent with the gradual decrease in their cell numbers observed after day 13. Such an effect was not observed in Caeser et al., 2019, where CD40 and IL-21 signalling were constitutively provided resulting in persistent cell growth and proliferation *in vitro* for up to 120 days. Thus, GC-associated conditions seem to support MYC and BCL2-mediated *in vitro*

transformation more efficiently than the conditions tested in this study which were permissive for PC differentiation.

In addition, these two different experimental settings utilized different initial B cell subsets to assess MYC-BCL2 overexpression. GC B cells were used by Caeser et al., 2019 while in the present study memory B cells were the initial population undergoing viral transductions. GC B cells contain dividing cells especially if they are derived from the dark zone while memory B cells comprise a resting population (345). In addition, these two B cell subsets originate from different stages in the B cell differentiation process, maybe demonstrating distinct chromatin landscape and epigenetic modifications (346, 347). Thus, if the MYC-BCL2 overexpression effect is dependent on cell-intrinsic parameters the above-mentioned differences in the starting population should be taken into consideration. To investigate experimentally this hypothesis an approach would be to culture the memory B cells upon MYC-BCL2 transductions into constitutive CD40 and IL-21 signalling, recapitulating the culture conditions utilized in Caeser et al., 2019. Such an approach would not interrogate the effect of MYC-BCL2 overexpression on PC differentiation, which was the aim of this study, hence it was not experimentally pursued. However, it could provide an understanding of the molecular requirements of MYC and BCL2 deregulation to drive *in vitro* transformation in different B cell subsets.

To get a better understanding of the observed lack of MYC-dependent transformation in our model system, additional aspects could have been further experimentally explored. In malignant cells, MYC deregulation can occur via its overexpression upon chromosomal translocations, gene amplification or mutations that enhance its function and protein stability (35, 252). Protein overexpression of MYC was confirmed at day 6. In addition, enforced MYC-mediated gene expression changes were observed in the *MYC-t2A-BCL2* transduced cells by day 6. These findings supported that transductions with the generated retroviral vectors at day 2 of the model system have successfully resulted in MYC hyperfunction. This allowed us to proceed with the assessment of its impact on PC differentiation acutely. However, constitutive overexpression of MYC protein was not validated at later time points of the model system. Based on our gene expression data, *MYC* and *BCL2* transcripts were maintained at higher levels than the controls for up to day 20. Thus, the most possible explanation for the observed lack of transformation in the model system is that MYC was overexpressed but not necessarily mediating its full oncogenic activity in the culture. This could indicate that MYC overexpression in combination with BCL2 would require specific extracellular signals to support and mediate their oncogenic activity and drive transformation. The present study showed that these signals do not include the assessed conditions permissive for PC differentiation.

6.2 The impact of MYC overexpression on plasma cell differentiation programmes

An interesting observation was that upon MYC overexpression in the model system, the MYCwt transduced cells could not efficiently adjust their resources and protein synthesis to respond to both their enhanced metabolic and antibody secretion needs at the same time. Instead, they were forced to adjust to the MYC-mediated metabolic reprogramming over the secretory pathway induced in a PC. The deletion mutants of MB0 and MBII are evidence of this effect and showed that with overexpression of deficient MYC mutants, that cannot drive the full MYC hyperfunction, the cells responded better to their secretory reprogramming needs. This finding suggested that during PC differentiation the transcriptional programmes regulating metabolic responses act antagonistically to the secretory pathway in an enforced MYC deregulation context.

The above hypothesis also fits with our observation of *XBP1* and immunoglobulin gene repression in the MYC-BCL2 overexpressing cells. An interesting idea to explore would be if ectopic expression of XBP1 would rescue the impaired secretory output upon MYC overexpression. Given the requirement of XBP1 for PC antibody secretion, that would test and validate if the reduced antibody secretion observed by overexpressed MYC is directly driven by *XBP1* repression (155, 156). One potential outcome is that XBP1 ectopic expression could improve antibody secretion in MYC overexpressing cells. However, given the observed adaptation of the cells on MYC hyperfunction driving metabolic reprogramming, another potential outcome could be that ectopic XBP1 expression would not suffice to restore antibody secretion in the model system under sustained MYC hyperfunction. Investigation of such an experimental approach would provide a better understanding of the ongoing regulation between overexpressed MYC and XBP1 in the model system.

6.3 MYC hyperfunction effect on human plasma cell differentiation

Another interesting phenotype was the repression of *FBXW7* by MYCwt in the overexpression setting tested under PC differentiation conditions. *FBXW7* had reduced expression upon ΔMB0 overexpression and normal expression when the MBII was deleted while no difference was observed in the ΔMBI. Even though these data were not shown, this finding indicated that both MB0 and MBII were required for its full repression. Also, it suggested that MYC might negatively regulate the activation of its degradation via the proteasome when overexpressed by transcriptionally inhibiting *FBXW7*. That could result in inhibition of MYC ubiquitination and recognition from the proteasome. Such a mechanism could enhance the levels

of MYC protein available in the cell, delaying its turnover. This could act as an additional mechanism to the already identified genetic aberrations in the *MYC* locus including chromosomal translocations, gene amplification, and mutations suggesting a synergistic mechanism to MYC deregulation to enhance its oncogenic activity.

MYC binding on its target genes has not been assessed in the present study. It is known that MYC binding is not equivalent to MYC-mediated gene expression (221). Thus, RNA-sequencing was considered a more valuable source of information to address the main hypothesis of this study and to compare the impact on MYC hyperfunction between the different mutants. No disruption in the ability of MYC to bind to the DNA is expected in the tested mutants (215, 221, 275). That could be further validated with luciferase assays to verify MYC DNA binding in the developed mutants and gene expression induction. Based on the RNA-sequencing results discussed in this study, efficient but differential gene expression of MYC targets was validated in the T58I, WT, *Δ*MBI and *Δ*MB0, *Δ*MBII, MBII-4aa mut and MBII-W135A mutants. Additional information regarding MYC hyperfunction under conditions permissive for PCs could be provided by a ChIP-seq experiment. Such an approach would reveal the different DNA sites bound by MYC in the model system across the time course and between all the mutants tested. Thus, the ability of MYC to directly bind on regulatory elements of genes that were identified as repressed upon MYCwt overexpression such as *XBP1*, immunoglobulin genes or *FBXW7*, could provide information on their direct or indirect regulation by MYC. ChIP-seq would further verify the ability of MBII mutants to bind to the DNA and confirm that the loss of MYC hyperfunction upon MBII deletion is mechanistically driven and not because of disruption in the MYC:MAX DNA binding. In addition, it would be of interest to see if the different mutants would bind to different MYC targets or if they will demonstrate different abundance between similar targets compared to MYCwt. Such an approach could provide a better understanding of our findings currently supporting that hyperfunctional MYC in the model system did not act as a global amplifier but induced the expression of specific targets.

6.4 MYC hyperfunction and its interaction with TRRAP

In the model system, overexpression of MYC with *Δ*MBII has been validated to disrupt MYC hyperfunction under conditions permissive for PC differentiation. Several studies have supported that the MBII plays a critical role in MYC-mediated transformation and function. Ectopic expression of a MYCER tamoxifen-inducible allele with a deleted MBII domain in human fibroblasts revoked the MYC transactivation ability in target genes and the MYC-mediated transformation activity of Rat1a cells (348). Deletion of the MBII in

rat embryonic fibroblasts revealed loss of MYC oncogenic transformation but maintained its transactivation activity in synthetic promoters (210). A similar result was observed in transformation assays conducted in Rat1a cells with reduced colony formation to be observed in ΔMBII (234). Also, the same study showed reduced proliferation and MYC-induced apoptosis upon MBII deletion. However, MYC with a deleted MBII differentially regulated the expression of endogenous MYC targets being able to induce the activation of *Cad* and the repression of *Gadd45a* but not the repression of *c-Myc* (234). Thus, contradictory results were observed regarding the contribution of MBII to MYC transactivation activity in the different systems. The findings of the present study indicated that overexpression of ΔMBII resulted in significantly reduced MYC-mediated gene expression suggesting a requirement of an intact MBII and W135 for efficient MYC transactivation activity.

The molecular mechanisms through which MYC mediates its normal and oncogenic activity remain unclear. It has been suggested that MYC interactome is essential for its transactivation and transformation activity. An *in vivo* study overexpressing MYC ΔMBII suggested that the MBII was required for tumour initiation through chromatin remodelling via its co-factors (240). One critical co-factor of MYC interacting with its MBII domain is TRRAP (248). TRRAP is a component of different complexes, and its interaction with the HATs GCN5 or TIP60 could result in chromatin remodelling via histone acetylation. Thus, TRRAP/HAT complexes have a critical role in the initiation of transcription (329). A BioID-based mass spectrometry study showed that cells overexpressing MYC and treated with TRRAP-specific small interfering RNAs (siRNAs) lost similar interactors as the samples with a deleted MBII domain (240). Such findings suggest that the loss of TRRAP interaction could be responsible for the impaired MYC hyperfunction observed in the ΔMBII or MBII mutants tested here. In our findings, despite having mentioned that ΔMBII, DCMW/AAAA, or W135A could result in loss of TRRAP interaction, no direct experimental proof has been provided. MYC and TRRAP Co-IPs in total or nuclear protein lysates of the transduced cells could examine the direct loss of TRRAP interaction. In addition, mass spectrometry analysis of MYC complexes derived from the Co-IP experiments could identify other proteins involved in complexes of TRRAP while in interaction with MYC in a MYC deregulation setting.

While Co-IPs might reveal that TRRAP interaction is lost in our ΔMBII or MBII mutants, this would not assess that the observed effect on PC differentiation upon MYC hyperfunction is mediated specifically by TRRAP. Thus, in addition, siRNAs of TRRAP should be tested in cells overexpressing MYCwt to assess if a similar phenotype and transcriptional profile to the ΔMBII or MBII mutants will be acquired upon disruption of TRRAP interaction. However, as TRRAP is the best-described interactor with MYC MBII, a

reasonable hypothesis is that the *Δ*MBII or MBII mutants' phenotype is dependent on TRRAP interaction and that when this interaction is lost MYC function is impaired in an overexpression context in PC differentiation.

6.5 The requirement of MBII and MB0 domains in MYC hyperfunction

Deletion mutants of the TAD MBs showed that loss of function in the MBII domain resulted in an almost non-functional MYC in an overexpression context. Previous studies have shown that MBII is required for all MYC biological activities and functions, especially in an overexpression context (212, 234). At the same time, MB0 was essential for the full MYC hyperfunction effect to be conferred in the model system. An interesting result was described by Wasylishen et al., 2011 (314), showing that in an immortalized lung fibroblast cell line, which was also further transformed with TERT, LT and ST oncoproteins, the proliferation rate and MYC-mediated transformation activity were similar between the MYCwt and both their *Δ*MBII or W135E MYC mutants (314). This result was not recapitulated in Rat1a cells or in additional not progressively transformed *in vitro* models. The authors of this study suggested the hypothesis that MBII is only essential for tumour initiation and not required for tumour progression. Such a model was mechanistically supported more recently by Kalkat et al., 2018 (240) suggesting that MBII supports tumour initiation via its TRRAP/HATs recruitment to modify the chromatin and the MB0 is essential for tumour growth via its direct interaction with TFIIF promoting transcriptional elongation. Such findings augment our understanding of the unelucidated molecular mechanisms through which MYC mediates its oncogenic activity.

The present study indicated that the MBs in MYC TAD follow the hierarchical contribution of MBII, MB0 and lastly, MBI on MYC hyperfunction-mediated phenotype, gene expression, and antibody secretion in the model system. When MBII was deleted the intact MB0 in *ΔMBII-t2A-BCL2* condition did not suffice to drive the hyperfunctional MYC effect. On the contrary, deletion of the MB0 impaired but did not completely abolish the overexpressed MYC effect on PC differentiation. Based on these findings we conclude that the MBII is indispensable for MYC hyperfunction while at the same time, it does not suffice for the full MYC hyperfunction to be conferred and requires also an intact MB0. Thus, we speculate that initiation of MYC hyperfunction is not possible without an intact MBII domain. In parallel, full MYC hyperfunction requires both the MBII and the MB0 domains of MYC to be functional. We propose that MB0 confers its function primarily after an initial signal, usually provided through the MBII-dependent MYC hyperfunction. This hypothesis agrees with what has been previously suggested by Wasylishen et al.,

2011 and Kalkat et al., 2018 (240, 314) expanding their observation in a MYC overexpression but not transformation-based setting, as validated and explored in this study.

6.6 MYC therapeutic targeting via its protein-protein interactions

MYC is a potent oncogene involved in 70% of human cancers (206). Thus, it is considered a promising target for cancer treatment but with no inhibitors approved to date for clinical use. Targeting MYC therapeutically has been proven a challenge since it lacks a catalytic site which deteriorated the discovery of small molecule MYC inhibitors. Omomyc is a promising MYC antagonist and the only MYC inhibitor currently tested on clinical trials (199, 264). It is a dominant negative MYC protein with four amino acids mutated in the region where MYC would interact with MAX (264). Thus, MAX binds with higher affinity to Omomyc resulting in MYC:MAX complex formation inhibition and abolishment of MYC function. It has been previously reported that MYC is considered undruggable and new therapeutic strategies are of urgent need for the treatment of MYC-associated cancers (199). An alternative approach is featuring MYC indirect targeting via its PPIs (214). The present study has indicated the importance of W135 in the DCMW motif of MBII for MYC function upon its deregulation. W135 is the most highly conserved amino acid in the MBII domain of MYC and the only tryptophan (W) (204). In addition, it is not recurrently mutated in BL in comparison to other residues in the MBII such as F138 and S146 (213, 349). This further supports its importance in MYC hyperfunction as also demonstrated by the findings of our study.

W135 is located in the core of MBII and has been implicated with TRRAP binding via a predicted exposed loop formed by the DCMW motif to interact with TRRAP (330). The present study has demonstrated that the point mutation W135A sufficed to abolish the hyperfunctional MYC effect on human PC differentiation. We would like to propose W135 as a promising point in MYC to be further investigated for its indirect therapeutic targeting with a focus on MYC MBII-dependent PPIs. Multiple complexes are associated with TRRAP but the actual mechanism of how they contribute to mediate MYC function in a normal or an oncogenic context remains unelucidated. Evidence of MYC:TRRAP interaction via its W135 in a transformation experimental setting could provide valuable information on the co-factors mediating the deregulated MYC downstream signalling. In our model system, MYC overexpression did not result in transformation but it could provide a suitable platform to investigate MYC:TRRAP interaction via W135 in a deregulation context. Such an approach could provide valuable insights into the MBII-PPIs-based mechanisms for MYC therapeutic targeting.

While both the MBII and its DCMW motif have been suggested as promising sites to be targeted therapeutically in MYC protein (204, 323), our findings also showed reduced MYC hyperfunction upon overexpression of ΔMB0. MYC interactome via its MB0 is less studied but our data show that a consistent level of MYC-mediated regulation is dependent on its MB0. Also, our GO analysis and PGCNA modular representation of genes upregulated in MYCwt in comparison to the MSCV-backbone control when the MB0 was intact, showed distinct ontologies to the upregulated genes dependent on an intact MBI. This suggested that MB0 drives distinct gene regulation to the MBI and also the MBII based on our gene expression results and posits the MB0 as a promising domain for MYC therapeutic targeting. Deletion of the MB0 and interactome analysis based on a BioID-focused mass spectrometry approach provided valuable information on the interactome of MYC via its MB0 (240). Interestingly, loss of TRRAP interaction was observed upon MB0 deletion in this system as well as upon deletion of the MBII. However, more components of the TRRAP/GCN5 and TRRAP/TIP60 complexes were identified as lost in ΔMBII than in ΔMB0 (240). This could indicate that MB0 and MBII function through both shared and distinctive interactors. The present study suggests that deletion of the MB0 weakened the effect of MYC hyperfunction and did not result in its complete abrogation observed in ΔMBII. Thus, MYC therapeutic targeting via both its MBII and MB0 PPIs may be an alternative approach to successfully inhibit MYC oncogenic activity utilizing synergistic and combination of drugs-based therapy.

6.7 The hypothesis of long-lived plasma cell cell cycle re-entry and modelling plasma cell neoplasia *in vitro*

Upon MYC-BCL2 enforced overexpression into the cells utilizing retroviral transductions on day 2, no additional mitogenic challenge was introduced in the model. A set of activation conditions, previously established in the laboratory (unpublished data) act as mitogenic signals that are potent to mediate cell cycle re-entry in long-lived PCs generated *in vitro*. An interesting hypothesis regarding the cell of origin in PC neoplasia and myeloma initiation suggests that an abnormal long-lived PC clone carrying a primary oncogenic event maintains a lower threshold of cell cycle re-entry in comparison to healthy PCs (350). Thus, upon mitogenic challenge provided by signals in the bone marrow niche, an abnormal PC could re-enter the cell cycle and progress into myelomagenesis. Such a hypothesis could have been tested into MYC-BCL2 overexpressing cells to assess the potential of cell cycle re-entry in *in vitro* PCs carrying oncogenic events. Even though MYC-BCL2 overexpression extended proliferation no transformation was established. Challenging the MYC-BCL2 overexpressing cells with the mitogenic/activation conditions at a

stage later to day 31, when they have exited the cell cycle, could provide an answer to the lower cell cycle re-entry threshold hypothesis in a PC setting.

MYC is not a driver oncogenic event in PC malignancies. Instead, both *MYC* and *BCL2* have been previously identified as secondary oncogenic events in PC cancers and MM (14, 54, 87, 197). Thus, the developed model system comprises a proof of principle for the overexpression of oncogenic combinations in *in vitro* differentiated human PCs. Overexpression of driver oncogenic events in MM, such as *CCND1*, *CCND3*, or *MAF*, could be accomplished by retroviral transduction on day 2. New intriguing questions regarding the early stages of human PC neoplasia could be investigated in such an experimental setup. Utilizing the mitogenic challenge approach, the hypothesis of cell cycle re-entry could be interrogated in the context of the deregulation of driver events in myelomagenesis.

The model system could also provide a suitable platform to model PC neoplasia. To this extent, a combination of oncogenes known as primary and secondary events in MM could be overexpressed *in vitro* to assess PC transformation and to further explore the cell cycle re-entry hypothesis. In more detail, double transductions of a retroviral vector containing the cDNA sequence of a primary event such as *CCND1* could be co-transduced with a MYCERT2 retroviral vector. This experimental setup would result in acute overexpression of CCND1 post-transduction while inducible MYC overexpression would be regulated by tamoxifen treatment at a later time point such as day 13, where the PC phenotype has been acquired. In a simplistic *in vitro* approach, CCND1 overexpression at day 6 would mimic an abnormal MGUS PC clone and a secondary event, such as inducible MYC overexpression at day 13 would model progression to SMM. The first hypothesis to be assessed in such an experimental setting is its ability to drive transformation in the *in vitro* generated PCs. The cell cycle re-entry hypothesis could be also studied in this context. Would the inducible overexpression of a secondary event, such as MYC, drive cell cycle re-entry in an abnormal clone overexpressing a primary event, upon cell cycle exit is established in the culture? In addition, would a mitogenic challenge be required for cell cycle re-entry to be achieved in PCs with deregulated oncogenes? If not, would a mitogenic challenge augment the oncogenic activity in regard to cell cycle re-entry? The developed model system could provide experimental proof in such unelucidated questions contributing to a better understanding of early molecular mechanisms in PC neoplasia.

An alternative approach to modelling PC neoplasia *in vitro* would be to generate lentiviral constructs containing cDNA sequences of *MYC* alone or in combination with other secondary events in MM such as *KRAS*, *FAM46C*, *TP53*, *DIS3* and assess *in vitro* PC transformation (57, 68). In this context, lentiviral vectors will be required to achieve transductions of non-dividing cells at the later time point of day 13 in the

culture. Oncogenic combinations of primary and secondary events that could lead to *in vitro* PC transformation could be used to generate murine xenografts and to investigate myeloma progression *in vivo*. Thus, the current model system has valuable potential to be used in studies investigating myeloma initiation mechanisms aiming at its early prevention and therapeutic intervention.

6.8 Conclusion remarks

In this study, MYC overexpression with BCL2 did not result in *in vitro* transformation of human PCs under conditions permissive for PC differentiation. This contrasted with the previous study by Caeser et al., 2019 (277) and implied that additional mitogenic pathways such as those provided by CD40:CD40L interaction are needed to drive B cell transformation. In addition, the initial memory B cell population acquired an abnormal antibody secreting cell phenotype and MYC-BCL2 overexpression severely perturbed but did not completely block the ongoing PC differentiation process. There were transcriptional and phenotypical changes resulting in aberrant PC features and increased cell size and number accompanied by extended proliferation and prolonged cell cycle exit. MYC hyperfunction drove metabolic over secretory reprogramming and induced repression of *XBP1* and its UPR-related targets. Also, the MYC overexpressing cells had impaired secretory output which to our understanding is regulated transcriptionally since significant transcriptional repression of the immunoglobulin genes was also mediated by MYC overexpression.

A hierarchical order of contribution to the MYC hyperfunction effect was identified for the MBs contained in MYC TAD. MBI domain was dispensable for the overexpressed MYC-mediated effect on human PC differentiation. In contrast, an intact MB0 was essential for the overexpressed MYC to confer its full hyperactivity. Finally, the loss of MBII function abolished the ability of deregulated MYC to impact PC differentiation. Thus, in our overexpression but non-transformation-based setting, the impact of MYC depended on an intact MBII and the full MYC hyperfunction effect required both the MBII and MB0 domains. Specific amino acids involved in the MBII-dependent MYC hyperfunction were identified. W135 of the core DCMW motif in the heart of MBII was essential for the MYC-mediated effect on PC differentiation in an overexpression context.

References

1. Carsetti R. The development of B cells in the bone marrow is controlled by the balance between cell-autonomous mechanisms and signals from the microenvironment. J Exp Med. 2000;191(1):5-8.
2. Chapuy B, Stewart C, Dunford AJ, Kim J, Kamburov A, Redd RA, et al. Molecular subtypes of diffuse large B cell lymphoma are associated with distinct pathogenic mechanisms and outcomes. Nat Med. 2018;24(5):679-90.
3. Basso K, Dalla-Favera R. Germinal centres and B cell lymphomagenesis. Nat Rev Immunol. 2015;15(3):172-84.
4. Alizadeh AA, Eisen MB, Davis RE, Ma C, Lossos IS, Rosenwald A, et al. Distinct types of diffuse large B-cell lymphoma identified by gene expression profiling. Nature. 2000;403(6769):503-11.
5. Klanova M, Klener P. BCL-2 Proteins in Pathogenesis and Therapy of B-Cell Non-Hodgkin Lymphomas. Cancers (Basel). 2020;12(4).
6. Chaudhari K, Rizvi S, Syed BA. Non-Hodgkin lymphoma therapy landscape. Nat Rev Drug Discov. 2019;18(9):663-4.
7. Pasqualucci L, Khiabanian H, Fangazio M, Vasishtha M, Messina M, Holmes AB, et al. Genetics of follicular lymphoma transformation. Cell Rep. 2014;6(1):130-40.
8. Nguyen L, Papenhausen P, Shao H. The Role of c-MYC in B-Cell Lymphomas: Diagnostic and Molecular Aspects. Genes (Basel). 2017;8(4).
9. Kuehl WM, Bergsagel PL. Molecular pathogenesis of multiple myeloma and its premalignant precursor. J Clin Invest. 2012;122(10):3456-63.
10. Alaggio R, Amador C, Anagnostopoulos I, Attygalle AD, Araujo IBO, Berti E, et al. The 5th edition of the World Health Organization Classification of Haematolymphoid Tumours: Lymphoid Neoplasms. Leukemia. 2022;36(7):1720-48.
11. Dalla-Favera R, Bregni M, Erikson J, Patterson D, Gallo RC, Croce CM. Human c-myc onc gene is located on the region of chromosome 8 that is translocated in Burkitt lymphoma cells. Proc Natl Acad Sci U S A. 1982;79(24):7824-7.
12. Love C, Sun Z, Jima D, Li G, Zhang J, Miles R, et al. The genetic landscape of mutations in Burkitt lymphoma. Nat Genet. 2012;44(12):1321-5.
13. Pasqualucci L, Trifonov V, Fabbri G, Ma J, Rossi D, Chiarenza A, et al. Analysis of the coding genome of diffuse large B-cell lymphoma. Nat Genet. 2011;43(9):830-7.
14. Shou Y, Martelli ML, Gabrea A, Qi Y, Brents LA, Roschke A, et al. Diverse karyotypic abnormalities of the c-myc locus associated with c-myc dysregulation and tumor progression in multiple myeloma. Proc Natl Acad Sci U S A. 2000;97(1):228-33.
15. Taub R, Kirsch I, Morton C, Lenoir G, Swan D, Tronick S, et al. Translocation of the c-myc gene into the immunoglobulin heavy chain locus in human Burkitt lymphoma and murine plasmacytoma cells. Proc Natl Acad Sci U S A. 1982;79(24):7837-41.
16. Grande BM, Gerhard DS, Jiang A, Griner NB, Abramson JS, Alexander TB, et al. Genome-wide discovery of somatic coding and noncoding mutations in pediatric endemic and sporadic Burkitt lymphoma. Blood. 2019;133(12):1313-24.
17. Lopez C, Burkhardt B, Chan JKC, Leoncini L, Mbulaiteye SM, Ogwang MD, et al. Burkitt lymphoma. Nat Rev Dis Primers. 2022;8(1):78.
18. Mbulaiteye SM, Pullarkat ST, Nathwani BN, Weiss LM, Rao N, Emmanuel B, et al. Epstein-Barr virus patterns in US Burkitt lymphoma tumors from the SEER residual tissue repository during 1979-2009. APMIS. 2014;122(1):5-15.

19. Abate F, Ambrosio MR, Mundo L, Laginestra MA, Fuligni F, Rossi M, et al. Distinct Viral and Mutational Spectrum of Endemic Burkitt Lymphoma. PLoS Pathog. 2015;11(10):e1005158.
20. Kaymaz Y, Oduor CI, Yu H, Otieno JA, Ong'echa JM, Moormann AM, et al. Comprehensive Transcriptome and Mutational Profiling of Endemic Burkitt Lymphoma Reveals EBV Type-Specific Differences. Mol Cancer Res. 2017;15(5):563-76.
21. Panea RI, Love CL, Shingleton JR, Reddy A, Bailey JA, Moormann AM, et al. The whole-genome landscape of Burkitt lymphoma subtypes. Blood. 2019;134(19):1598-607.
22. Richter J, Schlesner M, Hoffmann S, Kreuz M, Leich E, Burkhardt B, et al. Recurrent mutation of the ID3 gene in Burkitt lymphoma identified by integrated genome, exome and transcriptome sequencing. Nat Genet. 2012;44(12):1316-20.
23. Schmitz R, Young RM, Ceribelli M, Jhavar S, Xiao W, Zhang M, et al. Burkitt lymphoma pathogenesis and therapeutic targets from structural and functional genomics. Nature. 2012;490(7418):116-20.
24. Blum KA, Lozanski G, Byrd JC. Adult Burkitt leukemia and lymphoma. Blood. 2004;104(10):3009-20.
25. Ferry JA. Burkitt's lymphoma: clinicopathologic features and differential diagnosis. Oncologist. 2006;11(4):375-83.
26. Wildes TM, Farrington L, Yeung C, Harrington AM, Foyil KV, Liu J, et al. Rituximab is associated with improved survival in Burkitt lymphoma: a retrospective analysis from two US academic medical centers. Ther Adv Hematol. 2014;5(1):3-12.
27. Boerma EG, Siebert R, Kluin PM, Baudis M. Translocations involving 8q24 in Burkitt lymphoma and other malignant lymphomas: a historical review of cytogenetics in the light of todays knowledge. Leukemia. 2009;23(2):225-34.
28. Dalla-Favera R, Lombardi L, Pelicci PG, Lanfrancone L, Cesarman E, Neri A. Mechanism of activation and biological role of the c-myc oncogene in B-cell lymphomagenesis. Ann N Y Acad Sci. 1987;511:207-18.
29. Grau M, Lopez C, Martin-Subero JI, Bea S. Cytogenomics of B-cell non-Hodgkin lymphomas: The "old" meets the "new". Best Pract Res Clin Haematol. 2023;36(4):101513.
30. Salaverria I, Siebert R. The gray zone between Burkitt's lymphoma and diffuse large B-cell lymphoma from a genetics perspective. J Clin Oncol. 2011;29(14):1835-43.
31. Aukema SM, Kreuz M, Kohler CW, Rosolowski M, Hasenclever D, Hummel M, et al. Biological characterization of adult MYC-translocation-positive mature B-cell lymphomas other than molecular Burkitt lymphoma. Haematologica. 2014;99(4):726-35.
32. Aukema SM, Theil L, Rohde M, Bauer B, Bradtke J, Burkhardt B, et al. Sequential karyotyping in Burkitt lymphoma reveals a linear clonal evolution with increase in karyotype complexity and a high frequency of recurrent secondary aberrations. Br J Haematol. 2015;170(6):814-25.
33. Ott G, Rosenwald A, Campo E. Understanding MYC-driven aggressive B-cell lymphomas: pathogenesis and classification. Blood. 2013;122(24):3884-91.
34. Sander S, Calado DP, Srinivasan L, Kochert K, Zhang B, Rosolowski M, et al. Synergy between PI3K signaling and MYC in Burkitt lymphomagenesis. Cancer Cell. 2012;22(2):167-79.
35. Xia Y, Zhang X. The Spectrum of MYC Alterations in Diffuse Large B-Cell Lymphoma. Acta Haematol. 2020;143(6):520-8.
36. Shimkus G, Nonaka T. Molecular classification and therapeutics in diffuse large B-cell lymphoma. Front Mol Biosci. 2023;10:1124360.
37. Wright G, Tan B, Rosenwald A, Hurt EH, Wiestner A, Staudt LM. A gene expression-based method to diagnose clinically distinct subgroups of diffuse large B cell lymphoma. Proc Natl Acad Sci U S A. 2003;100(17):9991-6.
38. Rosenwald A, Wright G, Chan WC, Connors JM, Campo E, Fisher RI, et al. The use of molecular profiling to predict survival after chemotherapy for diffuse large-B-cell lymphoma. N Engl J Med. 2002;346(25):1937-47.

39. Shi Y, Han Y, Yang J, Liu P, He X, Zhang C, et al. Clinical features and outcomes of diffuse large B-cell lymphoma based on nodal or extranodal primary sites of origin: Analysis of 1,085 WHO classified cases in a single institution in China. Chin J Cancer Res. 2019;31(1):152-61.
40. Tavakkoli M, Barta SK. 2024 Update: Advances in the risk stratification and management of large B-cell lymphoma. Am J Hematol. 2023;98(11):1791-805.
41. Gandhi S. Diffuse Large B-Cell Lymphoma (DLBCL) Clinical Presentation. MedScape. 2023.
42. Coiffier B, Lepage E, Briere J, Herbrecht R, Tilly H, Bouabdallah R, et al. CHOP chemotherapy plus rituximab compared with CHOP alone in elderly patients with diffuse large-B-cell lymphoma. N Engl J Med. 2002;346(4):235-42.
43. Tilly H, Morschhauser F, Sehn LH, Friedberg JW, Trneny M, Sharman JP, et al. Polatuzumab Vedotin in Previously Untreated Diffuse Large B-Cell Lymphoma. N Engl J Med. 2022;386(4):351-63.
44. Miao Y, Medeiros LJ, Li Y, Li J, Young KH. Genetic alterations and their clinical implications in DLBCL. Nat Rev Clin Oncol. 2019;16(10):634-52.
45. Reddy A, Zhang J, Davis NS, Moffitt AB, Love CL, Waldrop A, et al. Genetic and Functional Drivers of Diffuse Large B Cell Lymphoma. Cell. 2017;171(2):481-94 e15.
46. Lohr JG, Stojanov P, Lawrence MS, Auclair D, Chapuy B, Sougnez C, et al. Discovery and prioritization of somatic mutations in diffuse large B-cell lymphoma (DLBCL) by whole-exome sequencing. Proc Natl Acad Sci U S A. 2012;109(10):3879-84.
47. Morin RD, Mendez-Lago M, Mungall AJ, Goya R, Mungall KL, Corbett RD, et al. Frequent mutation of histone-modifying genes in non-Hodgkin lymphoma. Nature. 2011;476(7360):298-303.
48. Zhang J, Grubor V, Love CL, Banerjee A, Richards KL, Mieczkowski PA, et al. Genetic heterogeneity of diffuse large B-cell lymphoma. Proc Natl Acad Sci U S A. 2013;110(4):1398-403.
49. Schmitz R, Wright GW, Huang DW, Johnson CA, Phelan JD, Wang JQ, et al. Genetics and Pathogenesis of Diffuse Large B-Cell Lymphoma. N Engl J Med. 2018;378(15):1396-407.
50. Wright GW, Huang DW, Phelan JD, Coulibaly ZA, Roulland S, Young RM, et al. A Probabilistic Classification Tool for Genetic Subtypes of Diffuse Large B Cell Lymphoma with Therapeutic Implications. Cancer Cell. 2020;37(4):551-68 e14.
51. Lacy SE, Barrans SL, Beer PA, Painter D, Smith AG, Roman E, et al. Targeted sequencing in DLBCL, molecular subtypes, and outcomes: a Haematological Malignancy Research Network report. Blood. 2020;135(20):1759-71.
52. Rajkumar SV. Multiple myeloma: 2022 update on diagnosis, risk stratification, and management. Am J Hematol. 2022;97(8):1086-107.
53. Hideshima T, Mitsiades C, Tonon G, Richardson PG, Anderson KC. Understanding multiple myeloma pathogenesis in the bone marrow to identify new therapeutic targets. Nat Rev Cancer. 2007;7(8):585-98.
54. Kumar SK, Rajkumar V, Kyle RA, van Duin M, Sonneveld P, Mateos MV, et al. Multiple myeloma. Nat Rev Dis Primers. 2017;3:17046.
55. Kyle RA, Remstein ED, Therneau TM, Dispenzieri A, Kurtin PJ, Hodnefield JM, et al. Clinical course and prognosis of smoldering (asymptomatic) multiple myeloma. N Engl J Med. 2007;356(25):2582-90.
56. Bergsagel PL, Kuehl WM. Chromosome translocations in multiple myeloma. Oncogene. 2001;20(40):5611-22.
57. Lohr JG, Stojanov P, Carter SL, Cruz-Gordillo P, Lawrence MS, Auclair D, et al. Widespread genetic heterogeneity in multiple myeloma: implications for targeted therapy. Cancer Cell. 2014;25(1):91-101.
58. Walker BA, Wardell CP, Melchor L, Hulkki S, Potter NE, Johnson DC, et al. Intraclonal heterogeneity and distinct molecular mechanisms characterize the development of t(4;14) and t(11;14) myeloma. Blood. 2012;120(5):1077-86.
59. Akhmetzyanova I, McCarron MJ, Parekh S, Chesi M, Bergsagel PL, Fooksman DR. Dynamic CD138 surface expression regulates switch between myeloma growth and dissemination. Leukemia. 2020;34(1):245-56.

60. Durie BGM, Hoering A, Abidi MH, Rajkumar SV, Epstein J, Kahanic SP, et al. Bortezomib with lenalidomide and dexamethasone versus lenalidomide and dexamethasone alone in patients with newly diagnosed myeloma without intent for immediate autologous stem-cell transplant (SWOG S0777): a randomised, open-label, phase 3 trial. Lancet. 2017;389(10068):519-27.
61. Facon T, Kumar S, Plesner T, Orlowski RZ, Moreau P, Bahlis N, et al. Daratumumab plus Lenalidomide and Dexamethasone for Untreated Myeloma. N Engl J Med. 2019;380(22):2104-15.
62. Gay F, Palumbo A. Management of disease- and treatment-related complications in patients with multiple myeloma. Med Oncol. 2010;27 Suppl 1:S43-52.
63. Manier S, Salem KZ, Park J, Landau DA, Getz G, Ghobrial IM. Genomic complexity of multiple myeloma and its clinical implications. Nat Rev Clin Oncol. 2017;14(2):100-13.
64. Bergsagel PL, Kuehl WM, Zhan F, Sawyer J, Barlogie B, Shaughnessy J, Jr. Cyclin D dysregulation: an early and unifying pathogenic event in multiple myeloma. Blood. 2005;106(1):296-303.
65. Chapman MA, Lawrence MS, Keats JJ, Cibulskis K, Sougnez C, Schinzel AC, et al. Initial genome sequencing and analysis of multiple myeloma. Nature. 2011;471(7339):467-72.
66. Bolli N, Avet-Loiseau H, Wedge DC, Van Loo P, Alexandrov LB, Martincorena I, et al. Heterogeneity of genomic evolution and mutational profiles in multiple myeloma. Nat Commun. 2014;5:2997.
67. Walker BA, Boyle EM, Wardell CP, Murison A, Begum DB, Dahir NM, et al. Mutational Spectrum, Copy Number Changes, and Outcome: Results of a Sequencing Study of Patients With Newly Diagnosed Myeloma. J Clin Oncol. 2015;33(33):3911-20.
68. Bolli N, Biancon G, Moarii M, Gimondi S, Li Y, de Philippis C, et al. Analysis of the genomic landscape of multiple myeloma highlights novel prognostic markers and disease subgroups. Leukemia. 2018;32(12):2604-16.
69. Bustoros M, Sklavenitis-Pistofidis R, Park J, Redd R, Zhitomirsky B, Dunford AJ, et al. Genomic Profiling of Smoldering Multiple Myeloma Identifies Patients at a High Risk of Disease Progression. J Clin Oncol. 2020;38(21):2380-9.
70. Oben B, Froyen G, Maclachlan KH, Leongamornlert D, Abascal F, Zheng-Lin B, et al. Whole-genome sequencing reveals progressive versus stable myeloma precursor conditions as two distinct entities. Nat Commun. 2021;12(1):1861.
71. Boiarsky R, Haradhvala NJ, Alberge JB, Sklavenitis-Pistofidis R, Mouhieddine TH, Zavidij O, et al. Single cell characterization of myeloma and its precursor conditions reveals transcriptional signatures of early tumorigenesis. Nat Commun. 2022;13(1):7040.
72. Manolov G, Manolova Y. Marker band in one chromosome 14 from Burkitt lymphomas. Nature. 1972;237(5349):33-4.
73. Adams JM, Harris AW, Pinkert CA, Corcoran LM, Alexander WS, Cory S, et al. The c-myc oncogene driven by immunoglobulin enhancers induces lymphoid malignancy in transgenic mice. Nature. 1985;318(6046):533-8.
74. Hann SR, King MW, Bentley DL, Anderson CW, Eisenman RN. A non-AUG translational initiation in c-myc exon 1 generates an N-terminally distinct protein whose synthesis is disrupted in Burkitt's lymphomas. Cell. 1988;52(2):185-95.
75. Lopez C, Kleinheinz K, Aukema SM, Rohde M, Bernhart SH, Hubschmann D, et al. Genomic and transcriptomic changes complement each other in the pathogenesis of sporadic Burkitt lymphoma. Nat Commun. 2019;10(1):1459.
76. Perry AM, Crockett D, Dave BJ, Althof P, Winkler L, Smith LM, et al. B-cell lymphoma, unclassifiable, with features intermediate between diffuse large B-cell lymphoma and burkitt lymphoma: study of 39 cases. Br J Haematol. 2013;162(1):40-9.
77. Bertrand P, Bastard C, Maingonnat C, Jardin F, Maisonneuve C, Courel MN, et al. Mapping of MYC breakpoints in 8q24 rearrangements involving non-immunoglobulin partners in B-cell lymphomas. Leukemia. 2007;21(3):515-23.

78. Chong LC, Ben-Neriah S, Slack GW, Freeman C, Ennishi D, Mottok A, et al. High-resolution architecture and partner genes of MYC rearrangements in lymphoma with DLBCL morphology. Blood Adv. 2018;2(20):2755-65.
79. Rosenwald A, Bens S, Advani R, Barrans S, Copie-Bergman C, Elsensohn MH, et al. Prognostic Significance of MYC Rearrangement and Translocation Partner in Diffuse Large B-Cell Lymphoma: A Study by the Lunenburg Lymphoma Biomarker Consortium. J Clin Oncol. 2019;37(35):3359-68.
80. Cucco F, Barrans S, Sha C, Clipson A, Crouch S, Dobson R, et al. Distinct genetic changes reveal evolutionary history and heterogeneous molecular grade of DLBCL with MYC/BCL2 double-hit. Leukemia. 2020;34(5):1329-41.
81. Pasqualucci L, Dalla-Favera R. Genetics of diffuse large B-cell lymphoma. Blood. 2018;131(21):2307-19.
82. Scott DW, King RL, Staiger AM, Ben-Neriah S, Jiang A, Horn H, et al. High-grade B-cell lymphoma with MYC and BCL2 and/or BCL6 rearrangements with diffuse large B-cell lymphoma morphology. Blood. 2018;131(18):2060-4.
83. Swerdlow SH, Campo E, Pileri SA, Harris NL, Stein H, Siebert R, et al. The 2016 revision of the World Health Organization classification of lymphoid neoplasms. Blood. 2016;127(20):2375-90.
84. Campo E, Jaffe ES, Cook JR, Quintanilla-Martinez L, Swerdlow SH, Anderson KC, et al. The International Consensus Classification of Mature Lymphoid Neoplasms: a report from the Clinical Advisory Committee. Blood. 2022;140(11):1229-53.
85. Roschewski M, Phelan JD, Wilson WH. Molecular Classification and Treatment of Diffuse Large B-Cell Lymphoma and Primary Mediastinal B-Cell Lymphoma. Cancer J. 2020;26(3):195-205.
86. Hu S, Xu-Monette ZY, Tzankov A, Green T, Wu L, Balasubramanyam A, et al. MYC/BCL2 protein coexpression contributes to the inferior survival of activated B-cell subtype of diffuse large B-cell lymphoma and demonstrates high-risk gene expression signatures: a report from The International DLBCL Rituximab-CHOP Consortium Program. Blood. 2013;121(20):4021-31; quiz 4250.
87. Barwick BG, Gupta VA, Vertino PM, Boise LH. Cell of Origin and Genetic Alterations in the Pathogenesis of Multiple Myeloma. Front Immunol. 2019;10:1121.
88. Avet-Loiseau H, Gerson F, Magrangeas F, Minvielle S, Harousseau JL, Bataille R, et al. Rearrangements of the c-myc oncogene are present in 15% of primary human multiple myeloma tumors. Blood. 2001;98(10):3082-6.
89. Chesi M, Robbiani DF, Sebag M, Chng WJ, Affer M, Tiedemann R, et al. AID-dependent activation of a MYC transgene induces multiple myeloma in a conditional mouse model of post-germinal center malignancies. Cancer Cell. 2008;13(2):167-80.
90. Jovanovic KK, Roche-Lestienne C, Ghobrial IM, Facon T, Quesnel B, Manier S. Targeting MYC in multiple myeloma. Leukemia. 2018;32(6):1295-306.
91. Mitchell JS, Li N, Weinhold N, Forsti A, Ali M, van Duin M, et al. Genome-wide association study identifies multiple susceptibility loci for multiple myeloma. Nat Commun. 2016;7:12050.
92. Shaffer AL, Emre NC, Lamy L, Ngo VN, Wright G, Xiao W, et al. IRF4 addiction in multiple myeloma. Nature. 2008;454(7201):226-31.
93. Valera A, Balague O, Colomo L, Martinez A, Delabie J, Taddesse-Heath L, et al. IG/MYC rearrangements are the main cytogenetic alteration in plasmablastic lymphomas. Am J Surg Pathol. 2010;34(11):1686-94.
94. De Silva NS, Klein U. Dynamics of B cells in germinal centres. Nat Rev Immunol. 2015;15(3):137-48.
95. Ise W, Kurosaki T. Plasma cell differentiation during the germinal center reaction. Immunol Rev. 2019;288(1):64-74.
96. Nutt SL, Hodgkin PD, Tarlinton DM, Corcoran LM. The generation of antibody-secreting plasma cells. Nat Rev Immunol. 2015;15(3):160-71.

97. Kometani K, Nakagawa R, Shinnakasu R, Kaji T, Rybouchkin A, Moriyama S, et al. Repression of the transcription factor Bach2 contributes to predisposition of IgG1 memory B cells toward plasma cell differentiation. Immunity. 2013;39(1):136-47.
98. Cooper MD. The early history of B cells. Nat Rev Immunol. 2015;15(3):191-7.
99. Nemazee D. Mechanisms of central tolerance for B cells. Nat Rev Immunol. 2017;17(5):281-94.
100. Pieper K, Grimbacher B, Eibel H. B-cell biology and development. J Allergy Clin Immunol. 2013;131(4):959-71.
101. van Zelm MC, Szczepanski T, van der Burg M, van Dongen JJ. Replication history of B lymphocytes reveals homeostatic proliferation and extensive antigen-induced B cell expansion. J Exp Med. 2007;204(3):645-55.
102. Murphy KW, C. Janeway's Immunobiology. 9th ed. Garland Science 2017.
103. Schatz DG, Oettinger MA, Baltimore D. The V(D)J recombination activating gene, RAG-1. Cell. 1989;59(6):1035-48.
104. Repasky JA, Corbett E, Boboila C, Schatz DG. Mutational analysis of terminal deoxynucleotidyltransferase-mediated N-nucleotide addition in V(D)J recombination. J Immunol. 2004;172(9):5478-88.
105. Meffre E, Casellas R, Nussenzweig MC. Antibody regulation of B cell development. Nat Immunol. 2000;1(5):379-85.
106. Grawunder U, Leu TM, Schatz DG, Werner A, Rolink AG, Melchers F, et al. Down-regulation of RAG1 and RAG2 gene expression in preB cells after functional immunoglobulin heavy chain rearrangement. Immunity. 1995;3(5):601-8.
107. Matthias P, Rolink AG. Transcriptional networks in developing and mature B cells. Nat Rev Immunol. 2005;5(6):497-508.
108. Radbruch A, Muehlinghaus G, Luger EO, Inamine A, Smith KG, Dorner T, et al. Competence and competition: the challenge of becoming a long-lived plasma cell. Nat Rev Immunol. 2006;6(10):741-50.
109. Obukhanych TV, Nussenzweig MC. T-independent type II immune responses generate memory B cells. J Exp Med. 2006;203(2):305-10.
110. Liao W, Hua Z, Liu C, Lin L, Chen R, Hou B. Characterization of T-Dependent and T-Independent B Cell Responses to a Virus-like Particle. J Immunol. 2017;198(10):3846-56.
111. Vinuesa CG, Chang PP. Innate B cell helpers reveal novel types of antibody responses. Nat Immunol. 2013;14(2):119-26.
112. DeFranco AL, Rookhuizen DC, Hou B. Contribution of Toll-like receptor signaling to germinal center antibody responses. Immunol Rev. 2012;247(1):64-72.
113. Rawlings DJ, Schwartz MA, Jackson SW, Meyer-Bahlburg A. Integration of B cell responses through Toll-like receptors and antigen receptors. Nat Rev Immunol. 2012;12(4):282-94.
114. Koch G, Benner R. Differential requirement for B-memory and T-memory cells in adoptive antibody formation in mouse bone marrow. Immunology. 1982;45(4):697-704.
115. Laidlaw BJ, Cyster JG. Transcriptional regulation of memory B cell differentiation. Nat Rev Immunol. 2021;21(4):209-20.
116. Young C, Brink R. The unique biology of germinal center B cells. Immunity. 2021;54(8):1652-64.
117. Akkaya M, Kwak K, Pierce SK. B cell memory: building two walls of protection against pathogens. Nat Rev Immunol. 2020;20(4):229-38.
118. Garside P, Ingulli E, Merica RR, Johnson JG, Noelle RJ, Jenkins MK. Visualization of specific B and T lymphocyte interactions in the lymph node. Science. 1998;281(5373):96-9.
119. O'Connor BP, Vogel LA, Zhang W, Loo W, Shnider D, Lind EF, et al. Imprinting the fate of antigen-reactive B cells through the affinity of the B cell receptor. J Immunol. 2006;177(11):7723-32.

120. Paus D, Phan TG, Chan TD, Gardam S, Basten A, Brink R. Antigen recognition strength regulates the choice between extrafollicular plasma cell and germinal center B cell differentiation. J Exp Med. 2006;203(4):1081-91.
121. Klein U, Dalla-Favera R. Germinal centres: role in B-cell physiology and malignancy. Nat Rev Immunol. 2008;8(1):22-33.
122. MacLennan IC, Toellner KM, Cunningham AF, Serre K, Sze DM, Zuniga E, et al. Extrafollicular antibody responses. Immunol Rev. 2003;194:8-18.
123. Taylor JJ, Pape KA, Jenkins MK. A germinal center-independent pathway generates unswitched memory B cells early in the primary response. J Exp Med. 2012;209(3):597-606.
124. Dal Porto JM, Haberman AM, Kelsoe G, Shlomchik MJ. Very low affinity B cells form germinal centers, become memory B cells, and participate in secondary immune responses when higher affinity competition is reduced. J Exp Med. 2002;195(9):1215-21.
125. Schwickert TA, Victora GD, Fooksman DR, Kamphorst AO, Mugnier MR, Gitlin AD, et al. A dynamic T cell-limited checkpoint regulates affinity-dependent B cell entry into the germinal center. J Exp Med. 2011;208(6):1243-52.
126. Shih TA, Meffre E, Roederer M, Nussenzweig MC. Role of BCR affinity in T cell dependent antibody responses in vivo. Nat Immunol. 2002;3(6):570-5.
127. Petersone L, Wang CJ, Edner NM, Fabri A, Nikou SA, Hinze C, et al. IL-21 shapes germinal center polarization via light zone B cell selection and cyclin D3 upregulation. J Exp Med. 2023;220(10).
128. Dvorscek AR, McKenzie CI, Robinson MJ, Ding Z, Pitt C, O'Donnell K, et al. IL-21 has a critical role in establishing germinal centers by amplifying early B cell proliferation. EMBO Rep. 2022;23(9):e54677.
129. Hipp N, Symington H, Pastoret C, Caron G, Monvoisin C, Tarte K, et al. IL-2 imprints human naive B cell fate towards plasma cell through ERK/ELK1-mediated BACH2 repression. Nat Commun. 2017;8(1):1443.
130. Johnson-Leger C, Christenson JR, Holman M, Klaus GG. Evidence for a critical role for IL-2 in CD40-mediated activation of naive B cells by primary CD4 T cells. J Immunol. 1998;161(9):4618-26.
131. Moens L, Tangye SG. Cytokine-Mediated Regulation of Plasma Cell Generation: IL-21 Takes Center Stage. Front Immunol. 2014;5:65.
132. Kurosaki T, Kometani K, Ise W. Memory B cells. Nat Rev Immunol. 2015;15(3):149-59.
133. Basso K, Klein U, Niu H, Stolovitzky GA, Tu Y, Califano A, et al. Tracking CD40 signaling during germinal center development. Blood. 2004;104(13):4088-96.
134. Zhang Y, Tech L, George LA, Acs A, Durrett RE, Hess H, et al. Plasma cell output from germinal centers is regulated by signals from Tfh and stromal cells. J Exp Med. 2018;215(4):1227-43.
135. Nieuwenhuis P, Opstelten D. Functional anatomy of germinal centers. Am J Anat. 1984;170(3):421-35.
136. Allen CD, Okada T, Cyster JG. Germinal-center organization and cellular dynamics. Immunity. 2007;27(2):190-202.
137. MacLennan IC. Germinal centers. Annu Rev Immunol. 1994;12:117-39.
138. Victora GD, Dominguez-Sola D, Holmes AB, Deroubaix S, Dalla-Favera R, Nussenzweig MC. Identification of human germinal center light and dark zone cells and their relationship to human B-cell lymphomas. Blood. 2012;120(11):2240-8.
139. Victora GD, Schwickert TA, Fooksman DR, Kamphorst AO, Meyer-Hermann M, Dustin ML, et al. Germinal center dynamics revealed by multiphoton microscopy with a photoactivatable fluorescent reporter. Cell. 2010;143(4):592-605.
140. Shlomchik MJ, Luo W, Weisel F. Linking signaling and selection in the germinal center. Immunol Rev. 2019;288(1):49-63.
141. Gatto D, Brink R. The germinal center reaction. J Allergy Clin Immunol. 2010;126(5):898-907; quiz 908-8.

142. Calado DP, Sasaki Y, Godinho SA, Pellerin A, Kochert K, Sleckman BP, et al. The cell-cycle regulator c-Myc is essential for the formation and maintenance of germinal centers. Nat Immunol. 2012;13(11):1092-100.
143. Dominguez-Sola D, Victora GD, Ying CY, Phan RT, Saito M, Nussenzweig MC, et al. The proto-oncogene MYC is required for selection in the germinal center and cyclic reentry. Nat Immunol. 2012;13(11):1083-91.
144. Holmes AB, Corinaldesi C, Shen Q, Kumar R, Compagno N, Wang Z, et al. Single-cell analysis of germinal-center B cells informs on lymphoma cell of origin and outcome. J Exp Med. 2020;217(10).
145. Victora GD, Nussenzweig MC. Germinal Centers. Annu Rev Immunol. 2022;40:413-42.
146. McCarron MJ, Park PW, Fooksman DR. CD138 mediates selection of mature plasma cells by regulating their survival. Blood. 2017;129(20):2749-59.
147. Sanderson RD, Lalor P, Bernfield M. B lymphocytes express and lose syndecan at specific stages of differentiation. Cell Regul. 1989;1(1):27-35.
148. Dienz O, Rincon M. The effects of IL-6 on CD4 T cell responses. Clin Immunol. 2009;130(1):27-33.
149. Stephenson S, Care MA, Doody GM, Tooze RM. APRIL Drives a Coordinated but Diverse Response as a Foundation for Plasma Cell Longevity. J Immunol. 2022;209(5):926-37.
150. Nutt SL, Taubenheim N, Hasbold J, Corcoran LM, Hodgkin PD. The genetic network controlling plasma cell differentiation. Semin Immunol. 2011;23(5):341-9.
151. Chu VT, Berek C. The establishment of the plasma cell survival niche in the bone marrow. Immunol Rev. 2013;251(1):177-88.
152. Yoshida T, Mei H, Dorner T, Hiepe F, Radbruch A, Fillatreau S, et al. Memory B and memory plasma cells. Immunol Rev. 2010;237(1):117-39.
153. Nutt SL, Heavey B, Rolink AG, Busslinger M. Commitment to the B-lymphoid lineage depends on the transcription factor Pax5. Nature. 1999;401(6753):556-62.
154. Calfon M, Zeng H, Urano F, Till JH, Hubbard SR, Harding HP, et al. IRE1 couples endoplasmic reticulum load to secretory capacity by processing the XBP-1 mRNA. Nature. 2002;415(6867):92-6.
155. Reimold AM, Iwakoshi NN, Manis J, Vallabhajosyula P, Szomolanyi-Tsuda E, Gravallese EM, et al. Plasma cell differentiation requires the transcription factor XBP-1. Nature. 2001;412(6844):300-7.
156. Reimold AM, Ponath PD, Li YS, Hardy RR, David CS, Strominger JL, et al. Transcription factor B cell lineage-specific activator protein regulates the gene for human X-box binding protein 1. J Exp Med. 1996;183(2):393-401.
157. Basso K, Dalla-Favera R. Roles of BCL6 in normal and transformed germinal center B cells. Immunol Rev. 2012;247(1):172-83.
158. Le Gallou S, Caron G, Delaloy C, Rossille D, Tarte K, Fest T. IL-2 requirement for human plasma cell generation: coupling differentiation and proliferation by enhancing MAPK-ERK signaling. J Immunol. 2012;189(1):161-73.
159. Shaffer AL, Lin KI, Kuo TC, Yu X, Hurt EM, Rosenwald A, et al. Blimp-1 orchestrates plasma cell differentiation by extinguishing the mature B cell gene expression program. Immunity. 2002;17(1):51-62.
160. Ochiai K, Muto A, Tanaka H, Takahashi S, Igarashi K. Regulation of the plasma cell transcription factor Blimp-1 gene by Bach2 and Bcl6. Int Immunol. 2008;20(3):453-60.
161. Klein U, Casola S, Cattoretti G, Shen Q, Lia M, Mo T, et al. Transcription factor IRF4 controls plasma cell differentiation and class-switch recombination. Nat Immunol. 2006;7(7):773-82.
162. Ochiai K, Maienschein-Cline M, Simonetti G, Chen J, Rosenthal R, Brink R, et al. Transcriptional regulation of germinal center B and plasma cell fates by dynamical control of IRF4. Immunity. 2013;38(5):918-29.
163. Shapiro-Shelef M, Calame K. Regulation of plasma-cell development. Nat Rev Immunol. 2005;5(3):230-42.

164. Sciammas R, Shaffer AL, Schatz JH, Zhao H, Staudt LM, Singh H. Graded expression of interferon regulatory factor-4 coordinates isotype switching with plasma cell differentiation. Immunity. 2006;25(2):225-36.
165. Angelin-Duclos C, Cattoretti G, Lin KI, Calame K. Commitment of B lymphocytes to a plasma cell fate is associated with Blimp-1 expression in vivo. J Immunol. 2000;165(10):5462-71.
166. Lin KI, Angelin-Duclos C, Kuo TC, Calame K. Blimp-1-dependent repression of Pax-5 is required for differentiation of B cells to immunoglobulin M-secreting plasma cells. Mol Cell Biol. 2002;22(13):4771-80.
167. Klein U, Tu Y, Stolovitzky GA, Keller JL, Haddad J, Jr., Miljkovic V, et al. Transcriptional analysis of the B cell germinal center reaction. Proc Natl Acad Sci U S A. 2003;100(5):2639-44.
168. Basso K, Dalla-Favera R. BCL6: master regulator of the germinal center reaction and key oncogene in B cell lymphomagenesis. Adv Immunol. 2010;105:193-210.
169. Shaffer AL, Yu X, He Y, Boldrick J, Chan EP, Staudt LM. BCL-6 represses genes that function in lymphocyte differentiation, inflammation, and cell cycle control. Immunity. 2000;13(2):199-212.
170. Phan RT, Saito M, Basso K, Niu H, Dalla-Favera R. BCL6 interacts with the transcription factor Miz-1 to suppress the cyclin-dependent kinase inhibitor p21 and cell cycle arrest in germinal center B cells. Nat Immunol. 2005;6(10):1054-60.
171. Finkin S, Hartweger H, Oliveira TY, Kara EE, Nussenzweig MC. Protein Amounts of the MYC Transcription Factor Determine Germinal Center B Cell Division Capacity. Immunity. 2019;51(2):324-36 e5.
172. Hetz C, Zhang K, Kaufman RJ. Mechanisms, regulation and functions of the unfolded protein response. Nat Rev Mol Cell Biol. 2020;21(8):421-38.
173. Tellier J, Shi W, Minnich M, Liao Y, Crawford S, Smyth GK, et al. Blimp-1 controls plasma cell function through the regulation of immunoglobulin secretion and the unfolded protein response. Nat Immunol. 2016;17(3):323-30.
174. Kozutsumi Y, Segal M, Normington K, Gething MJ, Sambrook J. The presence of malfolded proteins in the endoplasmic reticulum signals the induction of glucose-regulated proteins. Nature. 1988;332(6163):462-4.
175. Shaffer AL, Shapiro-Shelef M, Iwakoshi NN, Lee AH, Qian SB, Zhao H, et al. XBP1, downstream of Blimp-1, expands the secretory apparatus and other organelles, and increases protein synthesis in plasma cell differentiation. Immunity. 2004;21(1):81-93.
176. Todd DJ, McHeyzer-Williams LJ, Kowal C, Lee AH, Volpe BT, Diamond B, et al. XBP1 governs late events in plasma cell differentiation and is not required for antigen-specific memory B cell development. J Exp Med. 2009;206(10):2151-9.
177. Lin KI, Tunyaplin C, Calame K. Transcriptional regulatory cascades controlling plasma cell differentiation. Immunol Rev. 2003;194:19-28.
178. Xie H, Tang CH, Song JH, Mancuso A, Del Valle JR, Cao J, et al. IRE1alpha RNase-dependent lipid homeostasis promotes survival in Myc-transformed cancers. J Clin Invest. 2018;128(4):1300-16.
179. Lee AH, Iwakoshi NN, Glimcher LH. XBP-1 regulates a subset of endoplasmic reticulum resident chaperone genes in the unfolded protein response. Mol Cell Biol. 2003;23(21):7448-59.
180. Zhao N, Cao J, Xu L, Tang Q, Dobrolecki LE, Lv X, et al. Pharmacological targeting of MYC-regulated IRE1/XBP1 pathway suppresses MYC-driven breast cancer. J Clin Invest. 2018;128(4):1283-99.
181. Sheng X, Nenseth HZ, Qu S, Kuzu OF, Frahnow T, Simon L, et al. IRE1alpha-XBP1s pathway promotes prostate cancer by activating c-MYC signaling. Nat Commun. 2019;10(1):323.
182. Kaloni D, Diepstraten ST, Strasser A, Kelly GL. BCL-2 protein family: attractive targets for cancer therapy. Apoptosis. 2023;28(1-2):20-38.
183. Carrington EM, Zhan Y, Brady JL, Zhang JG, Sutherland RM, Anstee NS, et al. Anti-apoptotic proteins BCL-2, MCL-1 and A1 summate collectively to maintain survival of immune cell populations both in vitro and in vivo. Cell Death Differ. 2017;24(5):878-88.

184. Bhattacharya S, Ray RM, Johnson LR. STAT3-mediated transcription of Bcl-2, Mcl-1 and c-IAP2 prevents apoptosis in polyamine-depleted cells. Biochem J. 2005;392(Pt 2):335-44.
185. Strasser A, Harris AW, Huang DC, Krammer PH, Cory S. Bcl-2 and Fas/APO-1 regulate distinct pathways to lymphocyte apoptosis. EMBO J. 1995;14(24):6136-47.
186. Kale J, Osterlund EJ, Andrews DW. BCL-2 family proteins: changing partners in the dance towards death. Cell Death Differ. 2018;25(1):65-80.
187. Petros AM, Olejniczak ET, Fesik SW. Structural biology of the Bcl-2 family of proteins. Biochim Biophys Acta. 2004;1644(2-3):83-94.
188. Shamas-Din A, Brahmbhatt H, Leber B, Andrews DW. BH3-only proteins: Orchestrators of apoptosis. Biochim Biophys Acta. 2011;1813(4):508-20.
189. Kapoor I, Bodo J, Hill BT, Hsi ED, Almasan A. Targeting BCL-2 in B-cell malignancies and overcoming therapeutic resistance. Cell Death Dis. 2020;11(11):941.
190. Inoue T, Shinnakasu R, Kawai C, Ise W, Kawakami E, Sax N, et al. Exit from germinal center to become quiescent memory B cells depends on metabolic reprograming and provision of a survival signal. J Exp Med. 2021;218(1).
191. Peperzak V, Slinger E, Ter Burg J, Eldering E. Functional disparities among BCL-2 members in tonsillar and leukemic B-cell subsets assessed by BH3-mimetic profiling. Cell Death Differ. 2017;24(1):111-9.
192. Slomp A, Peperzak V. Role and Regulation of Pro-survival BCL-2 Proteins in Multiple Myeloma. Front Oncol. 2018;8:533.
193. Liu YJ, Mason DY, Johnson GD, Abbot S, Gregory CD, Hardie DL, et al. Germinal center cells express bcl-2 protein after activation by signals which prevent their entry into apoptosis. Eur J Immunol. 1991;21(8):1905-10.
194. Shen Y, Iqbal J, Huang JZ, Zhou G, Chan WC. BCL2 protein expression parallels its mRNA level in normal and malignant B cells. Blood. 2004;104(9):2936-9.
195. Ladanyi M, Wang S, Niesvizky R, Feiner H, Michaeli J. Proto-oncogene analysis in multiple myeloma. Am J Pathol. 1992;141(4):949-53.
196. Galteland E, Sivertsen EA, Svendsrud DH, Smedshammer L, Kresse SH, Meza-Zepeda LA, et al. Translocation t(14;18) and gain of chromosome 18/BCL2: effects on BCL2 expression and apoptosis in B-cell non-Hodgkin's lymphomas. Leukemia. 2005;19(12):2313-23.
197. Puertas B, Gonzalez-Calle V, Sobejano-Fuertes E, Escalante F, Rey-Bua B, Padilla I, et al. Multiple myeloma with t(11;14): impact of novel agents on outcome. Blood Cancer J. 2023;13(1):40.
198. Das SK, Lewis BA, Levens D. MYC: a complex problem. Trends Cell Biol. 2023;33(3):235-46.
199. Llombart V, Mansour MR. Therapeutic targeting of "undruggable" MYC. EBioMedicine. 2022;75:103756.
200. Madden SK, de Araujo AD, Gerhardt M, Fairlie DP, Mason JM. Taking the Myc out of cancer: toward therapeutic strategies to directly inhibit c-Myc. Mol Cancer. 2021;20(1):3.
201. Liu R, Shi P, Wang Z, Yuan C, Cui H. Molecular Mechanisms of MYCN Dysregulation in Cancers. Front Oncol. 2020;10:625332.
202. Huang M, Weiss WA. Neuroblastoma and MYCN. Cold Spring Harb Perspect Med. 2013;3(10):a014415.
203. Meyer N, Penn LZ. Reflecting on 25 years with MYC. Nat Rev Cancer. 2008;8(12):976-90.
204. Tu WB, Helander S, Pilstal R, Hickman KA, Lourenco C, Jurisica I, et al. Myc and its interactors take shape. Biochim Biophys Acta. 2015;1849(5):469-83.
205. Dhanasekaran R, Deutzmann A, Mahauad-Fernandez WD, Hansen AS, Gouw AM, Felsher DW. The MYC oncogene - the grand orchestrator of cancer growth and immune evasion. Nat Rev Clin Oncol. 2022;19(1):23-36.

206. Wang C, Zhang J, Yin J, Gan Y, Xu S, Gu Y, et al. Alternative approaches to target Myc for cancer treatment. Signal Transduct Target Ther. 2021;6(1):117.
207. Qiu X, Boufaied N, Hallal T, Feit A, de Polo A, Luoma AM, et al. MYC drives aggressive prostate cancer by disrupting transcriptional pause release at androgen receptor targets. Nat Commun. 2022;13(1):2559.
208. Thomas LR, Wang Q, Grieb BC, Phan J, Foshage AM, Sun Q, et al. Interaction with WDR5 promotes target gene recognition and tumorigenesis by MYC. Mol Cell. 2015;58(3):440-52.
209. Dong Y, Tu R, Liu H, Qing G. Regulation of cancer cell metabolism: oncogenic MYC in the driver's seat. Signal Transduct Target Ther. 2020;5(1):124.
210. Brough DE, Hofmann TJ, Ellwood KB, Townley RA, Cole MD. An essential domain of the c-myc protein interacts with a nuclear factor that is also required for E1A-mediated transformation. Mol Cell Biol. 1995;15(3):1536-44.
211. Herbst A, Hemann MT, Tworkowski KA, Salghetti SE, Lowe SW, Tansey WP. A conserved element in Myc that negatively regulates its proapoptotic activity. EMBO Rep. 2005;6(2):177-83.
212. Stone J, de Lange T, Ramsay G, Jakobovits E, Bishop JM, Varmus H, et al. Definition of regions in human c-myc that are involved in transformation and nuclear localization. Mol Cell Biol. 1987;7(5):1697-709.
213. Hinds JW, Feris EJ, Wilkins OM, Deary LT, Wang X, Cole MD. S146L in MYC is a context-dependent activating substitution in cancer development. PLoS One. 2022;17(8):e0272771.
214. Lourenco C, Resetca D, Redel C, Lin P, MacDonald AS, Ciaccio R, et al. MYC protein interactors in gene transcription and cancer. Nat Rev Cancer. 2021;21(9):579-91.
215. Blackwood EM, Eisenman RN. Max: a helix-loop-helix zipper protein that forms a sequence-specific DNA-binding complex with Myc. Science. 1991;251(4998):1211-7.
216. Blackwell TK, Huang J, Ma A, Kretzner L, Alt FW, Eisenman RN, et al. Binding of myc proteins to canonical and noncanonical DNA sequences. Mol Cell Biol. 1993;13(9):5216-24.
217. Amati B, Dalton S, Brooks MW, Littlewood TD, Evan GI, Land H. Transcriptional activation by the human c-Myc oncoprotein in yeast requires interaction with Max. Nature. 1992;359(6394):423-6.
218. Mao DY, Watson JD, Yan PS, Barsyte-Lovejoy D, Khosravi F, Wong WW, et al. Analysis of Myc bound loci identified by CpG island arrays shows that Max is essential for Myc-dependent repression. Curr Biol. 2003;13(10):882-6.
219. Wu S, Cetinkaya C, Munoz-Alonso MJ, von der Lehr N, Bahram F, Beuger V, et al. Myc represses differentiation-induced p21CIP1 expression via Miz-1-dependent interaction with the p21 core promoter. Oncogene. 2003;22(3):351-60.
220. Xia Y, Liu Y, Yang C, Simeone DM, Sun TT, DeGraff DJ, et al. Dominant role of CDKN2B/p15INK4B of 9p21.3 tumor suppressor hub in inhibition of cell-cycle and glycolysis. Nat Commun. 2021;12(1):2047.
221. Kress TR, Sabo A, Amati B. MYC: connecting selective transcriptional control to global RNA production. Nat Rev Cancer. 2015;15(10):593-607.
222. Eberhardy SR, D'Cunha CA, Farnham PJ. Direct examination of histone acetylation on Myc target genes using chromatin immunoprecipitation. J Biol Chem. 2000;275(43):33798-805.
223. Frank SR, Schroeder M, Fernandez P, Taubert S, Amati B. Binding of c-Myc to chromatin mediates mitogen-induced acetylation of histone H4 and gene activation. Genes Dev. 2001;15(16):2069-82.
224. Stine ZE, Walton ZE, Altman BJ, Hsieh AL, Dang CV. MYC, Metabolism, and Cancer. Cancer Discov. 2015;5(10):1024-39.
225. Rahl PB, Lin CY, Seila AC, Flynn RA, McCuine S, Burge CB, et al. c-Myc regulates transcriptional pause release. Cell. 2010;141(3):432-45.
226. Baluapuri A, Wolf E, Eilers M. Target gene-independent functions of MYC oncoproteins. Nat Rev Mol Cell Biol. 2020;21(5):255-67.

227. Sabo A, Kress TR, Pelizzola M, de Pretis S, Gorski MM, Tesi A, et al. Selective transcriptional regulation by Myc in cellular growth control and lymphomagenesis. Nature. 2014;511(7510):488-92.
228. Walz S, Lorenzin F, Morton J, Wiese KE, von Eyss B, Herold S, et al. Activation and repression by oncogenic MYC shape tumour-specific gene expression profiles. Nature. 2014;511(7510):483-7.
229. Lin CY, Loven J, Rahl PB, Paranal RM, Burge CB, Bradner JE, et al. Transcriptional amplification in tumor cells with elevated c-Myc. Cell. 2012;151(1):56-67.
230. Nie Z, Hu G, Wei G, Cui K, Yamane A, Resch W, et al. c-Myc is a universal amplifier of expressed genes in lymphocytes and embryonic stem cells. Cell. 2012;151(1):68-79.
231. Hann SR, Dixit M, Sears RC, Sealy L. The alternatively initiated c-Myc proteins differentially regulate transcription through a noncanonical DNA-binding site. Genes Dev. 1994;8(20):2441-52.
232. Amati B, Brooks MW, Levy N, Littlewood TD, Evan GI, Land H. Oncogenic activity of the c-Myc protein requires dimerization with Max. Cell. 1993;72(2):233-45.
233. Dang CV, McGuire M, Buckmire M, Lee WM. Involvement of the 'leucine zipper' region in the oligomerization and transforming activity of human c-myc protein. Nature. 1989;337(6208):664-6.
234. Oster SK, Mao DY, Kennedy J, Penn LZ. Functional analysis of the N-terminal domain of the Myc oncoprotein. Oncogene. 2003;22(13):1998-2010.
235. Akifuji C, Iwasaki M, Kawahara Y, Sakurai C, Cheng YS, Imai T, et al. MYCL promotes iPSC-like colony formation via MYC Box 0 and 2 domains. Sci Rep. 2021;11(1):24254.
236. Lutterbach B, Hann SR. Hierarchical phosphorylation at N-terminal transformation-sensitive sites in c-Myc protein is regulated by mitogens and in mitosis. Mol Cell Biol. 1994;14(8):5510-22.
237. Salghetti SE, Muratani M, Wijnen H, Futcher B, Tansey WP. Functional overlap of sequences that activate transcription and signal ubiquitin-mediated proteolysis. Proc Natl Acad Sci U S A. 2000;97(7):3118-23.
238. Sears R, Leone G, DeGregori J, Nevins JR. Ras enhances Myc protein stability. Mol Cell. 1999;3(2):169-79.
239. Yada M, Hatakeyama S, Kamura T, Nishiyama M, Tsunematsu R, Imaki H, et al. Phosphorylation-dependent degradation of c-Myc is mediated by the F-box protein Fbw7. EMBO J. 2004;23(10):2116-25.
240. Kalkat M, Resetca D, Lourenco C, Chan PK, Wei Y, Shiah YJ, et al. MYC Protein Interactome Profiling Reveals Functionally Distinct Regions that Cooperate to Drive Tumorigenesis. Mol Cell. 2018;72(5):836-48 e7.
241. Agrawal P, Yu K, Salomon AR, Sedivy JM. Proteomic profiling of Myc-associated proteins. Cell Cycle. 2010;9(24):4908-21.
242. Koch HB, Zhang R, Verdoodt B, Bailey A, Zhang CD, Yates JR 3rd, et al. Large-scale identification of c-MYC-associated proteins using a combined TAP/MudPIT approach. Cell Cycle. 2007;6(2):205-17.
243. Ullius A, Luscher-Firzlaff J, Costa IG, Walsemann G, Forst AH, Gusmao EG, et al. The interaction of MYC with the trithorax protein ASH2L promotes gene transcription by regulating H3K27 modification. Nucleic Acids Res. 2014;42(11):6901-20.
244. Sabo A, Amati B. Genome recognition by MYC. Cold Spring Harb Perspect Med. 2014;4(2).
245. Pineda-Lucena A, Ho CS, Mao DY, Sheng Y, Laister RC, Muhandiram R, et al. A structure-based model of the c-Myc/Bin1 protein interaction shows alternative splicing of Bin1 and c-Myc phosphorylation are key binding determinants. J Mol Biol. 2005;351(1):182-94.
246. Wei Y, Resetca D, Li Z, Johansson-Akhe I, Ahlner A, Helander S, et al. Multiple direct interactions of TBP with the MYC oncoprotein. Nat Struct Mol Biol. 2019;26(11):1035-43.
247. Wei Y, Redel C, Ahlner A, Lemak A, Johansson-Akhe I, Houliston S, et al. The MYC oncoprotein directly interacts with its chromatin cofactor PNUTS to recruit PP1 phosphatase. Nucleic Acids Res. 2022;50(6):3505-22.
248. McMahon SB, Van Buskirk HA, Dugan KA, Copeland TD, Cole MD. The novel ATM-related protein TRRAP is an essential cofactor for the c-Myc and E2F oncoproteins. Cell. 1998;94(3):363-74.

249. Doyon Y, Selleck W, Lane WS, Tan S, Cote J. Structural and functional conservation of the NuA4 histone acetyltransferase complex from yeast to humans. Mol Cell Biol. 2004;24(5):1884-96.
250. McMahon SB, Wood MA, Cole MD. The essential cofactor TRRAP recruits the histone acetyltransferase hGCN5 to c-Myc. Mol Cell Biol. 2000;20(2):556-62.
251. Wood MA, McMahon SB, Cole MD. An ATPase/helicase complex is an essential cofactor for oncogenic transformation by c-Myc. Mol Cell. 2000;5(2):321-30.
252. D'Avola A, Kluckova K, Finch AJ, Riches JC. Spotlight on New Therapeutic Opportunities for MYC-Driven Cancers. Onco Targets Ther. 2023;16:371-83.
253. Zhang N, Ichikawa W, Faiola F, Lo SY, Liu X, Martinez E. MYC interacts with the human STAGA coactivator complex via multivalent contacts with the GCN5 and TRRAP subunits. Biochim Biophys Acta. 2014;1839(5):395-405.
254. Dai MS, Arnold H, Sun XX, Sears R, Lu H. Inhibition of c-Myc activity by ribosomal protein L11. EMBO J. 2007;26(14):3332-45.
255. Kim JW, Zeller KI, Wang Y, Jegga AG, Aronow BJ, O'Donnell KA, et al. Evaluation of myc E-box phylogenetic footprints in glycolytic genes by chromatin immunoprecipitation assays. Mol Cell Biol. 2004;24(13):5923-36.
256. Vander Heiden MG, Cantley LC, Thompson CB. Understanding the Warburg effect: the metabolic requirements of cell proliferation. Science. 2009;324(5930):1029-33.
257. Bae S, Oh B, Tsai J, Park PSU, Greenblatt MB, Giannopoulou EG, et al. The crosstalk between MYC and mTORC1 during osteoclastogenesis. Front Cell Dev Biol. 2022;10:920683.
258. Betz C, Hall MN. Where is mTOR and what is it doing there? J Cell Biol. 2013;203(4):563-74.
259. Wullschleger S, Loewith R, Hall MN. TOR signaling in growth and metabolism. Cell. 2006;124(3):471-84.
260. Csibi A, Lee G, Yoon SO, Tong H, Ilter D, Elia I, et al. The mTORC1/S6K1 pathway regulates glutamine metabolism through the eIF4B-dependent control of c-Myc translation. Curr Biol. 2014;24(19):2274-80.
261. Hsieh AL, Walton ZE, Altman BJ, Stine ZE, Dang CV. MYC and metabolism on the path to cancer. Semin Cell Dev Biol. 2015;43:11-21.
262. Ramsay G, Evan GI, Bishop JM. The protein encoded by the human proto-oncogene c-myc. Proc Natl Acad Sci U S A. 1984;81(24):7742-6.
263. Farrell AS, Sears RC. MYC degradation. Cold Spring Harb Perspect Med. 2014;4(3).
264. Lama D, Vosselman T, Sahin C, Liano-Pons J, Cerrato CP, Nilsson L, et al. A druggable conformational switch in the c-MYC transactivation domain. Nat Commun. 2024;15(1):1865.
265. Minella AC, Clurman BE. Mechanisms of tumor suppression by the SCF(Fbw7). Cell Cycle. 2005;4(10):1356-9.
266. Boi D, Rubini E, Breccia S, Guarguaglini G, Paiardini A. When Just One Phosphate Is One Too Many: The Multifaceted Interplay between Myc and Kinases. Int J Mol Sci. 2023;24(5).
267. Popov N, Schulein C, Jaenicke LA, Eilers M. Ubiquitylation of the amino terminus of Myc by SCF(beta-TrCP) antagonizes SCF(Fbw7)-mediated turnover. Nat Cell Biol. 2010;12(10):973-81.
268. Cao Z, Fan-Minogue H, Bellovin DI, Yevtodiyenko A, Arzeno J, Yang Q, et al. MYC phosphorylation, activation, and tumorigenic potential in hepatocellular carcinoma are regulated by HMG-CoA reductase. Cancer Res. 2011;71(6):2286-97.
269. Raman D, Chong SJF, Iskandar K, Hirpara JL, Pervaiz S. Peroxynitrite promotes serine-62 phosphorylation-dependent stabilization of the oncoprotein c-Myc. Redox Biol. 2020;34:101587.
270. Welcker M, Orian A, Jin J, Grim JE, Harper JW, Eisenman RN, et al. The Fbw7 tumor suppressor regulates glycogen synthase kinase 3 phosphorylation-dependent c-Myc protein degradation. Proc Natl Acad Sci U S A. 2004;101(24):9085-90.
271. Bahram F, von der Lehr N, Cetinkaya C, Larsson LG. c-Myc hot spot mutations in lymphomas result in inefficient ubiquitination and decreased proteasome-mediated turnover. Blood. 2000;95(6):2104-10.

272. Mahani A, Arvidsson G, Sadeghi L, Grandien A, Wright APH. Differential Transcriptional Reprogramming by Wild Type and Lymphoma-Associated Mutant MYC Proteins as B-Cells Convert to a Lymphoma Phenotype. Cancers (Basel). 2021;13(23).
273. Conacci-Sorrell M, McFerrin L, Eisenman RN. An overview of MYC and its interactome. Cold Spring Harb Perspect Med. 2014;4(1):a014357.
274. Nie Z, Guo C, Das SK, Chow CC, Batchelor E, Simons SSJ, et al. Dissecting transcriptional amplification by MYC. Elife. 2020;9.
275. Schwinkendorf D, Gallant P. The conserved Myc box 2 and Myc box 3 regions are important, but not essential, for Myc function in vivo. Gene. 2009;436(1-2):90-100.
276. Feris EJ, Hinds JW, Cole MD. Luminescence complementation technology for the identification of MYC:TRRAP inhibitors. Oncotarget. 2021;12(21):2147-57.
277. Caeser R, Di Re M, Krupka JA, Gao J, Lara-Chica M, Dias JML, et al. Genetic modification of primary human B cells to model high-grade lymphoma. Nat Commun. 2019;10(1):4543.
278. Caeser R, Gao J, Di Re M, Gong C, Hodson DJ. Genetic manipulation and immortalized culture of ex vivo primary human germinal center B cells. Nat Protoc. 2021;16(5):2499-519.
279. Donnelly MLL, Hughes LE, Luke G, Mendoza H, Ten Dam E, Gani D, et al. The 'cleavage' activities of foot-and-mouth disease virus 2A site-directed mutants and naturally occurring '2A-like' sequences. J Gen Virol. 2001;82(Pt 5):1027-41.
280. Kim JH, Lee SR, Li LH, Park HJ, Park JH, Lee KY, et al. High cleavage efficiency of a 2A peptide derived from porcine teschovirus-1 in human cell lines, zebrafish and mice. PLoS One. 2011;6(4):e18556.
281. Terenin IM, Smirnova VV, Andreev DE, Dmitriev SE, Shatsky IN. A researcher's guide to the galaxy of IRESs. Cell Mol Life Sci. 2017;74(8):1431-55.
282. Cocco M, Stephenson S, Care MA, Newton D, Barnes NA, Davison A, et al. In vitro generation of long-lived human plasma cells. J Immunol. 2012;189(12):5773-85.
283. Stephenson S, Care MA, Fan I, Zougman A, Westhead DR, Doody GM, et al. Growth Factor-like Gene Regulation Is Separable from Survival and Maturation in Antibody-Secreting Cells. J Immunol. 2019;202(4):1287-300.
284. Walker BA, Mavrommatis K, Wardell CP, Ashby TC, Bauer M, Davies FE, et al. Identification of novel mutational drivers reveals oncogene dependencies in multiple myeloma. Blood. 2018;132(6):587-97.
285. Vardaka P, Page E, Care MA, Stephenson S, Kemp B, Umpierrez M, et al. Enforced MYC expression selectively redirects transcriptional programs during human plasma cell differentiation. bioRxiv doi: 101101/20240418589889. 2024.
286. Dobin A, Davis CA, Schlesinger F, Drenkow J, Zaleski C, Jha S, et al. STAR: ultrafast universal RNA-seq aligner. Bioinformatics. 2013;29(1):15-21.
287. Li B, Dewey CN. RSEM: accurate transcript quantification from RNA-Seq data with or without a reference genome. BMC Bioinformatics. 2011;12:323.
288. Love MI, Huber W, Anders S. Moderated estimation of fold change and dispersion for RNA-seq data with DESeq2. Genome Biol. 2014;15(12):550.
289. RDC. R: A Language and Environment for Statistical Computing. Vienna Austria R Foundation for Statistical Computing. 2008(1(09/18/2009):ISBN 3-900051-07-0).
290. Soneson C, Love MI, Robinson MD. Differential analyses for RNA-seq: transcript-level estimates improve gene-level inferences. F1000Res. 2015;4:1521.
291. Zhu A, Ibrahim JG, Love MI. Heavy-tailed prior distributions for sequence count data: removing the noise and preserving large differences. Bioinformatics. 2019;35(12):2084-92.
292. Care MA, Westhead DR, Tooze RM. Parsimonious Gene Correlation Network Analysis (PGCNA): a tool to define modular gene co-expression for refined molecular stratification in cancer. NPJ Syst Biol Appl. 2019;5:13.

293. Huang da W, Sherman BT, Lempicki RA. Systematic and integrative analysis of large gene lists using DAVID bioinformatics resources. Nat Protoc. 2009;4(1):44-57.
294. Sherman BT, Hao M, Qiu J, Jiao X, Baseler MW, Lane HC, et al. DAVID: a web server for functional enrichment analysis and functional annotation of gene lists (2021 update). Nucleic Acids Res. 2022;50(W1):W216-W21.
295. Chen EY, Tan CM, Kou Y, Duan Q, Wang Z, Meirelles GV, et al. Enrichr: interactive and collaborative HTML5 gene list enrichment analysis tool. BMC Bioinformatics. 2013;14:128.
296. Kuleshov MV, Jones MR, Rouillard AD, Fernandez NF, Duan Q, Wang Z, et al. Enrichr: a comprehensive gene set enrichment analysis web server 2016 update. Nucleic Acids Res. 2016;44(W1):W90-7.
297. Xie Z, Bailey A, Kuleshov MV, Clarke DJB, Evangelista JE, Jenkins SL, et al. Gene Set Knowledge Discovery with Enrichr. Curr Protoc. 2021;1(3):e90.
298. Fairlie WD, Lee EF. Co-Operativity between MYC and BCL-2 Pro-Survival Proteins in Cancer. Int J Mol Sci. 2021;22(6).
299. Punnoose EA, Leverson JD, Peale F, Boghaert ER, Belmont LD, Tan N, et al. Expression Profile of BCL-2, BCL-XL, and MCL-1 Predicts Pharmacological Response to the BCL-2 Selective Antagonist Venetoclax in Multiple Myeloma Models. Mol Cancer Ther. 2016;15(5):1132-44.
300. Pelletier N, Casamayor-Palleja M, De Luca K, Mondiere P, Saltel F, Jurdic P, et al. The endoplasmic reticulum is a key component of the plasma cell death pathway. J Immunol. 2006;176(3):1340-7.
301. Huber W, von Heydebreck A, Sultmann H, Poustka A, Vingron M. Variance stabilization applied to microarray data calibration and to the quantification of differential expression. Bioinformatics. 2002;18 Suppl 1:S96-104.
302. Agarwal E, Altman BJ, Seo JH, Ghosh JC, Kossenkov AV, Tang HY, et al. Myc-mediated transcriptional regulation of the mitochondrial chaperone TRAP1 controls primary and metastatic tumor growth. J Biol Chem. 2019;294(27):10407-14.
303. Farrell M, Fairfield H, Karam M, D'Amico A, Murphy CS, Falank C, et al. Targeting the fatty acid binding proteins disrupts multiple myeloma cell cycle progression and MYC signaling. Elife. 2023;12.
304. Tesi A, de Pretis S, Furlan M, Filipuzzi M, Morelli MJ, Andronache A, et al. An early Myc-dependent transcriptional program orchestrates cell growth during B-cell activation. EMBO Rep. 2019;20(9):e47987.
305. Wu KJ, Grandori C, Amacker M, Simon-Vermot N, Polack A, Lingner J, et al. Direct activation of TERT transcription by c-MYC. Nat Genet. 1999;21(2):220-4.
306. Yustein JT, Liu YC, Gao P, Jie C, Le A, Vuica-Ross M, et al. Induction of ectopic Myc target gene JAG2 augments hypoxic growth and tumorigenesis in a human B-cell model. Proc Natl Acad Sci U S A. 2010;107(8):3534-9.
307. Ochiai K, Katoh Y, Ikura T, Hoshikawa Y, Noda T, Karasuyama H, et al. Plasmacytic transcription factor Blimp-1 is repressed by Bach2 in B cells. J Biol Chem. 2006;281(50):38226-34.
308. Ma Y, Hendershot LM. Herp is dually regulated by both the endoplasmic reticulum stress-specific branch of the unfolded protein response and a branch that is shared with other cellular stress pathways. J Biol Chem. 2004;279(14):13792-9.
309. Misiewicz M, Dery MA, Foveau B, Jodoin J, Ruths D, LeBlanc AC. Identification of a novel endoplasmic reticulum stress response element regulated by XBP1. J Biol Chem. 2013;288(28):20378-91.
310. Oda Y, Okada T, Yoshida H, Kaufman RJ, Nagata K, Mori K. Derlin-2 and Derlin-3 are regulated by the mammalian unfolded protein response and are required for ER-associated degradation. J Cell Biol. 2006;172(3):383-93.
311. Lancho O, Herranz D. The MYC Enhancer-ome: Long-Range Transcriptional Regulation of MYC in Cancer. Trends Cancer. 2018;4(12):810-22.
312. Moreau P, Voillat L, Benboukher L, Mathiot C, Dumontet C, Robillard N, et al. Rituximab in CD20 positive multiple myeloma. Leukemia. 2007;21(4):835-6.

313. Robillard N, Wuilleme S, Moreau P, Bene MC. Immunophenotype of normal and myelomatous plasma-cell subsets. Front Immunol. 2014;5:137.
314. Wasylishen AR, Stojanova A, Oliveri S, Rust AC, Schimmer AD, Penn LZ. New model systems provide insights into Myc-induced transformation. Oncogene. 2011;30(34):3727-34.
315. Pan Y, van der Watt PJ, Kay SA. E-box binding transcription factors in cancer. Front Oncol. 2023;13:1223208.
316. Adhikary S, Eilers M. Transcriptional regulation and transformation by Myc proteins. Nat Rev Mol Cell Biol. 2005;6(8):635-45.
317. Eilers M, Eisenman RN. Myc's broad reach. Genes Dev. 2008;22(20):2755-66.
318. Wang H, Hammoudeh DI, Follis AV, Reese BE, Lazo JS, Metallo SJ, et al. Improved low molecular weight Myc-Max inhibitors. Mol Cancer Ther. 2007;6(9):2399-408.
319. Sun XX, Li Y, Sears RC, Dai MS. Targeting the MYC Ubiquitination-Proteasome Degradation Pathway for Cancer Therapy. Front Oncol. 2021;11:679445.
320. Arnold HK, Zhang X, Daniel CJ, Tibbitts D, Escamilla-Powers J, Farrell A, et al. The Axin1 scaffold protein promotes formation of a degradation complex for c-Myc. EMBO J. 2009;28(5):500-12.
321. Yeh E, Cunningham M, Arnold H, Chasse D, Monteith T, Ivaldi G, et al. A signalling pathway controlling c-Myc degradation that impacts oncogenic transformation of human cells. Nat Cell Biol. 2004;6(4):308-18.
322. Zhang Q, West-Osterfield K, Spears E, Li Z, Panaccione A, Hann SR. MB0 and MBI Are Independent and Distinct Transactivation Domains in MYC that Are Essential for Transformation. Genes (Basel). 2017;8(5).
323. Hann SR. MYC cofactors: molecular switches controlling diverse biological outcomes. Cold Spring Harb Perspect Med. 2014;4(9):a014399.
324. Grant PA, Duggan L, Cote J, Roberts SM, Brownell JE, Candau R, et al. Yeast Gcn5 functions in two multisubunit complexes to acetylate nucleosomal histones: characterization of an Ada complex and the SAGA (Spt/Ada) complex. Genes Dev. 1997;11(13):1640-50.
325. Cole MD. The myc oncogene: its role in transformation and differentiation. Annu Rev Genet. 1986;20:361-84.
326. Spencer CA, Groudine M. Control of c-myc regulation in normal and neoplastic cells. Adv Cancer Res. 1991;56:1-48.
327. Liberzon A, Birger C, Thorvaldsdottir H, Ghandi M, Mesirov JP, Tamayo P. The Molecular Signatures Database (MSigDB) hallmark gene set collection. Cell Syst. 2015;1(6):417-25.
328. Shim H, Dolde C, Lewis BC, Wu CS, Dang G, Jungmann RA, et al. c-Myc transactivation of LDH-A: implications for tumor metabolism and growth. Proc Natl Acad Sci U S A. 1997;94(13):6658-63.
329. Cowling VH, Cole MD. Mechanism of transcriptional activation by the Myc oncoproteins. Semin Cancer Biol. 2006;16(4):242-52.
330. Feris EJ, Hinds JW, Cole MD. Formation of a structurally-stable conformation by the intrinsically disordered MYC:TRRAP complex. PLoS One. 2019;14(12):e0225784.
331. Chen Y, Sun XX, Sears RC, Dai MS. Writing and erasing MYC ubiquitination and SUMOylation. Genes Dis. 2019;6(4):359-71.
332. Vervoorts J, Luscher-Firzlaff J, Luscher B. The ins and outs of MYC regulation by posttranslational mechanisms. J Biol Chem. 2006;281(46):34725-9.
333. Conacci-Sorrell M, Ngouenet C, Anderson S, Brabletz T, Eisenman RN. Stress-induced cleavage of Myc promotes cancer cell survival. Genes Dev. 2014;28(7):689-707.
334. Conacci-Sorrell M, Ngouenet C, Eisenman RN. Myc-nick: a cytoplasmic cleavage product of Myc that promotes alpha-tubulin acetylation and cell differentiation. Cell. 2010;142(3):480-93.
335. Nakagawa M, Takizawa N, Narita M, Ichisaka T, Yamanaka S. Promotion of direct reprogramming by transformation-deficient Myc. Proc Natl Acad Sci U S A. 2010;107(32):14152-7.

336. Kim SY, Herbst A, Tworkowski KA, Salghetti SE, Tansey WP. Skp2 regulates Myc protein stability and activity. Mol Cell. 2003;11(5):1177-88.
337. Salghetti SE, Caudy AA, Chenoweth JG, Tansey WP. Regulation of transcriptional activation domain function by ubiquitin. Science. 2001;293(5535):1651-3.
338. von der Lehr N, Johansson S, Wu S, Bahram F, Castell A, Cetinkaya C, et al. The F-box protein Skp2 participates in c-Myc proteosomal degradation and acts as a cofactor for c-Myc-regulated transcription. Mol Cell. 2003;11(5):1189-200.
339. Hydbring P, Castell A, Larsson LG. MYC Modulation around the CDK2/p27/SKP2 Axis. Genes (Basel). 2017;8(7).
340. Arpin C, Dechanet J, Van Kooten C, Merville P, Grouard G, Briere F, et al. Generation of memory B cells and plasma cells in vitro. Science. 1995;268(5211):720-2.
341. Randall TD, Heath AW, Santos-Argumedo L, Howard MC, Weissman IL, Lund FE. Arrest of B lymphocyte terminal differentiation by CD40 signaling: mechanism for lack of antibody-secreting cells in germinal centers. Immunity. 1998;8(6):733-42.
342. Satpathy S, Shenoy GN, Kaw S, Vaidya T, Bal V, Rath S, et al. Inhibition of terminal differentiation of B cells mediated by CD27 and CD40 involves signaling through JNK. J Immunol. 2010;185(11):6499-507.
343. Ding BB, Bi E, Chen H, Yu JJ, Ye BH. IL-21 and CD40L synergistically promote plasma cell differentiation through upregulation of Blimp-1 in human B cells. J Immunol. 2013;190(4):1827-36.
344. Ettinger R, Sims GP, Fairhurst AM, Robbins R, da Silva YS, Spolski R, et al. IL-21 induces differentiation of human naive and memory B cells into antibody-secreting plasma cells. J Immunol. 2005;175(12):7867-79.
345. Inoue T, Kurosaki T. Memory B cells. Nat Rev Immunol. 2024;24(1):5-17.
346. Lai AY, Mav D, Shah R, Grimm SA, Phadke D, Hatzi K, et al. DNA methylation profiling in human B cells reveals immune regulatory elements and epigenetic plasticity at Alu elements during B-cell activation. Genome Res. 2013;23(12):2030-41.
347. Moroney JB, Vasudev A, Pertsemlidis A, Zan H, Casali P. Integrative transcriptome and chromatin landscape analysis reveals distinct epigenetic regulations in human memory B cells. Nat Commun. 2020;11(1):5435.
348. Zhang XY, DeSalle LM, McMahon SB. Identification of novel targets of MYC whose transcription requires the essential MbII domain. Cell Cycle. 2006;5(3):238-41.
349. Kuttler F, Ame P, Clark H, Haughey C, Mougin C, Cahn JY, et al. c-myc box II mutations in Burkitt's lymphoma-derived alleles reduce cell-transformation activity and lower response to broad apoptotic stimuli. Oncogene. 2001;20(42):6084-94.
350. Tooze RM. A replicative self-renewal model for long-lived plasma cells: questioning irreversible cell cycle exit. Front Immunol. 2013;4:460.

Appendix

Appendix 1 – Vector map of pHIT60 construct

pHIT60 vector was provided by the group of Dr. Daniel Hodson.

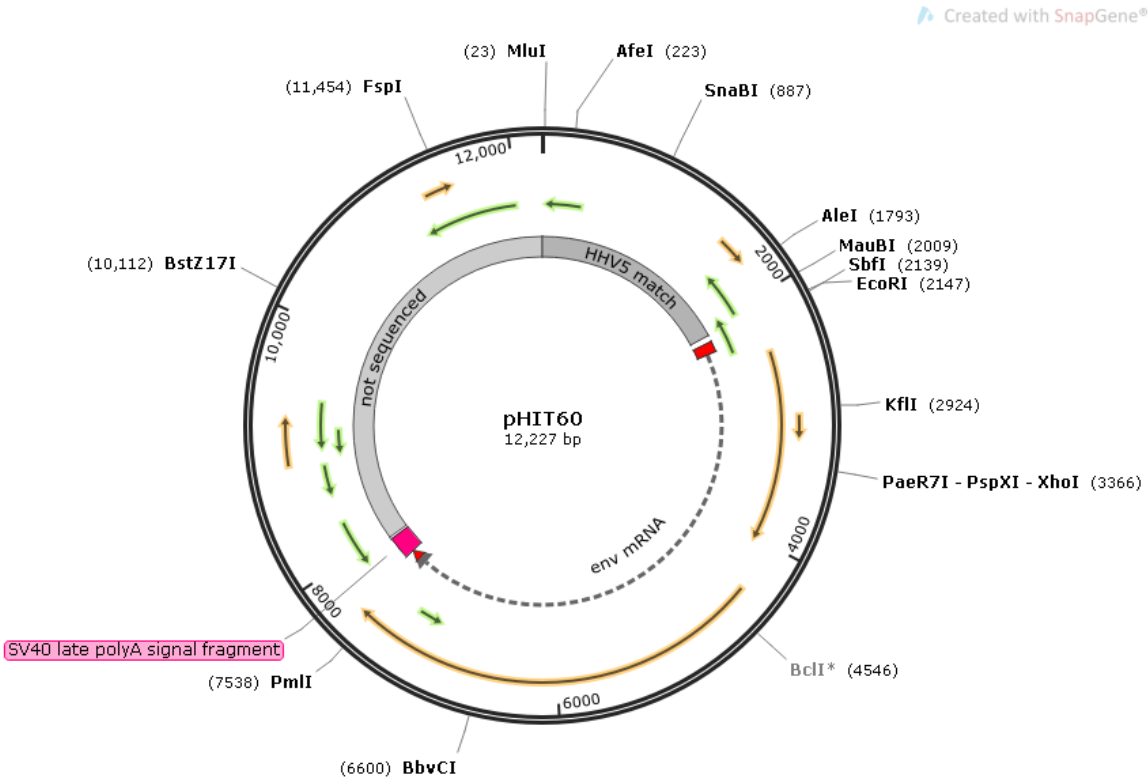

Appendix 2 – Vector map of GALV-MTR construct

GALV-MTR vector was provided by the group of Dr. Daniel Hodson.

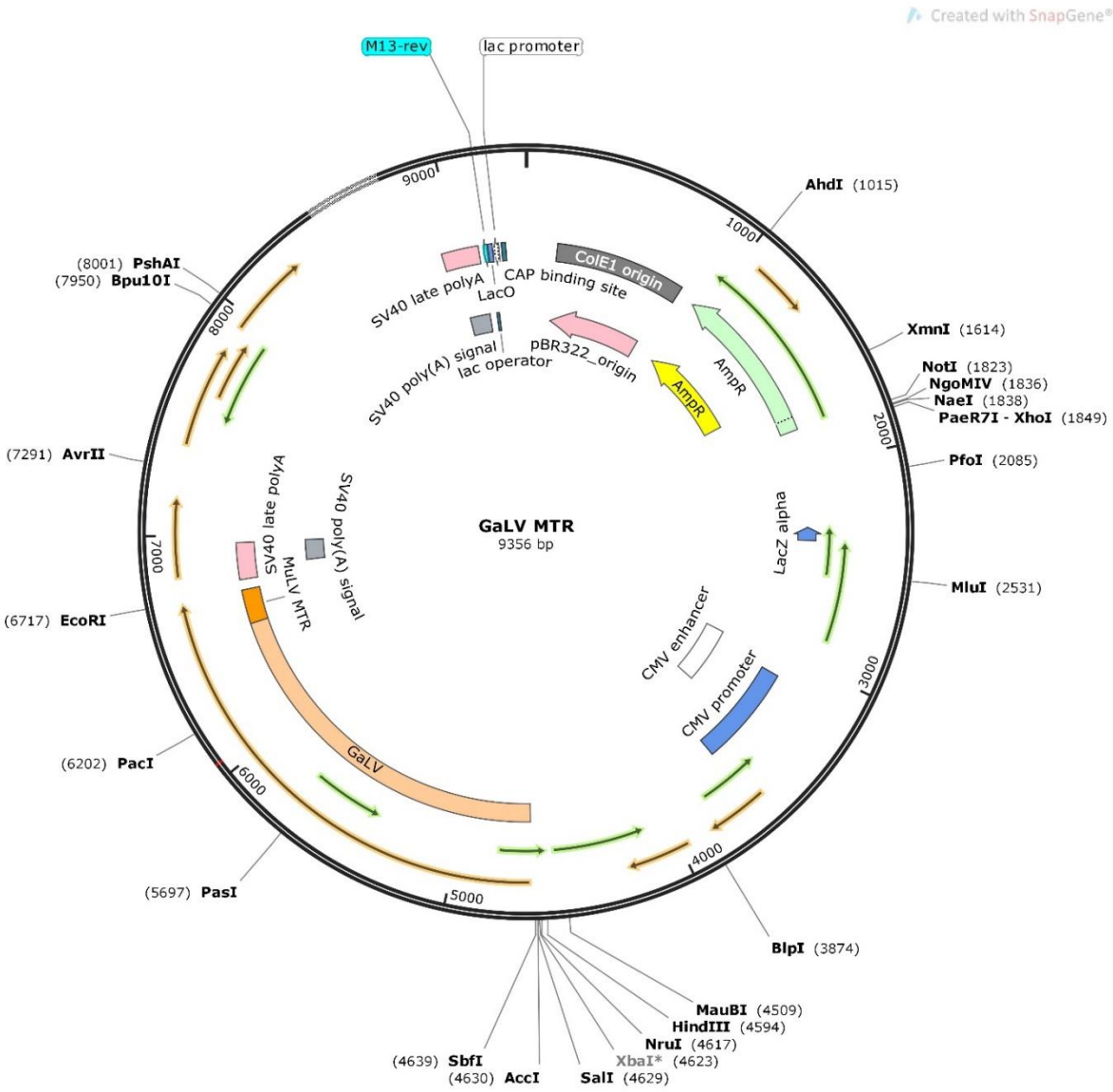

Appendix 3 – Vector map of MSCV-IRES-huCD2 backbone

MSCV-IRES-huCD2 backbone vector was provided by the group of Dr. Daniel Hodson. Diagnostic digest was conducted using the unique restriction enzymes XhoI and SalI at 1,416 and 2,870 bp respectively.

Appendix 4 – Vector map of T58I-t2A-BCL2 construct

MYC T58I-t2A-BCL2 vector was provided by the group of Dr. Daniel Hodson. Available on Addgene (#135306). Diagnostic digest was conducted using the unique restriction enzymes XhoI and SalI. Cloning of designed *MYC* mutants was conducted using the restriction enzymes XhoI and EcoRI.

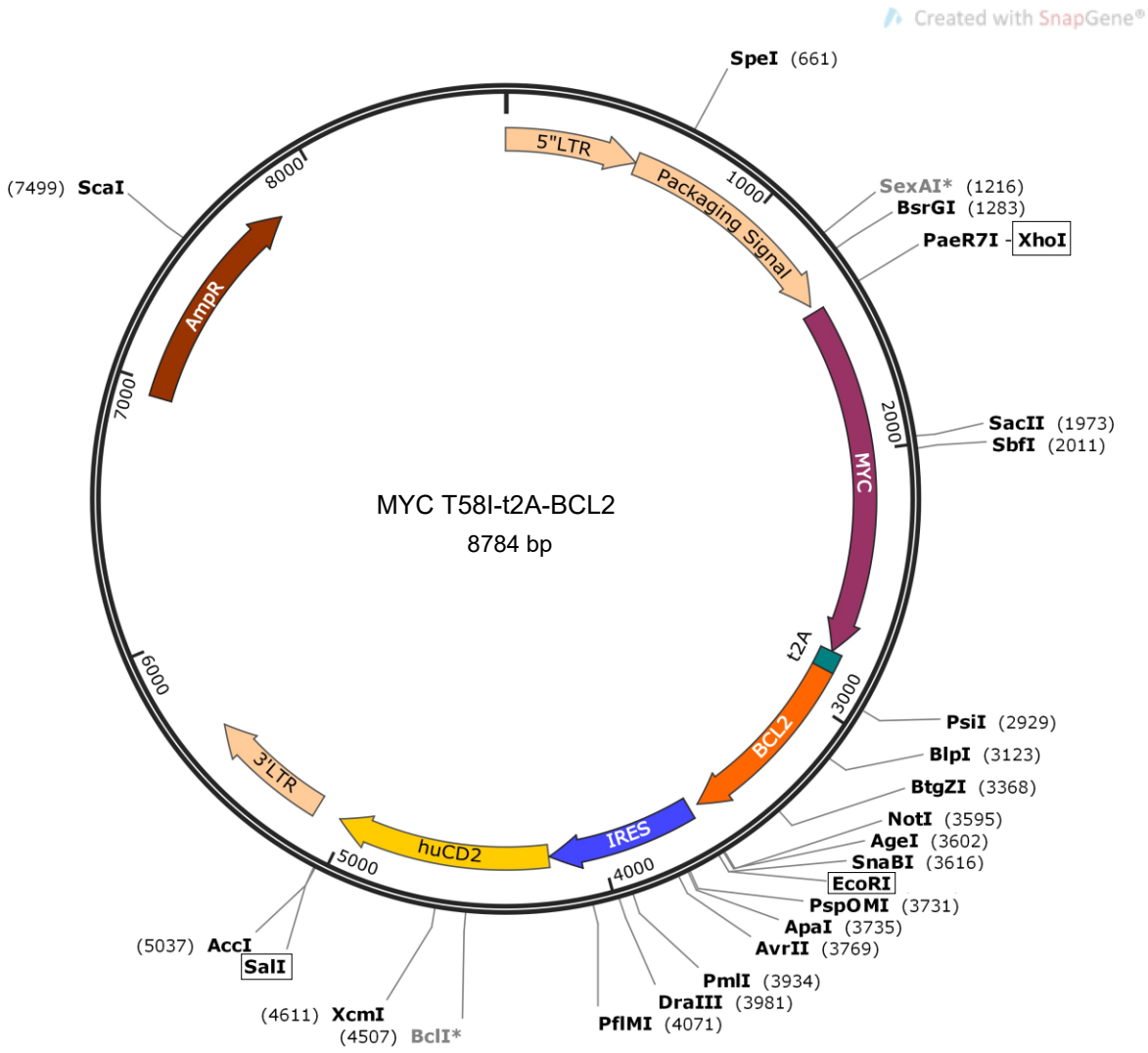

Appendix 5 – DNA sequence of the T58I-t2A-BCL2 insert

DNA sequence of insert (5’ -> 3’) with color coded codons corresponding to: XhoI- Kozak- MYC isoform 1 (15 amino acid extension)- glycine-serine enhanced T2A linker sequence- T2A- BCL2- spacer- EcoRI

CTCGAGGTTGCCACCATGGATTTTTTTCGGGTAGTGGAAAACCAGCAGCCTCCCGCGACGATGCCCCTCAACGTTAG
CTTCACCAACAGGAACTATGACCTCGACTACGACTCGGTGCAGCCGTATTTCTACTGCGACGAGGAGGAGAACTTCT
ACCAGCAGCAGCAGCAGAGCGAGCTGCAGCCCCCGGCGCCCAGCGAGGATATCTGGAAGAAATTCGAGCTGCTGC
CCATCCCGCCCCTGTCCCCTAGCCGCCGCTCCGGGCTCTGCTCGCCCTCCTACGTTGCGGTCACACCCTTCTCCCTTCG
GGGAGACAACGACGGCGGTGGCGGGAGCTTCTCCACGGCCGACCAGCTGGAGATGGTGACCGAGCTGCTGGGAG
GAGACATGGTGAACCAGAGTTTCATCTGCGACCCGGACGACGAGACCTTCATCAAAAACATCATCATCCAGGACTGT
ATGTGGAGCGGCTTCTCGGCCGCCGCCAAGCTCGTCTCAGAGAAGCTGGCCTCCTACCAGGCTGCGCGCAAAGACA
GCGGCAGCCCGAACCCCGCCCGCGGCCACAGCGTCTGCTCCACCTCCAGCTTGTACCTGCAGGATCTGAGCGCCGC
CGCCTCAGAGTGCATCGACCCCTCGGTGGTCTTCCCCTACCCTCTCAACGACAGCAGCTCGCCCAAGTCCTGCGCCTC
GCAAGACTCCAGCGCCTTCTCTCCGTCCTCGGATTCTCTGCTCTCCTCGACGGAGTCCTCCCCGCAGGGCAGCCCCG
AGCCCCTGGTGCTCCATGAGGAGACACCGCCCACCACCAGCAGCGACTCTGAGGAGGAACAAGAAGATGAGGAAG
AAATCGATGTTGTTTCTGTGGAAAAGAGGCAGGCTCCTGGCAAAAGGTCAGAGTCTGGATCACCTTCTGCTGGAGG
CCACAGCAAACCTCCTCACAGCCCACTGGTCCTCAAGAGGTGCCACGTCTCCACACATCAGCACAACTACGCAGCGC
CTCCCTCCACTCGGAAGGACTATCCTGCTGCCAAGAGGGTCAAGTTGGACAGTGTCAGAGTCCTGAGACAGATCAG
CAACAACCGAAAATGCACCAGCCCCAGGTCCTCGGACACCGAGGAGAATGTCAAGAGGCGAACACACAACGTCTT
GGAGCGCCAGAGGAGGAACGAGCTAAAACGGAGCTTTTTTGCCCTGCGTGACCAGATCCCGGAGTTGGAAAACAA
TGAAAAGGCCCCCAAGGTAGTTATCCTTAAAAAAGCCACAGCATACATCCTGTCCGTCCAAGCAGAGGAGCAAAAG
CTCATTTCTGAAGAGGACTTGTTGCGGAAACGACGAGAACAGTTGAAACACAAACTTGAACAGCTACGGAACTCTT
GTGCGAACGGATCCGGCAGCGGCGGGGAAGGAAGGGGCTCCCTGCTCACCTGCGGCGACGTGGAAGAGAACCCC
GGACCTATGGCGCACGCTGGGAGAACAGGGTACGATAACCGGGAGATAGTGATGAAGTACATCCATTATAAGCTGTC
GCAGAGGGGCTACGAGTGGGATGCGGGAGATGTGGGAGCCGCTCCTCCTGGTGCCGCTCCCGCACCGGGCATCTT
CTCCTCCCAGCCTGGGCACACGCCTCATCCAGCCGCATCCCGGGATCCTGTCGCCAGGACCTCGCCTCTGCAGACAC
CGGCTGCTCCTGGAGCTGCTGCAGGACCTGCGCTCAGCCCGGTGCCACCTGTGGTCCACCTGACCCTCCGCCAGGC
CGGCGACGACTTCTCCCGCCGCTACCGCCGCGACTTCGCCGAGATGTCCAGCCAGCTGCACCTGACGCCCTTCACCG
CGCGGGGACGCTTTGCCACGGTGGTGGAGGAGCTCTTCAGGGACGGGGTGAACTGGGGGAGGATTGTGGCCTTC
TTTGAGTTCGGTGGGGTCATGTGTGTGGAGAGCGTCAACCGGGAGATGTCGCCCCTGGTGGACAACATCGCCCTGT
GGATGACTGAGTACCTGAACCGGCACCTGCACACCTGGATCCAGGATAACGGAGGCTGGGATGCCTTTGTGGAACT
GTACGGCCCCAGCATGCGGCCTCTGTTTGATTTCTCCTGGCTGTCTCTGAAGACTCTGCTCAGTTTGGCCCTGGTGGG
AGCTTGCATCACCCTGGGTGCCTATCTGGGCCACAAGTGATAGAACGCGGCCGCACCGGTGGATCCTACGTAGAATT
C

Appendix 6 – DNA sequence of the WT-t2A-BCL2 insert

DNA sequence of insert (5’ -> 3’) with color coded codons corresponding to: XhoI- Kozak- MYC isoform 2 (MB0, MBI, MBII)- glycine-serine enhanced T2A linker sequence- T2A- BCL2- spacer- EcoRI

CTCGAGGTTGCCACCATGCCCCTCAACGTTAGCTTCACCAACAGGAACTATGACCTCGACTACGACTCGGTGCAGCC
GTATTTCTACTGCGACGAGGAGGAGAACTTCTACCAGCAGCAGCAGCAGAGCGAGCTGCAGCCCCCGGCGCCCAG
CGAGGATATCTGGAAGAAATTCGAGCTGCTGCCCACCCCGCCCCTGTCCCCTAGCCGCCGCTCCGGGCTCTGCTCGC
CCTCCTACGTTGCGGTCACACCCTTCTCCCTTCGGGGAGACAACGACGGCGGTGGCGGGAGCTTCTCCACGGCCGA
CCAGCTGGAGATGGTGACCGAGCTGCTGGGAGGAGACATGGTGAACCAGAGTTTCATCTGCGACCCGGACGACGA
GACCTTCATCAAAAACATCATCATCCAGGACTGTATGTGGAGCGGCTTCTCGGCCGCCGCCAAGCTCGTCTCAGAGA
AGCTGGCCTCCTACCAGGCTGCGCGCAAAGACAGCGGCAGCCCGAACCCCGCCCGCGGCCACAGCGTCTGCTCCAC
CTCCAGCTTGTACCTGCAGGATCTGAGCGCCGCCGCCTCAGAGTGCATCGACCCCTCGGTGGTCTTCCCCTACCCTCT
CAACGACAGCAGCTCGCCCAAGTCCTGCGCCTCGCAAGACTCCAGCGCCTTCTCTCCGTCCTCGGATTCTCTGCTCTC
CTCGACGGAGTCCTCCCCGCAGGGCAGCCCCGAGCCCCTGGTGCTCCATGAGGAGACACCGCCCACCACCAGCAGC
GACTCTGAGGAGGAACAAGAAGATGAGGAAGAAATCGATGTTGTTTCTGTGGAAAAGAGGCAGGCTCCTGGCAAA
AGGTCAGAGTCTGGATCACCTTCTGCTGGAGGCCACAGCAAACCTCCTCACAGCCCACTGGTCCTCAAGAGGTGCC
ACGTCTCCACACATCAGCACAACTACGCAGCGCCTCCCTCCACTCGGAAGGACTATCCTGCTGCCAAGAGGGTCAAG
TTGGACAGTGTCAGAGTCCTGAGACAGATCAGCAACAACCGAAAATGCACCAGCCCCAGGTCCTCGGACACCGAG
GAGAATGTCAAGAGGCGAACACACAACGTCTTGGAGCGCCAGAGGAGGAACGAGCTAAAACGGAGCTTTTTTGCC
CTGCGTGACCAGATCCCGGAGTTGGAAAACAATGAAAAGGCCCCCAAGGTAGTTATCCTTAAAAAAGCCACAGCAT
ACATCCTGTCCGTCCAAGCAGAGGAGCAAAAGCTCATTTCTGAAGAGGACTTGTTGCGGAAACGACGAGAACAGTT
GAAACACAAACTTGAACAGCTACGGAACTCTTGTGCGAACGGATCCGGCAGCGGCGGGGAAGGAAGGGGCTCCCT
GCTCACCTGCGGCGACGTGGAAGAGAACCCCGGACCTATGGCGCACGCTGGGAGAACAGGGTACGATAACCGGGA
GATAGTGATGAAGTACATCCATTATAAGCTGTCGCAGAGGGGCTACGAGTGGGATGCGGGAGATGTGGGAGCCGCT
CCTCCTGGTGCCGCTCCCGCACCGGGCATCTTCTCCTCCCAGCCTGGGCACACGCCTCATCCAGCCGCATCCCGGGAT
CCTGTCGCCAGGACCTCGCCTCTGCAGACACCGGCTGCTCCTGGAGCTGCTGCAGGACCTGCGCTCAGCCCGGTGC
CACCTGTGGTCCACCTGACCCTCCGCCAGGCCGGCGACGACTTCTCCCGCCGCTACCGCCGCGACTTCGCCGAGATG
TCCAGCCAGCTGCACCTGACGCCCTTCACCGCGCGGGGACGCTTTGCCACGGTGGTGGAGGAGCTCTTCAGGGAC
GGGGTGAACTGGGGGAGGATTGTGGCCTTCTTTGAGTTCGGTGGGGTCATGTGTGTGGAGAGCGTCAACCGGGAG
ATGTCGCCCCTGGTGGACAACATCGCCCTGTGGATGACTGAGTACCTGAACCGGCACCTGCACACCTGGATCCAGGA
TAACGGAGGCTGGGATGCCTTTGTGGAACTGTACGGCCCCAGCATGCGGCCTCTGTTTGATTTCTCCTGGCTGTCTCT
GAAGACTCTGCTCAGTTTGGCCCTGGTGGGAGCTTGCATCACCCTGGGTGCCTATCTGGGCCACAAGTGATAGAACG
CGGCCGCACCGGTGGATCCTACGTAGAATTC

Appendix 7 – DNA sequence of the ΔMB0-t2A-BCL2 insert

DNA sequence of insert (5’ -> 3’) with color coded codons corresponding to: XhoI- Kozak- MYC isoform 2 (ΔMB0, MBI, MBII)- glycine-serine enhanced T2A linker sequence- T2A- BCL2- spacer- EcoRI

CTCGAGGTTGCCACCATGCCCCTCAACGTTAGCTTCACCAACAGGAACTATGACCTCGACCAGCAGCAGCAGAGA
GCGAGCTGCAGCCCCCGGCGCCCAGCGAGGATATCTGGAAGAAATTCGAGCTGCTGCCCACCCCGCCCCTGTCCCC
TAGCCGCCGCTCCGGGCTCTGCTCGCCCTCCTACGTTGCGGTCACACCCTTCTCCCTTCGGGGAGACAACGACGGCG
GTGGCGGGAGCTTCTCCACGGCCGACCAGCTGGAGATGGTGACCGAGCTGCTGGGAGGAGACATGGTGAACCAG
AGTTTCATCTGCGACCCGGACGACGAGACCTTCATCAAAAACATCATCATCCAGGACTGTATGTGGAGCGGCTTCTCG
GCCGCCGCCAAGCTCGTCTCAGAGAAGCTGGCCTCCTACCAGGCTGCGCGCAAAGACAGCGGCAGCCCGAACCCC
GCCCGCGGCCACAGCGTCTGCTCCACCTCCAGCTTGTACCTGCAGGATCTGAGCGCCGCCGCCTCAGAGTGCATCGA
CCCCTCGGTGGTCTTCCCCTACCCTCTCAACGACAGCAGCTCGCCCAAGTCCTGCGCCTCGCAAGACTCCAGCGCCTT
CTCTCCGTCCTCGGATTCTCTGCTCTCCTCGACGGAGTCCTCCCCGCAGGGCAGCCCCGAGCCCCTGGTGCTCCATGA
GGAGACACCGCCCACCACCAGCAGCGACTCTGAGGAGGAACAAGAAGATGAGGAAGAAATCGATGTTGTTTCTGT
GGAAAAGAGGCAGGCTCCTGGCAAAAGGTCAGAGTCTGGATCACCTTCTGCTGGAGGCCACAGCAAACCTCCTCA
CAGCCCACTGGTCCTCAAGAGGTGCCACGTCTCCACACATCAGCACAACTACGCAGCGCCTCCCTCCACTCGGAAGG
ACTATCCTGCTGCCAAGAGGGTCAAGTTGGACAGTGTCAGAGTCCTGAGACAGATCAGCAACAACCGAAAATGCAC
CAGCCCCAGGTCCTCGGACACCGAGGAGAATGTCAAGAGGCGAACACACAACGTCTTGGAGCGCCAGAGGAGGA
ACGAGCTAAAACGGAGCTTTTTTGCCCTGCGTGACCAGATCCCGGAGTTGGAAAACAATGAAAAGGCCCCCAAGGT
AGTTATCCTTAAAAAAGCCACAGCATACATCCTGTCCGTCCAAGCAGAGGAGCAAAAGCTCATTTCTGAAGAGGACT
TGTTGCGGAAACGACGAGAACAGTTGAAACACAAACTTGAACAGCTACGGAACTCTTGTGCGAACGGATCCGGCA
GCGGCGGGGAAGGAAGGGGCTCCCTGCTCACCTGCGGCGACGTGGAAGAGAACCCCGGACCTATGGCGCACGCT
GGGAGAACAGGGTACGATAACCGGGAGATAGTGATGAAGTACATCCATTATAAGCTGTCGCAGAGGGGCTACGAGT
GGGATGCGGGAGATGTGGGAGCCGCTCCTCCTGGTGCCGCTCCCGCACCGGGCATCTTCTCCTCCCAGCCTGGGCA
CACGCCTCATCCAGCCGCATCCCGGGATCCTGTCGCCAGGACCTCGCCTCTGCAGACACCGGCTGCTCCTGGAGCTG
CTGCAGGACCTGCGCTCAGCCCGGTGCCACCTGTGGTCCACCTGACCCTCCGCCAGGCCGGCGACGACTTCTCCCG
CCGCTACCGCCGCGACTTCGCCGAGATGTCCAGCCAGCTGCACCTGACGCCCTTCACCGCGCGGGGACGCTTTGCC
ACGGTGGTGGAGGAGCTCTTCAGGGACGGGGTGAACTGGGGGAGGATTGTGGCCTTCTTTGAGTTCGGTGGGGT
CATGTGTGTGGAGAGCGTCAACCGGGAGATGTCGCCCCTGGTGGACAACATCGCCCTGTGGATGACTGAGTACCTG
AACCGGCACCTGCACACCTGGATCCAGGATAACGGAGGCTGGGATGCCTTTGTGGAACTGTACGGCCCCAGCATGC
GGCCTCTGTTTGATTTCTCCTGGCTGTCTCTGAAGACTCTGCTCAGTTTGGCCCTGGTGGGAGCTTGCATCACCCTGG
GTGCCTATCTGGGCCACAAGTGATAGAACGCGGCCGCACCGGTGGATCCTACGTAGAATTC

Appendix 8 – DNA sequence of the ΔMBI-t2A-BCL2 insert

DNA sequence of insert (5’ -> 3’) with color coded codons corresponding to: XhoI- Kozak- MYC isoform 2 (MB0, ΔMBI, MBII)- glycine-serine enhanced T2A linker sequence- T2A- BCL2- spacer- EcoRI

CTCGAGGTTGCCACCATGCCCCTCAACGTTAGCTTCACCAACAGGAACTATGACCTCGACTACGACTCGGTGCAGCC
GTATTTCTACTGCGACGAGGAGGAGAACTTCTACCAGCAGCAGCAGCAGAGCGAGCTGCAGCCCCCGGCGAGCCG
CCGCTCCGGGCTCTGCTCGCCCTCCTACGTTGCGGTCACACCCTTCTCCCTTCGGGGAGACAACGACGGCGGTGGC
GGGAGCTTCTCCACGGCCGACCAGCTGGAGATGGTGACCGAGCTGCTGGGAGGAGACATGGTGAACCAGAGTTTC
ATCTGCGACCCGGACGACGAGACCTTCATCAAAAACATCATCATCCAGGACTGTATGTGGAGCGGCTTCTCGGCCGC
CGCCAAGCTCGTCTCAGAGAAGCTGGCCTCCTACCAGGCTGCGCGCAAAGACAGCGGCAGCCCGAACCCCGCCCG
CGGCCACAGCGTCTGCTCCACCTCCAGCTTGTACCTGCAGGATCTGAGCGCCGCCGCCTCAGAGTGCATCGACCCCT
CGGTGGTCTTCCCCTACCCTCTCAACGACAGCAGCTCGCCCAAGTCCTGCGCCTCGCAAGACTCCAGCGCCTTCTCTC
CGTCCTCGGATTCTCTGCTCTCCTCGACGGAGTCCTCCCCGCAGGGCAGCCCCGAGCCCCTGGTGCTCCATGAGGAG
ACACCGCCCACCACCAGCAGCGACTCTGAGGAGGAACAAGAAGATGAGGAAGAAATCGATGTTGTTTCTGTGGAA
AAGAGGCAGGCTCCTGGCAAAAGGTCAGAGTCTGGATCACCTTCTGCTGGAGGCCACAGCAAACCTCCTCACAGCC
CACTGGTCCTCAAGAGGTGCCACGTCTCCACACATCAGCACAACTACGCAGCGCCTCCCTCCACTCGGAAGGACTAT
CCTGCTGCCAAGAGGGTCAAGTTGGACAGTGTCAGAGTCCTGAGACAGATCAGCAACAACCGAAAATGCACCAGCC
CCAGGTCCTCGGACACCGAGGAGAATGTCAAGAGGCGAACACACAACGTCTTGGAGCGCCAGAGGAGGAACGAG
CTAAAACGGAGCTTTTTTGCCCTGCGTGACCAGATCCCGGAGTTGGAAAACAATGAAAAGGCCCCCAAGGTAGTTAT
CCTTAAAAAAGCCACAGCATACATCCTGTCCGTCCAAGCAGAGGAGCAAAAGCTCATTTCTGAAGAGGACTTGTTGC
GGAAACGACGAGAACAGTTGAAACACAAACTTGAACAGCTACGGAACTCTTGTGCGAACGGATCCGGCAGCGGCG
GGGAAGGAAGGGGCTCCCTGCTCACCTGCGGCGACGTGGAAGAGAACCCCGGACCTATGGCGCACGCTGGGAGA
ACAGGGTACGATAACCGGGAGATAGTGATGAAGTACATCCATTATAAGCTGTCGCAGAGGGGCTACGAGTGGGATGC
GGGAGATGTGGGAGCCGCTCCTCCTGGTGCCGCTCCCGCACCGGGCATCTTCTCCTCCCAGCCTGGGCACACGCCTC
ATCCAGCCGCATCCCGGGATCCTGTCGCCAGGACCTCGCCTCTGCAGACACCGGCTGCTCCTGGAGCTGCTGCAGGA
CCTGCGCTCAGCCCGGTGCCACCTGTGGTCCACCTGACCCTCCGCCAGGCCGGCGACGACTTCTCCCGCCGCTACCG
CCGCGACTTCGCCGAGATGTCCAGCCAGCTGCACCTGACGCCCTTCACCGCGCGGGGACGCTTTGCCACGGTGGTG
GAGGAGCTCTTCAGGGACGGGGTGAACTGGGGGAGGATTGTGGCCTTCTTTGAGTTCGGTGGGGTCATGTGTGTG
GAGAGCGTCAACCGGGAGATGTCGCCCCTGGTGGACAACATCGCCCTGTGGATGACTGAGTACCTGAACCGGCACC
TGCACACCTGGATCCAGGATAACGGAGGCTGGGATGCCTTTGTGGAACTGTACGGCCCCAGCATGCGGCCTCTGTTT
GATTTCTCCTGGCTGTCTCTGAAGACTCTGCTCAGTTTGGCCCTGGTGGGAGCTTGCATCACCCTGGGTGCCTATCTG
GGCCACAAGTGATAGAACGCGGCCGCACCGGTGGATCCTACGTAGAATTC

Appendix 9 – DNA sequence of the ΔMBII-t2A-BCL2 insert

DNA sequence of insert (5’ -> 3’) with color coded codons corresponding to: XhoI- Kozak- MYC isoform 2 (MB0, MBI, ΔMBII)- glycine-serine enhanced T2A linker sequence- T2A- BCL2- spacer- EcoRI

CTCGAGGTTGCCACCATGCCCCTCAACGTTAGCTTCACCAACAGGAACTATGACCTCGACTACGACTCGGTGCAGCC
GTATTTCTACTGCGACGAGGAGGAGAACTTCTACCAGCAGCAGCAGCAGAGCGAGCTGCAGCCCCCGGCGCCCAG
CGAGGATATCTGGAAGAAATTCGAGCTGCTGCCCACCCCGCCCCTGTCCCCTAGCCGCCGCTCCGGGCTCTGCTCGC
CCTCCTACGTTGCGGTCACACCCTTCTCCCTTCGGGGAGACAACGACGGCGGTGGCGGGAGCTTCTCCACGGCCGA
CCAGCTGGAGATGGTGACCGAGCTGCTGGGAGGAGACATGGTGAACCAGAGTTTCATCTGCGACCCGGACGACGA
GACCTTCATCAAAAACCTCGTCTCAGAGAAGCTGGCCTCCTACCAGGCTGCGCGCAAAGACAGCGGCAGCCCGAAC
CCCGCCCGCGGCCACAGCGTCTGCTCCACCTCCAGCTTGTACCTGCAGGATCTGAGCGCCGCCGCCTCAGAGTGCAT
CGACCCCTCGGTGGTCTTCCCCTACCCTCTCAACGACAGCAGCTCGCCCAAGTCCTGCGCCTCGCAAGACTCCAGCG
CCTTCTCTCCGTCCTCGGATTCTCTGCTCTCCTCGACGGAGTCCTCCCCGCAGGGCAGCCCCGAGCCCCTGGTGCTCC
ATGAGGAGACACCGCCCACCACCAGCAGCGACTCTGAGGAGGAACAAGAAGATGAGGAAGAAATCGATGTTGTTT
CTGTGGAAAAGAGGCAGGCTCCTGGCAAAAGGTCAGAGTCTGGATCACCTTCTGCTGGAGGCCACAGCAAACCTC
CTCACAGCCCACTGGTCCTCAAGAGGTGCCACGTCTCCACACATCAGCACAACTACGCAGCGCCTCCCTCCACTCGG
AAGGACTATCCTGCTGCCAAGAGGGTCAAGTTGGACAGTGTCAGAGTCCTGAGACAGATCAGCAACAACCGAAAAT
GCACCAGCCCCAGGTCCTCGGACACCGAGGAGAATGTCAAGAGGCGAACACACAACGTCTTGGAGCGCCAGAGGA
GGAACGAGCTAAAACGGAGCTTTTTTGCCCTGCGTGACCAGATCCCGGAGTTGGAAAACAATGAAAAGGCCCCCA
AGGTAGTTATCCTTAAAAAAGCCACAGCATACATCCTGTCCGTCCAAGCAGAGGAGCAAAAGCTCATTTCTGAAGAG
GACTTGTTGCGGAAACGACGAGAACAGTTGAAACACAAACTTGAACAGCTACGGAACTCTTGTGCGAACGGATCCG
GCAGCGGCGGGGAAGGAAGGGGCTCCCTGCTCACCTGCGGCGACGTGGAAGAGAACCCCGGACCTATGGCGCAC
GCTGGGAGAACAGGGTACGATAACCGGGAGATAGTGATGAAGTACATCCATTATAAGCTGTCGCAGAGGGGCTACG
AGTGGGATGCGGGAGATGTGGGAGCCGCTCCTCCTGGTGCCGCTCCCGCACCGGGCATCTTCTCCTCCCAGCCTGG
GCACACGCCTCATCCAGCCGCATCCCGGGATCCTGTCGCCAGGACCTCGCCTCTGCAGACACCGGCTGCTCCTGGAG
CTGCTGCAGGACCTGCGCTCAGCCCGGTGCCACCTGTGGTCCACCTGACCCTCCGCCAGGCCGGCGACGACTTCTCC
CGCCGCTACCGCCGCGACTTCGCCGAGATGTCCAGCCAGCTGCACCTGACGCCCTTCACCGCGCGGGGACGCTTTG
CCACGGTGGTGGAGGAGCTCTTCAGGGACGGGGTGAACTGGGGGAGGATTGTGGCCTTCTTTGAGTTCGGTGGG
GTCATGTGTGTGGAGAGCGTCAACCGGGAGATGTCGCCCCTGGTGGACAACATCGCCCTGTGGATGACTGAGTACC
TGAACCGGCACCTGCACACCTGGATCCAGGATAACGGAGGCTGGGATGCCTTTGTGGAACTGTACGGCCCCAGCAT
GCGGCCTCTGTTTGATTTCTCCTGGCTGTCTCTGAAGACTCTGCTCAGTTTGGCCCTGGTGGGAGCTTGCATCACCCT
GGGTGCCTATCTGGGCCACAAGTGATAGAACGCGGCCGCACCGGTGGATCCTACGTAGAATTC

Appendix 10 – DNA sequence of the MBII 4aa mut-t2A-BCL2 insert

DNA sequence of insert (5’ -> 3’) with color coded codons corresponding to: XhoI- Kozak- MYC isoform 2 (ΔMBII: DCMW/AAAA)- glycine-serine enhanced T2A linker sequence- T2A- BCL2- spacer- EcoRI

CTCGAGGTTGCCACCATGCCCCTCAACGTTAGCTTCACCAACAGGAACTATGACCTCGACTACGACTCGGTGCAGCC
GTATTTCTACTGCGACGAGGAGGAGAACTTCTACCAGCAGCAGCAGCAGAGCGAGCTGCAGCCCCCGGCGCCCAG
CGAGGATATCTGGAAGAAATTCGAGCTGCTGCCCACCCCGCCCCTGTCCCCTAGCCGCCGCTCCGGGCTCTGCTCGC
CCTCCTACGTTGCGGTCACACCCTTCTCCCTTCGGGGAGACAACGACGGCGGTGGCGGGAGCTTCTCCACGGCCGA
CCAGCTGGAGATGGTGACCGAGCTGCTGGGAGGAGACATGGTGAACCAGAGTTTCATCTGCGACCCGGACGACGA
GACCTTCATCAAAAACATCATCATCCAGGCCGCCGCCGCCAGCGGCTTCTCGGCCGCCGCCAAGCTCGTCTCAGAGA
AGCTGGCCTCCTACCAGGCTGCGCGCAAAGACAGCGGCAGCCCGAACCCCGCCCGCGGCCACAGCGTCTGCTCCAC
CTCCAGCTTGTACCTGCAGGATCTGAGCGCCGCCGCCTCAGAGTGCATCGACCCCTCGGTGGTCTTCCCCTACCCTCT
CAACGACAGCAGCTCGCCCAAGTCCTGCGCCTCGCAAGACTCCAGCGCCTTCTCTCCGTCCTCGGATTCTCTGCTCTC
CTCGACGGAGTCCTCCCCGCAGGGCAGCCCCGAGCCCCTGGTGCTCCATGAGGAGACACCGCCCACCACCAGCAGC
GACTCTGAGGAGGAACAAGAAGATGAGGAAGAAATCGATGTTGTTTCTGTGGAAAAGAGGCAGGCTCCTGGCAAA
AGGTCAGAGTCTGGATCACCTTCTGCTGGAGGCCACAGCAAACCTCCTCACAGCCCACTGGTCCTCAAGAGGTGCC
ACGTCTCCACACATCAGCACAACTACGCAGCGCCTCCCTCCACTCGGAAGGACTATCCTGCTGCCAAGAGGGTCAAG
TTGGACAGTGTCAGAGTCCTGAGACAGATCAGCAACAACCGAAAATGCACCAGCCCCAGGTCCTCGGACACCGAG
GAGAATGTCAAGAGGCGAACACACAACGTCTTGGAGCGCCAGAGGAGGAACGAGCTAAAACGGAGCTTTTTTGCC
CTGCGTGACCAGATCCCGGAGTTGGAAAACAATGAAAAGGCCCCCAAGGTAGTTATCCTTAAAAAAGCCACAGCAT
ACATCCTGTCCGTCCAAGCAGAGGAGCAAAAGCTCATTTCTGAAGAGGACTTGTTGCGGAAACGACGAGAACAGTT
GAAACACAAACTTGAACAGCTACGGAACTCTTGTGCGAACGGATCCGGCAGCGGCGGGGAAGGAAGGGGCTCCCT
GCTCACCTGCGGCGACGTGGAAGAGAACCCCGGACCTATGGCGCACGCTGGGAGAACAGGGTACGATAACCGGGA
GATAGTGATGAAGTACATCCATTATAAGCTGTCGCAGAGGGGCTACGAGTGGGATGCGGGAGATGTGGGAGCCGCT
CCTCCTGGTGCCGCTCCCGCACCGGGCATCTTCTCCTCCCAGCCTGGGCACACGCCTCATCCAGCCGCATCCCGGGAT
CCTGTCGCCAGGACCTCGCCTCTGCAGACACCGGCTGCTCCTGGAGCTGCTGCAGGACCTGCGCTCAGCCCGGTGC
CACCTGTGGTCCACCTGACCCTCCGCCAGGCCGGCGACGACTTCTCCCGCCGCTACCGCCGCGACTTCGCCGAGATG
TCCAGCCAGCTGCACCTGACGCCCTTCACCGCGCGGGGACGCTTTGCCACGGTGGTGGAGGAGCTCTTCAGGGAC
GGGGTGAACTGGGGGAGGATTGTGGCCTTCTTTGAGTTCGGTGGGGTCATGTGTGTGGAGAGCGTCAACCGGGAG
ATGTCGCCCCTGGTGGACAACATCGCCCTGTGGATGACTGAGTACCTGAACCGGCACCTGCACACCTGGATCCAGGA
TAACGGAGGCTGGGATGCCTTTGTGGAACTGTACGGCCCCAGCATGCGGCCTCTGTTTGATTTCTCCTGGCTGTCTCT
GAAGACTCTGCTCAGTTTGGCCCTGGTGGGAGCTTGCATCACCCTGGGTGCCTATCTGGGCCACAAGTGATAGAACG
CGGCCGCACCGGTGGATCCTACGTAGAATTC

Appendix 11 – DNA sequence of the MBII W135A-t2A-BCL2 insert

DNA sequence of insert (5’ -> 3’) with color coded codons corresponding to: XhoI- Kozak- MYC isoform 2 (ΔMBII: W135A)- glycine-serine enhanced T2A linker sequence- T2A- BCL2- spacer- EcoRI

CTCGAGGTTGCCACCATGCCCCTCAACGTTAGCTTCACCAACAGGAACTATGACCTCGACTACGACTCGGTGCAGCC
GTATTTCTACTGCGACGAGGAGGAGAACTTCTACCAGCAGCAGCAGCAGAGCGAGCTGCAGCCCCCGGCGCCCAG
CGAGGATATCTGGAAGAAATTCGAGCTGCTGCCCACCCCGCCCCTGTCCCCTAGCCGCCGCTCCGGGCTCTGCTCGC
CCTCCTACGTTGCGGTCACACCCTTCTCCCTTCGGGGAGACAACGACGGCGGTGGCGGGAGCTTCTCCACGGCCGA
CCAGCTGGAGATGGTGACCGAGCTGCTGGGAGGAGACATGGTGAACCAGAGTTTCATCTGCGACCCGGACGACGA
GACCTTCATCAAAAACATCATCATCCAGGACTGTATGGCCAGCGGCTTCTCGGCCGCCGCCAAGCTCGTCTCAGAGA
AGCTGGCCTCCTACCAGGCTGCGCGCAAAGACAGCGGCAGCCCGAACCCCGCCCGCGGCCACAGCGTCTGCTCCAC
CTCCAGCTTGTACCTGCAGGATCTGAGCGCCGCCGCCTCAGAGTGCATCGACCCCTCGGTGGTCTTCCCCTACCCTCT
CAACGACAGCAGCTCGCCCAAGTCCTGCGCCTCGCAAGACTCCAGCGCCTTCTCTCCGTCCTCGGATTCTCTGCTCTC
CTCGACGGAGTCCTCCCCGCAGGGCAGCCCCGAGCCCCTGGTGCTCCATGAGGAGACACCGCCCACCACCAGCAGC
GACTCTGAGGAGGAACAAGAAGATGAGGAAGAAATCGATGTTGTTTCTGTGGAAAAGAGGCAGGCTCCTGGCAAA
AGGTCAGAGTCTGGATCACCTTCTGCTGGAGGCCACAGCAAACCTCCTCACAGCCCACTGGTCCTCAAGAGGTGCC
ACGTCTCCACACATCAGCACAACTACGCAGCGCCTCCCTCCACTCGGAAGGACTATCCTGCTGCCAAGAGGGTCAAG
TTGGACAGTGTCAGAGTCCTGAGACAGATCAGCAACAACCGAAAATGCACCAGCCCCAGGTCCTCGGACACCGAG
GAGAATGTCAAGAGGCGAACACACAACGTCTTGGAGCGCCAGAGGAGGAACGAGCTAAAACGGAGCTTTTTTGCC
CTGCGTGACCAGATCCCGGAGTTGGAAAACAATGAAAAGGCCCCCAAGGTAGTTATCCTTAAAAAAGCCACAGCAT
ACATCCTGTCCGTCCAAGCAGAGGAGCAAAAGCTCATTTCTGAAGAGGACTTGTTGCGGAAACGACGAGAACAGTT
GAAACACAAACTTGAACAGCTACGGAACTCTTGTGCGAACGGATCCGGCAGCGGCGGGGAAGGAAGGGGCTCCCT
GCTCACCTGCGGCGACGTGGAAGAGAACCCCGGACCTATGGCGCACGCTGGGAGAACAGGGTACGATAACCGGGA
GATAGTGATGAAGTACATCCATTATAAGCTGTCGCAGAGGGGCTACGAGTGGGATGCGGGAGATGTGGGAGCCGCT
CCTCCTGGTGCCGCTCCCGCACCGGGCATCTTCTCCTCCCAGCCTGGGCACACGCCTCATCCAGCCGCATCCCGGGAT
CCTGTCGCCAGGACCTCGCCTCTGCAGACACCGGCTGCTCCTGGAGCTGCTGCAGGACCTGCGCTCAGCCCGGTGC
CACCTGTGGTCCACCTGACCCTCCGCCAGGCCGGCGACGACTTCTCCCGCCGCTACCGCCGCGACTTCGCCGAGATG
TCCAGCCAGCTGCACCTGACGCCCTTCACCGCGCGGGGACGCTTTGCCACGGTGGTGGAGGAGCTCTTCAGGGAC
GGGGTGAACTGGGGGAGGATTGTGGCCTTCTTTGAGTTCGGTGGGGTCATGTGTGTGGAGAGCGTCAACCGGGAG
ATGTCGCCCCTGGTGGACAACATCGCCCTGTGGATGACTGAGTACCTGAACCGGCACCTGCACACCTGGATCCAGGA
TAACGGAGGCTGGGATGCCTTTGTGGAACTGTACGGCCCCAGCATGCGGCCTCTGTTTGATTTCTCCTGGCTGTCTCT
GAAGACTCTGCTCAGTTTGGCCCTGGTGGGAGCTTGCATCACCCTGGGTGCCTATCTGGGCCACAAGTGATAGAACG
CGGCCGCACCGGTGGATCCTACGTAGAATTC

Appendix 12 – Ethical approval reference number

A representative copy of amendment 1 in the Ethical approval, with reference number 07/Q1206/47. A-C indicates the order of pages.

A

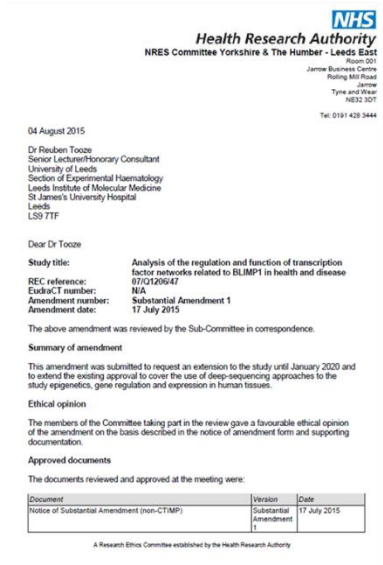

NHS
Health Research Authority
NRES Committee Yorkshire & The Humber - Leeds East
Room 001
Jarrow Business Centre
Rolling Mill Road
Jarrow
Tyne and Wear
NE32 3DT

Tel: 0191 428 3444

04 August 2015

Dr Reuben Tooze
Senior Lecturer/Honorary Consultant
University of Leeds
Section of Experimental Haematology
Leeds Institute of Molecular Medicine
St James's University Hospital
Leeds
LS9 7TF

Dear Dr Tooze

Study title: Analysis of the regulation and function of transcription factor networks related to BLIMP1 in health and disease
REC reference: 07/Q1206/47
EudraCT number: N/A
Amendment number: Substantial Amendment 1
Amendment date: 17 July 2015

The above amendment was reviewed by the Sub-Committee in correspondence.

Summary of amendment

This amendment was submitted to request an extension to the study until January 2020 and to extend the existing approval to cover the use of deep-sequencing approaches to the study epigenetics, gene regulation and expression in human tissues.

Ethical opinion

The members of the Committee taking part in the review gave a favourable ethical opinion of the amendment on the basis described in the notice of amendment form and supporting documentation.

Approved documents

The documents reviewed and approved at the meeting were:

Document	Version	Date
Notice of Substantial Amendment (non-CT/MP)	Substantial Amendment 1	17 July 2015

A Research Ethics Committee established by the Health Research Authority

B

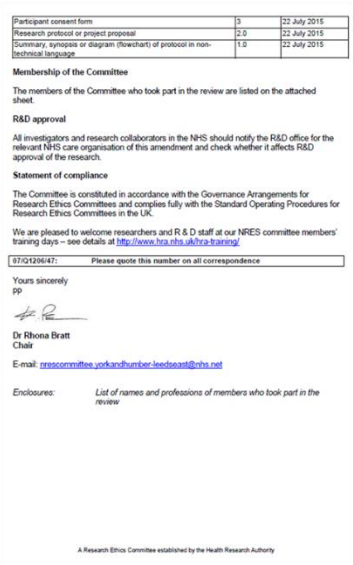

Participant consent form	3	22 July 2015
Research protocol or project proposal	2.0	22 July 2015
Summary, synopsis or diagram (flowchart) of protocol in non-technical language	1.0	22 July 2015

Membership of the Committee

The members of the Committee who took part in the review are listed on the attached sheet.

R&D approval

All investigators and research collaborators in the NHS should notify the R&D office for the relevant NHS care organisation of this amendment and check whether it affects R&D approval of the research.

Statement of compliance

The Committee is constituted in accordance with the Governance Arrangements for Research Ethics Committees and complies fully with the Standard Operating Procedures for Research Ethics Committees in the UK.

We are pleased to welcome researchers and R & D staff at our NRES committee members' training days – see details at http://www.hra.nhs.uk/hra-training/

07/Q1206/47: **Please quote this number on all correspondence**

Yours sincerely
pp

Dr Rhona Bratt
Chair

E-mail: nrescommittee.yorkandhumber-leedseast@nhs.net

Enclosures: *List of names and professions of members who took part in the review*

A Research Ethics Committee established by the Health Research Authority

C

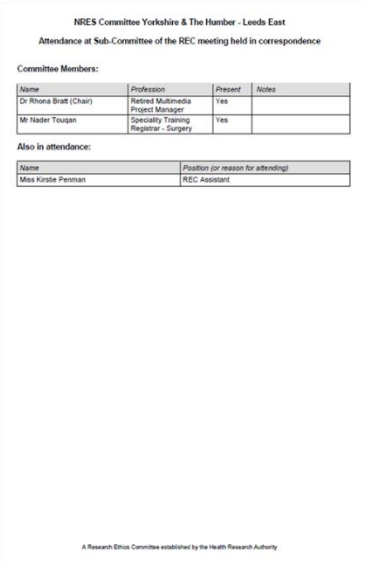

NRES Committee Yorkshire & The Humber - Leeds East

Attendance at Sub-Committee of the REC meeting held in correspondence

Committee Members:

Name	Profession	Present	Notes
Dr Rhona Bratt (Chair)	Retired Multimedia Project Manager	Yes	
Mr Nader Tougan	Speciality Training Registrar - Surgery	Yes	

Also in attendance:

Name	Position (or reason for attending)
Miss Kirstie Penman	REC Assistant

A Research Ethics Committee established by the Health Research Authority

Appendix 13 – Ethical approval IRAS reference

A representative copy of the IRAS reference 187050 in Ethical approval; A-D indicates the order of pages.

A

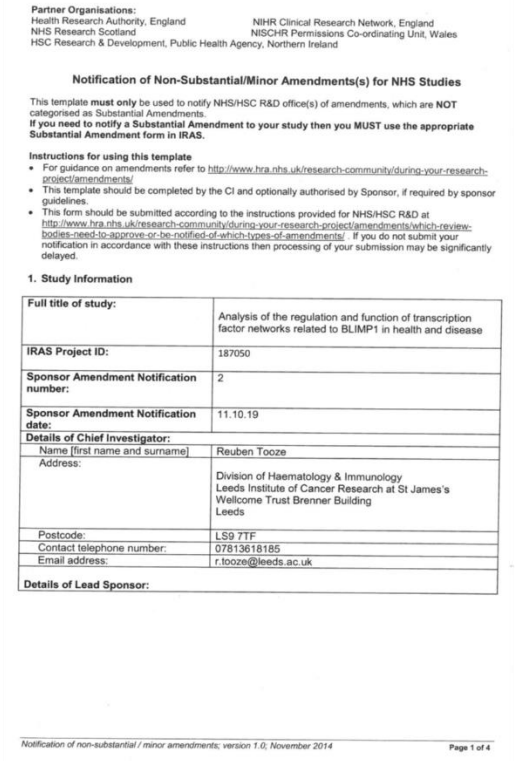

Partner Organisations:
Health Research Authority, England — NIHR Clinical Research Network, England
NHS Research Scotland — NISCHR Permissions Co-ordinating Unit, Wales
HSC Research & Development, Public Health Agency, Northern Ireland

Notification of Non-Substantial/Minor Amendments(s) for NHS Studies

This template **must only** be used to notify NHS/HSC R&D office(s) of amendments, which are **NOT** categorised as Substantial Amendments.
If you need to notify a Substantial Amendment to your study then you MUST use the appropriate Substantial Amendment form in IRAS.

Instructions for using this template

- For guidance on amendments refer to http://www.hra.nhs.uk/research-community/during-your-research-project/amendments/
- This template should be completed by the CI and optionally authorised by Sponsor, if required by sponsor guidelines.
- This form should be submitted according to the instructions provided for NHS/HSC R&D at http://www.hra.nhs.uk/research-community/during-your-research-project/amendments/which-review-bodies-need-to-approve-or-be-notified-of-which-types-of-amendments/ . If you do not submit your notification in accordance with these instructions then processing of your submission may be significantly delayed.

1. Study Information

Full title of study:	Analysis of the regulation and function of transcription factor networks related to BLIMP1 in health and disease
IRAS Project ID:	187050
Sponsor Amendment Notification number:	2
Sponsor Amendment Notification date:	11.10.19
Details of Chief Investigator:	
Name [first name and surname]	Reuben Tooze
Address:	Division of Haematology & Immunology Leeds Institute of Cancer Research at St James's Wellcome Trust Brenner Building Leeds
Postcode:	LS9 7TF
Contact telephone number:	07813618185
Email address:	r.tooze@leeds.ac.uk
Details of Lead Sponsor:	

Notification of non-substantial / minor amendments; version 1.0; November 2014 — Page 1 of 4

B

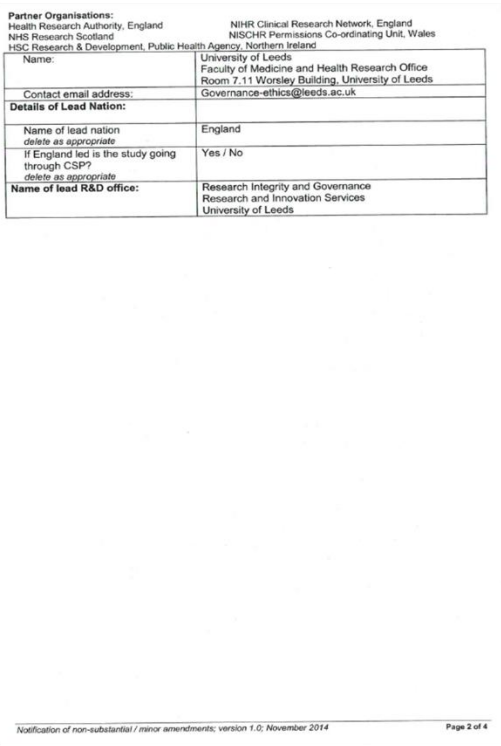

Partner Organisations:
Health Research Authority, England — NIHR Clinical Research Network, England
NHS Research Scotland — NISCHR Permissions Co-ordinating Unit, Wales
HSC Research & Development, Public Health Agency, Northern Ireland

Name:	University of Leeds Faculty of Medicine and Health Research Office Room 7.11 Worsley Building, University of Leeds
Contact email address:	Governance-ethics@leeds.ac.uk
Details of Lead Nation:	
Name of lead nation *delete as appropriate*	England
If England led is the study going through CSP? *delete as appropriate*	Yes / No
Name of lead R&D office:	Research Integrity and Governance Research and Innovation Services University of Leeds

Notification of non-substantial / minor amendments; version 1.0; November 2014 — Page 2 of 4

C

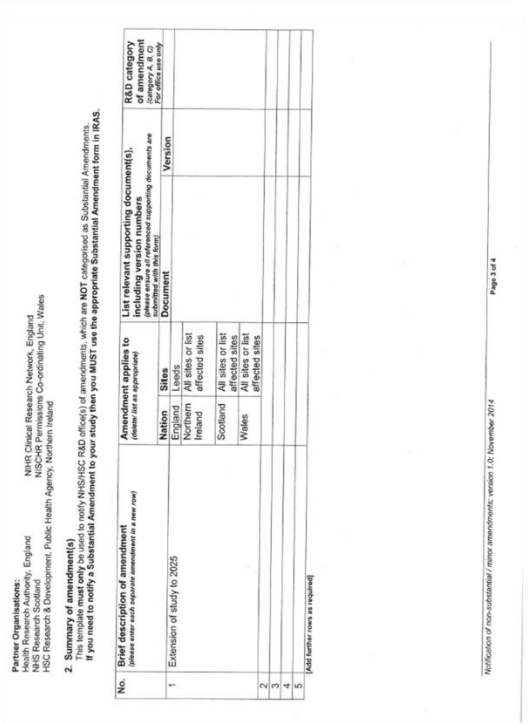

Partner Organisations:
Health Research Authority, England — NIHR Clinical Research Network, England
NHS Research Scotland — NISCHR Permissions Co-ordinating Unit, Wales
HSC Research & Development, Public Health Agency, Northern Ireland

2. Summary of amendment(s)
This template **must only** be used to notify NHS/HSC R&D office(s) of amendments, which are **NOT** categorised as Substantial Amendments.
If you need to notify a Substantial Amendment to your study then you MUST use the appropriate Substantial Amendment form in IRAS.

No.	Brief description of amendment *(please enter each separate amendment in a new row)*	Amendment applies to *(delete list as appropriate)*		List relevant supporting document(s), including version numbers *(please ensure all referenced supporting documents are submitted with this form)*		R&D category of amendment *(category A, B, C) For office use only*
		Nation	Sites	Document	Version	
1	Extension of study to 2025	England	Leeds			
		Northern Ireland	All sites or list affected sites			
		Scotland	All sites or list affected sites			
		Wales	All sites or list affected sites			
2						
3						
4						
5	[Add further rows as required]					

Notification of non-substantial / minor amendments; version 1.0; November 2014 — Page 3 of 4

D

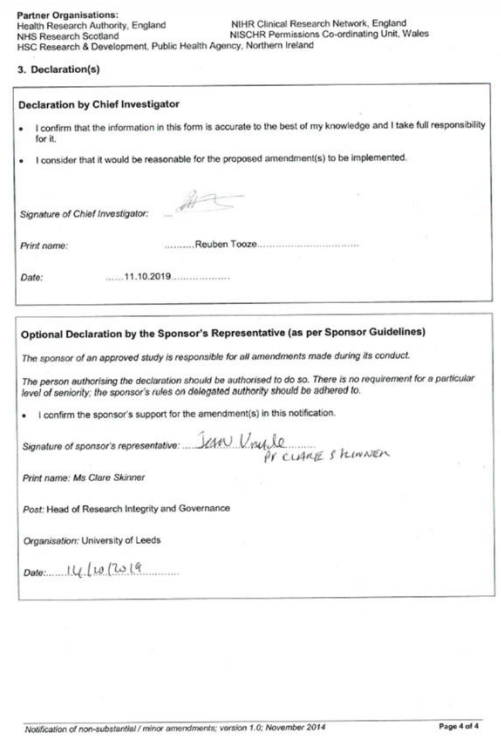

Partner Organisations:
Health Research Authority, England — NIHR Clinical Research Network, England
NHS Research Scotland — NISCHR Permissions Co-ordinating Unit, Wales
HSC Research & Development, Public Health Agency, Northern Ireland

3. Declaration(s)

Declaration by Chief Investigator

- I confirm that the information in this form is accurate to the best of my knowledge and I take full responsibility for it.
- I consider that it would be reasonable for the proposed amendment(s) to be implemented.

Signature of Chief Investigator: ...

Print name: .....Reuben Tooze.....

Date: .....11.10.2019.....

Optional Declaration by the Sponsor's Representative (as per Sponsor Guidelines)

The sponsor of an approved study is responsible for all amendments made during its conduct.

The person authorising the declaration should be authorised to do so. There is no requirement for a particular level of seniority; the sponsor's rules on delegated authority should be adhered to.

- I confirm the sponsor's support for the amendment(s) in this notification.

Signature of sponsor's representative: ..... Jean Vaule pp CLARE S SKINNER

Print name: Ms Clare Skinner

Post: Head of Research Integrity and Governance

Organisation: University of Leeds

Date: ..... 14/10/2019 .....

Notification of non-substantial / minor amendments; version 1.0; November 2014 — Page 4 of 4

Appendix 14 – Ethical approval amendment confirmation

A representative copy of the email confirming the amendment in the ethical approval.

IRAS [No IRAS Project ID entered]. Amendment categorisation and implementation information

LN LEEDSEAST, Nrescommitteeyorkandhumber- (HEALTH RESEARCH AUTHORITY)<nrescommittee.yorkandhumber-leedseast@nhs.net>

To: Reuben Tooze

Amendment Categorisation and Implementation Information

Dear Dr Tooze,

Short Study Title:	BLIMP1 related transcription factor network in health and disease 1
Date complete amendment submission received:	14th October 2019
Amendment No./ Sponsor Ref:	Non-Substantial Amendment 2, 11/10/2019
Amendment Date:	14 October 2019
Amendment Type:	Non-substantial
Outcome of HRA and HCRW Assessment	**This email also constitutes HRA and HCRW Approval for the amendment,** and you should not expect anything further.
Implementation date in NHS organisations in England and Wales	35 days from date amendment information together with this email, is supplied to participating organisations **(providing conditions are met)**
For NHS/HSC R&D Office information	
Amendment Category	A

Thank you for submitting an amendment to your project. We have now categorised your amendment and please find this, as well as other relevant information, in the table above.

What should I do next?

Please read the information in IRAS, which provides you with information on how and when you can implement your amendment at NHS/HSC sites in each nation, and what actions you should take now.

If you have participating NHS/HSC organisations in any other UK nations please note that **we will** forward the amendment submission to the relevant national coordinating function(s).

If not already provided, please email to us any regulatory approvals (where applicable) once available.

When can I implement this amendment?

You may implement this amendment in line with the information in IRAS. Please note that you may only implement changes described in the amendment notice.

Who should I contact if I have further questions about this amendment?

If you have any questions about this amendment please contact the relevant national coordinating centre for advice:

- England – hra.amendments@nhs.net
- Northern Ireland – research.gateway@hscni.net
- Scotland – nhsg.NRSPCC@nhs.net
- Wales – HCRW.amendments@wales.nhs.uk

Additional information on the management of amendments can be found in the IRAS guidance.

User Feedback

The Health Research Authority is continually striving to provide a high quality service to all applicants and sponsors. You are invited to give your view of the service you have received and the application procedure. If you wish to make your views known please use the feedback form available on the HRA website: http://www.hra.nhs.uk/about-the-hra/governance/quality-assurance/.

Please do not hesitate to contact me if you require further information.

Kind regards

Miss Jane Harker
Approvals Administrator
Health Research Authority
Ground Floor | Skipton House | 80 London Road | London | SE1 6LH
E.hra.amendments@nhs.net
W. www.hra.nhs.uk

Sign up to receive our newsletter HRA Latest.